DE GRUYTER

METALS, MICROBES, AND MINERALS: THE BIOGEOCHEMICAL SIDE OF LIFE

Edited by Peter M. H. Kroneck and Martha E. Sosa Torres

Series edited by Astrid Sigel, Eva Freisinger, Roland K. O. Sigel

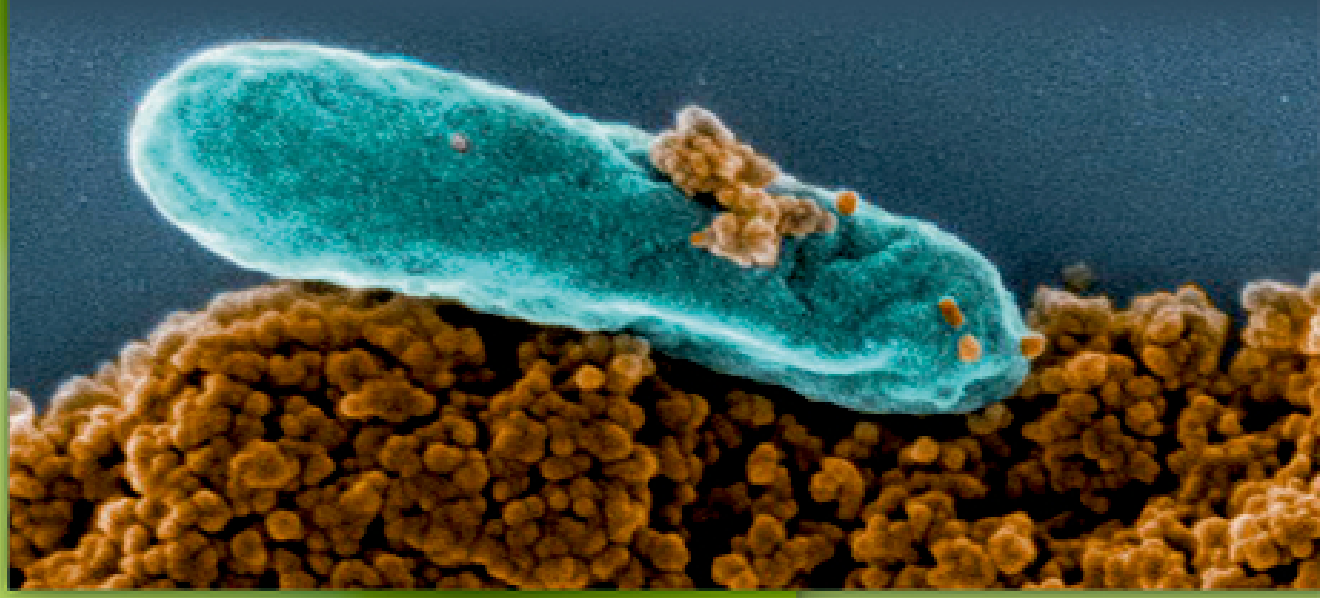

METAL IONS IN LIFE SCIENCES 21

Astrid Sigel, Eva Freisinger, Roland K. O. Sigel
Metal Ions in Life Sciences 21

Metal Ions in Life Sciences

Edited by
Astrid Sigel, Eva Freisinger and Roland K. O. Sigel

Volume 21

Guest Editors:
Peter M. H. Kroneck and Martha E. Sosa Torres

Metals, Microbes, and Minerals: The Biogeochemical Side of Life

DE GRUYTER

Series Editors

Astrid Sigel
Department of Chemistry
Inorganic Chemistry
University of Basel
Spitalstrasse 51
CH-4056 Basel
Switzerland
<astrid.sigel@unibas.ch>

Eva Freisinger and Roland K. O. Sigel
Department of Chemistry
University of Zürich
Winterthurerstrasse 190
CH-8057 Zürich
Switzerland
<freisinger@chem.uzh.ch>
<roland.sigel@chem.uzh.ch>

Guest Editors

Peter M. H. Kroneck
Fachbereich Biologie
Universität Konstanz
Universitätsstrasse 10
D-78457 Konstanz
Germany
<peter.kroneck@uni-konstanz.de>

Martha E. Sosa Torres
Departamento de Química
Inorgánica y Nuclear
Facultad de Química
Universidad Autónoma de México
Ciudad Universitaria
México, D.F. 04510
México
<mest@unam.mx>

ISBN 978-3-11-058890-3
e-ISBN (PDF) 978-3-11-058977-1
e-ISBN (EPUB) 978-3-11-058893-4
ISSN 1559-0836
e-ISSN 1868-0402
DOI: 10.1515/9783110588903

Library of Congress Control Number: 2020941700

Bibliographic information published by the Deutsche Nationalbibliothek
The Deutsche Nationalbibliothek lists this publication in the Deutsche Nationalbibliografie; detailed bibliographic data are available on the Internet at http://dnb.dnb.de.

Cover illustration: The figure shows the soil bacterium *Shewanella oneidensis* MR-1 (courtesy A. Kappler, University of Tübingen; Chapter 7).

Typesetting: Meta Systems Publishing & Printservices GmbH, Wustermark, Germany
Printing and binding: CPI books GmbH, Leck

For further volumes: www.mils-WdG.com
www.degruyter.com

About the Editors

Peter M. H. Kroneck received his Diploma in Chemistry from the University of Basel (Switzerland) and his PhD from the University of Konstanz (Germany). He worked as a postdoctoral student with Jack T. Spence, Utah State University (Logan, USA), and he was a visiting professor with Helmut Beinert, University of Wisconsin (Madison, USA), with Israel Pecht, Weizmann Institute of Science (Rehovot, Israel), with William E. Antholine, National EPR Center, Medical College of Wisconsin (Milwaukee, USA), and in 2012 he was the Robert Noyce Professor at Grinnell College (Grinnell, USA). He was the head of the Bioinorganic Research Group at the University of Konstanz, where he became a Professor of Biochemistry in 1989. In 2002, he received the Medal of the European Society of Biological Inorganic Chemistry; in 2009 he was the first Non-US scientist who chaired the Gordon Research Conference "Metals in Biology". His group's research activities have focused on structural and spectroscopic properties of copper, iron, molybdenum and tungsten enzymes and their functional roles in the biogeochemical cycles of nitrogen and sulfur.

Martha E. Sosa Torres is Full Professor of Chemistry at the Universidad Nacional Autónoma de México (UNAM, Mexico). She received her Bachelor and Master Degree in Chemistry summa cum laude from UNAM, and her PhD from the University College London (U.K.) working with Martin L. Tobe. She did postdoctoral work with Martin Hughes, King's College London (U.K.), and she was a visiting professor at the University of Konstanz and the University of Freiburg in Germany. She received several prestigious fellowships from international institutions. In 2008, she organized the Summer School "Metal Ions in Biology – Key Elements of Life" in Cuernavaca (Mexico) sponsored by the German Academic Exchange Service (DAAD). Her research is directed towards the understanding of inorganic reaction mechanisms, with focus on dioxygen activation. Her group is interested in the spectroscopic, magnetic, and structural analysis of metal complexes, in the properties of metalloenzymes, and in Multi-Frequency Electron Paramagnetic Resonance. Furthermore, she explores multi-functional materials based on transition metal compounds including lanthanide complexes.

Astrid Sigel has studied languages; she was an Editor of the *Metal Ions in Biological Systems* series (until Volume 44) and also of the "Handbook on Toxicity of Inorganic Compounds" (1988), the "Handbook on Metals in Clinical and Analytical Chemistry" (1994; both with H. G. Seiler), and the "Handbook on

Metalloproteins" (2001; with Ivano Bertini). She is also an Editor of the *MILS* series from Volume 1 on, and she coauthored about 50 papers on topics in Bioinorganic Chemistry.

Eva Freisinger is Associate Professor for Bioinorganic Chemistry and Chemical Biology (2018) at the Department of Chemistry at the University of Zürich, Switzerland. She obtained her doctoral degree (2000) from the University of Dortmund, Germany, working with Bernhard Lippert and spent three years as a postdoc at SUNY Stony Brook, USA, with Caroline Kisker. Since 2003, she performs independent research at the University of Zürich where she held a Förderungsprofessur of the Swiss National Science Foundation from 2008 to 2014. In 2014, she received her *Habilitation* in Bioinorganic Chemistry. Her research is focused on the study of plant metallothioneins with an additional interest in the sequence-specific modification of nucleic acids. Together with Roland Sigel she chaired the 12th European Bioinorganic Chemistry Conference (2014 in Zürich, Switzerland) and the 19th International Conference on Biological Inorganic Chemistry (2019 in Interlaken, Switzerland). She also serves on several Advisory Boards for international conference series; since 2014 she is the Secretary of the European Bioinorganic Chemistry Conferences (EuroBICs), and an Editorial Board Member of the *Journal of Inorganic Biochemistry*. She joined the group of editors of the *MILS* series from Volume 18 on.

Roland K. O. Sigel is Full Professor (2016) of Chemistry at the University of Zürich, Switzerland. In the same year he became Vice Dean of Studies (B.Sc./M.Sc.) and in 2017 he was elected Dean of the Faculty of Science. From 2003 to 2008 he was endowed with a Förderungsprofessur of the Swiss National Science Foundation, and he is the recipient of an ERC Starting Grant 2010. He received his doctoral degree summa cum laude (1999) from the University of Dortmund, Germany, working with Bernhard Lippert. Thereafter, he spent nearly three years at Columbia University, New York, USA, with Anna Marie Pyle (now Yale University). During the six years abroad he received several prestigious fellowships, and he was awarded the EuroBIC Medal in 2008 and the Alfred Werner Prize (SCS) in 2009. 2015–2019 he was the Secretary of the Society of Biological Inorganic Chemistry (SBIC) and since 2018 he is the Secretary of the International Conferences of Biological Inorganic Chemistry (ICBICs). His research focuses on the structural and functional role of metal ions in ribozymes, especially group II introns, regulatory RNAs, and on related topics. He is also an Editor of Volumes 43 and 44 of the *MIBS* series and of the *MILS* series from Volume 1 on.

Historical Development and Perspectives of the Series *Metal Ions in Life Sciences*[*]

It is old wisdom that metals are indispensable for life. Indeed, several of them, like sodium, potassium, and calcium, are easily discovered in living matter. However, the role of metals and their impact on life remained largely hidden until inorganic chemistry and coordination chemistry experienced a pronounced revival in the 1950s. The experimental and theoretical tools created in this period and their application to biochemical problems led to the development of the field or discipline now known as *Bioinorganic Chemistry*, *Inorganic Biochemistry*, or more recently also often addressed as *Biological Inorganic Chemistry.*

By 1970 *Bioinorganic Chemistry* was established and further promoted by the book series *Metal Ions in Biological Systems* founded in 1973 (edited by H. S., who was soon joined by A. S.) and published by Marcel Dekker, Inc., New York, for more than 30 years. After this company ceased to be a family endeavor and its acquisition by another company, we decided, after having edited 44 volumes of the *MIBS* series (the last two together with R. K. O. S.) to launch a new and broader minded series to cover today's needs in the *Life Sciences.* Therefore, the Sigels' new series is entitled

Metal Ions in Life Sciences.

After publication of 16 volumes (since 2006) with various publishers during the past 10 years, we are happy to join forces now in this still growing endeavor with Walter de Gruyter GmbH, Berlin, Germany, a most experienced Publisher in the *Sciences.*

The development of *Biological Inorganic Chemistry* during the past 40 years was and still is driven by several factors; among these are (i) attempts to reveal the interplay between metal ions and hormones or vitamins, etc., (ii) efforts regarding the understanding of accumulation, transport, metabolism, and toxicity of metal ions, (iii) the development and application of metal-based drugs,

---

* Reproduced with some alterations by permission of John Wiley & Sons, Ltd., Chichester, UK (copyright 2006) from pages v and vi of Volume 1 of the series *Metal Ions in Life Sciences* (MILS-1).

(iv) biomimetic syntheses with the aim to understand biological processes as well as to create efficient catalysts, (v) the determination of high-resolution structures of proteins, nucleic acids, and other biomolecules, (vi) the utilization of powerful spectroscopic tools allowing studies of structures and dynamics, and (vii), more recently, the widespread use of macromolecular engineering to create new biologically relevant structures at will. All this and more is reflected in the volumes of the series *Metal Ions in Life Sciences.*

The importance of metal ions to the vital functions of living organisms, hence, to their health and well-being, is nowadays well accepted. However, in spite of all the progress made, we are still only at the brink of understanding these processes. Therefore, the series *Metal Ions in Life Sciences* links coordination chemistry and biochemistry in their widest sense. Despite the evident expectation that a great deal of future outstanding discoveries will be made in the interdisciplinary areas of science, there are still "language" barriers between the historically separate spheres of chemistry, biology, medicine, and physics. Thus, it is one of the aims of this series to catalyze mutual "understanding".

It is our hope that *Metal Ions in Life Sciences* continues to prove a stimulus for new activities in the fascinating "field" of *Biological Inorganic Chemistry.* If so, it will well serve its purpose and be a rewarding result for the efforts spent by the authors.

Astrid Sigel and Helmut Sigel
Department of Chemistry, Inorganic Chemistry
University of Basel, CH-4056 Basel, Switzerland

Roland K. O. Sigel
Department of Chemistry
University of Zürich, CH-8057 Zürich, Switzerland

October 2005
and September 2016

Preface to Volume 21

Metals, Microbes, and Minerals: The Biogeochemical Side of Life

Microorganisms are found in almost every conceivable niche of the Earth. Antoni van Leeuwenhoek from Delft, universally acknowledged as the father of microbiology, saw the *animalcules* with his hand-lens microscope in 1674. Through their metabolic activity, they affect the chemistry and physical properties of their surroundings. They play key roles in carbon and nutrient cycling, in animal (including human) and plant health, in agriculture and the global food web. Undoubtedly, microbes played an important role in the evolution of the Earth and its atmosphere. It is the aim of this book to introduce the reader to the world of microorganisms, and to recognize the role they have played in the history of the Earth, and still play in altering our environment.

Studies of microbial interactions with geological media advance the field of *Geomicrobiology*. Most likely life had a rocky start according to expert Robert Hazen. How could *dead minerals* have assisted the emergence of life? The answer is chemistry. Minerals grow from simple molecules into ordered structures; critical transformations might not have been possible without the help of minerals acting as containers, scaffolds, templates, catalysts, and reactants.

Recently, a consortium of scientists published a *Consensus Statement* concerning climate change and microorganisms. It is now well established that human activities cause unprecedented animal and plant extinctions, surprisingly microorganisms are generally not discussed in the context of climate change. They date back to the origin of life on Earth, at least 3.8 billion years ago, and they will likely exist well beyond any future extinction events. Unless humans appreciate the importance of microbial processes, they fundamentally limit their understanding of Earth's biosphere and response to climate change and thus jeopardize efforts to create an environmentally sustainable future.

Metal Ions in Life Sciences, Volume 21 Guest Editors: Peter M. H. Kroneck and Martha E. Sosa Torres
Series Editors: Astrid Sigel, Eva Freisinger, and Roland K. O. Sigel

https://doi.org/10.1515/9783110589771-202

Chapter 1 introduces the reader to the complex and fascinating microbial world. As potent chemists and geoengineers, microbes had a significant influence on the history of the Earth. And they still do, in altering our environment. Their presence within geologic media had a profound effect on themselves and on the chemical and physical properties of the surrounding environment. Note that nowadays a remarkable number of microbially catalyzed reactions have been explored down to the level of enzyme structure, active site architecture, and specific roles of neighboring amino acid residues.

Global element cycles are in the focus of *Chapter 2*. Prokaryotes (classical Bacteria and Archaea) enable not only simple exergonic redox reactions to proceed but also couple exergonic with endergonic reactions, to perform biosynthesis. Microbial transformations can be highly specific and can direct reactions towards single types of products, such as the stereospecific production of one enantiomer, an important application in nowadays biotechnology. Therefore, they hold great promise for future applications in degradative and biosynthetic activities.

Chapter 3 emphasizes that biological processes leave an "imprint" in the form of non-equilibrium isotope distributions in metabolites, which have been intensively studied in sediments of various Earth ages. A central finding is that isotope fractionation occurs with high variability. Three different scales are investigated, (i) the enzyme level, (ii) the cell level, and (iii) the ecosystem level. The isotope fractionation of carbon from CO_2 in water oxidizing phototrophs, and the fractionation of sulfur from sulfate during microbial reduction of sulfate to hydrogen sulfide are discussed and fodder for future integration across these scales is provided.

The *in situ* detection and visualization of metals within cells and tissues is addressed in *Chapter 4*. Advances in imaging techniques, notably improved detection sensitivity and spatial resolution, enable metal imaging from the mesoscale down to the nanoscale size regime. The most important techniques for quantifying and visualizing biological metals are reviewed. Direct detection approaches (X-ray fluorescence microscopy, secondary ion mass spectrometry, laser-ablation inductively coupled mass spectrometry) and indirect imaging methods (fluorescence microscopy, magnetic resonance imaging) are discussed in detail.

Metal-bearing minerals are an integral part of almost all "metabolism-first"-type scenarios for the emergence of life as highlighted in *Chapter 5*. Metabolism-first scenarios stand in opposition to primordial soup hypotheses which envisage prebiotic synthesis of organic molecules as building blocks enabling life to come into being. A critical analysis of the historical roots of these emergence of life hypotheses points out fundamental inconsistencies, thus it is necessary to appeal to basic thermodynamic principles to provide rigorous guidelines for developing contradiction-free models. Combining these guidelines with the current understanding of biological energy conversion, arguably the process most fundamental to all life, strongly suggests an expansion of previous mineral-based scenarios.

Chapter 6 centers on magnetotactic bacteria, which form so-called magnetosomes, intracellular organelles consisting of ferrimagnetic crystals which sequester and biomineralize large amounts of iron in specific membrane-enclosed com-

partments. Magnetosome biosynthesis is under spatio-temporal control by specific factors and functions. The resulting cellular dipole moment acts like a compass needle which aligns the cell in the geomagnetic field. Magnetotaxis appears to facilitate the navigation of the actively swimming bacterial cells along vertical redox gradients within stratified sediments of natural waters. Recent knowledge on the diversity and ecology of magnetotactic bacteria is summarized as is the process of magnetosome biomineralization.

Chapter 7 elucidates important aspects of microbial life on iron. Reduced and oxidized iron compounds are present in virtually all of Earth's environments. Fe is essential to all (micro)organisms because it is a key constituent of numerous metalloenzymes. It can be used as an electron donor, or acceptor, by microorganisms for metabolic redox reactions which generate energy and drive growth. In this chapter it is discussed how different types of Fe(II)-oxidizing (aerobic, microaerophilic, anoxygenic phototrophic, anaerobic nitrate-reducing) and Fe(III)-reducing (ammonium-oxidizing, organic matter-oxidizing, methanotrophic, sulfur-oxidizing) microorganisms use the oxidation and reduction of Fe(II) and Fe(III), respectively, to generate energy and to produce biomass.

In *Chapter 8* recent advances in the field of extracellular redox chemistry are summarized. Life depends on metals and their redox transformations within the biologically accessible potential range. These transformations influence their mobility in water, their bioavailability, their toxicity, and their affinity towards biomolecules. The current state of the art is surveyed regarding the interaction between living organisms and metals with respect to the mechanisms of microbial assimilatory metal uptake, with special emphasis on iron. Direct metal uptake by membrane transporters and indirect metal uptake by metallophores are addressed. The implications of the extracellular redox chemistry of microbes for the environment, health, and biotechnology are discussed, including open questions that reveal new possibilities for diverse applications.

Metal ions have driven many of biology's catalytic processes since life first evolved, however, this advantage is a double-edged sword. Some metal ions are essential but also toxic if not processed properly, and others are non-essential but toxic if available. These aspects are in the focus of *Chapter 9*. The molecular methods that microorganisms have developed to deal with toxic metal ions (Cr, Ag, Au, Cd, Hg) are covered as are the toxic effects of the nutrient metals under dis-homeostasis. Toxic but rare or unavailable elements are not covered, yet brief introductions to some non-nutrient but highly toxic metals and metalloids of groups 13–15, Al, Tl, Pb, As, and Bi are included.

Chapter 10 focuses on rare earth elements essential for our daily life. Just think of their use in high technologies like cellular phones and computers, and the use in renewable energy applications. Their interaction with biomolecules and living organisms, and the exploitation of their photo-physical properties for a range of applications in biochemistry and medicine have been studied for many decades. Yet, an entirely new area of research has emerged in the past ten years after it was established that many bacteria utilize certain rare earth elements in their metabolism. The chapter gives an overview on the most recent developments with an account of the more established uses of rare earth elements in biochemistry, biomining, and medicine.

In conclusion, Volume 21 of the *Metal Ions in Life Sciences* series offers a wealth of in-depth information about the world of microorganisms and their important role in all aspects of life. Unique chemical reactions have been discovered which employ novel sophisticated transition metal centers. They have been explored to the level of enzyme structure, active site architecture, and specific roles of neighboring amino acid residues, and can be understood nowadays at atomic resolution.

It is the study of microbial interactions with geological media, which advances the field of *Geomicrobiology*. Significant advances in the understanding of these novel metal centers, such as CuA and CuZ present in nitrous oxide reductase, the coupled siroheme-[4Fe-4S] cluster of dissimilatory sulfite reductase, the super catalyst cytochrome P_{450} heme thiolate, or the Fe- and V,Mo Fe-S clusters of nitrogenase to name a few, have been achieved by the application of powerful spectroscopic and biochemical techniques, as also discussed in greater detail in Volume 20 of *Metal Ions in Life Sciences*, entitled *Transition Metal Ions and Sulfur: A Strong Relationship for Life.*

Peter M. H. Kroneck
Martha E. Sosa Torres

Contents

Contributors to Volume 21

Numbers in parentheses indicate the pages on which the authors' contributions begin.

Frauke Baymann Aix Marseille University, CNRS, BIP (UMR 7281), 31 chemin Joseph-Aiguier, F-13402 Marseille, Cedex 20, France <baymann@imm.cnrs.fr> (135)

Stefanie Becker Geomicrobiology, Department of Geosciences, Universität Tübingen, Schnarrenbergstrasse 94–96, D-72074 Tübingen, Germany <stefanie.becker@geo.uni-tuebingen.de> (185)

Elbert Branscomb Carl R. Woese Institute for Genomic Biology, and Department of Physics, University of Illinois, Urbana, IL 61801, USA <brnscmb@illinois.edu> (135)

Lena J. Daumann Department Chemie, Ludwigs-Maximilians-Universität, Butenandtstrasse 5, D-81377 München, Germany, <lena.daumann@lmu.de> (299)

Simon Duval Aix Marseille University, CNRS, BIP (UMR 7281), 31 chemin Joseph-Aiguier, F-13402 Marseille, Cedex 20, France <sduval@imm.cnrs.fr> (135)

Allison M. L. Enright Geomicrobiology, Department of Geosciences, Universität Tübingen, Schnarrenbergstrasse 94–96, D-72074 Tübingen, Germany <allison.m.enright@gmail.com> (185)

Christoph J. Fahrni School of Chemistry and Biochemistry, Petit Institute for Bioengineering and Bioscience, Georgia Institute of Technology, Atlanta, GA 30332, USA <fahrni@chemistry.gatech.edu> (81)

Shefali Harankhedkar School of Chemistry and Biochemistry, Petit Institute for Bioengineering and Bioscience, Georgia Institute of Technology, Atlanta, GA 30332, USA (81)

Andreas Kappler Geomicrobiology, Department of Geosciences, Universität Tübingen, Schnarrenbergstrasse 94–96, D-72074 Tübingen, Germany <andreas.kappler@uni-tuebingen.de> (185)

Peter M. H. Kroneck Department of Biology, University of Konstanz, D-78457 Konstanz, Germany <peter.kroneck@uni-konstanz.de> (1)

Ricardo O. Louro Instituto de Tecnologia Química e Biológica António Xavier, Universidade NOVA de Lisboa, Av. da República EAN, PT-2780-157 Oeiras, Portugal <louro@itqb.unl.pt> (229)

Shawn McGlynn Earth-Life Science Institute, Tokyo Institute of Technology, Ookayama, Tokyo, 152-8559, Japan <mcglynn@elsi.jp> (59)

Arielle Nabatilan School of Chemistry and Biochemistry, Petit Institute for Bioengineering and Bioscience, Georgia Institute of Technology, Atlanta, GA 30332, USA (81)

Wolfgang Nitschke Aix Marseille University, CNRS, BIP (UMR 7281), 31 chemin Joseph-Aiguier, F-13402 Marseille, Cedex 20, France <nitschke@imm.cnrs.fr> (135)

Huub J. M. Op den Camp Department of Microbiology/72, Faculty of Science, Radboud University Nijmegen, Heyendaalseweg 135, P.O. Box 9010, NL-6525 AJ Nijmegen, The Netherlands <h.opdencamp@science.ru.nl> (299)

Catarina M. Paquete Instituto de Tecnologia Química e Biológica António Xavier, Universidade NOVA de Lisboa, Av. da República EAN, PT-2780-157 Oeiras, Portugal <cpaquete@itqb.unl.pt> (229)

Michael J. Russell NASA Astrobiology Institute, Ames Research Center, California, USA, and Dipartimento di Chimica, Università degli Studi di Torino, via P. Giuria 7, I-10125 Turin, Italy <michaeljrussel80@gmail.com> (135)

Bernhard Schink Department of Biology, University of Konstanz, D-78457 Konstanz, Germany <bernhard.schink@uni-konstanz.de> (33)

Barbara Schoepp-Cothenet Aix Marseille University, CNRS, BIP (UMR 7281), 31 chemin Joseph-Aiguier, F-13402 Marseille, Cedex 20, France <schoepp@imm.cnrs.fr> (135)

Dirk Schüler Department of Microbiology, University of Bayreuth, D-95447 Bayreuth, Germany <dirk.schueler@uni-bayreuth.de> (159)

Martha E. Sosa Torres Departamento de Química Inorgánica y Nuclear, Facultad de Química, Universidad Nacional Autónoma de México, Ciudad Universitaria, México, D.F. 04510, México <mest@unam.mx> (1)

Inês B. Trindade Instituto de Tecnologia Química e Biológica António Xavier, Universidade NOVA de Lisboa, Av. da República EAN, PT-2780-157 Oeiras, Portugal <ines.trindade@itqb.unl.pt> (229)

René Uebe Department of Microbiology, University of Bayreuth, D-95447 Bayreuth, Germany <rene.uebe@uni-bayreuth.de> (159)

Anthony G. Wedd School of Chemistry and Bio21 Molecular Science and Biotechnology Institute, University of Melbourne, Parkville, Victoria 3010, Australia <agw@unimelb.edu.au> (271)

Zhiguang Xiao Melbourne Dementia Research Centre, Florey Institute of Neuroscience and Mental Health, The University of Melbourne, Parkville, Victoria 3052, Australia, <zhiguang.xiao@florey.edu.au> (271)

Jiyao Yu School of Chemistry and Biochemistry, Petit Institute for Bioengineering and Bioscience, Georgia Institute of Technology, Atlanta, GA 30332, USA (81)

Kilian Zuchan Aix Marseille University, CNRS, BIP (UMR 7281), 31 chemin Joseph-Aiguier, F-13402 Marseille, Cedex 20, France <kzuchan@imm.cnrs.fr> (135)

Titles of Volumes 1–44 in the *Metal Ions in Biological Systems* Series

edited by the SIGELs
and published by Dekker/Taylor & Francis (1973–2005)

Volume 1: **Simple Complexes**
Volume 2: **Mixed-Ligand Complexes**
Volume 3: **High Molecular Complexes**
Volume 4: **Metal Ions as Probes**
Volume 5: **Reactivity of Coordination Compounds**
Volume 6: **Biological Action of Metal Ions**
Volume 7: **Iron in Model and Natural Compounds**
Volume 8: **Nucleotides and Derivatives: Their Ligating Ambivalency**
Volume 9: **Amino Acids and Derivatives as Ambivalent Ligands**
Volume 10: **Carcinogenicity and Metal Ions**
Volume 11: **Metal Complexes as Anticancer Agents**
Volume 12: **Properties of Copper**
Volume 13: **Copper Proteins**
Volume 14: **Inorganic Drugs in Deficiency and Disease**
Volume 15: **Zinc and Its Role in Biology and Nutrition**
Volume 16: **Methods Involving Metal Ions and Complexes in Clinical Chemistry**
Volume 17: **Calcium and Its Role in Biology**
Volume 18: **Circulation of Metals in the Environment**
Volume 19: **Antibiotics and Their Complexes**
Volume 20: **Concepts on Metal Ion Toxicity**
Volume 21: **Applications of Nuclear Magnetic Resonance to Paramagnetic Species**
Volume 22: **ENDOR, EPR, and Electron Spin Echo for Probing Coordination Spheres**
Volume 23: **Nickel and Its Role in Biology**
Volume 24: **Aluminum and Its Role in Biology**
Volume 25: **Interrelations Among Metal Ions, Enzymes, and Gene Expression**
Volume 26: **Compendium on Magnesium and Its Role in Biology, Nutrition, and Physiology**
Volume 27: **Electron Transfer Reactions in Metalloproteins**

Volume 28: **Degradation of Environmental Pollutants by Microorganisms and Their Metalloenzymes**
Volume 29: **Biological Properties of Metal Alkyl Derivatives**
Volume 30: **Metalloenzymes Involving Amino Acid-Residue and Related Radicals**
Volume 31: **Vanadium and Its Role for Life**
Volume 32: **Interactions of Metal Ions with Nucleotides, Nucleic Acids, and Their Constituents**
Volume 33: **Probing Nucleic Acids by Metal Ion Complexes of Small Molecules**
Volume 34: **Mercury and Its Effects on Environment and Biology**
Volume 35: **Iron Transport and Storage in Microorganisms, Plants, and Animals**
Volume 36: **Interrelations Between Free Radicals and Metal Ions in Life Processes**
Volume 37: **Manganese and Its Role in Biological Processes**
Volume 38: **Probing of Proteins by Metal Ions and Their Low-Molecular-Weight Complexes**
Volume 39: **Molybdenum and Tungsten. Their Roles in Biological Processes**
Volume 40: **The Lanthanides and Their Interrelations with Biosystems**
Volume 41: **Metal Ions and Their Complexes in Medication**
Volume 42: **Metal Complexes in Tumor Diagnosis and as Anticancer Agents**
Volume 43: **Biogeochemical Cycles of Elements**
Volume 44: **Biogeochemistry, Availability, and Transport of Metals in the Environment**

Contents of Volumes in the *Metal Ions in Life Sciences* Series

edited by the SIGELs

Volumes 1–4

published by John Wiley & Sons, Ltd., Chichester, UK (2006–2008)
<http://www.Wiley.com/go/mils>
<http://www.wiley.com/WileyCDA/Section/id-300350.html>

Volumes 5–9

published by the Royal Society of Chemistry, Cambridge, UK (2009–2011)
since 2015 by Walter de Gruyter GmbH, Berlin, Germany
<http://www.bioinorganic-chemistry.org/mils> <http://www.mils-WdG.com>

Volumes 10–16

published by Springer Science & Business Media BV, Dordrecht, The Netherlands (2012–2014; MILS-10 to MILS-14)
and by Springer International Publishing AG, Cham, Switzerland (2015–2016; MILS-15 and MILS-16)
<http://www.bioinorganic-chemistry.org/mils>

and from Volume 17 on

published by Walter de Gruyter GmbH, Berlin, Germany
<http://www.mils-WdG.com>

Volume 1: Neurodegenerative Diseases and Metal Ions

Volume 2: Nickel and Its Surprising Impact in Nature

Volume 3: The Ubiquitous Roles of Cytochrome P450 Proteins

Volume 4: Biomineralization. From Nature to Application

Volume 5: Metallothioneins and Related Chelators

Volume 6: Metal-Carbon Bonds in Enzymes and Cofactors

Volume 7: Organometallics in Environment and Toxicology

Volume 9: Structural and Catalytic Roles of Metal Ions in RNA

Volume 10: Interplay between Metal Ions and Nucleic Acids

Volume 11: Cadmium: From Toxicity to Essentiality

Volume 12: Metallomics and the Cell
Guest Editor: Lucia Banci

Volume 13: Interrelations between Essential Metal Ions and Human Diseases

Volume 16: The Alkali Metal Ions: Their Roles for Life

Volume 17: Lead: Its Effects on Environment and Health

Comments and suggestions with regard to contents, topics, and the like for future volumes of the series are welcome.

1

Introduction: From Rocks to Living Cells

Martha E. Sosa Torres [1] ***and Peter M. H. Kroneck*** [2]

[1]Departamento de Química Inorgánica y Nuclear, Facultad de Química, Universidad Nacional Autónoma de México, Ciudad Universitaria, México, D.F. 04510, México
<mest@unam.mx>

[2]Department of Biology, University of Konstanz, D-78457 Konstanz, Germany
<peter.kroneck@uni-konstanz.de>

Abstract: Microorganisms are found in almost every conceivable niche of the Earth. They populate every habitable environment, and through their metabolic activity, affect the chemistry and physical properties of their surroundings. They are outstanding chemists and geoengineers, and they did this for billions of years, thus playing an important role in the evolution of the Earth and its atmosphere. Their presence within geologic media has a profound effect on themselves and on the chemical and physical properties of the surrounding environment. Obviously, today spectacular scientific breakthroughs take place between the boundaries of

Metal Ions in Life Sciences, Volume 21 Guest Editors: Peter M. H. Kroneck and Martha E. Sosa Torres
Series Editors: Astrid Sigel, Eva Freisinger, and Roland K. O. Sigel

https://doi.org/10.1515/9783110589771-001

the disciplines of Geology, Paleontology, Chemistry, Physics, and Biology, and new scientific disciplines come up, such as Astrobiology and Geomicrobiology. It is the aim of this chapter to introduce the reader to the fascinating world of microorganisms, and to recognize their important role they have played in the history of the Earth, and still play, in altering our environment. A remarkable number of reactions catalyzed by microbial enzymes have been explored down to the level of protein structure, active site architecture, and specific roles of neighboring amino acid residues. Thus, a lot of once *obscure microbiology* can be understood nowadays at the atomic level. Notably, numerous geochemical processes observed in the past were discovered through recent years to be catalyzed by microbes, except for those occurring at temperatures beyond 120 °C, the thermal borderline of living organisms. It is the study of microbial interactions with geological media, which advances the exciting field of Geomicrobiology. To speak with microbiologist Bernhard Schink, author of the chapter entitled *Microbes: Masters of the Global Element Cycles*: "If – after all the great discoveries in chemistry through the last 150 years – chemists may have been tempted to claim "it is all chemistry out there" I tend to oppose: "it is all microbiology – using a highly refined microbial biochemistry".

Keywords: catalysis · geomicrobiology · great oxidation event · history of earth · metals · microbes · minerals · surface

1. INTRODUCTION: FROM MICROBES TO METALLOENZYMES

When one ponders on the question 'Why did we, inorganic chemists by training, choose the title *Metals, Microbes, and Minerals: The Biogeochemical Side of Life* for this volume of the METAL IONS IN LIFE SCIENCES (MILS) series, several options come up. Firstly, based on what we learned from our activity as guest-editors for Volume 14 *The Metal-Driven Biogeochemistry of Gaseous Compounds in the Environment* [1], Volume 15 *Sustaining Life on Planet Earth: Metalloenzymes Mastering Dioxygen and Other Chewy Gases* [2], and Volume 20 *Transition Metals and Sulfur: A Strong Relationship for Life* [3], we felt that this was a timely and important topic. The most powerful motivation, however, resulted from the interaction with numerous pioneering researchers of microbiology and bioinorganic chemistry over several decades, either through experiments in the laboratory or thanks to fruitful discussions at international conferences and workshops. In first place come Norbert Pfennig (Department of Biology, University of Konstanz) [4, 5], Walter G. Zumft (Institute of Molecular Microbiology, Karlsruhe Institute of Technology) [6, 7], and Helmut Beinert, (Biochemistry Department, University of Wisconsin-Madison) [8, 9]. Guided by Norbert Pfennig (Figure 1), a survey was made in 1983 together with Helmut Beinert of components of sulfur-reducing bacteria, such as "Spirillum 5175", that can be detected by electron paramagnetic resonance spectroscopy. "Spirillum 5175" was later described as the type strain of the new genus and species *Sulfurospirillum deleyianum* [10–14].

These early studies have opened up new and fascinating areas of research with exciting discoveries. Enzymes with novel transition metal centers (Fe, Cu, Mo, W) and unique catalytic properties (Equations 1–4) (Figures 2–5) could be purified

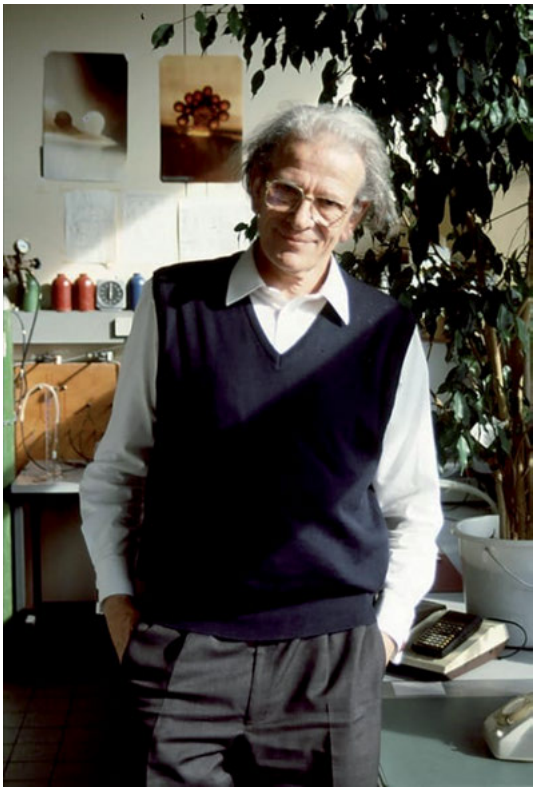

Figure 1. Norbert Pfennig (1925–2008), Professor of Microbiology, Department of Biology, University of Konstanz [4, 5, 13].

from both anaerobic and aerobic microorganisms [15], and were characterized in collaboration with microbiologists E. Bock (Hamburg), H. Cypionka (Konstanz/Oldenburg), J. E. Escamilla Marván (Mexico City), J. Harder (Bremen), H. Huber (Regensburg), D. Jendrossek (Stuttgart), A. Kröger (Frankfurt), B. Schink (Konstanz; see also Chapter 2), J. Simon (Frankfurt/Darmstadt), K. O. Stetter (Regensburg), D. A. Webster (Chicago), and W. G. Zumft (Karlsruhe) [16–39].

$$N_2O + 2H^+ + 2e^- \rightarrow N_2 + H_2O \quad (1)$$
copper sulfide enzyme N_2OR (Figure 2)

$$NO_2^- + 8H^+ + 6e^- \rightarrow NH_4^+ + 2H_2O \quad (2)$$
multi-heme enzyme CCNIR (Figure 3)

$$C_2H_2 + H_2O \rightarrow CH_3CHO \quad (3)$$
tungsten-iron sulfur enzyme WAH (Figure 4)

$$SO_3^{2-} + 8H^+ + 6e^- \rightarrow H_2S + 3H_2O \quad (4)$$
siroheme-iron sulfur enzyme DSIR (Figure 5)

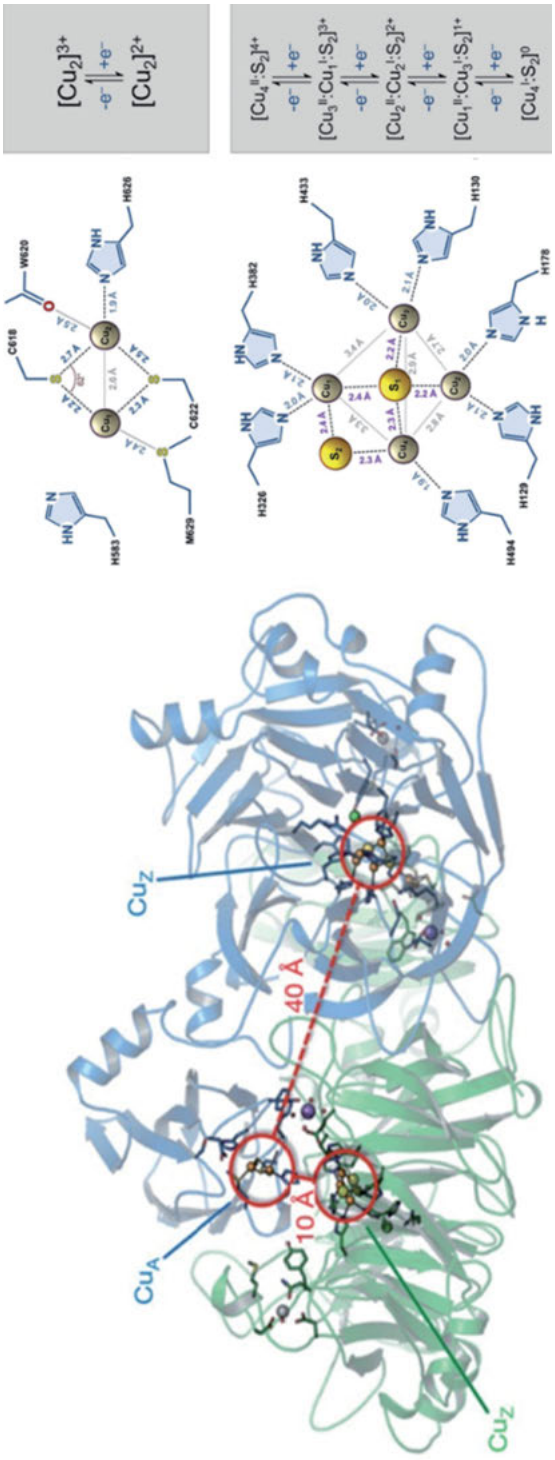

Figure 2. Microbial enzymes hosting novel transition metal active sites. Cu-dependent nitrous oxide reductase (N_2OR) of *Pseudomonas stutzeri* (PDB 3SBR), overall structure of head-to-tail dimer (**left**) and CuA and CuZ centers (**right**) [38, 39].

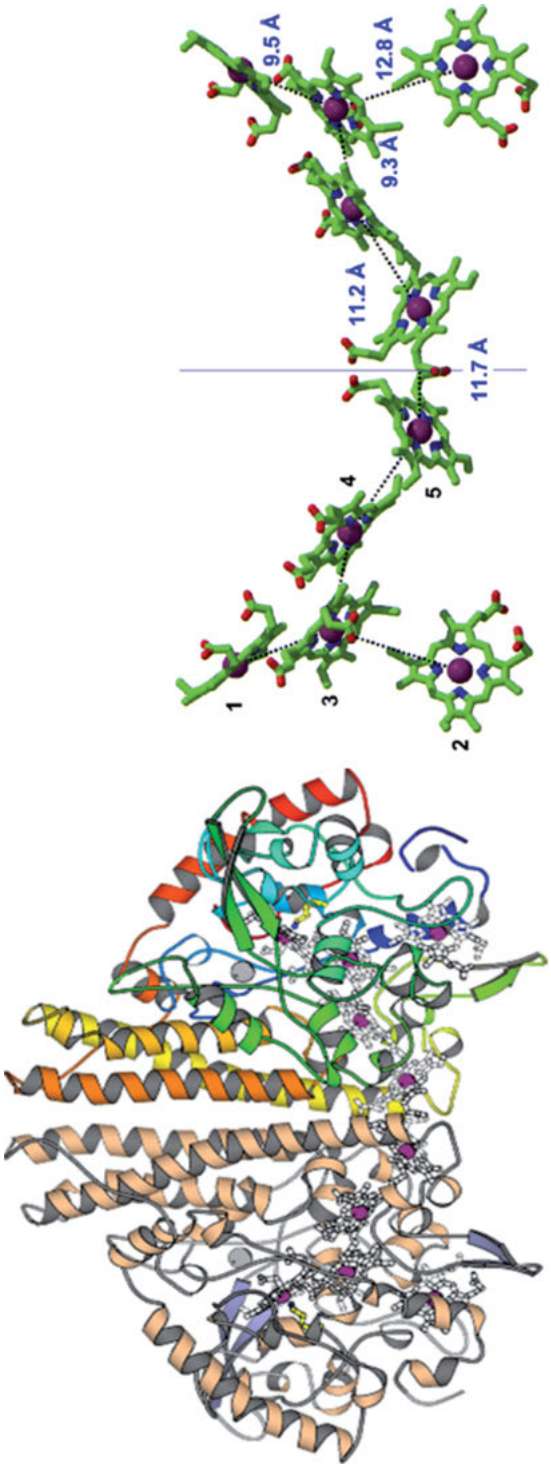

Figure 3. Microbial enzymes hosting novel transition metal active sites. Cytochrome *c* nitrite reductase (CCNIR) of *Wolinella succinogenes* (PDB 1FS7), overall structure of α_2 homodimer (**left**) and array of heme centers (5 per monomer) including active site heme 1 (**right**) [31–33].

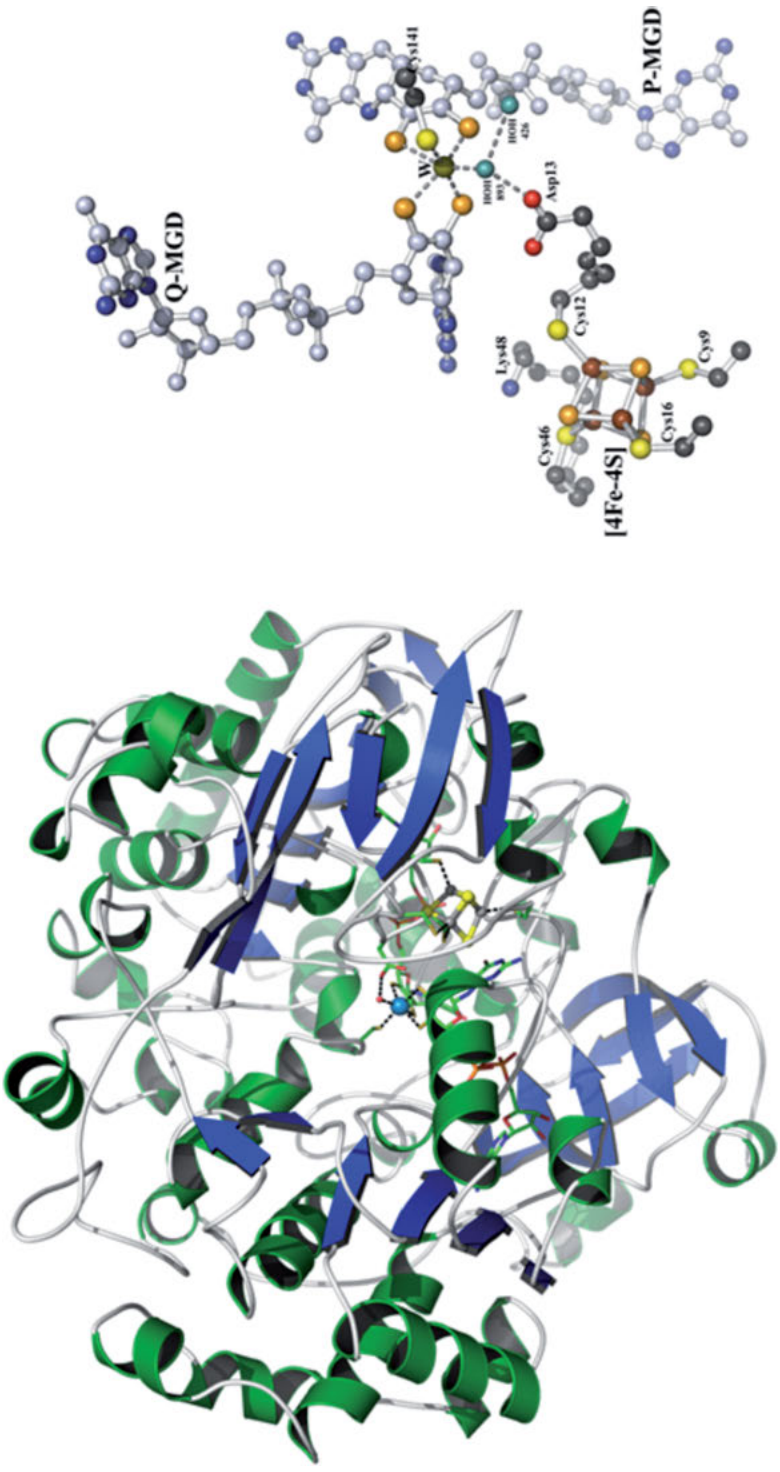

Figure 4. Microbial enzymes hosting novel transition metal active sites. W-dependent acetylene hydratase (WAH) of *Pelobacter acetylenicus* (PDB 2E7Z), overall structure of monomer (**left**) and tungsten active site (**right**) [26, 29, 30].

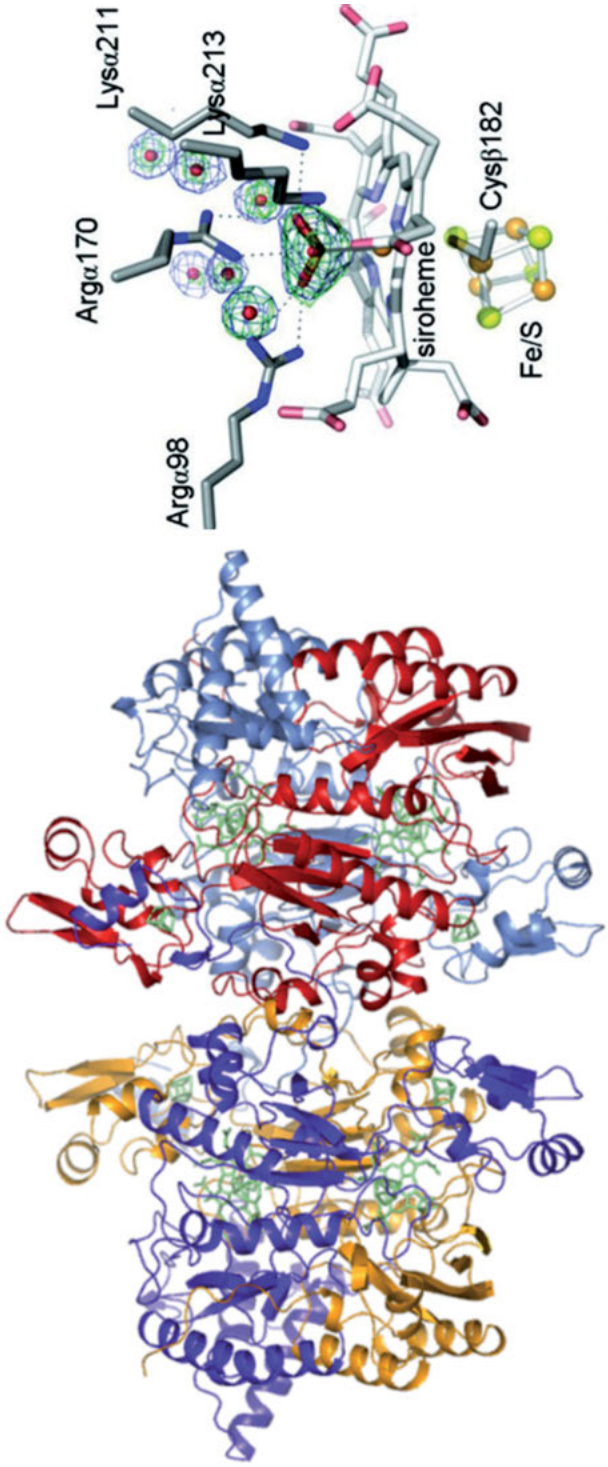

Figure 5. Microbial enzymes hosting novel transition metal active sites. Dissimilatory siroheme-[4Fe-4S] dependent sulfite reductase (DSIR) of *Archaeoglobus fulgidus* (PDB 3MMC), overall structure of $\alpha_2\beta_2$ heterotetramer (**left**) and coupled siroheme-[4Fe-4S] active site (**right**) [18, 20, 21, 33].

Second in this context, we have to bring up the name of international patent lawyer Günter Wächtershäuser, chemist by training and Honorary Professor at the University of Regensburg, and his intriguing Iron-Sulfur World theory. His ideas, if correct, mean that scientists seeking to understand the origin of life on Earth should focus on the chemistry that takes place on the surface of minerals, particularly in hot environments like the deep undersea volcanoes that gash the ocean floor [40]. The theory assumes that life began on minerals with an anabolic metabolism of synthetic, autocatalytic carbon fixation cycles, with the oxidative formation of pyrite (FeS_2) from Fe(II) sulfide (FeS) and H_2S providing the reducing power to the pioneer metabolism (Equation 5).

$$FeS + H_2S \rightarrow FeS_2 + 2\,H^+ + 2\,e^- \,(= H_2) \qquad \Delta G^0 = -41.9\ \text{kJ/Lmol} \quad (5)$$

The organic compounds were retained on or in the mineral base as ligands of the transition metal centers with a flow retention time in correspondence with their mineral bonding strength thereby defining an autocatalytic "surface metabolism", producing more complex organic compounds, more complex pathways, and more complex catalytic centers (see Chapter 5) [41–48].

In this chapter we intend to introduce the reader to the fascinating world of microorganisms, and to stress the important role they have played in the history of the Earth, and still play, in altering our environment. A remarkable number of reactions catalyzed by microbial enzymes have been explored down to the level of protein structure, active site architecture, and specific roles of neighboring amino acid residues. Thus, a lot of once *obscure microbiology* can be understood nowadays at the atomic level. Notably, numerous geochemical processes observed in the past were discovered through recent years to be catalyzed by microbes, except for those occurring at temperatures beyond 120 °C, the thermal borderline of living organisms. In view of the vast literature accumulated and still accumulating in the field, we suggest for introduction the books by world-renowned experts Robert Hazen (Clarence Robinson Professor of Earth Science at George Mason University) entitled "The Story of Earth", and Donald Canfield (Professor of Ecology at the University of Southern Denmark) entitled "Oxygen: A Four Billion Year History" [49, 50]. Furthermore, we recommend Volume 4 of the MILS series "Biomineralization: From Nature to Application" published in 2008 [51]. The discussion will be centered to some extent on the role of metals and their interaction within and outside of the microbial cell, and the impact of microbes hosting numerous sophisticated metalloenzymes on the environment. To stay updated with the rapidly advancing field, broader perspectives and more including the work of experts in this vibrant research area are available in a number of very informative and authoritative reviews [52–61].

2. EARLY LIFE CHEMISTRY AND CATALYSTS: CAN WE FIND THEIR TRACES IN ROCKS?

The Critical Zone (CZ) is the Earth's outer shell where all the fundamental physical, chemical, and biological processes critical for sustaining life occur and

interact. As microbes in this zone drive many of these biogeochemical cycles, understanding their impact on life-sustaining processes starts with an understanding of their biodiversity. Microbes are found throughout the CZ, down to 5 km below the surface, but their functional roles change with depth due to habitat complexity, e.g., variability in pore spaces, H_2O, O_2, and nutrients. Abundances of prokaryotes and microeukaryotes decrease significantly by orders of magnitude with depth. The relatively low abundance of microeukaryotes in the deep subsurface suggests that they are limited in space, nutrients, are unable to cope with O_2 limitations, or some combination thereof. Since deep regions of the CZ have limited access to recent photosynthesis-derived carbon, microbes there depend on deposited organic material or a chemolithoautotrophic metabolism that allows for a complete food chain, independent of the surface, although limited energy flux means cell growth may take tens to thousands of years. Microbes are found in all regions of the CZ and can mediate important biogeochemical processes. With the recent "omics" technologies at hand, microbial ecologists have new tools to link the composition and function of *in situ* microbial communities. These methods can be used to search for new metabolic pathways relevant to biogeochemical nutrient cycling, and to determine how the activity of microorganisms can affect transport of carbon, particulates, and reactive gases between and within CZ regions [62].

Today, many spectacular scientific breakthroughs take place between the boundaries of the previously august and familiar disciplines of Geology, Astronomy, Paleontology, Chemistry, Physics, and Biology, each symbolically separated into their own buildings on most university campuses. Each discipline has not only a faculty with its own rules and boundaries, but entire fields with their own vocabularies and favored methods of disseminating information coming from research. Furthermore, as science advances quickly, new scientific disciplines have come up, such as Astrobiology and Geomicrobiology, which barely existed before the 1990s [63–79]. For example, the recognition of the important role that microorganisms play in altering our environment, advanced the field of Geomicrobiology, the study of microbial interactions with geologic media, significantly [70–76].

Despite the importance of carbon atoms linked together to build biological macromolecules, such as proteins (carbon-based life), simple molecules that exist as gases, have had the greatest influence on the history of life: dioxygen (O_2), carbon dioxide (CO_2), methane (CH_4), and hydrogen sulfide (H_2S). Sulfur, in fact, may have been the single most important of all elements in dictating the nature and history of life on Earth [77–79]. Earth is over 4,500 million years old [80–83]. Note that in discussing geological time, 1 Gyr is 10^9 years, 1 Myr is 10^6 years, see also the discussion published by The International Union of Pure and Applied Chemistry (IUPAC), and the International Union of Geological Sciences (IUGS) [84]. Probably in the early stage, occasional impacts might have heated the ocean over 100 °C. Consequently, only hyperthermophiles, organisms optimally living in water at 80–110 °C, would have survived. Early hyperthermophile life, probably near hydrothermal systems, may have been non-photosynthetic, and many housekeeping proteins and biochemical processes may have an original hydrothermal heritage. The development of anoxygenic and then oxy-

genic photosynthesis would have allowed life to escape the hydrothermal setting. By about 3,500 million years ago, most of the principal biochemical pathways had evolved, and were global in scope [79, 85–87]. In 1999, Brocks and colleagues reported molecular fossils that expanded the geological record of eukaryotic biology and confirmed that cyanobacteria lived in Archean environments, which produced O_2 that transformed our planetary surface [82, 88]. In 2017, Dodd and associates described putative fossilized microorganisms that are at least 3,770 million and possibly 4,280 million years old, in ferruginous sedimentary rocks from northern Quebec, Canada [89–91]. This may be the oldest known sign of life on Earth. The tiny hematite tubes are as much as 4,280 million years old, and they are stunningly similar to structures produced by microbes living around undersea hydrothermal vents. The microscopic metallic detritus, plus chemical signatures associated with ancient metabolisms, would push back the date at which life arose on Earth; see also the article in National Geographic by N. Drake [89–92].

2.1. Mineral Surfaces and Microbes

"The farther back you can look, the farther forward you are likely to see" — Winston Churchill.

Exactly how life on Earth began remains a burning scientific question until today (see Chapter 5). The simple truth is, there were rocks and minerals on Earth before there was life. In 2013 Robert Hazen (Carnegie Institution's Geophysical Laboratory and George Mason University), cataloged the 420 minerals that likely characterized Earth's Hadean Eon, that is the planet's first 550 million years. These minerals comprise a mere 8 % of the diversity of minerals we see on Earth today, a complexity that is a direct result of the interplay between rock and life over geological time [93]. The Earth has always been a restless, evolving planet. Even today the air, the oceans, and the land are changing, perhaps at a pace unequaled in our planet's recent past.

From the geological point of view the Earth's surface is continuously changing. An igneous rock is transformed under the action of high pressure or heat into a metamorphic rock, and both igneous and metamorphic rocks can be eroded into a sedimentary rock. As all rocks on the Earth's surface are recycled, a rock's type gives information about the way it was made, while its mineralogical composition informs about its chemical nature. Clay minerals are ubiquitous on our planet, they are also abundant in the matrix of many primitive chondrites, present in interplanetary dust particles, and have been described on Mars in the form of ferromagnesian smectite. On Earth, during the Hadean and early Archean, when life originated, over 30 different clay minerals have been described with a large distribution in hydrothermal deposits. As clay minerals have a high affinity for organic molecules and can act as catalysts, they were proposed to play important roles in the origins of life on Earth, whether life emerged at hydrothermal vents, at active serpentinizing sites, on dry land exposed to ultraviolet sunlight, or in evaporative environments [94, 95].

Earth's natural libraries reveal a multibillion-year story of coevolution shared by elements, minerals, rocks, and life. The more we examine Earth's rich rock record, the more we see how the natural world, both living and non-living, has transformed itself again and again. The early evolution of Earth was a consequence of two intertwined chemical realities: (i) Cosmochemistry, that is making the elements, and (ii) Petrochemistry, that is making rocks, says leading expert Robert Hazen [96]. He and colleagues examined the roles of minerals in the origin of life, with a focus on mineral-catalyzed organic synthesis and interactions between biomolecules and mineral surfaces, also called "mineral evolution" and "mineral ecology" [93, 97–101].

When life arose on Earth, a complex mineral world was already present, ready to interact with the first biomolecules via their surfaces which are the obligation zone of contact with the outside world. How it directed chemical evolution has been the subject of much speculation. Specific roles for minerals have been invoked for the emergence of the three main distinguishing features of life, information storage, metabolism, and compartmentalization. One idea was that clays, not only guided the first steps toward life, but actually were the first living organisms, storing information in the sequence of their layers. While there is little evidence for this far-reaching claim, mineral surfaces may have supplied selectivity in adsorption and/or polymerization, thus selecting a subset in the space of possible proteins and nucleic acids. A lot remains to be understood concerning the molecular structure of relevant surfaces and the precise mechanisms of their interactions with biomolecules [93–102].

Concerning the emergence of metabolic activity, mineral surfaces are well-known as efficient catalysts (routinely applied in industrial heterogeneous catalysis) but they can also have played the role of alternate reaction media, offering thermochemical conditions different from those in solution, and allowing to harnessing macroscopic gradients and cyclical variations in temperature and humidity to produce the molecular-level imbalances that are characteristic of life. This includes the storage of chemical energy in the form of molecular-scale concentration gradients and the appearance of proto-metabolic cycles including reactions with mineral surfaces, some vestigial remains of which could perhaps still be found in metabolism. Minerals may also have played a role in compartmentalization, opposing the dilution process that would otherwise have destroyed emerging prebiotic systems [103–114]. Any type of adsorption has the potential to maintain high local concentration, but the micro-, meso-, and macroporosity of minerals from zeolite to pumice, and the tunable porosity of clay minerals, seem most attractive in this respect, as discussed in two special issues of open-access journal *Life* [60, 114].

2.2. Microbes, Minerals, and Electron Transfer

Life and element cycling on Earth depend on redox chemistry, that is oxidation and reduction of inorganic and organic compounds [115]. Understanding of biogeochemical electron transfer reactions is crucial for predicting and protecting

environmental health (see Chapters 7, 8, and 9). Energy can be released and stored via the oxidation of both organic and inorganic electron donors by microorganisms coupled to the reduction of electron acceptors, such as humic substances, Fe-bearing minerals, transition metals, metalloids, and actinides. Environmental redox processes play key roles in the formation and dissolution of mineral phases, redox cycling of trace elements and their host minerals often control the release or sequestration of inorganic compounds. Redox processes control the chemical speciation, bioavailability, toxicity, and mobility of elements, such as C, N, P, S, Cr, Fe, Mn, Co, Cu, As, Sb, Se, Hg, Tc, and U. Humic substances and mineral surfaces can catalyze the redox transformation and degradation of organic compounds [115].

Microbes interact with metals and minerals in natural and synthetic environments, altering their physical and chemical state, with metals and minerals also able to affect microbial growth, activity, and survival [116]. Application of microbial processes by the mineral industry, so-called biohydrometallurgy, predates the understanding of the role of microorganisms in metals extraction, commonly referred to as bioleaching. Undoubtedly, microbial processes were at work to leach the copper from sulfide minerals, which the rustics were able to recover by the process now known as precipitation on iron [117]. It has been known for a long time that the rate of oxidation of a number of sulfide minerals, e.g., pyrite (FeS_2), is markedly accelerated by Fe-oxidizing bacteria, such as *Thiobacillus ferrooxidans*, and related species. They play important roles in geochemical mineral transformations, in problems of water pollution associated with acid mine drainage, in the leaching and recovery of valuable metals from metal sulfide ores, and in eliminating pyritic sulfur from coal [118–126].

Many minerals are biogenic in origin, and their formation is of global significance, they provide important structural components for numerous microbial groups [127]. Furthermore, metal–mineral–microbe interactions are fundamental to microbial biomineralization, the collective processes by which organisms form minerals since the dawn of life on Earth. The biologically-mediated organization of aqueous ions into amorphous and crystalline compounds resulted in materials that were as simple as adventitious precipitates or as complex as exquisitely fabricated structures that meet specialized functionalities. This phenomenon is widespread in biology and mediated by bacteria, protists, fungi, plants, and animals [64, 67, 128–133].

2.3. Microbes, Metals, and Radionuclides

It is well established that microorganisms are able to reduce metal compounds. Microbes that couple growth to the reduction of a metal, such as manganese (Mn) can play an important role in the biogeochemistry of certain anaerobic environments. For example, *Alteromonas putrefaciens* MR-1, coupled its growth to the reduction of Mn oxides only under anaerobic conditions. The characteristics of this process were consistent with a biological reduction of Mn, suggesting that this bacterium used Mn oxide as a terminal electron acceptor [134].

Dissimilatory metal-reducing bacteria can transfer electrons to insoluble metallic compounds in natural habitats and to the surface of terminal acceptors outside the cell to support their respiratory metabolism, in a process designated extracellular electron transfer (EET) [135]. These microbes gained notoriety from the time it was realized that they represent excellent targets for bioremediation of contaminated sediments, soils, and ground waters, and, most important, as promising producers in microbial fuel cells. Bacteria from the genus *Shewanella* and *Geobacter* gained lots of attention for EET studies, as understanding EET mechanisms is crucial to develop and improve their biotechnological applications (see Chapters 7 and 8). The isopotential window that allows a smooth electron flow from the cell interior to the exterior might constitute the *modus operandi* of dissimilatory metal-reducing bacteria for which it may be beneficial to minimize dissipation of free energy across electron transfer networks. Such a *modus operandi* can explain the large abundance of multiheme *c*-type cytochromes (see Figure 3, CCNIR) participating in EET in these microorganisms.

Obviously, the presence of several redox centers in a single protein is advantageous for electron transfer by (i) increasing the reduction power of the cells, (ii) expanding the protein redox-active windows via heme–heme interactions between neighboring redox centers, and (iii) facilitating electron transfer across large distances without the need for transient recognition and binding between successive physiological partners. This clearly contrasts with proteins containing a single redox center, which have a range of redox activity limited by the Nernst curve [135]. In tropical iron ore regions, biologically-mediated reduction of crystalline iron oxides drives ongoing iron cycling that contributes to the stability of surface duricrusts.

Most recently [136], a glucose-fermenting microbial consortium capable of reducing at least 27 mmol/L iron oxide goethite could be enriched, its metagenome analysis led to the recovery of a metagenome assembled genome of an iron reducer belonging to the genus *Telmatospirillum*. Notably, the *Telmatospirillum* genome encoded putative metal transfer reductases and a novel, multi-heme outer membrane cytochrome for EET. With goethite, short chain fatty acid production shifted significantly in favor of acetate rather than propionate, suggesting goethite works as hydrogen sink in the culture. Stimulating microbial fermentation has potential to drive reduction of crystalline iron oxides, the rate limiting step for iron duricrust re-formation [136].

Microbes play important roles in the environmental fate of toxic metals and radionuclides with a multiplicity of mechanisms as integral components of natural biogeochemical cycles [137]. A diverse group of specialized Bacteria and Archaea can use such activities to conserve energy for growth in the absence of O_2. Clearly, respiratory metal reduction has opened up numerous important areas of research. These transformations play crucial roles in the cycling of both inorganic and organic species in a range of environments and, if harnessed, may offer the basis for innovative biotechnological processes. Interactions between microorganisms and minerals at the nanoscale have a major impact on the geochemical cycling of metals, such as iron and manganese. Hereby, Fe(III) minerals are often the dominant terminal electron acceptor for microbial metabolism in

anoxic subsurface sediments, and play a defining role in controlling the mobility of trace elements through the Fe(III)/Fe(II) redox couple, with *Geobacter* as one major key player(discussed in detail in Chapters 7 and 8) [138–142]. Pyrite (FeS_2) is the most abundant sulfide mineral on Earth, it is frequently associated with coals and Cu, Co, Ni, and Zn sulfide ores. Its oxidation is usually undesirable in commercial processes (net acid generating bio-heaps, coal, petroleum refining), an environmental issue known as acid mine drainage. Consequently, the role of bacteria in FeS_2 oxidation is necessary for commercial applications and environmental protection [143].

The biology of metal-transforming microorganisms is of fundamental and applied importance for our understanding of past and present biogeochemical processes on Earth and in the Universe [144]. Clay minerals and metal oxides are essential parts of the soil matrix and strongly influence the structure of microbial communities and the formation of biogeochemical interfaces in soils. For example, metal oxides have significant impacts on alkane-degrading community structure and the effects increased during soil maturation [74]. Recently, several studies have examined the effects of soil minerals on the viability of bacterial cells. For example, montmorillonite remarkably improved the metabolic activity of *Pseudomonas putida*, whereas kaolinite and goethite significantly inhibited the activity [106]. The mineralosphere, which has been defined as the specific interface and habitat encompassing the rocks and the surrounded soil, is under the influence of minerals. Along with biofilm formation, bacterial surface properties, including adsorbability, hydrophobicity, and nutrient capture, underwent change accordingly, and the changes could be enlarged in the subsequent processes.

Biogeochemical interactions between microorganisms and minerals at the nanoscale have a major impact on the geochemical cycling of bulk (e.g., Fe and Mn) and trace elements (e.g., As and Cr) in the subsurface. The significance of microbes in the biogeochemical Mn and Fe cycles has gained broad appreciation, with particular interest to the reduction of oxidized Mn and Fe compounds. The complete oxidation of organic substances or H_2 coupled to the reduction of Mn or Fe oxides could be demonstrated in sediments and pure cultures, and numerous of bacteria have been isolated that grow with oxidized Mn or Fe compounds as sole terminal electron acceptor. Fe(III) minerals are often the dominant terminal electron acceptor for microbial metabolism in anoxic subsurface sediments, and play a defining role in controlling the mobility of trace elements through the Fe(III)/Fe(II) redox couple [145, 146].

Metals are keys to all aspects of our daily life. Their increasing demand puts a permanent pressure on natural resources [147]. Due to a rapidly changing society, a growing world population, and new technologies and future products, an increasing demand of metals has to be expected. The primary production and industrial processing of metals and widespread use in many products and industry resulted in the release of many metals to the environment. The pollution with toxic metals is mainly caused by the release of the metals in effluent waters from mines, landfills, factories, and metal refineries. Further, current recycling rates are low for many technical products and rare metals. Recycling has become increasingly difficult due to the complexity of products and diverse interactions

within recycling systems. Especially many modern electronic products contain small amounts of metals with a complex composition that complicates their recovery. Despite valuable elements electronic wastes contain many environmental organic or inorganic contaminants such as polychlorinated biphenyls, polycyclic aromatic hydrocarbons, Sb, Cr, Ni, and others that potentially can be released to the environment.

Further, the promoted "low carbon technologies" that are considered as environmentally friendly such as wind turbines, solar cells, energy-saving light bulbs, fuel cells, and catalytic converters require rare and precious metals. Currently, the majority of these elements are mined and extracted from primary or in highly energy-intensive processes. Mining activities have a great impact on environmental conditions, they lead to elevated levels of metals in surrounding soil and water courses, resulting in destruction of vegetation and crops. Further, there are severe concerns regarding the availability of these elements in the future due to their low abundance and difficulty to access. Biological approaches can contribute to solve some of these problems by enhancing metal recovery from technical waste products, processing wastes, industrial waste waters, and other secondary sources. Microorganisms developed many processes that influence biogeochemical cycles of elements, e.g., bio-weathering, microbial reduction, biomineralization and bioprecipitation, or bioaccumulation. These processes provided by nature can be used as tools for many clean industrial processes, recovery of metals, novel bio-based materials, bioremediation, but also "green" recycling processes [148].

3. THE GREAT OXIDATION EVENT

Dioxygen (O_2) is considered one of the most important elements on Earth. In short terms, it means life, aerobes use O_2 to conserve the energy they have to gain from their environment [149]. The evolution of O_2-producing cyanobacteria was arguably *the most significant event in the history of life after the evolution of life itself*, says geologist Donald Canfield, Professor of Ecology at the University of Southern Denmark. Dioxygen is a potent oxidant whose accumulation into the atmosphere forever changed the surface chemistry of the Earth. It is also a preferred electron acceptor used in the respiration of countless different organisms that conduct a wide variety of different metabolisms. Thus, relationships between life, O_2, and Earth surface chemistry become obvious [150]. Aerobic organisms (in contrast to anaerobic organisms), including humans, animals, and plants, depend on it to conserve the energy, without O_2 these organisms cannot support an active lifestyle [150–154]. From a biological point of view, *the* most important oxygen compound on Earth is water, H_2O. It is the source of almost all the dioxygen in the atmosphere, moderates the climate of the Earth, and acts as an excellent solvent for biomolecules.

What makes O_2 so special? In the ground state O_2 is a diradical ($^3O_2$; triplet O_2) and is paramagnetic, it can enter many organic and inorganic reactions. In a way, O_2 is a strange molecule, for all its ubiquity. Oxygen's two least strongly held electrons, responsible for most of its chemistry, have available to them two

anti-bonding π* orbitals. Clearly, its appearance in the atmosphere changed the course of evolution on Earth. However, compared to other oxygen radicals, such as the superoxide anion ($O_2^{\bullet -}$), the hydroxyl radical ($^{\bullet}OH$) and the peroxide radical ($^{\bullet}OOH$), triplet O_2 is surprisingly unreactive. Along these lines, O_2 in its first excited state ($^1O_2$; singlet O_2) which is diamagnetic and lies 95 kilojoules above the triplet ground state, is much more reactive [154, 155]. Dioxygen gas does not react with itself or the other main component of our atmosphere, dinitrogen (N_2), under normal conditions. However, the effect of ultraviolet light upon O_2 is to form the blue gas ozone, O_3, the second allotrope of oxygen. Basically, atmospheric O_2 is controlled by the geochemical cycles of carbon and sulfur, as proposed (Equations 6 and 7) almost two centuries ago [156–161].

$$CO_2 + H_2O \rightarrow HCHO + O_2 \quad (6)$$

$$2\,Fe_2O_3 + 8\,SO_4^{2-} + 16\,H^+ \rightarrow 15\,O_2 + 4\,FeS_2 + 8\,H_2O \quad (7)$$

The initial increase of O_2 in the atmosphere, its build-up in the ocean, its increase to near-modern levels in the sea and air, and its cause-and-effect relationship with life are among the most heavily disputed stories in the history of the Earth (Figure 6) [162]. Dioxygen seems to be present everywhere, it makes up approximately 21 % of the current atmosphere. However, free O_2 was anything but plentiful during the first half of Earth's 4.5-billion-year history. Evidence for a permanent rise to appreciable concentrations of O_2 in the atmosphere approximately 2.3 billion years, now known as the Great Oxidation Event (GOE), left clear fingerprints in the rocks and is now deeply entrenched in our understanding of the early Earth [150, 162–164].

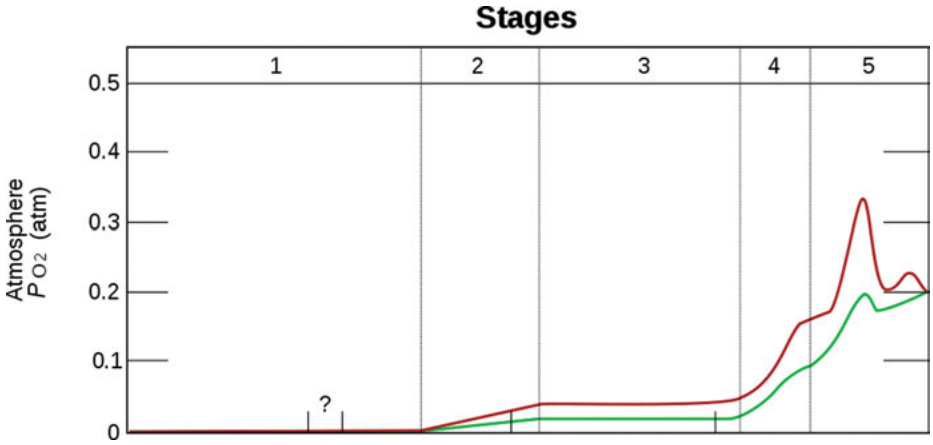

Figure 6. Estimated evolution of atmospheric PO_2. The upper red and lower green lines represent the range of the estimates. The stages are stage 1 (3.85–2.45 Gyr ago (Ga)), stage 2 (2.45–1.85 Ga), stage 3 (1.85–0.85 Ga), stage 4 (0.85–0.54 Ga), and stage 5 (0.54 Ga–present) [161]. Permission for reusing this file granted by H. Holland, Wikipedia, license under GFDL.

Biological, chemical, and physical processes interacting on and beneath the Earth's surface determine the concentration of O_2 and variations in O_2 distribution, both temporal and spatial. In the present-day Earth system, the process that releases O_2 to the atmosphere (photosynthesis) and the processes that consume O_2 (aerobic respiration, sulfide mineral oxidation, oxidation of reduced volcanic gases) result in large fluxes of O_2 to and from the atmosphere [165]. Loss of natural vegetation and the burning of fossil fuels lead to changes of our atmosphere at an alarming rate, with two interconnected themes receiving the most attention: (i) the rise in atmospheric carbon dioxide (CO_2) concentration, and (ii) the escalation of global temperatures. These changes are accompanied by natural phenomena with potentially catastrophic consequences, such as unpredictable climate subsystems and rising sea levels from polar ice cap recession. Although this does not currently appear to be a priority for environmental concern, there is yet another change already underway, and that is the so-called global deoxygenation. Although the current volume of O_2 in our atmosphere is still pretty high, it is diminishing inexorably [166].

The atmosphere has apparently been oxygenated since the GOE approximately 2.4 Ga ago, with the beginning of the photosynthetic O_2 production still heavily disputed [164–167]. However, geological and geochemical evidence from older sedimentary rocks indicates that oxygenic photosynthesis evolved well before this oxygenation event. Fluid-inclusion oils detected in approximately 2.45 Ga old sandstones contained hydrocarbon biomarkers evidently sourced from similarly ancient kerogen, preserved without subsequent contamination, and derived from organisms producing and requiring molecular oxygen. Molybdenum and rhenium abundances and sulfur isotope systematics of slightly older (2.5 Ga) kerogenous shales document a transient pulse of atmospheric O_2. As early as approximately 2.7 Ga, stromatolites and biomarkers from evaporative lake sediments deficient in exogenous reducing power strongly imply that oxygen-producing cyanobacteria had already evolved. Even at approximately 3.2 Ga, thick and widespread kerogenous shales are consistent with aerobic photoautrophic marine plankton, and uranium–lead data obtained from approximately 3.8 Ga old sediments suggest that this metabolism could have arisen by the start of the geological record. Hence, the hypothesis that oxygenic photosynthesis evolved well before the atmosphere became permanently oxygenated seems well-supported [168].

Pre-photosynthetic niches were meagre with a much lower productivity compared to modern photosynthesis. Serpentinization and volcanism reliably provided H_2, methanogens and acetogens reacted CO_2 with H_2 to conserve energy and to produce organic matter. These skills pre-adapted a bacterium for anoxygenic photosynthesis, probably starting with H_2 in lieu of an oxygen acceptor. Use of reduced iron(II) and sulfide followed as abundant O_2 acceptors, allowing productivity to approach modern levels. Cyanobacteria evolved O_2 production, but they did not immediately dominate the Earth. Eventually, both anoxygenic and oxygenic photosynthesis oxidized much of the Earth's crust and supplied sulfate to the ocean. The process of anoxygenic photosynthesis remained important until there was enough O_2 in down welling seawater to quantitatively oxidize massive sulfides at mid-ocean ridge axes. The evolution of oxygenic photosynthesis is

generally accepted as the ultimate cause of the GOE, but it has proved difficult to constrain the timing of this evolutionary innovation.

The oxidation of manganese in the water column requires substantial free O_2 concentrations, and thus any indication that manganese oxides were present in ancient environments would imply that oxygenic photosynthesis was ongoing. Manganese oxides are not commonly preserved in ancient rocks, but there is a large fractionation of Mo isotopes associated with the sorption of Mo onto the Mn oxides that would be retained. These experimental results suggest that O_2 from oxygenic photosynthesis started to accumulate in shallow marine settings at least half a billion years before the accumulation of significant levels of atmospheric oxygen [154, 169]. In order to illuminate the history of Mn-dependent water splitting, the behavior of the ancient Mn cycle was examined using newly obtained scientific drill cores through an early Paleoproterozoic succession (2.415 Ga) preserved in South Africa. Applying microscale X-ray spectroscopic techniques coupled to optical and electron microscopy and carbon isotope ratios, it could be shown that the Mn was hosted exclusively in carbonate mineral phases derived from reduction of Mn oxides during diagenesis of primary sediments. Additional observations revealed that the original Mn-oxide phases were not produced by reactions with O_2. These results point to a different high-potential oxidant and suggest that the oxidative branch of the manganese cycle predates the rise of O_2, and provide strong support for the hypothesis that the water-oxidizing complex of photosystem II evolved from an earlier transitional photosystem capable of single-electron oxidation reactions of manganese [170].

The anoxic deep open ocean was rich in free iron during the Proterozoic, but this iron remained effectively inaccessible since a photosynthetic expansion would have quenched its own supply. Near the Proterozoic-Phanerozoic boundary, bioenergetics innovations allowed eukaryotic photosynthesis to expand into the deep open oceans and onto the continents, where nutrients are inherently harder to come by. Key insights into the ecological rise of eukaryotic photosynthesis emerge from analyses of marine *Synechococcus* and *Prochlorococcus*, abundant marine picocyanobacteria whose ancestors colonized the oceans in the Neoproterozoic. The reconstructed evolution of *Prochlorococcus* reveals a sequence of innovations that ultimately produced a form of photosynthesis more like that of green plant cells than other cyanobacteria. Innovations increased the energy flux of cells, thereby enhancing their ability to acquire sparse nutrients, and as by-product also increased the production of organic carbon waste. Some of these organic waste products in turn had the ability to chelate iron and make it bioavailable, thereby indirectly pushing the oceans through a transition from an anoxic state rich in free iron to an oxygenated state with organic carbon-bound iron [171].

4. CALCIUM IN REDOX ENZYMES

Calcium (Ca; atomic number 20, electron configuration $[Ar]4s^2$, Ca^{2+} [Ar]) is an essential element needed in large quantities in the human body. As an alkaline earth metal, Ca is a reactive metal that forms a dark oxide-nitride layer

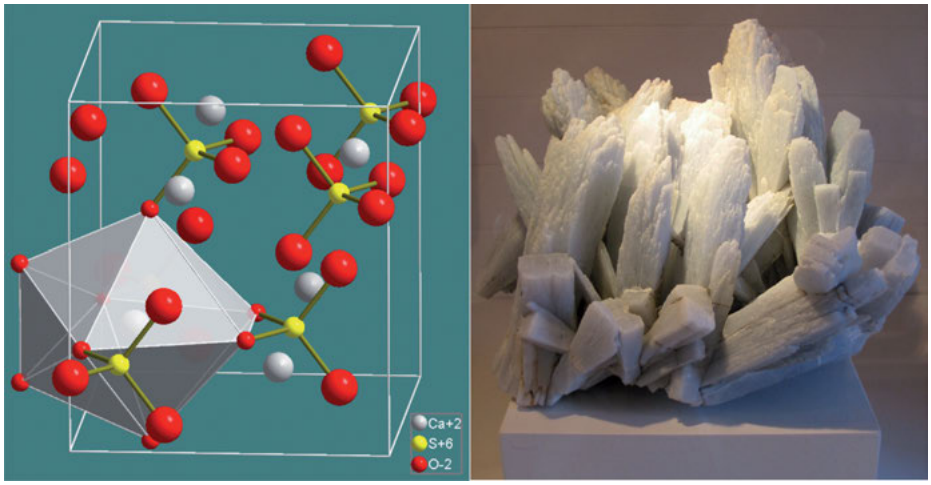

Figure 7. Anhydrite ($CaSO_4$). **Left**: Schematic representation of molecular formula. **Right**: Anhydrite mineral from Naica Mine, Chihuahua, Mexico. Permission for reusing these figures granted by Materialscientist at English Wikipedia, CC BY-SA 3.0.

when exposed to air. Its physical and chemical properties are most similar to its heavier homologues strontium (Sr) and barium (Ba). It is the fifth-most abundant element in the Earth's crust and the third-most abundant metal, after iron (Fe) and aluminum (Al). Notably, Ca is the most abundant metal and the fifth-most abundant element in the human body [172].

The Ca^{2+} ion acts as an electrolyte and is vital to the health of the muscular, circulatory, and digestive systems. It is indispensable to the building of bone, and supports synthesis and function of blood cells. Ca^{2+} regulates the contraction of muscles, nerve conduction, and the clotting of blood. Consequently, intra- and extracellular Ca^{2+} levels are tightly regulated by the body. The element can play this role because the Ca^{2+} ion forms stable coordination complexes with many organic compounds, especially proteins. It also forms compounds with a wide range of solubilities, enabling the formation of the skeleton [51]. Ca^{2+} is an important second messenger in the regulation of the cell life cycle in addition to being an essential component in biomineralization. Ca^{2+} mediates its action in regulation by binding to Ca^{2+} receptors/proteins that in turn regulate signal transduction, enzymatic activity, and protein stability. Owing to the fast progress in genomic information and structural biological studies, our understanding of calcium-binding proteins has been greatly expanded. Since the early 1990s, the three-dimensional structures of calcium-binding proteins have been extended to more than 1000 today and calcium-binding proteins are found in every cellular compartment [173].

Among the most important minerals containing the element Ca, are those of the carbonate family. Rocks, such as limestone ($CaCO_3$), dolomite ($CaMg(CO_3)_2$), and marble, are quarried for their calcium carbonate content, heated to produce quick lime (CaO) which is used for cement and many other industrial purposes.

Calcium sulfates ($CaSO_4$), such as gypsum and anhydrite, anhydrous calcium sulfate (Figure 7), are used for creating plasterboard for construction along with many other uses. Fluorite (CaF_2) is used primarily as a flux, it is also used as a source of fluorine to create hydrofluoric acid (https://www.mindat.org/element/Calcium) [174].

Notably, though not redox-active ([Ar] electron configuration), the Ca^{2+} ion is an important constituent in several biological metal redox centers. Most prominent example is the $CaMn_4O_5$ cluster of the oxygen evolving complex (OEC) of photosystem II (PS II) (Figure 8). Dioxygen, key to all aerobic life, is abundant in the Earth atmosphere because of its constant regeneration by photosynthetic water splitting, which is catalyzed by PS II (Equation 8).

$$2\,H_2O \rightarrow O_2 + 4\,H^+ + 4\,e^- \qquad \text{PS II } CaMn_4O_5 \text{ (Figure 8)} \tag{8}$$

PS II is a multi-peptide membrane protein complex embedded in the thylakoid membrane, involved in photosynthetic H_2O splitting and O_2 evolution, one of the most important, life-sustaining chemical processes on Earth. PS II is usually found as a dimer, with each monomer hosting more than 20 peptides and about

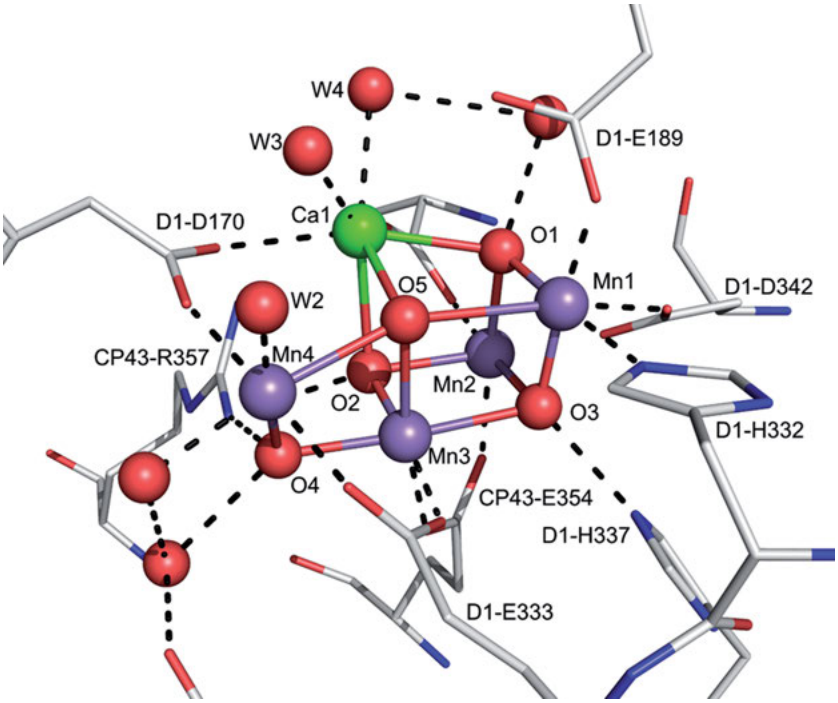

Figure 8. X-ray crystal structure of the $CaMn_4O_5$ core of the oxygen evolving complex of photosystem II at a resolution of 1.9 Å (PDB 3WU2) [175, 176]. Reprinted by permission from *Nature*, Crystal structure of oxygen-evolving photosystem II at a resolution of 1.9 Å, Y. Umena, K. Kawakami, J.-R. Shen, N. Kamiya, *Nature* **2011**, *473*, 55–60.

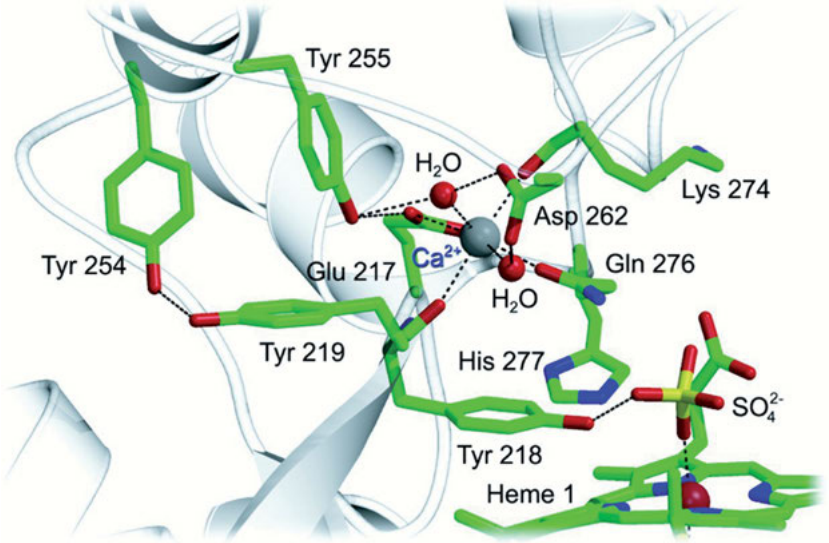

Figure 9. The highly conserved Ca^{2+} site in CCNIR of *Wolinella succinogenes* bridges two stretches of protein that hold active site residues; a set of conserved tyrosine residues might play a role in radical stabilization during catalysis (PDB 1FS7) [31, 32].

100 cofactors, including chlorophylls, quinones, carotenoids, and lipids. The OEC cycles through five intermediate S states (S_0 to S_4, known as the Kok cycle) that corresponds to the abstraction of four successive electrons from the OEC.

Once four oxidizing equivalents are accumulated (S_4 state), a spontaneous reaction occurs that results in the release of O_2 and the formation of the most reduced state, the S_0 state. Upon further light excitation, the initial S_1 state is formed once again, and the catalytic cycle is resumed. Strontium (Sr) can functionally replace Ca in the OEC and, therefore, Sr XAS studies of the $SrMn_4O_5$ cluster helped to study the structural changes of the native $CaMn_4O_5$ cluster [175, 176].

The multi-electron, multi-proton transfer enzyme cytochrome *c* nitrite reductase (CCNIR) (Equation 2) (Figure 9) [31, 32, 177–181], certain classes of heme peroxidases [182–189], and the bacterial pyrroloquinoline quinone-dependent alcohol dehydrogenases (see Chapter 10) [24, 190–194], represent further important examples and coordinate Ca^{2+} ions in strictly conserved binding sites which are important for catalysis.

The Ca^{2+} binding site of CCNIR, a homodimer harboring five *c*-type heme centers in each monomer, is an essential structural feature in the overall architecture of the enzyme, and the region surrounding the Ca binding site is one of the most highly conserved parts of the whole sequence. This is easily understood for Tyr-218, which is an active site residue that can directly interact with substrate. It can be rationalized that the Ca^{2+} ligands Lys-274 and Gln-276 immediately precede another active site residue, His-277, such that the calcium bridges two stretches of protein that hold key residues for catalysis. Furthermore, both

Lys-274 and Gln-276 take part in forming the active site cavity, whose electrostatic surface potential is presumably essential for guiding substrate influx and product efflux (Figure 9).

The detoxification of reactive oxygen species (ROS) is a major task for any organism growing in a microaerobic or aerobic habitat. Thus, a series of enzymes evolved that can reduce, cleave, or disproportionate such ROS. For peroxides (H_2O_2, ROOR), the heme cofactor has proven to be an excellent tool, and beside the well-characterized monofunctional peroxidases, there exist *c*-type diheme enzymes found exclusively in prokaryotes [182, 183]. Heme peroxidases oxidize a variety of substrates using hydrogen peroxide (H_2O_2), such as cytochrome *c* peroxidase, horseradish peroxidase, and ascorbate peroxidase. The resting Fe(III) form of the enzyme reacts with H_2O_2 to form the so-called Compound I, a Fe(IV)=O species, which reacts further to oxidize the substrate. Usually, they contain a single non-covalently bound heme, and they have been categorized into three classes based on sequence alignments and biological origin [182, 185, 186]. Class I, the intracellular peroxidases, includes yeast cytochrome *c* peroxidase and a number of plant and bacterial peroxidases. Secretory fungal peroxidases form class II. These enzymes are monomeric glycoproteins with four conserved disulfide bridges and two conserved calcium sites. The secretory plant peroxidases, or classical plant peroxidases form class III. Peanut peroxidase, a class III enzyme, binds two Ca^{2+} ions at the so-called distal and proximal sites. The proximal Ca^{2+} is 13.4 Å from the heme iron, the distal Ca^{2+} is 16.0 Å from the iron. In bacterial *c*-type diheme peroxidases (functional homodimers; each monomer has two connected cytochrome *c*-like domains, each with one heme group covalently attached via thioether bonds) the two heme groups within a monomer are separated by a Fe–Fe distance of ≈21 Å. Two Ca^{2+} binding sites with different affinities have been identified, the occupancy of these sites not only affects electron transfer between the two heme centers, but also seems to influence the equilibrium of inactive monomers and active dimers, underlining the important role of calcium [182–189].

So-called quinoprotein alcohol dehydrogenases use the pyrroloquinoline quinone cofactor coordinated to a Ca^{2+} cation (PQQ-Ca^{2+}) to catalyze the oxidation of alcohols RCH_2OH to the corresponding aldehydes RCHO. The catalytic cycle is thought to involve a hydride (H^-) transfer from RCH_2OH to $PQQ_{ox}-Ca^{2+}$, resulting in the generation of RCHO and $PQQ_{red}-Ca^{2+}$, re-oxidation of the cofactor by a *c*-type cytochrome proceeds in two sequential steps via the PQQ radical [124, 190–194].

Last but not least, a Ca^{2+} ion was found to play a key role in the assembly of Cu-dependent nitrous oxide reductase (N_2OR), a head-to-tail homodimer carrying the dinuclear CuA mixed-valent electron transfer center [$CuA^{1.5+}-CuA^{1.5+}$] and the tetranuclear [4Cu2S] CuZ catalytic site (Equation 1) (Figure 2) [195]. Its maturation largely occurs in the periplasm and includes the insertion of at least one Ca^{2+} ion per monomer. In the absence of Ca^{2+}, substantial parts of the enzyme surrounding the binding sites for the copper ions revealed structural disorder. Reconstitution of the mixed-valent CuA site was possible *in vitro* but required the presence of Ca^{2+} ions for a stable insertion of the center. An excess of Ca^{2+}

prevented copper insertion, and the structural analysis of the Ca^{2+} apo-N_2OR revealed that the cation is sufficient to structure the disordered regions of the protein.

5. OUTLOOK AND FUTURE DIRECTIONS

How life exactly arose on the young Earth, remains disputed. Most likely, life had a rocky start, the first living entity must have been crafted from air, water, and rock. Originally, it seemed that nothing could be more lifeless than a rock. So how could rocks, in other words minerals, have assisted the emergence of life? The answer is chemistry. Minerals grow from simple molecules into an ordered structure because of chemical reactions, critical transformations might not have been possible without the help of minerals acting as containers, scaffolds, templates, catalysts, and reactants [196–199].

Most recently, a large consortium of expert scientists published a *Consensus Statement* concerning climate change and microorganisms [200]. It is now well established that human activities and their effects on the climate and environment cause unprecedented animal and plant extinctions. Clearly, they cause loss in biodiversity, and endanger animal and plant life on Earth. Losses of species, communities and habitats are comparatively well researched, documented, and publicized. By contrast, microorganisms are generally not discussed in the context of climate change, particularly the effect of climate change on microorganisms. Microorganisms play key roles in carbon and nutrient cycling, animal (including human) and plant health, agriculture and the global food web. They live in all environments on Earth that are occupied by macroscopic organisms, and they are the sole life forms in other environments, such as the deep subsurface and 'extreme' environments.

Microorganisms date back to the origin of life on Earth at least 3.8 billion years ago, and they will likely exist well beyond any future extinction events. Although microorganisms are crucial in regulating climate change, they are rarely in the focus of climate change studies and are not considered in policy development. Their immense diversity and varied responses to environmental change make determining their role in the ecosystem challenging. In this *Consensus Statement*, the links between microorganisms, macroscopic organisms and climate change are illustrated, and put humanity on notice that the microscopic majority can no longer be the unseen elephant in the room. Unless humans learn to appreciate the importance of microbial processes, they fundamentally limit their understanding of Earth's biosphere and response to climate change and thus jeopardize efforts to create an environmentally sustainable future [200].

In summary, Geomicrobiology will continue to be a rich and important field of research [201–212]. Determining and understanding the world of microorganisms have greatly advanced a variety of fields and our understanding of unusual chemical reactions and novel catalytic metal sites, such as the one-megadalton metalloenzyme complex in *Geobacter metallireducens* which is involved in benzene

ring reduction beyond the biological redox window [210], or the trinuclear copper catalytic center of the thiocyanate dehydrogenase (Equation 9),

$$N{\equiv}C{-}S^- + H_2O \rightarrow N{\equiv}C{-}O^- + S^0 + 2\,H^+ + 2\,e^- \quad (9)$$

isolated from the haloalkaliphilic sulfur-oxidizing bacterium of the genus *Thioalkalivibrio* ubiquitous in saline alkaline soda lakes [211].

ACKNOWLEDGMENTS

This volume of the *Metal Ions in Life Sciences* is the result of numerous fruitful collaborations of many years in the laboratory and inspiring discussions at international conferences with great colleagues and highly talented students mentioned in this chapter. Our deepest thanks go to Norbert Pfennig who introduced one of us (PK) to this fascinating world of microorganisms which then sparked the idea to collaborate with researchers in the field, Heribert Cypionka, Oliver Einsle, Ulrich Ermler, Günter Fritz, Bernhard Schink, Karl O. Stetter, Julia Steuber, Dale Webster, Friederich Widdel, and Walter G. Zumft, to name a few. The authors are grateful for continuous financial support by CONACYT and DGAPA-UNAM (MEST), and Deutsche Forschungsgemeinschaft and Universität Konstanz (PK).

ABBREVIATIONS AND DEFINITIONS

CCNIR	cytochrome *c* nitrite reductase
CZ	critical zone
DSIR	dissimilatory siroheme-[4Fe-4S] sulfite reductase
EET	extracellular electron transfer
Ga	billion years (gigayears = 10^9 years); geological time, 1 Gyr is 10^9 years, 1 Myr is 10^6 years
GOE	great oxidation event
LUCA	last universal common ancestor
N_2OR	Cu-dependent nitrous oxide reductase
OEC	oxygen evolving complex (photosynthesis)
PDB	Protein Data Bank; https://www.rcsb.org/
PQQ	pyrroloquinoline quinone cofactor
PS II	photosystem II
ROS	reactive oxygen species
WAH	W-dependent acetylene hydratase
XAS	X-ray absorption spectroscopy

REFERENCES

1. *The Metal-Driven Biogeochemistry of Gaseous Compounds in the Environment*, Vol. 14 of *Metal Ions in Life Sciences*, Guest-Eds P. M. H. Kroneck, M. E. Sosa Torres,

Series Eds A. Sigel, H. Sigel, R. O. K. Sigel, Springer Science + Business Media, Dordrecht, NL, **2014**.
2. *Sustaining Life on Planet Earth: Metalloenzymes Mastering Dioxygen and Other Chewy Gases*, Vol. 15 of *Metal Ions in Life Sciences*, Guest-Eds P. M. H. Kroneck, M. E. Sosa Torres, Series Eds A. Sigel, H. Sigel, R. O. K. Sigel, Springer International Publishing, Cham, Switzerland, **2015**.
3. *Transition Metals and Sulfur: A Strong Relationship for Life*, Vol. 20 of *Metal Ions in Life Sciences*, Guest-Eds M. E. Sosa Torres, P. M. H. Kroneck, Series Eds A. Sigel, E. Freisinger, R. O. K. Sigel, Walter de Gruyter GmbH, Berlin, Germany, **2020**.
4. H. G. Trüper, N. Pfennig, *Characterization and Identification of the Anoxygenic Phototrophic Bacteria*, in *The Prokaryotes*, Eds M. P. Starr, H. Stolp, H. G. Trüper, A. Balows, H. G. Schlegel, Springer, Berlin, Heidelberg, **1981**, pp. 299–312.
5. N. Pfennig, *Annu. Rev. Microbiol.* **1993**, *47*, 1–29.
6. W. G. Zumft, *The Denitrifying Prokaryotes*, in *The Prokaryotes. A Handbook on the Biology of Bacteria, Ecophysiology, Isolation, Identification, Applications*, 2nd ed., Eds A. Balows, H. G. Trüper, M. Dworkin, W. Harder, K. H. Schleifer, Springer, New York, **1992**, pp. 554–582.
7. W. G. Zumft, *Microbiol. Mol. Biol. Rev.* **1997**, *61*, 533–616.
8. H. Beinert, *These are the Moments when we Live ! From Thunberg Tubes and Manometry to Phone, Fax and Fedex*, in *Selected Topics in the History of Biochemistry: Personal Recollections. IV*, Eds E. C. Slater, R. Jaenicke, G. Semenza, *Comprehensive Biochemistry*, *38*, Elsevier Science B.V., Amsterdam, NL, **1995**, pp. 193–258.
9. N. Kresge, R. D. Simoni, R. L. Hill, *J. Biol. Chem.* **2009**, *284*, p e4.
10. R. Bache, P. M. H. Kroneck, H. Merkle, H. Beinert, *Biochim. Biophys. Acta* **1983**, *722*, 417–426.
11. A. Zöphel, M. C. Kennedy, H. Beinert, P. M. H. Kroneck, *Arch. Microbiol.* **1988**, *150*, 72– 77.
12. A. Zöphel, M. C. Kennedy, H. Beinert, P. M. H. Kroneck, *Eur. J. Biochem.* **1991**, *195*, 849–856.
13. W. Schumacher, P. M. H. Kroneck, N. Pfennig, *Arch. Microbiol.* **1992**, *158*, 287–293.
14. E. Eisenmann, J. Beuerle, K. Sulger, P. M. H. Kroneck, W. Schumacher, *Arch. Microbiol.* **1995**, *164*, 180–185.
15. O. Einsle, G. B. Seiffert, M. E. Sosa Torres, P. M. H. Kroneck, *Biospektrum* **2006**, *12*, 346–349.
16. M. Meincke, E. Bock, D. Kastrau, P. M. H. Kroneck, *Arch. Microbiol.* **1992**, *158*, 127–131.
17. H. Sass, J. Steuber, M. Kroder, P. M. H. Kroneck, H. Cypionka, *Arch. Microbiol.* **1992**, *158*, 418–421.
18. J. Steuber, H. Cypionka, P. M. H. Kroneck, *Arch. Microbiol.* **1994**, *162*, 255–260.
19. G. Fritz, A. Roth, A. Schiffer, T. Büchert, G. Bourenkov, H. D. Bartunik, H. Huber, K. O. Stetter, P. M. H. Kroneck, U. Ermler, *Proc. Natl. Acad. Sci. USA* **2002**, *99*, 1836–1841.
20. A. Schiffer, K. Parey, E. Warkentin, K. Diederichs, H. Huber, K. O. Stetter, P. M. H. Kroneck, U. Ermler, *J. Mol. Biol.* **2008**, *379*, 1063–1074.
21. K. Parey, G. Fritz, U. Ermler, P. M. H. Kroneck, *Metallomics* **2013**, *5*, 302–317.
22. A. Steinbach, S. Fraas, J. Harder, E. Warkentin, P. M. H. Kroneck, U. Ermler, *FEBS J.* **2012**, *279*, 1209–1219.
23. S. Gómez Manzo, A. A. González Valdez, J. Oria Hernández, H. Reyes Vivas, R. Arreguín Espinosa, P. M. H. Kroneck, M. E. Sosa Torres, J. E. Escamilla Marván, *FEMS Microbiol. Lett.* **2012**, *328*, 106–113.
24. S. Gómez Manzo, A. Solano Peralta, J. P. Saucedo Vázquez, J. E. Escamilla Marván, P. M. H. Kroneck, M. E. Sosa Torres, *Biochemistry* **2010**, *49*, 2409–2415.

25. G. Schmitt, G. Seiffert, P. M. H. Kroneck, R. Braaz, D. Jendrossek, *Microbiology* **2010**, *156*, 2537–2548.
26. R. U. Meckenstock, R. Krieger, S. Ensign, P. M. H. Kroneck, B. Schink, *Eur. J. Biochem.* **1999**, *264*, 176–182.
27. W. Reichenbecher, A. Rüdiger, P. M. H. Kroneck, B. Schink, *Eur. J. Biochem.* **1996**, *237*, 406–413.
28. A. Messerschmidt, H. Niessen, D. Abt, O. Einsle, B. Schink, P. M. H. Kroneck, *Proc. Natl. Acad. Sci. USA* **2004**, *101*, 11571–11576.
29. G. B. Seiffert, G. M. Ullmann, A. Messerschmidt, B. Schink, P. M. H. Kroneck, O. Einsle, *Proc. Natl. Acad. Sci. USA* **2007**, *104*, 3073–3077.
30. R. Rabus, M. Boll, J. Heider, R. U. Meckenstock, W. Buckel, O. Einsle, U. Ermler, B. T. Golding, R. P. Gunsalus, P. M. H. Kroneck, M. Krüger, T. Lueders, B. M. Martins, F. Musat, H. H. Richnow, B. Schink, J. Seifert, M. Szaleniec, T. Treude, G. M. Ullmann, C. Vogt, M. von Bergen, H. Wilkes, *J. Mol. Microbiol. Biotechnol.* **2016**, *26*, 5–28.
31. O. Einsle, A. Messerschmidt, P. Stach, G. P. Bourenkov, H. D. Bartunik, R. Huber, P. M. H. Kroneck, *Nature* **1999**, *400*, 476–480.
32. O. Einsle, P. Stach, A. Messerschmidt, J. Simon, A. Kröger, R. Huber, P. M. H. Kroneck, *J. Biol. Chem.* **2000**, *275*, 39608–39616.
33. J. Simon, P. M. H. Kroneck, *Adv. Microbial Physiol.* **2013**, *62*, 45–117.
34. P. M. H. Kroneck, W. Jakob, D. A. Webster, R. DeMaio, *Biol. Metals* **1991**, *4*, 119–125.
35. W. Jakob, D. A. Webster, P. M. H. Kroneck, *Arch. Biochem. Biophys.* **1992**, *292*, 29–33.
36. C. L. Coyle, W. G. Zumft, P. M. H. Kroneck, H. Körner, W. Jakob, *Eur. J. Biochem.* **1985**, *153*, 459–467.
37. O. Farver, P. M. H. Kroneck, W. G. Zumft, I. Pecht, *Proc. Natl. Acad. Sci. USA* **2003**, *100*, 7622–7625.
38. W. G. Zumft, P. H. H. Kroneck, *Adv. Microbial Physiol.* **2007**, *52*, 107–227.
39. A. Pomowski, W. G. Zumft, P. M. H. Kroneck, O. Einsle, *Nature* **2011**, *477*, 234–238.
40. N. Wade, *Scientist at Work: Gunter Wachtershauser. Amateur Shakes Up Ideas On Recipe For Life*, *New York Times* **1997**, April 22. https://www.nytimes.com/1997/04/22/science/amateur-shakes-up-ideas-on-recipe-for-life.html. accessed at March 18, 2020.
41. G. Wächtershäuser, *Proc. Natl. Acad. Sci. USA* **1990**, *87*, 200–204.
42. G. Wächtershäuser, *Origin of Life: RNA World versus Autocatalytic Anabolism*, in *The Prokaryotes*, Vol. 1, Eds M. Dworkin, S. Falkow, E. Rosenberg, K. H. Schleifer, E. Stackebrandt, Springer, New York, **2006**, pp. 275–283.
43. G. Wächtershäuser, *Chemistry & Biodiversity* **2007**, *4*, 584–602.
44. L. Sydowa, P. C. Bennetta, D. K. Nordstrom, *Procedia Earth and Planetary Science* **2017**, *17*, 504 – 507.
45. M. J. Russell, W. Martin, *Trends Biochem. Sci.* **2004**, *29*, 358–363.
46. K. Pedersen, *FEMS Microbiol. Lett.* **2000**, *185*, 9–16.
47. R. J. Garwood, *Palaeontology Online* **2012**, *2*, Article 11, 1-14.
48. M. J. Russell, L. M. Barge, R. Bhartia, D. Bocanegra, P. J. Bracher, E. Branscomb, R. Kidd, S. McGlynn, D. H. Meier, W. Nitschke, T. Shibuya, S. Vance, L.White, I. Kanik, *Astrobiology* **2014**, *14*. doi: 10.1089/ast.2013.1110T.
49. R. M. Hazen, *The Story of Earth. The First 4.5 Billion Years from Stardust to Living Planet*, Penguin Books, Penguin Group, New York, USA, **2013**.
50. D. E. Canfield, *Oxygen: A Four Billion Year History*, Princeton University Press, Princeton, USA, **2014**.
51. *Biomineralization: From Nature to Application*,Vol. 4 of *Metal Ions in Life Sciences*, Eds A. Sigel, H. Sigel, R. K. O. Sigel, John Wiley & Sons, Chichester, UK, **2008**.

52. C. White, J. A. Sayer, G. M. Gadd, *FEMS Microbiol. Rev.* **1997**, *20*, 503–516.
53. J. L. Kirschvink, J. W. Hagadorn, *A Grand Unified Theory of Biomineralization*, in *The Biomineralisation of Nano- and Micro-Structures*, Ed. E. Bäuerlein, Wiley-VCH Verlag GmbH, Weinheim, Germany, **2000**, pp. 139–150.
54. *Thermophiles: The Keys to Molecular Evolution and the Origin of Life?*, Eds J. Wiegel, M. W. W. Adams, Taylor & Francis Ltd., London, UK, **2003**.
55. B. M. Tebo, J. R. Bargar, B. G. Clement, G. J. Dick, K. J. Murray, D. Parker, R. Verity, S. M.Webb, *Annu. Rev. Earth Planet. Sci.* **2004**, *32*, 287–328.
56. R. M. Hazen, *Elements* **2005**, *1*, 135–137.
57. D. Rumble, in *Chemical Evolution across Space and Time*, Eds L. Zaikowski, J. M. Friedrich, *ACS Symp. Ser.* **2008**, *981*, 261–281.
58. G. M. Gadd, *Microbiology* **2010**, *156*, 609–643.
59. S. Maruyama, M. Ikoma, H. Genda, K. Hirose, T. Yokoyama, M. Santosh, *Geoscience Frontiers* **2013**, *4*, 141e165.
60. Y. Li, N. Kitadai, R. Nakamura, *Life* **2018**, *8*, 46. doi: 10.3390/life8040046.
61. D. R. Lovley, D. J. F. Walker, *Front. Microbiol*. **2019**, *10*, 2078. doi: 10.3389/fmicb. 2019.02078.
62. D. M. Akob, K. Küsel, *Biogeosciences* **2011**, *8*, 3531–3543.
63. K. Konhauser, *Introduction to Geomicrobiology*, Blackwell Science Ltd., Oxford, UK, **2007**.
64. *Fundamentals of Geobiology*, Eds A. H. Knoll, D. E. Canfield, K. O. Konhauser, Blackwell Publishing Ltd., Oxford, UK, **2012**.
65. E. A. Atekwana, L. D. Slater, *Rev. Geophys.* **2009**, *47*, RG4004. doi: 10.1029/2009RG 000285.
66. L. A.Warren, M. E. Kauffman, *Science* **2003**, *299*, 1027–1029.
67. N. Sahai, *Elements* **2007**, *3*, 381–384.
68. W. Zhao, Z. Xu, N. Sahai, *Biogeochemistry*, in *Molecular Modeling of Geochemical Reactions: An Introduction*, Ed J. D. Kubicki, Wiley, Hoboken, USA, **2016**, pp. 311–339.
69. E. Pennisi, *Science* **2002**, *296*, 1058–1060.
70. C. Ash, B. Hanson, C. Norman, *Science* **2002**, *296*, 1055.
71. D. K. Newman, J. F. Banfield, *Science* **2002**, *296*, 1071–1077.
72. A.-L. Reysenbach, E. Shock, *Science* **2002**, *296*, 1077–1082.
73. L. A. Warren, M. E. Kauffman, *Science* **2003**, *299*, 1027–1028.
74. B. Schink, *Engineering in Life Sciences* **2006**, *6*, 3, 228–233.
75. A. Steinbach, S. Schulz, J. Giebler, S. Schulz, G. J. Pronk, I. Kögel-Knabner, H. Harms, L. Y. Wick, M. Schloter, *ISME J.* **2015**, *9*, 1687–1691.
76. P. Ward, J. Kirschvink, *A New History of Life: The Radical New Discoveries about the Origins and Evolution of Life on Earth*, Bloomberry Press, New York, USA, **2015**.
77. N. Lane, *The Vital Question. Why is life the way it is?* Profile Books, London, UK, **2015**.
78. M. E. Sosa Torres, A. Rito Morales, A. Solano Peralta, P. M. H. Kroneck, *Met. Ions Life Sci.* **2020**, *20*, 19–49.
79. E. G. Nisbet, N. H. Sleep, *Nature* **2001**, *409*, 1083–1091.
80. M. Schidlowski, *Nature* **1988**, *333*, 313–318.
81. A. H. Knoll, *Science* **1999**, *285*, 1025–1026.
82. J. J. Brocks, G. A. Logan, R. Buick, R. E. Summons, *Science* **1999**, *285*, 1033–1036.
83. E. T. McGuinness, *Chem. Rev.* **2010**, *110*, 5191–5215.
84. N. E. Holden, M. L. Bonardi, P. De Bièvre, P. R. Renne, I. M. Villa, *Pure Appl. Chem.* **2011**, *83*, 1159–1162.

85. R. Bolhar, B. S. Kamber, S. Moorbath, C. M. Fedo, M. J. Whitehouse, *Earth Planet. Sci. Lett.* **2004**, *222*, 43–60.
86. W. Martin, J. Baross, D. Kelley, M. J. Russell, *Nature Rev. Microbiol.* **2008**, *6*, 805–814.
87. S. I. Castro-Contreras, M. K. Gingras, E. Pecoits, N. R. Aubet, D. Petrash, S. M. Castro-Contreras, G. Dick, N. Planavsky, K. O. Konhauser, *PALAIOS* **2014**, *29*, 192–209.
88. R. E. Blankenship, H. Hartman, *Trends Biochem. Sci.* **1998**, *23*, 94–97.
89. M. S. Dodd, D. Papineau, T. Grenne, J. F. Slack, M. Rittner, F. Pirajno, J. O'Neil, C. T. S. Little, *Nature* **2017**, *543*, 60–64.
90. M. S. Dodd, D. Papineau, F. Pirajno, Y. Wan, J. A. Karhu, *Nature Comm.* **2019**, *10*, 5022. doi: 10.1038/s41467-019-12975-z.
91. J. O'Neil, R. W. Carlson, D. Papineau, E. Y. Levine, D. Francis, *The Nuvvuagittuq Greenstone Belt: A Glimpse of Earth's Earliest Crust*, in *Earth's Oldest Rocks*, Eds M. Van Kranendonk, V. Bennett, E. Hoffmann, Elsevier, Amsterdam, Netherlands, **2019**, pp. 349–374. doi: 10.1016/B978-0-444-63901-1.00016-2.
92. N. Drake, *National Geographic* **2017**; https://www.nationalgeographic.com/news/2017/03/oldest-life-earth-iron-fossils-canada-vents-science/; accessed at March 18, 2020.
93. R. M. Hazen, *Am. J. Sci.* **2013**, *313*, 807–843.
94. S. I. Ramírez Jiménez, *Met. Ions Life Sci.* **2014**, *14*, 1–14.
95. U. Pedreira-Segade, J. Hao, A. Razafitianamaharavo, M. Pelletier, V. Marry, S. Le Crom, L. J. Michot, I. Daniel, *Life* **2018**, *8*, 59. doi: 10.3390/life8040059.
96. R. M. Hazen, D. Papineau, W. Bleeker, R. Downs, J. M. Ferry, T. J. McCoy, D. A. Sverensky, H. Yang, *Am. Mineralogist* **2008**, *93*, 693–1720.
97. R. M. Hazen, *The Emergence of Chemical Complexity: An Introduction*, in *Chemical Evolution across Space & Time*, Eds L. Zaikowski, J. M. Friedrich, American Chemical Society, Washington, DC, USA, **2008**, pp. 2–13.
98. R. M. Hazen, *Chemical Evolution: An Introduction*, in *Chemical Evolution II: From the Origins of Life to Modern Society*, Eds L. Zaikowski, J. M. Friedrich, S. R. Seidel, American Chemical Society, Washington, DC, USA, **2009**, pp. 3–12. doi: 10.1021/bk-2009-1025.fw001.
99. R. M. Hazen, D. A. Sverjensky, *Cold Spring Harb. Perspect. Biol.* **2010**, *2*, a002162.
100. R. M. Hazen, J. M. Ferry, *Elements* **2010**, *6*, 9–12.
101. R. M. Hazen, *Geochemical Origins of Life*, in *Fundamentals of Geobiology*, 1st ed., Eds A. H. Knoll, D. E. Canfield, K. O. Konhauser, Blackwell Publishing Ltd., Oxford, UK, **2012**.
102. M. Ramstedt, L. Leone, A. Shchukarev, *Bacterial Surfaces in Geochemistry – How Can X-ray Photoelectron Spectroscopy Help?* in *Analytical Geomicrobiology: A Handbook of Instrumental Techniques*, Eds J. P. L. Kenney, H. Veeramani, D. S. Alessi, Cambridge University Press, Cambridge, UK, **2019**, pp. 262–287. doi: 10.1017/9781107707399.011.
103. K. Hickman-Lewis, F. Westall, B. Cavalazzi, *Traces of Early Life From the Barberton Greenstone Belt, South Africa*, in *Earth's Oldest Rocks*, Eds M. J. Van Kranendonk, V. C. Bennett, J. Elis Hoffmann, Elsevier B.V., Amsterdam, NL, **2019**, pp. 1029–1058; https://doi.org/10.1016/B978-0-444-63901-1.00042-3; accessed at March 18, 2020.
104. M. Ivarsson, T. Sallstedt, D.-T. Carlsson, *Front. Earth Sci.* **2019**, *7*, 91. doi: 10.3389/feart.2019.00091.
105. Q. Li, B. Yang, J. Zhu, H. Jiang, J. Li, R. Zhang, W. Sand, *Minerals* **2018**, *8*, 406. doi: 10.3390/min8090406.
106. H. Wu, W. Chen, X. Rong, P. Cai, K. Dai, Q. Huang, *Geomicrobiol. J.* **2014**, *31*, 590–596.

107. B. Rincón-Tomás, B. Khonsari, D. Mühlen, C. Wickbold, N. Schäfer, D. Hause-Reitner, M. Hoppert, J. Reitner, *Intern. J. Astrobiol.* **2016**, *15*, 219–229. doi: 10.1017/S1473550416000264.
108. P. Dalai, N. Sahai, *Trends Biochem. Sci.* **2019**, *44*, 331–341.
109. E. L. Shock, *Economic Geology* **2009**, *104*, 1235–1248.
110. F. Mapelli, R. Marasco, A. Balloi, E. Rolli, F. Cappitelli, D. Daffonchio, S. Borin, *J. Biotechnol.* **2012**, *157*, 473–481.
111. N. Sahai, H. Kaddour, P. Dalai, Z. Wang, G. Bass, M. Gao, *Sci. Rep.* **2017**, *7*, 43418. doi: 10.1038/srep43418.
112. S. Uroz, C. Calvaruso, M.-P. Turpault, P. Frey-Klett, *Trends Microbiol.* **2009**, *17*, 378–387.
113. D. Schulze-Makuch, D. Wagner, S. P. Kounaves, K. Mangelsdorf, K. G. Devine, J.-P. de Vera, P. Schmitt-Kopplin, H.-P. Grossart, V. Parron, M. Kaupenjohann, A. Galy, B. Schneider, A. Airo, J. Frösler, A. F. Davila, F. L. Arens, L. Cáceres, F. Solís Cornejo, D. Carrizo, L. Dartnell, J. DiRuggiero, M. Flury, L. Ganzert, M. O. Gessner, P. Grathwohl, L. Guan, J. Heinz, M. Hess, F. Keppler, D. Maus, C. P. McKay, R. U. Meckenstock, W. Montgomery, E. A. Oberlin, A. J. Probst, J. S. Sáenz, T. Sattler, J. Schirmack, M. A. Sephton, M. Schloter, J. Uhl, B. Valenzuela, G. Vestergaard, L. Wörmer, P. Zamorano, *Proc. Natl. Acad. Sci. USA* **2018**, *115*, 2670–2675.
114. M. Fiore, *Life* **2019**, *9*, 73. doi: 10.3390/life9030073.
115. T. Borch, R. Kretzschmar, A. Kappler, P. Van Cappellen, M. Ginder-Vogel, A. Voegelin, K. Campbell, *Environ. Sci. Technol.* **2010**, *44*, 15–23.
116. F. K. Crundwell, *Hydrometallurgy* **2003**, *71*, 75–81.
117. M. P. Silverman, H. L. Ehrlich, *Adv. Appl. Microbiol.* **1964**, *6*, 153–206.
118. M. P. Silverman, *J. Bacteriol.* **1967**, *94*, 1046–1051.
119. K. Bosecker, *FEMS Microbiol. Rev.* **1997**, *20*, 591 – 604.
120. G. J. Olson, J. A. Brierley, C. L. Brierley, *Appl. Microbiol. Biotechnol.* **2003**, *63*, 249–257.
121. H. Tao, L. Dongwei, *Biotech. Rep.* **2014**, *4*, 107–119.
122. A. Schippers, P.-G. Jozsa, W. Sand, *Appl. Environm. Mictobiol.* **1996**, *62*, 3424–3431.
123. A. Schippers, W. Sand, *Appl. Environm. Mictobiol.* **1999**, *65*, 319–321.
124. C. L. Brierley, J. A. Brierley, *Appl. Microbiol. Biotechnol.* **2013**, *97*, 7543–7552.
125. R. Zhang, S. Hedrich, C. Ostertag-Henning, A. Schippers, *Hydrometallurgy* **2018**, *178*, 215–223.
126. E. Pakostova, B. M. Grail, D. B. Johnson, *Hydrometallurgy* **2018**, *179*, 36–43.
127. G. M. Gadd, J. A. Raven, *Geomicrobiol. J.* **2010**, *27*, 491–519.
128. D. A. Bazylinski, *Bacterial Mineralization*, in *Encyclopedia of Materials: Science and Technology*, Eds K. H. J. Buschow, R. Cahn, M. Flemings, B. Ilschner, E. Kramer, S. Mahajan, P. Veyssiere, Elsevier, Amsterdam, NL, **2001**, pp. 441–448.
129. D. Kumari, X.-Y. Qian, X. Pan, V. Achalx, Q. Li, G. M. Gadd, *Adv. Appl. Microbiol.* **2016**, *94*, 79–108; doi: 10.1016/bs.aambs.2015.12.002.
130. H. L. Ehrlich, *Earth-Science Rev.* **1998**, *45*, 45–60.
131. H. L. Ehrlich, *Geomicrobiol. J.* **1999**, *16*, 135–153.
132. Y. N. Vodyanitskii, S. A. Shoba, *Moscow University Soil Science Bulletin* **2015**, *70*, 89–97.
133. G. M. Gadd, *Curr. Op. Biotechnol.* **2000**, *11*, 271–279.
134. C. R. Myers, K. H. Nealson, *Science* **1988**, *240*, 1319–1321.
135. T. C. Santos, M. A. Silva, L. Morgado, J. M. Dantas, C. A. Salgueiro, *Dalton Trans.* **2015**, *44*, 9335–9344.
136. E. J. Gagen, J. Zaugg, G. W. Tyson, G. Southam, *Front. Microbiol.* **2019**, *10*, 2938. doi: 10.3389/fmicb.2019.02938.
137. J. R. Lloyd, *FEMS Microbiol. Rev.* **2003**, *27*, 411–425.

138. D. R. Lovley, T. Ueki, T. Zhang, N. S. Malvankar, P. M. Shrestha, K. A. Flanagan, M. Aklujkar, J. E. Butler, L. Giloteaux, A.-E. Rotaru, D. E. Holmes, A. E. Franks, R. Orellana, C. Risso, K. P. Nevin, *Adv. Microb. Physiol.* **2011**, *59*, 1–100.
139. E. D. Melton, E. D. Swanner, S. Behrens, C. Schmidt, A. Kappler, *Nature Rev. Microbiol.* **2014**, *12*, 797–808.
140. H. F. Downie, J. P. Standerwick, L. Burgess, L. S. Natrajan, J. R. Lloyd, *Res. Microbiol.* **2018**, *169*, 582–589.
141. C. Bryce, N. Blackwell, C. Schmidt, J. Otte, Y.-M. Huang, S. Kleindienst, E. Tomaszewski, M. Schad, V. Warter, C. Peng, J. M. Byrne, A. Kappler, *Environ. Microbiol.* **2018**, *20*, 3462–3483.
142. H. Liu, J. Xia, Z. Nie, C. Mac, L. Zheng, C. Hong, Y. Zhao, W. Wend, *Minerals Engineering* **2016**, *98*, 80–89.
143. C. Liu, Y. Jia, H. Sun, Q. Tan, X. Niu, X. Leng, R. Ruan, *Sci. Rep.* **2017**, *7*, 5032. doi: 10.1038/s41598-017-04420-2.
144. D. Kölbl, M. Pignitter, V. Somoza, M. P. Schimak, O. Strbak, A. Blazevic, T. Milojevic, *Front. Microbiol.* **2017**, *8*, 1918. doi: 10.3389/fmicb.2017.01918.
145. W. Ma, D. Peng, S. L. Walker, B. Cao, C.-H. Gao, Q. Huang, P. Cai, *npj Biofilms and Microbiomes* **2017**, *3*, 4. doi: 10.1038/s41522-017-0013-6.
146. B. Thamdrup, *Adv. Microbiol. Ecol.* **2000**, *16*, 41–84. doi: 10.1007/978-1-4615-4187-5_2.
147. UNEP, 2013. *Metal Recycling: Opportunities, Limits, Infrastructure*, a report of the working group on the global metal flows to the international resource panel. Eds M. A. Reuter, C. Hudson, A. van Schaik, K. Heiskanen, C. Meskers, C. Hagelüken, Working Group on the Global Metal Flows, UNEP, Nairobi, Kenya, **2013**.
148. K. Pollmann, S. Kutschke, S. Matys, J. Raff, G. Hlawacek, F. L. Lederer, *Biotech. Adv.* **2018**, *36*, 1048–1062.
149. N. Lane, *Oxygen.The Molecule that Made the World*, Oxford University Press, Oxford, UK, **2002**.
150. D. E. Canfield, *Annu. Rev. Earth Planet. Sci.* **2005**, *33*, 1–36.
151. W. T. Borden, R. Hoffmann, T. Stuyver, B. Chen, *J. Am. Chem. Soc.* **2017**, *139*, 9010–9018.
152. R. K. Thauer, K. Jungermann, K. Decker, *Bact. Rev.* **1977**, *41*, 100–180.
153. F. Kracke, I. Vassilev, J. O. Krömer, *Front. Microbiol.* **2015**, *6*, 575. doi: 10.3389/fmicb.2015.00575.
154. M. E. Sosa Torres, J. P. Saucedo-Vázquez, P. M. H. Kroneck, *Met. Ions Life Sci.* **2015**, *15*, 1–12.
155. R. R. Ramsay, *Chem. Texts* **2019**, *5*, 9. doi: 10.1007/s40828-019-0085-4.
156. J. J. Ebelmen, *Ann. Rev. Mines* **1845**, *12*, 627–654.
157. R. M. Garrels, A. Lermann, *Proc. Natl. Acad. Sci. USA* **1981**, *78*, 4652–4656.
158. Robert M. Garrels, A. Lerman, *Am. J. Sci.* **1984**, *284*, 989–1007.
159. R. A. Berner, S. T. Petsch, *Science* **1998**, *282*, 1426–1427.
160. H. D. Holland, *Geochim. Cosmochim. Acta* **2002**, *66*, 3811–3826.
161. H. D. Holland, *Phil. Trans. Roy. Soc. B* **2006**, *361*, 903–915. doi: 10.1098/rstb.2006.1838.
162. R. A. Berner, *Nature* **2003**, *426*, 323–326.
163. N. M. Bergman, T. M. Lenton, A. J. Watson, *Am. J. Sci.* **2004**, *304*, 397– 437.
164. T. W. Lyons, C. T. Reinhard, N. J. Planavsky, *Nature* **2014**, *506*, 307–315.
165. S. Zhang, X. Wang, H. Wang, C. J. Bjerrum, E. U. Hammarlund, T. W. Dahl, D. E. Canfield, *Proc. Natl. Acad. Sci. USA* **2016**, *113*, E2552–E2553.
166. S. Zhang, X. Wang, H. Wang, C. J. Bjerrum, E. U. Hammarlund, M. M. Costa, J. N. Connelly, B. Zhang, J. Su, D. E. Canfield, *Proc. Natl. Acad. Sci. USA* **2016**, *113*, 1731–1736.
167. N. J. Planavsky, D. B. Cole, C. T. Reinhard, C. Diamond, G. D. Love, G. Luo, S. Zhang, K. O. Konhauser, T. W. Lyons, *Proc. Natl. Acad. Sci. USA* **2016**, *113*, E2550–E2551.

168. S. Crowe, L. Døssing, N. Beukes, M. Bau, S. J. Kruger, R. Frei, D. E. Canfield, *Nature* **2013**, *501*, 535–538.
169. N. J. Planavsky, D. Asael, A. Hofmann, C. T. Reinhard, S. V. Lalonde, A. Knudsen, X. Wang, F. Ossa Ossa, E. Pecoits, A. J. B. Smith, N. J. Beukes, A. Bekker, T. M. Johnson, K. O. Konhauser, T. W. Lyons, O. J. Rouxel, *Nature Geoscience* **2014**, *7*, 283–286.
170. J. E. Johnson, S. M. Webb, K. Thomas, S. Ono, J. L. Kirschvink, W. W. Fischer, *Proc. Natl. Acad. Sci. USA* **2013**, *110*, 11238–11243.
171. R. Braakman, *Peer J.* **2019**, *7*, e27269v2. doi: 10.7287/peerj.preprints.27269v2.
172. R. C. Ropp, *Encyclopedia of the Alkaline Earth Compounds*, Elsevier, Oxford, UK, **2013**, pp. 12–15.
173. J. J. Yang, W. Yang, *Calcium-Binding Proteins*, in *Encyclopedia of Inorganic Chemistry*, 1st ed., John Wiley & Sons, Ltd., Hoboken, USA, **2006**. doi: 10.1002/0470862106.ia032.
174. G. M. Friedman, *Classification of Sediments and Sedimentary Rocks*, in *Encyclopedia of Sediments and Sedimentary Rocks. Encyclopedia of Earth Sciences Series*, Eds G. V. Middleton, M. J. Church, M. Coniglio, L. A. Hardie, F. J. Longstaffe, Springer, Dordrecht, NL, **1978**.
175. Y. Umena, K. Kawakami, J.-R. Shen, N. Kamiya, *Nature* **2011**, *473*, 55–60.
176. J. Yano, J. Kern, V. K. Yachandra, H. Nilsson, S. Koroidov, J. Messinger, *Met. Ions Life Sci.* **2015**, *15*, 13–43.
177. P. Stach, P., O. Einsle, W. Schumacher, E. Kurun, P. M. H. Kroneck, *J. Inorg. Biochem.* **2000**, *79*, 381–385.
178. V. A. Bamford, H. C. Angove, H. E. Seward, A. J. Thomson, J. A. Cole, J. N. Butt, A. M. Hemmings, D. J. Richardson, *Biochemistry* **2002**, *41*, 2921–2931.
179. D. Bykov, F. Neese, *Inorg. Chem.* **2015**, *54*, 9303–9316.
180. C. A. Cunha, S. Macieira, J. M. Dias, G. Almeida, L. L. Goncalves, C. Costa, J. Lampreia, R. Huber, J. J. Moura, I. Moura, M. J. Romao, *J. Biol. Chem.* **2006**, *278*, 17455–17465.
181. O. Einsle, A. Messerschmidt, R. Huber, P. M. H. Kroneck, F. Neese, *J. Am. Chem. Soc.* **2002**, *124*, 11737–11745.
182. D. J. Schuller, N. Ban, R. B van Huystee, A. McPherson, T. L Poulos, *Structure* **1996**, *4*, 311–321.
183. A. Brausemann, J. Seidel, A. Wüst, O. Einsle, *Multiheme Peroxidases*, in *Heme Peroxidases*, Eds E. L. Raven, H. B. Dunford, RSC Publishing, Oxford, UK, **2015**, pp. 113–132.
184. C. A. Bonagura, B. M. Bhaskar, M. Sundaramoorthy, T. L. Poulos, *J. Biol. Chem.* **1999**, *274*, 37827–37833.
185. B. D. Howes, A. Feis, L. Raimondi, C. Indiani, G. Smulevich, *J. Biol. Chem.* **2001**, *276*, 40704–40711.
186. P. E .M. Siegbahn, M. R. A. Blomberg, *Theoret. Comput. Chemistry* **2001**, *9*, 95–143.
187. K. E. Ellis, J. Seidel, O. Einsle, S. J. Elliott, *Biochemistry* **2011**, *50*, 4513–4520.
188. M. Laberge, Q. Huang, R. Schweitzer-Stenner, J. Fidy, *Biophys. J.* **2003**, *84*, 2542–2552.
189. C. I. Nnamchi, G. Parkin, I. Efimov, J. Basran, H. Kwon, D. A. Svistunenko, J. Agirre, B. N. Okolo, A. Moneke, B. C. Nwanguma, P. C. E. Moody, E. L. Raven, *J. Biol. Inorg. Chem.* **2016**, *21*, 63–70.
190. A. R. Gvozdev, I. A. Tukhvatullin, R. I. Gvozdev, *Biochemistry (Moscow)* **2012**, *77*, 843–856.
191. A. Oubrie, H. J. Rozeboom, K. H. Kalk, E. G. Huizinga, B. W. Dijkstra, *J. Biol. Chem.* **2002**, *277*, 3727–3732.
192. C. W. M. Kay, B. Mennenga, H. Görisch, R. Bittl, *J. Biol. Chem.* **2006**, *281*, 1470–1476.
193. H. Toyama, F. S. Mathews, O. Adachi, K. Matsushita, *Arch. Biochem. Biophys.* **2004**, *428*, 10–21.

194. A. M. Shiller, E. W. Chan, D. J. Joung, M. C. Redmond, J. D. Kessler, *Sci. Rep.* **2017**, *7*, 10389. doi: 10.1038/s41598-017-11060-z.
195. L. K. Schneider, O. Einsle, *Biochemistry* **2016**, *55*, 1433–1440.
196. R. M. Hazen, *Scientific American* **2001**, *271*, 77–85.
197. R. M. Hazen, D. S. Sholl, *Nat. Materials* **2003**, *2*, 367–374.
198. R. M. Hazen, *Surface Science* **2014**, *629*, 11–14.
199. T. Fornaro, A. Steele, J. Robert Brucato, *Life* **2018**, *8*, 56. doi: 10.3390/life8040056.
200. R. Cavicchioli, W. J. Ripple, K. N. Timmis, F. Azam, L. R. Bakken, M. Baylis, M. J. Behrenfeld, A. Boetius, P. W. Boyd, A. T. Classen, T. W. Crowther, R. Danovaro, C. M. Foreman, J. Huisman, D. A. Hutchins, J. K. Jansson, D. M. Karl, B. Koskella, D. B. Mark Welch, J. B. H. Martiny, M. A. Moran, V. J. Orphan, D. S. Reay, J. V. Remais, V. I. Rich, B. K. Singh, L. Y. Stein, F. J. Stewart, M. B. Sullivan, M. J. H. van Oppen, S. C. Weaver, E. A. Webb, N. S. Webster, *Nat. Rev. Microbiol.* **2019**, *17*, 569–586.
201. D. Wacey, M. R. Kilburn, M. Saunders, J. Cliff, M. D. Brasier, *Nat. Geoscience* **2011**, *4*, 698–702. doi: 10.1038/NGEO1238.
202. M. G Pachiadaki, M. M. Yakimov, V. LaCono, E. Leadbetter, V. Edgcomb, *ISME J.* **2014**, *8*, 2478–2489.
203. C. J. Castelle, J. F. Banfield, *Cell* **2018**, *172*, 1181–1197.
204. J. E. Hallsworth, *Nat. Ecol. Evol.* **2019**, *3*, 1503–1504.
205. A. Spang, C. W. Stairs, N. Dombrowski, L. Eme, J. Lombard, E. F. Caceres, C. Greening, B. J. Baker, T. J. G. Ettema, *Nat. Microbiol.* **2019**, *4*, 1138–1148.
206. K. W. Seitz, N. Dombrowski, L. Eme, A. Spang, J. Lombard, J. R. Sieber, A. P. Teske, T. J. G. Ettema, B. J. Baker, *Nat. Comm.* **2019**, *10*, 1822. doi: 10.1038/s41467-019-09364-x.
207. S. D'Hondt, R. Pockalny, V. M. Fulfer, A. J. Spivack, *Nat. Comm.* **2019**, *10*, 3519. doi: 10.1038/s41467-019-11450-z.
208. A. J. Kessler, Y.-J. Chen, D. W. Waite, T. Hutchinson, S. Koh, M. E. Popa, J. Beardall, P. Hugenholtz, P. L. M. Cook, C. Greening, *Nat. Microbiol.* **2019**, *4*, 1014–1023.
209. A. O. Leu, C. Cai, S. J. McIlroy, G. Southam, V. J. Orphan, Z. Yuan, S. Hu, G. W. Tyson, *ISME J.* **2020**, *14*, 698–702.
210. S. G. Huwiler, C. Löffler, S. E. L. Anselmann, H.-J. Stärk, M. von Bergen, J. Flechsler, R. Rachel, M. Boll, *Proc. Natl. Acad. Sci. USA* **2019**, *116*, 2259–2264.
211. T. V. Tikhonova, D. Y. Sorokin, W. R. Hagen, M. G. Khrenova, G. Muyzer, T. V. Rakitina, I. G. Shabalin, A. A. Trofimov, S. I. Tsallagov, V. O. Popov, *Proc. Natl. Acad. Sci. USA* **2020**, *117*, 5280–5290.
212. J. Li, P. Mara, F. Schubotz, J. B. Sylvan, G. Burgaud, F. Klein, D. Beaudoin, S. Ying Wee, H. J. B. Dick, S. Lott, R. Cox, L. A. E. Meyer, M. Quémener, D. K. Blackman, V. P. Edgcomb, *Nature* **2020**, *579*, 250–255.

2

Microbes: Masters of the Global Element Cycles

Bernhard Schink

Department of Biology, University of Konstanz, D-78457 Konstanz
<bernhard.schink@uni-konstanz.de>

Metal Ions in Life Sciences, Volume 21 Guest Editors: Peter M. H. Kroneck and Martha E. Sosa Torres
Series Editors: Astrid Sigel, Eva Freisinger, and Roland K. O. Sigel

https://doi.org/10.1515/9783110589771-002

Abstract: Prokaryotes, i.e., classical Bacteria and Archaea, are excellent catalysts which enable not only simple exergonic redox reactions to proceed but can also couple exergonic with endergonic reactions, e.g., in biosynthesis. As true for all biochemical processes, microbial transformations can be highly specific and can direct reactions specifically towards single types of highly defined products, e.g., to the production of only one type of enantiomeric product. Microbes can combine endergonic activations at the beginning of a reaction chain with exergonic steps at a later stage in a transformation sequence. With the enormous breadth of microbially catalyzed reactions, nearly every energetically feasible reaction can be catalyzed by microbial activities, and numerous reactions that were considered in the past as purely chemical processes have been found later to depend on microbial activities. Through microbial growth, the catalytically active biomass can dynamically adapt to the needs of specific transformation processes, depending on the amount of energy derived in the respective reactions. Given the broad diversity of their reaction capacities, microbes hold great promise for applications in degradative and biosynthetic activities, also in the future.

Keywords: anaerobic bacteria · fermentation · lithotrophic oxidation · microbial degradation · microbial growth · minimum energy quantum · redox reactions

1. INTRODUCTION: MICROBES AS CATALYSTS

Microbes are an extremely heterogeneous and metabolically versatile group of organisms. In this chapter, I will focus on metabolic activities of Bacteria and so-called Archaeobacteria or Archaea which both together are defined as prokaryotes because they do not contain a membrane-surrounded nucleus (Greek *karyon*) but their genetic material is organized in one or few rings of DNA that are present free in the cytoplasm. Different from cells of eukaryotic organisms such as animals and plants which contain real nuclei, prokaryotes exhibit an enormous metabolic versatility, beyond the well-known processes of aerobic respiration or oxygenic photosynthesis that higher organisms do. They can live in the absence of molecular oxygen (O_2), either by fermentations or anaerobic respirations, they can use inorganic compounds as electron donors or acceptors, no matter if they are accessible as dissolved compounds or not, they can handle quite inert substrates such as hydrocarbons or dinitrogen, and they can live at extremes of heat, cold, acidity, alkalinity, salinity or water shortage. Due to their

small cell size (in the range of one to few μm), their surface-to-volume ratio is very high and with this, their metabolic activity and their rate of interaction with their surroundings are typically high. Prokaryotes cannot take up particulate substrates by, e.g., phagocytosis as eukaryotic protozoa do; thus, polymeric or otherwise non-dissolved substrates have to be depolymerized or otherwise be metabolized outside the cell.

Microbes act in nature as chemical catalysts. Needless to say, they cannot do wonders (although many of us sometimes think they do); they can only catalyze reactions that are thermodynamically feasible. As good catalysts, they speed up reactions that would otherwise occur also purely chemically, e.g., the corrosion of metallic iron. They can also allow exergonic reactions to proceed that would never proceed on their own, e.g., the oxidation of organic matter with O_2. Actually, this is perhaps the most important niche of biotic activities in general: to overcome the kinetic hindrance of metastable reaction systems. As it is true for biochemical reactions in general, enzyme-catalyzed reactions not only allow thermodynamically feasible reactions to occur, but they also direct them into a certain direction, e.g., produce stereospecifically only one enantiomer of a chiral compound, not a mix of both (racemate).

A very essential feature of biochemical reaction systems, not only in this context, is their ability to couple exergonic and endergonic reactions. Endergonic reactions, e.g., substrate activations at the beginning of a reaction chain, can be enabled by exergonic steps that proceed later in the process, typically by transfer of coenzymes or reactive co-reactants such as phosphoryl groups. With this, many substrates become metabolically accessible that otherwise are hard to attack. Similarly, microbial growth, i.e., the (endergonic) biosynthesis of microbial biomass, is fueled by the simultaneous (exergonic) degradation of, e.g., organic matter with O_2 as electron acceptor. Even more elegantly, the energy needed for growth can be derived from light reactions as in phototrophic bacteria, no matter whether they are oxygenic (O_2-producing) or anoxygenic, i.e., oxidizing organic or reduced sulfur compounds. It is worth mentioning at this point that nearly all organic matter on Earth derives directly or indirectly from photosynthetic activities. Phototrophs, both anoxygenic and oxygenic ones, were also responsible for the dramatic oxidation event around two billion years ago which changed the so far reduced state of our Earth's crust and atmosphere from an entirely reduced to a largely oxidized state, including the accumulation of sulfate (SO_4^{2-}) in seawater, of Fe(III) oxides in Banded Iron Formations (BIFs), and of dioxygen in our atmosphere [1, 2]. These gigantic changes of our world's chemistry are due to the efficient coupling of prokaryotic light reactions with the endergonic oxidation of sulfide (S^{2-}), iron(II), and water, with carbon dioxide (CO_2) as oxidant that was concomitantly reduced to organic cell material [1].

Many of the processes to be considered in this chapter are catalyzed in the absence of O_2, by strictly anaerobic microbes that are sensitive to O_2. Dioxygen and its metabolic derivatives, such as hydrogen peroxide (H_2O_2), superoxide ($O_2^{\bullet -}$) and hydroxyl radicals ($HO^{\bullet}$), destroy or inactivate many anaerobic enzymes, coenzymes or metastable reaction intermediates very quickly. The development of techniques for strictly anoxic handling of microbial cultures in the

late 1960ies [3] and transfer of these handling strategies also to cell-free extracts and enzyme preparations opened the door to an unbelievably colorful spectrum of biochemical reactions that are unique to the anaerobic world, and many of these reactions also provide insights into the early evolution of biochemistry and of life in general [4–7]. In the present chapter, I will use a few examples of microbial processes to demonstrate what we can learn still today from these witnesses of early life evolution, looking not only at the reactions themselves but also at the microbes that use them and often also create the reaction conditions under which the respective enzymes operate.

2. THE BIOCHEMICAL "REDOX TOWER"

Nearly all types of energy metabolism are redox reactions between electron donors and acceptors of different redox potentials. This is also true for fermentations which can be defined as redox processes of carbon compounds which undergo dismutation reactions to more reduced and more oxidized products. Since energy yields in anaerobic processes are much lower than in aerobic respirations, the majority of substrate is transformed in the energy metabolism. This is the main job of the respective organisms where they earn the "money", i.e., the ATP they need for the synthesis of cell matter and growth. Most biochemically catalyzed redox reactions operate within a redox range of –420 mV to +810 mV at neutral pH (Figure 1), with very few exceptions outside this range.

2.1. Aerobic and Anaerobic Respirations

Figure 1 gives a general overview of redox systems used by microbial activities. Oxidation of organic compounds on the upper left side releases electrons that are delivered to an acceptor on the right side, e.g., dioxygen. The electrons are channeled through various carrier systems indicated in the middle of this figure, mostly resulting in the formation of ATP via proton translocations through respiratory enzymes in the cytoplasmic membrane. Sugars are excellent electron donors allowing a maximum of ATP formation in the respiratory chain; electrons from acetate or partly degraded organic matter such as humic compounds (calculated as phenol equivalent) or hydrocarbons have to feed a major part of their electrons into the respiratory chain at a more positive redox potential than NADH, e.g., at the quinone level, resulting in a smaller ATP yield.

On the side of the electron acceptors, a broad variety of alternative oxidants can be applied. We find these alternatives spatially organized, e.g., in a lake sediment. Whereas aerobic respiration dominates in the top few millimeters, nitrate (NO_3^-) reduction to either dinitrogen (N_2) gas or to ammonia/ammonium (NH_3/NH_4^+) takes over below this layer, followed by reduction of Fe(III) or Mn(IV) oxides to Fe^{2+} and Mn^{2+} ions, reduction of sulfate to hydrogen sulfide (H_2S) and finally reduction of CO_2 to methane (CH_4) [8]. This redox sequence

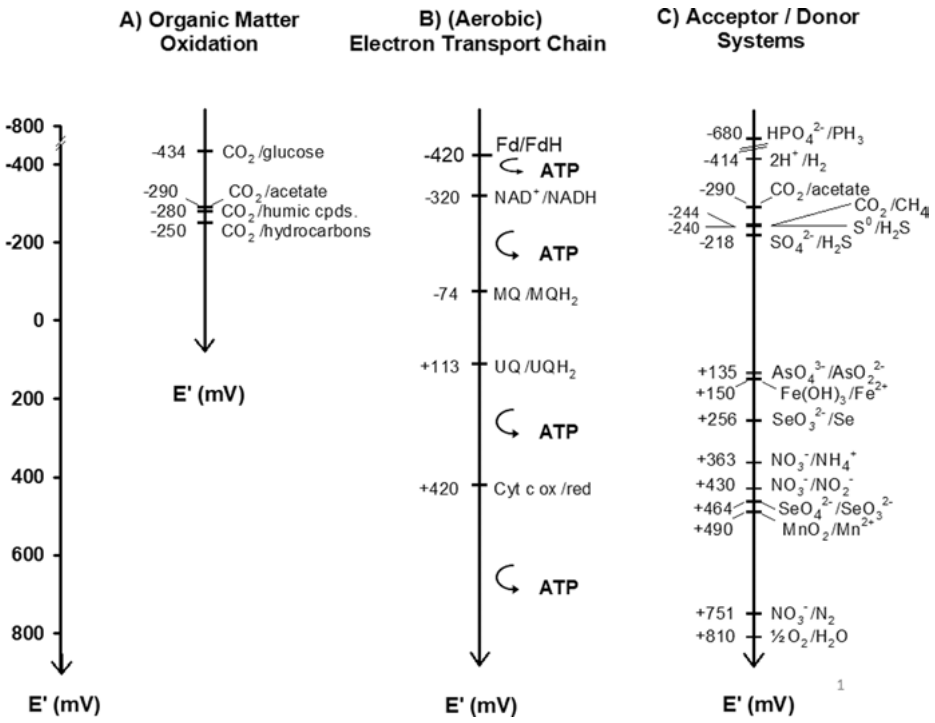

Figure 1. Redox potentials (E′, pH 7.0) of biologically relevant electron donors and acceptors, including important electron carriers inside the cell. Fd, Ferredoxin; MQ, menaquinone; UQ, ubiquinone; cyt, cytochrome. Modified after [99].

stretches over 10–20 cm depth within a freshwater sediment and can extend over several meters in deep ocean sediments, depending on the availability of organic matter from primary production. In marine sediments, the zone of sulfate reduction is far bigger than in freshwater sediments since seawater contains more than 100 times more sulfate than freshwater (28 mM versus 100–200 μM, respectively). The sequence of these alternative redox processes is determined by the redox potentials of the respective redox systems in play (Figure 1), with the most positive (most energy-yielding) process served first and others sequentially following. It goes without saying that the energy (ATP) yields of the respective reduction processes decrease with the decreasing redox potential of the acceptor system, with about 3 ATP per electron pair with NADH as donor and O_2 as acceptor, and less than one ATP with the redox couple NADH plus sulfate. The sequence extends in the opposite direction in, e.g., a groundwater plume in soil at an oil contamination site, with the most reduced zone at the contamination site itself. The predominant redox reactions can be localized in sediment profiles with specific electrodes as far as surface-active reagents (H_2, Fe^{2+}, H_2S, O_2) are involved.

The reduction of CO_2 to CH_4 or to acetate (CH_3COO^-) both are exciting examples of refined microbial biochemistry which both involve metals in the

final product formation reactions. The release of CH_4 from a sulfur-bound methyl residue is catalyzed inside a water-free pocket in the methyl-coenzyme M reductase enzyme in a reversible reaction involving a redox change of a corrinoid-bound nickel ion [9, 10]. The key reaction of CO_2 reduction to CH_3COO^- (homoacetogenesis) is catalyzed by an enzyme complex involving the reduction of CO_2 to a nickel-bound carbon monoxide (Ni-CO) which is subsequently combined with a methyl residue to form an acetyl-nickel intermediate which is thiolytically cleaved to form acetyl-coenzyme A [11, 12]. The reaction is mimicked in the Monsanto process of technical acetic acid synthesis from methanol and carbon monoxide with rhodium as catalyst which is run at large scale at pressures of 30–60 bar and 150–200 °C [13]. The CO dehydrogenase/acetyl-CoA synthase complex does basically the same at much milder conditions. It is widespread in the world of strict anaerobes and operates in many functions: (i) in the acetogenic energy metabolism of the homoacetogens as mentioned above, (ii) in the assimilatory synthesis of acetyl-CoA in numerous autotrophic anaerobes, (iii) in acetate cleavage by acetate-degrading methanogens, and (iv) in acetate oxidation by most completely-oxidizing sulfate reducers. It is a key enzyme of anaerobic metabolism that is found both in classical Bacteria and in Archaea and may count among the oldest enzymes in the evolution of life, therefore.

Beyond the "classical" electron acceptors mentioned, also other redox-active compounds can be used as electron acceptors. Among those are oxides of metals and metalloids such as CrO_4^{2-}, SeO_4^{2-}, SeO_3^{2-} or AsO_4^{3-}. Reductive transformation of these toxic compounds to less toxic or to water-insoluble derivatives is being applied for groundwater restoration or drinking water treatment in naturally or artificially contaminated regions [14, 15].

2.2. Lithotrophic Oxidations

The reduced derivatives formed in the anaerobic respiration processes mentioned above will either move on their own by molecular diffusion or will be transported with groundwater currents earlier or later to more oxidized zones of the underground where they meet reactants of higher redox potentials, most prominently again dioxygen. The energy spans for redox reactions that open up between reactants under these conditions are being exploited nearly always by microbial metabolic activities, so-called lithotrophic oxidations (Greek *lithos*: rock, mineral). Thus, CH_4, H_2S, Fe^{2+}, Mn^{2+}, NH_4^+, Cr^{3+}, SeO_3^{2-}, AsO_2^{2-} and others can be reoxidized to the respective more oxidized forms, and the available energy be exploited for microbial ATP synthesis and growth. While CH_4 and NH_4^+ are comparably stable and require serious biochemical efforts for activation (see Section 2.5) the others react nearly spontaneously with O_2 and other oxidants such as Fe(III) oxides or nitrite (NO_2^-). Whereas oxidation of CH_4, H_2S, Fe^{2+}, Mn^{2+}, and NH_4^+ with O_2 has been described many years ago, beginning with Sergey N. Winogradsky's seminal work [16–18], other options such as oxidation of CH_4 with SO_4^{2-}, NO_3^- or Fe(III) have been described only recently

[19–21], and the same applies to O_2-independent ammonia oxidation [22] and NO_3^--dependent oxidation of Fe(II) [23].

The couple phosphate/phosphine (PO_4^{3-}/PH_3) has an extremely low redox potential, overall –680 mV at pH 7.0 (Figure 1). Nonetheless, several reports claim that bacterial cultures reduced phosphate to phosphine with simultaneous oxidation of organic matter. It is obvious from comparison of the redox potentials that this would be a highly endergonic process that could never feed a bacterium. In none of these claims the product PH_3 was ever reliably identified; mostly, a "garlic-like odor" (probably due to formed thiols) was taken as proof (see overview in [24, 25]). In general, phosphorus does not change its redox state in biochemistry and stays nearly always at the redox state P(V), i.e., as PO_4^{3-}. Nonetheless, PO_4^{3-} can be reduced biochemically to the P(III) or P(I) state in the biosynthesis of phosphonate lipids and secondary metabolites, e.g., the naturally occurring herbicide glufosinate (phosphinothricin, $C_5H_{11}NO_4P^-$), but these syntheses are highly ATP-consuming [24]. On the other hand, reduced phosphorus compounds, due to their very low redox potential, can be potent electron donors for microbial life. A sulfate-reducing bacterium was isolated which couples the oxidation of phosphite (HPO_3^{2-}) to the reduction of sulfate and obviously exploits the available energy of this redox reaction quite efficiently [26, 27]. Several other bacteria can use HPO_3^{2-} or hypophosphite ($H_2PO_2^-$) as phosphorus source for cell matter synthesis [28] and with this exploit phosphorus sources that are available in today's environment only at low amounts but at higher solubility than phosphate, and may have played a more important role in the early phase of life's evolution [29].

Lithotrophic oxidation can also be taken over by phototrophic bacteria, provided that light penetrates down to sediments or water layers where, e.g., HS^- is available, such as in shallow stagnant water bodies. So far, light-dependent oxidation (with CO_2 as electron acceptor, which is reduced to cell mass) has been described for H_2O (oxygenic photosynthesis of cyanobacteria and green plants), H_2S [30], Fe^{2+} [31], and NO_2^- [32]. Analogous processes with Mn^{2+}, NH_4^+ or CH_4 as electron donor have not been described yet; thus, one of the "missing lithotrophs" that Broda anticipated [33] is still missing today.

3. REDOX REACTIONS WITH METALS

3.1. Iron Reduction and Oxidation in Acidic and Neutral Environments

Iron is the fourth most abundant element in the Earth's crust, and iron minerals make up a substantial amount of soils and sediments. In acidic environments, e.g., in volcanic sulfur springs at pH 2 and lower, both Fe^{3+} und Fe^{2+} ions are well soluble, and redox transitions between both are mechanistically easy (see Chapter 7). The transition from the Fe(III) to the Fe(II) state and back represents an essential redox process also in neutral sediments and waters, which has implications also on the availability (solubility) of iron ions for microbial growth.

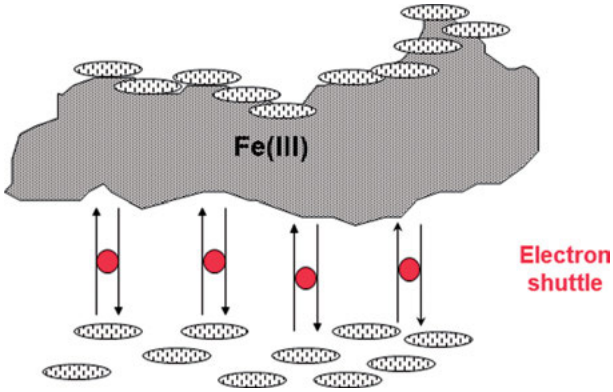

Figure 2. Reduction of Fe(III) oxide by direct cell attachment or via dissolved electron carriers. (Courtesy by Dr. Kristina Straub, with permission).

At neutral pH under reducing conditions, the Fe^{2+} ion is still rather well soluble; precipitation with sulfide to form FeS, or with carbonate to $FeCO_3$, still leaves Fe^{2+} ions in the micromolar range in solution. In the oxidized Fe(III) state at neutral pH, iron forms oxides and hydroxides of extremely low solubility, thus necessitating refined and highly costly strategies for aerobic organisms to secure their iron needs for cell matter synthesis, e.g., for iron-containing enzymes such as heme and iron-sulfur proteins [34]. Use of iron oxides as electron acceptors at neutral pH requires huge amounts of Fe(III) and precludes a costly uptake into the cells, thus the electrons have to be delivered outside the cell. So far, two different strategies have been discovered how this electron transfer can be accomplished (Figure 2).

Some bacteria use dissolved electron carriers to transfer electrons to the iron mineral surface that either are present in the surroundings, e.g., humic compounds [35] or dissolved sulfur species of various redox states [36], or they use compounds that they synthesize themselves for this purpose, e.g., phenazines [37]. Other bacteria have to attach directly to the iron oxides and deliver the metabolic electrons in direct surface contact or via electrically conductive pili, so-called "nanowires" (see Chapter 8). The way how electrons are transmitted inside such nanowires is still unclear; electrons might hop through series of iron complexes, e.g., cytochromes, from source to sink [38], or closely arranged aromatic ring structures might act as electrical conductants, comparable to the electrical conduction in graphite [39] (see Chapter 8).

Solubility problems arise also in iron oxidation at neutral pH. Specialists for this kind of metabolism are representatives of the genus *Gallionella* which are found in nature as rusty orange-red viscous pillows in small ditches and ponds where slightly acidic Fe^{2+}-rich groundwater meets O_2-rich surface waters. These bacteria release the formed Fe(III) oxyhydroxide (FeO(OH)) only at one site on their cell surface thus producing screw-like bands of iron oxides with small contents of proteins, thus avoiding that the entire cell covers itself with "rust" that would preclude further metabolic activity [40, 41]. The screw-like threads

produced this way form the mentioned viscous pillows which limit convective access of O_2 to the Fe^{2+}-rich water. With this, the bacteria largely prevent direct chemical oxidation of Fe^{2+} ions with O_2 that otherwise might outcompete the bacterial activity.

3.2. Extracellular Electron Transfer

Similar to the delivery of electrons to insoluble Fe(III) oxides described above, iron-reducing and also other bacteria can transfer electrons to an anode which, if coupled to a suitable cathode, allows to close an electrical circuit. In such a system, the bacteria facilitate electron transfer from, e.g., organic matter via the electric conductant to, e.g., dioxygen as terminal acceptor, and the electric potential difference between both can partially be sequestered for electrical work (Figure 3) [42, 43].

This concept is already being applied for advanced wastewater treatment strategies [44]. Microbes can as well transfer electrons directly from metallic surfaces and deliver them to external acceptors, e.g., in bacterial enhanced metal corrosion with either SO_4^{2-} or O_2 as electron acceptor [45]. Alternatively, microbes can settle on the cathode side to take up cathode-derived electrons for reduction of CO_2 to CH_4, thus converting excess electricity from wind or solar power plants into CH_4 as a storeable energy carrier [46]. Unfortunately, such systems work only on a small scale so far, and their efficiency in energy translation is rather limited.

The reduction of elemental sulfur (S^0) by anaerobic bacteria is another challenge due to its extremely low solubility. In this case, the reaction product H_2S helps to stimulate sulfur respiration by dissolution of S^0 to polysulfide (S_n^{2-}) that

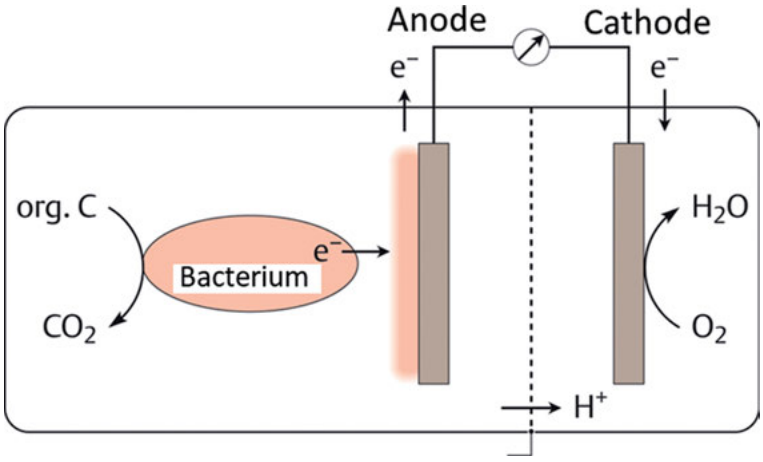

Figure 3. A microbial fuel cell including microbial cells attached to the anode. Modified after [100].

can be used by most sulfur reducers as an electron acceptor [47]. The formed H_2S does not accumulate as such in natural environments but reacts with Fe^{2+} ions to form black precipitates of FeS. In deeper sediment layers, FeS is further converted to FeS_2 (pyrite) as a very stable end product. Formation of pyrite in sediments has long been considered as a purely chemical process which uses either Fe(III) or S^0 sulfur as a co-substrate [48]. Recent results indicate that FeS_2 formation from FeS could as well be catalyzed in a microbial process according to the Wächtershäuser reaction (Equation 1) [49].

$$FeS + H_2S \rightarrow FeS_2 + H_2 \quad (1)$$

This process probably involves extracellular electron transfer reactions due to the very low solubility of the iron sulfides, perhaps through a reversal of H_2-dependent sulfur respiration [47].

4. ACTIVATION OF INERT SUBSTRATES

4.1. Dinitrogen

The industrial synthesis of ammonia from N_2 and H_2 in the so-called Haber-Bosch process, despite being an exergonic reaction, requires high temperature (450 °C) and high pressure (300 bar) to become efficient. Numerous Bacteria and Archaea catalyze this process, also called nitrogen fixation, at normal temperature and pressure using the enzyme nitrogenase. This enzyme requires reduced ferredoxin as electron donor and ATP as an energy source, and employs molybdenum and iron in its catalytic center [50]. Higher organisms never learned to produce nitrogenase themselves, but numerous plants established quite intimate cooperations with nitrogen-fixing bacteria to exploit this important prokaryotic metabolic capacity for themselves, e.g., in the well-known leguminous plant-*Rhizobium* symbiosis [51]. The exact reaction mechanism of nitrogen reduction by this enzyme has not been understood yet, but the molybdenum metal obviously plays a central role in it; some bacteria use alternatively a vanadium nitrogenase [50]. Efficient mimicking of the microbial nitrogenase enzyme system for technical application at large scale would be highly desirable since the Haber-Bosch process requires enormous amounts of energy (about 2 % of the global human energy budget).

4.2. Ammonia

Ammonia once released through decomposition of biomass, especially of proteins, is stable under air. Its oxidation in soil and oxygen-rich waters is initiated by Bacteria and Archaea through the action of ammonia monooxygenase. This enzyme uses dioxygen as co-substrate and introduces one oxygen atom into the

ammonia substrate to form hydroxylamine (NH_2OH). The second oxygen atom of O_2 is reduced to water with additional two electrons from a reductant XH_2 that have to be replenished in the further oxidation process (Equation 2).

$$NH_3 + O_2 + XH_2 \rightarrow NH_2OH + H_2O + X \quad (2)$$

Such oxygenase reactions are highly exergonic ($\Delta G'_0 \approx -350\ kJ\ mol^{-1}$) and irreversible; they can be considered as "incomplete combustions" of the substrate molecule. Nonetheless, this costly activation of an otherwise inert substrate molecule creates a specific niche for the microbes specialized on this type of metabolism. Oxygenases in general are employed in aerobic microbial biochemistry for the activation of inert substrates. The additionally supplied electrons are needed to produce an iron-bound peroxide residue in the enzyme which renders the oxygen even more aggressive for its attack on the inert substrate molecule [52].

Removal of bound reduced nitrogen is an important step in the wastewater treatment technology. In efforts to improve the conventional process of aerobic ammonia oxidation and subsequent denitrification, it was found that ammonia was also removed by an oxygen-independent process through reaction with nitrite, the "Anammox" process (Equation 3) [22].

$$NH_3 + NO_2^- + H^+ \rightarrow N_2 + 2\,H_2O \quad (3)$$

This highly exergonic reaction ($\Delta G'_0 = -410\ kJ\ mol^{-1}$) is well known in chemistry as nitrogen symproportionation (comproportionation). The bacteria catalyzing this process have not yet been obtained in pure culture, but the biochemistry has been basically elucidated in enriched cell material and by metagenomics analysis. It was shown that NO_2^- is first reduced to nitric oxide (NO) which attacks the NH_3 molecule to form hydrazine (N_2H_4) as the first intermediate that is subsequently oxidized to N_2 [53]. To protect the bacterial cytoplasm from the highly reactive and toxic NO and N_2H_4, the described reactions proceed inside cell-internal compartments, so-called anammoxosomes.

4.3. Saturated Aliphatic Hydrocarbons

Aerobic oxidation of saturated hydrocarbons ($R\text{-}CH_3$) is initiated, similar to ammonia, by a monooxygenase reaction (Equation 4) [54]. Again, the further oxidation steps have to replenish

$$R\text{-}CH_3 + O_2 + XH_2 \rightarrow R\text{-}CH_2OH + H_2O + X \quad (4)$$

the additional electrons (from XH_2) consumed in the initial activation reaction. With the simplest hydrocarbon methane (R = H), the further oxidation leads via formaldehyde (H_2CO) and formic acid (HCOOH) to CO_2. With higher alkanes, the oxygenase attacks preferentially the terminal carbon atom, and the further degradation proceeds via beta-oxidation of the resulting fatty acids.

Saturated hydrocarbons (alkanes) can also be degraded in the absence of dioxygen. Anaerobic methane oxidation under strictly anoxic conditions with sulfate as electron acceptor proceeds as a reversal of methane formation (methyl coenzyme M reductase; see Section 2.1). The initial attack on CH_4 happens in a water-free pocket inside the methyl coenzyme M reductase enzyme, probably by the thiyl radical end of coenzyme M [55, 56] to form methyl coenzyme M; the methyl group is further oxidized to CO_2. For anaerobic oxidation of higher hydrocarbons, the alkane molecules can be added to fumarate through a glycine radical-catalyzed reaction to form alkyl-succinate [57] which is further degraded by CoA activation and β-oxidation.

4.4. Aromatic Hydrocarbons

Aromatic cyclic hydrocarbons, such as benzene (C_6H_6) or naphthalene ($C_{10}H_8$), are difficult to attack due to their highly delocalized, perfectly symmetric π electron system that is comparably stable due to its high resonance energy (151 kJ mol^{-1} C_6H_6, 255 kJ mol^{-1} $C_{10}H_8$). There are basically two different strategies to attack these structures. Aerobic bacteria pull electrons out of the ring structure with O_2 as a co-substrate (di-oxygenase reaction) to form a dihydrodiol and subsequently a catechol derivative in which the π electron system is sufficiently localized to allow further oxidative attack and ring cleavage [52, 58]. In contrary, anaerobic bacteria attack the aromatic substrate, preferentially benzoate (C_6H_5-COO^-), after CoA activation in a reductive manner, pushing further electrons into the ring and with that, abolishing the aromatic character. Different from the analogous Birch reduction of benzene which requires metallic sodium as reductant (E'_0= –2.7 V) in nonaqueous solution, the biological reduction of benzoyl-CoA, due to its slight polarization by the neighboring carbonyl group, proceeds at E'_0 = –500 mV in two one-electron steps and leads to a cyclohexadiene derivative that can further undergo defined reduction and hydratation reactions [59]. Thus, the stability of the delocalized π electron system can be overcome either by oxidation or by reduction, depending on the availability of O_2 or strongly reducing conditions. Benzene derivatives with two or three hydroxyl groups can form keto-enol tautomers and therefore can undergo direct reduction without CoA activation [59, 60].

5. COMBINATION OF ENDERGONIC AND EXERGONIC REACTIONS

In classical glycolysis, sugars are activated at the beginning through phosphorylation to form sugar phosphates. This serves two functions: It makes the substrate easier accessible for the subsequent cleavage and redox reactions, and it prevents the now charged substrate molecule from escaping out of the cell by diffusion. Of course, the ATP invested at the beginning has to be recovered at the end of

the reaction sequence, e.g., in the reactions of phosphoglycerate kinase and pyruvate kinase. Organic acids are often activated by group transfer with coenzyme A as activating agent, transferring the energy-rich thioester linkage directly from one acyl residue to another one in CoA transferase reactions as, e.g., in both pathways of lactate fermentation to propionate and acetate [61].

5.1. Dissimilatory Reduction of Sulfate

The reduction of sulfate to hydrogen sulfide is an important anaerobic respiratory process, especially in marine sediments where sulfate is available in huge amounts (28 mM in seawater). Whereas the overall process can accept electrons on average at –218 mV standard potential (Figure 1) the first step from sulfate to sulfite has a standard redox potential of –527 mV at pH 7.0 and cannot be served directly with electrons derived from oxidation of organic matter or from dihydrogen [62]. Therefore, sulfate-reducing microorganisms first spend ATP in an activation of SO_4^{2-} to form adenosine 5′-phosphosulfate (APS) and pyrophosphate (PP_i) (Equation 5):

$$SO_4^{2-} + ATP \rightarrow APS + PP_i \quad (5)$$

Since the equilibrium of this reaction is still on the left side, PP_i is hydrolyzed to two molecules of inorganic phosphate (P_i) to shift the equilibrium to the right. The subsequent reduction of APS to AMP plus sulfite (SO_3^{2-}) has a standard redox potential of –60 mV, and its reduction, as well as the further reduction of SO_3^{2-} to S^{2-} ($E_0' = -116$ mV) is easy to accomplish by dissimilatory sulfite reductase with electrons at the NADH or the menaquinone level (Figure 1). The sulfite reductase reaction is an interesting case of a transfer of six electrons, with a protein trisulfide carrying zero-valent sulfur (RS-S^0-SR) formed as reaction intermediate [63, 64]. Of course, the initial activation of SO_4^{2-} to APS and the implicit shift of the redox potentials of SO_4^{2-}/SO_3^{2-} reduction to APS/SO_3^{2-} (a shift of 470 mV redox potential difference!) has to be paid for by investment of two ATP equivalents ($ATP \rightarrow AMP + 2\,P_i$), and this investment has to be earned again in subsequent electron transport phosphorylation steps. This is a classic example of substrate activation through investment of energy at the beginning that has to be regained at the end, thus making a substrate accessible that otherwise could not be used at all.

5.2. Reversed Electron Transport

In several biochemical processes, electrons have to be transported against the electrochemical potential, from a more positive to a more negative level. Of course, this requires energy. The phenomenon of “reversed electron transport” has been described already in the mid 1960s for phototrophic bacteria and several chemolithotrophic bacteria [65–67] which both have to reduce NAD^+ for

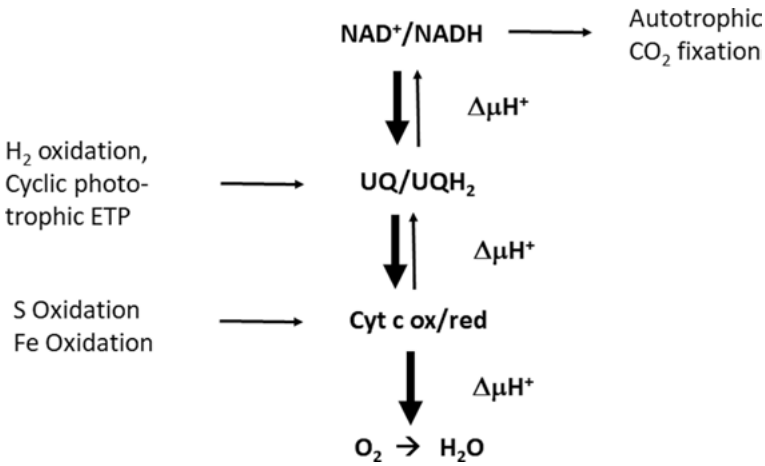

Figure 4. Direct and reversed electron flow at the prokaryotic cytoplasmic membrane.

autotrophic CO_2 fixation in the Calvin cycle, but have electrons available only at the level of quinones or even a more positive potential (Figure 1). Understanding this phenomenon became possible only after the Mitchell theory [68] provided the concept of separation of redox reactions and ATP synthesis and their connection through a charged membrane acting as a chemical capacitor. Exergonic electron transport processes establish through proton translocation a charge across the membrane that supplies the necessary energy for ATP synthesis in the ATP synthase complex. Reversal of this system allows a "reversed electron transport", e.g., from quinones to NADH to be energized through ATP hydrolysis. Similarly, exergonic electron transport, either by the cytochrome bc_1 complex or cytochrome oxidase, can directly energize endergonic electron transport from quinones to NADH (Figure 4). This way, redox reactions at different redox potential ranges can energetically support each other in a manner that only a highly organized arrangement of different redox systems in an energetically connected structure such as the cytoplasmic membrane of prokaryotic cells can provide.

5.3. Electron Bifurcation

Another fascinating device connecting exergonic and endergonic redox processes is electron bifurcation. In the ethanol-plus-acetate-fermenting bacterium *Clostridium kluyveri*, the exergonic reaction chain from ethanol (C_2H_5OH) to butyrate ($C_3H_7COO^-$) plus caproate ($C_5H_{11}COO^-$) has to "pull" the endergonic conversion of a minor amount of ethanol to acetate plus H_2, including the concomitant synthesis of ATP in the acetate kinase reaction (Figure 5a), obviously without a direct energetic linkage between these two reaction paths [69]. The problem was solved in 2008 with the discovery that the NADH electrons derived

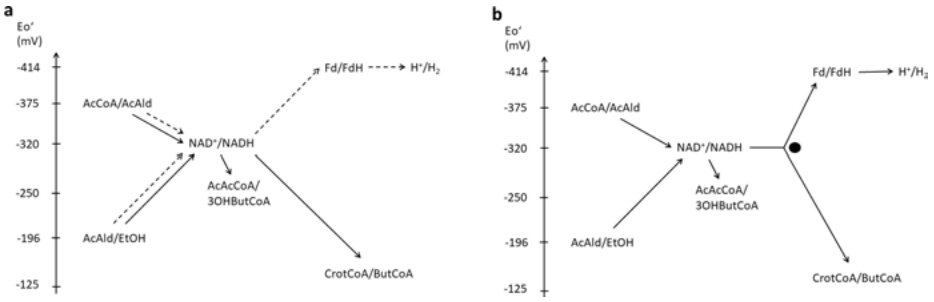

Figure 5. Electron flow in the energy metabolism of *Clostridium kluyveri*: (**a**) without electron bifurcation, (**b**) with an electron-bifurcating EtfAB enzyme complex (black dot).

in ethanol oxidation are stoichiometrically distributed between a low-potential ferredoxin ($E_0^{'}$ = –500 mV) and the high-potential reduction of crotonyl-CoA to butyryl-CoA ($E_0^{'}$ = –125 mV) (Figure 5b) [70]. The EtfAB complex catalyzing this "bifurcation" reaction contains a flavin as electron carrier which can deliver the electrons at two different redox potentials [70]. Such EtfAB complexes can operate reversibly in the direction of "bifurcation" or "confurcation" and have proven as excellent solutions to an understanding of energetically relevant key steps in numerous anaerobic metabolic processes, including homoacetogenesis, methanogenesis, and sulfate reduction [71–73].

6. AUTOCATALYTIC ADJUSTMENT OF CATALYTIC CAPACITY

Different from chemical catalysts, microbes multiply on their own and, with that, adapt their catalytic capacity to the substrate transformation needs. This applies to natural situations where microbes with special metabolic capacities grow just where these capacities are needed, and they die off when the respective job is done. This is true in a wastewater treatment plant where degradation capacities for specific wastewater contents supplied, e.g., by an industrial customer, will grow with the supply of these substrates, and will decline again when they are not needed anymore. Thus, such catalytic activities adapt to their respective job needs.

6.1. Microbial Growth Associated with Energy Metabolism

Microbial growth is most often directly associated with the availability of a growth substrate. An easily degradable organic substrate most often covers the energy needs for growth and also supplies the necessary organic carbon for cell matter synthesis. Specific substrates require the induction of specific enzymes for their degradation, and the induction pattern of degradative enzymes often helps to elucidate degradation pathways via proteomic techniques. Nonetheless,

problems may arise if energy and cell carbon are not both supplied by the same substrate as, e.g., especially with the lithotrophic bacteria discussed in Section 2.2; they receive their energy from oxidation of an inorganic electron donor but need CO_2 for synthesis of their cell material, thus, utilization of one substrate may be limited by lack of the other one. Microbial growth also depends on the supply of nitrogen compounds, phosphate, vitamins, trace elements, etc., and lack of either one may seriously limit the turnover of a substrate although the latter is available at huge excess.

Enrichment strategies used in the laboratory for selection of lithotrophic microbes most often use CO_2 as sole carbon source because the simultaneous supply of an inorganic and an organic electron source may be counterproductive with respect to the intended selection. In nature, however, lithotrophic microbes running their energy metabolism with an inorganic electron donor may prefer to use organic compounds for cell matter synthesis, but our classical enrichment strategies would not select for such microbes. In the anaerobic world, such combinations of lithotrophic energy metabolism with heterotrophic carbon assimilation are quite common: most known hydrogen-oxidizing methanogens or sulfate reducers depend on acetate plus CO_2 as co-substrates for cell matter synthesis.

6.2. Co-Metabolism

In some cases, especially with stable or synthetic compounds, it happens that the initial attack on a substrate does not lead to a product that the respective organism can use any further. "Promiscuous" enzymes produced by one organism may attack also substrates that the respective organism cannot handle. We have seen in Sections 4.1 and 4.2 that aerobic degradation of both CH_4 and NH_4^+ is initiated by oxygenases, and since both molecules are of nearly identical size and shape a methane-oxidizing bacterium may also oxidize NH_4^+ to NH_2OH (Equation 2) but cannot metabolize it any further, and the same applies to an ammonium-oxidizing microbe converting CH_4 to CH_3OH (Equation 4) and no further either. Similarly, methane-oxidizing bacteria oxidize ethane (C_2H_6) to ethanol (C_2H_5OH) and excrete it because they cannot handle ethanol any further. For such "non-productive" transformations the term "co-metabolism" has been coined [74], and such activities may play a major role in the environment in the transformation of synthetic compounds, so-called "xenobiotics" [75] as long as specific strategies for "productive" degradation of such compounds are lacking and only side activities of promiscuous enzymes may cause modifications of these substrates. It is obvious that in these cases there is no positive correlation between substrate transformation and microbial growth, even if a further microbe may happily use the intermediate thus produced. Even worse, in the described cases of alkane versus ammonium oxidation, the respective side activity of the degradative enzyme is even detrimental to the producing organism because these monooxygenases consume electrons in these non-productive side reactions and divert them from the original (productive) metabolism of the producer. Application of non-specific monooxygenases in partial degradation of, e.g., halogenated

hydrocarbons, requires either supplementation with pre-grown cells or the simultaneous supply of a "productive" substrate, therefore, to provide the necessary reducing power in the initial oxygenation and the necessary energy (and carbon) for growth and maintenance of the producing cell [76].

6.3. The "Minimum Energy" Debate

How much energy does a microbial cell need for growth? Synthesis of ATP under physiological conditions in a bacterial cell, implying also irreversible steps in a metabolic reaction chain, requires –60 to –70 kJ mol^{-1} ATP [69]. Membrane-bound enzyme complexes, so-called ATPases, convert reversibly ATP to ADP + P_i, with concomitant translocation of protons (in some cases Na^+ ions) across the cytoplasmic membrane. The stoichiometry of these reversible transformations is in most cases 3–4 H^+ (or Na^+ ions) per ATP synthesized or hydrolyzed [77, 78] and with this, the minimum amount of energy required for synthesis of ATP in small increments comes to –15 to –20 kJ mol^{-1}. Reactions yielding less energy can proceed, of course, but they cannot support growth of a bacterium and, with this, cannot produce a positive correlation between substrate transformation and growth, i.e., adaptation of catalytic capacities to the amounts of substrate to be transformed.

The exact value of the "minimum amount of energy for life" has been discussed repeatedly through recent years. There are several examples of anaerobic bacteria that run their energy metabolism with energy yields close to the minimum value defined above [79–81] and also free-energy calculations based on quantitative analysis of pool sizes of reaction intermediates in dynamic equilibrium in methanogenic processes within lake sediments or bioreactors converge in the same range [82, 83]. Even in the extremely energy-poor situation of microbial communities in the marine deep subsurface, minimum energy yields in the range of –10 kJ mol^{-1} substrate transformation have been calculated which may partly be explained by low phosphorylation potentials inside the microbial cells and combinations of Na^+- and H^+-driven energy couplings [84, 85].

A minimum amount of –20 kJ per mol can be brought about, e.g., by a two-electron redox reaction with a potential difference of ~100 mV (Figure 1). An example is the oxidation of ferredoxin with NAD^+ as electron acceptor catalyzed by the so-called Rnf complex that has become essential in the energy metabolism of many strict anaerobes [86]. In the opposite direction, the Rnf complex provides an energy-dependent "reversed electron transport" from NADH to ferredoxin in phototrophic and aerobic bacteria capable of nitrogen fixation, to supply low-potential electrons for the splitting of the N,N triple bond to produce ammonia [87]. The list of redox potentials shown in Figure 1 suggests some examples of electron donor and acceptor combinations that should allow microbial energy conservation but perhaps have never been tried.

7. SPECIFICITIES AND LIMITS OF ENZYME-CATALYZED REACTIONS

7.1. Stereospecificity and Substrate Affinity

Enzymes do not only catalyze reactions that are thermodynamically possible, they most often also direct the reaction into a specific direction. The discovery of biochemical stereoselectivity goes back to Louis Pasteur who worked in the 1860s on tartrate that he received from winemakers. He observed that in an aqueous solution of a (thermally produced) racemic mixture of *D*- and *L*-tartrate only the *D*-enantiomer was degraded by microbes whereas the *L*-enantiomer remained in solution [88]. He attributed this selective discrimination to a "*vis vitalis*", a specific ability that is inherent only to living organisms. The fact that enzymes discriminate between stereo isomers (enantiomers) of otherwise identical compounds has established the central role that enzymes and enzymatically active microbes play in the biotechnological production of organic compounds, including lactic acid, food additives, vitamins, pharmaceuticals, and many others. Modern chemical catalysts try to substitute for enzymes in some of these processes, but they hardly ever reach the degree of enantioselectivity that the three-dimensional architecture of a reaction center inside a protein can achieve.

Microbial enzymes do not only show high substrate specificity, they typically also show high substrate affinity and bind their respective substrates even at very low concentrations. It is not always clear which structural and chemical properties determine this affinity. As an example, I mention hydrogenases which reversibly bind the smallest known molecule, dihydrogen (H_2), either for its release or for its activation, and which are found in numerous aerobic or strictly anaerobic Bacteria and Archaea. Many hydrogenases contain nickel and iron in their catalytic centers, others have only iron as catalytic centers. These enzymes catalyze the release of electrons from H_2 and *vice versa* with minimal overpotentials [89], much more efficient than, e.g., a platinum catalyst, a property that makes them interesting especially for applications in technical dihydrogen or solar energy conversion and storage.

The affinity of hydrogenases for H_2 differs between different H_2-metabolizing microbes and determines, e.g., the dihydrogen pools and with this the bioenergetics of fermenting communities that cooperate in anaerobic methane formation via syntrophic "interspecies hydrogen transfer" [79]. The recently discovered nickel-iron hydrogenase of a *Mycobacterium* sp. from soil represents an extreme case. It was found to bind and oxidize H_2 at 50 and 130 pM concentration and with this contributes to the removal of this trace gas from our atmosphere [90]. Threshold concentrations of other hydrogenases (and their half-saturation constants K_m) are about 10–100 times higher and therefore these enzymes cannot participate in the oxidation of H_2 at atmospheric concentration levels [91]. So far, the structural or chemical properties determining this high substrate affinity remain unknown.

7.2. Operation in Reaction Chains and Their Limitations

From the early work by Winogradsky [18] it is known that the microbial oxidation of NH_3 to NO_3^- requires a cooperation of two different microorganisms (see Section 4.2). One bacterium, e.g., *Nitrosomonas* sp., oxidizes NH_3 to NO_2^-, hereafter another bacterium, e.g., *Nitrobacter* sp., oxidizes NO_2^- to NO_3^- in a second step. This strange division of labor between two metabolically different organisms remained enigmatic for many years. Why is there not a bacterium that does the entire oxidation from NH_3 to NO_3^-? Costa et al. [92] provided a convincing explanation for this phenomenon. Since enzymes are rather spacious macromolecules, and since the space inside a bacterial cell is limited, the number of enzyme molecules of every single type (which determines the maximal specific reaction rate and with this the ATP synthesis rate) competes against the number of steps that can be run within a reaction chain. Thus, short reaction chains would allow higher rates of ATP production and *vice versa*. It was concluded that long reaction chains would be advantageous especially at low reaction rates. Consequently, bacteria oxidizing NH_3 completely to NO_3^- ("*Comammox* bacteria") were finally enriched in biofilm reactors at low growth rate [93, 94], different from the "classical" enrichment strategies that select for fast-growing organisms. The example shows that long reaction lines can be detrimental under conditions of low energy supply; in this case, a modular organization of functions into different reaction units may allow a significant increase in turnover efficiency.

Division of labor between metabolically different organisms is a common feature especially found among anaerobic microbes. Conversion of polymeric biomass to CH_4 and CO_2 in a sediment or a bioreactor requires the cooperation of at least three to four different metabolic types (guilds) of microbes, including primary fermenters, secondary fermenters, homoacetogens, and methanogens [79]. The reason why never a single organism was found so far that could convert cellulose directly to CH_4 and CO_2 may be the same as with the nitrification story told above. The reaction chain of glycolysis – after cellulose depolymerization outside the cell – and that of CH_4 formation from H_2 and CH_3COO^- together would include many enzymatic steps that would render the total transformation activity low. Such organisms could be enriched preferentially in oligotrophic sediments at low substrate supply and unlimited detention times. At higher turnover rates, the well-known modular multi-step organization is obviously the better choice for faster substrate turnover and ATP synthesis, especially in the extremely energy-limited situation of methanogenic microbial communities.

8. CONSEQUENCES OF MICROBIAL REDOX ACTIVITIES

Due to their high surface-to-volume ratio and the implication of high metabolic activity, microorganisms not only take advantage of metabolic chances that nature provides, but they also shape their environment as a consequence of their activity.

8.1. Redox Heterogeneity Inside a Bacterial Colony

Cells forming a bacterial colony on a Petri dish may appear to run their energy metabolism entirely by aerobic respiration. Measurement of dioxygen distribution inside such colonies by micro electrodes revealed that the majority of the inhabitants of such a colony may be strongly O_2-limited and even entirely O_2-deprived in its lower part. Actually, a bacterial "film" as thin as 50 μm (about 50 cell layers!) in the upper colony part suffices to consume the dioxygen content from air-saturated to entirely anoxic within a substrate-supplied colony [95], thus forcing the lower cell layers to either switch to anaerobic fermentation or to give up their energy metabolism entirely if they do not have another choice. What is true for a bacterial colony in the laboratory applies as well at large scale to natural environments. Since the solubility of O_2 in aqueous solution is rather limited, and since its diffusive transport is often slow compared to the rate of its consumption, O_2 concentration becomes quickly limiting, e.g., in a lake sediment, and below a few millimeters in depth we find entirely anoxic conditions. The same applies to a waste dumpsite where huge amounts of organic matter are decomposed, or to soils, especially if excess water prevents convective oxygen transport as especially true for rice paddies. In all these cases, anaerobic processes will prevail in the degradation of organic matter, according to the "biochemical redox tower" mentioned above (Section 2.1). If we further consider digestive tracts of animals which are nearly entirely O_2-depleted it becomes obvious that a major part, perhaps the majority of organic matter in nature, is degraded anaerobically, applying the biochemical toolbox of anaerobes rather than O_2-dependent oxygenase and oxidase reactions.

8.2. Aerobic Sulfide Oxidation in a Marine Sediment: Kinetic Aspects

A special case of aerobic versus anaerobic metabolic transformation is the natural cycling of sulfur compounds. Sulfate is a common electron acceptor in anoxic sediments, and its reduction produces major amounts of hydrogen sulfide, especially in marine sediments. Part of this H_2S reacts with Fe^{2+} ions to form FeS, the black material that accumulates in such places. Another part of H_2S diffuses upwards and will finally meet free dioxygen. The chemical reaction of H_2S with O_2 at neutral pH leads to a mix of S^0, SO_3^{2-}, $S_2O_3^{2-}$ (thiosulfate) and other sulfur compounds. Specialized aerobic bacteria such as *Beggiatoa* spp. oxidize H_2S completely to SO_4^{2-}, but they have to compete against the chemical reaction mentioned above. The way how they do this has been demonstrated in model experiments in test tubes in which a soft agar mimics the sediment structure (Figure 6) [96].

In both test tubes, H_2S diffuses upwards against O_2 which diffuses from the top to the bottom. In the left, non-inoculated test tube, O_2 and H_2S will accumulate to substantial concentrations in the overlap zone and become depleted due to chemical oxidation of H_2S by O_2 as described above. The right test tube was

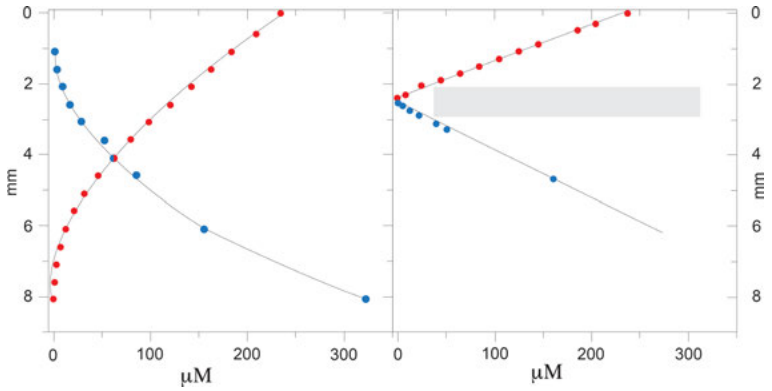

Figure 6. Distribution gradients of dioxygen (red dots) and hydrogen sulfide (blue dots) in agar-stabilized media with a sulfide source at the bottom and air from the top, after incubation for 3–4 days. **Left**: Non-inoculated control tube; **right**: tube inoculated with *Beggiatoa* cells; shaded area: enrichment of *Beggiatoa* cells; figure produced from data published by Nelson and associates [96].

inoculated with *Beggiatoa* cells that have grown through three days of incubation and form a whitish layer just where O_2 and H_2S meet. These bacteria act as an efficient catalyst which intensifies the reaction of H_2S with O_2 to SO_4^{2-}. In contrast to the non-inoculated test tube, O_2 and H_2S meet in the growth zone only to a minimum extent showing that the (biochemically) catalyzed process operates much more efficiently at low reactant concentrations than the non-catalyzed chemical reaction does. The gradient slopes of both reactants are significantly steeper in the inoculated test tube, indicating about three times higher reaction rates compared to the control test tube. Thus, the bacteria not only enhance the rate of O_2-dependent H_2S oxidation, they also separate the oxidized from the sulfide-supplied reduced part of the sediment and outcompete entirely the chemical H_2S oxidation process. At dynamic equilibrium, the H_2S oxidation rate is determined by the diffusion kinetics of the reactants, and even the reaction stoichiometry (1 : 2) can be calculated from the slopes of both distribution gradients according to Fick's law.

Due to the high reactivity of H_2S, its accumulation in deeper sediment layers leads to a general decrease of the measurable redox potential, in the range of $E_0' = -200$ mV. These electrons can be tapped by, e.g., a platinum electrode which, if connected to another electrode acting as a cathode in an air-saturated solution, establishes an electron flux that can provide electrical energy. Exactly this concept is being exploited by so-called cable bacteria, a novel type of sulfide-oxidizing bacteria that grow in cell chains of several thousand cells up to 2–3 cm (!) long, thus connecting the sulfide-rich sediment layers with the oxygen-saturated sediment surface [97]. It is not entirely clear yet how all cells in these chains manage to satisfy their energy needs. They are connected by thin fibers that may be electrically conducive and guide electrons from all deeper cells to the top cells that are exposed to oxygen [98]. These cable bacteria are another fascinat-

ing example of the ways how microbes exploit chemical and physical potentials for their energy metabolism.

9. CONCLUSIONS

This chapter was written by a microbiologist who focuses his research on the activities of microbes in natural and semi-natural environments. Many microbially catalyzed reactions have been elucidated through the recent four decades down to the level of enzyme structure, reaction center architecture, involvement of amino acid residues, metals and metal complexes, thus, a lot of "obscure microbiology" has turned into bright chemistry. On the other hand, many geochemical processes observed in the past were found through recent years to be catalyzed by microbes, except for those occurring at temperatures beyond 120 °C, the thermal borderline of living organisms. If – after all the great discoveries in chemistry through the last 150 years – chemists may have been tempted to claim "it is all chemistry out there" I tend to oppose: "it is all microbiology – using a highly refined microbial biochemistry".

Some reactions in microbial biochemistry, e.g., the acetyl CoA synthase reaction, were found to mimic metal-catalyzed reactions known from classical synthetic chemistry, but the bacteria run this process under far milder conditions, at normal pressure and ambient temperature. Others, such as nitrogenase or hydrogenase reactions, may prove as models for chemical processes to be optimized to higher efficiency in the future than through the conventional chemistry at hand so far, e.g., in fertilizer production or energy supply and storage. Microbiology provides an amazingly diverse toolbox of enzymes for application in a new world of "mild" synthetic chemistry. Microbes most often grow on demand and can supply their complex biochemistry at low cost according to the needed capacity. This applies to comparably simple processes such as microbial wastewater treatment and freshwater supply, biogas production, or ore leaching. Fermentations leading to solvents and organic acids have been used in food production and preservation already for millennia. Biosynthetic processes, such as the production of secondary metabolites including vitamins, antibiotics and further pharmaceuticals, require more refined control of culture purity and process operation. There is a lot of promise for fruitful cooperation of chemists and microbiologists for our future!

ACKNOWLEDGMENTS

This article is based on achievements of many years of cooperation with highly talented students and coworkers. I appreciate as well numerous inspiring discussions with my colleagues Rolf Thauer, Wolfgang Buckel, Peter Dimroth, Peter Kroneck, Georg Fuchs, Norbert Pfennig, Ralph Wolfe, Hans Günter Schlegel, Friedrich Widdel, Andreas Brune, Andreas Kappler, Ben Griffin, and David

Schleheck. My thanks go to all of them, as well as to the University of Konstanz and to the Deutsche Forschungsgemeinschaft for continuous financial support.

ABBREVIATIONS

AMP	adenosine 5′-monophosphate
APS	adenosine 5′-phosphosulfate
ATP	adenosine 5′-triphosphate
DNA	deoxyribonucleic acid
NAD^+	nicotinamide adenine dinucleotide, oxidized
NADH	nicotinamide adenine dinucleotide, reduced
P_i	inorganic phosphate
PP_i	pyrophosphate

REFERENCES

1. J. M. Hayes, J. R. Waldbauer, *Phil. Trans. Roy. Soc. B* **2006**, *361*, 931–950.
2. A. Kappler, C. Pasquero, K. O. Konhauser, D. K. Newman, *Geology* **2005**, *33*, 865–868.
3. R. E. Hungate, *Methods inMicrobiology* **1969**, *3*, 117–132.
4. N. Lane, W. F. Martin, *Cell* **2012**, *151*, 1406–1416.
5. W. F. Martin, F. L. Sousa, *Cold Spring Harbor Perspect. Biol.* **2016**, *8*, 18.
6. W. F. Martin, R. K. Thauer, *Cell* **2017**, *168*, 953–955.
7. P. Schönheit, W. Buckel, W. F. Martin, *Trends in Microbiology* **2016**, *24*, 12–25.
8. B. Schink, *Naturwissenschaften* **1989**, *76*, 364–372.
9. U. Ermler, W. Grabarse, S. Shima, M. Goubeaud, R. K. Thauer, *Science* **1997**, *278*, 1457–1462.
10. S. W. Ragsdale, *Met. Ions Life Sci.* **2014**, *14*, 125–145.
11. S. W. Ragsdale, E. Pierce, *Biochim. Biophy. Acta* **2008**, *1784*, 1873–1898.
12. M. Can, F. A. Armstrong, S. W. Ragsdale, *Chem. Rev.* **2014**, *114*, 4149–4174.
13. H. Cheung, R. S. Tanke, G. P. Torrence, *Acetic Acid*, in *Ullmann's Encyclopedia of Industrial Chemistry*, Wiley-VCH, Weinheim, **2002**. doi: 10.1002/14356007.a01_45.
14. T. Borch, R. Kretzschmar, A. Kappler, P. Van Cappellen, M. Ginder-Vogel, A. Voegelin, K. Campbell, *Environ. Sci. Technol.* **2010**, *44*, 15–23.
15. J. M. Byrne, A. Kappler, *Microb Biotechnol.* **2017**, *10*, 1098–1101.
16. S. Winogradsky, *Botanische Zeitung* **1887**, *45*, 489–507.
17. S. Winogradsky, in *Beiträge zur Morphologie und Physiologie der Bacterien*, Heft I: *Zur Morphologie und Physiologie der Schwefelbacterien*, Verlag A. Felix, Leipzig, **1888**.
18. S. N. Winogradsky, *Compt. Rend. Acad. Sci. (Paris)* **1890**, *110*, 1013–1016.
19. A. Boetius, K. Ravenschlag, C. J. Schubert, D. Rickert, F. Widdel, A. Gieseke, R. Amann, B. B. Jørgensen, U. Witte, O. Pfannkuche, *Nature* **2000**, *407*, 623–626.
20. K. F. Ettwig, M. K. Butler, D. Le Paslier, E. Pelletier, S. Mangenot, M. M. M. Kuypers, F. Schreiber, B. E. Dutilh, J. Zedelius, D. de Beer, J. Gloerich, H. J. C. T. Wessels, T. van Alen, F. Luesken, M. L. Wu, K. T. van de Pas-Schoonen, H. J. M. Op den Camp, E. M. Janssen-Megens, K.-J. Francoijs, H. Stunnenberg, J. Weissenbach, M. S. M. Jetten, M. Strous, *Nature* **2010**, *464*, 543–548.

21. A. A. Raghoebarsing, A. Pol, K. T. van de Pas-Schoonen, A. J. P. Smolders, K. F. Ettwig, W. I. C. Rijpstra, S. Schouten, J. S. Sinninghe Damsté, H. J. M. Op den Camp, M. S. M.Jetten, M. Strous, *Nature* **2006**, *440*, 918–921.
22. M. Strous, J. G. Kuenen, M. S. M. Jetten, *Appl. Environ. Microbiol.* **1999**, *65*, 3248–3250.
23. K. L. Straub, M. Benz, B. Schink, F. Widdel, *Appl. Environ. Microbiol.* **1996**, *62*, 1458–1460.
24. B. Schink, D. Simeonova, *Geomicrobial Interactions with Phosphorus*, in *Ehrlich's Geomicrobiology*, 6th ed., Eds H. L. Ehrlich, D. K. Newman, A. Kappler, CRC Press, Boca Raton, FL, USA, **2015**, pp. 265–279.
25. B. Schink, *Met. Ions Biol. Systems* **2005**, *43*, 179–200.
26. B. Schink, V. Thiemann, H. Laue, M. W. Friedrich, *Arch. Microbiol.* **2002**, *177*, 381–391.
27. B. Schink, M. Friedrich, *Nature* **2000**, *406*, 37.
28. A. K. White, W. W. Metcalf, *Annu. Rev. Microbiol.* **2007**, *61*, 379–400.
29. A. W. Schwartz, *Phil. Trans. Roy. Soc. B.* **2006**, *361*, 1743–1749.
30. N. Pfennig, *Annu. Rev. Microbiol.* **1967**, *21*, 285–324.
31. F. Widdel, S. Schnell, S. Heising, A. Ehrenreich, B. Assmus, B. Schink, *Nature* **1993**, *362*, 834–836.
32. B. M. Griffin, J. Schott, B. Schink, *Science* **2007**, *316*, 1870.
33. E. Broda, *Zeitschr. Allgem. Mikrobiol.* **1977**, *17*, 491–493.
34. V. Braun, K. Hantke, *Curr. Opin. Chem. Biol.* **2011**, *15*, 328–334.
35. D. R. Lovley, J. D. Coates, E. L. Blunt, E. L. Harris, E. J. P. Phillips, J. C. Woodward, *Nature* **1996**, *382*, 445–448.
36. K. L. Straub, B. Schink, *Appl. Environ. Microbiol.* **2004**, *70*, 5744–5749.
37. M. E. Hernandez, A. Kappler, D. K. Newman, *Appl. Environ. Microbiol.* **2004**, *70*, 921–928.
38. M. Y. El–Naggar, G. Wanger, K. M. Leung, T. D. Yuzvinsky, G. Southam, J. Yang, W. M. Lau, K. H. Nealson, Y. A. Gorby, *Proc. Natl. Acad. Sci. USA* **2010**, *107*, 18127–18131.
39. K. Xiao, N. S. Malvankar, C. J. Shu, E. Martz, D. R. Lovley, X. Sun, *Sci. Rep.* **2016**, *6*, 9.
40. S. Kucera, R. S. Wolfe, *J. Bacteriol.* **1957**, *74*, 344–349.
41. H. H. Hanert, *The Genus Gallionella*, in *The Prokaryotes*, Eds M. Dworkin, S. Falkow, E. Rosenberg, K. H. Schleifer, E. Stackebrandt, Springer, New York, **2006**, doi: 10.1007/0-387-30747-8_46.
42. K. Dolch, J. Danzer, T. Kabbeck, B. Bierer, J. Erben, A. H. Förster, J. Maisch, P. Nick, S. Kerzenmacher, J. Gescher, *Bioresource Technology* **2014**, *157*, 284–292.
43. T. Jafary, W. R. W. Daud, M. Ghasemi, B. H. Kim, J. M. Jahim, M. Ismail, S. S. Lim, *Renew. Sust. Energ. Rev.* **2015**, *47*, 23–33.
44. H. Liu, R. Ramnarayanan, B. E. Logan, *Environ. Sci. Technol.* **2004**, *38*, 2281–2285.
45. H. Venzlaff, D. Enning, J. Srinivasan, K. J. J. Mayrhofer, A. W. Hassel, F. Widdel, M. Stratmann, *Corrosion Sci.* **2013**, *66*, 88–96.
46. F. Mayer, F. Enzmann, A. M. Lopez, D. Holtmann, *Bioresource Technology* **2019**, *289*. doi: 10.1016/j.biortech.2019.121706.
47. R. Schauder, A. Kröger, *Arch Microbiol.* **1993**, *159*, 491–497.
48. D. Rickard, G. W. Luther, *Chem. Rev.* **2007**, *107*, 514–562.
49. J. Thiel, J. M. Byrne, A. Kappler, B. Schink, M. Pester, *Proc. Natl. Acad. Sci. USA* **2019**, *116*, 6897–6902.
50. C. C. Lee, M. W. Ribbe, Y. Hu, *Met. Ions Life Sci.* **2014**, *14*, 147–176.
51. P. Vanrhijn, J. Vanderleyden, *Microbiol. Rev.* **1995**, *59*, 124–142.
52. S. Fetzner, R. A. Steiner, *Appl. Microbiol. Biotechnol.* **2010**, *86*, 791–804.

53. B. Kartal, N. M. de Almeida, W. J. Maalcke, H. J. M. Op den Camp, M. S. M. Jetten, J. T. Keltjens, *FEMS Microbiol. Rev.* **2013**, *37*, 428–461.
54. P. E. M. Siegbahn, *J. Biol. Inorg. Chem.* **2001**, *6*, 27–45.
55. S. Scheller, M. Goenrich, R. K. Thauer, B. Jaun, *J. Am. Chem. Soc.* **2013**, *135*, 14975–14984.
56. R. K. Thauer, *Curr. Opin. Microbiol.* **2011**, *14*, 292–299.
57. H. Wilkes, W. Buckel, B. T. Golding, R. Rabus, *J. Mol. Microbiol. Biotechnol.* **2016**, *26*, 138–151.
58. B. G. Malmstroem, *Annu. Rev. Biochem.* **1982**, *51*, 21–59.
59. G. Fuchs, M. Boll, J. Heider, *Nature Rev. Microbiol.* **2011**, *9*, 803–816.
60. B. Philipp, B. Schink, *Environ. Microbiol. Rep.* **2012**, *4*, 469–478.
61. D. White, *The Physiology and Biochemistry of Prokaryotes*, Oxford University Press, New York, Oxford, **1995**.
62. H. D. Peck, J. Legall, J. Vanbeeumen, *Phil. Trans. Roy. Soc. B-Biol. Sci.* **1982**, *298*, 443–466.
63. A. A. Santos, S. S. Venceslau, F. Grein, W. D. Leavitt, C. Dahl, D. T. Johnston, I. A. C. Pereira, *Science* **2015**, *350*, 1541–1545.
64. J. Simon, P. M. H. Kroneck, *Adv. Microb. Physiol.* **2013**, *62*, 45–117.
65. M. I. H. Aleem, *J. Bacteriol.* **1966**, *91*, 729–736.
66. M. I. H. Aleem, *Biochim. Biophys. Acta* **1966**, *113*, 216–224.
67. K. Knobloch, J. H. Eley, M. I. H. Aleem, *Arch. Mikrobiol.* **1971**, *80*, 97–114.
68. P. Mitchell, *Biol. Rev.* **1966**, *41*, 445–501.
69. R. K. Thauer, K. Jungermann, K. Decker, *Bacteriol. Rev.* **1977**, *41*, 100–180.
70. F. Li, J. Hinderberger, H. Seedorf, J. Zhang, W. Buckel, R. K. Thauer, *J. Bacteriol.* **2008**, *190*, 843–850.
71. W. Buckel, R. K. Thauer, *Chem. Rev.* **2018**, *118*, 3862–3886.
72. W. Buckel, R. K. Thauer, *Front. Microbiol.* **2018**, *9*, 24.
73. G. Herrmann, E. Jayamani, G. Mai, W. Buckel, *J. Bacteriol.* **2008**, *190*, 784–791.
74. R. S. Horvath, *Bacteriol. Rev.* **1972**, *36*, 146–155.
75. L. Gonzalez-Gil, D. Krah, A. K. Ghattas, M. Carballa, A. Wick, L. Helmholz, J. M. Lema, T. A. Ternes, *Water Res.* **2019**, *152*, 202–214.
76. L. Semprini, *Curr. Opin. Biotechnol.* **1997**, *8*, 296–308.
77. S. Engelbrecht, W. Junge, *FEBS Lett.* **1997**, *414*, 485–491.
78. C. von Ballmoos, A. Wiedenmann, P. Dimroth, *Annu. Rev. Biochem.* **2009**, *78*, 649–672.
79. B. Schink, *Microbiol. Mol. Biol. Rev.* **1997**, *61*, 262–280.
80. B. Schink, N. Pfennig, *Arch. Microbiol.* **1982**, *133*, 209–216.
81. B. Schink, A. J. M. Stams, *Syntrophism among Prokaryotes*, in *The Prokaryotes*, Eds M. Dworkin, S. Falkow, E. Rosenberg, K. H. Schleifer, E. Stackebrandt, Springer, New York, **2006**, pp. 309–335.
82. D. Montag, B. Schink, *Appl. Environ. Microbiol.* **2018**, *84*, e01572–18.
83. B. Schink, D. Montag, A. Keller, N. Müller, *Environ. Microbiol. Rep.* **2017**, *9*, 189–202.
84. M. A. Lever, K. L. Rogers, K. G. Lloyd, J. Overmann, B. Schink, R. K. Thauer, T. M. Hoehler, B. B. Jørgensen, *FEMS Microbiol. Rev.* **2015**, *39*, 688–728.
85. V. Müller, V. Hess, *Front. Microbiol.* **2017**, *8*, 7.
86. E. Biegel, S. Schmidt, J. M. Gonzalez, V. Müller, *Cell Mol. Life Sci.* **2011**, *68*, 613–634.
87. H. S. Jeong, Y. Jouanneau, *J. Bacteriol.* **2000**, *182*, 1208–1214.
88. L. Pasteur, *Compt. Rend. Acad. Sci. Paris* **1858**, *46*, 615–618.
89. A. Parkin, *Met. Ions Life Sci.* **2014**, *14*, 99–124.

90. C. Greening, M. Berney, K. Hards, G. M. Cook, R. Conrad, *Proc. Natl. Acad. Sci. USA* **2014**, *111*, 4257–4261.
91. R. Conrad, *Microbiol. Rev.* **1996**, *60*, 609–640.
92. E. Costa, J. Perez, J. U. Kreft, *Trends in Microbiology* **2006**, *14*, 213–219.
93. H. Daims, E. V. Lebedeva, P. Pjevac, P. Han, C. Herbold, M. Albertsen, N. Jehmlich, M. Palatinszky, J. Vierheilig, A. Bulaev, R. H. Kirkegaard, M. von Bergen, T. Rattei, B. Bendinger, P. H. Nielsen, M. Wagner, *Nature* **2015**, *528*, 504–509.
94. M. van Kessel, D. R. Speth, M. Albertsen, P. H. Nielsen, H. J. M. Op den Camp, M. Kartal, M. S. M. Jetten, S. Lucker, *Nature* **2015**, *528*, 555–559.
95. A. C. Peters, J. W. T. Wimpenny, J. P. Coombs, *J. Gen. Microbiol.* **1987**, *133*, 1257–1263.
96. D. C. Nelson, B. B. Jørgensen, N. P. Revsbech, *Appl. Environ. Microbiol* **1986**, *52*, 225–233.
97. C. Pfeffer, S. Larsen, J. Song, M. D. Dong, F. Besenbacher, R. L. Meyer, K. U. Kjeldsen, L. Schreiber, Y. A. Gorby, M. Y. El-Naggar, K. M. Leung, A. Schramm, N. Risgaard-Petersen, L. P. Nielsen, *Nature* **2012**, *491*, 218–221.
98. J. T. Bjerg, H. T. S. Boschker, S. Larsen, D. Berry, M. Schmid, D. Millo, P. Tataru, F. J. R. Meysman, M. Wagner, L. P. Nielsen, A. Schramm, *Proc. Natl. Acad. Sci. USA* **2018**, *115*, 5786–5791.
99. B. Schink, *Anaerobic Transformation Processes, Microbiology*, in *Encyclopedia of Geobiology*, Eds J. Reitner, V. Thiel, Springer, Dordrecht, The Netherlands, **2011**, pp. 48–53.
100. B. Schink, *Allgemeine Mikrobiologie*, Chapter 20, 9th ed., Ed. G. Fuchs, Thieme, Stuttgart, Germany, **2014**.

3

Biological Isotope Fractionation and Earth History: From Enzymes, to Cells, to Ecosystems

Shawn E. McGlynn

Earth-Life Science Institute, Tokyo Institute of Technology, Tokyo, 152–8550, Japan
<mcglynn@elsi.jp>

Metal Ions in Life Sciences, Volume 21 Guest Editors: Peter M. H. Kroneck and Martha E. Sosa Torres
Series Editors: Astrid Sigel, Eva Freisinger, and Roland K. O. Sigel

https://doi.org/10.1515/9783110589771-003

Abstract: Biological processes often leave an "imprint" of their presence in the form of non-equilibrium isotope distributions in metabolites. These distributions (i.e., fractionations) have been intensively studied in sediments corresponding to various Earth ages, as well as in laboratory-based culture studies. A central finding has been that isotope fractionation occurs with high variability, leading to questions of what drives this. In this chapter we discuss some sources of this variability. To build a picture of this, we deal with three different scales: the enzyme level, the cell level, and the ecosystem level. To compare and contrast, we discuss the isotope fractionation of carbon from CO_2 in water-oxidizing phototrophs which utilize the Calvin cycle (i.e., the Calvin–Benson–Bassham cycle), and the fractionation of sulfur in sulfate during microbial sulfate reduction to hydrogen sulfide. Overall, we attempt to provide some background and fodder for future integration across these scales, where it is the collective challenge of researchers from multiple disciplines – who study across these scales – to elucidate what a particular isotope ratio observed in a natural system may represent.

Keywords: carbon fixation · enzymes · metabolic reversibility · microbial sulfate reduction · photosynthesis · reaction energetics · respiration · stable isotopes

1. EARTH HISTORY AND STABLE ISOTOPE BIOGEOCHEMISTRY

The oldest material record of life on Earth is made of rocks and minerals. Within these, microfossils can suggest the existence of life (e.g., [1–3]), but microbial life is generally not well-preserved during lithification (becoming a mineral or rock). In addition to these microfossils, biogenic sedimentary mounds called stromatolites – explained as laminated sediments of lithified microbes – also attest to the presence of life on the earlier Earth [4]. The visible record of life is not without controversy however [5–7], and supplementing the record of life in deep time are stable isotope distributions. The oldest evidence of a particular physiology – microbial methane formation – was found in the form of trapped methane with ratios of $^{13}C/^{12}C$ carbon coincident with biological methane formation [8]. Going further, the oldest putative evidence of life on Earth is in the form of $^{13}C/^{12}C$ carbon ratios suggestive of biological fractionation [9].

The distribution of stable isotopes can provide a "fingerprint" of source and process, and this is valuable for the analysis of both ancient and contemporary samples. For example, isotope measurements can enable sourcing of food and drink [10–12].

This chapter introduces the reader to a multi-level perspective of biological isotope fractionation which can be applied to contemporary and deep time questions. We focus on the application of isotope fractionation in biological processes at the enzyme and cell levels, and touch on the ecosystem scale. We discuss sulfur isotope fractionation during microbial sulfate reduction, which is a major component of the Earth's current sulfur cycle. In discussing carbon, we focus on carbon fixation through the Calvin cycle which operates in autotrophic oxygen-producing photosynthetic organisms (and also in non-photosynthetic organisms such as some aerobic iron oxidizing-bacteria [13]). Similar discussions to those below could also be made for other processes involving carbon and sulfur, and also for other stable isotope systems, for example nitrogen.

1.1. Isotopes Through Time: The Example of Sulfur in Sulfate and Pyrite

On the present Earth, sulfate (SO_4^{2-}) is the most abundant electron acceptor for life [14]. Sulfur has four stable isotopes: ^{32}S, ^{33}S, ^{34}S, and ^{36}S, and variations in the isotopic content of materials can record the activity of biological processes (see [15, 16] for review). Most sulfur is in the form of ^{32}S and ^{34}S, which are referred to as the "major isotopes". ^{33}S and ^{36}S are referred to as the "minor" isotopes. Microbial metabolisms involving sulfur are thought to have an ancient history as evidenced by the preservation of sulfur isotope signals coincident with their presence in deep time [16, 17] (Figure 1, [16, 18–28]). Why does this vary through time? Many hypotheses could be entertained.

2. A STABLE ISOTOPE PRIMER: THE 'LANGUAGE' OF ISOTOPE FRACTIONATION

2.1. How Isotope Values Between Molecules Are Calculated and Expressed

Below we briefly detail how variations in isotope content are discussed in the geochemical literature. Notes prepared by John Hayes on "An Introduction to Isotopic Calculations" will be useful for any reader who is new to isotopes [29], and the reader is directed there for a more thorough discussion.

2.2. Delta Notation

A natural way of comparing isotope abundances in a sample is through a ratio, for example the ratio of $^{13}C/^{12}C$. It is useful to have a standard frame of reference to make comparisons (like the Vienna Canyon Diablo Troilite (VCDT) men-

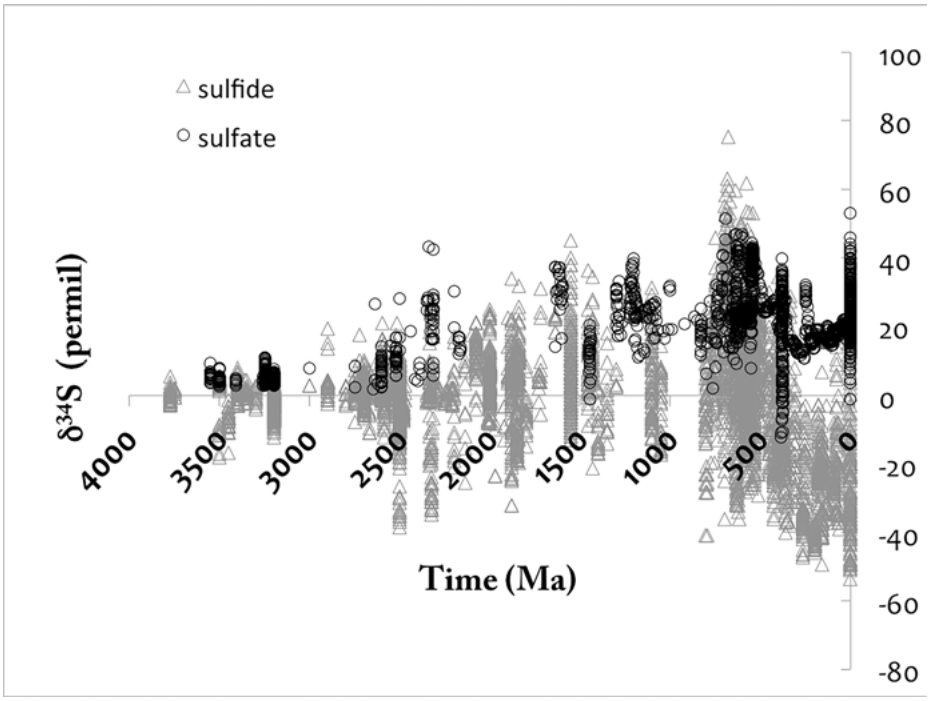

Figure 1. Sulfur isotope values of sulfide and sulfate through time. Sulfide is in the form of pyrite, and the values are normalized to a standard of Vienna Canyon Diablo Troilite (VCDT); a common reference from which to measure variation. Data are re-plotted from [18], which was compiled from [16, 19] and supplemented with data from [20–28]. Ma refers to millions of years before the present.

tioned in the caption of Figure 1 for sulfur). This is done by comparing isotope ratios in a sample of interest to isotope ratios that are present in a standard, and becomes a ratio of ratios. Since differences in isotope abundances can be quite small, differences are typically presented not in units of *per cent* (1/100), but in units of *per mille* (1/1000). Recall that a miligram is 1/1000 of a gram, and that millimolar is 1/1000 of molar.

The delta notation allows for a comparison of ratios where isotope abundances can be expressed in comparison to a standard as in Equation (1):

$$\delta = (\text{ratio(sample)}/\text{ratio(standard)}) - 1) \cdot 1000 \quad (1)$$

The units of δ are *per mille*, ‰.

2.3. Equilibrium Isotope Fractionation

Differences in the formation energies of molecules lead to the chemical potential for a reaction to occur. During a chemical reaction, the concentrations of mole-

cules adjust until the energy on both sides of a chemical equation become equal. In the case of molecules whose atoms can be formed from more than a single isotope, the energy differences between isotopically substituted molecules results in a difference in chemical potentials, which subsequently leads to differences in final concentrations of the isotopically substituted molecules when energy is equal across a chemical reaction. This final (at equilibrium) difference in concentrations of isotopically substituted molecules gives rise to the equilibrium isotope effect (EIE).

Equilibrium isotope values are usually written as fractionation factors, which are a ratio of ratios corresponding to the isotopic equilibrium. For example, for an isotope exchange between two molecules A and B, we could consider Equation (2),

$$AL + BH \rightleftharpoons BL + AH \tag{2}$$

where L and H indicate the heavier and the lighter version of the isotope, respectively. The fractionation factor is a way of expressing ratios of isotopes (usually written as alpha, α) and can be calculated from the above introduced delta (δ) (Equation 1). One way of expressing the difference in heavy and light isotopes in the above equation would be to write alpha as the ratio of heavy to light in the molecule A, divided by the ratio of heavy to light isotope in B (Equation 3):

$$\alpha_{(A/B)} = (AH/AL)/(BH/BL) \tag{3}$$

As a further example, for the molecule thiosulfate ($S_2O_3^{2-}$), we could consider sulfur isotope equilibration between the two sulfurs in thiosulfate, considering the major isotopes (Equation 4)

$$^{34}S\text{-}^{32}SO_3^{2-} + {}^{32}S\text{-}^{32}SO_3^{2-} \rightleftharpoons {}^{32}S\text{-}^{32}SO_3^{2-} + {}^{32}S\text{-}^{34}SO_3^{2-} \tag{4}$$

and write a ratio of ratios for α as below, considering the two sulfurs (Equation 5):

$$\alpha(S/SO_3^{2-}) = \frac{^{34}S \,/\, ^{32}S}{^{34}SO_3^{2-} \,/\, ^{32}SO_3^{2-}} \tag{5}$$

Another example which occurs more quickly than the above at room temperature in the absence of catalysts is the equilibration of sulfur isotopes between sulfur in two of the forms of sulfide (SH^-, H_2S) written below (Equation 6):

$$^{34}SH^- + {}^{32}SH_2 \rightleftharpoons {}^{32}SH^- + {}^{34}SH_2 \tag{6}$$

Again, α would be the ratio of species A to species B, which could be either SH^- or SH_2.

Sometimes, instead of writing α which corresponds to the fractionation factor, the related enrichment factor is written, usually with an epsilon (ε) (Equation 7):

$$\varepsilon = \alpha - 1 \tag{7}$$

2.4. Kinetic Isotope Fractionation

Energy differences of chemical intermediates which occur during a reaction can be shown along an axis of the "reaction coordinate", which depicts the energy of reactants, intermediates, and products. Depending on the mechanism of reaction, the path between reactants and products can be different. For differently isotopically substituted molecules, the energy difference from the ground state to the intermediate state varies with isotope substitution, leading to a kinetic *rate difference* between isotopically substituted molecules. Mechanistic information can be extracted from the differences in rate between isotopically substituted reactants. The interested reader is directed to more in depth treatments [30, 31]. For the current discussion, the difference in rate between different isotopically substituted molecules is the important concept.

In the case of a kinetic isotope effect (KIE), we can express the kinetic fractionation factor as a ratio of rates between the two different isotopes. A normal kinetic isotope effect occurs when the heavier isotope reacts more slowly than the lighter isotope, and an inverse isotope effect occurs when the heavier isotope reacts more quickly than the lighter isotope. At chemical equilibrium, the forward and reverse rates of a reaction are equal, and forward and reverse kinetic isotope effects cancel out, leaving the equilibrium isotope effect (EIE) (Equation 8):

$$\mathrm{EIE} = \mathrm{KIE}_{\mathrm{fwd}} - \mathrm{KIE}_{\mathrm{rev}} \tag{8}$$

2.5. Rayleigh Distillation Model for Isotope Fractionation During an Enzyme Assay

Enzymes in the laboratory are typically studied at conditions where the substrate is abundant, and the product starting concentration is zero. The reaction can be started in different ways, for example by adding substrate, some cofactor, or the enzyme catalyst itself. Under these initial rate conditions which occur before product has accumulated, the reaction may be unidirectional. For the discussion of isotopes, which might be fractionated kinetically as substrate is converted to product, this unidirectional characteristic is important since it means that when the ratio of isotopes in substrate and product are measured, the abundances are derived from the starting composition, and the forward catalytic fractionation factor, without "contamination" (or confusion!) from the reverse reaction, or equilibrium fractionation.

Under the above conditions, where the starting amount of substrate defines the sum amount of both the substrate and product during the course of the assay,

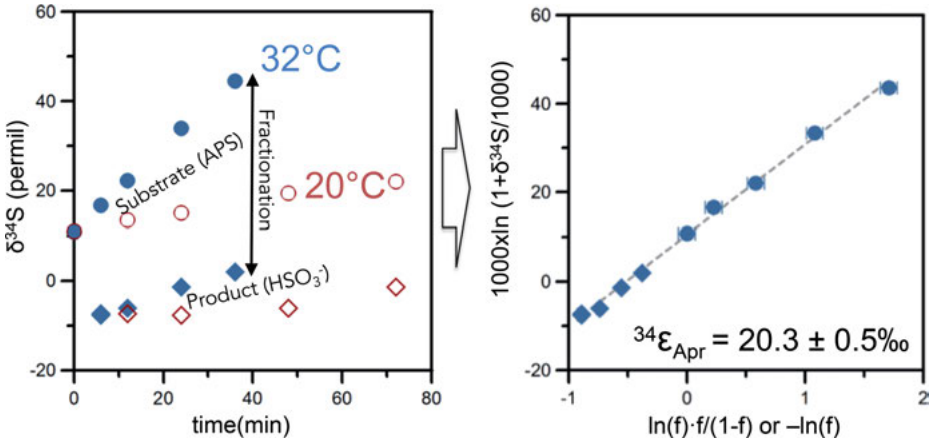

Figure 2. Example application of a Rayleigh distillation model applied to a closed system for kinetic isotope fractionation analysis of the enzyme APS reductase. On the **left**, change in the isotope composition of the substrate and product occurs as the enzyme-catalyzed reaction proceeds. On the **right**, the isotope composition of substrate and product are re-plotted against an x-axis which shows a natural log-transformed (ln) amount of substrate remaining (f), or product formed, and the slope of the line $^{34}\varepsilon_{(product/reactant)}$ corresponds to the ongoing fractionation between isotope pools in the substrate and product, following an equation of the form $\delta = \delta_{initial} + {}^{34}\varepsilon_{(product/reactant)} \bullet \ln(f)$. The assay shown on the left was conducted at 32 °C and 20 °C, and the corresponding Rayleigh distillation model approximation [32] for the 32 °C experiment is shown on the right. The figure is modified from [18], which was published under a Creative Commons Attribution 4.0 International License http://creativecommons.org/licenses/by/4.0/.

the system is a closed kinetic system, where a Rayleigh distillation model can be applied (Figure 2). Here, if a reaction were to proceed irreversibly to completion, the isotope composition of the product approaches the initial isotope composition of the substrate (though for an *in vitro* enzyme reaction, maintaining irreversibility to 100 % reaction completion may be unlikely). If the isotope ratio of the substrate and product are measured during the course of such a reaction, these can be plotted against an axis which describes the extent of the reaction, yielding a straight line whose slope estimates the apparent kinetic isotope effect (Figure 2). The reader is referred to [29, 32] for more background and the necessary mathematical description for application.

3. AN ENZYME PRIMER: THE 'LANGUAGE' OF ENZYME KINETICS

Biological reaction rates often occur at rates which are orders of magnitude faster than their non-biological counterparts. Critically, they can occur with varying degrees of net directionality, but since biology is a non-equilibrium process

where molecules "flow" through metabolic pathways, some net directionality always occurs through metabolism. This flow of molecules is accomplished by the activity of enzymes, and can lead to an isotope effect, where the kinetic isotope effect is the ratio of the respective forward and backward rate constants. Depending on its position in metabolism, its kinetic properties, and the state of a cell, an enzyme might act as an equilibrator and quicken the establishment of an equilibrium isotope effect between molecules, or on the other hand it might be unidirectional and display only the kinetic component (the kinetic isotope effect). At, or between, these two (EIE and KIE), isotopes will be partitioned.

Enzymes enhance the rate of reaction by lowering activation barriers. In solution, a pool of enzymes may be exposed to higher or lower concentrations of a substrate. If the substrate concentration is low relative to the enzyme concentration, there are many enzyme molecules that are not in the process of performing reactions. On the other hand, if the concentration of substrate is high in comparison to the enzyme, all the enzyme molecules might be carrying out reactions. In this case they can be said to be "saturated". Describing this, we follow Noor et al.'s useful review [33] and the reader is directed there for further information.

Mathematically, the degree of enzyme saturation, and the propensity of a given enzyme to become saturated can be written as in Equation (9) where C represents capacity,

$$C = s/(K_s + s) \tag{9}$$

where s is the concentration of substrate and K_s is a concentration of s which relates the velocity of reaction to the concentration of substrate (K_s is the half saturation constant, often written as K_m, referring to the Michaelis constant in Michaelis-Menten kinetics). However, enzymes produce products (p), and these can be included as a term by re-writing Equation (9) as given in Equation (10):

$$C = \frac{s/K_s}{(1 + s/K_s + p/K_p)} \tag{10}$$

where K_p is the product half saturation constant for the product, and p is the concentration of product. These terms can be thought of as saturation, or capacity [33]. When the concentration of s is large, the reaction velocity is not modulated by K_s. All the available enzymes are occupied by substrate and the enzyme is saturated. If more substrate is added to the solution, there will not be a change in the observed reaction rate. The velocity is at a limit (referred to as V_{max} in kinetic discussions). When s is small compared with K_s, there are many enzyme molecules not performing reactions. There is "capacity" to perform more reactions, and if more s is added to the solution, an increase in observed reaction rate will occur proportionally to the amount of s added.

Every catalyst has its own turnover number, that is, the number of reactions that it can perform per unit time. The maximum reaction rate that can be achieved by a catalyst in solution will be (Equation 11),

$$V = K_{cat} \cdot E \tag{11}$$

where V is the observed reaction rate (velocity), K_{cat} is the turnover number (with units of inverse time), and E is the concentration of catalyst.

When the overall velocity observed is modulated by the degree of saturation, the above equations can be combined (Equations 12 and 13):

$$V = E \cdot K_{cat} \cdot C \tag{12}$$

$$V = E \cdot K_{cat} \cdot \frac{s/K_s}{(1 + s/K_s + p/K_p)} \tag{13}$$

It is routine for biochemists to study enzymes under conditions of very low product concentrations (p starts at zero at time zero). In that case the capacity term of Equation (13) reduces to the simplified capacity form of Equation (9) above. In this condition, it is typical to hold the concentration of E constant, and perform multiple experiments where the starting concentration of a substrate s is varied from low to high. In this way, the relationship between enzyme turnover number, and saturation can be determined, as demonstrated by Michaelis and Menten and others.

The above discussion captures much of the kinetics and was fundamental to the development of enzymology. In addition to kinetics however, all chemical processes also have a thermodynamic component which dictates the directionality of the reaction: forward versus reverse, or the case of equilibrium where the forward and reverse rates are equal. In biochemical experiments within the lab, enzymes are most frequently assayed at high thermodynamic driving energies; the Gibbs energy of reaction is large and negative. However, it is important to consider how the rate of a reaction might change with thermodynamics, and the energetic "distance" to equilibrium encountered in an enzyme assay.

Since the thermodynamic favorability of a chemical reaction can be understood from the basis of formation energies and the reaction product and substrate ratios, it is possible to rearrange the Gibbs free energy of reaction equation to a form which expresses the forward and reverse rate ratio, as developed below, where $\Delta G^{0\prime}$ is the reaction energy at standard state, R is the universal gas constant, and T is temperature.

Bassham and Krause recognized this in their study of algal photosynthetic carbon fixation, where they noted that the ratio of rates for a forward and reverse reaction should change together proportionately, starting from the condition of equilibrium where the forward rate equals the reverse [34]. They wrote the equilibrium constant K_{eq} as a ratio of forward and reverse rates, and by combining this with the reaction quotient, were able to derive an expression which relates the Gibbs energy of reaction with the reversibility following the Equations (14)–(18):

$$\Delta G_{rxn} = \Delta G^{0\prime} - RT \cdot \ln([\text{substrate}]/[\text{product}]) \tag{14}$$

$$\Delta G_{rxn} = -RT\ln K' - RT \cdot \ln([\text{substrate}]/[\text{product}]) \tag{15}$$

$$\Delta G_{rxn} = -RT\ln(k'fwd/k'rev) - RT \cdot \ln([\text{substrate}]/[\text{product}]) \tag{16}$$

$$\Delta G_{rxn} = -RT\ln(k'fwd \cdot [substrate])/(k'rev \cdot [product]) \quad (17)$$

$$\Delta G_{rxn} = -RT\ln(fwd.\ rate)/(rev.\ rate) \quad (18)$$

Predicted ratios of forward to reverse rates in relationship to the Gibbs energy of reaction are plotted in Figure 3, and take the form of the relationship between K_{eq} and standard reaction energy. This assumption of changing proportionality in forward and reverse rates, as it relates to the energy of the reaction in the cell (what Bassham and Krause [34] called the "steady state" energy), allowed them to quantify the ratio of forward and reverse rates at different reaction energies, and thus identify potential sites of metabolic regulation.

More recently, the above relationship derived from rate proportionality in a steady state open system (i.e., a living cell) was incorporated into enzyme kinetic models, allowing for energy of reaction to be understood as modulator of catalyzed rate [33, 35].

Re-writing Equation (14) as Equation (19),

$$\Delta G_{rxn} = \Delta G^{0\prime} + RT \cdot \ln([product]/[substrate]) \quad (19)$$

we see (Equation 20) that

$$\frac{(p/s)}{K'_{eq}} = e^{\Delta G_{rxn}/RT} \quad (20)$$

where p and s are the product and substrate concentrations. This follows because Equation (21) holds

$$\Delta G^{0\prime} = -RT\ln K'_{eq} \quad (21)$$

If we write (Equation 22)

$$D = 1 - e^{\Delta G_{rxn}/RT} \quad (22)$$

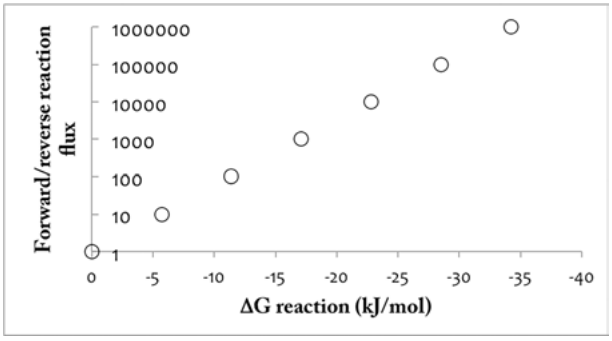

Figure 3. Expected ratios of forward to reverse reaction rates as a function of ΔG_{rxn}.

we have an expression where the directionality D varies between 0 and 1. When ΔG_{rxn} is large and negative, the expression approaches 1, but when ΔG_{rxn} goes to 0, D approaches zero and the reaction is at equilibrium with no net forward or reverse reaction velocity. Since equilibrium is the state when a reaction's forward and reverse rates are equal, this expression can be used to modify the above kinetic expressions *in accord to their net directionality.* The typical case of *in vitro* biochemically is a thermodynamically very favorable case: ΔG_{rxn} is large and negative and the expression is equal to 1. However, when ΔG_{rxn} becomes smaller and approaches zero, the reaction approaches equilibrium and opposite reaction rates: the reaction becomes more reversible, until $\Delta G_{rxn} = 0$, D = 0, and the velocity of the reaction = 0, as in Equation (23) [33]:

$$V = E \cdot K_{cat} \cdot \frac{s/K_s}{(1 + s/K_s + p/K_p)} \cdot (1 - e^{\Delta G_{rxn}/RT}) \tag{23}$$

4. ENZYMATIC STABLE ISOTOPE FRACTIONATION: ENZYMES ARE NOT IRREVERSIBLE CATALYSTS

Since the thermodynamics of a reaction dictates the reversibility of a reaction, this also dictates how isotopes will be fractionated by an enzyme when it is strongly driven, or close to equilibrium. We can consider that the observed fractionation of isotopes in a chemical reaction will be related to the KIE and the EIE as in Equation (24) [36]:

$$F = KIE_{fwd} + x \cdot (EIE - KIE_{fwd}) \tag{24}$$

where F is the observed fractionation, and x is the reversibility, that is, the ratio of rates of reactant formed from product, to product formed from reactant, derived from the discussion above [33–35] (Equation 25):

$$x = v^-/v^+ = e^{\Delta G_{rxn}/RT} \tag{25}$$

Thinking about the relationship between equilibrium and kinetic isotope fractionation in Equation (24) above, we can see that at large negative values of ΔG_{rxn}, the reversibility of the reaction x approaches zero, and F is equal to KIE_{fwd}. When $\Delta G_{rxn} = 0$, the ratio of the forward and reverse rates is one, and the F is equal to the EIE value. Given an open system which does not quantitatively convert substrate to product, observed fractionation values of a chemical reaction will occur between the KIE and EIE values, making their determination a primary constraint on understanding biological isotope fractionation. This approach was developed by Wing and Halevy [36], and a more detailed discussion of this concept of reversibility with enzyme catalyzed reactions in the context of reaction energies is given in [35].

Below, we discuss carbon isotope fractionation during CO_2 reduction by the enzyme ribulose-1,5-bisphosphate carboxylase/oxygenase (RuBisCo) which oc-

curs in a number of autotrophs, and also sulfur isotopes as they are fractionated during microbial respiration on sulfate. These two systems are used as models to discuss how the kinetic and thermodynamic relationships above can manifest in organismal isotope fractionations. Key questions to keep in mind while reading are: is this enzyme rate determining in the metabolism? And: what is the reversibility of the enzyme in the metabolism that it operates within?

4.1. Enzymology of the Calvin Cycle, A Central Role for RuBisCO?

CO_2 fixation in oxygenic photosynthetic organisms occurs by the continual regeneration of ribulose bisphosphate, which is the substrate for carboxylation by the RuBisCo enzyme. The enzyme is a member of a larger family of enolases [37, 38]. Overall, the Calvin cycle uses enzyme reactions found in glycolysis and the pentose phosphate pathways. Four reactions that are unique to the Calvin cycle link the glycolysis and pentose phosphate components: (i) RuBisCO, which carboxylates ribulose bisphosphate, (ii) an aldolase, which combines erythrose 4-phosphate and dihydroxyacetone phosphate, (iii) a phosphatase, which dephosphorylates the sedoheptulose diphosphate product of the former reaction, and (iv) a kinase, which phosphorylates ribulose 5-phosphate in an ATP-dependent reaction. An up to date description of the Calvin cycle and a brief history of its discovery is provided in a recent and useful article [39].

Although other enzymes in the Calvin cycle are involved in the formation and breaking of bonds to CO_2-derived carbon, agreement in the carbon isotope composition of tomato plants and isotope fractionation observed by the RuBisCo enzyme (from spinach) was suggestive that the RuBisCo enzyme is a major control on the biomass carbon isotope composition of organisms which employ the Calvin cycle [40]. Subsequent work indicated that variation in fractionation exists [31, 41], and furthermore that some of this variation can be attributed to differences in transition state energy between enzymes [31].

4.2. Microbial Respiration on Sulfate Involves Three Primary Enzymes: Sat, Apr, Dsr

Sulfur isotope fractionation during microbial respiration has been intensively investigated at the level of laboratory microbial populations, as well as cell extracts/lysates (e.g., [42–44]). Models of sulfur isotope fractionation have supplied rationale as to the cellular conditions under which fractionation values occur [36, 45, 46], and recently, the kinetic isotope effects of the enzymes involved in sulfate reduction have begun to be investigated [18, 47].

Microbial sulfate reduction is accomplished by three enzymes, which together results in the eight electron reduction of sulfate to sulfide [48]. The reactions are catalyzed by (i) sulfate adenylyltransferase (EC# 2.7.7.4, Sat), (ii) the FAD and

[4Fe-4S] cluster binding adenylylsulfate reductase (EC# 1.8.99.2, Apr), and (iii) dissimilatory sulfite reductase (EC# 1.8.99.5, Dsr) which harbors a siroheme linked to a [4Fe-4S] cluster. The reactions catalyzed by each enzyme (neglecting the protons) are: the activation of sulfate by Sat [49] (Equation 26)

$$\text{sulfate} + \text{ATP} \rightleftharpoons \text{adenosine 5′-phosphosulfate} + \text{diphosphate} \quad (26)$$

This is followed by a two-electron reduction of adenosine 5′-phosphosulfate (APS) to form sulfite by Apr [50, 51] (Equation 27):

$$\text{adenosine 5′-phosphosulfate} + 2\,e^- \rightleftharpoons SO_3^{2-} + \text{AMP} \quad (27)$$

After the formation of sulfite, DsrABC together participate in the six-electron reduction of sulfite to sulfide (Equation 28):

$$SO_3^{2-} + 6\,H^+ + 6\,e^- \rightleftharpoons 3\,H_2O + S^{2-} \quad (28)$$

This reaction occurs by the two-electron reduction of sulfite by DsrAB to produce protein-bound sulfur (S^0) on DsrC, which is coordinated by two CysSH residues [52, 53] (Equation 29):

$$SO_3^{2-} + 2\,e^- + \text{DsrC(CysSH)}_2 \rightleftharpoons \text{DsrC(CysS-S}^0\text{-SCys)} + 3\,H_2O \quad (29)$$

This is followed by a four-electron reduction of the bound sulfur and Cys residues to produce sulfide (HS^-) and regenerate the thiol form of Dsr, DsrC(CysSH)_2 (Equation 30):

$$\text{DsrC(CysS-S}^0\text{-S-Cys)} + 4\,e^- + 3\,H^+ \rightleftharpoons \text{DsrC(CysSH)}_2 + HS^- \quad (30)$$

Since the first step of microbial sulfate reduction does not involve the formation or breaking of a bond to the sulfur atom, it can be speculated that the Sat enzyme may not have a large KIE associated with it. On the other hand, the Apr and Dsr enzymes both involve bond formation and breaking events at the sulfur atom.

The first enzyme in the sulfate reduction pathway to be investigated with the goal of understanding KIE was the DsrAB complex [47]. This enzyme catalyzes the reduction of sulfite to intermediate reduction state products such as thiosulfate ($S_2O_3^{2-}$), trithionate ($S_3O_6^{2-}$) [53]. Working with the bacterium *Desulfovibrio vulgaris* str. Hildenborough, experiments conducted in the absence of DsrC gave the opportunity to isolate the initial two electron reduction step by measuring the $^{34}S/^{32}S$ isotope value changes in sulfite and the reduced sulfur of $S_3O_6^{2-}$ and $S_2O_3^{2-}$ during enzyme assay [47]. The apparent isotope fractionation factor was determined to be 15.3 ± 2‰ ($2\,\sigma$), in contrast to the predicted value for the whole enzyme complex of 50‰ [45]. Importantly, this work also estimated sulfur isotope fractionation by the DsrAB enzyme purified from the Archaeon *Archaeoglobus fulgidus*, giving the first insight into potential evolutionary variability of isotope fractionation at the enzyme level. The obtained result was

within error of the bacterial enzyme, suggesting that perhaps the sulfur isotope fractionation by the Dsr enzyme may not vary as a function of enzyme sequence evolution.

Later, the Apr enzyme isolated from *Desulfovibrio vulgaris* Miyazaki was determined to have an apparent isotope effect of 20.3‰ ± 0.5‰ at 32 °C [18]. The results of this measurement were discussed in the context of the cell energetic state and the isotope fractionation between sulfate and sulfide in laboratory studies, as well as in the rock record. The first enzyme of the sulfate reduction pathway, Sat, has not yet been evaluated for isotope fractionation.

5. METABOLIC STABLE ISOTOPE FRACTIONATION: ORGANISMS ARE NOT ENZYMES

Inside the cell, the concentration of metabolites can vary by condition and time. This means that a given enzyme may or may not be operating kinetically at saturated state, and also that the concentration of product is not zero (as assumed in Equation 9). Other than this difference in kinetic state of the catalyst, variation in metabolite concentration alters the thermodynamic potential of the reaction, and can lead to conditions where the reaction is not unidirectional and occurs with some reversibility (Equation 25). Together, this variability requires that the full spectrum from kinetic unsaturated to saturated states, as well as near equilibrium to effectively irreversible be considered. If the concentrations of individual enzyme substrates and products are known, then together with the EIE and enzyme KIE values, the isotope ratios of each metabolite, and that of the whole cell summed reaction, can be calculated [36].

How can the concentrations of each substrate and product be known however? One way is to directly measure them, as has been done for the case of the sulfate-reducing bacterium *Desulfovibrio alaskensis* [54], and the alga *Chlorella pyrenoidosa* [34]. A separate way other than direct measurement would be to predict the concentrations, and if this prediction can be made, then together with the KIE and EIE values, inference on the isotope ratios of species in the cell can be made as described for the case of microbial sulfate reduction [36].

5.1. Reaction Step Energetics in the Calvin Cycle

Bassham and Krause determined the steady state concentration of metabolites in the photosynthetic carbon reduction cycle which later became known as the Calvin cycle [34] (Figure 4). These energetics were re-evaluated subsequently using density functional theory estimates of formation energies [55]. In either the original, or the later estimate of reaction step energetics, the step performed by RuBisCo is the most exergonic. In the later estimate, the RuBisCo step was estimated to operate at around –130 kJ/mol, making it perhaps the most exergonic chemical reaction in biology.

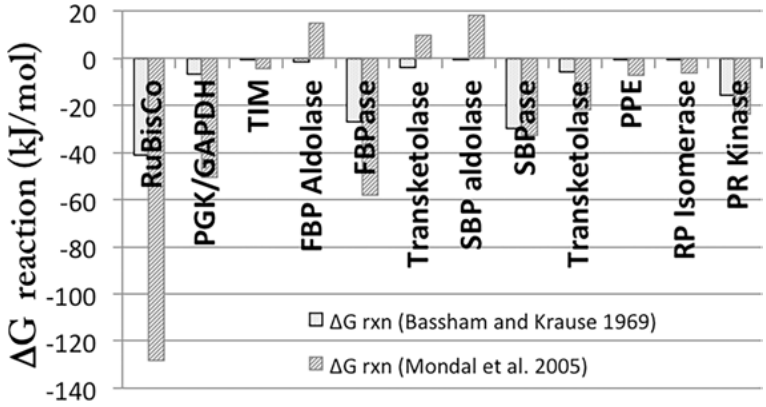

Figure 4. ΔG energy values of reactions in the Calvin cycle calculated from steady state metabolite concentration values in *Chlorella pyrenoidosa* and reported previously [34, 55]. The enzyme abbreviations and names are: RuBisCo; PGK/GAPDH, phosphoglycerate kinase + glyceraldehyde 3-phosphate dehydrogenase; TIM, triosephosphate isomerase; FBP aldolase, fructose bisphosphate aldolase; FBPase, fructose-1,6-biphosphatase; transketolase; SBP aldolase, sedoheptulosebisphosphate aldolase; SBPase, sedoheptulosebisphosphatase; PPE, pentosphosphate epimerase; RP isomerase, ribosephosphate isomerase; PR kinase, phosphoribulokinase. Transketolase features twice in the figure, acting first on glyceraldehyde 3-P and fructose-6P (step 6), and second on glyceraldehyde 3-phosphate and sedoheptulose-7P (step 9).

As noted by Bassham and Krause [34], there are four highly exergonic steps in the cycle given their calculated energetics: Rubisco, FBP aldolase, SBP phosphatase, and PR kinase. The combined kinase and dehydrogenase steps could also be included in with the more recent calculations of Mondal et al. [55]. These reactions are expected to be highly irreversible. Among these four, the step with the lowest energy associated with the reaction, PR kinase, has an energy of –15.8 kJ/mol, which corresponds to a ratio of forward to reverse reaction fluxes in the cell of 612. At –41 kJ/mol, the RuBisCo step of CO_2 fixation is expected to have a ratio of forward to reverse rates of 15, 378, 228 (see Figure 3 for the expected relationship between G_{rxn} and reaction flux). These exergonic steps are also steps on which metabolic control is exerted [56–58]; the other steps exist close to equilibrium and substrates and products can easily "spill" from one side of the reaction equation to the other.

From the perspective of carbon isotope fractionation in the Calvin cycle, these energy data are highly relevant. First, as a net reaction, the Calvin cycle can be considered as the synthesis of phosphoglyceraldehyde from three molecules of carbon dioxide (Equation 31):

$$3\,CO_2 + 9\,ATP + 6\,NADPH + 5\,H_2O \rightleftharpoons \text{D-glyceraldehyde 3-phosphate} + 9\,ADP + 6\,NADP + 8\,P_i \quad (31)$$

At the concentrations of substrates measured by Bassham and Krause [34], the reaction energy is estimated to be –289 kJ/mol for the above reaction. It is highly

directional in the forward direction, and this ensures that the substrate of RuBisCo (ribulose 1,5-bisphosphate) is present as the substrate for CO_2 fixation. Indeed, at 2.04 mM, ribulose 1,5-bisphosphate was the most abundant compound measured by Bassham and Krause.

5.2. Reaction Step Energetics During Microbial Sulfate Reduction

One remarkable characteristic of sulfate reducing microbes is the wide range of observed growth rates. In the laboratory, respiration rates on sulfate can be as high as in the 10's or 100's femtomol SO_4^{2-} reduced per cell per day (fmol cell^{-1} day^{-1}), but in the natural environment, this value can be as low as 10^{-4} fmol cell^{-1} day^{-1} [59]. Translating these rates into electrons per second, the low end of 10^{-4} fmol SO_4^{2-} cell^{-1} s^{-1} corresponds to ~8 e$^-$ cell^{-1} s^{-1}. At the high end of 100 fmol SO_4^{2-} cell^{-1} s^{-1}, the value is 8,000,000 e$^-$ cell^{-1} s^{-1}, indicating a remarkable ability to accommodate a varying current through the respiratory chain. From a thermodynamic perspective, microbes that respire sulfate are also capable of respiring on sulfate to about –20 kJ/mol reaction energy and possibly less in syntrophic conditions [60, 61] (as calculated from concentrations of SO_4^{2-} and the corresponding electron donor).

On a per reaction basis, energies can be estimated using measurements of intracellular metabolites [54]. Although the electron donor to the Apr and Dsr steps is not known, it is likely a compound with a potential similar to menaquinol [62]. With estimated intracellular concentrations and an assumed redox state of an electron donor, the energies of the three steps of sulfate reduction can be calculated and are shown in the figure below for one possible state (Figure 5). It is clear that the Apr step is the single largely exergonic step in these conditions, and that the Sat and Dsr steps are close to equilibrium, and thus reversible.

The individual enzymes discussed above have been purified, and their kinetic properties determined. Following from this, a steady state model of sulfate reduction was previously constructed [36], which allowed a prediction of the steady state concentrations of the intermediates of sulfate reduction to be made. With concentrations calculated, the transformation into Gibbs energy of reaction could be made. By estimating the kinetic sulfur isotope fractionation expected at each step (KIE), and with knowledge of the EIE [67], sufficient information was available to relate microbial respiration rates and extracellular sulfate concentrations, to the predicted value of whole cell isotope fractionation. This model compared well to previous studies where microbes were grown at variable rates and the sulfur isotopes of sulfate and sulfide determined [25, 27, 68]. Importantly, multiple parameters affect isotope fractionation, and no single step can be singled out that controls fractionation across rate, energy, and concentration regimes [36].

Later, in an extension to this modeling work, the free parameter of the model was altered to investigate the possible potential range of electron donors in the metabolism [62]. This allowed an inference of which electron donors might actu-

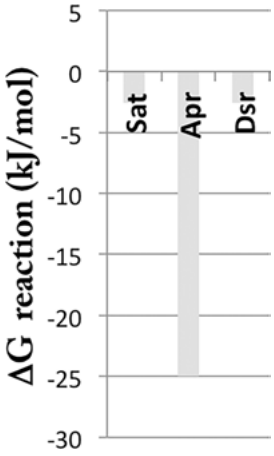

Figure 5. ΔG energy values of reactions of microbial sulfate reduction, estimated by Equilibrator [63–66] from metabolite concentration values estimated from *Desulfovibrio alaskensis* [54]. The input concentrations for the calculation were: sulfate: 10 mM, sulfite: 0.005 mM, sulfide: 0.005 mM, ATP: 5 mM, AMP: 0.5 mM, phosphate: 1 mM, APS: 0.05 mM, menaquinol: 2 mM, menaquinone: 0.1 mM. The first step of sulfate activation was written to incorporate hydrolysis of the produced pyrophosphate.

ally be responsible for delivering electrons onto Apr and Dsr, since variability in this is directly related to the reversibility, through the Nernst equation. In this way, an inference into the fundamental physiological process of the cell could be made through the analysis of isotopes [62].

6. ECOLOGICAL STABLE ISOTOPE FRACTIONATION: ECOSYSTEMS ARE NOT ORGANISMS

In the above sections, we have focused on cells, and the components of cells (enzymes), in discussing the partitioning of sulfur and carbon isotopes without considering simple facts of reality such as (i) the depletion of a substrate in a reservoir, (ii) competing reactions which may act on the substrate or product of individual reactions, or (iii) cycling of substrates and products. In the natural environment, these processes and others can confound interpretations based on isotopes.

How open or closed a system of interest is can have a major effect on the resulting isotope abundances in materials. In a simple case, if a system becomes closed, it is possible to have quantitative consumption of a substrate to a product, and such a quantitative conversion takes the isotopes with it. Thus, a system's "openness" can result in variation in observed fractionation, and this can be recorded in environments which have experienced variable sedimentation rates over time [69, 70].

7. WAYS FORWARD AND FUTURE ISSUES

Understanding equilibrium and kinetic isotope effects is important for our understanding of the distributions of biologically fractionated isotopes seen in nature. But these alone are not enough to understand distributions observed in the environment. Information on the metabolic network of individual cells, the concentration of the substrate in the environment, the state of these cells (energetically, nutritionally, etc.), and the open-ness or closed-ness of a system can all modulate isotope ratios. Going further, cells operate within ecosystems, not as isolated entities, interconverting and exchanging their products, and sometimes fractionation isotopes in the process. It is the collective challenge of researchers from multiple disciplines – who study across all of these scales – to elucidate what a particular isotope ratio may represent.

New observations continue to adjust our understanding of how isotopes are partitioned both today, and in the past, by biological processes. For example, recent observations of a sulfide-oxidizing organism revealed a previously unknown ability of organisms of this type to mediate large fractionations of the element [71]. As knowledge of enzyme KIE and metabolic pathways (including their topology, flux rates, and thermodynamic properties) continues to grow, better understandings of biological isotope fractionations in relationship to physiology will be possible. It may be possible to estimate the physiological state of contemporary and ancient cells from these isotope measurements. Gaining an understanding of potential evolutionary variability in enzyme-mediated KIE might be one way of uniting the molecular record of life with the historical, geological record.

ACKNOWLEDGMENTS

I thank Boswell Wing, David Fike, Yuichiro Ueno, Mayuko Nakagawa, Min Sub Sim, and Dave Johnston for many past and continuing conversations on isotope biogeochemistry. I thank Boswell Wing for contributing to the overall outline of this manuscript and for comments along the way, as well as Min Sub Sim for comments on the manuscript. Support by JSPS KAKENHI Grant No.18H01325, and NSF Award No. 1724300 is acknowledged.

ABBREVIATIONS

ADP	adenosine 5′-diphosphate
Apr	adenylylsulfate reductase
APS	adenosine 5′-phosphosulfate
ATP	adenosine 5′-triphosphate
Dsr	dissimilatory sulfite reductase
EIE	equilibrium isotope effect

ΔG_{rxn}	Gibbs energy of reaction
KIE	kinetic isotope effect
NADP	nicotinamide adenine dinucleotide phosphate
NADPH	dihydronicotinamide-adenine dinucleotide phosphate
P_i	inorganic phosphate, PO_4^{3-}
RuBisCo	ribulose-1,5-bisphosphate carboxylase/oxygenase
Sat	sulfate adenylyltransferase
VCDT	Vienna Canyon Diable Troilite

REFERENCES

1. J. W. Schopf, A. B. Kudryavtsev, D. G. Agresti, T. J. Wdowiak, A. D. Czaja, *Nature* **2002**, *416*, 73–76.
2. J. W. Schopf, A. B. Kudryavtsev, *Gondwana Res.* **2012**, *22*, 761–771.
3. K. Sugitani, K. Lepot, T. Nagaoka, K. Mimura, M. Van Kranendonk, D. Z. Oehler, M. R. Walter, *Astrobiology* **2010**, *10*, 899–920.
4. A. C. Allwood, M. R. Walter, B. S. Kamber, C. P. Marshall, I. W. Burch, *Nature* **2006**, *441*, 714–718.
5. A. C. Allwood, M. T. Rosing, D. T. Flannery, J. A. Hurowitz, C. M. Heirwegh, *Nature* **2018**, *563*, 241–244.
6. M. D. Brasier, O. R. Green, A. P. Jephcoat, A. K. Kleppe, M. J. Van Kranendonk, J. F. Lindsay, A. Steele, N. V. Grassineau, *Nature* **2002**, *416*, 76–81.
7. J. P. Grotzinger, D. H. Rothman, *Nature* **1996**, *383*, 423.
8. Y. Ueno, K. Yamada, N. Yoshida, S. Maruyama, Y. Isozaki, *Nature* **2006**, *440*, 516–519.
9. E. A. Bell, P. Boehnke, T. M. Harrison, W. L. Mao, *Proc. Natl. Acad. Sci. USA* **2015**, *112*, 14518–14521.
10. C. Bauer-Christoph, H. Wachter, N. Christoph, A. Roßmann, L. Adam, *Z. für Leb.-Forsch. A* **1997**, *204*, 445–452.
11. W. Meier-Augenstein, H. F. Kemp, S. M. L. Hardie, *Food Chem.* **2012**, *133*, 1070–1074.
12. A. Santato, D. Bertoldi, M. Perini, F. Camin, R. Larcher, *J. Mass Spectrom.* **2012**, *47*, 1132–1140.
13. S. M. McAllister, R. M. Moore, A. Gartman, G. W. Luther, D. Emerson, C. S. Chan, *FEMS Microbiol. Ecol.* **2019**, *95*. doi: 10.1093/femsec/fiz015.
14. J. M. Hayes, J. R. Waldbauer, *Philos. Trans. R. Soc. Lond. B. Biol. Sci.* **2006**, *361*, 931–950.
15. D. E. Canfield, *Rev. Mineral. Geochem.* **2001**, *43*, 607–636.
16. D. A. Fike, A. S. Bradley, C. V. Rose, *Annu. Rev. Earth Planet. Sci.* **2015**, *43*, 593–622.
17. Y. Shen, R. Buick, D. E. Canfield, *Nature* **2001**, *410*, 77–81.
18. M. S. Sim, H. Ogata, W. Lubitz, J. F. Adkins, A. L. Sessions, V. J. Orphan, S. E. McGlynn, *Nat. Commun.* **2019**, *10*, 44. doi: 10.1038/s41467-018-07878-4.
19. D. E. Canfield, J. Farquhar, *Proc. Natl. Acad. Sci. USA* **2009**, *106*, 8123–8127.
20. A. Crémière, H. Strauss, M. Sebilo, W.-L. Hong, O. Gros, S. Schmidt, J. Tocny, F. Henry, S. Gontharet, A. M. Laverman, *Chem. Geol.* **2017**, *454*, 67–79.
21. W. P. Gilhooly, C. T. Reinhard, T. W. Lyons, *Geochim. Cosmochim. Acta* **2016**, *189*, 1–23.
22. M. L. Gomes, M. T. Hurtgen, *Geochim. Cosmochim. Acta* **2015**, *157*, 39–55.

23. M. L. Gomes, D. T. Johnston, *Geochim. Cosmochim. Acta* **2017**, *205*, 331–359.
24. N. Knossow, B. Blonder, W. Eckert, A. V. Turchyn, G. Antler, A. Kamyshny, *Geochem. Trans.* **2015**, *16*, 7. doi: 10.1186/s12932-015-0021-5.
25. W. D. Leavitt, I. Halevy, A. S. Bradley, D. T. Johnston, *Proc. Natl. Acad. Sci. USA* **2013**, *110*, 11244–11249.
26. A. Pellerin, T. H. Bui, M. Rough, A. Mucci, D. E. Canfield, B. A. Wing, *Geochim. Cosmochim. Acta* **2015**, *149*, 152–164.
27. M. S. Sim, T. Bosak, S. Ono, *Science* **2011**, *333*, 74–77.
28. H. S. Weber, B. Thamdrup, K. S. Habicht, *Front. Earth Sci.* **2016**, *4*.
29. J. Hayes, *An Introduction to Isotopic Calculations*, Woods Hole Oceanographic Institution, Woods Hole, MA 02543, USA, **2004**.
30. *Isotope Effects In Chemistry and Biology*, Eds A. Kohen, H.-H. Limbach, CRC Press, Boca Raton, **2006**.
31. D. B. McNevin, M. R. Badger, S. M. Whitney, S. von Caemmerer, G. G. B. Tcherkez, G. D. Farquhar, *J. Biol. Chem.* **2007**, *282*, 36068–36076.
32. A. Mariotti, J. C. Germon, P. Hubert, P. Kaiser, R. Letolle, A. Tardieux, P. Tardieux, *Plant Soil.* **1981**, *62*, 413–430.
33. E. Noor, A. Flamholz, W. Liebermeister, A. Bar-Even, R. Milo, *FEBS Lett.* **2013**, *587*, 2772–2777.
34. J. A. Bassham, G. H. Krause, *Biochim. Biophys. Acta* **1969**, *189*, 207–221.
35. D. A. Beard, H. Qian, *PLoS ONE* **2007**, *2*.
36. B. A. Wing, I. Halevy, *Proc. Natl. Acad. Sci. USA* **2014**, *111*, 18116–18125.
37. T. J. Erb, J. Zarzycki, *Curr. Opin. Biotechnol.* **2018**, *49*, 100–107.
38. F. R. Tabita, T. E. Hanson, H. Li, S. Satagopan, J. Singh, S. Chan, *Microbiol. Mol. Biol. Rev.* **2007**, *71*, 576–599.
39. T. D. Sharkey, *Photosynth. Res.* **2019**, *140*, 235–252.
40. R. Park, S. Epstein, *Geochim. Cosmochim. Acta* **1960**, *21*, 110–126.
41. M. F. Estep, F. R. Tabita, P. L. Parker, C. V. Baalen, *Plant Physiol.* **1978**, *61*, 680–687.
42. J. Detmers, V. Brüchert, K. S. Habicht, J. Kuever, *Appl. Environ. Microbiol.* **2001**, *67*, 888–894.
43. I. R. Kaplan, S. C. Rittenberg, *J. Gen. Microbiol.* **1964**, *34*, 195–212.
44. A. Kemp, H. Thode, *Geochim. Cosmochim. Acta* **1968**, *32*, 71–91.
45. B. Brunner, S. M. Bernasconi, *Geochim. Cosmochim. Acta* **2005**, *69*, 4759–4771.
46. C. E. Rees, *Geochim. Cosmochim. Acta* **1973**, *37*, 1141–1162.
47. W. D. Leavitt, A. S. Bradley, A. A. Santos, I. A. C. Pereira, D. T. Johnston, *Front. Microbiol.* **2015**, *6*, 1392. doi: 10.3389/fmicb.2015.01392.
48. *Sulfate-Reducing Bacteria*, Ed. L. L. Barton, 1st ed., Springer Science + Business Media, New York, **1995**.
49. O. Y. Gavel, S. A. Bursakov, J. J. Calvete, G. N. George, J. J. Moura, I. Moura, *Biochemistry* **1998**, *37*, 16225–16232.
50. G. Fritz, A. Roth, A. Schiffer, T. Büchert, G. Bourenkov, H. D. Bartunik, H. Huber, K. O. Stetter, P. M. H. Kroneck, U. Ermler, *Proc. Natl. Acad. Sci. USA* **2002**, *99*, 1836–1841.
51. J. Lampreia, I. Moura, M. Teixeira, H. D. Peck Jr, J. Legall, B. H. Huynh, J. J. Moura, *Eur. J. Biochem.* **1990**, *188*, 653–664.
52. T. F. Oliveira, C. Vonrhein, P. M. Matias, S. S. Venceslau, I. A. C. Pereira, M. Archer, *J. Biol. Chem.* **2008**, *283*, 34141–34149.
53. A. A. Santos, S. S. Venceslau, F. Grein, W. D. Leavitt, C. Dahl, D. T. Johnston, I. A. C. Pereira, *Science* **2015**, *350*, 1541–1545.
54. M. S. Sim, G. Paris, J. F. Adkins, V. J. Orphan, A. L. Sessions, *Geochim. Cosmochim. Acta* **2017**, *206*, 57–72.
55. D. Mondal, T. Sadhukhan, I. A. Latif, S. N. Datta, *J. Chem. Sci.* **2015**, *127*, 2231–2240.

56. R. G. Jensen, J. A. Bassham, *Biochim. Biophys. Acta.* **1968**, *153*, 227–234.
57. G. H. Krause, J. A. Bassham, *Biochim. Biophys. Acta.* **1969**, *172*, 553–565.
58. T. A. Pedersen, M. Kirk, J. A. Bassham, *Physiol. Plant* **1966**, *19*, 219–231.
59. T. M. Hoehler, B. B. Jørgensen, *Nat. Rev. Microbiol.* **2013**, *11*, 83–94.
60. T. M. Hoehler, M. J. Alperin, D. B. Albert, C. S. Martens, *Glob. Biogeochem. Cycles* **1994**, *8*, 451–463.
61. T. M. Hoehler, M. J. Alperin, D. B. Albert, C. S. Martens, *FEMS Microbiol. Ecol.* **2001**, *38*, 33–41.
62. C. B. Wenk, B. A. Wing, I. Halevy, *ISME J.* **2017**. doi: 10.1038/ismej.2017.185.
63. A. Flamholz, E. Noor, A. Bar-Even, R. Milo, *Nucleic Acids Res.* **2012**, *40*, D770–775.
64. E. Noor, A. Bar-Even, A. Flamholz, Y. Lubling, D. Davidi, R. Milo, *Bioinforma. Oxf. Engl.* **2012**, *28*, 2037–2044.
65. E. Noor, A. Bar-Even, A. Flamholz, E. Reznik, W. Liebermeister, R. Milo, *PLoS Comput. Biol.* **2014**, *10*, e1003483.
66. E. Noor, H. S. Haraldsdóttir, R. Milo, R. M. T. Fleming, *PLoS Comput. Biol.* **2013**, *9*. doi: 10.1371/journal.pcbi.1003098.
67. T. Otake, A. C. Lasaga, H. Ohmoto, *Chem. Geol.* **2008**, *249*, 357–376.
68. K. S. Habicht, M. Gade, B. Thamdrup, P. Berg, D. E. Canfield, *Science* **2002**, *298*, 2372–2374.
69. G. Claypool, *Geochem. Soc. Spec. Publ.* **2004**, *9*, 59–65.
70. V. Pasquier, P. Sansjofre, M. Rabineau, S. Revillon, J. Houghton, D. A. Fike, *Proc. Natl. Acad. Sci. USA* **2017**, *114*, 5941–5945.
71. A. Pellerin, G. Antler, S. A. Holm, A. J. Findlay, P. W. Crockford, A. V. Turchyn, B. B. Jørgensen, K. Finster, *Sci. Adv.* **2019**, *5*, eaaw1480. doi: 10.1126/sciadv.aaw1480.

4

Imaging Trace Metals in Biological Systems

Jiyao Yu, Shefali Harankhedkar, Arielle Nabatilan, and Christoph J. Fahrni

School of Chemistry and Biochemistry, Petit Institute for Bioengineering and Bioscience, Georgia Institute of Technology, Atlanta, GA 30332, USA
<fahrni@chemistry.gatech.edu>

Metal Ions in Life Sciences, Volume 21 Guest Editors: Peter M. H. Kroneck and Martha E. Sosa Torres
Series Editors: Astrid Sigel, Eva Freisinger, and Roland K. O. Sigel

https://doi.org/10.1515/9783110589771-004

Abstract: The in situ detection and visualization of trace metals within the complex environment of cells and tissues is instrumental for exploring the role of metals in biology. Advances in microanalytical imaging techniques, notably improved detection sensitivity and spatial resolution, enabled trace metal imaging from the mesoscale down to the nanoscale size regime. This chapter offers an overview of the most important techniques for quantifying and visualizing biological trace metals. In addition to direct detection approaches, including synchrotron X-ray fluorescence microscopy (SXRF), secondary ion mass spectrometry (SIMS), and laser-ablation inductively coupled mass spectrometry (LA-ICP-MS), indirect imaging methods based on fluorescence microscopy and magnetic resonance imaging (MRI), both of which rely on specifically designed probes, are discussed in detail. Each technique is introduced with a brief review of the underlying physical principles, followed by representative examples from the literature, and a discussion of the advantages and limitations. Particular emphasis was given to synchrotron X-ray fluorescence microscopy and microtomography for direct elemental quantifications, and laser confocal fluorescence microscopy for dynamic imaging of labile metal pools with fluorescent probes, including recent advances in ratiometric two-photon excitation microscopy.

Keywords: fluorescent probes · laser ablation inductively coupled mass spectrometry · magnetic resonance imaging · microtomography · secondary ion mass spectrometry · two-photon excitation microscopy · trace metals · X-ray fluorescence microscopy

1. INTRODUCTION

The desire to detect and visualize trace metals within complex biological systems can be traced back over a hundred years. One of the earliest accounts was published in 1867 by the German pathologist Max Perls, who described a histochemical stain for the detection of non-heme iron [1]. Owing to its simplicity, the method, commonly known as Perls' stain, is still widely used for the visualization of iron overload in tissues [2]. In the protocol, treatment with hydrochloric acid releases protein-bound Fe(III), which is then reacted with potassium ferrocyanide ($K_4[Fe(CN)_6]$) to form the intensely colored Prussian blue pigment. Today, an arsenal of microanalytical techniques with much-improved sensitivities are available for the in situ detection of trace metals in cells and tissues [3–5]. A selection of the most important methods is compiled in Table 1. These approach-

Table 1. Microanalytical techniques for the *in situ* imaging of metals in biological systems.[a]

Method	Limit of detection	Spatial resolution	Analytical depth
Direct Detection Methods			
SXRF	0.1–1 μg/g	10–200 nm	100–500 μm
PIXE	1–10 μg/g	0.2–2 μm	10–100 μm
EPXMA	0.1–1 mg/g	30 nm	0.1–1 μm
LA-ICP-MS	0.1 μg/g	1–50 μm	200 μm
SIMS	0.1 μg/g	30–50 nm	0.1 μm
Indirect Detection Methods[b]			
Bright-field microscopy	low μM	0.2–0.5 μm	0.01–1 μm
Fluorescence microscopy	pM to nM	0.2–0.5 μm	1–5 mm
MRI	high μM	25–100 μm	no limit

[a] Because the limit of detection, resolution, and analytical depth depend on multiple experimental parameters, the values provided represent only a general range.
[b] Indirect detection methods employ a molecular probe that interacts with exchangeable metal ions to produce a detectable response.

es vary not only in terms of their sensitivity but show considerable differences in the available spatial resolution and analytical depth. Thus, none of the techniques is superior in all aspects; instead, each offers specific advantages but also has some limitations. For example, synchrotron X-ray fluorescence microscopy (SXRF) provides excellent spatial resolution and detection sensitivity for subcellular studies; however, slow data acquisition times combined with beam time constraints render this method less than ideal for analyzing large tissue sections. Such specimens would be better imaged by laser ablation inductively coupled mass spectrometry (LA-ICP-MS), which offers much shorter acquisition times with a spatial resolution down to the low-micrometer range. Likewise, magnetic resonance imaging (MRI), which was specifically developed for biomedical applications, represents the method of choice for studying live organisms; however, the sensitivity and spatial resolution of this technique is not sufficient for studying trace metals at the single-cell level.

In addition to the differences in performance parameters, trace metal imaging techniques can be divided into two distinct categories based on whether the analyte is detected directly or indirectly with the help of a probe (Table 1). Direct detection techniques such as SXRF, SIMS, or LA-ICP-MS inform on the total trace metal distribution within a specimen and may yield quantitative data after calibration with a suitable reference standard. In contrast, indirect methods such as confocal fluorescence microscopy or MRI rely on a reporter molecule that selectively interacts with the metal ion of interest and then relays a signal to a detector. Although some biological metal cations are present as free hydrated ions, increasing evidence suggests that essential trace metals such as zinc and copper are buffered at very low concentrations [6–8]. These trace metals are therefore detected based on a competitive exchange equilibrium between the

probe and endogenous ligands. Moreover, some metal-binding sites might be buried within a protein scaffold and thus not accessible for exchange. For this reason, indirect methods cannot be used to quantify total trace metal levels in a biological system. Instead, they may serve as a functional assay to gather information regarding the exchangeable metal ion availability, which is specific to a particular probe.

The following sections provide an overview of the most widely used techniques for imaging trace metal ions in biological systems. For each technique, the physical principles and underlying concepts are introduced first, followed by representative examples from the current literature, including a brief discussion of challenges and limitations. Particular emphasis was given to recent developments in X-ray fluorescence microscopy as well as the design and application of synthetic fluorescent probes for dynamic imaging of trace metals in living systems.

2. SYNCHROTRON X-RAY FLUORESCENCE ELEMENTAL IMAGING

2.1. Physical Principle

Exposure of a biological sample to high-energy X-rays may result in the ionization of individual atoms. If the ionization process involves the ejection of a core-shell electron, it generates a vacancy that is rapidly filled by an electron from an outer shell (Figure 1A). Most of the time, the transition energy is released in the form of a photon to produce a fluorescence signal; however, the energy may also be transferred to another electron, which is then ejected with an energy equal to the transition energy minus its binding energy. This secondary electron ejection is called the Auger effect, named after the French physicist Pierre Auger (1899–1993). The ratio between the two decay modes defines the X-ray fluorescence yield, which increases with the atomic number Z [9]. As the fluorescence yield of light elements ($Z < 12$) is very weak, only elements heavier than silicon are routinely detected by X-ray fluorescence-based imaging techniques. Most importantly, the binding energy of the electrons involved in the relaxation process is proportional to the squared nuclear charge, thus producing an X-ray fluorescence spectrum that is characteristic for each element and that can be used as a unique signature to detect and quantify elements within chemically complex biological environments [10, 11].

The relaxation of a higher-energy electron follows the same transition dipole selection rules common to electronic spectroscopy with $\Delta l = \pm 1$, where l refers to the angular quantum number. For example, a vacancy in the K-shell upon excitation of a 1s ($l = 0$) core-shell electron would result in the relaxation of $2p_{3/2}$ or $2p_{1/2}$ electrons ($l = 1$) of the L-shell, thus producing two emission lines of slightly different energies (Figure 1B). Likewise, fluorescence may also result from relaxation of $3p_{3/2}$ or $3p_{1/2}$ electrons from the M-shell, albeit with lower intensity. The different emission lines are routinely indicated by the Siegbahn notation [12], where the symbol of the corresponding element is followed by the

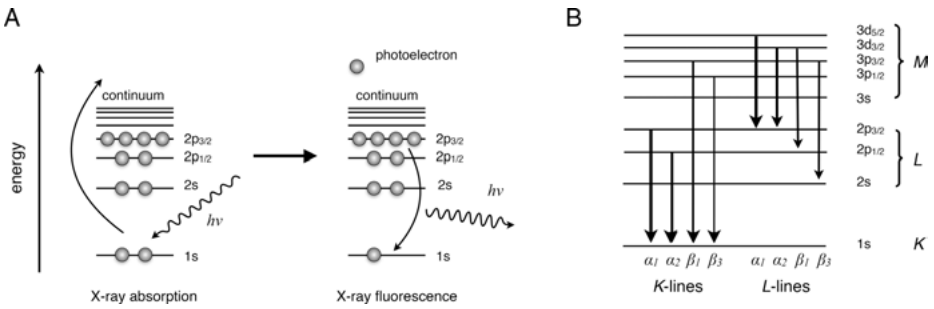

Figure 1. Principle of X-ray absorption and fluorescence. (**A**) Atomic orbital energy diagram illustrating the excitation of a 1s core-shell electron to yield a free photoelectron (left). The resulting orbital vacancy is populated by relaxation of an electron from a higher-energy orbital with simultaneous emission of a photon (right). (**B**) Major X-ray fluorescence emission lines for first-row transition metals. The arrow thickness indicates the intensity for each transition. The corresponding transition energies are compiled in Table 2.

name of the shell in which the initial vacancy occurred and a Greek letter indicating the relative intensity of the line. Accordingly, relaxation of the 2p electrons to the vacant K-shell produces the $K_{\alpha 1}$ and $K_{\alpha 2}$ lines with the strongest intensity, followed by the weaker $K_{\beta 1}$ and $K_{\beta 3}$ lines originating from the relaxation of a $3p_{3/2}$ electron. A selection of pertinent X-ray fluorescence transition energies, including K-shell fluorescence yields, for biologically relevant elements are compiled in Table 2.

Figure 2 shows the integrated X-ray fluorescence spectrum of a single 3T3 fibroblast acquired with a synchrotron X-ray source (see also Section 2.3). With an excitation energy of 10 keV, the spectrum reveals fluorescence peaks for all biologically relevant first-row transition metals, including Zn, Cu, and Fe. Because the energy resolution of the detector is not sufficient to resolve the $K_{\alpha 1}$ and $K_{\alpha 2}$ lines, they appear as a single broad emission band. Likewise, the two $K_{\beta 1}$ and $K_{\beta 3}$ lines are neither resolved and appear as less intense bands at higher energy compared to the corresponding K_{α} emissions. In addition to the elemental fluorescence, the spectrum also shows a strong scattering signal centered around the incident beam energy of 10 keV. The asymmetric shape of the signal is due to two overlapping contributions originating from elastic (Raleigh) and inelastic (Compton) scattering. Because Compton scattering exhibits a broad asymmetric profile and occurs at lower energy relative to the incident beam, it may extend into the spectral region of the elemental fluorescence. Nevertheless, by matching the Gaussian peaks to the characteristic X-ray emission lines of each element, the raw spectral data can be deconvoluted. To quantify the elemental content of bulk samples, the integrated Gaussian intensities are compared to those of an internal standard, for example, a xenobiotic element such as Ga(III) added to the sample. For SXRF imaging of individual specimens, the X-ray emission intensity can be calibrated by comparison with an external thin-film standard of known elemental content.

Table 2. X-ray fluorescence transition energies of biologically relevant elements.[a]

Element	Z	ω[b]	$K_{\alpha 1}$	$K_{\alpha 2}$	$K_{\beta 1,3}$	$K_{\beta 2}$	$L_{\alpha 1}$	$L_{\alpha 2}$	$L_{\beta 1}$
Na	11	0.023	1.041	1.041	1.067				
Mg	12	0.030	1.253	1.253	1.295				
Si	14	0.050	1.740	1.739	1.829				
P	15	0.063	2.013	2.012	2.136				
S	16	0.078	2.307	2.306	2.464				
Cl	17	0.097	2.622	2.620	2.815				
K	18	0.140	3.313	3.310	3.589				
Ca	20	0.163	3.691	3.687	4.012	–	0.341	0.341	0.345
V	23	0.243	4.951	4.944	5.426	–	0.511	0.511	0.519
Mn	25	0.308	5.898	5.887	6.489	–	0.637	0.637	0.649
Fe	26	0.340	6.403	6.390	7.057	–	0.705	0.705	0.718
Co	27	0.373	6.929	6.914	7.648	–	0.776	0.776	0.791
Ni	28	0.406	7.477	7.460	8.263	–	0.851	0.851	0.869
Cu	29	0.440	8.046	8.026	8.904	–	0.930	0.930	0.950
Zn	30	0.474	8.637	8.614	9.570	9.656	1.012	1.012	1.034
Se	34	0.589	11.220	11.179	12.494[c]	12.650	1.379	1.379	1.419
Br	35	0.618	11.922	11.876	13.289[c]	13.467	1.480	1.480	1.526
Mo	42	0.765	17.476	17.371	19.605[c]	19.962	2.293	2.289	2.394
I	53	0.884	28.607	28.312	32.289[c]	33.036	3.937	3.925	4.220
W	74	0.891	59.308	57.972	67.233[c]	69.089	8.396	8.334	9.671

[a] Data adopted from [13]. All energies are listed in units of keV.
[b] K-shell fluorescence yield reported in [9].
[c] $K_{\beta 1}$ transition energy.

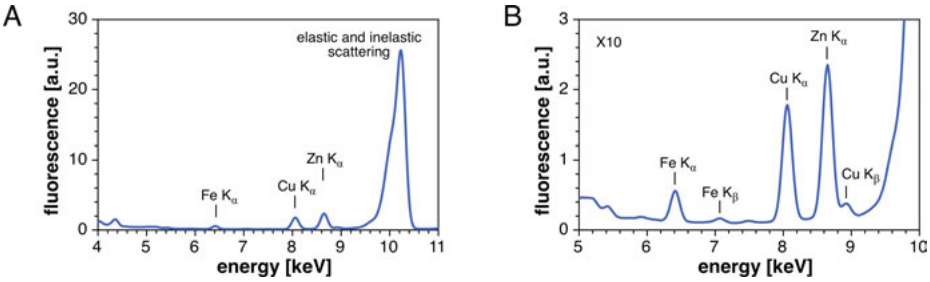

Figure 2. Integrated X-ray fluorescence emission spectrum of a 3T3 mouse fibroblast grown in copper-supplemented medium. The spectrum was acquired with an energy-dispersive detector using an incident beam energy of 10 keV (2-ID-D beam line, Argonne National Laboratory, Illinois, USA). (**A**) X-ray emission spectrum at full scale from 4–11 keV. (**B**) Spectrum of panel (A) shown at 10x magnification.

2.2. Sample Preparation Methods

The high-energy ionizing photon beam used in SXRF imaging would be destructive to live cells, and thus samples must be fixed and mounted on an X-ray-compatible substrate. Early SXRF imaging experiments were performed with

Formvar films supported on gold grids, a support material commonly employed in transmission electron microscopy [14, 15]. Produced from polyvinyl alcohol and formaldehyde, this carbon-based thermoplastic resin offers a low background absorption; however, due to the limited mechanical stability and softness, Formvar films may distort upon chemical fixation and break during data collection. As an alternative substrate, commercially available prolene films have been employed for elemental mapping of NIH-3T3 cells [16], and polycarbonate films have been successfully used for elemental imaging of PC12 cells by SXRF and particle-induced X-ray emission with a focused beam (micro-PIXE) [17]. The search for a biocompatible and more versatile substrate that also meets the requirements of X-ray fluorescence-based techniques led to silicon nitride (Si_3N_4) membranes, which have emerged as the preferred choice for cellular imaging. This non-toxic material offers mechanical stability similar to glass, and adherent cells can be directly cultured on Si_3N_4 membranes analogous to glass cover slips used in visible-light microscopy. The windows are optically transparent and can be used for correlative optical fluorescence microscopy studies. Unlike carbon-based polymeric materials, inorganic Si_3N_4 membranes can be employed in combination with synchrotron radiation-based Fourier transform infrared (SR-FTIR) spectroscopy for spatial mapping of proteins, lipids, or nucleic acids [18]. Commercial membranes are available in a broad range of sizes and thicknesses and typically free of metal contaminants, thus making Si_3N_4 an excellent choice for SXRF imaging studies.

In addition to choosing a suitable support material, biological samples must be fixed and dehydrated to preserve the structural integrity during exposure to the high-intensity photon flux in SXRF imaging. Early investigations of the elemental composition of rat brain sections revealed significant differences depending on the sample preparation technique. For example, chemical fixation with 10 % formalin followed by embedding in paraffin [19], a standard procedure used in preserving tissue for histopathological investigations, showed significantly lower levels for most elements, whereas fixation with formalin alone resulted in an unexpected increase of Fe, Cu, and Zn [19, 20]. Cryofixation by rapid-freeze immersion into liquid isopentane, ethane, or propane is, without a doubt, the best approach for preserving the native elemental composition of a biological specimen. After cryoimmobilization on a Si_3N_4 membrane, the frozen cells can either be lyophilized for imaging under ambient conditions or maintained at low temperature for transfer to an imaging beam line that is equipped with a cryo-stage [21]. While the cryofixation of hydrated cells represents, in principle, the best method for preserving the elemental composition, it requires specialized and expensive equipment that is not generally available. Moreover, this approach is still not devoid of potential artifacts, as cells must be rinsed with isotonic ammonium acetate or sucrose solution to remove inorganic salts and blotted to minimize the thickness of the surface film before plunge-freezing.

Several studies have been devoted to exploring whether conventional chemical fixation methods might preserve or alter the elemental composition of biological specimens [17, 21, 22]. Compared to cryopreservation, chemical fixation with 3 % paraformaldehyde resulted in a significant loss of diffusible elements such

as Cl, K, and Ca; however, the total levels of Fe, Cu, and Zn remained within the margin of cell-to-cell variations. Moreover, a combination of 1.5 % glutaraldehyde and 3 % paraformaldehyde yielded better preservation of P, S, Fe, Cu, and Zn levels than either fixative alone [17]. To remove extracellular contaminants, adherent monolayer cells must be washed before fixation. Considering the rapid kinetics of trace metal uptake and release [23], washing with a buffer solution might affect the intracellular elemental composition. Nevertheless, a systematic comparison of various rinse buffers, including isotonic ammonium acetate, Tris-glucose buffer, and Dulbecco's phosphate-buffered saline, revealed no statistically significant differences in total Fe, Cu, and Zn levels. Finally, a comparison of different dehydration methods showed that passive in-air drying of chemically fixed cells yielded better results than graded ethanol. In fact, chemical fixation and dehydration with ethanol or methanol should be avoided altogether as it leads to protein denaturation and membrane solubilization, both of which may result in substantially reduced levels for most elements, including S, Ca, Fe, and Cu [17].

In summary, rapid-freeze immersion offers far superior preservation of biologically relevant elements compared to chemical fixation [17, 21]; however, chemical fixation followed by in-air drying may still be employed as a convenient alternative approach, if the study does not require the detection and quantification of diffusible elements such as K, Ca, or Cl.

2.3. Elemental Imaging with Subcellular Resolution

For the elemental analysis of bulk samples, the photon flux of an X-ray tube is sufficient to yield an emission spectrum with good signal-to-noise ratio. Thus, bench top X-ray fluorescence elemental analysis instruments employ conventional vacuum tubes, which generate X-rays by colliding accelerated electrons from a high-voltage source with a material such as tungsten, molybdenum, or copper. However, the photon flux generated by this approach is too weak for the elemental mapping of individual cells with submicron resolution. For this purpose, the intense, focused beam of a synchrotron X-ray radiation source is required. In a synchrotron, electrons are accelerated to 99.9999998 % of the speed of light and then bent by a magnetic field (undulator) to produce X-rays within a narrow energy range and flux that is over a billion times greater than that of an X-ray tube. By focusing the X-ray beam to a narrow spot size, full X-ray emission spectra can be acquired from subcellular locations. Raster scanning of the specimen through the beam yields a two-dimensional hyperspectral data set from which the corresponding elemental density maps can be derived.

A schematic diagram of the components of a synchrotron X-ray fluorescence microscope is shown in Figure 3. Most synchrotron facilities around the globe offer several imaging beam lines covering a broad range of spatial resolutions and energy regimes. For example, the instrument at the 2-ID-E beam line of the Advanced Photon Source (Argonne National Laboratory, USA) is equipped with a double-monochromator to select photons within a tunable energy range between 8 and 20 keV and a Fresnel zone plate optics to focus the coherent X-ray beam to the sample surface. Named in honor of the original work by Augustin-

Jean Fresnel (1788–1827), a zone plate utilizes an uneven but radially symmetrical pattern of gold rings to generate a constructive interference pattern, which reduces the beam to a submicron focal spot. To achieve such a narrow focus, higher-order diffraction peaks are blocked by an aperture, which, however, also attenuates the overall photon throughput. To minimize scatter signals from air as well X-ray emission from ambient argon, the specimen is placed inside a helium-filled chamber. An x-y piezo-encoded stage is used to raster-scan the specimen through the focused beam with nanometer spatial precision, and a full X-ray emission spectrum is acquired at each position with an energy-dispersive multi-element detector positioned at 90 degrees relative to the incident beam. A beam monitor placed downstream of the microprobe is used to align the zone plate and sample along the beam trajectory. In place of a Fresnel zone plate, Kirkpatrick-Baez (KB) mirrors can be employed as focusing optics, which offer several orders of magnitude improved photon throughput [24]. In this setup, the X-ray beam is reflected and focused by two precision-engineered elliptical focusing mirrors, which are oriented perpendicular to each other. Because the fabrication of KB mirrors requires a machining tolerance in the low nanometer regime, their production remains challenging and costly. Nevertheless, with recent advances in X-ray optics fabrication, it is possible to manufacture KB mirrors that rival the beam profiles of zone plates [25, 26].

Elemental mapping of biological specimens with submicron resolution provides unique opportunities to gain insights into the spatial organization of transition metal ions at the single-cell level during normal and altered cell physiology. For example, X-ray fluorescence microscopy was employed to visualize the spatial redistribution of transition metals as cells progress through mitosis [27]. Such studies were previously limited to analyzing the elemental content of bulk samples, where cells had to be synchronized with drugs to increase the mitotic yield. By identifying the mitotic stage of cells based on the morphology of the cell nucleus, cells can be cultured under normal growth conditions, thus avoiding synchronization that might alter the overall cellular physiology. As illustrated with Figure 4 for a metaphase cell, X-ray emission spectra were acquired by raster-scanning with 0.3 μm step-size over an area of 107 × 75 pixels, thus producing a total of 7725 individual spectra comprised of 2048 data points with an energy resolution of approximately 10 eV. The total data acquisition time for this sample was around 3 hours. To generate individual elemental density maps, each raw X-ray emission spectrum was processed by Gaussian fitting, and the peaks were matched to the characteristic elemental X-ray emission lines as shown in Figure 4B. To derive quantitative elemental densities, the integrated photon counts were compared to the fluorescence intensity of a thin film standard. In Figure 4C, the final quantitative elemental maps are reproduced on a false-color scale with the corresponding density range indicated below each plot.

A comparison of the individual elemental maps provided intriguing insights into the subcellular elemental topography at the metaphase stage. For example, the high-density areas in the P map align well with the chromosome distribution. In contrast, the Zn and Cu maps show a complementary topography in which the highest-density areas appear in the centrosomal region adjacent to the meta-

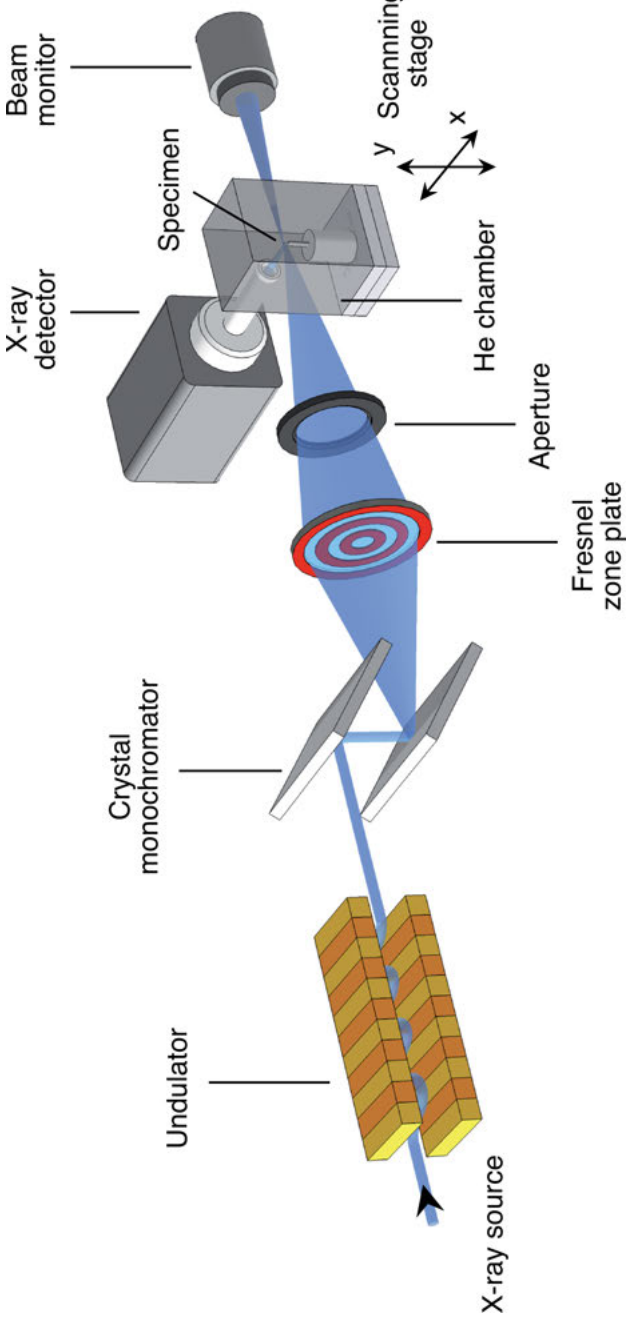

Figure 3. Schematic diagram of a synchrotron X-ray fluorescence microscope. After passing through a crystal monochromator to select the excitation energy, the X-ray beam is focused on the specimen with a Fresnel zone plate. An aperture is used to reject higher order diffraction peaks and scattered photons. The specimen is mounted on an x-y stage inside a helium-filled chamber and raster-scanned through the focused beam. Emitted photons are collected with an energy-dispersive detector to yield a two-dimensional hyperspectral data set from which quantitative elemental maps can be derived.

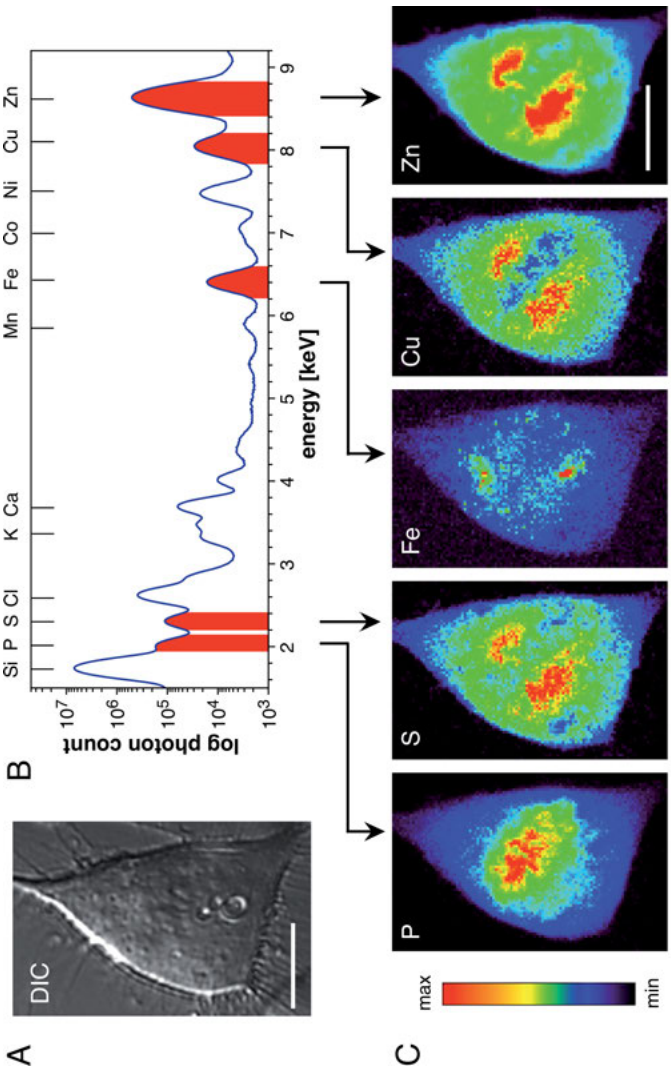

Figure 4. Subcellular elemental imaging of a 3T3 mouse fibroblast at the metaphase stage by synchrotron X-ray fluorescence microscopy. (**A**) DIC micrograph of the in-air dried cell. (**B**) Integrated X-ray fluorescence emission spectrum. (**C**) Raster-scanning of the cell at 0.3 µm step-size produced raw X-ray fluorescence spectra for each pixel. Two-dimensional elemental density maps were obtained by integrating the photon count of the raw spectra within the spectral region of the corresponding element indicated in panel B (red regions). The minimum and maximum density values of the false-color scale are indicated below each map. Scale bar: 10 µm.

phase plate. Both Zn and Cu parallel the S distribution, whereas the highest density areas of Fe show no apparent spatial correlation with any of the other elements. The integrated elemental densities also revealed an almost 3-fold increase of mitotic Zn levels compared to interphase cells, thus suggesting a prominent physiological role for Zn during cell division [27].

2.4. Imaging at the Nanoscale

Recent advances in X-ray focusing optics opened the window towards elemental imaging at the nanoscale. The challenges associated with realizing nanoscale spatial resolution, however, go beyond the development of nanofocusing optics. As the spot size decreases, fewer atoms are available for producing the X-ray emission profile. To maintain a satisfactory signal-to-noise ratio, a higher photon flux and increased detector sensitivity are therefore required. As the higher photon flux may increase radiation damage, hydrated biological samples should be imaged at cryogenic temperatures. Moreover, raster-scanning at the nanoscale also poses increased demands on the mechanical stability of the imaging stage. The Bionanoprobe, recently implemented at an undulator beam line of the Advanced Photon Source (Argonne, USA), successfully addressed these challenges [28]. Equipped with a Fresnel zone plate nanofocusing optics, the instrument offers a spatial resolution of 30 nm and employs a laser interferometer system to measure the position of the sample stage relative to the incident beam with an accuracy of a few nanometers. Full X-ray fluorescence spectra are acquired with a collimated four-element silicon drift detector at 90° relative to the incident beam. Vitrified biological samples can be loaded onto the cryo-stage through a sample exchange robot while maintaining the temperature well below the glass transi-

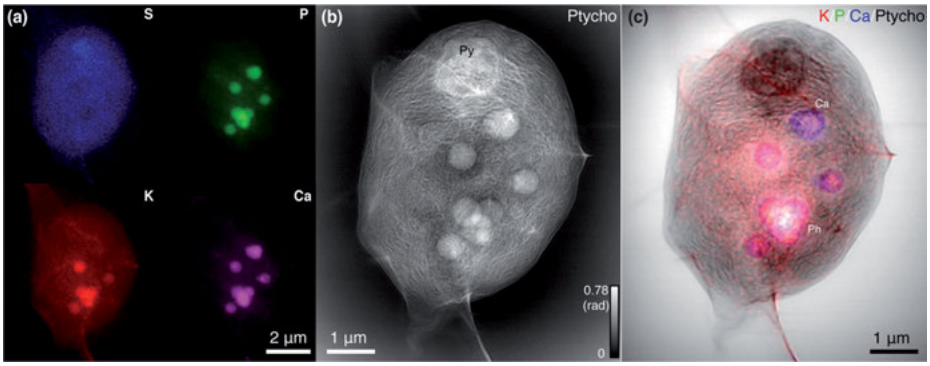

Figure 5. Nano-scale elemental imaging by synchrotron X-ray fluorescence microscopy. (**A**) Elemental distributions of P, S, K, and Ca within a frozen-hydrated *Chlamydomonas reinhardtii* cell at ~30 nm spatial resolution. (**B**) Phase image reconstructed via ptychography. (**C**) Color composite image showing an overlay of the SXR elemental maps and the ptychographic image. Reproduced with permission from [30]; copyright 2017, Springer Nature.

tion of water (135 K). To illustrate the performance of the instrument, Figure 5 shows nanoscale elemental maps of the unicellular green algae *Chlamydomonas reinhardtii*, as well as the corresponding phase image, which was reconstructed via ptychography [29, 30]. The electron-dense features in the ptychographic image revealed high densities of P and Ca in the fluorescence maps, presumably originating from polyphosphate bodies in which calcium is coordinated to polyphosphate [31].

More recently, a scanning X-ray microscope featuring a multilayer Laue lens with 15 nm $\times$ 15 nm spatial resolution was realized at the nanoprobe beamline of the National Synchrotron Light Source II (Brookhaven National Laboratory, USA) [32]. Similar to the Bionanoprobe, the instrument offers ptychography, differential phase contrast, and tomography imaging modalities. New manufacturing techniques enabled the fabrication of multilayer Laue lenses with a high numerical aperture (NA), which further reduced the beam size to a focal spot below 10 nm [33].

2.5. X-ray Fluorescence Microtomography

While scanning X-ray fluorescence microscopy is well-suited to study the colocalization of elemental distributions in cells or thin tissue sections, the lack of depth information may render the assignment of spatial relationships in thicker specimens ambiguous. Advances in X-ray optics and detector sensitivity significantly shortened the data acquisition time, which paved the way towards three-dimensional tomographic X-ray fluorescence imaging. Instead of relying on a single X-ray fluorescence scan, tomographic methods use a collection of projections at many angles to derive three-dimensional elemental distributions. Figure 6 illustrates the basic principle of X-ray fluorescence tomographic elemental imaging with a two-dimensional Shepp-Logan phantom as a sample object. As described above for two-dimensional elemental mapping (Figure 3), an energy-dispersive X-ray detector is oriented at a 90-degree angle relative to the incident beam trajectory. Analogous to absorption-based computed tomography (CT), the sample is mounted on a rotation stage, and parallel projections are acquired at equally spaced angles over 180 or 360 degrees. Thus, raster-scanning of the specimen along the x-axis direction yields at each position a full X-ray emission spectrum that represents the integrated fluorescence of all elements located along the incident beam path. The intensity projection that would result from a one-dimensional scan of the Shepp-Logan phantom at 0 degrees relative to the incident beam (z-axis) is shown in Figure 6 (bottom, left). The intensity projections for each angular position are then combined in a sinogram based on which the original 2D image can be reconstructed with a mathematical algorithm. By acquiring tomographic data sets at each position along the y-axis, individual reconstructed 2D elemental maps can be joined to generate full three-dimensional volumetric elemental maps.

The mathematical reconstruction of a two-dimensional image from an ensemble of one-dimensional projections is based on the Fourier slice theorem [34]. In

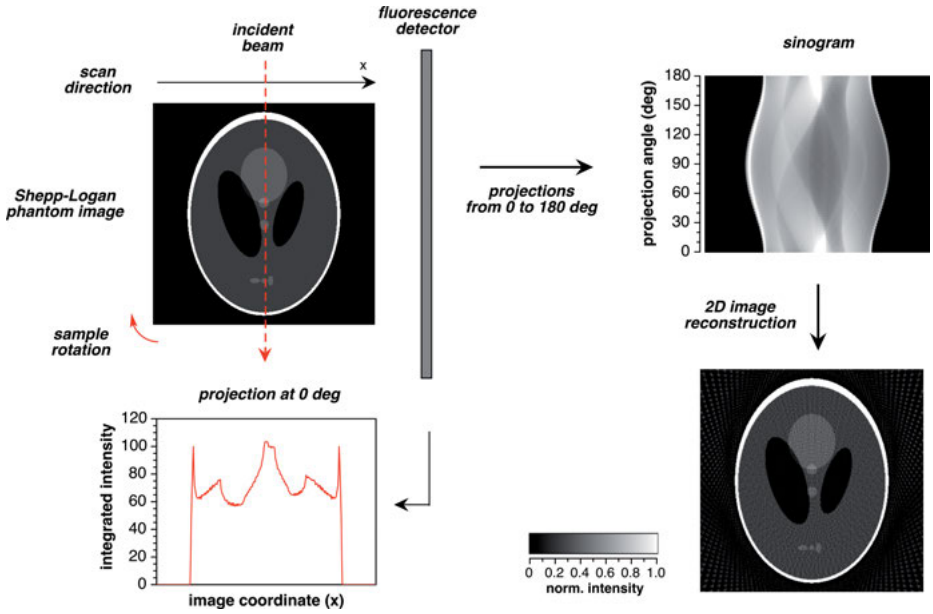

Figure 6. Principle of X-ray fluorescence tomography data acquisition and reconstruction illustrated with a 2D Shepp-Logan phantom image. Individual 1D intensity projections are recorded at a 90-degree angle relative to the incident beam by rotating the sample over 180 or 360 degrees. The intensity projections from each angle position are combined as a sinogram, based on which the original object can be reconstructed through a mathematical algorithm.

essence, the 1D Fourier transform of a projection is equal to a slice of the 2D Fourier transform of the object. Thus, with a sufficient number of projections, the original object can be reconstructed through a 2D inverse Fourier transform. The most common approach for the reconstruction of absorption CT data employs a filtered back-projection (FBP), which combines an inverse Radon transform with a ramp-filter to address image blurring introduced by the non-uniform sampling of the Fourier space [35]. However, this approach is not well-suited for the reconstruction of XRF tomographic data. Because of the much-weaker signal intensity, fluorescence data are not only noisier but also require longer acquisition times, which significantly limits the number of projections that can be acquired. Incomplete sampling of the Fourier space, in turn, introduces reconstruction artifacts. Additional challenges arise due to self-absorption of both the incident beam and emitted photons.

To reduce noise levels and minimize reconstruction artifacts, a number of iterative methods have been developed, such as the Algebraic Reconstruction Technique (ART) [36], the Simultaneous Iterative Reconstruction Technique (SIRT) [36], or the Maximum Likelihood Expectation Maximization Algorithm (MLEM) [37]. The MLEM algorithm, which was originally developed for the reconstruction of positron emission tomography data, assumes the same Poisson

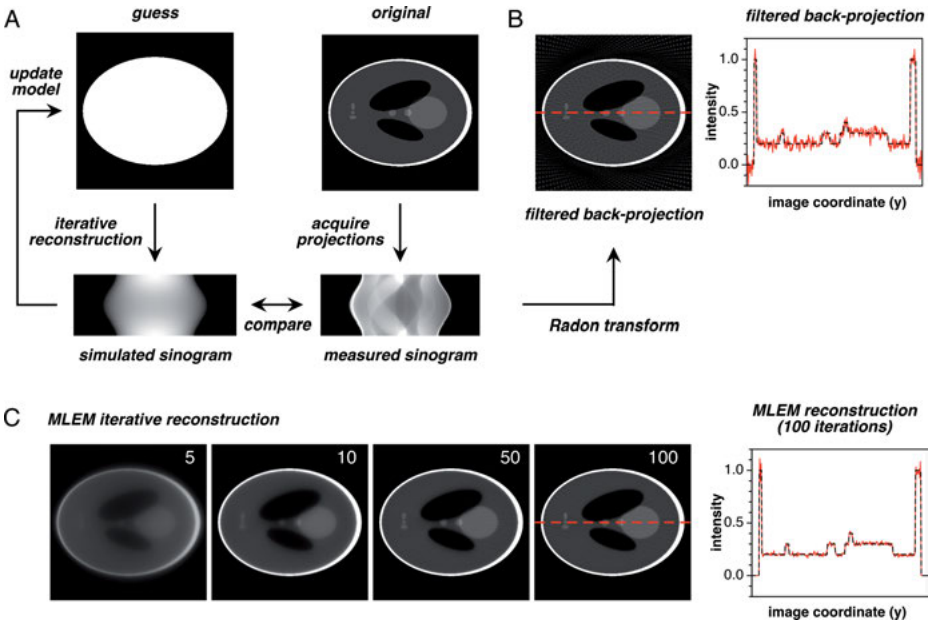

Figure 7. Reconstruction of XRF projections through an (**A**) iterative MLEM approach and (**B**) filtered back-projection (FBP) using the Radon transform. (**C**) With increasing number of iterations (shown for 5, 10, 50, and 100), the accuracy of the reconstruction improves and gradually converges to the original object. The plots to the right show intensity trajectories along the dashed red line in panels B and C, respectively.

noise statistics as observed in XRF. Reconstruction by iterative methods begins with a guessed model of the object, from which a projection (ART) or full sinogram (SIRT and MLEM) is mathematically generated (Figure 7A). After comparing the simulated data with the experimental projection or sinogram, the original model is updated by applying a correction function based on the back-projected changes. This process is repeated until the algorithm converges, at which point the projection or sinogram of the simulated model closely agrees with the experimental data set (Figure 7C). Compared to filtered back-projection (Figure 7B), the noise level of the MLEM-reconstructed model is significantly lower, as is evident from the corresponding intensity trajectories across the y-coordinate (Figure 7B/C).

The accuracy of tomographic reconstructions critically depends on the mechanical stability of the instrument as well as the sample integrity. To achieve the maximum resolution in the reconstructed data set, it is of paramount importance that the morphology of the specimen is retained and does not suffer radiation damage during data acquisition. For this reason, early XRF tomographic studies have focused on mechanically robust specimens such as seeds or diatoms [38, 39]. To visualize the 3D elemental distribution in soft tissue, the sample must be either cryopreserved or embedded in an X-ray-compatible matrix. The latter has been successfully demonstrated for zebrafish embryos at 24 and 48 hours

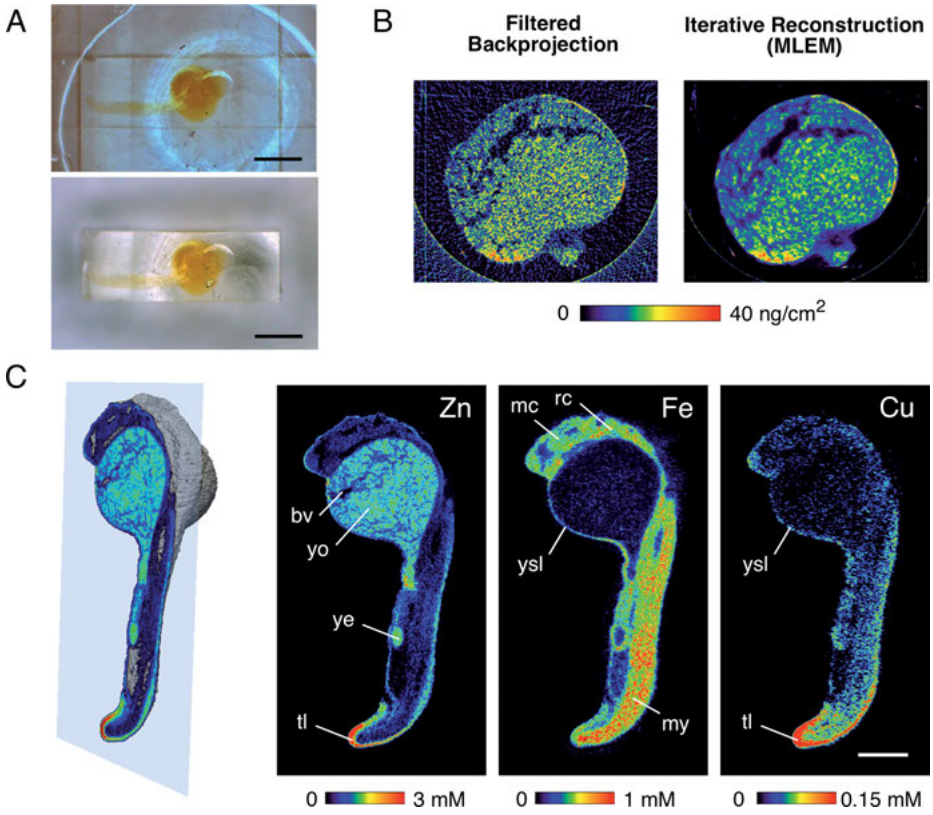

Figure 8. 3D imaging of zinc, iron, and copper in a zebrafish embryo (24 hours post fertilization) by XRF microtomography. (**A**) The embryo was cryo-embedded in Lowicryl (top) and excised from the resin block with a multiphoton laser microtome (bottom). Scale bar: 500 μm. (**B**) Filtered back-projection versus iterative MLEM reconstruction of the zinc density of a slice across the yolk region. (**C**) Full volumetric reconstruction of the Zn, Fe, and Cu densities illustrated for a sagittal section. Abbreviations: blood vessel (bv), mesencephalon (mc), myotome (my), rhombencephalon (rc), tail (tl), yolk extension (ye), yolk (yo), yolk syncytial layer (ysl). Scale bar 200 μm. Data adopted with permission from [40]; copyright 2014, Royal Society of Chemistry.

post-fertilization [40, 41], which were cryo-preserved by the progressive lowering of temperature (PLT) method, followed by freeze-substitution and polymerization in Lowicryl at –20 °C. The specimens were excised from the polymer block through contact-free sectioning using a multiphoton microtome (Figure 8A). Even though a total of 100 hours were required to collect a complete tomographic data set at a raster-scanned resolution of 2 μm, the sample integrity was not compromised. Iterative tomographic reconstruction yielded individual volumetric maps for Zn, Cu, and Fe, each of which entailed over 124 million individual voxels. Compared to simple FBP, the iterative MLEM algorithm resulted in much lower noise levels, as illustrated for a single slice across the yolk region

of the embryo (Figure 8B). The volumetric elemental maps provided intriguing insights into the 3D trace metal distributions with pronounced Zn and Cu densities at the tip of the tail, strikingly elevated Fe in the myotome and brain region, and a thin veneer of both Cu and Fe within the yolk syncytial layer (Figure 8C).

3. MASS SPECTROMETRY-BASED IMAGING TECHNIQUES

3.1. Secondary Ion Mass Spectrometry

Secondary ion mass spectrometry (SIMS) has been widely employed for analyzing the chemical composition of the surface from solid materials such as polymers [42], biomaterials [43], or thin films [44, 45]. By bombarding the specimen with an energetic ion beam, a process also referred to as sputtering, ions penetrate the surface layer and trigger the emission of a range of different particles (Figure 9A). While most of the sputtered material remains charge-neutral, a small fraction is ionized to yield either positively or negatively charged secondary ions. These ions are then guided to a mass spectrometer for analysis to provide detailed information about the elemental, isotopic, or molecular composition of the material. Unlike XRF-based chemical imaging, SIMS not only includes

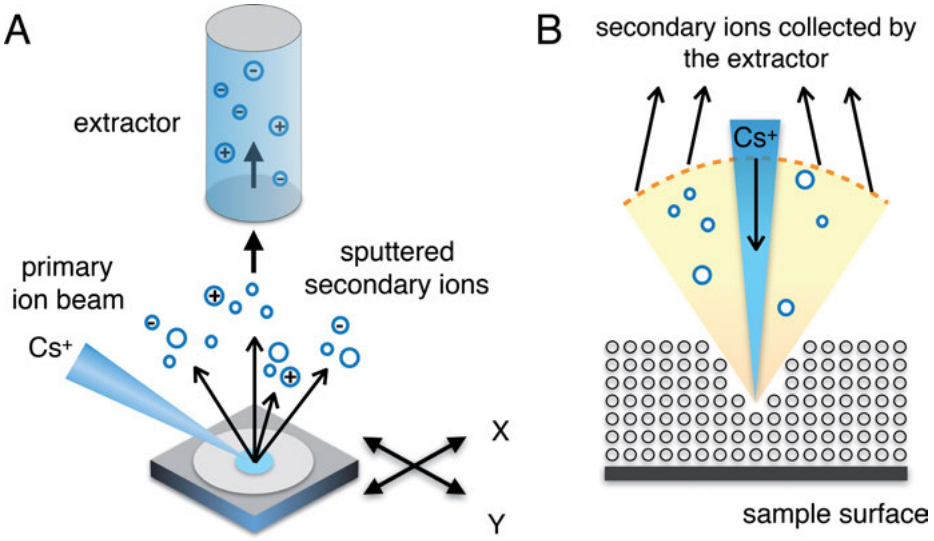

Figure 9. Principle of secondary ion mass spectrometry (SIMS) imaging. (**A**) A primary beam of focused Cs^+ ions triggers the ejection of fragments from the surface layer. Charged secondary ions are collected with an extractor and guided to a mass spectrometer for analysis. Raster-scanning of the sample with an x-y stage yields spatially resolved images of the surface composition. (**B**) In nano SIMS, the primary ion beam is oriented orthogonal to the surface to yield a narrower focus for much-increased spatial resolution below 50 nm.

information about elemental concentrations but may also inform on the molecular structure of the surface material. However, the high energy of the primary ion beam yields only small molecular fragments, thus limiting biological applications of SIMS to the analysis and identification of low-molecular-weight species. Analogous to XRF-based elemental imaging, the sample is raster-scanned on an x-y stage to produce images of the surface composition with a routine lateral resolution in the low micrometer range [46, 47].

Commercial SIMS instruments can be divided into three major classes: static SIMS, dynamic SIMS, and nano SIMS devices. Static SIMS or TOF-SIMS instruments employ a relatively low-count pulsed primary-ion beam such that each primary ion impacts only within a previously undisturbed area. The ensuing secondary ions are separated and analyzed based on their mass-to-charge ratio using a time-of-flight (TOF) or quadrupole-TOF (QTOF) mass spectrometer. Static SIMS instruments can achieve a high spatial resolution and may provide structural information for molecules with mass-to-charge ratios (m/z) of up to 1500. In contrast, dynamic SIMS employs a continuous primary-ion beam for sputtering, which inundates the uppermost surface with primary ions for sampling. The secondary ions are collected and sent to a magnetic sector or a quadrupole mass spectrometer for analysis. The dynamic range of dynamic SIMS is extensive and allows for the sensitive detection of fragments from the ppm to ppb concentration range. Finally, nano SIMS represents the highest resolution methodology and has evolved into a powerful tool for chemical imaging in the biological field. Nano SIMS instruments feature an improved ion optics to achieve a sub-50 nm lateral resolution, offer enhanced detection sensitivity, and allow for the simultaneous detection of up to seven mass signals [48]. With the development of the micro-cesium ion source, which has been commercialized by CAMECA, the incident angle of the primary ion beam was changed from 40 to 90 degrees relative to the sample surface while simultaneously extracting the secondary ions in a coaxial geometry (Figure 9B). As the orthogonal incident beam produces a circular rather than elliptical spot shape, the ion beam can be focused to a smaller size, which in turn results in a greatly enhanced lateral resolution. There are two different types of primary ion sources used in nano SIMS instruments: Cs^+ is the preferred choice for generating negatively charged secondary ions, and $^{16}O^-$ is employed for positively charged secondary ion analysis. The Cs^+ primary ion source also generates secondary electrons during the sputtering process. These secondary electrons can then be extracted and sent to a photomultiplier for simultaneous secondary-electron imaging. Nano SIMS also allows for quantitative imaging and depth profiling.

While the spatial resolution of conventional static SIMS represents the preferred choice for the analysis of tissue or multicellular colonies, nano SIMS enables imaging at the single-cell level to visualize subcellular details. For example, Ghosal et al. used nano SIMS to perform a 3D depth profile analysis of individual micrometer-sized bacterial spores [49]. The elemental maps revealed that phosphorous was localized in the center of the spores, whereas chlorine was found mostly in the outercoat. Similar to XRF elemental mapping with a synchrotron microprobe, nano SIMS can be used to derive spatial maps of biomet-

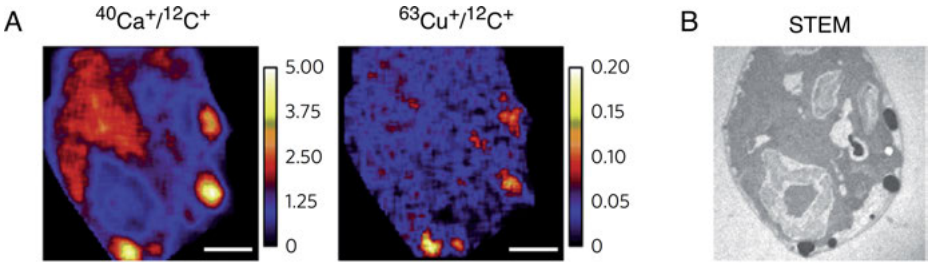

Figure 10. Subcellular nano SIMS imaging of copper-accumulating compartments in *Chlamydomonas reinhardtii.* Density maps for $^{40}Ca^{+}$ and $^{63}Cu^{+}$ (normalized to $^{12}C^{+}$) revealed that the two elements colocalize in zinc-limited cells. The areas of colocalization also coincide with electron-dense structures revealed by STEM in panel (**B**). Scale bars: 1 μm. Reproduced with permission from [50]; copyright 2014, Springer Nature.

als. For example, nano SIMS studies of the unicellular algae *Chlamydomonas reinhardtii* revealed copper accumulation and colocalization with calcium in lysosome-related organelles when cells were grown under zinc limiting conditions (Figure 10A). Sites with elevated copper levels also coincided with electron-dense structures visualized by scanning transition electron microscopy (STEM) (Figure 10B). The researchers inferred that the sequestration of copper into intracellular compartments might be a cellular response for preventing protein mis-metalation during zinc deficiency [50].

Although SIMS represents, without doubt, a very powerful tool for elemental and molecular imaging, there are several limitations to this technology. The ultra-high vacuum required for scanning restricts the type of specimens that can be analyzed, and the tightly focused ion beam significantly limits the total imaging area, typically just to a few mm^2. As the high-energy beam yields primarily small fragments, only limited molecular information can be derived. Finally, continuous bombardment with the primary ion beam destroys the sample surface, and it is therefore not possible to reproduce a scan of the same area for statistical evaluation.

3.2. Laser Ablation Inductively Coupled Plasma Mass Spectrometry

Laser ablation inductively coupled plasma mass spectrometry (LA-ICP-MS) represents another powerful imaging modality for analyzing the spatial distribution of trace metals in cells and tissues [51]. As implied by the name, the technique employs inductively coupled plasma mass spectrometry to quantify elemental concentrations. While this technique has been originally developed for the analysis of bulk samples, the development of new ionization techniques, improved separation systems, and more sensitive detectors made the in situ analysis of soft tissue possible. Since its introduction in 1985 [52], LA-ICP-MS has evolved into

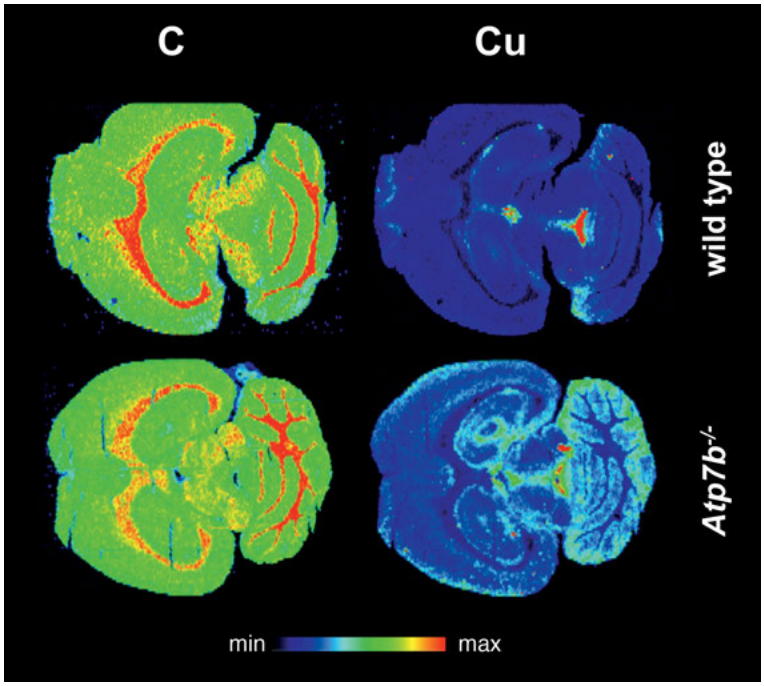

Figure 11. High-resolution LA-ICP-MS imaging of the copper distribution in a brain section of a mouse model of Wilson's disease ($Atp7b^{-/-}$, bottom row) and the corresponding wild-type (top row). The carbon map to the left served as internal standard for quantifying the copper levels. Color scale range from 0 to 20 μg/g Cu. Reproduced with permission from [61]; copyright 2014, Springer Nature.

a widely used analytical tool for multi-elemental analysis and offers a wide dynamic range combined with minimum sample preparation requirements [53]. Contrary to SIMS, tissues can be analyzed under ambient pressure without the need for a sophisticated vacuum system. Instead of using a high-energy ion beam, the material is excited with a pulsed laser, which causes rapid heating of the surface area and ablation of small particles [54]. The laser beam, typically a Nd:YAG laser with deep-UV output ($\lambda/4$ = 266 nm), irradiates the sample with high positional precision to ablate material only within the small focal area. Depending on the laser wavelength and fluence, particles with sizes ranging from 0.02 to 5 μm are produced [55]. The vaporized particles are then introduced into a plasma composed of ionized argon gas, which decomposes the particles into individual atomic ions [56]. The ions are subsequently analyzed in a mass spectrometer equipped with a quadrupole or double-focusing sector field mass analyzer. Similar to SXRF microscopy, the specimen is raster-scanned to produce elemental maps with lateral resolutions of around 1 μm [57] suitable for subcellular imaging [58]. As the amount of ablated material depends on several experimental parameters, such as the laser spot size, pulse rate, and scan speed, elemental

quantification is only possible through calibration with suitable reference standards [59].

Given the high sensitivity combined with a spatial resolution in the low micrometer range, LA-ICP-MS is especially well suited for analyzing large tissue sections that do not require subcellular detail as provided by SXRF microscopy. For example, LA-ICP-MS was employed to create an elemental atlas depicting quantitative maps of iron, copper, and zinc in a serially sectioned mouse brain [60]. To illustrate the application of LA-ICP-MS for the analysis of trace elements within complex biological tissues, Figure 11 shows high-resolution maps of the copper distribution within brain tissue sections of a Wilson's disease model mouse compared to wild-type [61]. The study revealed significant accumulation of copper in brain parenchyma but reduced levels in the periventricular region of the disease model. These data underscore the utility of LA-ICP-MS to visualize trace metal distributions in large tissue sections.

4. FLUORESCENCE IMAGING WITH METAL-ION SELECTIVE PROBES

4.1. Probing Cellular Metals with Synthetic Fluorescent Probes

Fluorescent probes are small organic molecules that reversibly bind to metal ions and respond with a change in their photophysical properties. They rank among the most widely used tools for detecting metal ions within a biological environment [62, 63]. Unlike all other techniques discussed in this chapter, fluorescent probes do not require specialized and expensive equipment; instead, they rely on conventional fluorescence microscopes for visualizing dynamic changes in metal ion concentrations. Because of their lipophilicity and low molecular weight, synthetic probes can enter cells through passive diffusion. This non-invasive imaging approach renders them the preferred tool for visualizing metal ions in live cells, tissues, and even whole organisms.

As illustrated in Figure 12, the molecular architecture of a fluorescent probe is composed of a binding site, which is tethered to a fluorophore reporter with a suitable spacer. Selective interaction of the metal ion with the binding site elicits either an intensity change or spectral shift, which can be monitored with a fluorescence microscope. Because analytes must bind to the probe to trigger a fluorescence change, non-labile metal ions such as those buried within proteins scaffolds cannot be detected by this method. In this regard, fluorescent probes should not be considered a cost-effective alternative to quantitative microanalytical techniques such as SXRF, SIMS, or LA-ICP MS imaging, but rather a complementary tool for exploring dynamic changes of labile metal ion pools.

As fluorescent probes respond to labile metal ions, an in-depth understanding of the underlying metal exchange equilibria is of fundamental importance [64]. Although the speciation of the exchangeable metal ion pool remains elusive, the

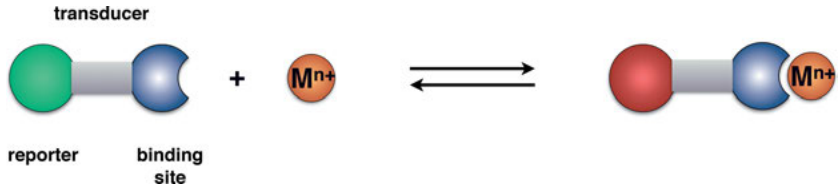

Figure 12. Schematic illustrating the design principle of a fluorescent probe. The probe senses a metal ion M^{n+} by engaging in a reversible binding equilibrium. Binding to the receptor site is communicated through a suitable transducing mechanism to a reporter fluorophore, which responds either with a change in fluorescence intensity or a spectral shift.

cellular concentration of free metal ions appears to be low, especially in the case of transition metal ions [7, 65]. Analogous to a pH buffer, an ensemble of polydisperse ligands is responsible for keeping the effective free metal ion concentration at a level that is much lower than the nominal concentration of the total exchangeable metal ion pool. Moreover, the buffered concentration depends on the nature of the metal ion and may also vary between cell types and organisms. For example, increasing evidence suggests that the exchangeable Zn(II) pool in mammalian cells is buffered at low nano- to high picomolar concentrations [8, 66], and recent imaging studies indicate low attomolar buffered concentrations for Cu(I), the predominant oxidation state of labile copper within the reducing cellular environment [6].

At a fundamental level, the magnitude of the fluorescence change upon metal binding is related to the change in fractional saturation, which refers to the ratio of metal-bound versus total probe concentration. As the probe engages in a competitive metal exchange equilibrium with endogenous ligands, the observed fluorescence response depends on its binding affinity relative to the buffered metal ion concentration. Figure 13 illustrates this dependence with a set of three simulated binding isotherms for probes with different dissociation constants, assuming a buffered metal ion concentration increase from 0.1 to 10 nM. A probe with a stability constant of log K = 9 (K_d = 1 nM), for example, would respond to such a concentration swing with an approximately 9-fold increase of the fractional saturation from ~10 to 90 % with a mid-point at 1 nM. In contrast, a higher-affinity probe with log K = 11 (K_d = 10 pM) would already attain near 90 % fractional saturation at the lowest metal ion concentration, and a lower-affinity probe with log K = 7 (K_d = 100 nM) would remain >90 % free, even at the highest metal ion concentration. Thus, the fluorescence response of the two probes with poorly matched affinities would be significantly smaller for the same change in buffered metal ion concentration. To ensure that the probe operates within the optimal dynamic range, it is therefore critical to evaluate its fractional saturation within the biological context. This can be accomplished by establishing the maximum and minimum probe response with suitable ionophores and membrane-permeant chelators.

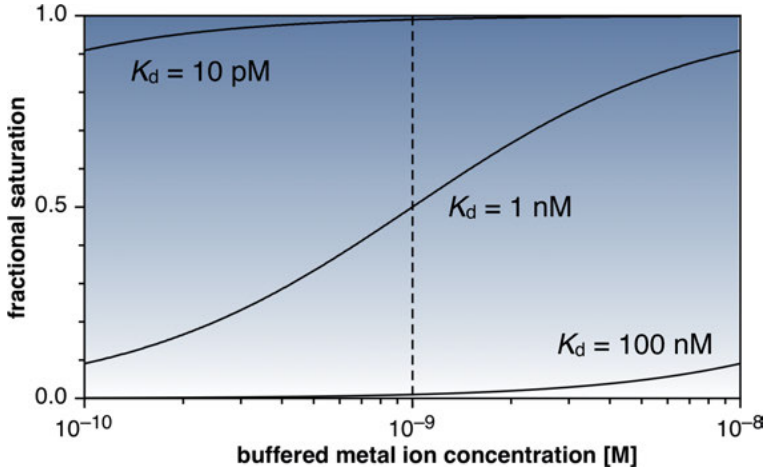

Figure 13. Simulated binding isotherms for three fluorescent probes with different metal dissociation constants (K_d) of 100 nM, 1 nM, and 10 pM. If the buffered metal ion concentration increases 100-fold from 100 pM to 10 nM, only the probe with a matched K_d of 1 nM responds with a large change in fractional saturation from 10 to 90 %. In contrast, the high-affinity probe is already saturated to 90 % at the lowest metal concentration, whereas the lower affinity probe does not bind beyond 10 % fractional saturation at the highest concentration.

4.2. Single-Wavelength Intensity-Based Probes

4.2.1. Fluorescence Switching Based on Photoinduced Electron Transfer

Fluorescent probes that respond with an increase in fluorescence intensity upon metal binding constitute presumably the most extensive class among currently available metal ion-responsive probes. As even small increases in the fluorescence intensity can be readily discerned by a photomultiplier detector, their dynamic range is typically wider compared to dual-wavelength probes that respond with a spectral shift (Section 4.3). While a broad range of design approaches have been developed to translate the metal-binding event into a measurable fluorescence increase, photoinduced electron transfer (PET) based fluorescence switching ranks among the most widely employed mechanisms. In this design approach, the metal ion chelator is attached to a fluorophore through a sigma-bond spacer that electronically decouples the two units from each other. In the absence of the metal ion, the chelator moiety acts as an electron donor (D) to promote an intramolecular electron transfer reaction to the excited fluorophore (A*) serving as the electron acceptor (Figure 14). The radical ion pair formed in the process subsequently undergoes charge recombination back to the ground state GS. Because charge recombination typically occurs without the emission of a photon, the fluorescence is effectively quenched. If a metal ion is coordinated to the chelator, the driving force for PET is reduced, and the fluorescence emis-

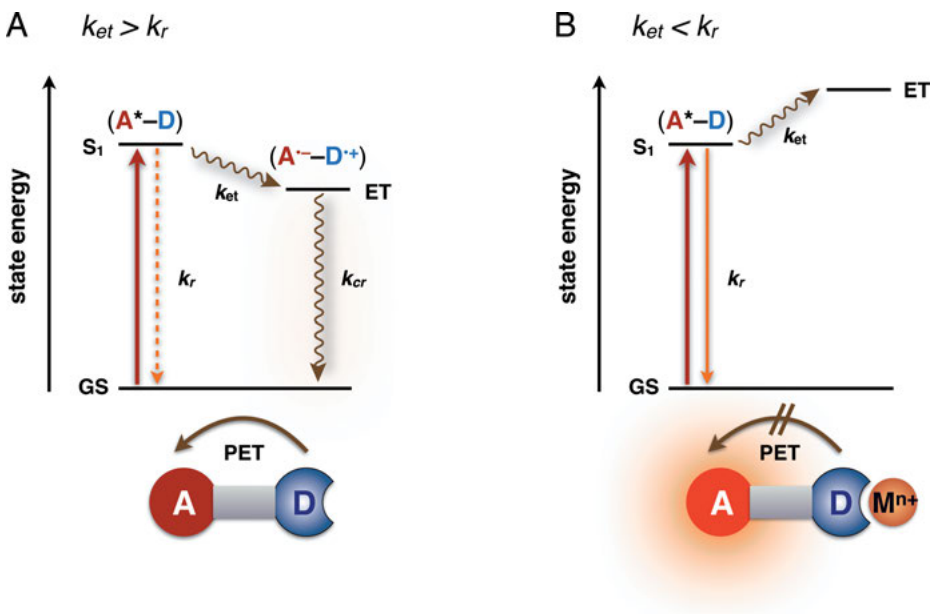

Figure 14. Simplified Jablonski diagram showing the mechanism of analyte-dependent photoinduced electron transfer (PET) fluorescence switching. (**A**) In the free probe, the electron rich donor (D) quenches the fluorescence of the excited fluorophore acting as an electron acceptor (A). Because the rate for electron transfer (k_{et}) is faster than radiative deactivation (k_r), the fluorescence is quenched through non-radiative charge-recombination (k_{cr}). (**B**) In the analyte-bound probe, PET is rendered unfavorable due to the increased potential of the donor (D) and the fluorescence is switched on ($k_r > k_{et}$). Abbreviations: Lowest-energy excited singlet state (S_1), ground state (GS), electron transfer state (ET).

sion from the excited fluorophore is restored. From the simplified energy diagram depicted in Figure 14, it becomes apparent that PET-induced fluorescence quenching only occurs if the rate for the excited-state electron transfer reaction (k_{et}) is faster than the rate for radiative deactivation (k_r). Conversely, in the metal-bound form, the fluorescence emission is only restored if k_{et} is sufficiently reduced over k_r. Moreover, because the metal ion is not in immediate contact with the fluorophore π-system, PET-based probes respond only with an increase in fluorescence without spectral shift.

4.2.2. Fluorescence Contrast Optimization

When employing fluorescent probes in cells and tissues, a large fluorescence contrast ratio between the free and metal-bound probe is advantageous. The inhomogeneous environment of biological samples inevitably affects the probe distribution and may produce artifacts, e.g., through sequestration into cellular compartments such as lipid droplets or acidic vesicles [67, 68]. With a small contrast ratio, it is very well possible that the emission intensity of the free but

sequestered probe might exceed that of the saturated probe. In addition to the fluorescence contrast, the molar brightness of the probe, defined by the product of the molar extinction coefficient at the excitation wavelength and the quantum yield of the metal-bound probe, is critical to avoid interference from cellular autofluorescence (see also Section 4.4.1). As evident from the Jablonski diagram in Figure 14, the fluorescence intensity of the probe is governed by the relative rates of the electron transfer quenching (k_{et}) and the rate of radiative decay (k_r) of the excited fluorophore. To achieve a large contrast ratio, metal coordination should therefore induce a significant reduction of k_{et} relative to k_r. According to Marcus theory, the kinetics for PET quenching is determined by its thermodynamic driving force [69]. The larger the energy gap between the emissive singlet state (S_1) and the charge-separated electron transfer state (ET), the more effective the fluorescence is quenched. Thus, the fluorescence contrast ratio increases with increasing change of the ET state energy relative to S_1 upon metal coordination. Ideally, the ET state should reside below S_1 to elicit fluorescence quenching of the free probe, but ascend above S_1 upon metal binding to restore maximum fluorescence [70, 71]. To design a probe with large fluorescence contrast, it is therefore critical to adjust the ET driving force such that an optimal balance of the relative state energies is achieved.

The driving force for PET quenching can be estimated based on the Rehm-Weller Equation (1), in which the energy of the ET state is approximated by the experimental ground-state donor and acceptor potentials $E(D^+/D)$ and $E(A/A^-)$, respectively and a work term, w_p, which captures the Coulomb stabilization energy of the formed radical ion pair within the respective solvent [72]. In polar solvents, this term is usually small due to dielectric screening. Because vibrational cooling usually occurs at a faster timescale than the ET process, the excited state energy S_1 can be approximated by E_{00}, the zero-zero transition energy between the vibrationally relaxed ground and excited states.

$$\Delta G_{ET} \approx E(D^+/D) - E(A/A^-) - E_{00} + w_p \quad (1)$$

In general, the donor potential $E(D^+/D)$ is defined by the type of metal chelator used for achieving the desired affinity and selectivity. Thus, the remaining parameters $E(A/A^-)$ and E_{00} can be used to tune the PET driving force for optimizing the contrast ratio. However, both parameters depend on the nature of the fluorophore, and in most cases, structural changes that alter the reduction potential $E(A/A^-)$ also affect the excited state energy E_{00} and vice versa. Nevertheless, some fluorophore platforms exhibit an electronic structure in which the HOMO and LUMO densities are sufficiently separated to allow for mostly independent tuning of these two parameters [73–75]. For example, in 1,3,5-triarylpyrazoline-based fluorophores, the HOMO densities are predominantly localized on the aryl ring attached in the 1-position of the pyrazoline ring system, whereas the LUMO densities are associated with the ring in the 3-position (Figure 15) [71]. As a consequence, the attachment of electron-withdrawing or donating substituents to the 1-aryl ring has a large effect on the excited state energy but only a small influence on the fluorophore reduction potential [75]. Despite the significant

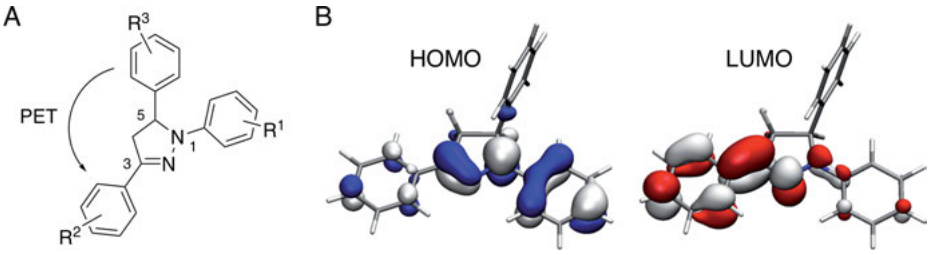

Figure 15. Structure (**A**) and molecular orbital densities (**B**) of the 1,3,5-triaryl-pyrazoline fluorophore platform. The aryl ring in the 5-position is electronically decoupled and can serve as a donor for PET-mediated fluorescence switching. The HOMO and LUMO densities were calculated based on density functional theory (B3LYP/6–31G(d)//B3LYP/6–311 + (2d,2p)). The density plots were generated with VMD [82] based on computational data from [71].

spatial separation of the HOMO and LUMO densities, pyrazolines still offer a significant molar extinction coefficient between 20,000–30,000 M^{-1} cm^{-1} [76]. Also, the 5-position of the pyrazoline ring-system can serve as an attachment point to introduce an electronically decoupled chelating unit (R^3) for designing PET-based metal-responsive probe (Figure 15A) [68, 76–81].

To illustrate the tunability of the pyrazoline fluorophore platform, the following section outlines the design and contrast optimization of a Cu(I)-responsive fluorescent probe [79]. Compared to non-redox active divalent transition metal ions, the selective detection of Cu(I) poses significant challenges due to potential interference from metal-mediated quenching pathways. Furthermore, coordination of the mono-cationic Cu(I) is expected to yield a significantly smaller differential increase of the donor potential $E(D^+/D)$ compared to divalent cations such as Zn(II) or Mg(II). Therefore, fine-tuning of the PET driving force is critical to achieve a large fluorescence contrast. Following the design concept outlined above, the pyrazoline fluorophore was functionalized in the 5-position with a Cu(I)-chelator composed of a mixed aza-thioether NS_3 coordination environment (Figure 16A). To maximize the increase in donor potential upon Cu(I)-binding, the aniline nitrogen was substituted only with a single thioether arm. With this ligand architecture, the aniline nitrogen can adopt a trigonal planar geometry for efficient resonance stabilization of the transient radical cation formed upon PET. In the Cu(I)-bound form, the aniline nitrogen is engaged in metal coordination and assumes a tetrahedral geometry, which no longer supports resonance stabilization. Thus, the conformational and electronic changes upon metal coordination work in concert to maximize suppression of PET quenching in favor of a large fluorescence contrast. To match the donor potential of the metal chelating unit with an appropriate acceptor, the 3-aryl ring of the pyrazoline fluorophore was functionalized with an electron-withdrawing cyano group. This modification lowers the acceptor potential by approximately 0.5 V compared to the corresponding unsubstituted derivative [71]. Finally, the excited state energy was adjusted step-wise by modifying the 1-aryl ring with fluoro

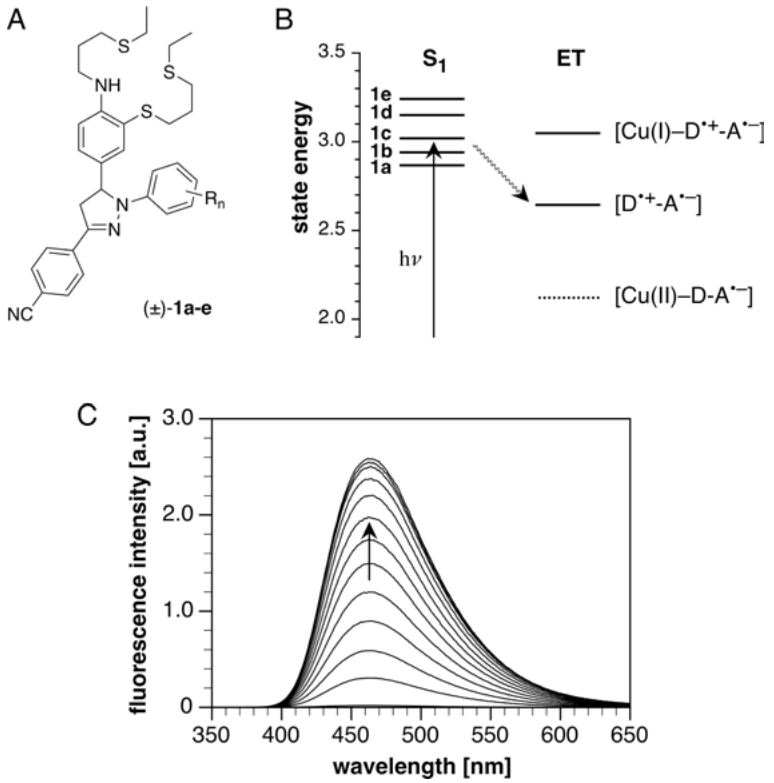

Figure 16. Design and contrast optimization of a Cu(I)-responsive probe based on electronic tuning of 1,3,5-triaryl pyrazolines [79]. (**A**) Molecular structure of the probe family **1a-e** featuring a thiaza-ligand as Cu(I) recognition site. (**B**) With increasing number of fluoro substituents R_n, the excited state energy S_1 increases in a step-wise fashion. Derivative **1c** offers the strongest PET driving force while still keeping the ET energy above S_1 upon Cu(I) coordination, thus producing a maximum 210-fold fluorescence enhancement. All pertinent photophysical data for probes **1a–e** are compiled in Table 3. (**C**) Fluorescence titration of **1c** (5 μM) with $[Cu(I)(CH_3CN)_4]PF_6$ in methanol (excitation at 362 nm). The arrow indicates the change upon Cu(I) addition.

substituents. As evident from the data compiled in Table 3, both the absorption and emission maxima moved towards shorter wavelength with increasing number of fluoro substituents; however, the acceptor potential remained centered at –2.19 ± 0.03 V. Concomitant with the increase of the excited state energy E_{00}, the PET driving force increased by 0.37 eV from ΔG_{et} = 0.18 eV to 0.55 eV (Figure 16B). With an intermediate driving force of 0.36 eV, derivative **1c** offers the optimal balance between the relative energies of excited state S_1 and the ET state. In the absence of Cu(I), the ET state resides significantly below S_1 to effectively quench the fluorescence emission but rises above S_1 upon Cu(I) binding, thus yielding a 210-fold fluorescence enhancement (Figure 16C). Time-resolved fluorescence studies revealed that radiative deactivation from S_1 is ap-

Table 3. Photophysical Data of Cu(I)-responsive pyrazoline probes **1a–e** in methanol at 298 K.[a]

	R_n	abs λ_{max} [nm]	em λ_{max} [nm]	E_{00} [b] [eV]	$E(A/A^-)$ [c] [V]	ΔG_{et} [d] [eV]	Φ_f [e]	E_f [f]
1a	3-F	391	486	2.86	–2.21	–0.18	0.57	34
1b	2,5-F_2	380	479	2.93	–2.18	–0.27	0.54	74
1c	2,3,5-F_3	371	463	3.01	–2.15	–0.36	0.49	210
1d	2,3,5,6-F_4	354	441	3.16	–2.21	–0.46	0.24	160
1e	2,3,4,5,6-F_5	346	432	3.23	–2.18	–0.55	0.21	n. d.

[a] Data adopted from [79].
[b] Zero-zero transition energy of the emissive state ($E_{00} = (E_{abs}(max) + E_{em}(max))/2$).
[c] Half-wave acceptor potential versus $Fc^{+/0}$ in acetonitrile (0.1 M Bu_4NPF_6, 298 K).
[d] PET driving force calculated based on the Rehm-Weller Equation (1) with $w_p = –0.045$ eV.
[e] Fluorescence quantum yield of the Cu(I)-saturated probe.
[f] Fluorescence enhancement factor (contrast ratio) between the free and Cu(I)-bound probe.

proximately 3-times faster than the rate of electron transfer quenching [79]. In contrast, the excited state energy of derivatives **1d** and **1e** reside both above the energy of the ET state in the Cu(I)-bound form, and for this reason, the fluorescence quantum yield does not fully recover, thus compromising the fluorescence contrast. Although Cu(I) would be expected to act as an efficient electron donor to promote formation of the charge-separated radical ion pair [Cu^{2+}–D–$A^{\bullet-}$] (Figure 16B), the kinetics for this pathway is too slow to compete with radiative deactivation, likely due to the large reorganization energy involved with the oxidation of Cu(I) to Cu(II).

Because probes **1a–e** are too lipophilic to dissolve in water without colloidal aggregation [68], the fluorescence properties were optimized in methanol, which is significantly different from an aqueous biological environment. Nevertheless, the same photophysical tuning concept was successfully applied towards optimizing the fluorescence contrast of water-soluble pyrazoline derivatives. Functionalized with hydroxymethyl and sulfonic acid functional groups, the Cu(I)-responsive fluorescent probe CTAP-3 offers, for example, a 180-fold fluorescence contrast with a quantum yield of 41 % and a limit of detection in the sub-part-per-trillion concentration range [83].

4.3. Dual-Wavelength Ratiometric Probes

4.3.1. Ratiometric Fluorescence Imaging

Fluorescent probes that respond with a significant chromatic shift in the excitation or emission spectra upon metal binding can be utilized for dual-wavelength ratiometric imaging. Instead of acquiring mere intensity changes at a single wavelength, ratiometric imaging relies on analyzing the ratio of fluorescence

intensities at two distinct excitation or emission wavelengths. By evaluating the ratio rather than absolute signal intensities, differences due to uneven cellular loading or photobleaching are canceled out. For this reason, ratiometric microscopy is less prone to artifacts than intensity-based imaging with single-wavelength probes. Moreover, the actual buffered metal ion concentration [M] can be directly estimated from the intensity ratio according to Equation (2),

$$[\mathrm{M}] = K_\mathrm{d}\left(\frac{R - R_\mathrm{min}}{R_\mathrm{max} - R}\right)\left(\frac{S_\mathrm{f}}{S_\mathrm{b}}\right) \tag{2}$$

where K_d refers to the dissociation constant of the probe-metal complex, R_min and R_max correspond to the minimum and maximum fluorescence intensity ratios of the free and metal-saturated probe, respectively, and S_f and S_b are instrument-dependent calibration constants [84]. If one of the acquisition wavelengths is assigned to the crossover point of the calibration spectra, the instrument-dependent term assumes unity and becomes obsolete. In this case, the fractional saturation f of the probe can be directly derived from the limiting ratios R_min and R_max according to Equation (3),

$$f = \left(\frac{R - R_\mathrm{min}}{R_\mathrm{max} - R_\mathrm{min}}\right) \tag{3}$$

where f is defined as the ratio of the metal-bound and total probe concentrations. Because it is easier to detect a fluorescence increase than a spectral shift, the dynamic range of ratiometric probes is inherently smaller compared to single-wavelength probes. It should also be noted that Equations (2) and (3) only apply to probes that reversibly coordinate the metal ion with a robust 1 : 1 binding stoichiometry.

While numerous single-wavelength probes have been developed for biologically relevant metal cations, the literature on ratiometric probes is comparatively sparse, even though ratiometric imaging microscopy was conceived more than 30 years ago [84]. Nevertheless, it is difficult to overstate the impact of the first ratiometric probes, in particular, fura-2 [84], on advancing our understanding of the role of Ca(II) in the central nervous system. As shown in Figure 17A, fura-2 is derived from the Ca(II)-selective chelator BAPTA (1,2-bis(*o*-aminophenoxy)ethane-*N,N,N′,N′*-tetraacetic acid), which is fused with an electron-deficient heterocyclic system to create a dipolar push-pull fluorophore architecture. The free probe features an excitation maximum of 362 nm, which shifts to 335 nm upon saturation with Ca(II). To maximize the ratio swing between the free and saturated probe, the fluorescence intensity ratio is routinely acquired with excitation at 340 and 380 nm (Figure 17B, red bars). Most recently, an LED-based illuminator that closely matches these excitation peaks was developed and successfully employed for visualizing spontaneous Ca(II)-transients in hippocampal neurons [85]. With a K_d of 135 nM (100 mM KCl, 20 °C, pH 7.1–7.2), fura-2 is well suited to capture dynamic Ca(II) fluxes in live cells. However,

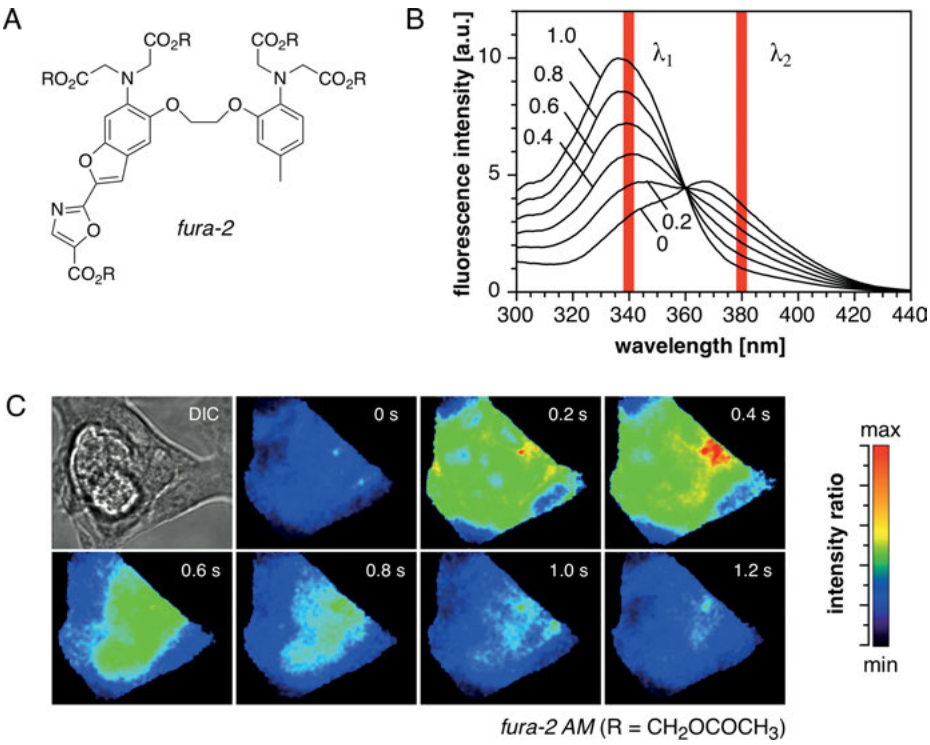

Figure 17. Ratiometric fluorescence imaging of Ca(II) ions. (**A**) Molecular structure of the Ca(II)-selective fluorescent probe fura-2. (**B**) Excitation spectra of fura-2 acquired at 510 nm as a function of the fractional saturation $f = [\text{Ca(II)-fura-2}]/[\text{fura-2}]_{\text{total}}$. (**C**) Dynamic imaging of a Ca(II)-wave in embryonic cardiomyocytes using fura-2 AM ester. DIC = differential interference contrast. The false-color intensity ratio micrographs illustrate the time-dependent progression of the Ca(II) wave. Adopted with permission from [87]; copyright 2007, Rockefeller University Press.

the charged carboxylic acid groups of fura-2 render the probe membrane impermeant, thus preventing its direct use for intracellular imaging. To enable cellular uptake through passive diffusion across the plasma membrane, the carboxylic acid groups can be masked as charge-neutral esters [86]. Upon cellular uptake, the masking groups are cleaved by non-specific esterases to yield the charged carboxylate anions, thus trapping the probe within cells and increasing the overall cellular retention. Due to their rapid hydrolysis kinetics, acetoxymethyl (AM) esters have been widely adopted as masking groups. Without a doubt, the ability to load a fluorescent probe into the cytosol of live cells represents a key development that revolutionized cell biology research [86]. As an example, Figure 17C shows the time-dependent progression of a Ca(II) wave in embryonic cardiomyocytes loaded with fura-2-AM [87]. The study revealed that periodic Ca(II) oscillations were local events, which generated action potentials responsible for the synchronization of electrical and mechanical signals.

4.3.2. Design of Ratiometric Fluorescent Probes

Compared to single-wavelength intensity-based probes, the body of literature on ratiometric fluorescent probes is modest, and only a few probes are commercially available. Several design principles have been described for inducing a chromatic shift of the fluorescence upon metal ion binding [88]. The original approach introduced by Tsien and coworkers with the Ca(II)-selective fluorescent probe fura-2 shown in Figure 17 employs a donor-acceptor substituted fluorophore architecture to produce a polarized intramolecular charge transfer (ICT) state upon photoexcitation [84]. In a polar solvent such as water, the polarized ICT state is stabilized through solvent-solute interactions, which are responsible for an unstructured emission band with a large Stokes shift. By employing the Lewis base heteroatom of a chelator both as metal-binding site and donor moiety of the fluorophore π-system, interaction of the metal ion decreases the degree of charge transfer, which in turn yields a higher-energy ICT state and a blue-shifted absorption and emission. As apparent from the molecular structure of fura-2 (Figure 17A), the aniline nitrogen of the BAPTA chelator serves as the electron donor that is responsible for modulating the energy of the ICT state upon Ca(II) binding.

As explained in detail in Section 4.4.3, the push-pull fluorophore architecture of fura-2 yields only a small chromatic shift in the emission response. Compared to excitation ratiometric microscopy, which requires rapid switching between two different excitation light sources, the instrumentation for emission-ratiometric sensing is less involved and thus the preferred imaging mode. Here, the fluorescence intensity of two emission channels can be measured without time delay by guiding the emitted photons through two band-pass filters with a beam splitter. To create fluorescent probes for emission-ratiometric sensing, several design concepts have been explored. For example, some fluorophores containing an intramolecular hydrogen bond undergo an excited-state intramolecular proton transfer (ESIPT) reaction to generate a tautomeric species with a strongly red-shifted emission [89]. If metal-coordination disrupts the intramolecular hydrogen bond, the ESIPT process is no longer operative, and the fluorophore emits with a strong blue-shift relative to the free probe [90, 91]. Another common approach for the design of emission-ratiometric probes utilizes a pair of fluorophores that interact through a Förster resonance energy transfer (FRET) mechanism in a metal-dependent fashion [88]. One of the fluorophores serves as a donor, which upon excitation emits at a wavelength that overlaps with the absorption spectrum of the second fluorophore acting as a FRET acceptor. Thus, excitation of the donor fluorophore produces a dual emission signal originating from both the donor and acceptor fluorophores. Several strategies have been realized to couple metal-binding to FRET efficiency, which depends on the donor-acceptor distance as well as the spectral overlap. This approach has been extensively utilized for the design of genetically encoded metal-responsive probes using fluorescent proteins as FRET pairs [92, 93].

4.4. Two-Photon Excitation Microscopy

4.4.1. Physical Principle

In two-photon excitation microscopy (TPEM), the fluorophore is excited by the simultaneous absorption of two photons in a single quantized event [94]. Analogous to one-photon excitation, fluorescence is emitted when the fluorophore returns to the ground state (Figure 18). As the energy of a photon is inversely proportional to its wavelength, fluorophores commonly employed in conventional fluorescence microscopy can be excited in the near-infrared region between 700 and 1000 nm [95]. The lower excitation energy reduces not only phototoxicity and photobleaching but also improves tissue penetration due to reduced Rayleigh scattering [96]. These properties are particularly advantageous for long-term imaging of live cells, tissues, or even whole organisms [97].

The theory of two-photon absorption was first developed by Maria Göppert-Mayer in 1931 [98], but only with the advent of lasers thirty years later, the phenomenon was experimentally demonstrated in a $CaF_2:Eu^{2+}$ crystal [99]. Because the probability for the simultaneous absorption of two photons is very low, two-photon excitation requires a very high photon flux that is only present within the small focal volume (Figure 18B) [100]. To achieve the photon density necessary for two-photon absorption while minimizing the average power exposure, a mode-locked femtosecond-pulsed Ti:sapphire laser is employed as the excitation source. As two-photon absorption is a non-linear process, the emitted fluorescence scales with the square of the excitation intensity and drops with the 4^{th} power as the distance z increases from the focal plane ($I \propto z^{-4}$). Thus, fluorophores located outside the focal plane are not excited, and TPEM, therefore, offers intrinsic optical sectioning capabilities for acquiring three-dimensional image stacks. By focusing the incident photons with a high numerical aperture (NA) objective, excitation volumes as small as 100 attoliters ($0.1\ \mu m^3$) can be achieved [101]. While conventional confocal microscopy also allows for optical sectioning by rejecting fluorescence from out-of-focus emitters with a pin-hole [102], the excitation beam still passes through the entire specimen and drops only with the squared distance from the focal plane (Figure 18A). As a consequence, fluorophores located outside the focal plane are still excited and are subjected to photobleaching or may promote phototoxicity. Moreover, many biomolecules absorb visible light [103], thus attenuating the excitation beam before it can reach the focal plane [102]. As the excited biomolecules may also fluoresce, the background fluorescence increases and reduces the overall imaging contrast.

While it might appear that TPEM differs from conventional fluorescence microscopy only in terms of the excitation mode, the fluorescence brightness of a fluorophore can vary significantly due to the different selection rules that apply for one- versus two-photon absorption. In general, the molecular brightness of a fluorophore is proportional to its quantum yield and absorption cross-section at the wavelength of excitation. Fluorophores with a large brightness enable imaging at lower concentrations, which minimizes photodamage to the sample at the laser power commonly used in TPEM (~ 5 mW at the objective lens)

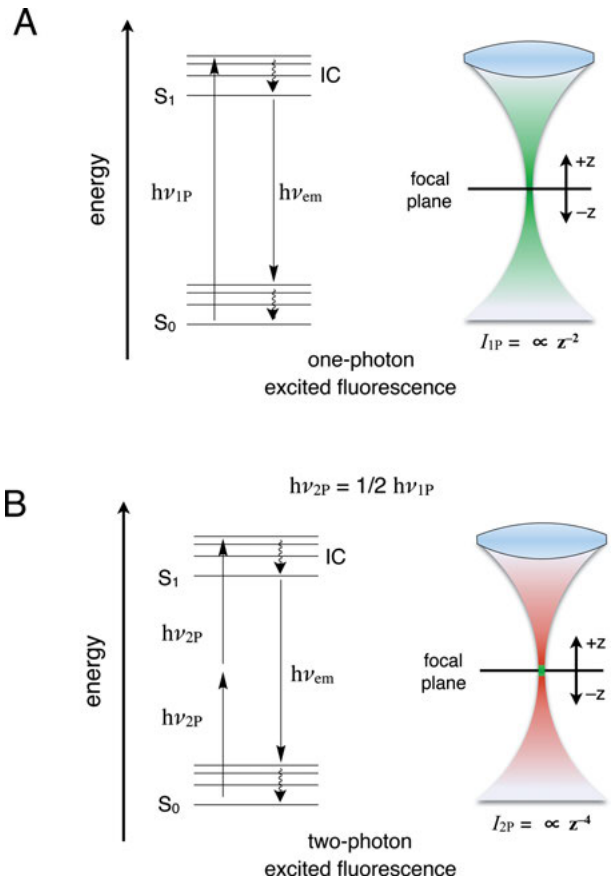

Figure 18. Principle of one-photon vs. two-photon excited fluorescence microscopy. (**A**) **Left**: Absorption of a single photon with energy $h\nu_{1P}$ promotes electronic excitation of a fluorophore from the ground state (S_0) to the first excited state (S_1). After vibrational cooling, the fluorophore emits a photon with slightly lower energy ($h\nu_{em} < h\nu_{1P}$). **Right**: Although the incident photon intensity decreases with the squared distance from the focal plane, out-of-focus emitters are still excited and contribute to background fluorescence, photobleaching, and phototoxicity. (**B**) **Left**: Simultaneous absorption of two photons yields the same excited state S_1 but with half of the photon energy. **Right**: Two-photon excited fluorescence (green) occurs only within the small focal volume where the photon density is sufficiently high.

[104]. While the quantum yield is mainly independent of the excitation mode, the absorption cross-section may vary significantly.

As illustrated with the data compiled in Table 4 for three common fluorophores employed in conventional fluorescence microscopy, their molecular brightness critically depends on the excitation mode. For ease of comparison, the relative brightness of each fluorophore has been normalized to the value of fluorescein. As is customary, the two-photon absorption cross-sections are listed in units of Göppert-

Table 4. One- and two-photon absorption properties of fluorophores commonly used in linear microscopy.

	one-photon abs		two-photon abs			rel. brightness[a]		
	λ_{max} [nm]	ε [10^4 M^{-1} cm^{-1}]	λ_{max} [nm]	δ [GM][b]	Φ_f[c]	1P	2P	Ref.
Fluorescein	490	7.6	790	47	0.93	1.00	1.00	[105]
Rhodamine 6G	530	11.6	700	120	0.95	1.56	2.61	[106]
BODIPY 492	500	7.9	920	15	0.95	1.06	0.31	[107]

[a] Brightness for one- (1P) and two-photon (2P) excited fluorescence emission relative to fluorescein (calculated as the product of absorption cross-section and quantum yield).
[b] Two-photon absorption cross-section at the wavelength indicated in column to the left. 1 GM = 10^{-50} cm^4 s $photon^{-1}$ $molecule^{-1}$.
[c] Fluorescence quantum yield.

Mayer (GM) where 1 GM corresponds to 10^{-50} cm^4 s $photon^{-1}$ $molecule^{-1}$. In one-photon excitation mode (1P), rhodamine 6G offers superior brightness with a value that is approximately 50 % higher compared to fluorescein or BODIPY 492. In two-photon excitation mode (2P), BODIPY is more than 3-times dimmer compared to fluorescein due to its lower absorption cross-section of 15 GM. In contrast, the favorable cross-section of rhodamine 6G of 120 GM renders its brightness more than 8-times higher compared to BODIPY and over 2-fold higher than fluorescein. This comparison underscores the importance of employing fluorescent probes and labels with a high two-photon absorption cross-section. Because the two-photon excited brightness of most biomolecule is low, TPEM yields a lower autofluorescence background and significantly improved imaging contrast over conventional linear fluorescence microscopy.

4.4.2. Design of Fluorescent Probes for Two-Photon Excitation Microscopy

As outlined in the previous section, fluorescent probes should offer a large 2PA cross-section to provide sufficient brightness for TPEM imaging applications. In general, the 2PA cross-section of a fluorophore increases with increasing charge transfer upon transitioning from the ground to the excited state [108, 109]. In the simplest case, a large excited-state charge polarization can be realized by substituting a conjugated π-system with electron-donating (D) and accepting (A) substituents to yield a dipolar fluorophore architecture. For example, when naphthalene is modified with an acetyl and dimethylamino group in the 2- and 6-positions, respectively, the 2PA cross-section increases by more than two orders of magnitude from 2.5 GM [110] to 302 GM for acedan **I** [111] (Figure 19A). Based on a simple two-state model that considers only the ground state S_0 and lowest-energy excited state S_1, the maximum absorption cross-section δ_{max} at the two-photon resonance energy ($E_1 = 2h\nu$) is proportional to the square of

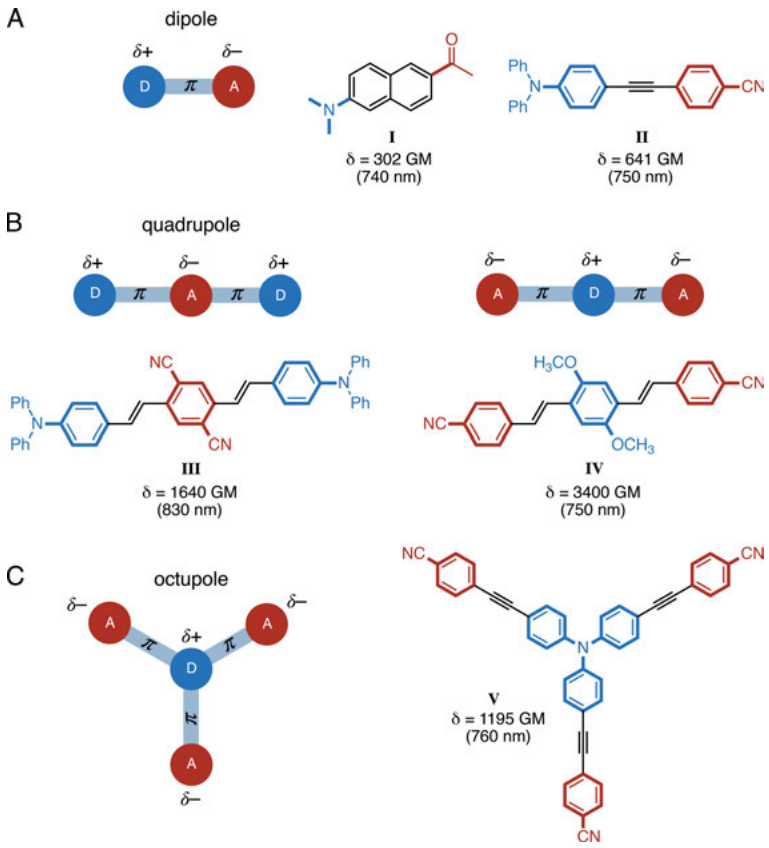

Figure 19. Molecular design principles for optimizing the two-photon absorption cross-section based on various arrangements of donor (D, blue) and acceptor (A, red) moieties tethered together through conjugated π-bridges (grey). (**A**) dipolar, (**B**) quadrupolar, and (**C**) octupolar fluorophore architectures, including representative structures and corresponding experimental 2PA cross-sections.

the transition dipole moment M_{01} and the change of the permanent dipole $\Delta\mu = \mu_1 - \mu_0$ moment between the ground and excited states as expressed by Equation (4)

$$\delta_{max} \propto \frac{(\Delta\mu)^2 M_{01}^2}{\Gamma} \tag{4}$$

where Γ corresponds to a damping factor describing the bandwidth of the $S_0 \rightarrow S_1$ transition.

From Equation (4) it becomes apparent that, in principle, the 2PA cross-section could be further increased by increasing the donor and acceptor strength of the terminal substituents or by extending the conjugation length of the push-pull

π-system as illustrated with the alkyne-bridged fluorophore **II** [112]. However, in polar solvents such as water, an increased excited state polarization also enhances solute-solvent interactions, which in turn may lower the 2PA cross-section and quantum yield, thus attenuating the overall brightness [113]. While the performance of dipolar fluorophores is often compromised in aqueous solutions, the 2PA cross-section and quantum yield of lipophilic probes might increase in cells by partitioning within lipid bilayers.

By tethering together multiple donor and acceptor moieties, push-pull architectures with further increased complexity can be created, including quadrupolar and octupolar geometries (Figure 19B and C). Fluorophores with a centrosymmetric arrangement of donor and acceptor groups exhibit an unusually large 2PA cross-section. Due to the dipole selection rules, excitation from the ground state S_0 to the lowest-energy excited state S_1 is symmetry forbidden. As a consequence, the lowest-energy excitation occurs only to the next higher-lying singlet state S_2, which is reached through a nonstationary "virtual state". Employing a three-state model encompassing S_0, S_1, and S_2, the 2PA cross-section δ_{max} at the 2PA resonance energy ($E_2 = 2\ h\nu$) is proportional to the squared transition dipole moments M_{01} and M_{12} as described by Equation (5)

$$\delta_{max} \propto \frac{M_{01}^2 M_{12}^2}{\left(E_1 - h\upsilon\right)\Gamma} \tag{5}$$

The bandwidth of the $S_0 \rightarrow S_2$ transition is again captured by the damping term Γ, which is approximately ~0.1 eV for many quadrupolar organic fluorophores. Because the centrosymmetric charge distribution results in a net-zero dipole moment in the ground and excited states, the permanent dipole term of Equation (4) is not present in Equation (5). Analogous to dipolar fluorophores, substitution with electron-donating and withdrawing groups dramatically increases the 2PA cross-section, as illustrated for the centrosymmetric fluorophores **III** and **IV** (Figure 19B). Despite the additional branch, the octupolar architecture **V** does not further boost the 2PA cross-section (Figure 19C); however, it still offers an approximately 2-fold improvement over the simple dipolar arrangement of **II**.

Although quadrupolar and octupolar fluorophores display much higher 2PA cross-sections than dipolar structures, the design of metal ion-responsive probes based on these architectures poses significant challenges. First, the linear geometry of the extended π-system promotes intermolecular interactions, which not only reduce the solubility in polar solvents but also promote self-aggregation. Second, a centrosymmetric architecture would require the incorporation of two analyte binding sites, either acting as donor or acceptor moieties. However, binding of a single analyte equivalent would compromise the symmetry, thus reducing the 2PA cross-section and complicating the quantitative evaluation of the emission response. Finally, to achieve a balanced 2PA cross-section and fluorescence brightness upon analyte binding, the magnitude of the transition dipole moments should be retained at a similar level. As illustrated with the aza-crown ether substituted distyrylbenzenes CR1 and CR2 (Figure 20), coordination of Mg(II) has a profound impact on the 2PA cross-section and brightness of these struc-

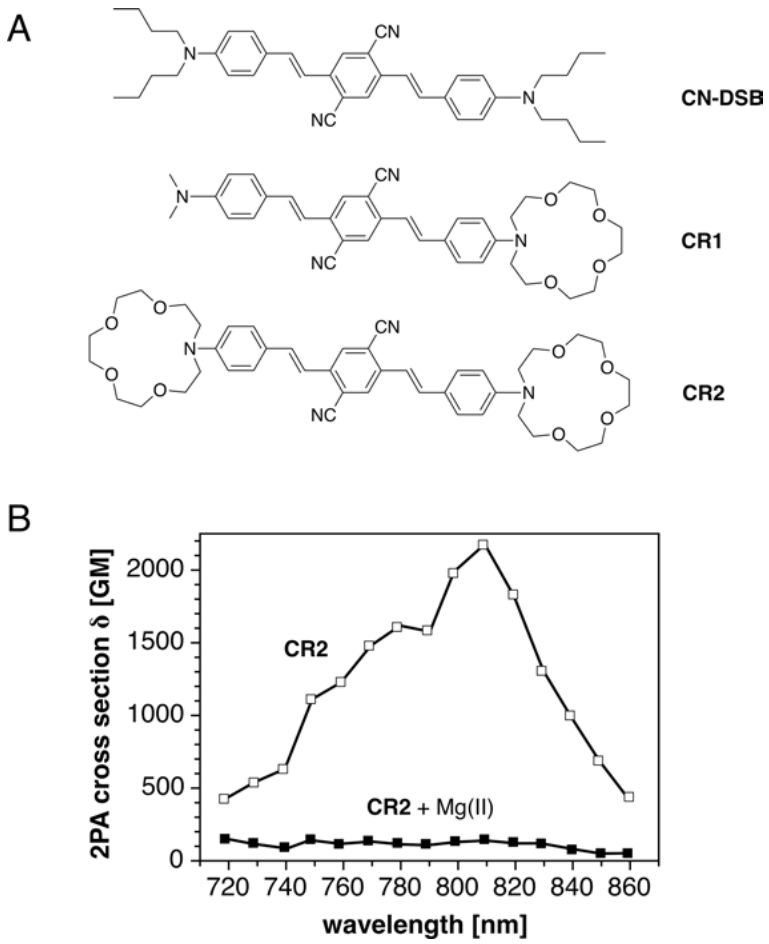

Figure 20. Two-photon excited fluorescence detection of metal ions with probes featuring conjugated push-pull π-systems. (**A**) Replacing the dibutylamino donor moieties of the parent fluorophore CN-DSB with one or two azacrown chelators yielded the Mg(II)-responsive probes CR1 and CR2. (**B**) The 2PA cross-section of CR2 dramatically decreased upon saturation with Mg(II) due to a reduction of the transition dipole moments. Data adopted with permission from [114]; copyright 2004, American Chemical Society.

tures [114]. While modification of the symmetric parent structure CN-DSB with a single crown ether binding site in CR1 reduced the 2PA cross-section only moderately from 2500 GM to 1800 GM, saturation with Mg(II) resulted in a 6-fold decrease to 300 GM (810 nm) and an over 30-fold reduction in overall brightness (Figure 20B). Moreover, the centrosymmetric probe CR2 exhibits a very large 2PA cross-section of 2150 GM (810 nm); however, saturation of both binding sites with Mg(II) diminished the 2PA cross-section to 45 GM resulting in an almost 50-fold reduction in brightness. In both compounds, coordination of Mg(II) reduced the donor strength of the crown ether moiety, which affected

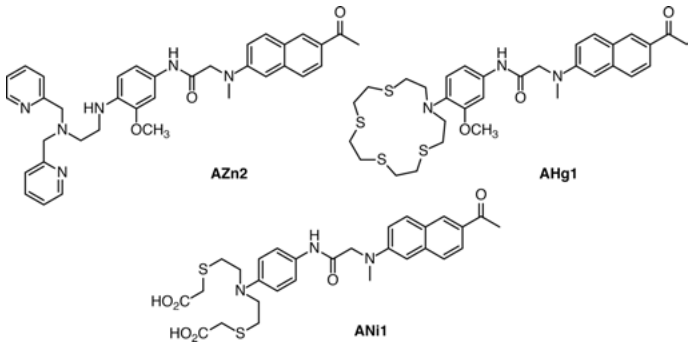

Figure 21. Fluorescent probes for two-photon microscopy employing the dipolar acedan fluorophore. Due to the modular probe architecture, the chelator moiety can readily be modified to create a range of probes with distinct metal ion selectivity, e.g., towards Zn(II) (AZn2), Hg(II) (AHg1), or Ni(II) (ANi1).

the 2PA cross-section due to the reduced transition dipole moment according to Equation (5).

Given the challenges associated with centrosymmetric architectures, simple dipolar fluorophores have emerged as the preferred choice for designing fluorescent probes, despite their lower 2PA cross-sections [115]. For example, the dipolar acedan fluorophore with its favorable 2PA cross-section has been extensively used for the design of fluorescent probes [116]. Based on a modular approach, a diverse array of metal ion selectivities was achieved simply by choosing the appropriate chelating moiety. As illustrated with Figure 21, the *N,N*-di(2-picolyl)ethylenediamine (DPEN) moiety of **AZn2** acts as a Zn(II)-selective receptor site with an apparent dissociation constant of 1.1 nM (pH 7.2, 0.1 M KCl) [117]. In the absence of Zn(II), the methoxy-substituted aryl ring serves as an electron-rich donor that effectively quenches the acedan fluorescence through a PET mechanism as described in Section 4.2. Upon saturation with Zn(II), the two-photon excited fluorescence increases 50-fold with a maximum intensity at 499 nm. With a 2PA cross-section of 140 GM at 780 nm and a quantum yield of 0.49, the Zn(II)-saturated form of **AZn2** is more than 2-fold brighter than fluorescein (Table 4). Applied in acute hippocampal slices, the probe revealed elevated labile Zn(II) pools in the stratum lucidum of the CA3 region and the hilus of the dentate gyrus. Combination with an electron-rich thiazacrown ether yielded **AHg1**, a Hg(II)-selective probe, which showed a 6-fold emission enhancement upon saturation with Hg(II) [118]. The probe was successfully used in TPEM to detect enhanced Hg(II) levels in live cells as well as organs isolated from fish (*Oryzias latipes*) that were exposed to 2 ppb of $HgCl_2$. Likewise, attachment of *N,N*-bis[2-(carboxymethyl)thioethyl]amine (CTEA) yielded a Ni(II)-responsive probe **ANi1** [119].

4.4.3. Ratiometric Two-Photon Excitation Microscopy

As outlined in Section 4.3, ratiometric imaging allows for visualizing dynamic changes of buffered metal ion concentrations in a semi-quantitative fashion, thus offering a distinct advantage over simple intensity-based fluorescence detection. However, only fluorescent probes that undergo a significant shift in the emission maximum are suitable for TPEM imaging. Although the Ti : sapphire femtosecond-pulsed lasers of commercial two-photon microscopes can be tuned to a specific wavelength, it is not possible to alternate rapidly between two different wavelengths. Therefore, fluorescent probes that respond only with a shift in the excitation but not emission wavelength cannot be used for two-photon excited ratiometric imaging. Despite large chromatic excitation shifts, the majority of metal-responsive ratiometric fluorescent probes used in conventional fluorescence microscopy, however, do not undergo a significant change of the peak emission wavelength upon metal binding. This is a direct consequence of the underlying fluorophore design, which relies on an intramolecular charge transfer state to produce the excitation ratiometric response upon metal binding (Figure 22A). By integrating the electron-rich Lewis base of a chelator into a push-pull fluorophore architecture, the energy of the charge transfer state becomes sensitive towards metal binding. Although the donor strength decreases upon metal binding in the ground state, a partial buildup of positive charge on the donor moiety in the excited state weakens the interaction with the metal ion through Coulomb repulsion. This, in turn, yields an excited-state polarization that is not much different compared to the metal-free probe. As a consequence, only the excitation but not the emission energy changes upon metal ion coordination to the donor. Consistent with this analysis, the absorption maximum of fura-2 (Figure 22B) undergoes a strong blue-shift from 362 nm to 335 nm, but a comparatively weak emission shift from 512 to 505 nm upon saturation with Ca(II) [84]. Moreover, the 2PA cross-section decreases from 12 GM to 1 GM (750 nm) upon saturation with Ca(II) [120], analogous to the attenuation observed for the centrosymmetric probes discussed above.

To design a probe that responds with an emission shift, it is necessary to circumvent the repulsive interaction between the fluorophore and the metal ion upon formation of the charge transfer state. A push-pull fluorophore architecture in which the acceptor rather than donor strength is modulated by metal binding offers a simple solution to this problem (Figure 22A) [121]. Contrary to the previous design, the partial buildup of negative charge on the acceptor site strengthens the fluorophore-metal ion interaction in the excited state, which should produce a significantly red-shifted emission spectrum. Although binding of a cation to an electron-deficient site might appear counterintuitive, some Lewis bases can serve both as metal donors and electron-deficient acceptors. For example, the Zn(II)-responsive ratiometric probe chromis-1 features a push-pull fluorophore architecture in which the pyridine ring acts as an electron-rich σ-donor for Zn(II)-coordination but also as a strong π-acceptor to produce a charge-transfer state upon photoexcitation (Figure 22B) [122]. Designed explicitly for ratiometric two-photon microscopy, chromis-1 undergoes a substantial shift

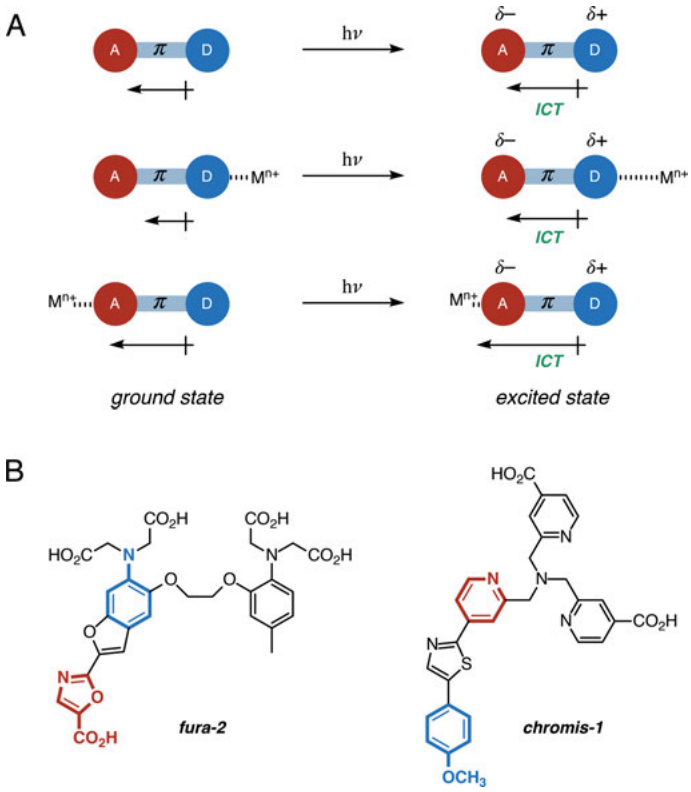

Figure 22. Design principles of ratiometric probes based on dipolar push-pull fluorophore architectures. (**A**) Metal (M^{n+}) coordination to the donor moiety decreases the dipole moment in the ground state compared to the unbound probe. In the excited state, Coulomb repulsion weakens the coordinative interaction to produce a similar polarization compared to the free probe and thus a small chromatic emission shift. In contrast, coordination to the acceptor increases the polarization of both, the ground and excited states, thus yielding red-shifted absorption and emission maxima. (**B**) Examples of ratiometric probes where the metal ion binds either to the donor (fura-2) or acceptor (chromis-1) sites. Only chromis-1 [122] produces a strong emission shift suitable for ratiometric TPEM.

of the emission maximum from 483 to 520 nm and retains a balanced 2PA cross-section around 20 GM upon saturation with Zn(II) (Figure 23A and B). The ethyl ester derivative of chromis-1 can readily cross lipid bilayers and has been successfully used for imaging changes of buffered Zn(II) levels in live 3T3 mouse fibroblasts by TPEM. As illustrated with Figure 23C, exposure of cells to the thiol-selective oxidant 2,2′-dithiodipyridine (DTDP) induced release of Zn(II) from endogenous pools as evident by the ratio change from 0.5 to about 1.3. Interestingly, the cytoplasmic buffered Zn(II) levels equilibrated back to the initial ratio within about 1 hour. Moreover, the probe revealed a pronounced reduction of cellular zinc availability as oligodendrocytes mature and differentiate to mature cells [121].

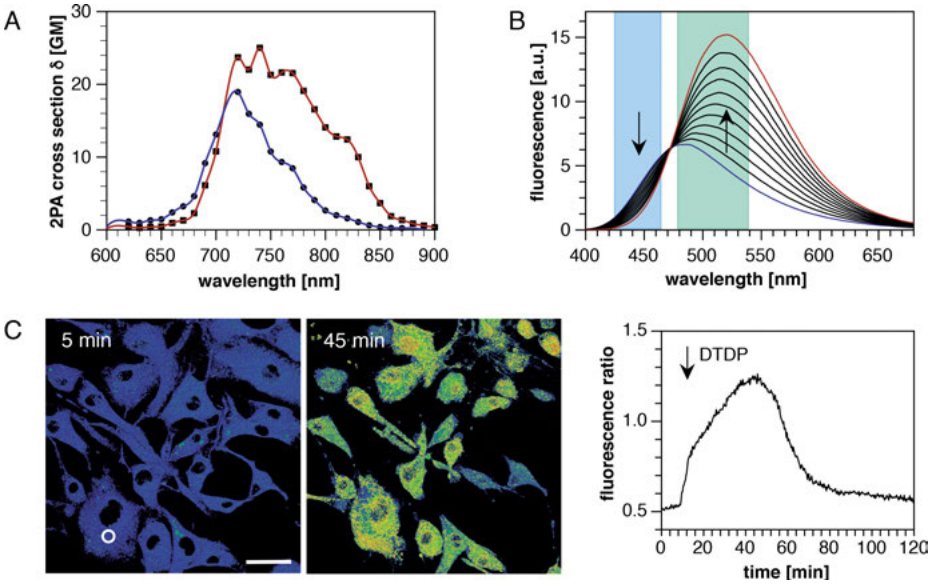

Figure 23. Ratiometric two-photon imaging of labile Zn(II) with chromis-1. (**A**) Two-photon absorption cross-section of the free (blue) and Zn(II)-bound form (red) of chromis-1 (pH 7.0, 0.1 M KCl, 25 °C). (**B**) Fluorescence emission response upon saturation with Zn(II) (excitation at 358 nm). (**C**) Emission-ratiometric two-photon imaging (excitation at 720 nm) of dynamic changes of labile Zn(II) in live 3T3 mouse fibroblasts before (left) and after (right) addition of 100 μM 2,2′-DTDP. The emission ratio (BP2/BP1) was calculated based on the integrated fluorescence intensities from 425 to 462 nm (BP1) and 478–540 nm (BP2). **Right**: Time course of the average ratio change within the ROI indicated with a white circle. Scale bar: 40 μm. Adopted with permission from [122]; copyright 2018, American Chemical Society.

5. MAGNETIC RESONANCE IMAGING

5.1. Physical Principle

Magnetic resonance imaging (MRI) ranks among the most widely used clinical imaging modalities and produces three-dimensional images with rich anatomical detail. Compared to positron emission tomography (PET) and X-ray absorption-based computed tomography (CT), MRI offers superior contrast and does not rely on ionizing radiation. The technique takes advantage of nuclear magnetic properties, typically the hydrogen nuclei of water. When exposed to a static magnetic field, the positively charged nuclei, composed of a single proton with spin I = 1/2, align their magnetic moment either parallel or anti-parallel to the field axis and produce two populations of slightly different energy. As shown in Figure 24A, the energy difference, commonly referred to as Zeeman splitting, increases with increasing field strength (B_0). At room temperature, the Boltzmann distribution (N_B/N_A) between the two populations approaches almost uni-

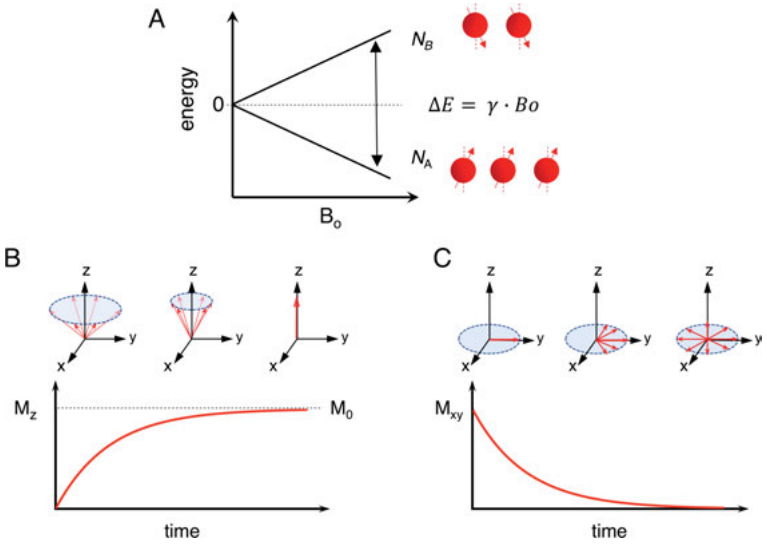

Figure 24. Principle of proton-based magnetic resonance imaging. (**A**) The hydrogen nuclei (protons) of water molecules align either parallel or anti-parallel to the axis of a static magnetic field (B_0). This yields two populations N_A and N_B of precessing nuclei with slightly different energies and thus a net bulk magnetization M_0. (**B**) Upon application of a short RF pulse, the net magnetization along the field axis (M_z) decreases but relaxes back to M_0 over time with time constant T_1, the longitudinal relaxation time. (**C**) The transverse component (M_{xy}) perpendicular to the field axis starts to de-phase with time constant T_2, the transverse relaxation time, as the precessing magnetic moment returns to the original orientation.

ty. Because only the excess number of spins in the lower-energy level can be excited, the probability of observing a transition through absorption of energy is quite small. For this reason, the sensitivity of nuclear magnetic resonance is much lower compared to fluorescence spectroscopy.

Nevertheless, the small but unequal occupancy of the two energy levels results in a bulk nuclear magnetization or magnetic moment, which is a collective property of the entire nuclear spin system of the sample. Upon application of a low-energy radio frequency (RF) pulse, this magnetic moment is brought out of alignment relative to the field axis and set into a precessional motion, which causes the emission of an RF signal. Its frequency is identical to the precessional frequency, also termed Larmor frequency, and is unique for each type of nucleus. After the bulk magnetic moment is brought out of alignment, the precessional motion gradually relaxes and reorients along the field axis, a process referred to as spin-lattice relaxation (Figure 24B). The rate at which the bulk magnetization (M) decays follows a first-order kinetics as described by Equation (6)

$$M_z = M_0(1 - e^{-t/T_1}) \tag{6}$$

where T_1 is the spin-lattice or longitudinal relaxation time, and M_0 refers to the original magnetization along the field axis. Because the relaxation rate depends

on the local environment, the detected MRI signal intensities vary between different types of tissues. Thus, a significant difference in the relaxation rate of neighboring tissue increases the contrast in the resulting image. In biological environments, T_1 ranges from a few tenths of a second to several seconds.

Besides the longitudinal relaxation of the magnetic moment, the transverse component (M_{xy}), which is oriented along the plane perpendicular to the field axis, starts to de-phase as the precessing magnetic moment returns to the original orientation (Figure 24C). Analogous to Equation (6), this process also follows a first-order kinetics as expressed by Equation (7)

$$M_{xy} = M_0 e^{-t/T_2} \tag{7}$$

where T_2 refers to the spin-spin or transverse relaxation time, and M_0 is again the original value of the bulk magnetization. As each relaxation mode is caused by a different mechanism, variations in the structure and composition of the environment produce different changes in the relaxation rates T_1 and T_2. Thus, by weighing the contributions of T_1 and T_2, a tissue-specific contrast can be achieved, which is of particular value for clinical imaging.

The relaxation rate of the magnetic moment can be enhanced by contrast agents, which are usually composed of a paramagnetic metal ion such as Mn(II), Fe(III), or Gd(III). After applying the RF pulse, the large fluctuating local magnetic field near the paramagnetic metal center increases the relaxation rate, thus resulting in an improved imaging contrast. The observed longitudinal and transverse relaxation rates both increase linearly with the concentration of the contrast agent [M] according to Equation (8)

$$\left(\frac{1}{T_n}\right)_{obs} = \left(\frac{1}{T_n}\right)_d + r_n[M] \qquad \text{with } n = 1,2 \tag{8}$$

where $(1/T_n)_d$ refers to the diamagnetic solvent relaxation rate in the absence of the paramagnetic contrast agent. The slope r_n is termed the relaxivity of the paramagnetic contrast agent and is usually expressed in units of $mM^{-1}\,s^{-1}$. The majority of contrast agents are based on kinetically inert Gd(III) complexes of multidentate ligands such as DOTA (see Figure 25A in Section 5.2) [123, 124]. With 7 unpaired electrons (S = 7/2), Gd(III)-based contrast agents are very effective at increasing both the longitudinal and transverse relaxation of water protons; however, because the dynamic range of $1/T_1$ in tissue is much larger compared to $1/T_2$, T_1-weighted MRI is the most common clinical imaging modality.

5.2. Design Principles of Metal Ion-Selective Magnetic Resonance Imaging Probes

Analogous to fluorescent probes, where analyte binding triggers an increase in fluorescence (Section 4.2), MRI probes respond with a change in relaxivity to generate an analyte-dependent imaging contrast [125]. Instead of using a fluorophore as a signal reporter (Figure 12), MRI probes employ a contrast agent whose relaxivity is modulated by interaction with the analyte [123, 126]. Likewise, MRI probes can only detect labile or exchangeable metal ions and are not suitable for quantitative measurements of total metal ion concentrations. A significant advantage of MRI over fluorescence-based imaging is the much increased analytical depth; however, the sensitivity of nuclear magnetic resonance is orders of magnitude lower. For common Gd(III)-based contrast agents, the limit of detection is around 30 μM [127]. To achieve a suitable MRI contrast, probes must therefore be employed at concentrations that are 10 to 100-times higher compared to fluorescence-based detection. Because the buffer depth or total concentration of the analyte should be higher than the probe concentration, the application of MRI is limited to visualizing only highly abundant metal ions.

To achieve a useful dynamic range, metal binding to the probe should trigger a significant change in relaxivity. The Gd(III)-promoted enhancement of the longitudinal relaxation rate $1/T_1$ can be attributed to direct inner-sphere interactions and outer-sphere contributions. As expressed by Equation (9), the inner-sphere longitudinal relaxation rate depends on several factors, including the number of coordinated water molecules (q) and their residence lifetime (τ_m) [128]. The parameters P_m refer to the mole fraction of coordinated water molecules, and T_{1m} corresponds to their longitudinal relaxation time.

$$\left(\frac{1}{T_1}\right) = \frac{qP_m}{T_{1m} + \tau_m} \tag{9}$$

Based on Equation (9), it becomes apparent that for very fast water exchange rates ($\tau_m \ll T_{1m}$), the observed relaxation rate is proportional to the number of coordinated water molecules (q) and their relaxation rate $1/T_{1m}$. This relationship provided the underlying rationale for the design of the first metal-ion responsive MRI probe DOPTA-Gd (Figure 25B) [129]. Similar to the ratiometric fluorescent probe fura-2 (Figure 17), DOPTA-Gd employs a functionalized BAPTA chelator to achieve a Ca(II)-selective MRI response through two attached Gd(III) reporters. Upon binding of Ca(II), the probe undergoes a coordinative rearrangement of the pendant iminoacetate arms, thus allowing water to bind directly to the Gd(III) center. As a consequence, the observed relaxivity increases over 80 % from 3.3 $mM^{-1}\,s^{-1}$ to 5.8 $mM^{-1}\,s^{-1}$. Inspired by this design principle, numerous MRI probes have been created to detect other biologically relevant metal ions [123, 126, 130].

As an alternative approach, several Gd(III)-based MRI probes have been developed based on modulating the rotational correlation time τ_r (Figure 25A). This

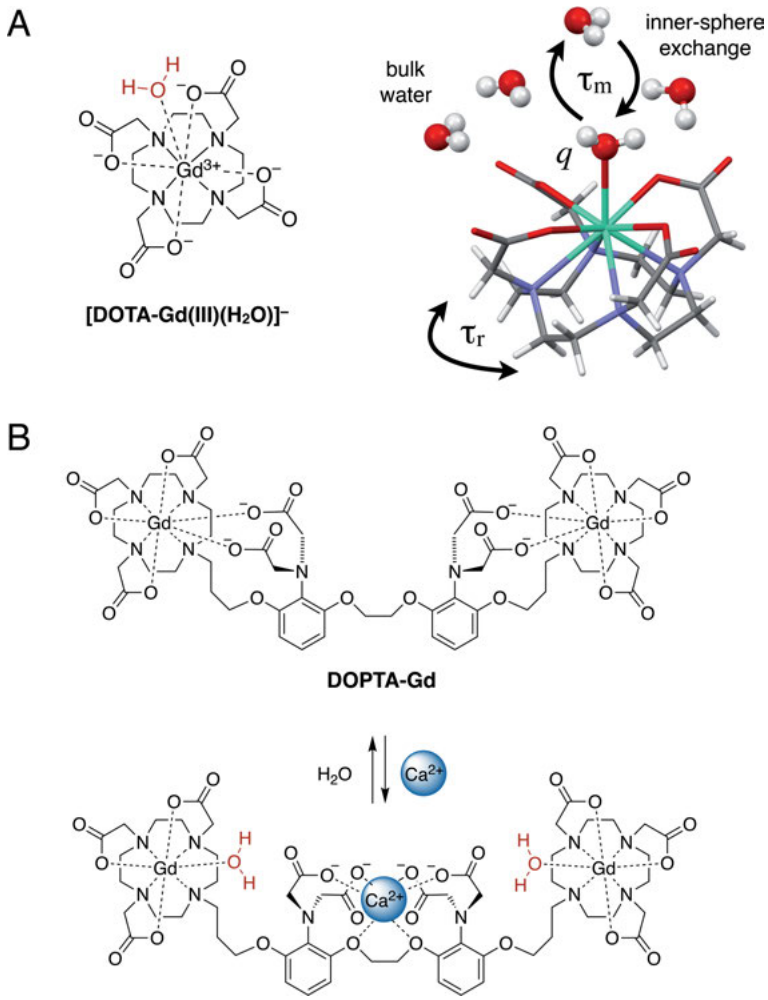

Figure 25. Design principle for metal-responsive MRI-probes. (**A**) The enhancement of the longitudinal relaxation (T1) of water protons by Gd(III) complexes depends on the number of coordinated water molecules (q), the rotational correlation time τ_r, and the lifetime of τ_m of Gd(III)-bound water. (**B**) The MRI probe DOPTA-Gd responses with an 80 % relaxivity enhancement upon saturation with Ca(II), achieved through a coordinative rearrangement of the iminodiacetic acid groups to allow water molecules (red) coordinate to the Gd(III) center.

can be achieved, for example, by metal ion-mediated ternary complex formation with a large protein whose rotational motion is inherently much slower. Based on this approach, the Gd(III) complex GD-CP207 was designed to interact with human serum albumin (HSA) in a Zn(II)-dependent fashion (Figure 26A). While the free probe does not bind significantly to HSA, it forms a robust ternary complex in the presence of Zn(II) to yield a nearly 2-fold increase in relaxivity [131]. This

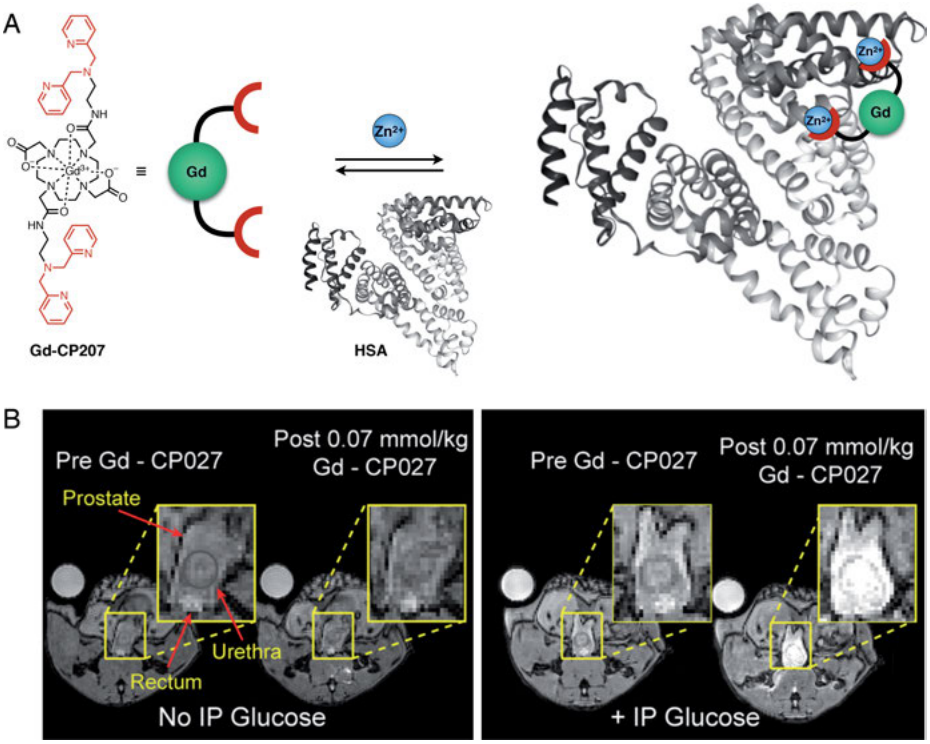

Figure 26. Design of a Zn(II)-responsive contrast agent based on modulation of the rotational correlation time τ_r. (**A**) In the presence of Zn(II), the MRI probe Gd-CP207 forms a ternary complex with human serum albumin, thus increasing the relaxivity by slowing down rotational tumbling. (**B**) Magnetic resonance imaging of glucose-stimulated Zn(II)-release in the mouse prostate. **Left**: In the absence of glucose, no contrast enhancement was observed upon injection of Gd-CP207. **Right**: After glucose stimulation, a dramatic contrast enhancement was observed in the dorsolateral prostate and the urethra (zoomed image). Data adopted with permission from [131]; copyright 2016, National Academy of Science.

contrast enhancement was successfully employed for visualizing differences in the glucose-stimulated Zn(II)-release from secretory prostate cells in a healthy and malignant mouse model [131] (Figure 26B). Recent correlative SXRF imaging studies provided detailed insights into the mechanism of the glucose-promoted zinc release [132]. A drawback of probes that modulate the MRI contrast based on changes in the rotational correlation time is their strong dependence on the magnetic field strength. While the image resolution increases at higher field strength, the effect of changing τ_r on the proton relaxation is substantially diminished. This challenge has been recently addressed with the development of a fast-field cycling MRI approach [133]. Instead of measuring the absolute difference of the proton relaxation rate within a static magnetic field, the method exploits the change of the longitudinal relaxation rate as the field strength is altered during

image acquisition. Based on this approach, an over 1.6-fold contrast enhancement was achieved for a Zn(II)-responsive MRI probe at a field strength of 3T, whereas conventional static MRI yielded no detectable contrast change [133].

6. CONCLUSIONS

Modern microanalytical techniques have become an indispensable tool for exploring trace metals in biological systems. While traditional methods for trace element quantifications were limited to the analysis of bulk samples, rapid technological advances led to significant improvements in detection limits and paved the way towards mapping spatial distributions of trace elements down to the nanoscale regime. With the ability to analyze frozen, hydrated samples, SXRF microscopy ranks among the most powerful techniques to visualize and quantify elemental distributions in biological samples across vast length scales from millimeter to submicron dimensions. Advances in X-ray optics and detector technologies significantly reduced data acquisition times and enabled high-resolution microtomography of specimens as large as zebrafish embryos [40]. However, SXRF imaging relies on sophisticated instrumentation that is only available at synchrotron beamlines, thus significantly limiting the number and size of samples that can be analyzed. For trace elemental mapping at the mesoscale, commercially available LA-ICP-MS instruments represent a formidable alternative to SXRF microscopy [134]. By imaging the trace metal distribution in serial sections, it is possible to reconstruct three-dimensional volumes [135], thus opening up the exciting prospect of creating metallomic atlases of entire organs. For subcellular imaging, the sensitivity of nano SIMS is comparable to routine SXRF microscopy; however, the narrow analytical depth requires sectioning of the specimen similar to electron microscopy. Because all of these techniques are limited to the analysis of fixed samples, the development of suitable preparation methods plays a central role in ensuring that the trace metal content and distribution are preserved as close as possible to the native state.

Among the techniques discussed in this chapter, only MRI and visible-light fluorescence microscopy are suitable to study the dynamics of endogenous trace metals in living organisms; however, both methods rely on chemical probes to detect the analyte and thus capture only the exchangeable metal ion pool that can interact with the probe. Although direct detection of Mn and Fe is feasible by quantitative MRI [136], it is best used in cases where only one of the paramagnetic metals undergoes a concentration change, and no other tissue features contribute to the MRI signal [137]. The unlimited analytical depth offered by MRI complements a major limitation of fluorescence microscopy when studying whole organisms, albeit at the expense of lower resolution and sensitivity. To address the sensitivity challenge of MRI, hyperpolarization of ^{13}C, ^{15}N, or ^{129}Xe nuclei ranks among the most promising approaches. In this technique, the net spin polarization is transiently enhanced above thermal equilibrium levels to achieve 4–5 orders of magnitude gains in detection sensitivity [138]. By labeling

chelators with ^{129}Xe, ^{13}C, or ^{15}N nuclei, various metal ion-responsive probes have been described [139–142]. As an alternative approach to MRI, photoacoustic molecular imaging (PAI) is emerging as a powerful biomedical imaging modality [143]. Based on the photoacoustic effect [144], this technique employs a pulsed near-infrared (NIR) light source to excite chromophores with large molar extinction coefficients. Thermal relaxation generates ultrasonic waves, which can be detected by ultrasound transducers to create a three-dimensional image. Compared to traditional NIR imaging, PAI benefits from the much weaker scattering of acoustic waves compared to light to produce a superior imaging contrast, although with a lower spatial resolution. Analogous to fluorescence imaging, the technique relies on specifically designed probes to detect an analyte of interest [145]. For example, if analyte-binding induces a large chromatic shift in molar absorptivity, the fractional saturation of the probe can be evaluated analogous to fluorescence-based ratiometric imaging (Section 4.3).

While indirect detection methods lack the ability to quantify total metal levels, they offer unique opportunities to tailor probe molecules towards specific applications. For example, the photophysical characteristics of an optical probe can be tuned for TPEM by enhancing the 2PA cross-section, or it may be optimized for alternative detection schemes, such as synchronously amplified fluorescence image recovery (SAFIRe) to suppress fluorescence background [146–148]. Moreover, target-specific tagging methods such as the SNAP-tag [149] or HaloTAG [150] provide opportunities to direct synthetic probes to specific locations within cells or even whole organisms [151, 152].

As each detection method offers distinct strengths (Table 1), the combination of multiple imaging modalities represents a particularly powerful approach to explore trace metal distributions across different length scales [153] and to cross-validate data acquired by different techniques [15, 132, 136]. To this end, the development of multimodal probes that can be visualized by several imaging techniques is especially valuable for bridging the limitations and harnessing the benefits of both direct and indirect detection methods. A cross-disciplinary approach involving the combination of different imaging techniques and bioanalytical methods holds also great promise to tackle another significant, yet mostly unsolved challenge, the in situ elucidation of the trace metal speciation. The integration of trace metal analysis by ICP-MS with mass spectrometry-based proteomics analyzes represents, for example, a particularly promising approach to tackle this complex problem [154]. Without a doubt, trace metal imaging techniques have matured into a vibrant research area and represent an indispensable tool for deciphering the complex role of metals within biological systems.

ACKNOWLEDGMENTS

Financial support from the National Institutes of Health (GM067169 and GM136404), the National Science Foundation (CHE-1306943), and the Georgia Institute of Technology is gratefully acknowledged.

ABBREVIATIONS AND DEFINITIONS

2PA	two-photon absorption
AM	acetoxymethyl
ART	algebraic reconstruction technique
BAPTA	1,2-bis(*o*-aminophenoxy)ethane-*N,N,N′,N′*-tetraacetic acid
CT	computed tomography
CTEA	*N,N*-bis[2-(carboxymethyl)thioethyl]amine
DOTA	tetraazacyclododecane-1,4,7,10-tetraacetic acid
DPEN	*N,N*-di(2-picolyl)ethylenediamine
DTDP	2,2′-dithiodipyridine
EPXMA	electron-probe X-ray microanalysis
ESIPT	excited-state intramolecular proton transfer
ET	electron transfer state
FRET	Förster resonance energy transfer
GM	Göppert-Mayer (unit)
HOMO	highest-energy occupied molecular orbital
HSA	human serum albumin
IC	internal conversion
ICP-MS	inductively-coupled plasma mass spectrometry
ICT	intramolecular charge transfer
KB	Kirkpatrick-Baez (mirror)
LA-ICP-MS	laser ablation-inductively coupled plasma mass spectrometry
LUMO	lowest-energy unoccupied molecular orbital
MLEM	maximum likelihood expectation maximization
MRI	magnetic resonance imaging
NA	numerical aperture
NIR	near-infrared
PAI	photoacoustic imaging
PET	photoinduced electron transfer
PIXE	particle induced X-ray emission
PLT	progressive lowering of temperature
QTOF	quadrupole time-of-flight
RF	radio frequency
SIMS	secondary ionization mass spectrometry
SIRT	simultaneous iterative reconstruction technique
SR-FTIR	synchrotron radiation-based Fourier transform infrared
STEM	scanning transition electron microscopy
SXRF	synchrotron-based X-ray fluorescence
TOF-MS	time-of-flight mass spectrometry
TPEM	two-photon excitation microscopy
XAS	X-ray absorption spectroscopy
XRF	X-ray fluorescence

REFERENCES

1. M. Perls, *Virchows Arch. Path. Anat.* **1867**, *39*, 42–48.
2. D. L. Schonberg, D. M. McTigue, *Exp. Neurol.* **2009**, *218*, 64–74.
3. R. McRae, P. Bagchi, S. Sumalekshmy, C. J. Fahrni, *Chem. Rev.* **2009**, *109*, 4780–4827.
4. V. L. Dressler, E. I. Müller, D. Pozebon, *Adv. Exp. Med Biol.* **2018**, *1055*, 139–181.
5. E. J. New, V. C. Wimmer, D. J. Hare, *Cell. Chem. Biol.* **2018**, *25*, 7–18.
6. M. T. Morgan, D. Bourassa, S. Harankhedkar, A. M. McCallum, S. A. Zlatic, J. S. Calvo, G. Meloni, V. Faundez, C. J. Fahrni, *Proc. Natl. Acad. Sci. USA* **2019**, *116*, 12167–12172.
7. T. D. Rae, P. J. Schmidt, R. A. Pufahl, V. C. Culotta, T. V. O'Halloran, *Science* **1999**, *284*, 805–808.
8. J. L. Vinkenborg, T. J. Nicolson, E. A. Bellomo, M. S. Koay, G. A. Rutter, M. Merkx, *Nat. Meth.* **2009**, *6*, 737–740.
9. M. O. Krause, *J. Phys. Chem. Ref. Data* **1979**, *8*, 307–327.
10. C. J. Fahrni, *Curr. Opin. Chem. Biol.* **2007**, *11*, 121–127.
11. M. J. Pushie, I. J. Pickering, M. Korbas, M. J. Hackett, G. N. George, *Chem. Rev.* **2014**, *114*, 8499–8541.
12. R. Jenkins, R. Manne, R. Robin, C. Senemaud, *X-Ray Spectrom.* **1991**, *20*, 149–155.
13. G. Johnson, E. W. White, *Amer. Soc. Test. Mater. Data Ser. DS-46* **1970**, *33*, 1–38.
14. H. H. Harris, A. Levina, C. T. Dillon, I. Mulyani, B. Lai, Z. H. Cai, P. A. Lay, *J. Biol. Inorg. Chem.* **2005**, *10*, 105–118.
15. L. Yang, R. McRae, M. M. Henary, R. Patel, B. Lai, S. Vogt, C. J. Fahrni, *Proc. Natl. Acad. Sci. USA* **2005**, *102*, 11179–11184.
16. S. Matsuyama, M. Shimura, H. Mimura, M. Fujii, H. Yumoto, Y. Sano, M. Yabashi, Y. Nishino, K. Tamasaku, T. Ishikawa, *X-Ray Spectrom.* **2009**, *38*, 89–94.
17. L. Perrin, A. Carmona, S. Roudeau, R. Ortega, *J. Anal. Atom. Spectrom.* **2015**, *30*, 2525–2532.
18. E. A. Carter, B. S. Rayner, A. I. McLeod, L. E. Wu, C. P. Marshall, A. Levina, J. B. Aitken, P. K. Witting, B. Lai, Z. H. Cai, S. Vogt, Y. C. Lee, C. I. Chen, M. J. Tobin, H. H. Harris, P. A. Lay, *Mol. Biosyst.* **2010**, *6*, 1316–1322.
19. J. Chwiej, M. Szczerbowska-Boruchowska, M. Lankosz, S. Wojcik, G. Falkenberg, Z. Stegowski, Z. Setkowicz, *Spectrochim. Acta B* **2005**, *60*, 1531–1537.
20. M. J. Hackett, J. A. McQuillan, F. El-Assaad, J. B. Aitken, A. Levina, D. D. Cohen, R. Siegele, E. A. Carter, G. E. Grau, N. H. Hunt, P. A. Lay, *Analyst* **2011**, *136*, 2941–2952.
21. S. Matsuyama, M. Shimura, M. Fujii, K. Maeshima, H. Yumoto, H. Mimura, Y. Sano, M. Yabashi, Y. Nishino, K. Tamasaku, Y. Ishizaka, T. Ishikawa, K. Yamauchi, *X-Ray Spectrom.* **2010**, *39*, 260–266.
22. Q. L. Jin, T. Paunesku, B. Lai, S. C. Gleber, S. Chen, L. Finney, D. Vine, S. Vogt, G. Woloschak, C. Jacobsen, *J. Microsc.* **2017**, *265*, 81–93.
23. S. M. Herd, J. Camakaris, R. Christofferson, P. Wookey, D. M. Danks, *Biochem. J.* **1987**, *247*, 341–347.
24. V. V. Lider, *J. Surf. Invest. X-Ray Synchr. Neutr. Tech.* **2019**, *13*, 670–682.
25. H. Mimura, Y. Takei, T. Kume, Y. Takeo, H. Motoyama, S. Egawa, Y. Matsuzawa, G. Yamaguchi, Y. Senba, H. Kishimoto, H. Ohashi, *Rev. Sci. Instrum.* **2018**, *89*, 093104.
26. H. Yumoto, T. Koyama, S. Matsuyama, Y. Kohmura, K. Yamauchi, T. Ishikawa, H. Ohashi, *Sci. Rep.* **2017**, *7*, 16408.
27. R. McRae, B. Lai, C. J. Fahrni, *Metallomics* **2013**, *5*, 52–61.
28. S. Chen, J. Deng, Y. Yuan, C. Flachenecker, R. Mak, B. Hornberger, Q. Jin, D. Shu, B. Lai, J. Maser, C. Roehrig, T. Paunesku, S. C. Gleber, D. J. Vine, L. Finney, J. VonOsinski, M. Bolbat, I. Spink, Z. Chen, J. Steele, D. Trapp, J. Irwin, M. Feser, E.

Snyder, K. Brister, C. Jacobsen, G. Woloschak, S. Vogt, *J. Synchrotron Radiat.* **2014**, *21*, 66–75.
29. J. Deng, D. J. Vine, S. Chen, Y. S. G. Nashed, Q. Jin, N. W. Phillips, T. Peterka, R. Ross, S. Vogt, C. J. Jacobsen, *Proc. Natl. Acad. Sci. USA* **2015**, *112*, 2314–2319.
30. J. Deng, D. J. Vine, S. Chen, Q. Jin, Y. S. G. Nashed, T. Peterka, S. Vogt, C. Jacobsen, *Sci. Rep.* **2017**, *7*.
31. Y. Komine, L. L. Eggink, H. Park, J. K. Hoober, *Planta* **2000**, *210*, 897–905.
32. E. Nazaretski, H. Yan, K. Lauer, N. Bouet, X. Huang, W. Xu, J. Zhou, D. Shu, Y. Hwu, Y. S. Chu, *J. Synchrotron Radiat.* **2017**, *24*, 1113–1119.
33. S. Bajt, M. Prasciolu, H. Fleckenstein, M. Domaracký, H. N. Chapman, A. J. Morgan, O. Yefanov, M. Messerschmidt, Y. Du, K. T. Murray, V. Mariani, M. Kuhn, S. Aplin, K. Pande, P. Villanueva-Perez, K. Stachnik, J. P. Chen, A. Andrejczuk, A. Meents, A. Burkhardt, D. Pennicard, X. Huang, H. Yan, E. Nazaretski, Y. S. Chu, C. E. Hamm, *Light Sci. Appl.* **2018**, *7*, 17162–17162.
34. P. E. Kinahan, M. Defrise, R. Clackdoyle, *Analytic Image Reconstruction Methods*, in Emission Tomography: The Fundamentals of PET and SPECT. Eds M. N. Wernick, J. N. Aarsvold, Elsevier, London, UK, **2004**, pp. 421–442.
35. G. L. Zeng, *Medical Image Reconstruction*, Higher Education Press, Beijing, and Springer, Heidelberg, **2010**.
36. R. Gordon, R. Bender, G. T. Herman, *J. Theor. Biol.* **1970**, *29*, 471–481.
37. L. A. Shepp, Y. Vardi, *IEEE Trans. Med. Imag.* **1982**, *1*, 113–122.
38. S. A. Kim, T. Punshon, A. Lanzirotti, L. Li, J. M. Alonso, J. R. Ecker, J. Kaplan, M. L. Guerinot, *Science* **2006**, *314*, 1295–1298.
39. M. D. de Jonge, C. Holzner, S. B. Baines, B. S. Twining, K. Ignatyev, J. Diaz, D. L. Howard, D. Legnini, A. Miceli, I. McNulty, C. J. Jacobsen, S. Vogt, *Proc. Natl. Acad. Sci. USA* **2010**, *107*, 15676–15680.
40. D. Bourassa, S. C. Gleber, S. Vogt, H. Yi, F. Will, H. Richter, C. H. Shin, C. J. Fahrni, *Metallomics* **2014**, *6*, 1648–1655.
41. D. Bourassa, S. C. Gleber, S. Vogt, C. H. Shin, C. J. Fahrni, *Metallomics* **2016**, *8*, 1122–1130.
42. X. W. Ren, L. T. Weng, C. M. Chan, K. M. Ng, *Anal. Chem.* **2012**, *84*, 8497–8504.
43. S. Jung, M. Foston, U. C. Kalluri, G. A. Tuskan, A. J. Ragauskas, *Angew. Chem. Int. Ed. Engl.* **2012**, *51*, 12005–12008.
44. O. J. G. M. Goor, H. M. Keizer, A. L. Bruinen, M. G. J. Schmitz, R. M. Versteegen, H. M. Janssen, R. M. A. Heeren, P. Y. W. Dankers, *Adv. Mater.* **2017**, *29*, 1604652.
45. M. S. Wagner, *Anal. Chem.* **2005**, *77*, 911–922.
46. J. S. Fletcher, S. Rabbani, A. Henderson, P. Blenkinsopp, S. P. Thompson, N. P. Lockyer, J. C. Vickerman, *Anal. Chem.* **2008**, *80*, 9058–9064.
47. J. S. Fletcher, J. C. Vickerman, *Anal. Bioanal. Chem.* **2010**, *396*, 85–104.
48. J. Nuñez, R. Renslow, J. B. Cliff, C. R. Anderton, *Biointerphases* **2018**, *13*, 03B301.
49. S. Ghosal, S. J. Fallon, T. J. Leighton, K. E. Wheeler, M. J. Kristo, I. D. Nutcheon, P. K. Weber, *Anal. Chem.* **2008**, *80*, 5986–5992.
50. A. Hong-Hermesdorf, M. Miethke, S. D. Gallaher, J. Kropat, S. C. Dodani, J. Chan, D. Barupala, D. W. Domaille, D. I. Shirasaki, J. A. Loo, P. K. Weber, J. Pett-Ridge, T. L. Stemmler, C. J. Chang, S. S. Merchant, *Nat. Chem. Biol.* **2014**, *10*, 1034–1042.
51. J. S. Becker, A. Matusch, B. Wu, *Anal. Chim. Acta* **2014**, *835*, 1–18.
52. A. L. Gray, *Analyst* **1985**, *110*, 551–556.
53. B. Hattendorf, C. Latkoczy, D. Günther, *Anal. Chem.* **2003**, *75*, 341A–347A.
54. R. E. Russo, X. L. Mao, S. S. Mao, *Anal. Chem.* **2002**, *74*, 70A–77A.
55. I. Horn, M. Guillong, D. Günther, *Appl. Surf. Sci.* **2001**, *182*, 91–102.
56. R. S. Houk, *Anal. Chem.* **1986**, *58*, 97A–105A.

57. H. A. Wang, D. Grolimund, C. Giesen, C. N. Borca, J. R. Shaw-Stewart, B. Bodenmiller, D. Günther, *Anal. Chem.* **2013**, *85*, 10107–10116.
58. S. J. M. Van Malderen, E. Vergucht, M. De Rijcke, C. Janssen, L. Vincze, F. Vanhaecke, *Anal. Chem.* **2016**, *88*, 5783–5789.
59. D. Hare, C. Austin, P. Doble, *Analyst* **2012**, *137*, 1527–1537.
60. D. J. Hare, J. K. Lee, A. D. Beavis, A. van Gramberg, J. George, P. A. Adlard, D. I. Finkelstein, P. A. Doble, *Anal. Chem.* **2012**, *84*, 3990–3997.
61. S. G. Boaru, U. Merle, R. Uerlings, A. Zimmermann, S. Weiskirchen, A. Matusch, W. Stremmel, R. Weiskirchen, *BMC Neurosci.* **2014**, *15*, 98.
62. J. A. Cotruvo Jr, A. T. Aron, K. M. Ramos-Torres, C. J. Chang, *Chem. Soc. Rev.* **2015**, *44*, 4400–4414.
63. X. Qian, Z. Xu, *Chem. Soc. Rev.* **2015**, *44*, 4487–4493.
64. C. J. Fahrni, D. Bourassa, R. Dikdan, *Metals in the Brain: Measurement and Imaging*, *Neuromethods*, Vol. 124, Ed. A. R. White, Springer, New York, USA **2017**, pp. 71–107.
65. Y. Hitomi, C. E. Outten, T. V. O'Halloran, *J. Am. Chem. Soc.* **2001**, *123*, 8614–8615.
66. A. M. Hessels, M. Merkx, *Metallomics* **2015**, *7*, 258–266.
67. K. A. Price, J. L. Hickey, Z. G. Xiao, A. G. Wedd, S. A. James, J. R. Liddell, P. J. Crouch, A. R. White, P. S. Donnelly, *Chem. Sci.* **2012**, *3*, 2748–2759.
68. M. T. Morgan, P. Bagchi, C. J. Fahrni, *J. Am. Chem. Soc.* **2011**, *133*, 15906–15909.
69. R. A. Marcus, N. Sutin, *Biochim. Biophys. Acta* **1985**, *811*, 265–322.
70. A. F. Chaudhry, M. Verma, M. T. Morgan, M. M. Henary, N. Siegel, J. M. Hales, J. W. Perry, C. J. Fahrni, *J. Am. Chem. Soc.* **2010**, *132*, 737–747.
71. J. Cody, S. Mandal, L. C. Yang, C. J. Fahrni, *J. Am. Chem. Soc.* **2008**, *130*, 13023–13032.
72. D. Rehm, A. Weller, *Isr. J. Chem.* **1970**, *8*, 259–271.
73. C. J. Fahrni, L. C. Yang, D. G. VanDerveer, *J. Am. Chem. Soc.* **2003**, *125*, 3799–3812.
74. R. Lincoln, L. E. Greene, K. Krumova, Z. Ding, G. Cosa, *J. Phys. Chem. A* **2014**, *118*, 10622–10630.
75. M. Verma, A. F. Chaudhry, C. J. Fahrni, *Org. Biomol. Chem.* **2009**, *7*, 1536–1546.
76. K. Rurack, L. Julia, B. Schulz, M. Maus, G. Reck, U. Resch-Genger, *J. Phys. Chem. A* **2000**, *104*, 6171–6188.
77. K. Rurack, *Spectrochim. Acta A* **2001**, *57*, 2161–2195.
78. M. Verma, A. F. Chaudhry, M. T. Morgan, C. J. Fahrni, *Org. Biomol. Chem.* **2010**, *8*, 363–370.
79. A. F. Chaudhry, S. Mandal, K. I. Hardcastle, C. J. Fahrni, *Chem. Sci.* **2011**, *2*, 1016–1024.
80. M. T. Morgan, P. Bagchi, C. J. Fahrni, *Dalton Trans.* **2013**, *42*, 3240–3248.
81. M. T. Morgan, S. Sumalekshmy, M. Sarwar, H. Beck, S. Crooke, C. J. Fahrni, *J. Phys. Chem. B* **2014**, *118*, 14196–14202.
82. W. Humphrey, A. Dalke, K. Schulten, *J. Mol. Graphics* **1996**, *14*, 33–38.
83. M. T. Morgan, A. M. McCallum, C. J. Fahrni, *Chem. Sci.* **2016**, *7*, 1468–1473.
84. G. Grynkiewicz, M. Poenie, R. Y. Tsien, *J. Biol. Chem.* **1985**, *260*, 3440–3450.
85. P. W. Tinning, A. J. P. M. Franssen, S. U. Hridi, T. J. Bushell, G. McConnell, *J. Microsc.* **2018**, *269*, 212–220.
86. R. Y. Tsien, *Nature* **1981**, *290*, 527–528.
87. P. Sasse, J. Zhang, L. Cleemann, M. Morad, J. Hescheler, B. K. Fleischmann, *J. Gen. Physiol.* **2007**, *130*, 133–144.
88. A. P. Demchenko, *J. Fluoresc.* **2010**, *20*, 1099–1128.
89. A. P. Demchenko, K. C. Tang, P. T. Chou, *Chem. Soc. Rev.* **2013**, *42*, 1379–1408.
90. M. M. Henary, C. J. Fahrni, *J. Phys. Chem. A* **2002**, *106*, 5210–5220.
91. M. M. Henary, Y. G. Wu, C. J. Fahrni, *Chem. Eur. J.* **2004**, *10*, 3015–3025.
92. J. L. Vinkenborg, M. S. Koay, M. Merkx, *Curr. Opin. Chem. Biol.* **2010**, *14*, 231–237.

93. K. P. Carter, A. M. Young, A. E. Palmer, *Chem. Rev.* **2014**, *114*, 4564–4601.
94. W. Denk, J. H. Strickler, W. W. Webb, *Science* **1990**, *248*, 73–76.
95. M. Pawlicki, H. A. Collins, R. G. Denning, H. L. Anderson, *Angew. Chem. Int. Ed. Engl.* **2009**, *48*, 3244–3266.
96. F. Helmchen, W. Denk, *Nat. Methods* **2005**, *2*, 932–940.
97. S. Skylaki, O. Hilsenbeck, T. Schroeder, *Nat. Biotechnol.* **2016**, *34*, 1137–1144.
98. M. Göppert-Mayer, *Ann. Phys.* **1931**, *9*, 273–294.
99. W. Kaiser, C. G. V. Garrett, *Phys. Rev. Lett.* **1961**, *7*, 229–231.
100. P. T. C. So, C. Y. Dong, B. R. Masters, K. M. Berland, *Annu. Rev. Biomed. Eng.* **2000**, *2*, 399–429.
101. W. R. Zipfel, R. M. Williams, W. W. Webb, *Nat. Biotechnol.* **2003**, *21*, 1368–1376.
102. P. G. Bush, D. L. Wokosin, A. C. Hall, *Front Biosci* **2007**, *12*, 2646–2657.
103. C. N. Pace, F. Vajdos, L. Fee, G. Grimsley, T. Gray, *Protein Sci.* **1995**, *4*, 2411–2423.
104. G. S. He, L. S. Tan, Q. Zheng, P. N. Prasad, *Chem. Rev.* **2008**, *108*, 1245–1330.
105. N. S. Makarov, M. Drobizhev, A. Rebane, *Opt. Express* **2008**, *16*, 4029–4047.
106. M. A. Albota, C. Xu, W. W. Webb, *Appl. Optics* **1998**, *37*, 7352–7356.
107. J. Mütze, V. Iyer, J. J. Macklin, J. Colonell, B. Karsh, Z. Petrášek, P. Schwille, L. L. Looger, L. D. Lavis, T. D. Harris, *Biophys. J.* **2012**, *102*, 934–944.
108. M. Albota, D. Beljonne, J. L. Brédas, J. E. Ehrlich, J. Y. Fu, A. A. Heikal, S. E. Hess, T. Kogej, M. D. Levin, S. R. Marder, D. McCord-Maughon, J. W. Perry, H. Röckel, M. Rumi, G. Subramaniam, W. W. Webb, X. L. Wu, C. Xu, *Science* **1998**, *281*, 1653–1656.
109. S. Sumalekshmy, C. J. Fahrni, *Chem. Mater.* **2011**, 823–830.
110. A. Bergman, J. Jortner, *Chem. Phys. Lett.* **1974**, *26*, 323–326.
111. D. Kim, H. Moon, S. H. Baik, S. Singha, Y. W. Jun, T. Wang, K. H. Kim, B. S. Park, J. Jung, I. Mook-Jung, K. H. Ahn, *J. Am. Chem. Soc.* **2015**, *137*, 6781–6789.
112. D. Cvejn, E. Michail, K. Seintis, M. Klikar, O. Pytela, T. Mikysek, N. Almonasy, M. Ludwig, V. Giannetas, M. Fakis, F. Bureš, *RSC Adv.* **2016**, *6*, 12819–12828.
113. H. Y. Woo, B. Liu, B. Kohler, D. Korystov, A. Mikhailovsky, G. C. Bazan, *J. Am. Chem. Soc.* **2005**, *127*, 14721–14729.
114. S. J. K. Pond, O. Tsutsumi, M. Rumi, O. Kwon, E. Zojer, J.-L. Brédas, S. R. Marder, J. W. Perry, *J. Am. Chem. Soc.* **2004**, *126*, 9291–9306.
115. H. M. Kim, B. R. Cho, *Chem. Rev.* **2015**, *115*, 5014–5055.
116. C. S. Lim, B. R. Cho, *Tetrahedron* **2015**, *71*, 8219–8249.
117. H. M. Kim, M. S. Seo, M. J. An, J. H. Hong, Y. S. Tian, J. H. Choi, O. Kwon, K. J. Lee, B. R. Cho, *Angew. Chem. Int. Ed. Engl.* **2008**, *47*, 5167–5170.
118. C. S. Lim, D. W. Kang, Y. S. Tian, J. H. Han, H. L. Hwang, B. R. Cho, *Chem. Commun.* **2010**, *46*, 2388–2390.
119. M. Y. Kang, C. S. Lim, H. S. Kim, E. W. Seo, H. M. Kim, O. Kwon, B. R. Cho, *Chem. Eur. J.* **2012**, *18*, 1953–1960.
120. D. L. Wokosin, C. M. Loughrey, G. L. Smith, *Biophys. J.* **2004**, *86*, 1726–1738.
121. S. Sumalekshmy, M. M. Henary, N. Siegel, P. V. Lawson, Y. G. Wu, K. Schmidt, J. L. Brédas, J. W. Perry, C. J. Fahrni, *J. Am. Chem. Soc.* **2007**, *129*, 11888–11889.
122. D. Bourassa, C. M. Elitt, A. M. McCallum, S. Sumalekshmy, R. L. McRae, M. T. Morgan, N. Siegel, J. W. Perry, P. A. Rosenberg, C. J. Fahrni, *ACS Sens.* **2018**, *3*, 458–467.
123. J. Wahsner, E. Gale, A. Rodríguez-Rodríguez, P. Caravan, *Chem. Rev.* **2019**, *119*, 957–1057.
124. H. Li, T. J. Meade, *J. Am. Chem. Soc.* **2019**, *141*, 17025–17041.
125. Z. Xu, C. Liu, S. Zhao, S. Chen, Y. Zhao, *Chem. Rev.* **2019**, *119*, 195–230.
126. E. L. Que, C. J. Chang, *Chem. Soc. Rev.* **2010**, *39*, 51–60.
127. P. Wedeking, C. H. Sotak, J. Telser, K. Kumar, C. A. Chang, M. F. Tweedle, *Magn. Reson. Imaging* **1992**, *10*, 97–108.

128. R. B. Lauffer, *Chem. Rev.* **1987**, *87*, 901–927.
129. W.-H. Li, S. E. Fraser, T. J. Meade, *J. Am. Chem. Soc.* **1999**, *121*, 1413–1414.
130. V. C. Pierre, S. M. Harris, S. L. Pailloux, *Acc. Chem. Res.* **2018**, *51*, 342–351.
131. M. V. Clavijo Jordan, S. T. Lo, S. Chen, C. Preihs, S. Chirayil, S. Zhang, P. Kapur, W. Li, L. M. De Leon-Rodriguez, A. J. Lubag, N. M. Rofsky, A. D. Sherry, *Proc. Natl. Acad. Sci. USA* **2016**, *113*, E5464–E5471.
132. V. Clavijo Jordan, A. Al-Ebraheem, K. Geraki, E. Dao, A. F. Martins, S. Chirayil, M. Farquharson, A. D. Sherry, *Inorg. Chem.* **2019**, *58*, 13654–13660.
133. M. Bödenler, K. P. Malikidogo, J. F. Morfin, C. S. Aigner, É. Tóth, C. S. Bonnet, H. Scharfetter, *Chem. Eur. J.* **2019**, *25*, 8236–8239.
134. K. M. Davies, D. J. Hare, S. Bohic, S. A. James, J. L. Billings, D. I. Finkelstein, P. A. Doble, K. L. Double, *Anal. Chem.* **2015**, *87*, 6639–6645.
135. B. Paul, D. J. Hare, D. P. Bishop, C. Paton, V. T. Nguyen, N. Cole, M. M. Niedwiecki, E. Andreozzi, A. Vais, J. L. Billings, L. Bray, A. I. Bush, G. McColl, B. R. Roberts, P. Adlard, D. I. Finkelstein, J. Hellstrom, J. M. Hergt, J. D. Woodhead, P. A. Doble, *Chem. Sci.* **2015**, *6*, 5383–5393.
136. K. L. Desmond, A. Al-Ebraheem, R. Janik, W. Oakden, J. M. Kwiecien, W. Dabrowski, R. Rola, K. Geraki, M. J. Farquharson, G. J. Stanisz, N. A. Bock, *NMR Biomed.* **2016**, *29*, 985–998.
137. N. A. Bock, F. F. Paiva, G. C. Nascimento, J. D. Newman, A. C. Silva, *Brain Res.* **2008**, *1198*, 160–170.
138. P. Nikolaou, B. M. Goodson, E. Y. Chekmenev, *Chem. Eur. J.* **2015**, *21*, 3156–3166.
139. N. Kotera, N. Tassali, E. Léonce, C. Boutin, P. Berthault, T. Brotin, J. P. Dutasta, L. Delacour, T. Traoré, D. Buisson, F. Taran, S. Coudert, B. Rousseau, *Angew. Chem. Int. Ed. Engl.* **2012**, *51*, 4100–4103.
140. H. Nonaka, R. Hata, T. Doura, T. Nishihara, K. Kumagai, M. Akakabe, M. Tsuda, K. Ichikawa, S. Sando, *Nat. Commun.* **2013**, *4*, 2411.
141. R. Hata, H. Nonaka, Y. Takakusagi, K. Ichikawa, S. Sando, *Chem. Commun.* **2015**, *51*, 12290–12292.
142. A. Mishra, G. Pariani, T. Oerther, M. Schwaiger, G. G. Westmeyer, *Anal. Chem.* **2016**, *88*, 10790–10794.
143. J. Yao, L. V. Wang, *Curr. Opin. Chem. Biol.* **2018**, *45*, 104–112.
144. A. G. Bell, *Am. J. Sci.* **1880**, *20*, 305–324.
145. H. J. Knox, J. Chan, *Acc. Chem. Res.* **2018**, *51*, 2897–2905.
146. C. I. Richards, J. C. Hsiang, R. M. Dickson, *J. Phys. Chem. B* **2010**, *114*, 660–665.
147. Y.-C. Chen, A. E. Jablonski, I. Issaeva, D. Bourassa, J.-C. Hsiang, C. J. Fahrni, R. M. Dickson, *J. Am. Chem. Soc.* **2015**, *137*, 12764–12767.
148. A. Jablonski, J. C. Hsiang, P. Bagchi, N. Hull, C. I. Richards, C. J. Fahrni, R. M. Dickson, *J. Phys. Chem. Lett.* **2012**, *3*, 3585–3591.
149. A. Keppler, H. Pick, C. Arrivoli, H. Vogel, K. Johnsson, *Proc. Natl. Acad. Sci. USA* **2004**, *101*, 9955–9959.
150. G. V. Los, L. P. Encell, M. G. McDougall, D. D. Hartzell, N. Karassina, C. Zimprich, M. G. Wood, R. Learish, R. F. Ohana, M. Urh, D. Simpson, J. Mendez, K. Zimmerman, P. Otto, G. Vidugiris, J. Zhu, A. Darzins, D. H. Klaubert, R. F. Bulleit, K. V. Wood, *ACS Chem. Biol.* **2008**, *3*, 373–382.
151. M. Kamiya, K. Johnsson, *Anal. Chem.* **2010**, *82*, 6472–6479.
152. K. J. Cash, C. Li, J. Xia, L. V. Wang, H. A. Clark, *ACS Nano* **2015**, *9*, 1692–1698.
153. C. M. Ackerman, P. K. Weber, T. Xiao, B. Thai, T. J. Kuo, E. Zhang, J. Pett-Ridge, C. J. Chang, *Metallomics* **2018**, *10*, 474–485.
154. M. Montes-Bayón, M. Sharar, M. Corte-Rodriguez, *TrAC Trends Anal. Chem.* **2018**, *104*, 4–10.

5

Minerals and the Emergence of Life

Simon Duval,[1] ***Kilian Zuchan,***[1] ***Frauke Baymann,***[1]
Barbara Schoepp-Cothenet,[1] ***Elbert Branscomb,***[2]
Michael J. Russell,[3, 4] ***and Wolfgang Nitschke***[1]

[1]Aix Marseille Univ, CNRS, BIP (UMR 7281), 31 chemin Joseph-Aiguier,
13402 Marseille Cedex 09, France
<sduval@imm.cnrs.fr>
<kzuchan@imm.cnrs.fr>
<baymann@imm.cnrs.fr>
<schoepp@imm.cnrs.fr>
<nitschke@imm.cnrs.fr>

[2]Carl R. Woese Institute for Genomic Biology, and Department of Physics,
University ofIllinois, Urbana, IL 61801, USA
<brnscmb@illinois.edu>

[3]NASA Astrobiology Institute, Ames Research Center, California, USA

[4]Dipartimento di Chimica, Università degli Studi di Torino, via P. Giuria 7, 10125 Turin, Italy
<michaeljrussell80@gmail.com>

Metal Ions in Life Sciences, Volume 21 Guest Editors: Peter M. H. Kroneck and Martha E. Sosa Torres
Series Editors: Astrid Sigel, Eva Freisinger, and Roland K. O. Sigel

https://doi.org/10.1515/9783110589771-005

Abstract: Metal-bearing minerals are an integral part of almost all "metabolism-first"-type scenarios for the emergence of life which consider that life is better defined by what it does than what it is made from. Since metals are formidable catalysts, these scenarios stipulate that early metabolic reactions (and prominently the reduction of CO_2 to yield biomass) were performed by (mainly transition) metals contained in certain minerals. Metabolism-first scenarios stand in opposition to primordial soup hypotheses which envisage prebiotic synthesis of organic molecules as building blocks for life to be the salient feature enabling life to come into being. A critical analysis of the historical roots of these emergence of life hypotheses highlights fundamental inconsistencies prompting us to appeal to basic thermodynamic principles to provide rigorous guidelines for developing contradiction-free models. Combining these guidelines with our present-day understanding of biological energy conversion, arguably the process most fundamental to all life, strongly suggests an expansion of previous mineral-based scenarios to include processes converting environmental redox tensions into phosphate-group-transfer disequilibria, i.e., the quintessential free energy converting mechanism of extant life. Based on their reported physicochemical and electrochemical properties, iron- (together with other transition metal-) based layered double oxyhydroxide (Fe-LDH) minerals such as fougerite are promising candidates to afford the required capacities and therefore may render previous mineral-based scenarios compliant with thermodynamic strictures.

Keywords: abiogenesis · alkaline hydrothermal vent · bioenergetics · disequilibrium converters · emergence of life · fougerite · green rust · greigite · mackinawite · transition metal clusters

1. BACK TO THE (THERMODYNAMIC) ROOTS OF LIFE

A contribution discussing a link between minerals and the emergence of life is, in the context of the prevalent scientific mindset, necessarily bound to raise eyebrows. Can there be anything more antithetical than organisms and rocks? And aren't organisms evidently, as already in their name, made up from organic matter, that is, hydrocarbons? Does that not imply that the reasons for why there

is life must be within the realm of organic chemistry while of course minerals are the epitomes of inorganic chemistry? The combination of bottom-up considerations (that is, thermodynamic requirements) and of top-down evidences (i.e., fundamental characteristics of biological energy conversion, also known as bioenergetics) has convinced us of the necessity to question the very foundations of an origin of life contingent on organic molecules and to rather adhere to the thermodynamic view. In this view, life emerged from environmental disequilibria in the form of processes carried out by transition metal-containing minerals, driven by the tendency to efficiently dissipate these disequilibria. In the following we will elaborate on our reasons to adopt this stance.

1.1. The Textbook Narrative: Life from Organic Molecules

The notion that life originated from a "primordial soup" of organic molecules is presently almost unconditionally embraced, from popular culture to the dedicated research communities. Space exploration outreach, for example, strongly capitalizes on the promise of finding the "organic building blocks" in extraterrestrial environments. These building blocks are considered to eventually have found their way to planet Earth where they engendered life. It all seems to make sense – but does it really or have we just grown accustomed to a narrative which in fact, as we will argue, from a thermodynamic perspective doesn't make sense? To understand the philosophical roots of the organic soup hypothesis, we need to go back 200 years to when Western thinking went through a conceptual upheaval with respect to its vision of life and non-life and to what distinguishes one from the other. Prior to Pasteur, abiogenesis and spontaneous generation, that is, the emergence of living things from abiotic matter, was nothing outrageous and taken to explain a plethora of empirical observations such as for example the emergence of fleas from dust [1]. In 1859 Pasteur did away with the concept of spontaneous generation [2] but thereby spontaneously generated a disturbing conundrum: what then is it that fundamentally distinguishes life from non-life? A plausible answer to this question was eventually afforded by the chemists who found that living organisms were mainly made up from hydrocarbons (proteins, lipids, sugars, etc.) which they accordingly called organic molecules yielding the nascence of the field of organic chemistry. It then was sensible and straightforward to posit that these organic molecules must somehow possess the ability to bring forward life, i.e., a "vital force". Vitalism was born and the majority of chemists and biologists, among them Louis Pasteur himself, adhered to this hypothesis as the most satisfactory way to make sense of all empirical evidences.

The advent of an atomistic understanding of chemistry at the beginning of the 20th century, however, dealt the death-blow to vitalism since there was nothing special to organic molecules as compared to their inorganic counterparts, apart from their higher structural complexity (a disputable claim in the light of some minerals we will discuss below) and no natural border between inorganic and organic chemistry could be defined. It is ironic that the detection of organic

molecules in numerous extraterrestrial settings from the surface of Titan [3] through comet atmospheres [4] to interstellar space [5] is still systematically interpreted as evidence that the seed for life on Earth may have come from outer space rather than as showing that there is nothing special to complex hydrocarbons and that their synthesis is just chemistry.

The notion that organic molecules are the defining characteristics of life and hence its prerequisites thus has somehow survived the demise of vitalism and it is this failure to acknowledge that there is nothing "life-specific" to hydrocarbons which rendered the persistence of organic soup scenarios to the present day possible. Such scenarios, however, face extraordinary hurdles when assessed within the framework of the physical sciences.

1.2. The Organic Soup's Primordial Problem with Thermodynamics

As pointed out by Erwin Schrödinger [6] already in 1944, and even earlier by Ludwig Boltzmann as well as numerous further physicists and physical chemists ever since [7–11], all living entities share the same characteristics. They generate order, that is, highly structured and regulated networks of processes, from disorder, i.e., relatively randomly distributed chemical elements (Figure 1). Therefore, they are entropy-decreasing phenomena. The second law of thermodynamics of course tells us that spontaneous lowering of entropy in closed (that is, fully isolated from their environment) systems is unlikely and that this unlikelihood steeply increases with the number of elements making up the system. This means that the probability of generating even extremely rudimentary cellular entities from organic soup settings is virtually zero (Figure 1) and this probability further decreases with each and every complexification of such rudimentary cells. Since we definitively know that there *is* life on our planet, its origin was, in the framework of organic soup hypotheses, infinitely unlikely but obviously still has happened. This would imply that the origin of life on Earth was a one-off event and there basically would be no chance to find life elsewhere in the universe.

Fortunately, we don't have to worry about all this since life is everything but a closed system! All living organisms depend on a continuous flux of free energy from their environment and therefore fully obey the requirements of the second law of thermodynamics. As already pointed out by Schrödinger, life must be a subsystem of a larger one which itself needs to be far from thermodynamic equilibrium. Life can exist because it accelerates the increase in entropy of the larger system, that is, takes it faster to its equilibrium state. The second law permits life to lower its own entropy (or, in other words, to generate order) if the increase of entropy of the larger system surpasses the entropy decrease within the subsystem Life.

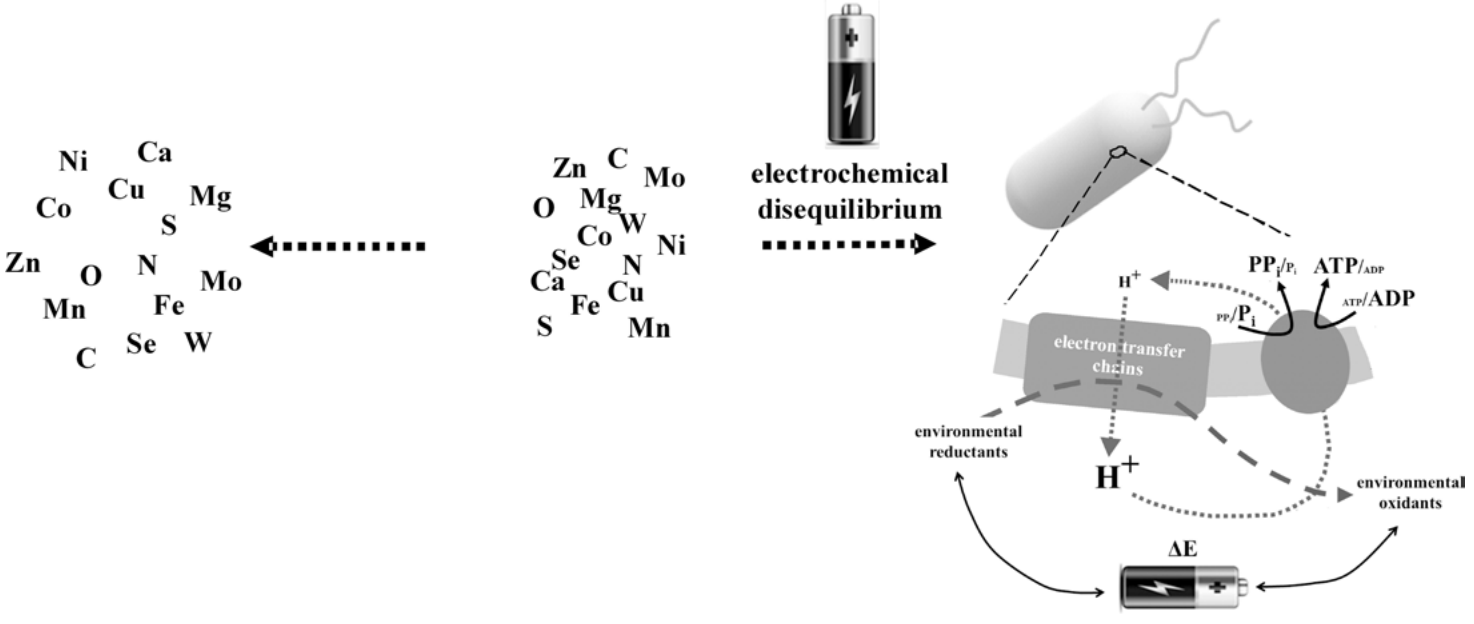

Figure 1. Schematic illustration of the main message emerging from the synthesis of far-from-equilibrium thermodynamics and bioenergetics in extant life. In the absence of environmental thermodynamic disequilibria, a random distribution of the elements involved in living systems can only be expected to become even more random (arrow to the left; note that the sample of elements is not exhaustive but reflects what appears most important to us for proper functioning of living cells). The situation is completely different if environmental disequilibria are available which can drive the formation of dissipative structures (arrow to the right), the raison d'être of which is, as is in their name, to more rapidly dissipate the environmental disequilibria. In extant biology, the driving disequilibrium is electrochemical (symbolized by the battery) and we consider that it also was when life emerged. In extant life, electrochemical free energy is transduced into far-from-equilibrium ratios of ATP to ADP or pyrophosphate (PP_i) to orthophosphate (P_i) (schematically depicted below the icon of a prokaryotic cell) which then drive all subsequent order-generating metabolic processes. It seems most parsimonious to us to assume the operation of a similar conversion process in nascent life.

1.3. Life Serves to Dissipate Environmental Disequilibria

Not only does the free energy flux from the environment into cellular organisms render life compatible with the second law of thermodynamics, it even provides a rationale why life did emerge in the first place. Science has recognized and characterized a plethora of phenomena which basically do what life does, i.e., generate transient low entropy entities which serve to increase the entropy of a larger system they are part of. Frequently cited examples are atmospheric phenomena such as tornados, convective structures ("Benard cells") or spatial and temporal structure formation in chemical reactions (such as the iconic Belousov-Zhapotinsky reaction). These entities are called dissipative structures [7] and are shown by far-from-equilibrium thermodynamics to spontaneously and necessarily emerge under appropriate conditions (for more details see [8]). From the thermodynamic point of view, life must be such a dissipative structure or it simply could not be. The true requirement permitting, but also driving, life to emerge therefore lies in the existence of environmental disequilibria and of the mechanisms converting these disequilibria into the ordered metabolism of cellular entities rather than the mere presence of organic molecules in a primordial soup.

However, would it not be possible to reconcile thermodynamics and primordial soup hypotheses by assuming that both, environmental disequilibria and organic molecules, were indispensable ingredients to life's emergence and that life wouldn't have appeared unless both were present at the same time?

The fact that life overwhelmingly consists of organic molecules at first glance seems to bolster this view. However, the detailed ways of functioning in biological energy conversion unraveled over the last few decades attribute the role of essential agents to low-abundancy entities, that is, metals (mainly transition metals) and clusters thereof, rather than to the bulk organic substance of cellular life. In doing so, they provide a rationale for the empirical observation microbiologists had made very early on: no "trace-elements", no growth! In the following we will have a closer look at what bioenergetics in extant life actually is about and how it works.

2. THE TOP-DOWN APPROACH: WHAT CAN WE LEARN FROM EXTANT LIFE?

2.1. Life Is Fueled by Electrochemical Disequilibria

The first major lesson to be gleaned from the diversity, but even more so from the underlying unicity of life's bioenergetic processes is that their free energy converting mechanisms universally exploit electrical tensions. While prokaryotes can indeed make a living from a bewildering variety of environmental sources of free energy, the molecular mechanisms they employ to this end are astonishingly homogeneous and the unifying aspect of all these free energy sources is that

they ultimately are electrochemical [12]. Such environmental (or, for the case of photosynthesis, light-induced) electrochemical disequilibria are alleviated *via* electron transfers from reducing towards oxidizing redox substrates (Figure 1). These electron transfer events are mediated by bioenergetic chains which serve as converters of redox free energy into extremely out-of-equilibrium ATP/ADP ratios driving the ensemble of endergonic chemical reactions which characterize life by their inherent decrease in entropy. The coupling between collapsing redox tensions and build-up of ATP/ADP disequilibria is generally mediated by a transmembrane proton (and occasionally sodium) gradient (Figure 1) which is generated by the electron transfer chains and which drives in return the phosphorylating systems, in most cases ATP synthases or H^+-translocating pyrophosphatases. High pyrophosphate (PP_i) to orthophosphate (P_i) levels can indeed play similar roles in certain prokaryotes as high ATP/ADP ratios do. All this can thus be likened to life being driven by an environmental battery [12] as depicted in Figure 1.

Biological energy conversion being fundamentally based on redox tensions raises the question of what is so special about electrochemical disequilibria. Part of the answer to this question may come down to the metastability of redox disequilibria were one-electron compounds need to react with strongly cooperative two-electron ones. A significant portion of environmental redox substrates in fact show strong redox cooperativity, such as the H_2/H^+, CO_2/formate, NO_3^-/NO_2^-, arsenate/arsenite couples, to name only the most common ones.

Such two-electron compounds react only extremely slowly with one-electron redox centers as a result of their highly destabilized semi-reduced form (for a discussion of this phenomenon see [13]). Extant life by the way heavily relies on this electrochemical principle which allows the extremely cooperative two-electron compound NAD(P)H (with a stability constant for the half-reduced form of $K_S = 10^{-20}$ [14]) to float freely in the cytoplasm without becoming unproductively, chaotically and rapidly oxidized by the plethora of one-electron centers (mostly iron sulfur centers) present within cytoplasmic enzymes. The very long persistence compared to biological timescales, of the above mentioned environmental electrochemical disequilibria leaves sufficient leeway for the enzymes constituting bioenergetic chains (and others) to mediate reactions between two- and one-electron compounds and to couple these reaction schemes to the generation of ion-motive membrane potentials. Of course, fully-fledged bioenergetic enzymes certainly were not available at the time of life's emergence. However, their redox active cores were! As we will argue in the following section, these active centers are mainly made up from metals.

2.2. Bioenergetic Enzymes: A Functional Inorganic Heart Cladded in an Organic Shell

The very first 3D structures of a few bioenergetic enzymes were resolved about 30 years ago but it took about 20 more years until eventually all key enzymes of eukaryotic, that is, mitochondrial and plastidic bioenergetic chains were known

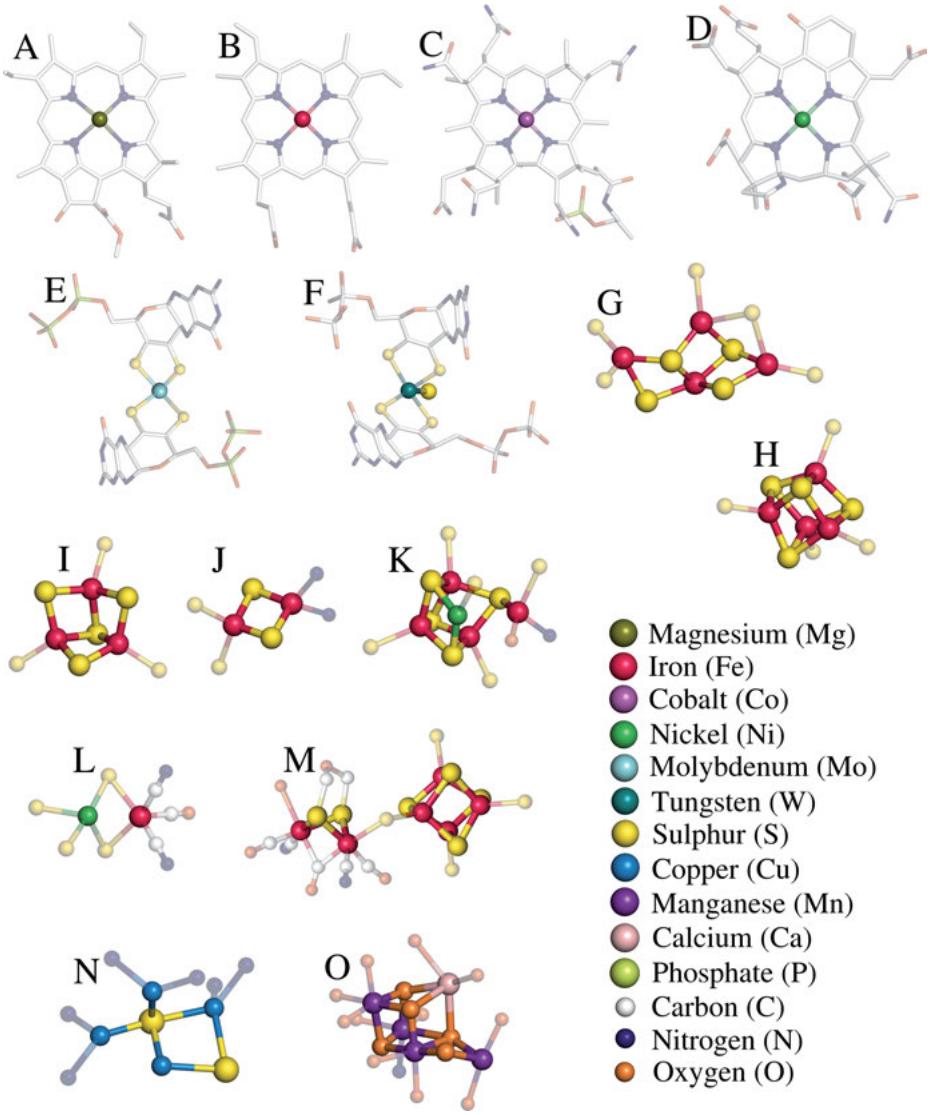

to atomic resolution. In the realm of the much more diverse bioenergetics of prokaryotes, only a fraction of all known bioenergetic enzymes have their 3D structures resolved so far. However, we had quite detailed pictures of the structural make-up of the catalytic centers in these bioenergetic complexes well before their atomic coordinates were determined by X-ray diffraction and cryo-electron-microscopy. These pictures were afforded by spectroscopic methods such as EPR, EXAFS, XANES, Mössbauer, and the likes, many of which specifically detect metals and metal ions. Quite detailed geometries of the catalytically active metal centers and clusters thereof (mostly composed of particularly redox-

Figure 2. The overwhelming majority of catalytic reactions involved in bioenergetic mechanisms of extant life is carried out by metal clusters in metalloenzymes. The figure intends to illustrate the diversity of involved metals and of the structural assembly of mixed-metal clusters present in metalloproteins (in a non-exhaustive way) and to emphasize that it is the metal part of metalloproteins that plays the crucial catalytic role rather than the protein part. Depicted centers are from the following 3D-structures (**A–D**: tetrapyrrol-ligated, **E–F**: pterin-ligated, **G–O**: ligated by specific amino acids) (**A**) Chlorophyll from PS I of *Pisum sativum* with Mg central ion (4Y28); (**B**) Heme from fumarate reductase of *Wolinella succinogenes* (2BS2); (**C**) Cobalamin (Vit. B_{12}) from the enzyme OxsB of *Bacillus megaterium* with cobalt in the active site (5UL3); (**D**) Factor F430 from methyl-CoM reductase of *Methanothermobacter marburgensis* containing nickel (3POT); (**E**) Molybdopterin cofactor of arsenite oxidase from *Alcaligenes faecalis* (1G8J); (**F**) Tungstopterin in formylmethanofuran dehydrogenase of *Methanothermobacter wolfeii* (5T5I); (**G**) Noncubane [4Fe-4S] cluster of heterodisulfide reductase/[Ni-Fe]-hydrogenase complex from *Methanothermococcus thermolithotrophicus* (5ODC); (**H**) Cubane [4Fe-4S] cluster from fumarate reductase of *Wolinella succinogenes* (2BS2); (**I**) [3Fe-4S] cluster from fumarate reductase of *Wolinella succinogenes* (2BS2); (**J**) Rieske [2Fe-2S] cluster in the Rieske/cyt*b* complex of *Rhodobacter sphaeroides* (2NUK); (**K**) [Ni-Fe-S] cluster from anaerobic CODH of *Carboxydothermus hydrogenoformans* (3B51); (**L**) [Ni-Fe] cluster in the hydrogenase of *Hydrogenophilus thermoluteolus* (5XFA); (**M**) [Fe-Fe] cluster in the hydrogenase of *Clostridium pasteurianum* (3C8Y); (**N**) Copper cluster of nitrous oxide reductase from *Pseudomonas stutzeri* (6RKZ); (**O**) Manganese cluster in PS II from *Thermosynechococcus vulcanus* (3WU2). The coordinating atoms are drawn proportionally smaller and transparent.

versatile transition metals) had thus been deduced long before the molecular architectures of the protein scaffolds holding these active centers became resolved. The emerging picture is that of inorganic metal centers performing the energy-converting processes and redox reactions with their protein environments mainly adjusting and optimizing the metal clusters' properties. Without pretending to be exhaustive, we have presented several of the metal centers playing essential roles in bioenergetic processes in Figure 2. While in many biochemistry textbooks enzymes are considered to be polypeptide chains which occasionally may recruit metals to improve catalysis, to the spectroscopists studying bioener-

getic enzymes it was always clear that the crucial action happened on the metal clusters and not on the polypeptide (with admittedly a few amino acids assisting metal-catalyzed redox processes such as, for example, in cytochrome oxidase and photosystem II).

Biological energy conversion, by thermodynamic standards the most fundamental process of life, in extant life employs also a few organic molecules such as quinones, flavins, and nicotinamides but remains first and foremost the business of a plethora of specialized inorganic entities, the diverse metal clusters. All this suggests that absolute abundance likely is a misleading criterion when looking for what is essential to life. As a provocative analogy, the high abundance of plastics in a computer should obviously not be taken as proof that it is these polymers rather than the semiconducting material which performs logical operations on binary states, i.e., the processes defining the apparatus.

3. STRUCTURAL AFFINITIES BETWEEN CATALYTIC CENTERS IN METALLOENZYMES AND SPECIFIC MINERALS

Despite all this, dedicated advocates of organic soup scenarios might well admit that the relevant processes are carried out by metal clusters but argue that it is the polypeptide chain that imposes their specific structural layout. This does not seem to be the case for the majority of studied metal clusters in metalloenzymes. As pointed out for example by Helmut Beinert [15, 16], many iron-sulfur clusters observed in enzymes also exist as inorganic entities in appropriate solvents. Inorganic models mimicking the geometries (and properties) of metal centers, metal clusters, and mixed-metal clusters in many metalloproteins have been synthesized and characterized. Even more tellingly from an evolutionary point of view, several biological clusters involved in pivotal types of free energy conversion have been observed to structurally resemble units making up the crystal lattices of certain minerals [17–21]. For these cases, life appears to merely have extracted these units from the bulk mineral by wrapping them in polypeptide chains [22, 23]. The most iconic mineral: biocluster similarities (see Figure 3) have been reviewed in the past, and we refer the reader to the relevant literature [19, 21]. The main minerals suggested to be parent to intriguing metal clusters in biology are greigite, mackinawite, and fougerite, all of which are extremely likely or certain to have been present in specific locations on the Hadean and early Archaean planet Earth, that is, when life is supposed to have emerged. In particular, these minerals were probably constituents of the chimneys formed at submarine alkaline hydrothermal vents, which in addition also feature electrochemical and pH gradients providing the *sine-qua-non* thermodynamic sources of free energy to drive life into being (cf. Section 1) and which have therefore been put forward as potential hatcheries of life [24–26]. The first mineral to be put forward as instrumental in an inorganic, metabolism-based emergence of life certainly was pyrite [27]. Pyrite has indeed been shown to perform a range of catalytic reac-

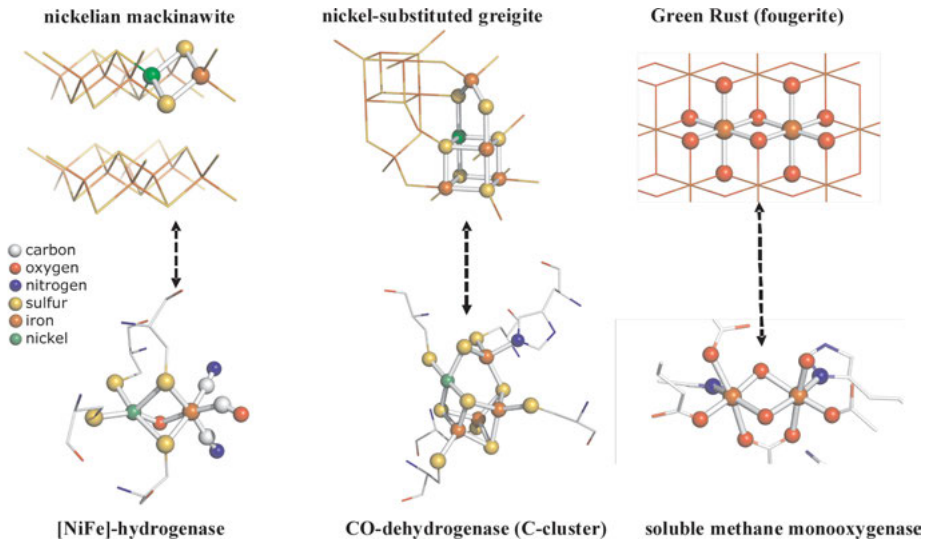

Figure 3. Structural resemblance between the catalytic metal clusters present in three key enzymes (bottom row) involved in substrate conversions with strong relevance to emergence of life scenarios and the minerals mackinawite, greigite, and fougerite (top row).

tions potentially pertinent to emergence of life scenarios. However, a close inspection of pyrite's crystal lattice does not immediately suggest structural similarities to metal centers in biological systems.

4. MINERAL-CATALYZED REACTIONS PERTINENT TO EMERGENCE OF LIFE SCENARIOS

Minerals, and in particular transition metal-containing ones, are renowned for their extraordinarily versatile catalytic abilities. However, only part of the manifold chemical reactions mediated by minerals is of obvious relevance to the problem of life's emergence. We have collected a subset of reactions which appear most noteworthy to us in the context of the emergence of life scenarios dealt with in this contribution (Table 1).

Table 1. Reactions catalyzed by 3D sulfides and oxides, and a 2D oxyhydroxide (fougerite) and sulfide (mackinawite) expected to have occurred at a Hadean alkaline submarine vent as demonstrated in the lab or field. Reactions are depicted either at equilibrium or driven electrochemically [26]. All potentials are with respect to the normal hydrogen electrode.

Reaction		Mineral/Cation	Conditions	Refs
$H_2 \rightarrow 2\,H^{\bullet} \rightarrow 2\,H^+ + 2\,e^-$ $H_2S \rightarrow 2\,H^+ + 2\,e^- + S^0$	ELECTRONS	Unspecified Fe-S conductors	Induced/natural chimneys 309° to 4 °C, pH 4.8 to 7	[28]
$H_2 + CO_2 \rightarrow HCOOH$	FORMATE	Fe-Ni sulfides, Awaruite Ni_3Fe Greigite Fe_3S_4 Magnetite Fe_3O_4	120 °C, pH 5 to 11 100 °C, pH 5 to 11	[29–31]
$CO_2 + 2\,H^+ + 2\,e^- \rightarrow CO + H_2O$		Violarite $FeNi_2S_4$	25 °C, pH ~5.5 to 9.5 1.1 V	[32]
$CH_3S^- + CO + H_2O \rightarrow CH_3COO^- + H_2S$ *via* $CH_3SH + CO \rightarrow CH_3COSH$	ACETATE	FeS, NiS ($NiSO_4$)	100 °C, pH 6 to 9	[33]
$CO_2 + 2\,H_2 \rightarrow CH_3OH + H_2O$	METHANOL	Awaruite Ni_3Fe Greigite Fe_3S_4 Magnetite Fe_3O_4	100 °C, pH 5 to 11	[30]
$2CO_2 + 8\,H^+ + 8e^- \rightarrow CH_3COOH + 2\,H_2O$	ACETIC ACID	Greigite Fe_3S_4	25 °C, pH 6.5 + 0.2 V and 0.8 V	[34]
$3\,CO_2 + 2\,H_2 \rightarrow CH_3COCOOH$	PYRUVIC ACID	Magnetite Fe_3O_4 Awaruite Ni_3Fe	100 °C, pH 7 to 10	[30]
$3\,CO_2 + 10\,H^+ + 10\,e^- \rightarrow CH_3COCOOH + 3\,H_2O$	PYRUVIC ACID	Greigite Fe_3S_4	25 °C, pH 6.5 + 0.2 V ↔ 0.8 V	[35]

$NO_2^- + Fe^{2+} + 2H^+ \rightarrow NO + Fe^{3+} + H_2O$		Fougerite	25 °C, pH 6.6	[36]
$NO_3^- + 4H_2 \rightarrow NH_3 + 2H_2O + OH^-$		Fougerite	25 °C, pH 8	[37]
$R{\cdot}CO{\cdot}COO^- + NH_4Cl + H_2 \rightarrow R{\cdot}CH(NH_2)COO^- + H_2O + HCl$	AMINO ACIDS: ALA, GLU, PHE, TYR	FeS, $Fe(OH)_2$ (Mackinawite, White Rust?)	50° to 100 °C, pH 8.3 to 10.5	[38]
$CH_3CO{\cdot}COO^- + NH_3 + H_2 \rightarrow CH_3CH(NH_2)COO^- + H_2O$	ALANINE	Fougerite	50 °C, pH 9 to 11	[39]
$CH_3COPO_4^{2-} + HPO_4^{2-} \rightarrow HP_2O_7^{3-} + CH_3COO^-$	PYROPHOSPHATE	Goethite, α-FeOOH Vivianite, Fougerite	22 °C, pH 2.2 to 7.3	[40]

5. CATALYSIS AND DISEQUILIBRIUM CONVERTERS, METALS, AND QUINONES/FLAVINS: AN ATTEMPT AT DISENTANGLING THE KNOT

It appears important to us to emphasize the fundamental difference between catalysis and disequilibrium conversion. The very definition of catalysis implies that the catalyzed reaction is exergonic and thus would proceed even in the absence of the catalysts, only much more slowly. For example, the oxidation of molecular hydrogen by the nickel-iron ([NiFe]) cluster of certain hydrogenases in the presence of sufficiently oxidizing electron acceptors therefore represents straightforward catalysis. Members of so-called Group 4 [NiFe]-hydrogenases, by contrast, couple the redox interconversion of $H_2/2\,H^+$ to translocation of a cation over the cytoplasmic membrane [41] and therefore perform genuine disequilibrium conversion. Several key disequilibrium conversions in bioenergetics, however, require the crucial participation of aromatic organic molecules, quinones, and flavins. Both these aromats play crucial roles in the generation of out-of-equilibrium reductants *via* the process of electron bifurcation, the quinones mainly within the membrane-integral Rieske/cyt*b* complexes and flavins in a wide variety of soluble bioenergetic enzymes [13, 42–45]. Do these implications of quinones and flavins in disequilibrium-converting processes contradict the notion of primeval roles of metals in the emergence of life and instead bring the organics back to the forefront? Maybe but not necessarily. It has in fact been shown that molybdenum-based centers can in principle perform the cooperative two-electron reactions which are crucial to the mentioned roles played by quinones and flavins [46] and it has been argued that molybdenum (and/or tungsten) may have performed these reactions in nascent life [13, 44]. The environmental scarcity of Mo and W may then early on have forced life to devise (organic) alternatives to these metals resulting in quinones and flavins taking over the respective tasks.

Alternatively, these aromats may have been produced as side products in disequilibrium-converting processes performed by a specific mineral (see [47, 48] and Section 6) and thus may have been woven into the fabric of early metabolic reactions almost from the beginning. In any case, we would like to emphasize that, if quinones and flavins did indeed play pivotal roles already at life's onset, these roles would be dramatically different from those of organic building blocks envisaged by primordial soup scenarios. They rather would be dynamic actors in the prime processes of life's emergence: the conversion of electrochemical tensions into membrane potentials and onwards into high ATP/ADP ratios and the provision of out-of-equilibrium reductants (required for example for efficient CO_2 reduction).

6. ADDITIONAL LEVELS OF COMPLEXITY: LAYERED (CLAY-LIKE) MINERALS

In Figure 3 and Section 4 we have discussed a few examples of minerals structurally resembling specific active clusters in metalloproteins as well as bio-relevant processes they have been shown to carry out. The cases of greigite, mackinawite, and also pyrite have been discussed in the framework of metabolism-first scenarios for life's emergence since several decades [25, 49]. Relevant reactions in these minerals are basically surface chemistry since greigite, mackinawite, and pyrite are solids. The mineral fougerite, however, belongs to an entirely different structural class. These are the layered anionic clays with solvent-accessible interstitial galleries [47, 48, 50–54] (Figure 4). They distinguish themselves from solids such as greigite by several properties particularly pertinent to emergence-of-life scenarios:

- The surface area available for catalytic processes exceeds that of a solid crystal by orders of magnitude.
- Water activity within the interstitial spaces is substantially decreased with respect to bulk water [26] entailing displaced equilibria for chemical transformations [39] which involve uptake or release of water molecules.

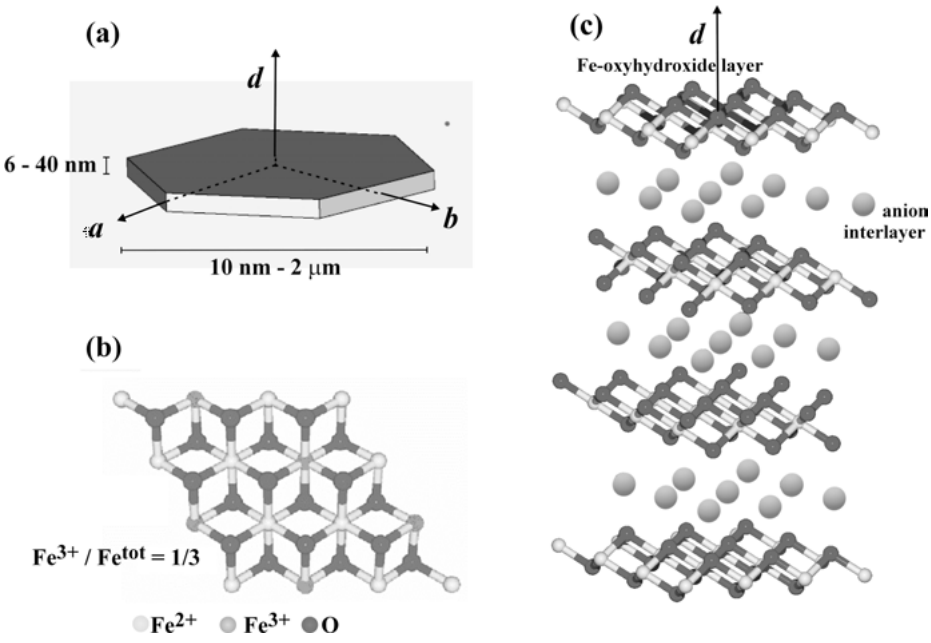

Figure 4. Overview of basic structural features of Green Rusts. The shape and typical dimensions of the hexagonal nanocrystals of GR are depicted in (**a**). (**b**) and (**c**) show top and sideviews, respectively, of the layered structure arising from an alternating series of Fe-oxyhydroxide strata and charge-compensating, anion-containing interstitial galleries.

- Local dielectric constants in the interlayer spaces differ strongly from that of bulk water due to the lowered water activity and restricted mobility of individual water molecules [55].
- Interstitial spaces can accommodate a variety of counterions with a wide range of bulkiness. Layered minerals therefore can swell and shrink to extraordinary extents in response to the chemical composition of their surrounding solvent.

Well aware of these enticing properties, the clay community has advocated a pivotal role of clays in life's emergence already since quite some time [56–60]. However, the considered minerals were mainly clays devoid of transition metals and hence redox-inactive and the relevant catalytic reactions therefore mostly revolved around surface-facilitated condensation reactions [60–62]. The mineral we single out here, i.e., fougerite, by contrast, uniquely combines the fascinating redox abilities of transition metal bearing solids such as greigite or mackinawite and the above-mentioned particularities of clay-like layered structures. Most intriguingly, fougerite couples redox and structural features in ways eerily reminiscent of bioenergetic systems as we shall detail below.

6.1. Fougerite and Green Rusts

Fougerite is the naturally occurring form of the synthetic mineral Green Rust (GR), known to the mineralogists since almost 100 years [56, 57]. GRs are layered double-hydroxide (LDH) minerals (sometimes also called double layered oxyhydroxides, to emphasize the coexistence of two distinct layers). In GR, the metals within the oxyhydroxide layers are Fe^{2+} and Fe^{3+} (with variable stoichiometry, see below) and the interstitial galleries contain ordered water molecules and small anions (Figure 4). We have described bio-relevant properties of GR in more detail recently [47] and will in the following focus on a few key features. Fougerite as a natural form of GRs is obviously less well-behaved than its synthetic counterparts with occasional Fe-sites being replaced by other divalent metal cations such as Ni, Mg, Al, and Zn [54]. While the mineralogists' GR samples are usually prepared with a single type of interstitial anion (such as chloride, carbonate, sulfate, etc.), fougerite certainly contains a mixture of all kinds of anions present in the respective environments. So far, in-depth characterizations of properties and reactivities have only been obtained for the synthetic GRs. It is safe to expect that the reactional versatility of fougerite surpasses that of GRs by a wide margin due to the pronounced variability of metal ions in the oxyhydroxide layers and of counterions in the interstitial spaces.

In contrast to solid minerals which tend to grow to truly macroscopic sizes, GR only forms nanocrystals with hexagonal crystal symmetry and typical dimensions in the range of several nanometers to 2,000 nanometers (Figure 4a). An average nanocrystal contains a few tens of Fe-oxyhydroxide layers. We emphasize that the smallest types of GR nanocrystals thus feature sizes comparable to those of typical bioenergetic enzymes. GRs' extraordinary physicochemical

peculiarities detailed below further narrow the gap between these inorganic structures and life.

6.1.1. Softness of Internal Structure

While crystals are commonly associated with rigidity, this picture is strongly inappropriate when dealing with GR (or clay-like minerals in general). Clay-like assemblages substantially morph in response to the chemical composition of their solvent environment. This is due to their interstitial spaces being contiguous with the outside bulk solvent and the resulting possibility of counterions with strongly differing bulkiness to diffuse into these galleries [54]. In GR, the best-studied examples are those of the so-called GR1 and GR2-variants containing chloride and sulfate counterions, respectively. The height of the interlayer space of GR1 is about 8 Å which swells to 12 Å during the sulfate-induced transition to GR2 while long-chain carbohydrate chains have been observed to push interlayer heights up to 40 Å and above [63]. The arrangement of counterions in the interlayer space also varies considerably. Spherical or "flat" anions (e.g., chloride, carbonate, hydroxide) tend to form a single interlayer in the middle of the interstitial galleries [64]. Tetragonal anions such as sulfate (and possibly phosphate), by contrast, arrange themselves into two superimposed interlayers [65]. Individual nanocrystals can harbor mixed populations of flat and tetragonal anions resulting in undulated geometries of layer/interlayer stacks (Figure 5 [54, 66]).

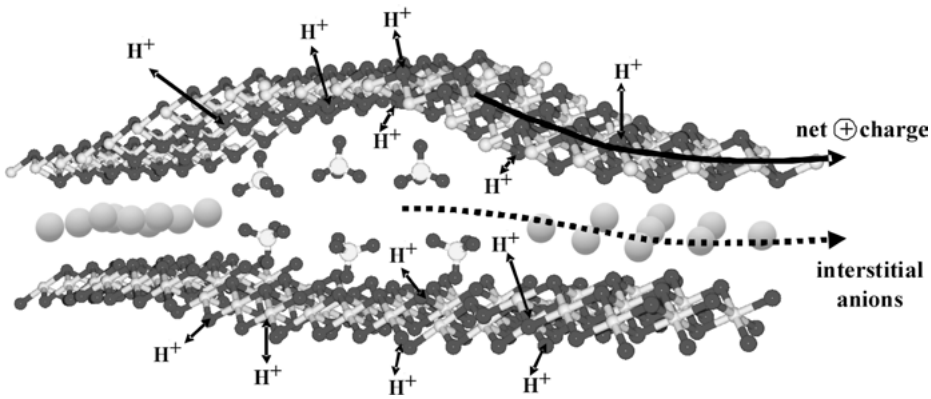

Figure 5. Schematic representation of two individual oxyhydroxide layers and their interstitial space of a Green Rust nanocrystal harboring mixed-type interstitial anions (that is, spherical ones resulting in GR1 with an interstitial height of about 8 Å and tetragonal ones yielding GR2 with heights of about 12 Å). Movement of charge in the Fe-oxyhydroxide layer will be accompanied by modifications in the p*K* values of the μ-bridging OH groups in the way that more oxidized (Fe^{3+}) sites are likely to induce deprotonation of their surrounding hydroxy groups and release of H^+ into the interstitial spaces. Movements of Fe^{3+} sites (corresponding to electron transfer in the opposite direction) within the layers are also expected to drag charge-compensating ions with them resulting in correlated movements of the interstitial anions.

6.1.2. *Redox Softness, Electron Transfer, and Proton-Coupled Redox Transitions*

As mentioned, iron-oxyhydroxide layers of GR are characterized by the coexistence of ferric and ferrous iron sites in the lattice. In the presence of oxygen, all iron sites are gradually converted to the ferric state resulting in the transformation of the typical GR layering into the true solids magnetite and goethite *via* lepidocrocite (still a layered mineral but devoid of anion interlayers). GRs thus are a metastable manifestation of iron oxides carving out a niche of existence in between the soluble Fe^{2+} oxides and the mentioned fully oxidized forms. In the absence of oxygen (or other oxidizing agents), GRs are long-term stable (that is, for months and years) in the range of Fe^{3+}/Fe^{tot} ratios ranging from 1/3 to 2/3 (see Figure 4b) [67]. However, GR samples can be taken to the fully oxidized (all Fe^{3+}) and fully reduced (all Fe^{2+}) states for minutes to hours without losing the GR-typical layering [68]. These shifts in reduction state correspond to effective electron transfer within the plane of the Fe-oxyhydroxide layer.

Altering the Fe^{3+}/Fe^{tot} ratio amounts to changing the net charge of the oxyhydroxide layers. To maintain their structural integrity in the face of growing charge imbalance, the GR nanocrystals can adjust the amount of compensating countercharges in the interlayer or, for the case of very high Fe^{3+}/Fe^{tot} values, deprotonate the μ-hydroxo bridges to result in μ-oxo-bridged structures (Figure 5). Oxidation of the layers is therefore accompanied by release of protons into the interlayer space (which certainly sounds familiar to the bioenergeticist). For the case of in-plane vectorial migration of Fe^{3+} sites, it is tempting to assume that the compensating counter-anions in the interlayer space will tend to be dragged along and thus move in the inverse direction of effective electron flow (Figure 5). Again, the analogies to phenomena in bioenergetic transmembrane transport are intriguing.

6.1.3. *Multi-Electron Redox Catalysis*

The catalytic versatility of GR is showcased in several dedicated review articles from the mineralogical community [64]. GR's abilities to mediate challenging multi-electron redox transformations appear of particular interest to emergence of life scenarios which try to obey the thermodynamic and bioenergetic strictures laid out in Sections 1 and 2. For example, GR has been shown to catalyze the 8-electron reduction of nitrate to ammonia [37] as well as several intermediate steps thereof [66]. These reactions are intriguing since, apart from producing strongly reduced nitrogen compounds required for instance in the synthesis of amino acids, they can produce highly reactive intermediates such as nitrogen oxide [66] or potentially hydrazine [47].

Although a plethora of GR-assisted redox transformations have been reported by the mineralogists, the list is almost certainly far from complete and GRs are likely to feature further intriguing reaction pathways. Naturally occurring fougerite can safely be expected to show even broader reactive abilities due to the presence of transition metals other than only iron. As indicated in Section 2

and Figure 3, the top-down lead from biology to GR arises from the structural resemblance between the catalytic center of members of the diiron hydroxylase superfamily and in particular of the enzyme "soluble methane monooxygenase" and the arrangement of the Fe-oxyhydroxide layers. The diversity of diiron hydroxylases may suggest further reaction schemes to be assayed in GR samples.

6.2. A Potential Bridge from the Inorganic World to Biology

The above listed properties of GRs are certainly fascinating and potentially important for emergence of life scenarios. However, as we have tried to convey in Sections 1 and 6 as well as in a recent article [48], none of these properties by themselves can rationalize an emergence of life which would be in line with the 2nd law of thermodynamics. Even the most intricate types of redox catalyses remain "catalyses", that is, they facilitate exergonic reactions rather than driving endergonic ones. What is required for credible emergence of life scenarios is the availability of disequilibria-converting processes, ideally somehow resembling the conversion of environmental redox tensions into phosphate group transfer disequilibria such as high ATP/ADP or PP_i/P_i ratios, as observed in real life [47]. We imagine that the synergy of GR's properties listed in Sections 6.1.1 to 6.1.3 may be able to bring forth such disequilibria-converting processes [39] and we have proposed tentative models in recent articles [47, 48].

However, we also consider that these scenarios are too speculative to be detailed in this contribution which we would like to keep as close as possible to empirical data, basic thermodynamic considerations, and undeniable structural analogies. The model we have proposed nevertheless serves as proof of principle that disequilibria-converting systems based on the synergy of fougerite, mackinawite and greigite and resembling actual biology can be conceived of. Our specific model may become falsified in the future *via* experimental results and replaced by other scenarios, but we strongly suspect that the discussed properties of the layered Fe-oxyhydroxide minerals will play pivotal roles also in these future scenarios.

7. CONCLUSION

Whether it was the presence of organic building blocks or the emergence of an ancestral metabolism based on mineral-borne inorganic metal clusters [17, 25, 27, 33, 38, 69] appears to be presently the main controversy animating the field of emergence of life research. While organic soup hypotheses have dominated the field since almost a century [70–72], the alternative current of thought is with us since quite some time, too [24] and many inorganic chemists shared David Garner's view that "It is the inorganic elements that bring organic chemistry to life" already several decades ago. Earlier emergence of life scenarios building on alkaline vent settings strongly relied on the inorganic nature of both the

redox substrates and the metal catalysts of certain types of prokaryotic energy metabolism to infer a close resemblance between these metabolisms and abiotic chemical reactions occurring in the vents [17, 73, 74].

In the past, more than half of the authors of the present contribution championed the alkaline hydrothermal vent scenario precisely because of the perceived similarity of catalytic reaction steps in the vent and in biological methano- and acetogenesis. We have since became convinced by the incontrovertible arguments from thermodynamics that abiogenesis cannot simply correspond to a speeding up of abiotic chemical reactions. Life's most fundamental nature as an entropy-lowering process requires the existence of conversion mechanisms transducing environmental disequilibria into the highly ordered factories of living cells. As we have tried to argue in this contribution, this stricture further strengthens the lead towards metal-containing minerals as midwives for nascent life but requires the inclusion of minerals which are able to couple redox reactions and mass transfer as well as to perform proton-coupled electron transfer.

ACKNOWLEDGMENTS

SD's and WN's work was supported by the CNRS (Défi Origines, grant SIAM). EB's contribution was partly supported by the NASA Astrobiology Institute under a cooperative agreement issued through the Science Mission directorate, no. NNH06ZDA001N (Universal Biology). MJR is supported by the National Aeronautics and Space Administration, through the NASA Astrobiology Institute under cooperative agreement issued through the Science Mission directorate; No. NNH13ZDA017C (Icy Worlds).

ABBREVIATIONS AND DEFINITIONS

ADP	adenosine 5′-diphosphate
ATP	adenosine 5′-triphosphate
CO_2	carbon dioxide
EPR	electron paramagnetic resonance
EXAFS	extended X-ray absorption fine structure
GR	Green Rust
K_S	stability constant of semireduced form of 2-electron compounds
LDH	layered double-hydroxide
Mo	molybdenum
NAD(P)H	nicotinamide adenine dinucleotide(phosphate), reduced
[NiFe]	nickel-iron
P_i	orthophosphate; inorganic phosphate; PO_4^{3-}
PP_i	pyrophosphate
W	tungsten
XANES	X-ray absorption near-edge spectroscopy

REFERENCES

1. Aristotle, *De Generatione Animalium* (*On the generation of animals*), 4th century BC.
2. J. R. Porter, *Bacteriol. Rev.* **1961**, *25*, 389–403.
3. C. D. Neish, A. Somogyi, M. A. Smith, *Astrobiology* **2010**, *10*, 337–347.
4. K. Altwegg, H. Balsiger, A. Bar-Nun, J. J. Berthelier, A. Bieler, P. Bochsler, C. Briois, U. Calmonte, M. R. Combi, H. Cottin, J. De Keyser, F. Dhooghe, B. Fiethe, S. A. Fuselier, S. Gasc, T. I. Gombosi, K. C. Hansen, M. Haessig, A. Jäckel, E. Kopp, A. Korth, L. Le Roy, U. Mall, B. Marty, O. Mousis, T. Owen, H. Rème, M. Rubin, T. Sémon, C. Y. Tzou, J. Hunter Waite, P. Wurz, *Sci. Adv.* **2016**, *27*, 2. doi: 10.1126/sciadv.1600285.
5. S. Kwok, *Orig. Life Evol. Biosph.* **2015**, *45*, 113–121.
6. E. Schrödinger, *What is life? The Physical Aspect of the Living Cell*, Cambridge University Press, Cambridge, **1944**.
7. G. Nicolis, Y. Prigogine, *Exploring Complexity*, St. Martin's Press, New York, **1989**.
8. D. Kondepudi, I. Prigogine, *Modern Thermodynamics; From Heat Engines to Dissipative Structures*, John Wiley & Sons, Chichester, UK, **1998**.
9. E. Branscomb, M. J. Russell, *Biochim. Biophys. Acta* **2013**, *1827*, 62–78.
10. E. Branscomb, T. Biancalani, N. Goldenfeld, M. J. Russell, *Physics Reports* **2017**, *677*, 1–60.
11. R. G. Endres, *Sci. Rep.* **2017**, *7*, 14437.
12. B. Schoepp-Cothenet, R. van Lis, A. Atteia, F, Baymann, L. Capowiez, A.-L. Ducluzeau, S. Duval, F. ten Brink, M. J. Russell, W. Nitschke, *Biochim. Biophys. Acta* **2013**, *1827*, 79–93.
13. F. Baymann, B. Schoepp-Cothenet, S. Duval, M. Guiral, M. Brugna, C. Baffert, M. J. Russell, W. Nitschke, *Front. Microbiol.* **2018**, *9*, 13577.
14. R. F. Anderson, *Biochim. Biophys. Acta* **1980**, *590*, 277–281.
15. H. Beinert, R. H. Holm, E. Münck, *Science* **1997**, *277*, 653–659.
16. H. Beinert, *J. Biol. Inorg. Chem.* **2000**, *5*, 2–15.
17. M. J. Russell, W. Martin, *Trends Biochem. Sci.* **2004**, *24*, 358–363.
18. W. Nitschke, M. J. Russell, *J. Mol. Evol.* **2009**, *69*, 481–496.
19. W. Nitschke, S. E. McGlynn, E. J. Milner-White, M. J. Russell, *Biochim. Biophys. Acta* **2013**, *1827*, 871–881.
20. M. J. Russell, L. M. Barge, R. Bhartia, D. Bocanegra, P. J. Bracher, E. Branscomb, R. Kidd, S. E. McGlynn, D. H. Meier, W. Nitschke, T. Shibuya, S. Vance, L. White, I. Kanik, *Astrobiology* **2014**, *14*, 308–343.
21. E. L. Shock, E. S. Boyd, *Elements* **2015**, *11*, 395–411.
22. E. J. Milner-White, M. J. Russell, *Biology Direct* **2008**, *3*, 3. doi: 10.1186/1745-6150-3-3.
23. E. J. Milner-White, *Interface focus* **2019**, *9*, 20190057.
24. M. J. Russell, A. J. Hall, A. G. Cairns-Smith, P. S. Braterman, *Nature* **1988**, *336*, 117.
25. M. J. Russell, A. J. Hall, *J. Geol. Soc. Lond.* **1997**, *154*, 377–402.
26. M. J. Russell, *Life* **2018**, *8*, 35.
27. G. Wächtershäuser, *System. Appl. Microbiol.* **1988**, *10*, 207–210.
28. M. Yamamoto, R. Nakamura, T. Kasaya, H. Kumagai, K. Suzuki, K. Takai, *Angew. Chem. Int. Ed.* **2017**, *56*, 5725–5728.
29. L. M. White, T. Shibuya, S. D. Vance, L. E. Christensen, T. Bhartia, R. Kidd, A. Hoffmann, G. D. Stucky, I. Kanik, M. J. Russell, *Astrobiology* **2020**, *20(3)*, in press.
30. M. Preiner, K. Igarashi, K. B. Muchowska, M. Yu, S. J. Varma, K. Kleinermanns, M. K. Nobu, Y. Kamagata, H. Tüysüz, J. Moran, W. F. Martin, *bioRxiv* **2019**, 682–955.
31. M. Preiner, J. C. Xavier, A. D. N. Vieira, K. Kleinermanns, J. F. Allen, W. F. Martin, *Interface focus* **2019**, *9*, 20190072.

32. A. Yamaguchi, M. Yamamoto, K. Takai, T. Ishii, K. Hashimoto, R. Nakamura, *Electrochim. Acta.* **2014**, *141*, 311–318.
33. C. Huber, G. Wächtershäuser, *Science* **1997**, *276*, 245–247.
34. N. Kitadai, R. Nakamura, M. Yamamoto, K. Takai, Y. Li, A. Yamaguchi, A. Gilbert, Y. Ueno, N. Yoshida, Y. Oono, *Sci.Adv.* **2018**, *4*, eaao7265.
35. A. Roldan, N. Hollingsworth, A. Roffrey, H. U. Islam, J. Goodall, C. R. A. Catlow, J. A. Darr, W. Bras, G. Sankar, K. B. Holt, G. Hogarth, N. H. de Leeuw, *Chem. Commun.* **2015**, *51*, 7501–7504.
36. H. C. Hansen, O. K. Borggaard, J. Sørensen, *Geochim. Cosmochim. Acta* **1994**, *58*, 2599–2608.
37. H. C. B. Hansen, *Appl. Clay Science* **2001**, *18*, 81–91.
38. C. Huber, G. Wächtershäuser, *Tetrahedron Lett.* **2003**, *4*, 1695–1697.
39. L. M. Barge, E. Flores, M. M. Baum, D. G. VanderVelde, M. J. Russell, *Proc. Natl Acad. Sci.* **2019**, *116*, 4828–4833.
40. Q. Wang, L. M. Barge, O. Steinbock, *Chem. Eur. J.* **2019**, *25*, 4732–4739.
41. R. Hedderich, L. Forzi, *J. Mol. Microbiol. Biotechnol.* **2005**, *10*, 92–104.
42. D. G. Nicholls, S. J. Ferguson, *Bioenergetics 4*, 4th edition, Academic Press, London, UK, **2013**.
43. W. Buckel, R. K. Thauer, *Biochim. Biophys. Acta* **2013**, *1827*, 94–113.
44. W. Nitschke, M. J. Russell, *Bioessays* **2012**, *34*, 106–109.
45. J. L. Yuly, C. E. Lubner, P. Zhang, D. N. Beratan, J. W. Peters, *Chem. Commun.* **2019**, *55*, 11823–11832.
46. S. Duval, J. M. Santini, D. Lemaire, F. Chaspoul, M. J. Russell, S. Grimaldi, W. Nitschke, B. Schoepp-Cothenet, *Biochim. Biophys. Acta* **2016**, *1857*, 1353–1362.
47. S. Duval, F. Baymann, B. Schoepp-Cothenet, F. Trolard, G. Bourrié, O. Grauby, E. Branscomb, M. J. Russell, W. Nitschke, *Interface focus* **2019**, *9*, 20190063. doi: 10.1098/rsfs.2019.0063.
48. S. Duval, E. Branscomb, F. Trolard, G. Bourrié, O. Grauby, V. Heresanu, B. Schoepp-Cothenet, M. J. Russell, W. Nitschke, *Applied Clay Sci.* **2020**, 195, 105737. doi: 10.1016/j.clay.2020.105737.
49. L. M. White, R. Bhartia, G. D. Stucky, I. Kanik, M. J. Russell, *Earth Planet. Sci. Lett.* **2015**, *430*, 105–114.
50. G. Arrhenius, *Interaction of Hydrous Minerals with Bioorganic Precursor Molecules*, in NASA Space Life Sciences Symposium, Washington DC, June 21–26, 1987, pp. 260–261.
51. G. O. Arrhenius, *Helv. Chim. Acta* **2003**, *86*, 1569–1586.
52. F. Trolard, G. Bourrié, M. Abdelmoula, P. Refait, F. Feder, *Clays and Clay Minerals* **2007**, *55*, 323–334.
53. J. M. R. Génin, R. Aïssa, A. Géhin, M. Abdelmoula, O. Benali, V. Ernstsen, G. Ona-Nguema, C. Upadhyay, C. Ruby, *Solid State Sciences* **2005**, *7*, 545–572.
54. M. I. Agnel, S. Grangeon, F. Fauth, E. Elkaïm, F. Claret, M. Roulet, F. Warmont, C. Tournassat, *Environm. Sci. Technol.* **2019**, *54*, 851–861.
55. E. Branscomb, M. J. Russell, *Interface Focus* **2019**, *9*, 20190061. doi: 10.1098/rsfs.2019.0061.
56. J. D. Bernal, D. R. Dasgupta, A. L. Mackay, *Nature* **1957**, *180*, 645–647.
57. J. D. Bernal, D. R. Dasgupta, A. L. Mackay, *Clay Minerals Bulletin* **1959**, *4*, 15–30.
58. A. G. Cairns-Smith, *Genetic Takeover and the Mineral Origins of Life*, Cambridge University Press, Cambridge, UK, **1982**.
59. D. H. Solomon, *Clays and Clay Minerals* **1968**, *16*, 31–39.
60. M. Rao, D. G. Odom, J. Oro, *J. Mol. Evol.* **1980**, *15*, 317–331.
61. D. G. Odom, M. Rao, J. G. Lawless, J. Oro, *J. Mol. Evol.* **1979**, *12*, 365–367.
62. N. Kitadai, K. Nishiuchi, *Astrobiology* **2019**, *19*, 1363–1376.

63. K. B. Ayala-Luis, C. B. Koch, H. C. B. Hansen, *Appl. Clay Sci.* **2010**, *48*, 334–341.
64. M. Usman, J. M. Byrne, A. Chaudhary, S. Orsetti, K. Hanna, C. Ruby, A. Kappler, S. B. Haderlein, *Chem. Rev.* **2018**, *118*, 3251–3304.
65. L. Simon, M. François, P. Refait, G. Renaudin, M. Lelaurain, J.-M. R. Génin, *Solid State Sci.* **2003**, *5*, 327–334.
66. D. Guerbois, G. Ona-Nguema, G. Morin, M. Abdelmoula, A. M. Laverman, J. M. Mouchel, K. Barthelemy, F. Maillot, J.Brest, *Environ. Sci. Technol.* **2014**, *48*, 4505–4514.
67. J.-M. R. Génin, P. Refait, G. Bourrié, M. Abdelmoula, F. Trolard, *Appl.Geochem.* **2001**, *16*, 559–570.
68. J.-M. R. Génin, C. Ruby, C. Upadhyay, *Solid State Sci.* **2006**, *8*, 1330–1343.
69. E. Camprubi, S. F. Jordan, R. Vasiliadou, N. Lane, *IUBMB Life* **2017**, *69*, 373–381.
70. J. B. S. Haldane, *Rationalist Annual* **1929**, *3*, 3–10.
71. A. I. Oparin, *Origin of Life*, McMillan, New York, **1938**.
72. S. L. Miller, H. C. Urey, *Science* **1959**, *130*, 245–251.
73. W. Martin, M. J. Russell, *Philos.Trans. Roy. Soc. London B* **2007**, *362*, 1887–925.
74. N. Lane, *The Vital Question. Energy, Evolution and the Origins of Complex Life*, Norton & Company, New York, USA, **2015**.

6

The Formation of Iron Biominerals in Magnetotactic Bacteria

René Uebe and Dirk Schüler

Department of Microbiology, University of Bayreuth,
Universitätsstrasse 30, D-95447 Bayreuth, Germany
<rene.uebe@uni-bayreuth.de>
<dirk.schueler@uni-bayreuth.de>

Metal Ions in Life Sciences, Volume 21 Guest Editors: Peter M. H. Kroneck and Martha E. Sosa Torres
Series Editors: Astrid Sigel, Eva Freisinger, and Roland K. O. Sigel

https://doi.org/10.1515/9783110589771-006

Abstract: Magnetotactic bacteria (MTB) form magnetosomes, which are intracellular organelles that consist of ferrimagnetic crystals of a magnetic mineral. To build these organelles, large amounts of iron are sequestered and biomineralized in specific membrane-enclosed intracellular compartments. Magnetosome biosynthesis is under spatio-temporal control by a number of specific factors and functions. The resulting cellular dipole moment acts like a compass needle which aligns the cell in the geomagnetic field. This magnetotaxis is assumed to facilitate the navigation of the actively swimming bacterial cells along vertical redox gradients within stratified sediments of natural waters, where MTB are highly abundant. In this contribution, we present some recent knowledge on the diversity and ecology of MTB and the process of magnetosome biomineralization, as well as some geochemical and palaeomagnetic implications of magnetosome formation.

Keywords: biomineralization · greigite · magnetite · magnetofossils · magnetosome · magnetotaxis

1. INTRODUCTION

A particularly remarkable example for the accumulation and biomineralization of metals is represented by the magnetosomes of magnetotactic bacteria (MTB). Magnetosomes are intracellular organelles which consist of ferrimagnetic membrane-enveloped crystals of a magnetic mineral, either magnetite or greigite, that are aligned in one or several linear chains (Figure 1) [1, 2]. To build these organelles, large amounts of iron are sequestered in specific membrane-enclosed intra-

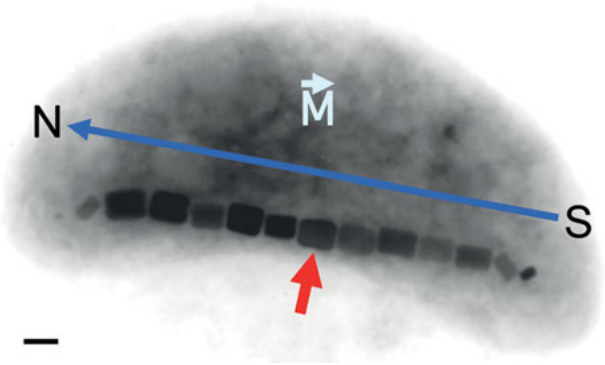

Figure 1. Electron micrograph of an uncultured magnetic vibrio collected from Lake Chiemsee (Germany). The arrow indicates the chain of magnetosomes, which confers a magnetic dipole moment (drawn in blue) to the cell.

cellular compartments. The resulting magnetic dipole moment acts like a compass needle which aligns the cell in the geomagnetic field while it actively swims. This "magnetotaxis" is assumed to facilitate the navigation of cells along vertical redox gradients within stratified sediments of natural waters, where MTB are highly abundant [3–5].

2. PHYLOGENETIC AND MORPHOLOGICAL DIVERSITY OF MAGNETOTACTIC BACTERIA

MTB display a huge diversity of cell morphologies, including rods, vibrios, spirilla, cocci, and even multicellular magnetic consortia (Figure 2) [6–9]. In addition to the presence of magnetosomes and despite of their phylogenetic, metabolic and morphological diversity, all known MTB have a Gram-negative type of cell wall, are motile by flagella, and have a microaerophilic or anaerobic lifestyle. While the majority of environmental MTB still cannot be cultured in the lab, they can be easily detected and collected from environmental samples by taking advantage of their conspicuous magnetically directed motility. This has facilitated numerous targeted metagenomic and single-cell genomic studies, which revealed a tremendous phylogenetic diversity. MTB do not represent a homogenous taxonomic group, but instead are distributed over several eubacterial taxa which contain non-magnetotactic species as well. The majority of MTB described so

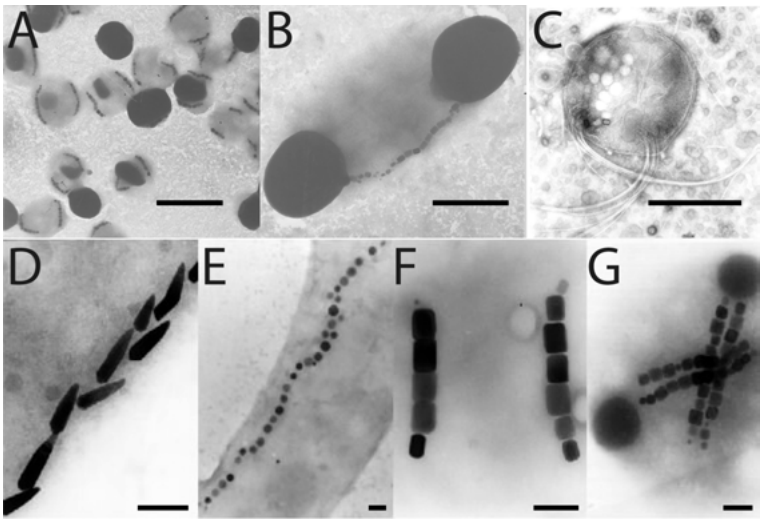

Figure 2. (**A–C**) Electron micrographs of different morphotypes of MTB collected from freshwater sediment samples, showing different magnetotactic cocci (**A**, **C**) and a large rod (**B**) (bars represent 1 μm). (**D–G**) Micrographs of magnetosome crystals from various magnetotactic bacteria, showing bullet-shaped (**D**), cubo-octahedral (**E**), and elongated prismatic morphologies (**F**, **G**) (bars represent 100 nm).

far belong to six subdivisions of Proteobacteria (α, γ, δ, ζ, η, and λ), some are affiliated with the *Nitrospirae* and *Omnitrophica* phyla [10–19], and even with some lineages within the deep-branching *Latescibacteria* and *Planctomycetes* [18]. Magnetosome biogenesis is thus a polyphyletic and possibly ancient trait [2, 9, 20].

3. STRUCTURE AND BIOMINERALIZATION OF MAGNETOSOMES

3.1. Magnetosome Structure

Magnetosome crystals vary widely with respect to their shape, size, number, and arrangement (Figure 2). MTB belonging to the α-, β-, η- and γ-Proteobacteria biomineralize highly regular crystals of magnetite (Fe_3O_4) with cubooctahedral or elongated prismatic morphologies. In contrast, MTB belonging to the δ-Proteobacteria biomineralize crystals of magnetite, greigite (Fe_3S_4), or both types of minerals [7, 8, 10, 21, 22]. Their magnetite crystals are bullet-shaped, and are structurally less perfect compared to the magnetite crystals produced by other Proteobacteria. Greigite crystals of the δ-Proteo-MTB are often equidimensional, with irregularly-shaped surfaces [23], and lack the morphological perfection of magnetite magnetosomes produced by other MTB. *Nitrospirae* and *Omnitrophica* MTB also biomineralize bullet-shaped magnetite crystals akin to those of the δ-Proteo-MTB, but are unable to form greigite crystals [12, 22, 24] (Figure 3).

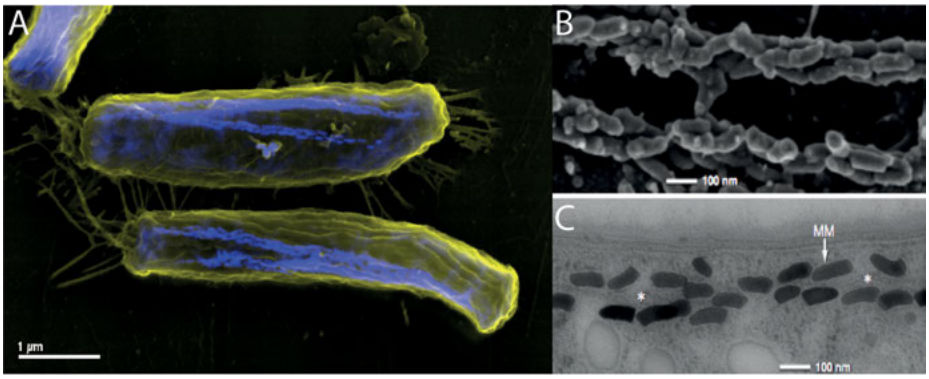

Figure 3. (**A**) Scanning electron micrograph of two cells of the uncultured '*Candidatus* M. bavaricum' from the *Nitrospirae* phylum. Magnetosome crystals consisting of magnetite are visualized by backscattered electrons (blue). The large rod-shaped cells contain several hundreds of magetosomes aligned in several bundles of chains. (**B**) Higher magnification scanning and (**C**) transmission electron micrographs of magnetosome chains of '*Ca.* M. bavaricum', revealing the bullet-shaped, slightly kinked morphology of the crystals. Micrographs by Gerhard Wanner, LMU München, modified after [24] and [25].

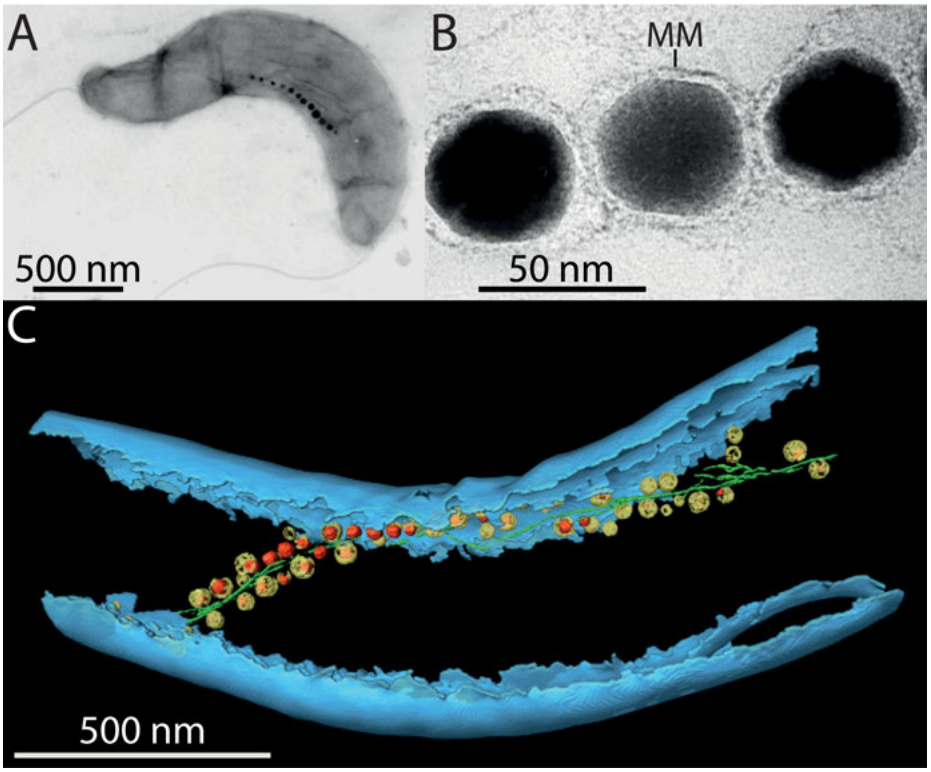

Figure 4. (**A**) Electron micrograph of a cell of the Alphaproteobacterium *Magnetospirillum gryphiswaldense.* (**B**) Electron micrograph of solated magnetosomes of *M. gryphiswaldense* showing the magnetosome membrane (MM) enveloping each magnetite crystal. (**C**) Segmented cryo-electron tomogram of a *M. gryphiswaldense* cell. The outer and cytoplasmic membranes are depicted in blue, magnetosome membranes in yellow, magnetite crystals in red and the cytoskeletal magnetosome filament in green. Tomogram by Oliver Raschdorf, LMU München/MPI Martinsried, modified after [62].

Most of the knowledge on the biomineralization of magnetosomes and its molecular control relies on studies of several species belonging to the α-proteobacterial genus *Magnetospirillum* (Figure 4A). In contrast to most other MTB, magnetospirilla can be reasonably well cultured in the lab in pure culture because of their versatile facultative anaerobic, chemo-organoheterotrophic lifestyle and moderate robustness against higher oxygen concentrations. Importantly, two species – *M. magneticum*, and *M. gryphiswaldense* – can be genetically manipulated and therefore served as models in many studies [26–31]. In both species, the magnetite crystals have a cubo-octahedral morphology with sizes of ~35–50 nm (Figure 4B) [32, 33]. Magnetite grains within this size range are in the stable single magnetic-domain state in which all elementary magnetic dipoles of the crystals are permanently aligned parallel to each other [34, 35]. Since magnetite crystals of magnetospirilla are also characterized by a highly controlled crystallo-

graphic structure and narrow size distribution, they exhibit exceptionally strong magnetic properties [36]. The possibility to display additional functional moieties on their surface by chemical or genetic coupling makes them also attractive as biogenic magnetic particles in a number of biomedical and biotechnical applications such as magnetic hyperthermia, as contrast agents in magnetic imaging techniques such as magnetic particle imaging and magnetic resonance imaging [37–41] and for magnetic drug targeting [42, 43].

A prerequisite for high quality magnetite particles is the precise control over the iron concentration as well as the redox and pH conditions during biomineralization. In magnetospirilla and probably all other MTB, this is achieved by compartmentalization of the biomineralization reaction within 10–70 nm large magnetosome vesicles that are formed by a 5–6 nm thick proteinaceous phospholipid bilayer, the magnetosome membrane (MM). Cryo-electron tomography revealed that at least some MMs are contiguous with the cytoplasmic membrane suggesting that vesicles are formed by invagination from the cytoplasmic membrane [26]. Consistent with this idea, the MM was found to have a lipid composition similar to the cytoplasmic membrane [44, 45], but contains a set of at least 30 specific proteins [44–48]. Recent genetic analyses confirmed that these proteins regulate magnetosome biogenesis which could be dissected into four separate steps: (i) Magnetosome membrane invagination and protein targeting, (ii) iron import into the vesicles, (iii) magnetite crystallization and crystal growth, and (iv) magnetosome chain formation.

These proteins are encoded by so-called *mam* (*magnetosome membrane*) and *mms* (*magnetosome membrane-specific*) gene clusters within a genomic island-like region (magnetosome island (MAI)), which was first discovered in *M. gryphiswaldense* [31, 49], but later found in all MTB studied so far. The MAI is highly variable between different species, but shares a universal set of core genes. Nine of these genes (*mamABEIKMOPQ*) are conserved in all MTB (including greigite producers), while a further gene, *mamL*, is also conserved in all magnetite producers [10]. This suggests that this minimal gene set encodes the universal core functions of magnetosome biosynthesis: The invagination of empty magnetosome membrane vesicles is controlled primarily by the cation diffusion facilitator MamBM heterodimer [50]. This generates a nano-reactor in which physicochemical conditions for biomineralization are tightly controlled. Next, iron is transported into the magnetosome vesicles by MamBM and others [50, 51]. Iron is then partially oxidized by the ferro-oxidase activity of MamE and MamP, which contain the *c*-type cytochrome "magnetochrome" domain unique to MTB [52–55]. This step is followed by mineral nucleation putatively regulated by MamO and MamI. MamQ and MamL are assumed to have as-yet uncharacterized functions in the control of crystal growth [56]. The highly conserved core protein MamA is not essential for biomineralization, but involved in formation of a "magnetosomal matrix" priming magnetosome biosynthesis [27, 57, 58]. Nascent particles are then concatenated into linear chains along a dynamic filamentous cytoskeletal network established by the actin-like MamK protein [26, 44, 59, 60], which in some MTB forms a more complex "Magnetoskeleton" together with other cytoskeletal constituents (Figure 4C) [61]. In addition to these

core proteins, further group-specific proteins are also encoded within the MAI clusters. These variable set of genes are speculated to account for the stunning diversity of magnetosome biomineralization observed in many environmental, mostly uncultured MTB, in a manner which so far is poorly understood.

3.2. Uptake and Intracellular Sequestration of Iron

Magnetotactic bacteria are able to accumulate large amounts of extracellular iron for the synthesis of intracellular magnetite or greigite crystals. The intracellular iron content of *M. gryphiswaldense*, for example, has been shown to account for up to 4 % of the cell dry weight [63]. '*Candidatus* Magnetobacterium bavaricum' an uncultured MTB which produces more than 1000 magnetosomes per cell (Figure 3), may even incorporate up to 10 % iron [64]. Thus, the cellular iron content of magnetosome-forming MTB is at least 100-times higher than that of non-magnetic bacteria such as *Escherichia coli* (0.027 % iron per dry weight, [65]). By contrast, the intracellular iron content of aerobically grown non-magnetic cells of *M. gryphiswaldense* was found to be similar to that of *E. coli* (0.02 to 0.06 % of dry weight) suggesting that magnetosomes contain up to 99 % of the cell-bound iron [44, 66]. In contrast, single-cell iron content and iron isotopic studies with *M. magneticum* revealed that magnetite accounts for only 50–80 % of the cellular iron [67–69]. Nevertheless, in both species huge increases of the intracellular iron content could be observed upon induction of magnetite biomineralization by oxygen depletion or addition of high iron concentrations which indicates that iron uptake is tightly coupled to magnetite biomineralization [66, 69].

For magnetite biosynthesis, extracellular iron can be taken up as Fe(III) or Fe(II) ions. Fe(III) iron ions, however, seem to be preferred as Fe(III) iron uptake proceeds at about 7-fold higher rates than Fe(II) iron uptake (0.43 versus 0.06 nmol min^{-1} mg cell dry $weight^{-1}$, respectively) [70, 71]. Under optimal conditions, i.e., magnetite biomineralization inducing low oxygen and high extracellular iron concentrations, iron uptake rates increase to about 0.8 to 1 nmol min^{-1} mg cell dry $weight^{-1}$ [71–73] which is one of the highest Fe uptakes rates in bacteria reported so far. It was thus speculated that complex cytoplasmic membrane iron uptake systems, different from known transport mechanisms in other microorganisms, are active in magnetospirilla and other MTBs [74]. However, no unique transporters that would be specific for MTB could be identified so far. Instead, several generic iron uptake systems commonly found in other Gram-negative bacteria were reported [75–79]. In addition, many of these identified iron uptake systems are only poorly conserved between different *Magnetospirillum* species. *M. magneticum*, for example, was reported to produce hydroxamate- and catechol-type siderophores whereas *M. magnetotacticum* forms only hydroxamate siderophores and *M. gryphiswaldense* seems to be unable to form siderophores at all [71, 77–80]. Furthermore, ferrous iron transporters of the FTR1 family are encoded in the genomes of *M. magneticum* and *M. magnetotacticum* but not in *M. gryphiswaldense*, which, on the other hand, harbors a Fe(III)

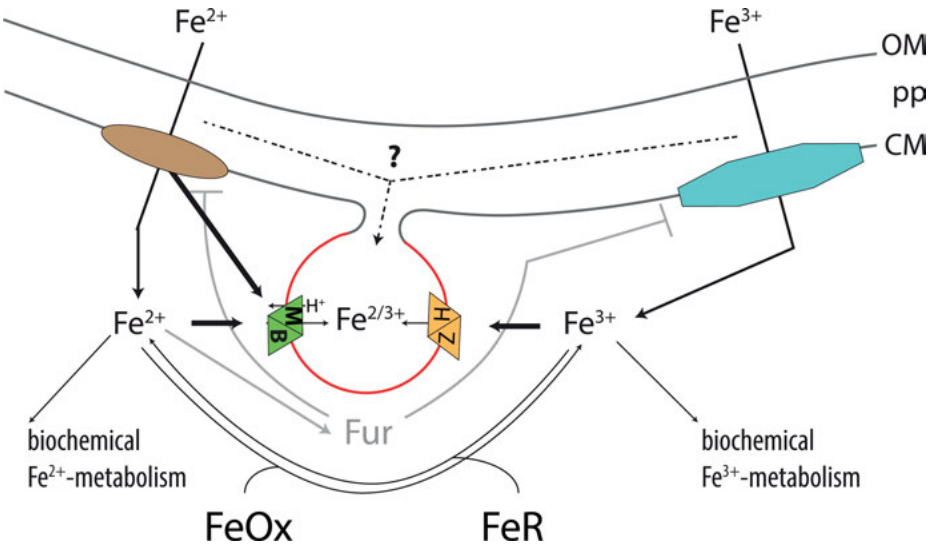

Figure 5. Model of iron uptake in magnetospirilla. Extracellular iron is imported into the cytoplasm by cytoplasmic membrane transporters. Subsequently, iron is transported into MM vesicles by magnetosome-specific transporters (Fe^{2+} is probably transported by MamB and MamM, and Fe^{3+} by MamH and MamZ; single letters denote respective Mam proteins). An alternative route might proceed directly from the periplasm (pp). Iron oxidases (FeOx) and reductases (FeR) regulate the intracellular Fe^{2+}/Fe^{3+} ratio. Fe^{2+} acts as a co-repressor of the ferric uptake regulator (Fur), which is a transcriptional regulator of iron import genes but not magnetosome genes.

iron-specific ABC transport system that is absent from *M. magneticum* and *M. magnetotacticum* [74, 80].

The only iron uptake system that appears to be universal among MTB is the Fe(II) iron transporter FeoB of which one copy is even encoded within the MAI [10], while another copy is usually encoded elsewhere in the genome. Notably, transcription of *feoB* and other Fe(II) iron transport systems are upregulated under microxic and high Fe(III) iron conditions in *M. magneticum* [74]. Thus, although magnetospirilla show only low Fe(II) iron uptake rates, Fe(II) iron uptake systems seem to be more abundant and important under magnetite-inducing conditions than Fe(III) iron uptake systems. In agreement with these findings, deletion of two different *feoB* genes in *M. gryphiswaldense* resulted in significantly decreased magnetite biomineralization [75, 76]. These results, furthermore, indicate that iron is first transported through the outer and inner membranes into the cell before it is imported into magnetosomes (Figure 5A). This MM-directed iron transport is likely catalyzed by two distinct import machineries. The first system is composed of MamB and MamM which are members of the ubiquitous cation diffusion facilitator family [50]. Members of this family are well known to transport divalent metal cations from the cytosol into organelles or out of the cell using electrochemical gradients (H^+ or K^+) as energy source [81]. In the case of MamB and MamM, the energy for Fe(II) iron trans-

port might be derived partly from protons which are generated within magnetosomes during magnetite biomineralization [63]. The second putative magnetosome-directed iron import system is composed of the major facilitator (MFS) superfamily proteins MamH and MamZ [51]. MFS transporters also use electrochemical gradients to energize transport of a single solute (uniport) or couple the movement of a substrate with a second substrate (antiport or symport) [82]. Since the iron-transporting role for MamH and MamZ is only based on indirect evidence [51], it is currently not known which species of iron is transported.

In agreement with an intracellular iron transport route, Mössbauer spectroscopy studies with *M. magnetotacticum* and *M. gryphiswaldense*, respectively, identified intracellular Fe(II) and Fe(III) iron species as putative intermediates of the iron biomineralization pathway [70, 83]. But although both studies identified similar iron metabolites, they proposed different iron biomineralization pathways. The *M. gryphiswaldense* study, for example, proposed that the intracellular Fe(III) iron species are membrane-bound ferrihydrite-containing ferritins which, together with a membrane-bound Fe(II) iron species, release iron at the MM to enable magnetite crystallization by fast coprecipitation of Fe^{2+} and Fe^{3+} [70]. It was furthermore suggested that iron is processed to the MM directly from the cell membranes without iron transport through the cytoplasm which implies that pathways for magnetite formation and biochemical iron uptake are distinct [70]. In contrast, data from *M. magnetotacticum* indicated that, after cellular import, Fe(II) iron is oxidized to a low-density hydrous Fe(III) oxide which is dehydrated to the precursor mineral ferrihydrite that is finally partially reduced to magnetite [83]. Interestingly, later X-ray absorption near edge structure and high-resolution transmission electron microscopy studies on magnetite biomineralization in *M. gryphiswaldense* and *M. magneticum* also revealed a ferritin-like ferrihydrite phase as a magnetite intermediate [84, 85] while mutational analysis or X-ray magnetic circular dichroism studies with *M. gryphiswaldense* proposed that magnetite forms by phase transition from other precursor minerals like the metastable ε-Fe_2O_3 and/or the thermodynamically stable α-Fe_2O_3 (hematite) phases [86, 87].

Thus, although many studies using different techniques tried to elucidate how MTB biomineralize magnetite, the exact pathway of iron uptake and magnetite biomineralization in MTB is still poorly understood. However, at least some clarification was recently achieved by a combination of Mössbauer spectroscopy and deletion mutagenesis in *M. gryphiswaldense*. It could be shown that the heterooligomeric iron storage protein bacterioferritin is identical with the putative ferritin-like ferrihydrite magnetite precursor, but dispensable for magnetite biomineralization and thus is not involved in the biomineralization pathway [88].

3.3. Redox Control and Magnetite Crystallization

Magnetite is a mixed-valence iron oxide ($Fe^{2+}Fe^{3+}_2O_4$) with a ratio of 1 : 2 between Fe(II) and Fe(III) iron. Since Fe(II) iron is rapidly oxidized by dioxygen, magnetite formation typically requires slightly negative redox potentials (i.e., –0.2 to –0.4 V) under neutral or basic pH conditions [63]. These low redox poten-

tials and pH conditions probably cannot be maintained under high O_2 concentrations or low external pH, respectively. Thus, *M. gryphiswaldense* fails to form magnetite under low pH or O_2 concentrations of more than 24 μM [73, 89].

The observation that under suboxic conditions magnetite biomineralization can be induced by uptake of either Fe(II) or Fe(III) iron indicates that cells possess mechanisms to adjust the correct Fe(II) to Fe(III) iron ratio. Indeed, several soluble ferrireductases that loosely associate with the cellular membrane were discovered in *M. gryphiswaldense* and *M. magnetotacticum*, suggesting that iron can be reduced before or after transport through the cytoplasmic membrane [90, 91]. Consistent with this idea, a membrane-bound pool of Fe(II) iron was identified by Mößbauer spectroscopic analyses [70]. Furthermore, the importance of iron reduction was shown by the inability of a ferrireductase double deletion mutant to biomineralize magnetite [92].

In addition to these iron-specific redox-active enzymes, magnetite biomineralization in *M. gryphiswaldense* is also affected by the overall redox status of the cell. For example, growth on carbon sources which are slightly more reduced than the average cell biomass (e.g., acetate) impaired magnetite biomineralization in *M. gryphiswaldense* [93]. Similarly, magnetite biomineralization was severely affected by deletion of respiratory chain constituents (*nap*, *nirS*, cbb_3] or the O_2-responsive transcriptional regulator gene *fnr* [93–96]. It has therefore been suggested that the periplasmic nitrate (NO_3^-) reductase Nap transfers electrons from the quinone pool to the magnetosomes via its CymA-like multiheme cytochrome subunit NapC [52]. In contrast, the subsequent enzyme of the denitrification pathway, the periplasmic nitrite (NO_2^-) reductase NirS, was found to use NO_2^- as an electron acceptor for the oxidation of Fe(II) iron *in vitro* and thus might serve as an iron oxidase *in vivo* [97]. More recent work on mixotrophic NO_3^--reducing Fe(II)-oxidizing bacteria, however, suggested that NO_2^- itself may abiotically oxidize Fe(II) during heterotrophic denitrification [98].

Besides these putative cellular iron oxidases and reductases, several proteins of the magnetosome membrane might also possess such activities. The major facilitator superfamily protein MamZ, for example, contains a heme *b*-binding YedZ-like domain with putative ferric reductase activity [51]. MamE, MamP, MamT, and MamX also contain redox-active *c*-type cytochrome-like domains, so-called magnetochrome domains [52]. Since purified MamP of *M. magneticum* was shown to contribute to the formation of Fe(III) ferrihydrite or mixed-valence iron oxides from Fe(II) iron *in vitro* this protein is suggested to act as an iron oxidase *in vivo* [53, 54]. Whether magnetochrome domains generally act as iron oxidases is currently not clear, since the magnetochrome deletion phenotypes differ significantly. Deletion mutants of *MamT* in *M. magneticum* and *M. gryphiswaldense*, for example, produce magnetite particles that are significantly smaller than those of the wild-type. In contrast, deletion of *MamP* in *M. magneticum* and *M. gryphiswaldense* caused the formation of very few magnetite particles with relatively large diameters which are flanked by small, irregular-shaped poorly crystalline particles [54, 56, 99]. Thus, further studies are required to clarify the individual role of the magnetochrome-containing proteins.

4. ENVIRONMENTAL AND BIOGEOCHEMICAL IMPLICATIONS OF MAGNETOSOME BIOMINERALIZATION

4.1. Ecology, Occurrence, and Distribution of Magnetotactic Bacteria

Numerous studies have documented the ubiquitous occurrence of MTB in many aquatic environments including lakes, rivers, creeks, ponds, estuaries, lagoons, swamps, wet soils, and intertidal zones. Because of their global distribution and magnetotactic behavior that enables their selective identification, collection and analysis directly from environmental sources and independent of cultivation, MTB were suggested as a useful model for addressing questions in microbial ecology and biogeography [17, 20]. Despite of the diversity of habitats, the general characteristics of environments where MTB are found in the highest numbers include a neutral to slightly alkaline pH, suboxic to anoxic conditions, the presence of dissolved iron, and the presence of sulfide (S^{2-}) for greigite-producing MTB [9, 13, 14, 21, 100–106]. More recent findings show that some MTB occupy extreme environments [107] including hot springs [108], or saline-alkaline lakes [103, 109]. In addition, MTB were detected in deep-sea environments [110, 111].

Contrary to what one might expect, the occurrence of MTB appears not to depend on particularly high concentrations of iron in the environment, and on the opposite, MTB are absent from environments with exceptionally high concentrations of iron such as iron-rich seeps and ditches as well as acid mine drainages [9, 13, 112]. In depth profiles of freshwater microcosm sediments, for example, the occurrence of MTB coincided with the availability of significant amounts (ca. 5–60 μM) of soluble Fe(II) [13]. Notably, this is roughly equivalent to the moderate micromolar iron concentrations (10–100 μM) which were found to saturate iron uptake and magnetite biomineralization in pure cultures of *M. gryphiswaldense* [66, 71].

The largest numbers of MTB are typically found at or slightly below the oxic-anoxic transition zone (OATZ) of sediments or chemically stratified water columns. Moreover, within the OATZ itself, different species of MTB occupy different positions that represent different specific chemical conditions at that depth. For example, MTB in microcosms with sediment samples from several ponds and lakes were found to occur in narrow, but very dense layers close to the OATZ and have been estimated to be among the locally most abundant microorganisms, occurring in numbers of up to 1.5×10^7 cells/cm^3, which corresponded to about 1% of the total bacterial cell number in the upper sediment layer [13]. In this study, the occurrence and abundance of diverse MTB was correlated to several geochemical parameters. For example, the occurrence of MTB was restricted to a narrow layer 5–15 mm below the sediment surface, which was overlapping or closely below the maximum oxygen and nitrate penetration depth. While different species showed different preferences within vertical gradients, the largest proportion of MTB was detected within the suboxic zone, and oxygen

was the main geochemical determinant for the vertical distribution of MTB [13]. Another study by He et al. [113] also suggested that different freshwater MTB species occupy distinctly different niches in sediment microcosms, and their horizontal positioning is heterogeneous and under constant flux.

A detailed profile analysis of the giant rod '*Ca.* M. bavaricum' (Figure 3) in sediments from a freshwater lake (Lake Chiemsee, Germany) revealed that the cells were located at one or two peaks of up to about 5×10^5 cells/mL within a rather narrow layer located 5–10 mm below the sediment surface, which again was correlated with low oxygen concentrations of about 5–30 μM O_2 [25]. Again, no clear correlation with other geochemical parameters was observed. In a previous study, this organism constituted approximately 30 % of the microbial biovolume in that layer in sediments from the same site [114].

In marine environments, MTB were reported to reach population densities of 10^3–10^5 cells mL^{-1} [115, 116]. Magnetite-producing MTB were most abundant at the top of the chemocline of the chemically stratified water column of a brackish pond (Salt pond, Massachusetts, USA). They peaked directly above a zone with maximal Fe(II) iron concentration, a distributional pattern typical for sulfide oxidizers. In contrast, greigite-producing MTB were predominantly found at lower depths at the base of the chemocline where sulfide became detectable [115, 117, 118]. Consistent with the prevalence of environmental MTB populations in narrow suboxic layers, cultures of magnetospirilla show a strong micro-aerotactic preference for low O_2 concentrations, and the formation of very sharp aerotactic bands is a common characteristic of several MTB when cultivated in O_2-gradients in semisolid agar media or observed in microcapillaries in laboratory conditions [5, 119–121].

In conclusion, the distribution of natural MTB populations in sediments, as well as the results from laboratory studies of cultured species suggest that MTB are typical gradient organisms, which derive energy for growth from the proximity of reductants (such as organic acids or reduced sulfur compounds) and oxidants (such as O_2, NO_3^-, or SO_4^{2-}) at a chemical interface, and occur in very narrow layers at particular locations relative to this interface [13, 14, 115]. From studies of the available laboratory cultures and metabolic predictions based on genomic analysis of uncultured MTB, it seems that all known MTB perform a respiratory type of metabolism. Depending on the particular species and environmental condition, they can oxidize simple organic compounds or reduced sulfur compounds in the presence of low concentrations of O_2 [122–124], or anaerobically with NO_3^- or SO_4^{2-}, and many MTB are capable of a chemolithoautotrophic lifestyle [12, 93, 125] and can fix molecular nitrogen (N_2) [12, 17, 126].

4.1.1. Association and Symbiosis of Magnetotactic Bacteria with Eukaryotes

Magnetosome-producing bacteria have been detected in marine bivalves and interpreted as symbionts that were incorporated by the host, and eventually lost the ability to swim and to build regular magnetosome chains [127]. Interestingly, this observation was interpreted as support for the hypothesis that the utilization of

symbiotic MTB may even underlie the magnetic sensing capability of higher animals, thus providing a possible explanation for the still-elusive magnetic sensor in metazoa [128]. However, the presence of magnetosomes (or their remnants) within bivalves was recently speculated to be likely more related to predation, rather than to symbiosis [129].

Diverse free-living protists, which exhibited a magnetotactic swimming behavior have been repeatedly observed to be present in the same microhabitats as MTB [115, 130–132]. Much like MTB, they migrated and accumulated at the edge of a hanging water drop in a magnetic field and contained magnetite particles with morphologies and dimensions similar to bacterial magnetosomes. However, for most of these observations it was suggested that the unusual magnetic response was most likely caused by the ingestion of MTB by grazing, rather than endogenous biomineralization of the protist itself. In fact, feeding predatory ciliates with magnetically purified multicellular MTB ('*Ca*. Magnetoglobus multicellularis') resulted in the accumulation and subsequent dissolution of the greigite magnetosomes within the acidic vacuoles of the ciliate [133]. Likewise, ciliates affiliated with the genus *Uronema* were able to ingest hundreds of MTB into acidic vacuoles and progressively became sensitive to magnetic fields in the same way as MTB. Thus, MTB grazing could be involved in recycling particulate iron back to a bioavailable form in the environment through dissolution [134].

In a more recent study [135], uncultured single-celled eukaryotic flagellates from two different Brazilian freshwater sites were observed harboring anisotropic bullet-shaped magnetite magnetosomes aligned in complex aggregations of multiple chains within the cell. Because of the unusually large size of the magnetosomes (twice as large as typical bacterial magnetosomes) and the absence of specific microcompartments typical of a bacterial cell, or digestive vacuoles, the observations rather supported the notion that magnetosomes indeed might originate from biomineralization by the eukaryote itself rather than ingested MTB, which however will require further verification by molecular methods [135].

Most recently, a genuinely symbiotic and magnetotactic protist belonging to the Euglenozoa was discovered in marine sediments [130]. In contrast to grazing magnetic protists, its magnetoreception was shown to be due to the presence of hundreds of ectosymbiotic Deltaproteobacteria biomineralizing magnetite magnetosomes aligned in regular chains. Unlike MTB grazers, the sensing and geolocalization in this biological system benefits both organisms thanks to the long-term cooperation established with the host, thereby forming a microbial magnetic holobiont. The partners' interdependency likely relies also on syntrophy based on the molecular H_2 provided by the protist that is being used by the bacteria to reduce sulfate in order to gain energy. Clearly, this spectacular discovery of magnetosome-producing holobionts has changed much of our vision of magnetoreception in unicellular eukaryotes as well as ecological niches of MTB [130].

4.2. Functions of Magnetosome Biomineralization

4.2.1. Magnetotaxis

The chain-like arrangement of magnetosome particles generates a magnetic dipole that passively rotates the bacterium into alignment with the Earth magnetic field as it swims actively by means of flagella. The most widely assumed function of this magnetotaxis is that navigating along the geomagnetic field allows MTB to more efficiently locate and maintain an optimal position within vertical chemical and redox gradients in water columns and sediments for survival and growth [9]. The overall direction of the Earth's field lines at any given location is the vectorial sum of the horizontal and vertical components of the geomagnetic field. At the equator, there is no vertical component, and the geomagnetic field lines are flat due to only the horizontal component. As one moves from the equator, toward either pole, the geomagnetic field lines deviate from the horizontal at an angle that increases to 90° at the poles where the horizontal component is absent [9]. Thus, geomagnetic field lines on most of Earth are inclined and provide a reliable path through vertically stratified redox gradients.

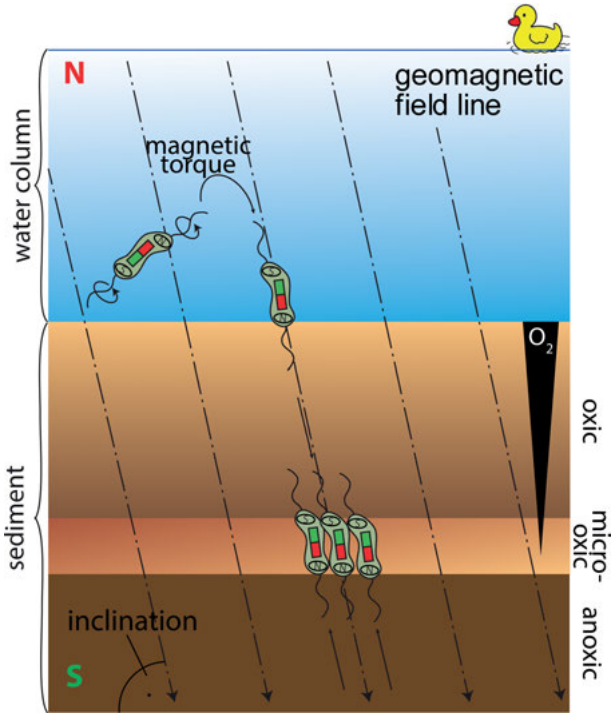

Figure 6. Model of magnetotaxis. The magnetic dipole moment caused by the magnetosome chain orients the cell parallel to the inclined geomagnetic field lines, much like a compass needle. This facilitates the search and positioning of the cell within vertical redox (e.g., O_2) gradients of aquatic sediments by active aerotactic swimming motility.

Most studies so far suggested that a low (micromolar) O_2 concentration is the most important factor determining vertical distribution of MTB within their native sediments and stratified water columns (Figure 6). To navigate efficiently within these gradients, MTB are thought to combine alignment with the geomagnetic field with aerotaxis to find zones with favorable O_2 and redox concentrations. The main benefit of this magneto-aerotaxis is that alignment to geomagnetic fields reduces random three-dimensional swimming walk to a linear movement along more or less vertical field lines. This likely represents a selective advantage in their natural habitat [2]. Under oxic conditions, that is, for example, when observed in the classical hanging drop, most MTB sampled from environmental sites generally display a preferred swimming polarity, which is mostly North-seeking on the Northern Hemisphere and South-seeking in the Southern Hemisphere. In the α-Proteo-MTB *M. gryphiswaldense* it was shown that swimming polarity can be reversed by sudden shifts from oxic to anoxic conditions and *vice versa* [5]. Thus, the inherited magnetic polarity bias in swimming facilitates an aerophobic reaction which upon exposure to harmful high O_2 concentrations in surface waters directs MTB efficiently downward along the inclined geomagnetic field lines toward micro- or anaerobic sediments. In *M. gryphiswaldense* (and probably other MTB) magneto-(micro)aerotaxis there is a direct molecular link between aerotactic sensing and the determination of magnetotactic polarity, through an unusually complex chemotactic sensory pathway. The function of magnetotaxis as a navigational mechanism is also strongly supported by the strict evolutionary optimization of magnetosomes as magnetic sensors: The magnetosome crystal size generally lies within the single magnetic-domain size range (35 to 120 nm) with the highest possible magnetic moment [63]. In addition, in most MTB, the magnetosomes are organized by a surprisingly complex cytoskeleton in one or several straight chains that add up their magnetic moments and are precisely positioned within the cell for most efficient magnetic navigation [5, 59, 61].

4.2.2. Other Putative Functions of Magnetosome Biomineralization

The theory of magnetotaxis as a navigational mechanism within the vertically inclined geomagnetic field is also supported by the predominant occurrence of North-seeking bacteria in the Northern Hemisphere, and South-seeking MTB in the Southern Hemisphere, which is consistent with the opposite directions of inclined field lines in the two hemispheres. Notwithstanding, MTB were also found to be abundant at the equator where South-seeking and North-seeking MTB appeared to be present in about equal concentrations [136]. However, because of the absence of any vertical inclination at the equator, the selective fitness advantage for magnetotaxis at this location is not obvious. In addition, several MTB, such as the large rod '*Ca.* M. bavaricum' biomineralize much more magnetosome particles as would be required for magnetotaxis (Figure 3) [24]. Therefore, besides magnetotaxis, other or additional potential advantages of producing magnetosomes have been suggested, which for instance include the detoxification of metal ions or reactive oxygen species which can form during oxygen respiration. During evolution, ancestral magnetosomes have been proposed

to play a primary role in scavenging reactive oxygen species which could react with magnetite, and synthesis of magnetosomes could potentially represent the first strategy developed by living organisms to scavenge the toxic effects of oxygen [137]. In fact, it was shown that magnetosomes of magnetospirilla may eliminate intracellular reactive oxygen species and exhibit peroxidase activity [138, 139].

A related role of magnetosomes that was proposed is the sequestration of toxic intracellular iron in a compact, non-hydrated, inert, and nontoxic form inside a vesicle [63]. It was also discussed whether iron biomineralized as magnetite or greigite could be resolubilized and used for metabolic requirements in iron starved cells [9]. However, experimental evidence supporting these hypotheses is still lacking.

4.2.3. The Magnetite Electrochemical Battery Hypothesis

It has also been speculated that MTB can use intracellular magnetite not only for orientation, but also for electron storage or as electron source to serve as an internal electrochemical battery to generate energy [140, 141]. Depending upon the geochemical conditions, mixed-valent Fe minerals, e.g., magnetite, contain varying amounts of Fe(II) and Fe(III) and therefore have the potential to function both as abiotic reductants and oxidants as well as electron donors or acceptors for Fe(II)-oxidizing and Fe(III)-reducing bacteria, respectively. Vertically aligned magnetic bacteria might actively cycle back and forth across redox gradients in their native sediments. In anoxic layers, the mineral core of magnetosomes could be reduced to magnetite, thereby "charging" the internal battery (by organic compounds, H_2, or HS^- as electron donors). While the bacterium is moving upward towards more oxic conditions, magnetite ($Fe^{2+}Fe_2^{3+}O_4$) will be become gradually oxidized and "discharged" to the ferrimagnetic spinel maghemite ($Fe_2^{3+}O_3$). The bacterium could then exploit the change in the redox state of the mineral to generate additional energy. Although this has been discussed with some controversy because of the relatively low energy yield in bacteria with only few magnetosome particles per cell [118], several preliminary observations seemed to be in line with this hypothesis. For instance, in lab cultures of *M. magneticum* grown in redox gradients magnetosomes from high O_2 conditions were more oxidized than those from low O_2 conditions, as the magnetosome battery hypothesis would predict [141], and some MTB with very high numbers of magnetosomes (up to 1000 per cell) such as '*Ca.*M. bavaricum' (Figure 3) in fact seem to fluctuate between oxidized and reduced sediment layers, resulting in a bimodal distribution [25]. Recent evidence has shown that Fe(III)-reducing and Fe(II)-oxidizing bacteria can use magnetite in such a capacity termed biogeobattery [142]. However, unambiguous experimental evidence for the magnetosome battery hypothesis is so far not available.

4.3. Magnetotactic Bacteria in Biogeochemical Cycling of Iron and Other Elements

Given their high abundance and ubiquitous occurrence, MTB are likely to play important roles in the geochemical cycling of iron, sulfur, nitrogen and carbon. As mentioned above, MTB are able to accumulate high amounts of iron from rather low ambient concentrations.

Due to the presence of magnetosomes, the intracellular iron content of MTB is about 100- to 1,000-fold higher than that in other microorganisms. The large amounts of Fe concentrated by MTB in intracellular magnetosomes (depending on the external iron concentration a maximum value of $\sim 10^{-6}$ ng of iron per cell) [69] indicate that nanomolar concentrations of Fe may be sequestered in biomass, considering their estimated population densities [115, 143]. It was estimated that globally MTB could generate $>10^{8}$ kg of magnetite per year [109, 144]. The stability of iron within magnetosomes, whether within cells or released from lysed cells in the environment, is also important to consider, as magnetite and greigite might represent either sources of bioavailable or unavailable sequestered iron, depending on whether these minerals are stable or dissolve under environmental conditions where they were deposited [145]. After cell death, magnetosome crystals are trapped into sediments that remove iron from the soluble pool. MTB may incorporate a significant fraction of the mass of dissolved iron transported to the ocean where dissolved iron limits nitrogen fixation and primary productivity [69]. In estuarine environments, MTB could act as a sink of iron and prevent accumulation of riverine dissolved iron in the ocean [146].

Besides iron, many MTB also are capable of intracellular accumulation of large amounts of other elements such as sulfur (S) and phosphorus (P) [109]. For example, in a recent study, Rivas-Lamelo et al. [147] showed that MTB of the *Magnetococcaceae* family accumulate large amounts of polyphosphates and appear as P hotspots in the particulate fraction at the oxic-anoxic interface in the water column of the meromictic ferruginous Lake Pavin, France. This high accumulation may also relate to the chemical conditions prevailing in the lake, and these magnetotactic cocci were suggested as new models playing a potentially important role in the phosphorus geochemical cycle. In another study, it was shown recently that bacterial polyphosphate inclusions within large MTB related to the genus *Magnetococcus* contribute substantially to the characteristic phosphorus peak observed within the suboxic zone of the Black Sea [148]. The bacteria contained about 25–35 % P, and it was proposed these large MTB shuttle up and down within the suboxic zone, scavenging phosphate (PO_4^{3-}) at the upper and releasing it at the lower boundary. In contrast to passive transport via metal oxides, this bacterial transport now provides a plausible explanation for the conspicuous phosphate profiles that had remained enigmatic until this study.

4.4. Bacterial Magnetosomes in the Geological Record: Crystallographic, Compositional, and Isotopic Signatures of "Magnetofossils"

After MTB bacteria die and become lysed (e.g., by bacteriophages or grazing predators), it is assumed that magnetosomes can be released as more or less intact magnetite crystals (Figure 7) [149–153]. Fossil magnetite from MTB was found to be well-preserved in suboxic freshwater sedimentary environments [154]. For comparison, magnetite dissolves easily in highly sulfidic environments, but a fraction can be preserved by formation of a pyrite coating [155]. In condi-

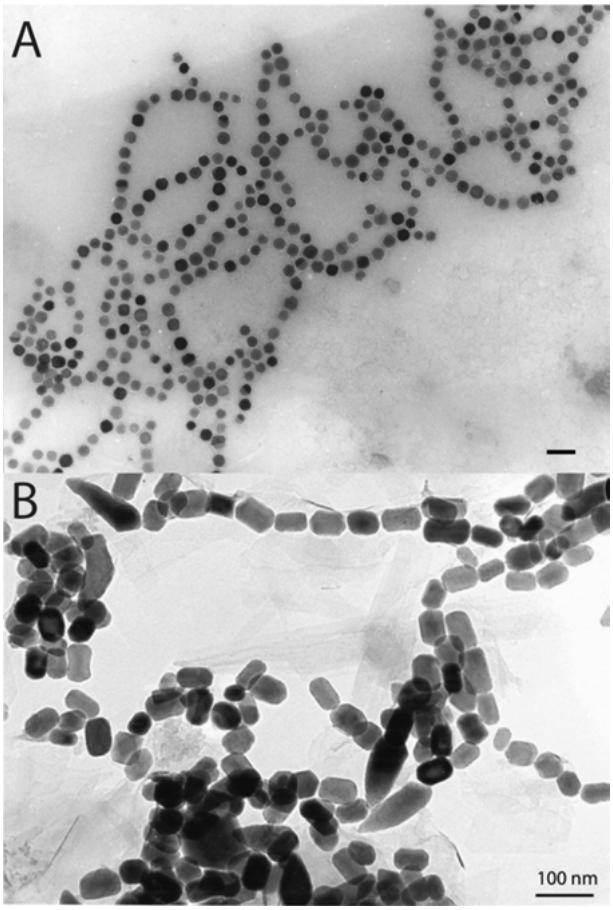

Figure 7. TEM micrographs of magnetosome crystals isolated from a lab culture of *M. gryphiswaldense* (**A**), and of magnetofossils (**B**) in a magnetic extract from Culver Cliff chalk. Magnetofossils have prismatic and irregular elongate magnetosome morphologies with some intact chains of prismatic crystals (*scale bars* = 100 nm). Figure 7B reproduced with permission from [157]; copyright 2008, Elsevier.

tions where magnetosome magnetite is assumed to be stable, the crystals have been used as a paleoenvironmental biomarker referred to as "magnetofossils", and considered as evidence for the previous presence of MTB in rocks as old as 700 million years [156] and even in ancient sediments of 2 billion years [145, 157]. These findings also suggest a significant role for MTB not only in present-day global iron cycling, but likely in the deposition of iron in sediments across geological history.

Magnetofossils can be identified by their characteristic morphologies, crystallinity, and sizes that are distinct from abiogenic magnetite, but resembling magnetosome particles isolated from lab cultures of extant MTB (Figure 7) [151, 158]. Greigite is also abundant and well-preserved in the rock record [159–161]. However, the distinctive morphology of magnetofossil greigite has not yet been used to distinguish it from inorganic greigite, although biogenic greigite crystals have been shown to display different size distributions than inorganic greigite [160]. Magnetofossils are important carriers of remnant magnetism both in the sedimentary and rock records [157, 162]. For example, it was estimated that about 10 % of the total magnetization in the uppermost sediment layer in Lake Chiemsee (Germany) is carried by bacterial magnetite [150]. MTB have even been suggested to be the source of magnetite chains found within the Martian meteorite ALH84001 [163], although this study was heavily debated and faced by growing skepticism [164].

Potential problems for using magnetosomes as biosignatures are due to the fact that diagenetic or metamorphic processes might result in changes to the magnetic properties of the mineral inclusions [165]. A combination of physical, mineralogical, and chemical characterization could be used to identify magnetite with trace element incorporations. In a recent study [166] the incorporation of 34 trace elements into magnetosomes formed by *Magnetospirillum magneticum* was analyzed, and it was found that biogenic magnetite is chemically very pure and incorporates 100 times less trace elements than synthetic magnetite. Alternatively, mass-dependent and -independent fractionation of Fe isotopes within magnetosomes might also be used as a potential proxy to investigate their ability to serve as biomarkers [67].

ACKNOWLEDGMENTS

This work was supported by the Deutsche Forschungsgemeinschaft (DFG) grants UE 200/1-1 to R.U., and Schu1080/9-2 to D.S., and the European Research Council (ERC) under the European Union's Horizon 2020 research and innovation program, grant agreement No 692637 to D.S.

ABBREVIATIONS

MAI	magnetosome island
MFS	major facilitator superfamily

MM	magnetosome membrane
MTB	magnetotactic bacteria
OATZ	oxic-anoxic transition zome
TEM	transmission electron microscopy

REFERENCES

1. R. P. Blakemore, *Science* **1975**, *190*, 377–379.
2. R. Uebe, D. Schüler, *Nat. Rev. Microbiol.* **2016**, *14*, 621–637.
3. D. Bazylinski, R. Frankel, *Nat. Rev. Microbiol.* **2004**, *2*, 217–230.
4. R. Blakemore, R. Frankel, A. Kalmijn, *Nature* **1980**, *286*, 384–385.
5. F. Popp, J. P. Armitage, D. Schüler, *Nat. Commun.* **2014**, *5*, 5398.
6. R. Wenter, G. Wanner, D. Schüler, J. Overmann, *Environ. Microbiol.* **2009**, *11*, 1493–1505.
7. M. Farina, D. Esquivel, H. G. P. Lins de Barros, *Nature* **1990**, *343*, 256–258.
8. S. Mann, N. H. C. Sparks, R. G. Board, *Adv. Microb. Physiol.* **1990**, *31*, 125–181.
9. C. T. Lefèvre, D. A. Bazylinski, *Microbiol. Mol. Biol. Rev.* **2013**, *77*, 497–526.
10. C. T. Lefèvre, D. Trubitsyn, F. Abreu, S. Kolinko, C. Jogler, L. G. P. de Almeida, A. T. R. de Vasconcelos, M. Kube, R. Reinhardt, U. Lins, D. Pignol, D. Schüler, D. A. Bazylinski, N. Ginet, *Environ. Microbiol.* **2013**, *15*, 2712–2735.
11. S. Kolinko, C. Jogler, E. Katzmann, G. Wanner, J. Peplies, D. Schüler, *Environ. Microbiol.* **2012**, *14*, 1709–1721.
12. S. Kolinko, M. Richter, F.-O. Glöckner, A. Brachmann, D. Schüler, *Environ. Microbiol.* **2016**, *18*, 21–37.
13. C. B. Flies, H. M. Jonkers, D. de Beer, K. Bosselmann, M. E. Böttcher, D. Schüler, *FEMS Microbiol. Ecol.* **2005**, *52*, 185–195.
14. C. B. Flies, J. Peplies, D. Schüler, *Appl. Environ. Microbiol.* **2005**, *71*, 2723–2731.
15. S. Spring, R. Amann, W. Ludwig, K. H. Schleifer, N. Petersen, *Syst. Appl. Microbiol.* **1992**, *15*, 116–122.
16. S. Spring, R. Amann, W. Ludwig, K. Schleifer, D. Schüler, K. Poralla, N. Petersen, *Syst. Appl. Microbiol.* **1994**, *17*, 501–508.
17. W. Lin, A. Deng, Z. Wang, Y. Li, T. Wen, L.-F. Wu, M. Wu, Y. Pan, *ISME J.* **2014**, *8*, 2463–2477.
18. W. Lin, W. Zhang, X. Zhao, A. P. Roberts, G. A. Paterson, D. A. Bazylinski, Y. Pan, *ISME J.* **2018**, *12*, 1508–1519.
19. C. T. Lefèvre, R. B. Frankel, F. Abreu, U. Lins, D. A. Bazylinski, *Environ. Microbiol.* **2011**, *13*, 538–549.
20. W. Lin, G. A. Paterson, Q. Zhu, Y. Wang, E. Kopylova, Y. Li, R. Knight, D. A. Bazylinski, R. Zhu, J. L. Kirschvink, Y. Pan, *Proc. Natl. Acad. Sci. USA* **2017**, *114*, 2171–2176.
21. C. T. Lefèvre, N. Menguy, F. Abreu, U. Lins, M. Pósfai, T. Prozorov, D. Pignol, R. B. Frankel, D. A. Bazylinski, *Science* **2011**, *334*, 1720–1723.
22. S. Kolinko, M. Richter, F.-O. Glöckner, A. Brachmann, D. Schüler, *Environ. Microbiol. Rep.* **2014**, *6*, 524–531.
23. M. Pósfai, C. T. Lefèvre, D. Trubitsyn, D. A. Bazylinski, R. B. Frankel, *Front. Microbiol.* **2013**, *4*, 344.
24. C. Jogler, G. Wanner, S. Kolinko, M. Niebler, R. Amann, N. Petersen, M. Kube, R. Reinhardt, D. Schüler, *Proc. Natl. Acad. Sci. USA* **2011**, *108*, 1134–1139.

25. C. Jogler, M. Niebler, W. Lin, M. Kube, G. Wanner, S. Kolinko, P. Stief, A. J. Beck, D. de Beer, N. Petersen, Y. Pan, R. Amann, R. Reinhardt, D. Schüler, *Environ. Microbiol.* **2010**, *12*, 2466–2478.
26. A. Komeili, Z. Li, D. K. Newman, G. J. Jensen, *Science* **2006**, *311*, 242–245.
27. A. Komeili, H. Vali, T. J. Beveridge, D. K. Newman, *Proc. Natl. Acad. Sci. USA* **2004**, *101*, 3839–3844.
28. D. Schultheiss, D. Schüler, *Arch. Microbiol.* **2003**, *179*, 89–94.
29. D. Schultheiss, M. Kube, D. Schüler, *Appl. Environ. Microbiol.* **2004**, *70*, 3624–3631.
30. M. Richter, M. Kube, D. Bazylinski, T. Lombardot, F. Glöckner, R. Reinhardt, D. Schüler, *J. Bacteriol.* **2007**, *189*, 4899–4910.
31. S. Ullrich, M. Kube, S. Schübbe, R. Reinhardt, D. Schüler, *J. Bacteriol.* **2005**, *187*, 7176–7184.
32. D. Murat, V. Falahati, L. Bertinetti, R. Csencsits, A. Körnig, K. Downing, D. Faivre, A. Komeili, *Mol. Microbiol.* **2012**, *85*, 684–699.
33. A. Lohße, S. Ullrich, E. Katzmann, S. Borg, G. Wanner, M. Richter, B. Voigt, T. Schweder, D. Schüler, *PLoS ONE* **2011**, *6*, e25561.
34. J. C. D. Ricci, J. L. Kirschvink, *J. Geophys. Res.* **1992**, *97*, 17309–17315.
35. R. F. Butler, S. Banerjee, *J. Geophys. Res.* **1975**, *80*, 4049–4058.
36. A. Fischer, M. Schmitz, B. Aichmayer, P. Fratzl, D. Faivre, *J. R. Soc. Interface* **2011**, *8*, 1011–1018.
37. A. Kraupner, D. Eberbeck, D. Heinke, R. Uebe, D. Schüler, A. Briel, *Nanoscale* **2017**, *9*, 5788–5793.
38. D. Heinke, A. Kraupner, D. Eberbeck, D. Schmidt, P. Radon, R. Uebe, D. Schüler, A. Briel, *Int. J. Mag. Part. Imag.* **2017**, *3*, 1706004.
39. R. Taukulis, M. Widdrat, M. Kumari, D. Heinke, M. Rumpler, É. Tompa, R. Uebe, A. Kraupner, A. Cebers, D. Schüler, M. Pósfai, A. M. Hirt, D. Faivre, *Magnetohydrodynamics* **2015**, *51*, 721–748.
40. E. Alphandéry, I. Chebbi, F. Guyot, M. Durand-Dubief, *Int. J. Hyperthermia* **2013**, *29*, 801–809.
41. E. Alphandéry, A. Idbaih, C. Adam, J.-Y. Delattre, C. Schmitt, F. Gazeau, F. Guyot, I. Chebbi, *J. Nanobiotechnol.* **2019**, *17*, 126.
42. E. Alphandéry, *Front. Bioeng. Biotechnol.* **2014**, *2*, 5.
43. E. B. Denkbaş, E. Çelik, E. Erdal, D. Kavaz, Ö. Akbal, G. Kara, C. Bayram, *Magnetically Based Nanocarriers in Drug Delivery*, in *Nanobiomaterials in Drug Delivery*, Ed. A. M. Grumezescu, William Andrew Publishing, Norwich, NY, **2016**, pp. 285–331.
44. K. Grünberg, E. C. Müller, A. Otto, R. Reszka, D. Linder, M. Kube, R. Reinhardt, D. Schüler, *Appl. Environ. Microbiol.* **2004**, *70*, 1040–1050.
45. Y. A. Gorby, T. J. Beveridge, R. Blakemore, *J. Bacteriol.* **1988**, *170*, 834–841.
46. K. Grünberg, C. Wawer, B. M. Tebo, D. Schüler, *Appl. Environ. Microbiol.* **2001**, *67*, 4573–4582.
47. M. Tanaka, Y. Okamura, A. Arakaki, T. Tanaka, H. Takeyama, T. Matsunaga, *Proteomics* **2006**, *6*, 5234–5247.
48. O. Raschdorf, F. Bonn, N. Zeytuni, R. Zarivach, D. Becher, D. Schüler, *J. Proteom.* **2018**, *172*, 88–99.
49. S. Schübbe, M. Kube, A. Scheffel, C. Wawer, U. Heyen, A. Meyerdierks, M. H. Madkour, F. Mayer, R. Reinhardt, D. Schüler, *J. Bacteriol.* **2003**, *185*, 5779–5790.
50. R. Uebe, K. Junge, V. Henn, G. Poxleitner, E. Katzmann, J. M. Plitzko, R. Zarivach, T. Kasama, G. Wanner, M. Pósfai, L. Böttger, B. Matzanke, D. Schüler, *Mol. Microbiol.* **2011**, *82*, 818–835.
51. O. Raschdorf, F. D. Müller, M. Pósfai, J. M. Plitzko, D. Schüler, *Mol. Microbiol.* **2013**, *89*, 872–886.

52. M. I. Siponen, G. Adryanczyk, N. Ginet, P. Arnoux, D. Pignol, *Biochem. Soc. Trans.* **2012**, *40*, 1319–1323.
53. M. I. Siponen, P. Legrand, M. Widdrat, S. R. Jones, W.-J. Zhang, M. C. Y. Chang, D. Faivre, P. Arnoux, D. Pignol, *Nature* **2013**, *502*, 681–684.
54. S. R. Jones, T. D. Wilson, M. E. Brown, L. Rahn-Lee, Y. Yu, L. L. Fredriksen, E. Ozyamak, A. Komeili, M. C. Y. Chang, *Proc. Natl. Acad. Sci. USA* **2015**, *112*, 3904–3909.
55. A. Taoka, Y. Eguchi, S. Mise, Z. Oestreicher, F. Uno, Y. Fukumori, *FEMS Microbiol. Lett.* **2014**, *358*, 21–29.
56. A. Lohße, S. Borg, O. Raschdorf, I. Kolinko, E. Tompa, M. Pósfai, D. Faivre, J. Baumgartner, D. Schüler, *J. Bacteriol.* **2014**, *196*, 2658–2669.
57. N. Zeytuni, E. Ozyamak, K. Ben-Harush, G. Davidov, M. Levin, Y. Gat, T. Moyal, A. Brik, A. Komeili, R. Zarivach, *Proc. Natl. Acad. Sci. USA* **2011**, *108*, E480-E487.
58. D. Yamamoto, A. Taoka, T. Uchihashi, H. Sasaki, H. Watanabe, T. Ando, Y. Fukumori, *Proc. Natl. Acad. Sci. USA* **2010**, *107*, 9382–9387.
59. M. Toro-Nahuelpan, F. D. Müller, S. Klumpp, J. M. Plitzko, M. Bramkamp, D. Schüler, *BMC Biol.* **2016**, *14*, 88.
60. O. Draper, M. E. Byrne, Z. Li, S. Keyhani, J. C. Barrozo, G. Jensen, A. Komeili, *Mol. Microbiol.* **2011**, *82*, 342–354.
61. M. Toro-Nahuelpan, G. Giacomelli, O. Raschdorf, S. Borg, J. M. Plitzko, M. Bramkamp, D. Schüler, F.-D. Müller, *Nat. Microbiol.* **2019**, *4*, 1978–1989.
62. O. Raschdorf, Y. Forstner, I. Kolinko, R. Uebe, J. M. Plitzko, D. Schüler, *PLoS Genet.* **2016**, *12*, e1006101.
63. D. Faivre, D. Schüler, *Chem. Rev.* **2008**, *108*, 4875–4898.
64. E. Bäuerlein, *Angew. Chem. Int. Ed.* **2003**, *42*, 614–641.
65. H. Abdul-Tehrani, A. J. Hudson, Y. S. Chang, A. R. Timms, C. Hawkins, J. M. Williams, P. M. Harrison, J. R. Guest, S. C. Andrews, *J. Bacteriol.* **1999**, *181*, 1415–1428.
66. D. Schüler, E. Bäuerlein, *J. Bacteriol.* **1998**, *180*, 159–162.
67. M. Amor, V. Busigny, P. Louvat, A. Gélabert, P. Cartigny, M. Durand-Dubief, G. Ona-Nguema, E. Alphandéry, I. Chebbi, F. Guyot, *Science* **2016**, *352*, 705–708.
68. M. Amor, V. Busigny, P. Louvat, M. Tharaud, A. Gélabert, P. Cartigny, J. Carlut, A. Isambert, M. Durand-Dubief, G. Ona-Nguema, E. Alphandéry, I. Chebbi, F. Guyot, *Geochim. Cosmochim. Acta* **2018**, *232*, 225–243.
69. M. Amor, M. Tharaud, A. Gélabert, A. Komeili, *Environ. Microbiol.* **2019**.
70. D. Faivre, L. H. Böttger, B. F. Matzanke, D. Schüler, *Angew. Chem. Int. Ed.* **2007**, *46*, 8495–8499.
71. D. Schüler, E. Bäuerlein, *Arch. Microbiol.* **1996**, *166*, 301–307.
72. D. Faivre, N. Menguy, M. Pósfai, D. Schüler, *Am. Mineral.* **2008**, *93*, 463–469.
73. C. Moisescu, S. Bonneville, S. Staniland, I. Ardelean, L. G. Benning, *Geomicrobiol. J.* **2011**, *28*, 590–600.
74. T. Suzuki, Y. Okamura, R. J. Calugay, H. Takeyama, T. Matsunaga, *J. Bacteriol.* **2006**, *188*, 2275–2279.
75. C. Rong, Y. Huang, W. Zhang, W. Jiang, Y. Li, J. Li, *Res. Microbiol.* **2008**, *159*, 530–536.
76. C. Rong, C. Zhang, Y. Zhang, L. Qi, J. Yang, G. Guan, Y. Li, J. Li, *J. Bacteriol.* **2012**, *194*, 3972–3976.
77. R. J. Calugay, H. Miyashita, Y. Okamura, T. Matsunaga, *FEMS Microbiol. Lett.* **2003**, *218*, 371–375.
78. R. J. Calugay, H. Takeyama, D. Mukoyama, Y. Fukuda, T. Suzuki, K. Kanoh, T. Matsunaga, *J. Biosci. Bioeng.* **2006**, *101*, 445–447.
79. L. C. Paoletti, R. P. Blakemore, *J. Bacteriol.* **1986**, *167*, 73–76.

80. R. Uebe, B. Voigt, T. Schweder, D. Albrecht, E. Katzmann, C. Lang, L. Böttger, B. Matzanke, D. Schüler, *J. Bacteriol.* **2010**, *192*, 4192–4204.
81. O. Kolaj-Robin, D. Russell, K. A. Hayes, J. T. Pembroke, T. Soulimane, *FEBS Lett.* **2015**, *589*, 1283–1295.
82. V. S. Reddy, M. A. Shlykov, R. Castillo, E. I. Sun, M. H. Saier, Jr., *FEBS J.* **2012**, *279*, 2022–2035.
83. R. Frankel, G. C. Papaefthymiou, R. P. Blakemore, W. O'Brian, *Biochim. Biophys. Acta* **1983**, *763*, 147–159.
84. J. Baumgartner, G. Morin, N. Menguy, T. Perez Gonzalez, M. Widdrat, J. Cosmidis, D. Faivre, *Proc. Natl. Acad. Sci. USA* **2013**, *110*, 14883–14888.
85. M. L. Fdez-Gubieda, A. Muela, J. Alonso, A. Garcia-Prieto, L. Olivi, R. Fernandez-Pacheco, J. M. Barandiaran, *ACS Nano* **2013**, *7*, 3297–3305.
86. Y. Zhang, T. Wen, F. Guo, Y. Geng, J. Liu, T. Peng, G. Guan, J. Tian, Y. Li, J. Li, J. Ju, W. Jiang, *Front. Microbiol.* **2017**, *8*, 208.
87. S. Staniland, B. Ward, A. Harrison, G. Van der Laan, N. Telling, *Proc. Natl. Acad. Sci. USA* **2007**, *104*, 19524–19528.
88. R. Uebe, F. Ahrens, J. Stang, K. Jäger, L. H. Böttger, C. Schmidt, B. F. Matzanke, D. Schüler, *mBio* **2019**, *10*, e02795–18.
89. U. Heyen, D. Schüler, *Appl. Microbiol. Biotechnol.* **2003**, *61*, 536–544.
90. M. Xia, J. Wei, Y. Lei, L. Ying, *Curr. Microbiol.* **2007**, *55*, 71–75.
91. Y. Noguchi, T. Fujiwara, K. Yoshimatsu, Y. Fukumori, *J. Bacteriol.* **1999**, *181*, 2142–2147.
92. C. Zhang, X. Meng, N. Li, W. Wang, Y. Sun, W. Jiang, G. Guan, Y. Li, *J. Bacteriol.* **2013**, *195*, 876–885.
93. Y. Li, E. Katzmann, S. Borg, D. Schüler, *J. Bacteriol.* **2012**, *194*, 4847–4856.
94. Y. Li, S. Bali, S. Borg, E. Katzmann, S. J. Ferguson, D. Schüler, *J. Bacteriol.* **2013**, *195*, 4297–4309.
95. Y. Li, O. Raschdorf, K. T. Silva, D. Schüler, *J. Bacteriol.* **2014**, *196*, 2552–2562.
96. Y. Li, M. Sabaty, S. Borg, K. T. Silva, D. Pignol, D. Schüler, *BMC Microbiol.* **2014**, *14*, 153.
97. T. Yamazaki, H. Oyanagi, T. Fujiwara, Y. Fukumori, *Eur. J. Biochem.* **1995**, *233*, 665–671.
98. N. Klueglein, F. Zeitvogel, Y.-D. Stierhof, M. Floetenmeyer, K. O. Konhauser, A. Kappler, M. Obst, *Appl. Environ. Microbiol.* **2014**, *80*, 1051–1061.
99. D. Murat, A. Quinlan, H. Vali, A. Komeili, *Proc. Natl. Acad. Sci. USA* **2010**, *107*, 5593–5598.
100. W. Lin, Y. Pan, *Environ. Microbiol. Rep.* **2015**, *7*, 237–242.
101. W. Lin, Y. Wang, B. Li, Y. Pan, *ISME J.* **2012**, *6*, 475–479.
102. C. T. Lefèvre, A. Bernadac, K. Yu-Zhang, N. Pradel, L.-F. Wu, *Environ. Microbiol.* **2009**, *11*, 1646–1657.
103. C. T. Lefèvre, R. B. Frankel, M. Pósfai, T. Prozorov, D. A. Bazylinski, *Environ. Microbiol.* **2011**, *13*, 2342–2350.
104. C. T. Lefèvre, N. Viloria, M. L. Schmidt, M. Pósfai, R. B. Frankel, D. A. Bazylinski, *ISME J.* **2012**, *6*, 440–450.
105. C. Jogler, W. Lin, A. Meyerdierks, M. Kube, E. Katzmann, C. Flies, Y. Pan, R. Amann, R. Reinhardt, D. Schüler, *Appl. Environ. Microbiol.* **2009**, *75*, 3972–3979.
106. S. Kolinko, G. Wanner, E. Katzmann, F. Kiemer, B. M. Fuchs, D. Schüler, *Environ. Microbiol.* **2013**, *15*, 1290–1301.
107. D. A. Bazylinski, C. T. Lefevre, *Life* **2013**, *3*, 295–307.
108. C. T. Lefèvre, F. Abreu, M. L. Schmidt, U. Lins, R. B. Frankel, B. P. Hedlund, D. A. Bazylinski, *Appl. Environ. Microbiol.* **2010**, *76*, 3740–3743.
109. W. Lin, Y. Pan, D. A. Bazylinski, *Environ. Microbiol. Rep.* **2017**, *9*, 345–356.

110. Y. Dong, J. Li, W. Zhang, W. Zhang, Y. Zhao, T. Xiao, L.-F. Wu, H. Pan, *Environ. Microbiol. Rep.* **2016**, *8*, 239–249.
111. H. Petermann, U. Bleil, *Earth. Planet. Sci. Lett.* **1993**, *117*, 223–228.
112. R. Blakemore, *Annu. Rev. Microbiol.* **1982**, *36*, 217–238.
113. K. He, S. A. Gilder, W. D. Orsi, X. Zhao, N. Petersen, *Appl. Environ. Microbiol.* **2017**, *83*, e01382–17.
114. S. Spring, R. Amann, W. Ludwig, K. Schleifer, H. van Gemerden, N. Petersen, *Appl. Environ. Microbiol.* **1993**, *50*, 2397–2403.
115. S. L. Simmons, D. A. Bazylinski, K. J. Edwards, *Environ. Microbiol.* **2007**, *9*, 2162–2174.
116. D. Bazylinski, A. Garratt-Reed, A. Abedi, R. Frankel, *Arch. Microbiol.* **1993**, *160*, 35–42.
117. S. L. Simmons, D. A. Bazylinski, K. J. Edwards, *Science* **2006**, *311*, 371.
118. S. L. Simmons, K. J. Edwards, *Geobiology of Magnetotactic Bacteria*, in *Magnetoreception and Magnetosomes in Bacteria*, Ed. D. Schüler, Springer, Berlin, Heidelberg, **2007**, pp. 77–102.
119. C. T. Lefèvre, M. Bennet, L. Landau, P. Vach, D. Pignol, D. A. Bazylinski, R. B. Frankel, S. Klumpp, D. Faivre, *Biophys. J.* **2014**, *107*, 527–538.
120. C. T. Lefèvre, P. A. Howse, M. L. Schmidt, M. Sabaty, N. Menguy, G. W. Luther, D. A. Bazylinski, *Environ. Microbiol. Rep.* **2016**, *8*, 1003–1015.
121. D. A. Bazylinski, T. J. Williams, C. T. Lefèvre, D. Trubitsyn, J. Fang, T. J. Beveridge, B. M. Moskowitz, B. Ward, S. Schübbe, B. L. Dubbels, B. Simpson, *Int. J. Syst. Evol. Microbiol.* **2013**, *63*, 1824–1833.
122. M. Dziuba, V. Koziaeva, D. Grouzdev, E. Burganskaya, R. Baslerov, T. Kolganova, A. Chernyadyev, G. Osipov, E. Andrianova, V. Gorlenko, B. Kuznetsov, *Int. J. Syst. Evol. Microbiol.* **2016**, *66*, 2069–2077.
123. D. Schüler, M. Köhler, *Zentralbl. Mikrobiol.* **1992**, *147*, 150–151.
124. T. Matsunaga, T. Sakaguchi, F. Tadokoro, *Appl. Microbiol. Biotechnol.* **1991**, *35*, 651–655.
125. R. Kawaguchi, J. G. Burgess, T. Sakaguchi, H. Takeyama, R. H. Thornhill, T. Matsunaga, *FEMS Microbiol. Lett.* **1995**, *126*, 277–282.
126. D. Bazylinski, A. J. Dean, D. Schüler, E. J. P. Phillips, D. R. Lovley, *Environ. Microbiol.* **2000**, *2*, 266–273.
127. S. C. Dufour, J. R. Laurich, R. T. Batstone, B. McCuaig, A. Elliott, K. M. Poduska, *ISME J.* **2014**, *8*, 2453–2462.
128. E. Natan, Y. Vortman, *Mov. Ecol.* **2017**, *5*, 22.
129. C. L. Monteil, C. T. Lefevre, *Trends Microbiol.* **2019**. doi: 10.1016/j.tim.2019.10.012.
130. C. L. Monteil, D. Vallenet, N. Menguy, K. Benzerara, V. Barbe, S. Fouteau, C. Cruaud, M. Floriani, E. Viollier, G. Adryanczyk, N. Leonhardt, D. Faivre, D. Pignol, P. López-García, R. J. Weld, C. T. Lefevre, *Nat. Microbiol.* **2019**, *4*, 1088–1095.
131. F. F. Torres de Araujo, M. A. Pires, R. B. Frankel, C. E. M. Bicudo, *Biophys. J.* **1986**, *50*, 375–378.
132. D. Bazylinski, D. R. Schlezinger, B. H. Howes, R. Frankel, S. S. Epstein, *Chem. Geol.* **2000**, *169*, 319–328.
133. J. L. Martins, T. S. Silveira, F. Abreu, K. T. Silva, I. D. da Silva-Neto, U. Lins, *Environ. Microbiol.* **2007**, *9*, 2775–2781.
134. C. L. Monteil, N. Menguy, S. Prévéral, A. Warren, D. Pignol, C. T. Lefèvre, *Appl. Environ. Microbiol.* **2018**, *84*, e02865–17.
135. P. Leão, L. Le Nagard, H. Yuan, J. Cypriano, I. Da Silva-Neto, D. A. Bazylinski, D. Acosta-Avalos, H. L. de Barros, A. P. Hitchcock, U. Lins, F. Abreu, *Environ. Microbiol.* **2019**, doi: 10.1111/1462-2920.14711.

136. R. Frankel, R. Blakemore, F. F. Torres de Araujo, D. Esquivel, J. Danon, *Science* **1981**, *212*, 1296.
137. C. T. Lefèvre, L.-F. Wu, *Trends Microbiol.* **2013**, *21*, 534–543.
138. F. F. Guo, W. Yang, W. Jiang, S. Geng, T. Peng, J. L. Li, *Environ. Microbiol.* **2012**, *14*, 1722–1729.
139. K. Li, C. Chen, C. Chen, Y. Wang, Z. Wei, W. Pan, T. Song, *Enzyme Microb. Technol.* **2015**, *72*, 72–78.
140. H. Vali, J. L. Kirschvink, *Observations of Magnetosome Organization, Surface Structure, and Iron Biomineralization of Undescribed Magnetic Bacteria: Evolutionary Speculations*, in *Iron Biominerals*, Eds R. B. Frankel, R. P. Blakemore, Springer, Boston, MA, **1991**, pp. 97–115.
141. R. E. Kopp, C. Z. Nash, J. L. Kirschvink, J. R. Leadbetter, *EOS Trans. AGU Fall Meet. Suppl.* **2004**, *85*, GP34-A06.
142. J. M. Byrne, N. Klueglein, C. Pearce, K. M. Rosso, E. Appel, A. Kappler, *Science* **2015**, *347*, 1473.
143. J. F. Stolz, H. C. W. Skinner, *Magnetotactic Bacteria: Biomineralization, Ecology, Sediment Magnetism, Environmental Indicator*, in *Biomineralization: Processes of Iron and Manganese; Modern and Ancient Environments*, Catena, Reiskirchen, **1992**, pp. 133–145.
144. W. Lin, D. A. Bazylinski, T. Xiao, L.-F. Wu, Y. Pan, *Environ. Microbiol.* **2014**, *16*, 2646–2658.
145. A. P. Roberts, *Earth-Sci. Rev.* **2015**, *151*, 1–47.
146. A. P. Chen, V. M. Berounsky, M. K. Chan, M. G. Blackford, C. Cady, B. M. Moskowitz, P. Kraal, E. A. Lima, R. E. Kopp, G. R. Lumpkin, B. P. Weiss, P. Hesse, N. G. F. Vella, *Nat. Commun.* **2014**, *5*, 4797.
147. S. Rivas-Lamelo, K. Benzerara, C. T. Lefèvre, C. L. Monteil, D. Jézéquel, N. Menguy, E. Viollier, F. Guyot, C. Férard, M. Poinsot, F. Skouri-Panet, N. Trcera, J. Miot, E. Duprat, *Geochem. Pers. Lett.* **2017**, *5*, 35–41.
148. H. N. Schulz-Vogt, F. Pollehne, K. Jürgens, H. W. Arz, S. Beier, R. Bahlo, O. Dellwig, J. V. Henkel, D. P. R. Herlemann, S. Krüger, T. Leipe, T. Schott, *ISME J.* **2019**, *13*, 1198–1208.
149. R. E. Kopp, B. P. Weiss, A. C. Maloof, H. Vali, C. Z. Nash, J. L. Kirschvink, *Earth Planet. Sci. Lett.* **2006**, *247*, 10–25.
150. M. Winklhofer, N. Petersen, *Paleomagnetism and Magnetic Bacteria*, in *Magnetoreception and Magnetosomes in Bacteria*, Ed. D. Schüler, Springer, Berlin, Heidelberg, **2007**, pp. 255–273.
151. N. Petersen, T. von Dobeneck, H. Vali, *Nature* **1986**, *320*, 611–615.
152. J. L. Kirschvink, H. A. Lowenstam, *Earth Planet. Sci. Lett.* **1979**, *44*, 193–204.
153. J. F. Stolz, S. R. Chang, J. L. Kirschvink, *Nature* **1986**, *321*, 849–851.
154. I. Snowball, L. Zillén, P. Sandgren, *Quater. Int.* **2002**, *88*, 13–19.
155. D. E. Canfield, R. A. Berner, *Geochim. Cosmochim. Acta* **1987**, *51*, 645–659.
156. S.-B. R. Chang, J. L. Kirschvink, *Annu. Rev. Earth Planet. Sci.* **1989**, *17*, 169–195.
157. R. E. Kopp, J. L. Kirschvink, *Earth-Sci. Rev.* **2008**, *86*, 42–61.
158. J. F. Stolz, D. R. Lovley, S. E. Haggerty, *J. Geophys. Res.* **1990**, *95*, 4355–4361.
159. A. P. Roberts, R. L. Reynolds, K. L. Verosub, D. P. Adam, *Geophys. Res. Lett.* **1996**, *23*, 2859–2862.
160. M. Pósfai, K. Cziner, E. Marton, P. R. Buseck, R. Frankel, D. Bazylinski, *Eur. J. Mineral.* **2001**, *13*, 691–703.
161. S.-J. Kao, C.-S. Horng, A. P. Roberts, K.-K. Liu, *Chem. Geol.* **2004**, *203*, 153–168.
162. D. Heslop, A. P. Roberts, L. Chang, M. Davies, A. Abrajevitch, P. de Deckker, *Earth. Planet. Sci. Lett.* **2013**, *382*, 58–65.

163. D. S. McKay, E. K. Gibson, Jr.,K. L. Thomas-Keprta, H. Vali, C. S. Romanek, S. J. Clemett, X. D. F. Chilier, C. R. Maechling, R. N. Zare, *Science* **1996**, *273*, 924–930.
164. P. R. Buseck, R. E. Dunin-Borkowski, B. Devouard, R. Frankel, M. R. McCartney, P. A. Midgley, M. Pósfai, M. Weyland, *Proc. Natl. Acad. Sci. USA* **2001**, *98*, 13490–13495.
165. M. Usman, J. M. Byrne, A. Chaudhary, S. Orsetti, K. Hanna, C. Ruby, A. Kappler, S. B. Haderlein, *Chem. Rev.* **2018**, *118*, 3251–3304.
166. M. Armor, V. Busigny, M. Durand-Dubief, M. Tharaud, G. Ona-Nguema, A. Gélabert, E. Alphandéry, N. Menguy, M. F. Benedetti, I Chebbi, F. Guyot, *Proc. Natl. Acad. Sci. USA* **2015**, *112*, 1699–1703.

7

Living on Iron

Stefanie Becker, Allison M. L. Enright, and Andreas Kappler

Geomicrobiology, Center for Applied Geoscience, University of Tübingen,
Schnarrenbergstrasse 94–96, D-72076 Tübingen, Germany
<andreas.kappler@uni-tuebingen.de>

Metal Ions in Life Sciences, Volume 21 Guest Editors: Peter M. H. Kroneck and Martha E. Sosa Torres
Series Editors: Astrid Sigel, Eva Freisinger, and Roland K. O. Sigel

https://doi.org/10.1515/9783110589771-007

Abstract: Reduced and oxidized iron is present in virtually all of Earth's environments. Iron is essential to all living organisms because it is a critical component of many biomolecules. It can also be used as an electron donor or terminal electron acceptor by microorganisms for metabolic redox reactions which generate energy and drive growth. In this chapter we introduce the environmental distribution and redox activity of iron and discuss how different types of Fe(II)-oxidizing (aerobic, microaerophilic, anoxygenic phototrophic, and anaerobic nitrate-reducing) and Fe(III)-reducing (ammonium-oxidizing, organic matter-oxidizing, methanotrophic, sulfur-oxidizing) microorganisms use the oxidation and reduction of Fe(II) and Fe(III), respectively, to generate energy and to produce biomass. In addition, we present some of the many biotechnological and environmental applications of iron-cycling microorganisms.

Keywords: biogeochemical iron cycling · geomicrobiology · heavy metal sequestration · microbial Fe(II) oxidation · microbial Fe(III) reduction

1. INTRODUCTION

1.1. Iron Speciation

Iron is present in the environment in the form of poorly crystalline and crystalline iron minerals, dissolved iron-organic-matter complexes, colloids, as well as dissolved ions [1]. The two main redox species relevant for environmental processes and biogeochemical iron cycling are Fe(III) and Fe(II) species. At pH 5.0–8.0 (circumneutral pH), Fe(III) is poorly soluble, with solubility products for Fe(III) minerals in the range of 10^{-38}–10^{-42}. Because of this, in the absence of Fe(III)-complexing ligands, concentrations of dissolved Fe^{3+} at circumneutral pH are in the low nM range. In contrast, at circumneutral pH, Fe(II) is relatively

soluble. Environmental concentrations of dissolved Fe^{2+} can be on the order of high μM or even low mM. This solubility is impacted by the rapid abiotic oxidation of Fe(II) in the presence of O_2; in fully aerated water, the half-life of Fe(II) is ~15 minutes [2]. By contrast, at pH < 4.0, both Fe^{3+} and Fe^{2+} are soluble, which makes iron redox transformations even more energetically favorable in low pH environments.

1.2. Iron Mineralogy

Fe(II) and Fe(III) mineral species are important to environmental microbiology, because of their global ubiquity, redox-activity, and their impact on biogeochemistry. Iron-bearing minerals present in soils and sediments include Fe(III) (oxyhydr)oxides, such as ferrihydrite ($Fe_{10}O_{14}(OH)_2$) [3], goethite (α-FeOOH), Fe(III) oxides (e.g., hematite, α-Fe_2O_3), and mixed-valent Fe(II)-Fe(III) oxides including magnetite (Fe_3O_4) and various green-rusts [4]. Common non-oxide Fe(II) minerals include siderite ($FeCO_3$), vivianite ($Fe_3(PO_4)_2$), pyrite (FeS_2), and mackinawite (FeS), as well as detrital minerals such as biotite, hornblende, and iron-containing clay minerals (e.g., illite, smectite, chlorite) [5]. Many iron-bearing minerals form as secondary phases during rock weathering, i.e., by a combination of physical, chemical, and biological processes.

The crystallinity and oxidation state of these minerals also have a dramatic impact on the bioavailability, especially in the case of Fe(III) [6], where being limited to solid-state electron acceptors means that the electron transfer processes must take place outside the cell, as the solid substrate cannot be assimilated into cells [6, 7]. Semi-conductive minerals, such as hematite and magnetite, can function as conductors to transfer electrons between different microbial species [7, 8].

1.3. The Effect of Iron Redox Potentials on Energy-Yielding Processes

Fe(II) can be oxidized to provide an electron for either: (i) chemolithotrophic microbial processes coupled to the reduction of O_2 or NO_3^-, and CO_2 fixation; or, (ii) photosynthesis and CO_2 fixation. By contrast, Fe(III) can act as a terminal electron acceptor for anaerobic respiration coupled to oxidation of organic and inorganic compounds (e.g., H_2, OM, NH_4^+, CH_4).

The potential of the Fe(II)/Fe(III) redox couple, and therefore the energy available for microbial processes, depends on the iron speciation and pH. It ranges from less than −400 mV (strongly reducing) to more than +700 mV (strongly oxidizing). This means that the iron species of both the oxidant and reductant effect the energetics of their corresponding chemotrophic process.

In the case of Fe(II) oxidation, the energy released is determined in part by whether the reductant is dissolved Fe^{2+}, a Fe(II)-organic matter (OM) complex, or a Fe(II)-containing mineral. Similarly, in case of Fe(III)-reduction, where

Fe(III) acts as the terminal electron acceptor, the energy released is determined in part by whether Fe^{3+} is dissolved (i.e., pH < 4.0), or present in either poorly crystalline or crystalline Fe(III) minerals (i.e., ferrihydrite or goethite; pH > 4.0).

Generally, more crystalline minerals such as hematite or goethite have lower (less positive/more negative) redox potentials and thus provide less energy than less crystalline minerals such as ferrihydrite or even dissolved Fe(III)-OM complexes.

In the case of photoautotrophic Fe(II)-oxidizing processes, the energy driving the redox processes is derived from light. As such, this process is not thermodynamically dependent on the oxidation of Fe(II). Instead, the amount of CO_2 fixed (and biomass produced) is stoichiometrically linked to the amount of the electron donor oxidized (see Section 2.2.1; Equation 6).

1.4. Significance of Iron to Global-Scale Biogeochemical Processes

Until the oxidation of Earth's oceans ca. 2.4 Ga, dissolved Fe(II) was highly concentrated in the oceans. This early abundance is thought to make Fe(II) oxidation one of the most ancient metabolic pathways exploited by microbes. This longevity, as well as the perpetual abundance of iron in modern terrestrial environments, has the consequence of linking the microbial iron cycle to global biogeochemical cycling of nitrogen, carbon, phosphate, oxygen, and sulfur [9–11]. The relatively large amount of energy available in the iron redox state transformations is likely the reason that microbes adopted Fe(II) as electron donor in phototrophic or chemosynthetic processes or Fe(III) as electron acceptor in anaerobic respiration [11]. It is important to note that high concentrations of iron are not always necessary to indicate the importance of biogeochemical iron cycling in a certain habitat. It has been shown that iron, and in particular, Fe-OM complexes, can be efficiently cycled by microbial and abiotic Fe(II)-oxidizing and Fe(III)-reducing processes [12–14]. An illustration of several mechanisms of microbial iron cycling is presented in Figure 1.

2. MICROBIAL GROWTH BY OXIDIZING IRON(II)

2.1. Chemolithotrophic Iron(II) Oxidation

Chemolithotrophic Fe(II)-oxidizing microorganisms gain energy from a redox reaction where Fe(II) is oxidized to Fe(III) and donates electrons to an oxidant with a more positive redox potential. The two-half reactions are spatially separated and coupled by an electron transport chain through the cytoplasmic membrane. During the process of electron transport, energy is released by redox reactions and coupled to the dislocation of H^+ over the cytoplasmic membrane, building up or maintaining the H^+ concentration gradient. This results in an

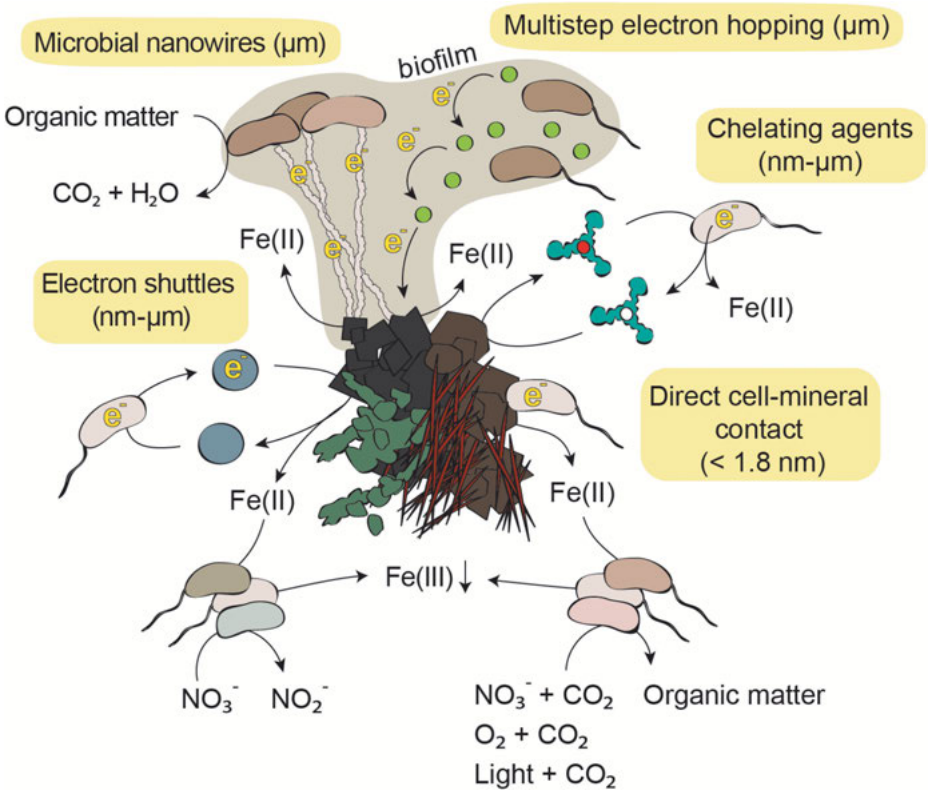

Figure 1. Illustration of processes involved in electron exchange between microbes, iron minerals, and dissolved iron. Mechanisms of electron transfer utilized for microbial Fe(III) reduction are highlighted in yellow. **Yellow top left**: Cells use microbial nanowires to directly attach to solid Fe(III)-bearing substrates, these nanowires are conductive. **Yellow top right**: Cells transfer electrons to redox-active intermediates, the electrons then can hop along a chain of small molecules which are quickly reoxidized and can cycle more electrons. **Yellow bottom left**: Cells donate electrons to redox-active electron shuttles, which in turn transfer electrons to the Fe(III)-bearing mineral substrate. **Yellow middle right**: Cells produce chelating ligands that complex with Fe(III), making it available for microbial reduction. **Yellow bottom right**: Cells in direct contact with their substrates of interest can transfer electrons directly to mineral surfaces. **Bottom left**: Fe(II) solely used as energy source by nitrate-dependent iron-oxidizing bacteria. **Bottom right**: Fe(II) used as electron donor for CO_2 fixation in organic matter by nitrate-dependent iron-oxidizing bacteria, microaerophilic and acidophilic bacteria, and phototrophs.

electrochemical proton gradient over the membrane and consequently to a proton motive force (PMF). The PMF powers an ATP synthase regenerating ATP by the phosphorylation of ADP. This mechanism of energy conservation is called electron transport-linked phosphorylation.

Considering redox processes like an energetic tower, electrons will move down a gradient of electrochemical potential to their oxidant in the course of electron

transport-linked phosphorylation. This is called a down-hill electron pathway. Anabolic processes (e.g., carbon assimilation) are essential for cell growth and proliferation, and require reducing agents, in particular, NADPH. Since these molecules are regenerated by reduction, a cell needs a consistent supply of electrons. However, the reducing potential of Fe(II) is insufficient to reduce $NAD(P)^+$ (NAD^+ or $NADP^+$). As such, the PMF is used to both: (i) to regenerate ATP, and, (ii) to power the up-hill pathway of $NAD(P)^+$ reduction. This mechanism is called reverse electron transport. The process of both down-hill (exergonic) and up-hill (endergonic) pathway is a bifurcated electron-transport chain.

2.1.1. Acidophilic Iron(II) Oxidation

2.1.1.1. Iron(II)-Driven Energy Conservation

For acidophilic Fe(II)-oxidizers, O_2 functions as a terminal electron acceptor in the energy conservation pathway (Equation 1). The half-reaction of Fe(II) oxidation takes place at the outer membrane (~pH 2) while the half-reaction of O_2 reduction takes place in the pH neutral cytoplasm (~pH 6.5) (Equation 1).

$$4\,Fe^{2+} + O_2 + 4\,H^+ \rightarrow 4\,Fe^{3+} + 2\,H_2O \quad (1)$$

Considering the pH dependence of redox potentials, the overall redox reaction seems thermodynamically unfavorable ($E_{m\ pH2}$ Fe(II)/Fe(III): ~ +0.77 V; $E_{m\ pH6.5}$ O_2/H_2O: ~ +0.82 V). However, as the reduction of O_2 to H_2O is localized in an environment with an overall pH of 2, the redox potential of the O_2/H_2O couple increases by 0.3 V ($E_{m\ pH2}$ O_2/H_2O: ~ +1.12 V). Because of this, the redox gradient of Fe(II) oxidation to Fe(III) and O_2 reduction to H_2O is positive and an overall exergonic reaction [15–17]. Additionally, the formation of H_2O from the reaction of reduced O_2 with protons, neutralizes protons that have entered the cell via the ATPase complex coming from a pH 2 environment. For this reason, the oxidative phosphorylation does theoretically not require additional H^+ transport against the pH gradient, although it is possible that the final oxidase translocates H^+ over the cytoplasmic membrane [16].

Maintaining a circumneutral cytoplasmic pH is a challenge for all acidophiles [18], and pH homeostasis in acidophiles was reviewed by Baker-Austin and Dopson in 2007 [19]. A neutral cytoplasmic pH is accomplished by maintaining a positive intracellular electrical potential; known as an inverted transmembrane electrical potential. Consequently, the electrical potential ($\Delta\Psi$) is unfavorable for the potential energy of the PMF, however, the net result facilitates a chemiosmotic mechanism of energy conservation. This means the PMF is entirely due to the pH gradient. In contrast, in neutrophiles, both the chemical potential (ΔpH) and the electrical potential ($\Delta\Psi$) contribute to the PMF. Down-hill electron transport supporting ATP synthesis and up-hill electron transport supporting reconstitution of reducing equivalents (e.g., NAD(P)H), are both connected to proton flux. Therefore, it is thought that these pathways are homeostatically regulated [20].

The genomics of Fe(II) oxidation and iron uptake strategies of acidophiles were reviewed by Bonnefoy and Holmes [20, 21]. Here, we discuss *Acidithiobacillus ferrooxidans,* the best-studied representative of the Fe(II)-oxidizing acidophiles. Multi-omic studies on *Leptospirillum ferriphilum* have been published by Christel et al. [22].

2.1.1.2. Environmental Distribution

Because abiotic Fe(II) oxidation (Fe(II) autoxidation by O_2) occurs rapidly at alkaline and neutral pH, it has been difficult to quantify the contribution of microbial Fe(II) oxidation, i.e., enzymatically catalyzed Fe(II) oxidation, at neutral pH. As such, aerobic microbial Fe(II) oxidation has been a subject of controversy for decades [23]. In contrast, this has not been an issue for the research on acidophilic Fe(II)-oxidizers [24, 25]. Acidophilic Fe(II)-oxidizers include members of the domain Bacteria and Archaea and have been identified in mesophilic environments such as mine drainage water [26] and thermophilic environments, such as solfatara fields and marine hydrothermal systems [27]. Examples for microorganisms isolated from these environments are listed in Table 1.

Table 1. Examples of mesophilic and thermophilic acidophilic aerobic Fe(II)-oxidizing microorganisms, including Bacteria and Archaea.

Bacteria		**Reference**
Mesophiles	*Acidithiobacillus ferrooxidans*	[23]
	Acidithiobacillus ferridurans	[288]
	Acidithiobacillus prosperus	[289]
	Leptospirillum ferrooxidans	[290]
	Metallogenium	[291]
	Ferromicrobium acidophilum	[292]
	Ferrovum myxofaciens	[293]
Thermophiles	*Sulfobacillus thermosulfidooxidans*	[294]
	Sulfobacillus acidophilus	[295, 296]
	Acidimicrobium ferrooxidans	[297, 298]
	Acidiferrobacter thiooxydans	[299]
Archaea		
Mesophiles	*Ferroplasma acidiphilum*	[300]
	Ferroplasma acidarmanus	[301]
	Ferroplasma thermophilum	[302]
Thermophiles	*Acidianus brierleyi*	[303]
	Sulfolobus acidocaldarius	[304]

2.1.1.3. *Acidithiobacillus ferrooxidans*

(a) Environmental impact and biotechnological application

At. ferrooxidans (basionym: *Thiobacillus ferrooxidans*) is a Gram-negative bacterium that oxidizes Fe(II) (di)sulfide minerals (i.e., pyrite or marcasite), thereby contributing to microbial sulfur cycling in the environment [23, 28]. Because bacterial pyrite oxidation results in the formation of ferric iron and sulfuric acid

which perpetuates dissolution of sulfide minerals, causing acid mine drainage and solubilizing metals from minerals [29–31]. *At. ferrooxidans'* ability to oxidize metals makes it interesting for industrial applications such as bioleaching of metals from ores or from electronic waste [32–38]. $FeSO_4$ oxidation catalyzed by *At. ferrooxidans* can be used to improve schwertmannite production [20]. Schwertmannite is a mineral that promotes the natural passivation of heavy metals and can be used to decrease environmental pollution [39–42].

(b) Metabolic pathway of Fe(II) oxidation

At. ferrooxidans became a model organism for acidophilic chemotrophic life and aerobic iron oxidation [16, 20, 43, 44]. Therefore, its iron respiration chain is one of the best-studied Fe(II) oxidation mechanisms. A model for up-hill and down-hill electron transport during Fe(II) oxidation by *At. ferrooxidans* is shown in Figure 2.

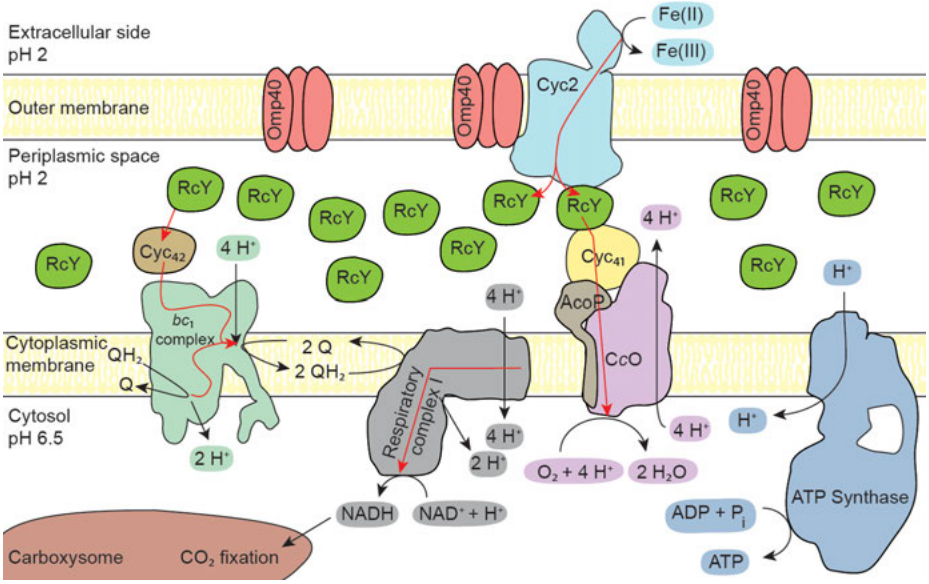

Figure 2. Model for electron transport from Fe(II) to the electron transport chain via free rusticyanin (RcY), and the respirasome in the cytoplasmic membrane. Fe(II) becomes oxidized by a high-molecular-weight cytochrome c_4 (Cyc2) located in the outer membrane. Cyc2 has been proposed to bind to a 40-kD major outer membrane protein (Omp40) [308]. In the course of the down-hill electron chain, the electrons are transported by the respirasome, compromising Cyc2, RcY, a dihemic cytochrome c_4 (Cyc_{41}), a green copper protein (AcoP) and an aa_3-type cytochrome *c* oxidase (C*c*O). C*c*O builds up the proton motive force which is used by either an ATP synthase to produce ATP from ADP and inorganic phosphate (P_i) or by the respiratory complex I to regenerate NADH. In the up-hill electron chain, it has been proposed that the electrons travel via RcY, Cyc_{42} and bc_1 complex which reduces quinone by using the proton motive force. The electron of reduced quinone can be then used to regenerate NADH by the respiratory complex I. The figure contains data from Li et al. [50], Castelle et al. [56], and Wang et al. [54].

The proposed iron respiratory chain (down-hill electron transport) is composed of five electron transfer proteins which are encoded by the *rus* operon [45, 46]. The Fe(II)-oxidation itself is hypothesized to take place extracellularly by an outer membrane high-molecular-weight cytochrome c_4 (Cyc2, encoded by *cyc2* [47, 48]). The harvested electrons are passed to rusticyanin (RcY), a type I blue copper protein which was found to form a complex with Cyc2 [49]. The abundance of RcY is relatively high compared to other cellular proteins [49]. Because of the cells' RcY concentration, it has been concluded that there is also free RcY present in the periplasm [49, 50]. At the next step, the electron is transferred via a dihemic cytochrome c_4 (Cyc_{41}, encoded by *cyc1*) [51] located in the periplasm, to an aa_3-type cytochrome *c* oxidase (C*c*O) that belongs to the subgroup of heme-copper O_2 reductases and spans the cytoplasmic membrane, where it reduces molecular oxygen to one molecule of water [52, 53]. The *rus* operon also encodes a green copper protein (AcoP: "acidophile C*c*O partner") of unknown function which interacts with C*c*O and Cyc_{41}. Two different functions have been proposed: (i) AcoP accepts electrons from Cyc_{41} as a linker to C*c*O [54, 55], (ii) as a chaperone-like protein to protect C*c*O against acidic damage [55].

The proteins encoded by the *rus* operon have been proposed to form a super-protein complex [45], which could be reconstituted [56], and has been termed respirasome. Looking at the relative ratios of the proteins involved in the respirasome and the periplasmic concentration of RcY, one can conclude that most of the RcY is either free or undergoes other protein-protein interactions. Free RcY has a redox midpoint potential of +490 mV (pH 4.8) which is increased upon protein complex formation with cytochrome c_4 to +590 mV (pH 4.8) [49]. Li et al. [50] observed that the entirety of all available respiratory electron transfer proteins is organized as a network that is reducing and oxidizing concomitantly at a common functional reduction potential. As stated by the authors, this observation stands in contrast to the proposed well-defined linear series of electron transfer accomplished by a respirasome. Considering that the experiments by Li et al. [50] were performed *in situ* and that the formation of a protein complex is highly specific, both findings are biologically relevant. Consequently, this leads to the hypothesis that the efficient electron transfer is based on a protein network influenced by both, specific interactions due to super-complex formation (respirasome) and non-specific interactions that can be traced back to the macromolecular crowding of electron transfer proteins in the periplasmic space [57]. The latter mechanism would explain how the organism can change between different electron donors without the observation of a lag phase. Considering the bifurcated chain, accomplishing both ATP formation and $NAD(P)^+$ reduction, the implementation of both models might be crucial for the understanding of the regulation of up- and down-hill pathways. The branching point of these pathways has been proposed to be at the level of RcY [58]. The electrons for $NAD(P)^+$ reduction are hypothesized to be transferred from RcY through a dihemic cytochrome c_4 (Cyc_{42}) [59], a bc_1 complex [60], the quinone pool, and a NAD(P)H dehydrogenase [48, 52, 61]. Cyc_{42} and the bc_1 complex are encoded by the *petI* operon.

2.1.2. Microaerophilic Iron(II) Oxidation

2.1.2.1. Iron(II)-Driven Energy Conservation

Microaerophilic Fe(II)-oxidizers are a group of bacteria which are proposed to be among the first to have taken advantage of rising levels of oxygen in the atmosphere [62]. This group of organisms grows in circumneutral environments and uses oxygen as electron acceptor to oxidize Fe(II) (Equation 1). Unlike at acidic pH; Fe^{3+} will subsequently react with water and precipitate Fe(III) (oxyhydr)oxide mineral phases (Equation 2).

$$10\,Fe^{3+} + 16\,OH^- \rightarrow Fe_{10}O_{14}(OH)_2\downarrow + 14\,H^+ \quad (2)$$

The Gibbs free energy ($\Delta G^{0'}$) yield from neutrophilic oxygen-dependent Fe(II) oxidation (oxidation of Fe^{2+} to Fe^{3+}) is relative low (-29 kJ mol^{-1}) compared with all other potential lithotrophic energy sources. However, considering that Fe^{3+} precipitates as a Fe(III) (oxyhydr)oxide at pH 7, the energetic yield doubles, which also shows that depending on the identity of the Fe(III) mineral product, the free energy can vary.

2.1.2.2. Environmental Distribution and Biomineral Formation

Fe(II) oxidation at circumneutral pH must overcome two challenges: (i) Fe(III) (oxyhydr)oxide precipitation during microbial Fe(II) oxidation causes cell encrustation, which can lead to cell death [63]; and (ii) autoxidation of Fe(II) by O_2. This process (autoxidation) is pH-dependent and in circumneutral-pH oxic waters, Fe(II) has a half-life of less than 15 minutes [2, 63].

To minimize Fe(II) autoxidation, neutrophilic Fe(II)-oxidizers typically grow in microoxic habitats, increasing the half-life of Fe(II) 300-fold [64]. Furthermore, OM-complexed Fe(II) slows autoxidation [65]. Microaerophilic Fe(II)-oxidizers are found in freshwater and marine iron-rich flocs and sediments, the rhizosphere of wetland plants and paddy soils [66, 67], interfaces of ground and surface water [68], slow moving streams [69, 70], creeks, ditches, and marine hydrothermal vents [71].

To prevent Fe(III) mineral encrustation of cells, microaerophilic Fe(II)-oxidizers produce extracellular biofilaments forming either sheaths, stalks, Y-shaped tubular filaments, or induce the formation of particulate Fe(III) (oxyhydr)oxides [70, 72–74] (Figure 3). Sheaths and stalks can, in turn be colonized (i.e., *Siderocapsa* [71, 75]). These colonies appear as spherical structures that are fibrillary and resemble rounded nests [71]. Model organisms for each type extracellular biofilament structure can be found in Table 2.

The characteristic extracellular twisted stalks can be easily spotted under a microscope and are evidence for the presence of *Gallionellaceae*, and thus are often used as indicator for microaerophilic Fe(II) oxidation activity [71, 72, 76]. Such stalks have been suggested to be found in ancient rock formations. If true, their presence would allow the reconstruction of geochemical conditions and the evolution of early microbial life, and provide evidence for the availability of reduced iron and oxygen on early Earth [62, 77]. However, this evidence is

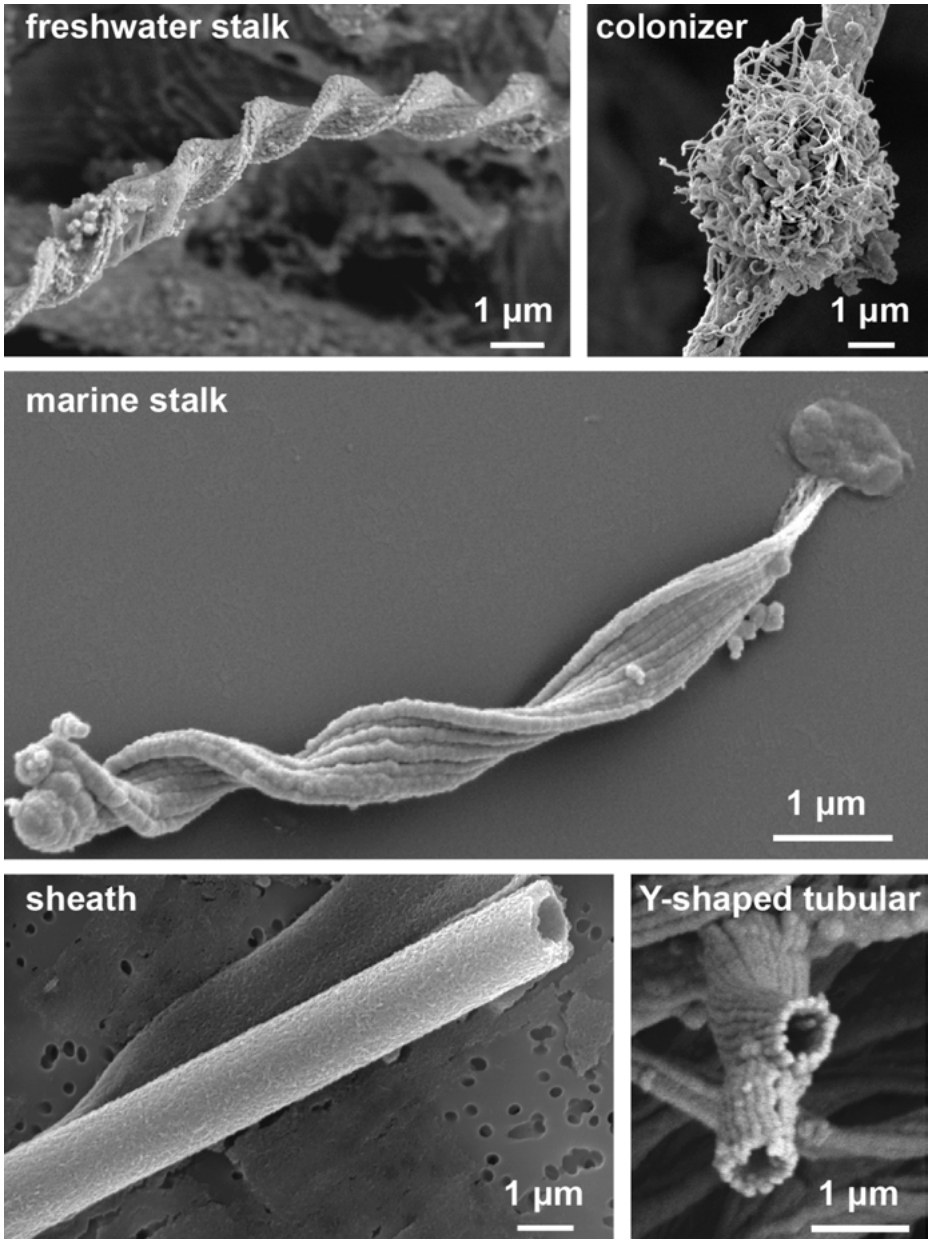

Figure 3. Morphologies of Fe(III) (oxyhydr)oxide biominerals known or suspected to be formed by microaerophilic Fe(II)-oxidizers. Micrographs were kindly provided by Clara Chan (University of Delaware, USA). The figure is modified from Chan et al. [71] and McAllister et al. [73].

Table 2. Examples of freshwater and marine microaerophilic Fe(II)-oxidizers sorted by Fe(III) (oxyhydr)oxide formation [79].

Freshwater microaerophilic Fe(II)-oxidizers (Betaproteobacteria)		
Fe(III) (oxyhydr)oxide-stalk-formers	**particulate Fe(III) (oxyhydr)oxides of no specific shape**	**Fe(III) (oxyhydr)oxide-sheath/-dreads-formers**
Ferriphaselus amnicola OYT1 [79] *Ferriphaselus* sp. R-1 [79] *Gallionella ferruginea* [71]	*Sideroxydans lithotrophicus* ES-1 [82] *Gallionella capsiferriformans* ES-2 [82]	*Leptothrix ochracea* [71] *Ferriphaselus amnicola* OYT1 [79] *Ferriphaselus* sp. R-1 [79]
Marine microaerophilic Fe(II)-oxidizers (Zetaproteobacteria)		
Fe(III) (oxyhydr)oxide-stalk-formers	**Fe(III) (oxyhydr)oxide-sheath/-dreads-formers**	**Y-shaped tubular filaments and colonizers**
Mariprofundus ferrooxydans PV-1 [305] *Mariprofundus* sp. M34 [306] *Mariprofundus* sp. EKF-M39 [306]	*Mariprofundus aestuarium* CP-5 [81] *Mariprofundus ferrinatatus* CP-8 [81]	Uncultured Zetaproteobacteria [71]

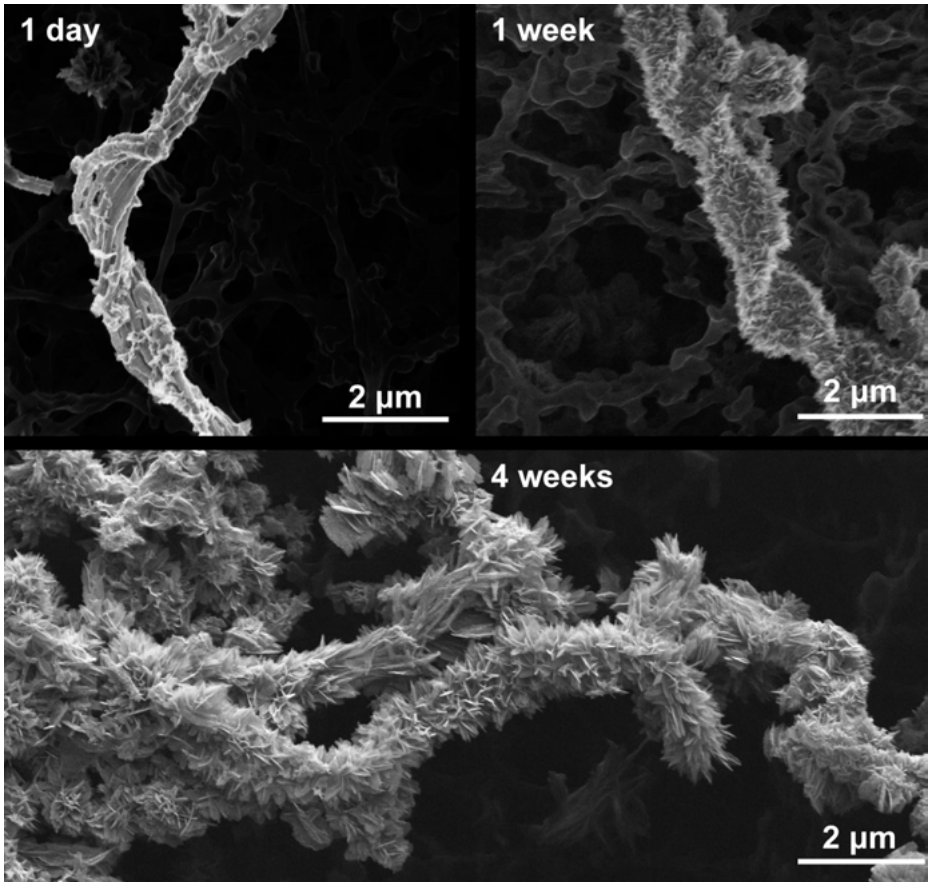

Figure 4. Aging twisted stalk produced by microaerophilic Fe(II)-oxidizing bacteria. Micrographs were collected by using a helium ion microscope and kindly provided by James Byrne (University of Bristol, UK). The figure is modified from Byrne et al. [72].

limited and still controversial. Stalk formation is proposed to be induced by acidic polysaccharide-containing fibrils excreted by the cell [78]. These fibrils then act as a template for Fe(III) (oxyhydr)oxide precipitation (Figure 4).

It is thought that the formation of stalks has the dual purpose of preventing cell encrustation and supporting cell mobility [79, 80]. The stalk anchors the cell to surfaces, and while the stalk grows, the cell moves forward, for example, towards an optimum O_2 concentration. Stalk formation has been observed for *Gallionella ferruginea* and most Zetaproteobacteria isolates. As stated previously, some microaerophilic Fe(II)-oxidizers produce other biomineral morphologies to avoid encrustation. For example, *Leptothrix ochracea*, *Mariprofundus ferrinatatus* CP-8, and *Mariprofundus aestuarium* CP-5 form shorter filaments that look like tubular sheaths [65, 73, 81]. Cultures of *Ferriphaselus amnicola* OYT1 and *Ferriphaselus* strain R-1 showed both stalks and tubular sheaths [79]. The freshwa-

ter Betaproteobacteria *Sideroxydans lithotrophicus* ES-1 and *Gallionella capsiferriformans* ES-2 do not form a specific shape of particulate Fe(III) (oxyhydr)oxides [82].

2.1.2.3. Biotechnological Application

Fe(III) (oxyhydr)oxides produced by neutrophilic Fe(II)-oxidizers have been investigated for their possible application in wastewater treatment as a metal remediation strategy [83] and in nanotechnology for their magneto-electronic applications as biosensors [84].

2.1.2.4. Metabolic Pathway of Iron(II) Oxidation

The neutrophilic Fe(II) oxidation metabolism has not been as extensively studied as acidophilic Fe(II) oxidation metabolism. Models for the metabolic pathway were proposed based on comparative genome studies; insights into freshwater and marine neutrophilic Fe(II)-oxidizers were published by Kato et al. in 2015 [79] and He et al. in 2017 [85]. A genomic study of marine neutrophilic Fe(II)-oxidizers, in particular Zetaproteobacteria, was published by McAllister et al. [73], and a comparative genomic study of freshwater neutrophilic Fe(II)-oxidizers was published by Emerson et al. [82].

Based on genome analysis, these researchers hypothesized, that either a homologous gene to *cyc2* or *mtoA/B* encodes the Fe(II) oxidase. Nevertheless, the authors also state that there might be an alternative Fe(II) oxidase, too. Since Cyc2 in *Acidithiobacillus ferrooxidans* was shown to oxidize Fe(II), its homologs are likely candidates for Fe(II) oxidation [56]. MtoA/B and MtrA/B of *Shewanella* spp. (Fe(III)-reducing bacteria, see Section 3.4.1.) are homologous proteins [86, 87]. MtrA/B is a porin-cytochrome complex located in the outer membrane and binds MtrC on the outside of the cell [88–91]. These proteins are involved in extracellular electron transfer linked to metal reduction (Mtr) [88–90]. If Fe(II)-oxidizers can oxidize Fe(II) on the outside of the cell instead of inside the cell, they could avoid intracellular mineral precipitation. Because of this, MtrA/B homologs such as MtoA/B, have also been proposed to be involved in metal oxidation (Mto). In addition to MtoA/B, Fe(II)-oxidizing homologs to MtrA/B include PioA/B in *Rhodopseudomonas palustris* strain TIE-1, a phototrophic Fe(II)-oxidizer (see Section 2.2) [92, 93].

Furthermore, MtoA has been demonstrated to be a decaheme cytochrome with Fe(II) oxidation activity *in vitro* by Liu et al. [93]. Based on the genomic analyses, microaerophilic Fe(II)-oxidizers have either a homologous protein to MtoA or Cyc2 functioning as Fe(II) oxidase with differing electron transport chains. In Figure 5 we present an overview of proposed Fe(II) oxidation models, corresponding to freshwater isolates and marine Zetaproteobacteria. He et al. presented a comparative genome analysis of neutrophilic Fe(II)-oxidizer where they suggest alternative Fe(II) oxidases [85]. Their findings indicate two novel porin-cytochrome *c* complexes, a transmembrane multicopper oxidase and a porin-multicopper complex as putative Fe(II) oxidases in addition to the commonly suggested transmembrane cytochrome *c* oxidase (similar to Cyc2) and the porin-cytochrome *c* complex (similar to MtoA/B and PioA/B).

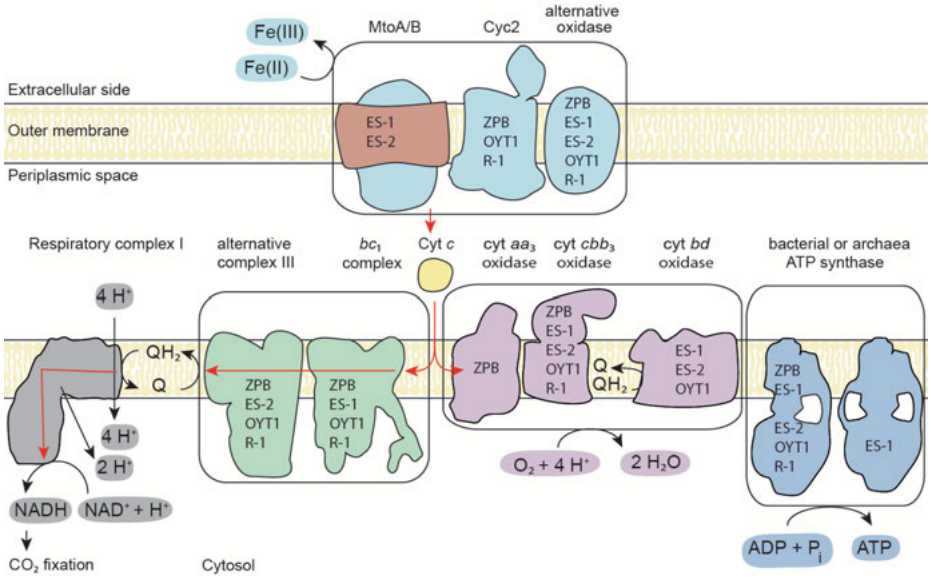

Figure 5. Model for electron transport from Fe(II) to the electron transport chain in the cytoplasmic membrane for the freshwater isolates *Sideroxydans lithotrophicus* ES-1 (ES-1) and *Gallionella capsiferriformans* ES-2 (ES-2) [82], *Ferriphaselus amnicola* OYT1 (OYT1) and *Ferriphaselus* sp. R-1 (R-1) [79], and for marine microaerophilic Fe(II)-oxidizing bacteria, in particular Zetaproteobacteria (ZPB) [73]. Proteins that have been suggested for one of these organisms are marked with the corresponding organisms short name in the site of the protein envelope. After oxidation of Fe(II) by an iron oxidase (light blue), the electron is passed to a *c*-type cytochrome (yellow) and from there it enters either the up-hill or down-hill electron chain. The alternative complex III or bc_1 complex (green) is proposed to pass the electrons to oxidized quinone by using the proton motive force. The NADH regeneration is catalyzed by the respiratory complex I (grey) by oxidizing reduced quinone and use of the proton motive force. Via the down-hill electron chain, the electrons are passed to their terminal electron acceptor oxygen, by an oxygen reductase (violet; respiratory oxidases). It should be noted that the *bd*-type cytochrome oxidase receives the electrons from reduced quinone but not directly from a *c*-type cytochrome as it is the case for the other shown oxidases. The ATP synthase phosphorylates ADP by the use of the proton motive force, generated by the oxygen reductase.

2.1.3. Nitrate-Reducing Iron(II) Oxidation

2.1.3.1. Iron(II)-Driven Energy Conservation

Nitrate-dependent Fe(II)-oxidizers couple enzymatic Fe(II) oxidation to the reduction of NO_3^- to NO_2^-, N_2, or NH_4^+ as a source of energy and electrons. The chemolithotrophic process of nitrate reduction to NO_2^- coupled to Fe(II) oxidation, has a proposed change in Gibbs free energy of -96.23 kJ mol^{-1} for standard conditions at pH 7 [94]. Equation (3) describes the nitrate-dependent Fe(II) oxidation with nitrate reduction to molecular nitrogen:

$$10\,Fe^{2+} + 2\,NO_3^- + 12\,H^+ \rightarrow 10\,Fe^{3+} + 2\,N_2 + 6\,H_2O \quad (3)$$

At circumneutral environments, Fe^{3+} will subsequently react with water and precipitate Fe(III) (oxyhydr)oxide mineral phases (Equation 2).

Fe(II) oxidation is not only observed due to direct enzymatic nitrate-reducing Fe(II) oxidation activity, but also due to heterotrophic denitrifying bacteria, reducing nitrate to nitrite. This process is called chemodenitrification and nitrite oxidizes Fe(II) abiotically.

The equations of nitrite production by denitrifying bacteria (Equation 4) and of abiotic Fe(II)-oxidation by nitrite to nitrous oxide (Equation 5) are as follows:

$$NO_3^- + 2\,e^- + 2\,H^+ \rightarrow NO_2^- + H_2O \quad (4)$$

$$20\,Fe^{2+} + 10\,NO_2^- + 17\,H_2O \rightarrow 2\,Fe_{10}O_{14}(OH)_2\downarrow + 5\,N_2O + 30\,H^+ \quad (5)$$

Heterotrophic denitrifying bacteria do not belong to the group of nitrate-reducing Fe(II)-oxidizers (NRFeOx). By contrast, in this case, Fe(II)-oxidation is an abiotic process, caused by nitrite released from the cells, and is not an enzymatic process [63]. The uncontrolled Fe(III) (oxyhydr)oxide precipitation at the cell

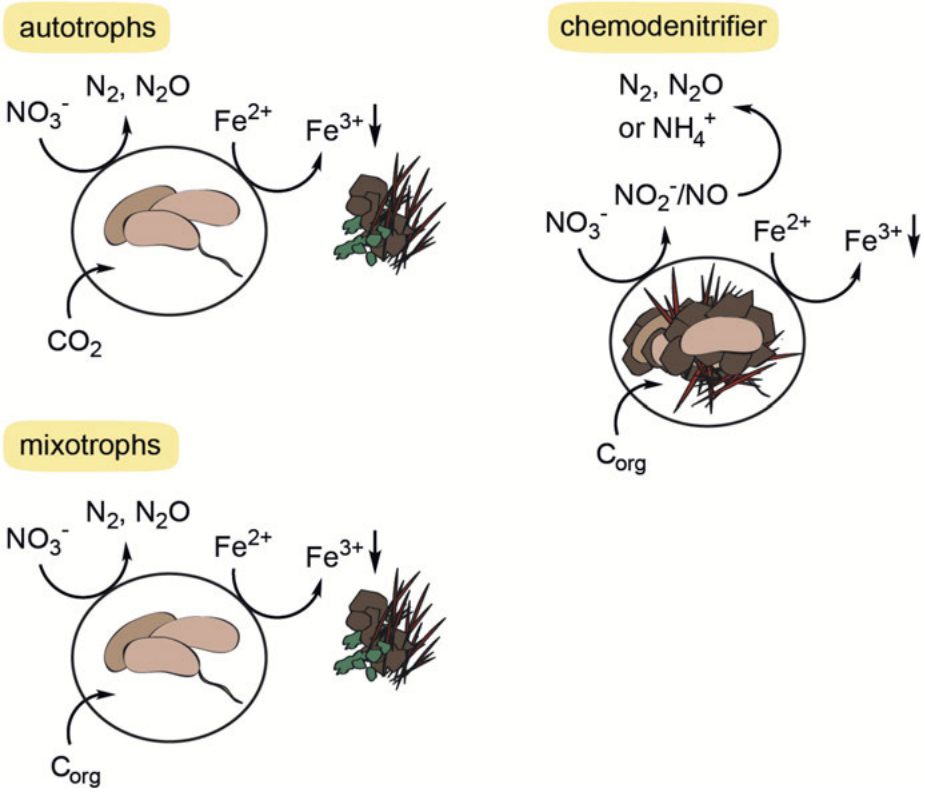

Figure 6. Schematic of autotrophic and mixotrophic NRFeOX, and heterotrophic denitrifiers.

surface, in their periplasm and cytoplasm [63, 95] can cause cell encrustation even leading to cell death (Figure 6).

In addition to these heterotrophic denitrifying bacteria indirectly oxidizing Fe(II), nitrate-reducing Fe(II) oxidation has been proposed for autotrophic and mixotrophic enrichment cultures and isolates. However, this remains controversial. A true autotrophic NRFeOx maintains its ability to conserve energy by nitrate-dependent Fe(II)-oxidation over several transfers into fresh autotrophic media and does not require any additional carbon source beyond CO_2 to building biomass. So far, this was only demonstrated for the enrichment culture KS by culture maintenance on autotrophic media over several years (in two different laboratories) and by incorporation of labelled CO_2 into biomass [96–99]. Most NRFeOx cultures are proposed to require addition of organic substrates for continuous Fe(II)-oxidation. These NRFeOx were termed 'mixotrophs'. By definition, this means that the cells use both organic and inorganic compounds as sources for carbon fixation and/or energy conservation. Depending on the context, mixotrophy can mean different combinations of obligate or facultative metabolic processes. However, so far, such a dependence on both inorganic and organic compounds for NRFeOx has not been demonstrated.

In the context of NRFeOx, mixotrophy has not been further defined beyond the dependence on organic substrates in combination with Fe(II)-oxidation. If some of these strains are true mixotrophs, the role of organic substrates (used during Fe(II)-oxidation) could be to regenerate reducing equivalents due to the lack of a reverse electron transport pathway linked to Fe(II)-oxidation. Further, it could be an essential substrate for CO_2 assimilation similar to acetate assimilation via the ethylmalonyl-CoA pathway. The metabolic mode of mixotrophic and autotrophic NRFeOx has been recently reviewed by Bryce et al. [100]. It must be noted that for all NRFeOx that have been called "mixotrophs", it seems more likely these strains are heterotrophic denitrifiers producing nitrite that is abiotically oxidizing Fe(II). There is currently no example of a true mixotrophic NRFeOx.

2.1.3.2. Environmental Distribution

Nitrate-dependent Fe(II)-oxidation has been observed for several pure and enrichment cultures derived from anoxic sediments and soils at circumneutral pH [11, 101]. Habitats where NRFeOx have been found include freshwater lake sediments [102], ponds, paddy soils [103], ditches, a brackish water lagoon [97], and groundwater aquifers [104, 105].

2.1.3.3. Biotechnological Application

Nitrate-reducing Fe(II)-oxidizing bacteria can be harnessed as a whole cell biocatalyst for the removal of nitrate pollution in groundwater [106]. High levels of nitrate in groundwater are caused by agricultural practices, in particular the application of inorganic fertilizer and animal waste [107, 108]. Nitrate pollution is causing environmental problems such as eutrophication of surface waters due to excess nutrients [109]. In subsurface environments or groundwater aquifers containing pyrite, NRFeOx could potentially couple pyrite oxidation to denitrification for nitrate removal [110, 111]. However, nitrate-reducing Fe(II)-oxidizing

bacteria may cause environmental problems due to the accumulation of NO_2^- or the release of N_2O gas. While NO_2^- in drinking water directly affects human health [112], N_2O is a greenhouse gas. Additionally, depending on the Fe(II) source (e.g., aqueous OM complexes) the identity of the reduced nitrogen species varies [113].

2.1.3.4. Metabolic Pathway of Iron(II) Oxidation

(a) Diversity of nitrate-reducing pathways

Microbial nitrate reduction is part of various metabolic pathways. Nitrate can be reduced to nitrite in a two-electron transfer step ($NO_3^- \rightarrow NO_2^-$) [114], to N_2 by full denitrification ($NO_3^- \rightarrow NO_2^- \rightarrow NO \rightarrow N_2O \rightarrow N_2$), or to ammonium by dissimilatory nitrate reduction to ammonium (DNRA; $NO_3^- \rightarrow NO_2^- \rightarrow NH_4^+$) [115]. Nitrite and ammonium, obtained by either of these processes can be further metabolized to N_2 by anaerobic ammonium oxidation (Anammox) ($NH_4^+ + NO_2^- \rightarrow N_2$) [116, 117]. Thus it is possible that NRFeOx have a common Fe(II) oxidation mechanism via homologs of MtoA/B or Cyc2 but differ in the metabolic pathway for nitrate reduction. The best model for the nitrate-reducing Fe(II)-oxidation mechanism is derived from metagenome analyses of the enrichment culture KS and genome analysis of *Gallionellaceae* sp., main Fe(II)-oxidizer of culture KS [85, 118].

(b) Culture KS and the proposed *Gallionellaceae* sp. Fe(II)-oxidation metabolic pathway

The enrichment culture KS was originally isolated from sediment in a freshwater pond in Bremen, Germany [97], it is a chemolithoautotrophic nitrate-reducing Fe(II)-oxidizing culture and has been used as a model system to study nitrate-reducing Fe(II)-oxidation. However, the putative Fe(II)-oxidizer, a species from the family *Gallionellaceae*, has not yet been isolated from this co-culture [119].

This *Gallionellaceae* sp. is closely related to *Sideroxydans lithotrophicus* ES-1, a microaerophilic Fe(II)-oxidizer. Culture KS also contains relatives of the heterotrophic nitrate-reducing bacteria *Comamonas badia*, *Parvibaculum lavamentivorans* and *Rhodanobacter thiooxidans* [120]. He et al. [118] analyzed the culture community composition and in particular the flanking community of two KS cultures maintained in different laboratories and demonstrated that the communities of these two subcultures of culture KS can indeed vary substantially but both subcultures still perform autotrophic nitrate-reducing Fe(II) oxidation [118]. The cultures were maintained on autotrophic media in both laboratories, at the University of Tübingen (Germany) and at the University of Wisconsin (Madison, USA), over several years. In KS-Madison, *Gallionellaceae* accounted for 42 % of the total community whereas *Gallionellaceae* of KS-Tübingen accounted for 96 % of the total community [85]. Since both cultures are able to grow autotrophically, the composition of the flanking community seems to have a minor impact on the predominant occurring *Gallionellaceae* sp. which is the putative Fe(II)-oxidizer. However, since the *Gallionellaceae* sp. has not been isolated, it is hypothesized that the flanking community has an essential role for

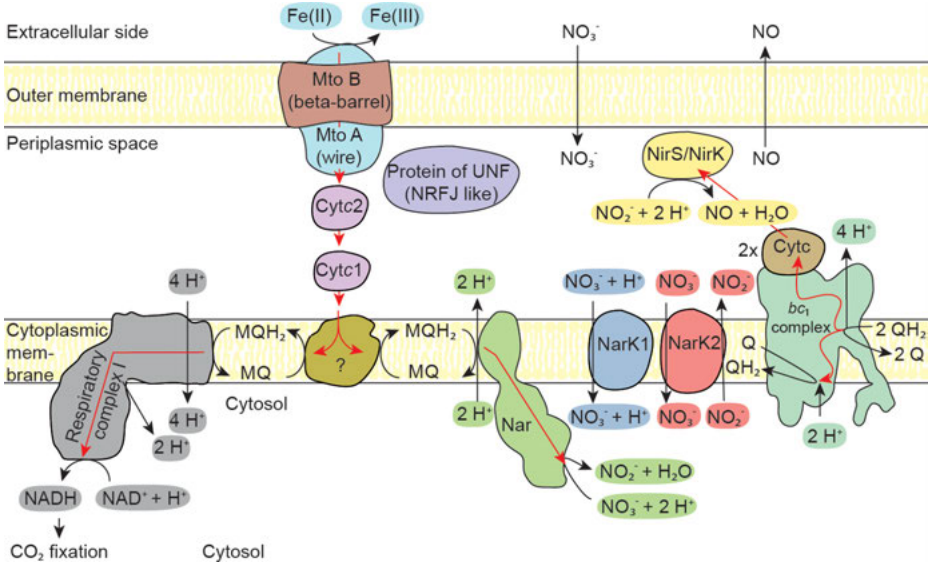

Figure 7. Schematic of nitrate-reducing Fe(II) oxidation pathway in culture KS. The figure is modified from Bryce et al. [100]. Fe(II) is oxidized by multiheme *c*-type cytochrome (MtoA) associated with a porin (MtoB). *c*-type cytochromes 1 and 2 (Cytc1 and Cytc2) are located in the same genome cluster as MtoAB and are therefore suggested being the next proteins in the electron chain. However, there is also a protein of unknown function (Protein of UNF) located in the same gene cluster. The electrons are proposed to reduce quinones via the bc_1 complex. This would require a proton motive force that might not be regenerated by the reduction of nitrate alone. Therefore, the figure shows a question mark for the reduction of the quinones. The quinones can be used by the respiratory complex I to regenerate NADH by using the proton motive force. The proton motive force is supposed to be built by the dissimilatory nitrate reductase complex (Nar) catalyzing the reaction of nitrate to nitrite. NarK1 and NarK2 are nitrate:nitrite antiporter. NirS and NirK are cytochrome cd_1- and copper-type nitrite reductase, respectively and catalyze the reduction of nitrite to nitric oxide.

the physiology of the main Fe(II)-oxidizer in the co-culture, e.g., these community members could degrade a toxic product derived from the Fe(II)-oxidation metabolism in *Gallionellaceae* sp.

The metabolic pathway model resulting from comparative genome analysis suggests that nitric oxide cannot be degraded by *Gallionellaceae* sp. as it lacks a nitric oxide reductase. However, the flanking community members have the genomic capability to reduce nitric oxide to N_2. The schematic of the proposed Fe(II)-oxidation metabolic pathway in culture KS is presented in Figure 7. The pathway is similar to the proposed pathways in *Sideroxydans* ES-1 and *Gallionella* ES-2 (Figure 5), suggesting a similar Fe(II)-oxidizing pathway in neutrophilic freshwater Fe(II)-oxidizers. The putative Fe(II)-oxidase is MtoA, which is thought to form a porin-cytochrome complex with MtoB. The *mtoB* gene is located downstream next to *mtoA*. The *mto* operon encodes two more cytochromes that are potentially involved in electron transfer as well.

After passing the electrons to the quinone pool they can enter either an up-hill electron transfer pathway via complex I resulting in NAD(P)H generation or a down-hill pathway towards nitrate and further nitrite reduction. It should be acknowledged that the neutrophilic Fe(II)-oxidation pathways remain speculative and are mainly based on *in silico* analysis. He et al. [85] published a genome study where several alternative putative Fe(II)-oxidases of neutrophilic Fe(II)-oxidizers are discussed [85]. Further information about putative Fe(II)-oxidases in nitrate-dependent Fe(II)-oxidizers can be found in the supplementary information of He et al. [118].

2.2. Phototrophic Iron(II)-Oxidation

2.2.1. Iron(II)-Driven Energy Conservation

Phototrophic Fe(II)-oxidizing bacteria, so-called photoferrotrophs, conserve light energy and reduce CO_2 to biomass by the use of electrons stemming from Fe(II). It is proposed that light does not support the oxidation of Fe(II), however, builds up a PMF that in turn powers the up-hill transportation of the electrons that reduce $NAD(P)^+$ to NAD(P)H. This process is anoxygenic, which means oxygen is not a product of phototrophic Fe(II)-oxidation, thus this metabolism is an example of anoxygenic photosynthesis. It may have evolved earlier than oxygenic photosynthesis [121, 122] and might be an ancestor in its evolution [123–125].

Fe(II)-oxidation by photoferrotrophy follows the stoichiometry described by Equation (6):

$$20\,Fe^{2+} + 5\,HCO_3^- + 22\,H_2O + C_n(H_2O)_m \xrightarrow{h\nu} Fe_{10}O_{14}(OH)_2\downarrow + C_{n+5}(H_2O)_{m+5} + 35\,H^+ \quad (6)$$

2.2.2. Environmental Distribution

Phototrophic Fe(II)-oxidizing bacteria can be isolated from freshwater sediments of ditches [126, 127], stratified lakes and marshes [128], and from marine sediments at the North Sea coast [129] and coastal marine sediments [130], among other locations. Examples are listed in Table 3 and an extended list was recently published by Bryce et al. [100].

2.2.3. Biological Availability of the Iron(II) Source

Rhodobacter ferrooxidans strain SW2, *Chlorobium ferrooxidans* strain KoFox and *Thiodictyon* sp. strain F4 were shown to metabolize dissolved Fe(II) and highly soluble minerals such as FeS and $FeCO_3$, but not poorly soluble Fe(II)-bearing minerals (e.g., Fe_3O_4 and FeS_2 [131]). There is evidence that another photoferrotroph, *Rhodopseudomonas palustris* strain TIE-1, can oxidize magnet-

Table 3. Cultures of phototrophic Fe(II)-oxidizers.

Freshwater strains	**Reference**
Rhodobacter ferrooxidans strain SW2	[126]
Rhodopseudomonas palustris strain TIE-1	[307]
Chlorobium ferrooxidans strain KoFox	[127]
Thiodictyon sp. strain F4	[128]
Rhodomicrobium vannielii strain BS-1	[154]
Marine strains	
Rhodovulum iodosum	[129]
Rhodovulum robiginosum	[129]
Chlorobium sp. strain N1	[130]

ite, however, the oxidation was shown to depend on the magnetite particle size [132]. Fe-OM complexes are suggested to play a significant role in biogeochemical iron cycling in the photic zones of aquatic environments [133]. Here, Fe(III)-OM reduction can be induced by abiotic photoreduction and Fe(II)-OM oxidation is promoted by photoferrotrophic bacteria. This suggests a light-driven cryptic iron cycle that may play a role in the photic zone of aquatic habitats [134]. A cryptic iron cycle is so-called because it describes such a rapid turnover of Fe(II) and Fe(III) that a change in their concentration cannot be measured using traditional sampling or analytical approaches. Despite rapid Fe(II) oxidation and Fe(III) re-reduction, the Fe(II) concentration would remain low and steady.

Cultivation studies with *Rhodopseudomonas palustris* strain TIE-1 demonstrated that: (i) Fe(II)-organic matter complexation promotes Fe(II)-oxidation in comparison to free Fe^{2+}, and, (ii) the choice of organic ligand influenced the bioavailability of Fe(II) [133, 134]. This might be due to different redox kinetics between Fe(II) and *c*-type cytochromes based on the organic ligand or free Fe^{2+}, respectively. Further steric effects of the complexing ligand could be an additional factor [135].

2.2.4. Environmental Impact

Microbial iron oxidation and reduction processes are tightly coupled and allow efficient iron cycling [136]. It is thought that one iron atom can undergo up to 300 redox cycles until it is converted to a bio-unavailable form [137]. In anoxic environments phototrophic and nitrate-reducing Fe(II) oxidation activity can play an especially important role in iron cycling [97, 138]. During phototrophic Fe(II) oxidation a variety of Fe(II) minerals can be oxidized and Fe(III) minerals can be formed, e.g., ferrihydrite, goethite, lepidocrocite, and magnetite [131]. If phototrophic Fe(II)-oxidizing bacteria colonized the early Earth, they may have contributed to the deposition of banded iron formations (BIFs), some of the most economically significant iron deposits worldwide [139–141].

2.2.5. Biotechnological Application

Photoferrotrophs are promising candidates for whole-cell catalysts in combination with electrodes as electron donors. It was demonstrated for *Rhodopseudomonas palustris* strain TIE-1 that electrons derived from solid-phase conductive matrices (e.g., electrodes) can be linked to carbon dioxide fixation by extracellular electron uptake [142]. Such a photoelectron autotrophic system was applied for producing bioplastic (polyhydroxybutyrates) [143].

2.2.6. Metabolic Pathway of Iron(II) Oxidation

The best studied photoferroautotrophic strains are the freshwater isolates *Rhodobacter ferrooxidans* strain SW2 and *Rhodopseudomonas palustris* strain TIE-1. Notably, they have different metabolic pathways for Fe(II)-oxidation and electron transport. In strain SW2, the *fox* operon; and, in strain TIE-1 the *pio* operon, have been shown to be essential for Fe(II)-oxidation.

The first gene in the *pio* operon encodes PioA, a decaheme *c*-type cytochrome. It is proposed to function as the Fe(II)-oxidase similar to Cyc2 in acidophilic Fe(II)-oxidizers [144]. Sequence analysis of PioA indicates that it is located in the periplasm because it lacks typical features of an outer membrane protein [144]. PioA has a putative secretory signal peptide (amino acids 1–40) [145] and can be further divided in a C-terminal domain that shows a multiheme cytochrome *c* family profile (amino acids 271–529) similar to MtrA and MtoA [92] and an N-terminal domain of unknown function (amino acids 41–270) which includes a glycine-rich region (amino acids 90–133) [146].

PioB and MtrB of *Shewanella* spp. (Fe(III)-reducing bacteria, see Section 3.4.1.) are homologous proteins. MtrB is an outer membrane porin with 26 transmembrane β-strands [91]. According to the high number of β-strands MtrB, and consequently its homologs (i.e., PioB and MtoB), are relatively large outer membrane porins. MtrA and B of the metal-reducing bacterium *Shewanella oneidensis* strain MR-1 are assembled in a porin-cytochrome complex. These findings are based on MtrA, MtrA/B, and MtrA/B/C models derived from small-angle x-ray scattering (SAXS) data [88–90]. The X-ray crystal structure of the whole Mtr complex from *Shewanella baltica* OS185 has been published recently by Edwards et al. [91]. Because of this, it has been suggested that PioB and PioA are assembled in a similar complex [85, 147], however, the localization of the N-terminal domain remains unclear.

The third gene in the *pio* operon encodes PioC, a putative high potential iron-sulfur protein (HiPIP). Its function is proposed to be an electron carrier from PioA to the photosynthetic reaction center (RC). However, HiPIPs could also substitute for cytochrome c_2 and therefore function as an electron carrier that shuttles electrons between the cytochrome bc_1 complex and the RC in the periplasm. In the case of strain TIE-1, the extracellular electrons derived from Fe(II)-oxidation are transferred to reducing equivalents and can finally be used for the reduction of CO_2 to build up biomass via the Calvin-Benson-Bassham cycle [142].

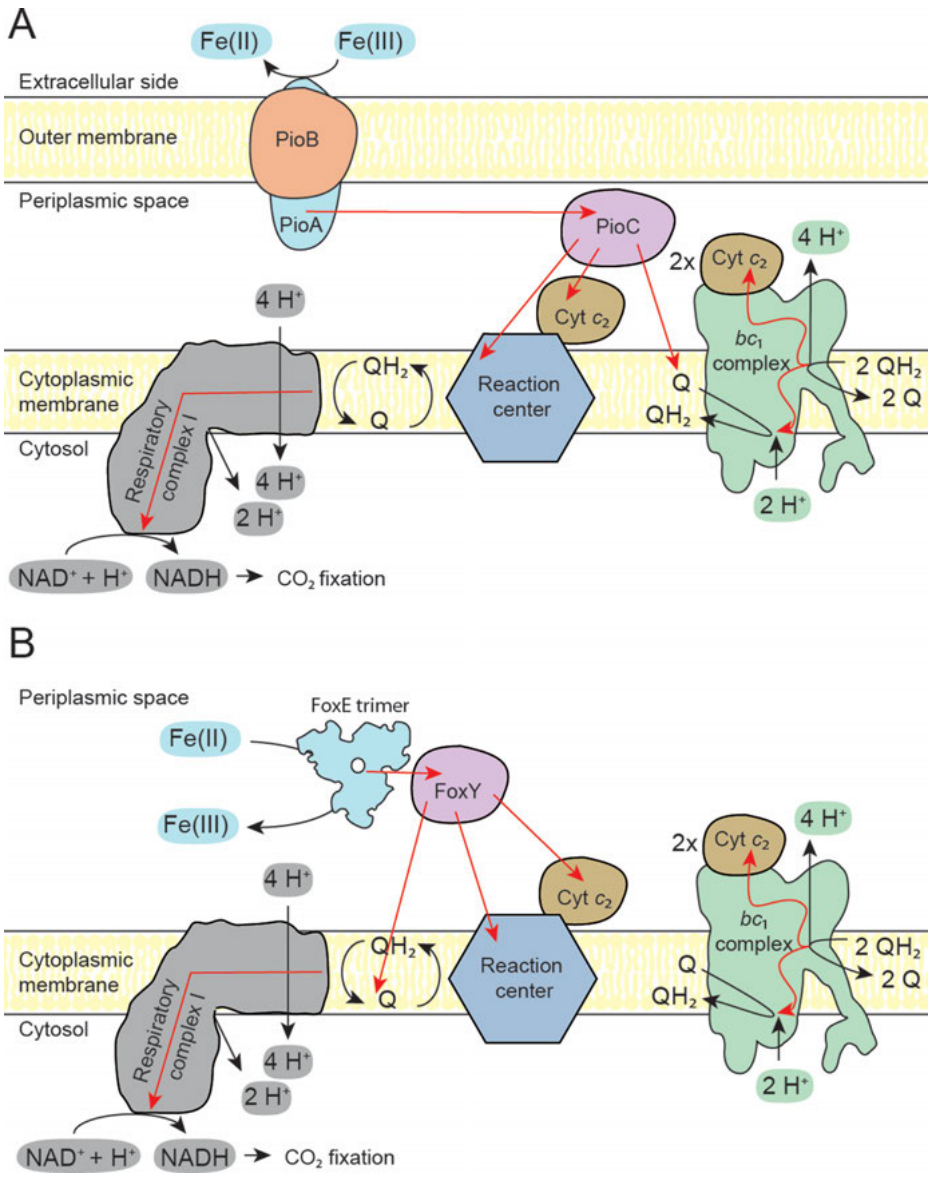

Figure 8. Schematic for electron transport from Fe(II) to the electron transport chain in the cytoplasmic membrane for the freshwater isolates *Rhodopseudomonas palustris* strain TIE-1 (A) and *Rhodobacter ferrooxidans* strain SW2 (B) [309]. FoxE is shown as a trimer [153].

The *fox* operon of strain SW2 encodes three essential proteins that are different to those encoded by the *pio* operon [148, 149] (Figure 8). The first gene in the *fox* operon encodes a *c*-type cytochrome, FoxE, and is the proposed Fe(II)-

oxidase. It has been shown that the protein is thermodynamically and kinetically able to perform Fe(II)-oxidation [149] and its location is hypothesized for the periplasm based on the lack of β-sheets and a lipoprotein profile, as is the case for Cyc2, OmcA or OmcB [47, 86, 148]. The suggested redox partner of FoxE is FoxY encoded by the second gene of the *fox* operon. The protein is similar to PioC and has a binding site for pyrroloquinoline quinone. According to its predicted isoelectric point (5.34), it is negatively charged at neutral pH, and therefore it could possibly interact with the convex side of the FoxE trimer. The last gene in the *fox* operon encodes a putative transport protein, FoxZ.

Strain SW2 seems to lack an extracellular electron transport system which stands in agreement with the observation, that it cannot oxidize solid Fe(II) phases [148].

All the proposed photoferrotrophic Fe(II)-oxidation pathways do not answer the question, why Fe(III) production does not lead to cell encrustation. Strain SW2 seems to oxidize Fe(II) in the periplasm, where it theoretically precipitates as Fe(III) (oxyhydr)oxide at pH 7. This would lead to mineral deposition inside the cell. However, experiments indicate that photoferrotrophs must have strategies to avoid mineral formation inside or on the cell [74, 126, 131, 150].

For strain TIE-1, the expression of genes involved in active efflux mechanisms upon Fe(II) addition and long period cultivations with Fe(II) was demonstrated by Bryce et al. [100]. It is possible that efflux proteins contribute to the mineralization away from the cell. Further, it is hypothesized that the cells produce Fe(III) chelators that transport Fe(III) to the outside of the cell [149]. This is consistent with the observation that: (i) strain SW2 grows better with nitrilotriacetic acid (NTA, a complexing agent) [148], and, (ii) the supernatant of Fe(II)-grown culture increases the solubility of Fe(III) [149, 151]. The chelators do not seem to be siderophores, as they have not been found in high concentrations in Fe(II)-grown cultures. Additionally, their synthesis would be energetically expensive [149]. It has been demonstrated that FoxE is active at low pH, thus a low-pH microenvironment around the cell could be an alternative strategy to avoid cell encrustation [152].

Pereira et al. [153] showed that the distances of hemes within the FoxE trimer structure are relatively large (16 Å, within the monomer; 22 Å, the closest heme between neighbors). Therefore, the authors propose a slow, intermolecular electron transfer that prevents product accumulation and further spontaneous Fe(III) precipitation in the cytosol. In general, it has been proposed that (i) not all photoferrotophs share the same strategy to avoid Fe(III) precipitation inside or at the surface of the cell, and, (ii) their strategies have different efficiencies [150, 154].

3. MICROBIAL GROWTH BY REDUCTION OF IRON(III)

Fe(III)-reducing microbes couple the reduction of Fe(III), including Fe(III) minerals and dissolved Fe(III)-OM complexes, to the oxidation of a variety of elec-

tron sources, including organic matter (OM), sulfur (S^0), ammonium (NH_4^+), methane (CH_4) or dihydrogen (H_2). Fe(III)-reducing microbes are phylogenetically diverse, and are present in virtually every environmental habitat on Earth, including soils, sediments, and subsurface environments. Combined with the abundance of iron in the Earth's crust, and the phylogenetic and spatial breadth of this process, these interactions, which underpin biogeochemical cycling for so many elements, make the Fe(III)-reduction metabolic process globally and geologically significant.

3.1. Dissimilatory Iron(III) Reduction

Dissimilatory Fe(III) reduction is a metabolic process where microbes obtain energy for growth and cellular maintenance by oxidizing organic (e.g., acetate, lactate, benzene) or inorganic (i.e., H_2) electron donors, and transferring electrons to minerals that contain Fe(III), thereby reducing the Fe(III). Myers and Nealson [155] first identified metal reduction as a cellular metabolic process linked to growth, in the year 1988.

Many types of microbes can perform Fe(III) reduction; the substrates used by microorganisms to reduce Fe(III) are varied and readily available in most terrestrial environments. Observed electron donors include organic compounds such as: glucose [156, 157], acetate [158, 159], and CH_4 [160]; as well as H_2 [161], NH_4^+ [162], S^0 [163, 164], and electrically conductive carbon materials; e.g., activated carbon [165, 166] and carbon cloth [167]. Fe(III)-bearing electron acceptors include minerals such as ferrihydrite [160, 168, 169] and magnetite [156, 157].

In addition, dissimilatory Fe(III)-reducing bacteria have been shown to be capable of degrading complex polysaccharides [170, 171]; thus, the potential exists for Fe(III)-reducing bacteria to participate directly in the metabolism of humic substances, in addition to oxidizing the products of hydrolytic and fermentative metabolism [172]. Coupling humic substance degradation to dissimilatory iron reduction dramatically increases the pathways for soil organic carbon degradation, since microbial Fe(III)-reduction can lead to the release of dissolved organic carbon associated with Fe(III)-oxide surfaces [173, 174].

3.2. Metabolic Pathways and Substrates

3.2.1. Fe-Ammox

Initially suggested in 2005 [175], Fe-ammox is a recently discovered metabolic pathway that links nitrogen and iron cycling by coupling the reduction of Fe(III) to ammonium oxidation [175–177]. This process has been observed in a forested riparian wetland in New Jersey [162, 175, 176, 178, 179], tropical upland soils [177], wetland soils in South Carolina [179], and various forested and wetland locations in Southern China, including paddy soils [179]. The Fe-ammox reaction appears to be more common in acidic, iron-rich wetland environments [162, 177–

180]. The stoichiometry for the Fe-ammox process with ferrihydrite as the iron source is described by Equation (7).

$$6\,Fe_{10}O_{14}(OH)_2 + 98\,H^+ + 11\,NH_4^+ \rightarrow 60\,Fe^{2+} + 80\,H_2O + 11\,NO_2^- \quad (7)$$

The first Fe-ammox bacterium, *Acidimicrobiaceae* sp. A6, was isolated and characterized by Huang and Jaffe in 2018 [162]. Fe-ammox may be an autotrophic Fe(III) reduction process [162], although at present, data does not support this.

3.2.2. Anaerobic Methane Oxidation and Methanotroph Symbiosis

Beal et al. [160] first observed the coupling of the reduction of Fe(III)-bearing minerals by Archaea to the anaerobic oxidation of methane (AOM). AOM is most often coupled to sulfate reduction. However, in low-sulfate environments where abundant reactive Fe(III)-(oxyhydr)oxide phases and CH_4 co-occur, such as in freshwater and brackish environments [181], the coupling of Fe(III)-reduction to AOM can act as a mechanism to remove CH_4, which is a potent greenhouse gas.

Summers et al. [182] demonstrated the direct involvement of microbial nanowires and multiheme *c*-type cytochromes in interspecies electron transfer, and identified the process of direct interspecies electron transfer. In the context of microbial Fe(III)-reduction coupled to methanogenesis, a syntrophic interaction requires a Fe(III)-reducing bacterium, which oxidizes OM to interspecies-transferable molecules, and a methanotrophic partner to scavenge the transferable molecules. The reaction proceeds as follows for the Fe(III) minerals, bernite (Equation 8) and goethite (Equation 9) [4].

$$CH_4 + 8\,Fe(OH)_3 + 15\,H^+ \rightarrow HCO_3^- + 8\,Fe^{2+} + 21\,H_2O \quad (8)$$

$$CH_4 + 8\,FeOOH + 15\,H^+ \rightarrow HCO_3^- + 8\,Fe^{2+} + 13\,H_2O \quad (9)$$

Several studies have subsequently shown evidence for CH_4-oxidation coupled to Fe(III)-reduction [181, 183, 184]. Most recently, Cai et al. demonstrated that the anaerobic methanotrophic Archaea, *Candidatus* "Methanoperedens ferrireducens" could directly couple AOM to Fe(III) reduction [169].

3.2.3. S^0-Oxidation Coupled to Iron(III)-Reduction

At pH < 4.0, Fe(III) is soluble, removing the barrier of a solid-phase electron acceptor for acidophilic bacteria [185]. Dissimilatory Fe(III)-reduction is widespread among moderately acidophilic and extremely acidophilic bacteria [186]; the best known bacterium which utilizes this metabolic pathway is *Acidothiobacillus ferroxidans*. This strain is important in bioleaching applications, and can contribute to the creation of acid mine drainage [164]. Brock and Gustafson

[187] reported that *A. ferrooxidans* anaerobically reduced Fe(III) using elemental sulfur as the electron donor, proposing bacterial growth (Equation 10) [164]:

$$S^0 + 6\,Fe^{3+} + 4\,H_2O \rightarrow HSO_4^- + 6\,Fe^{2+} + 7\,H^+ \quad (10)$$

3.3. Mechanisms of Iron(III)-Reduction

Two physical constraints act to direct the mechanisms of electron transfer adopted by Fe(III)-reducing microorganisms at circumneutral pH: (1) the poor solubility of Fe(III) (oxyhydr)oxide minerals, and (2) the maximum hopping distance of 1.8–2.0 nm [188] for an electron moving between redox-active molecules. Despite this, both *Shewanella* and *Geobacter* species can transfer electrons to Fe(III) minerals located at considerable (mm- to cm-scale) distances from the cell [189–192] via non-local electron transfer strategies [193]. Two mechanisms have been proposed for the extracellular transfer of electrons from the microorganism to solid surfaces. These are: (i) electron transfer via direct contact of outer-membrane enzymes (cytochromes) or with outer cell membrane structures, such as pili and nanowires; and (ii) the use of soluble electron shuttles, such as humic substances and quinones. *Geobacter* spp. can also use Fe(III) (oxyhydr)oxides as conductors for interspecies electron transfer [8].

3.3.1. Electron Shuttling by Humic Substances

The process of electron shuttling between the bacterial cell and Fe(III) minerals via redox-active organic matter happens in a two-step process. First, the microbe donates electrons to the electron shuttle, reducing it. Second, the electrons are abiotically donated from the reduced shuttle to the Fe(III) mineral [11, 172, 194–199]. Many of the redox-active organic compounds which are common in soils and sediments can be used as electron shuttles for dissimilatory iron reduction. These include humic substances [194], plant exudates [200], biochar [201], and antibiotics [172, 192].

The ability to reduce humic substances is not constrained to metal-respiring organisms: many bacterial groups, including fermenting bacteria, methanogens, sulfate reducers, halorespirers, and hyperthermophilic Archaea [202–205] in diverse environments, such as lake and marine sediments and pristine and contaminated wetland sediments, were shown to be able to transfer electrons to humic substances [194, 198, 206, 207]. Because of the environmental and phylogenetic ubiquity of humic substance reduction, the abiotic reduction of Fe(III) by electron shuttles implicates biogeochemical iron-redox transformations even for microorganisms lacking the enzymatic machinery to directly reduce Fe(III) [208].

3.3.2. Pili and Nanowires to Iron Minerals

Conductive, redox-active pili, often called nanowires, have been implicated in extracellular electron transfer in both *Shewanella* spp. and *Geobacter* spp. [209,

210]. These nanowires play a critical role in long-range (~10 μm) extracellular electron transfer for respiration (i.e., cell-to-mineral) [209, 211] and interspecies (i.e., cell-to-cell) electron exchange [182, 212]. Wang et al. [135] show that conductive *G. sulfurreducens* pili are chains solely composed of OmcS, a six-heme *c*-type cytochrome. The hemes are closely stacked along the micrometer length of the filament, establishing the molecular basis for electronic conductivity in these nanowires.

3.3.3. Enzymatics

Electron transport pathways for Fe(III) reduction in different microorganisms often contain functionally similar components, but are different in their biochemistry [11, 213]. Genome sequence information from *Shewanella* spp. [214] and *Geobacter* spp. [215] helped to identify the genes involved in Fe(III) reduction pathways. Porin-cytochrome homologs have been identified in all sequenced *Geobacter* species and in bacteria from six different phyla, including *Anaeromyxobacter dehalogenans* 2CP-1, '*Candidatus* Kuenenia stuttgartiensis', *Denitrovibrio acetiphilus* DSM12809, *Desulfurispirillum indicum* S5, *Ignavibacterium album* JCM16511, and *Thermovibrio ammonificans* HB-1 [7, 11].

Electrons that originate from intracellular catabolism are transferred to cell surface-localized *c*-type cytochromes, which catalyze the extracellular electron transfer for the reduction of Fe(III) (oxyhydr)oxides [216]. The outer membrane cytochromes are connected to respiratory electrons of the intracellular quinone pool by outer membrane porin-cytochrome complexes, such as MtrA, MtrB, and CymA [217, 218]. This is suggestive of a general design principle for transferring electrons during the extracellular reduction of Fe(III)-bearing minerals [219, 220].

3.4. Most Important Representatives of Iron(III)-Reducing Microorganisms

The most notable examples of Fe(III)-reducing microorganisms include *Geobacter* spp. [159, 221, 222], *Shewanella* spp. [155, 161, 223–226], *Albidiferax ferrireducens* (formerly known as *Rhodoferax*) [227], *Geothrix fermentans* [228], and various hyperthermophilic Archaea [205, 229, 230]. Among the isolated microorganisms, Fe(III)-reducing extremophiles including hyperthermophilic, thermophilic, psychrophilic, acidophilic and alkaliphilic Archaea and bacteria have been described in pure culture [9, 203, 231–235]. One such isolate (strain 121, member of Archaea, most closely related to *Pyrodictium occultum* and *Pyrobaculum aerophilum*) surviving in hydrothermal vents has pushed the upper temperature limit for life to 121 °C [203].

3.4.1. Shewanella spp.

Shewanella oneidensis MR-1 was among the first identified microorganisms capable of using minerals that contain Fe(III) as terminal electron acceptors [224,

225]. The genus *Shewanella* is widespread in sedimentary environments and is characterized by a wide metabolic diversity [224, 226, 236–239]. *Shewanella* spp. reduce ferrihydrite to Fe(II) with lactate or formate (Equation 11):

$$5\,CH_3CH(OH)COO^- + 2\,Fe_{10}O_{14}(OH)_2 + 35\,H^+ \rightarrow 20\,Fe^{2+} + 5\,CH_3COO^- + 5\,HCO_3^- + 22\,H_2O \quad (11)$$

S. oneidensis MR-1 produces and secretes flavins that mediate extracellular electron transfer and facilitate the interaction between bacteria and their solid ferric substrate [240–243]. These chemically reduced flavins are proposed to function as diffusive electron shuttles [240, 241, 243], redox-active compounds that can be reduced and then transfer electrons directly to minerals that contain Fe(III) [244, 245].

Genetic studies of *Shewanella* spp. revealed the direct involvement of six multiheme *c*-type cytochromes – CymA, Fcc3 (also known as FccA), MtrA, MtrC, OmcA, and a small tetraheme cytochrome (STC) – and the porin-like outer membrane protein MtrB in the extracellular reduction of minerals that contain Fe(III) [92, 242, 246–249]. CymA, Fcc3, MtrA, MtrB, MtrC, OmcA, and STC form a pathway that oxidizes quinol in the cytoplasmic membrane and transfers the released electrons across the entire width of the cell envelope to the surface of minerals [7]. MtrA, B, and C from a complex and their protein structure has been recently solved by Edwards et.al. using X-ray crystallography techniques [91].

3.4.2. Geobacter spp.

Microorganisms from the family *Geobacteraceae* play a significant role in environmental Fe(III) reduction and the oxidation of organic matter in circumneutral surface and subsurface environments. The metabolic activity of *Geobacter* spp. is flexible and varied. These taxa are capable of utilizing a broad variety of carbon sources for growth, including monoaromatic compounds [250, 251], alcohols and fatty acids [252], acetate, lactate, pyruvate, and formate. In addition, *Geobacter* spp. can completely mineralize organic carbon to CO_2 [222]. Of special interest for engineering applications, *Geobacter* spp. are capable of generating electricity by transferring electrons directly to electrodes.

Two examples of the stoichiometric reduction of Fe(III) coupled to the oxidation of organic matter (acetate; Equation 12) and the reductive formation of magnetite from ferrihydrite (Equation 13) are as follows:

$$CH_3COO^- + 8\,Fe^{3+} + 4\,H_2O \rightarrow 2\,HCO_3^- + 8\,Fe^{2+} + 9\,H^+ \quad (12)$$

$$5\,CH_3COO^- + 12\,Fe_{10}O_{14}(OH)_2 \rightarrow 40\,Fe_3O_4 + 5\,HCO_3^- + 5\,CO_2 + 17\,H_2O \quad (13)$$

G. sulfurreducens does not synthesize electron shuttle molecules but requires direct contact with an electron acceptor via conductive filaments for long-range

extracellular electron transfer [209]. However, *Geobacter* spp. are known to make use of electron shuttles if present (see e.g., *Geobacter metallireducens* [194]). *Geobacter* spp. secrete extracellular cytochromes, such as the hexaheme OmcS in *G. sulfurreducens.* These cytochromes have been associated with conductive pili nanowires [211, 253], which mediate the conduction of current along the length of the wire or function as a contact point for mineral Fe(III) reduction [254].

In addition to cytochromes, *G. sulfurreducens* requires the outer membrane porin OmpJ for Fe(III) reduction [255]. In *G. sulfurreducens* DL-1 and *G. sulfurreducens* PCA, the key players in electron transfer across the cell envelope include the putative quinol oxidases ImcH and CbcL in the cytoplasmic membrane [256, 257], PpcA and PpcD in the periplasm [258, 259], and OmaB, OmaC, OmcB and OmcC in the outer membrane. The latter form porin–cytochrome trans-outer membrane protein complexes with the porin-like outer membrane proteins OmbB and OmbC [219, 254, 260]. In addition to cytochromes, *G. sulfurreducens* requires the outer membrane porin OmpJ for Fe(III) reduction [255].

4. APPLICATIONS AND CONSEQUENCES

4.1. Link to Other Biogeochemical Cycles

As explained in the previous sections, iron cycling microorganisms have been shown to occur in various aquatic and terrestrial environments, using different species of Fe(II) and Fe(III) for energy generation and growth. However, these processes are not only relevant for biogeochemical iron cycling. Iron metabolism is closely linked to most other important biogeochemical cycles. The oxidation of organic molecules (including methane) during microbial Fe(III) reduction (respiration with Fe(III)) as well as CO_2 fixation during microbial Fe(II) oxidation (with nitrate or O_2 as electron acceptor) link the iron to the carbon cycle. Additionally, the sequestration of organic molecules by sorption and co-precipitation to Fe(III) minerals and the release of the organic carbon during reductive dissolution of these carbon-loaded Fe(III) minerals shows how Fe(III) minerals have the potential for controlling the cycling of carbon [261].

Furthermore, a series of abiotic and biotic reactions such as microbially-catalyzed nitrate-dependent Fe(II) oxidation (see Section 2.1.3.), enzymatic ammonium oxidation coupled to Fe(III) mineral reduction, or abiotic oxidation of Fe(II) by reactive nitrogen species (nitric oxide or nitrite) couple the iron to the nitrogen cycle. Similarly, the oxidation of several sulfur species (sulfide, elemental sulfur, etc.) can be linked abiotically and biotically to Fe(III) mineral reduction (see Section 3.2.3.), thus linking the iron cycle to the sulfur cycle.

4.2. Consequences for Pollutants

In addition to these connections of the biogeochemical iron cycle to all other major element cycles, iron-metabolizing microorganisms can also influence the

fate and environmental behavior of pollutants, in particular toxic metals. On the one hand, Fe(III)-reducing bacteria can directly interact with toxic metals such as chromium and uranium, and can be used for remediation purposes by reductive immobilization of Cr(VI) as Cr(III) oxide (Cr_2O_3) and U(VI) as U(IV) oxide (UO_2) [262]. On the other, Fe(III) mineral-reducing bacteria were shown to be responsible for reductive dissolution of arsenic-bearing Fe(III) minerals and thus mobilization of arsenic into ground water and drinking water [263, 264]. On the oxidative side, Fe(II)-oxidizing bacteria and the resulting biogenic Fe(III) (oxyhydr)oxides have been suggested to be useful for immobilizing toxic metals such as arsenic, for example in drinking water filters [265–267].

4.2.1. Bioremediation and Biotechnology

Fe(III)-reducing bacteria contribute to bioremediation and bioattenuation of many contaminants through a variety of processes. Both, *Shewanella* spp. and *Geobacter* spp. have been reported to directly respire a number of metals other than Fe(III) and Mn(IV), including U(VI) [268, 269], sequestering radioactive uranium in the solid phase as the oxidized form U(IV).

4.2.2. Oxidation of Hydrocarbons

Fe(III)-reducing microorganisms such as *Geobacter metallireducens* GS-15 and *Geobacter* strain Ben couple the oxidative degradation of aromatic hydrocarbon contaminants, such as benzoate, toluene, phenol and *p*-cresol, to the reduction of Fe(III) [250, 250, 270–275]. Acetate oxidation by *Geobacter sulfurreducens* PCA is also electrically coupled to the reductive degradation of the contaminant trichloroethene by *Desulfitobacterium* spp. and *Dehalococcoides* spp. through conductive minerals [276]. In hydrocarbon-contaminated groundwater, Amos et al. [277] were able to link Fe(III) reduction to the oxidation of CH_4 under anoxic conditions.

4.2.3. Sequestration of Heavy Metals

In addition to the direct respiration of metals, the microbially-mediated reduction of Fe(III) regulates the solubility and sequestration of heavy metals by causing the reduction, and subsequent precipitation of heavy metals in Fe(III) (oxyhydr)oxide minerals [278–280]. This is because Fe(II) is a strong reductant to many heavy metals. Minerals, such as Fe(III) (oxyhydr)oxides (e.g., goethite), hematite, or maghemite that contain microbially-formed Fe(II) also reduce, and thereby sequester Cr(VI), Se(IV), Se(VI), and Tc(VII). Further, some Cr(III) can be incorporated into the mineral structure [102, 168, 278, 281–285], and the precipitates provide a reactive surface for the adsorption of PO_4^{3-}, Zn(II), As(V), and Co(II) [286].

5. OUTLOOK AND FUTURE DIRECTIONS

Although a lot is known about microbial iron metabolisms, there are several fascinating new areas of research that emerged in the last years, which require study by the next generations of iron biogeochemists and iron geomicrobiologists. These areas include (i) the isolation, cultivation, and characterization of microbial representatives of new iron-related metabolisms, (ii) the mechanisms of electron transfer being utilized by iron-cycling bacteria, and (iii) the role of iron-metabolizing microbes in the environment.

One obvious research need is that microbial representatives of new iron-related metabolisms need to be isolated, cultured, and characterized. This includes autotrophic nitrate-reducing Fe(II)-oxidizing microorganisms where so far only one promising example exists (culture KS, see Section 2.1.3.4. (b) [98]). However, this culture is currently still a mixed culture, and most other cultures that have been suggested to be autotrophic are either questionable or have been shown to need an organic co-substrate for sustainable growth and cultivation [100]. The isolation of new autotrophic nitrate-reducing Fe(II)-oxidizers (including isolation of the Fe(II)-oxidizer from culture KS) will then also allow to study the Fe(II) oxidation mechanisms and enzymes in these systems. Additionally, isolating more novel strains capable of coupling methane and ammonium oxidation to Fe(III) reduction [160, 177, 287] will provide the opportunity to investigate these metabolisms in more detail and to evaluate their potential environmental relevance.

The mechanisms of electron transfer being exploited by iron-cycling bacteria are complex and varied, and recent discoveries about the underlying structures have accelerated in the last few years. This is a promising and important area of active research, as these complex microbial interactions are teased apart in detail. Finally, while links to nearly every known biogeochemical cycle have been established, current knowledge only scratches the surface of understanding the intricacies of the role of iron minerals and iron-cycling microbes in the environment.

ACKNOWLEDGMENTS

We would like to thank the Geomicrobiology Group members (University of Tübingen, Germany) for our scientific discussions. We are grateful for the experimental work, that has been done in order to achieve the knowledge, on which this chapter is based on. Thanks to the corresponding researchers for your contribution to a greater understanding of iron biogeochemistry. We thank Nia Blackwell, Casey Bryce, and Caroline Schmidt for their thoughtful reviews of this manuscript. Clara Chan and James Byrne are thanked for generously sharing their images.

ABBREVIATIONS AND DEFINITIONS

ADP	adenosine 5′-diphosphate
Anammox	anaerobic ammonium oxidation
AOM	anaerobic oxidation of methane
ATP	adenosine 5′-triphosphate
C*c*O	cytochrome *c* oxidase
Cyc	cytochrome *c*
DNRA	dissimilatory nitrate reduction to ammonium
EDTA	ethylenediaminetetraacetic acid
Fe-ammox	iron-reducing anaerobic oxidation of ammonium
HiPIPs	high potential iron-sulfur proteins
NADH	reduced nicotinamide adenine dinucleotide
NAD^+	nicotinamide adenine dinucleotide
$NADP^+$	nicotinamide adenine dinucleotide phosphate
NADPH	reduced nicotinamide adenine dinucleotide phosphate
NRFeOx	nitrate reducing Fe(II)-oxidizer
NTA	nitrilotriacetic acid
OM	organic matter
PMF	proton motive force
P_i	inorganic phosphate
RcY	rusticyanin
RC	photosynthetic reaction center
STC	small tetraheme cytochrome

REFERENCES

1. A. Kappler, D. Emerson, J. Gralnick, E. Roden, E. M. Muehe, *Geomicrobiology of Iron,* in *Geomicrobiology,* 2nd ed., CRC Press, 2015, 1–320.
2. D. Emerson, *Biochem. Soc. Trans.* **2012**, *40*, 1211–1216.
3. F. M. Michel, V. Barron, J. Torrent, M. P. Morales, C. J. Serna, J.-F. Boily, Q. Liu, A. Ambrosini, A. C. Cismasu, G. E. Brown, *Proc. Natl. Acad. Sci. USA* **2010**, *107*, 2787–2792.
4. R. M. Cornell, U. Schwertmann, *The Iron Oxides: Structure, Properties, Reactions, Occurrences and Uses,* Wiley-VCH Verlag GmbH & Co. KGaA, Weinheim, 2003.
5. R. Raiswell, D. E. Canfield, *Geochem. Pers.* **2012**, *1*, 1–220.
6. O. E. Oni, M. W. Friedrich, *Trends Microbiol.* **2017**, *25*, 88–90.
7. L. Shi, H. Dong, G. Reguera, H. Beyenal, A. Lu, J. Liu, H. Q. Yu, J. K. Fredrickson, *Nature Rev. Microbiol.* **2016**, *14*, 651–662.
8. S. Kato, K. Hashimoto, K. Watanabe, *Proc. Natl. Acad. Sci. USA* **2012**, *109*, 10042–10046.
9. D. R. Lovley, D. E. Holmes, K. P. Nevin, *Adv. Microb. Physiol.* **2004**, *49*, 219–286.
10. D. R. Lovley, *Microbiol. Mol. Biol. Rev.* **1991**, *55*, 259–287.
11. E. D. Melton, E. D. Swanner, S. Behrens, C. Schmidt, A. Kappler, *Nature Rev. Microbiol.* **2014**, *12*, 797–808.
12. J. S. Berg, D. Michellod, P. Pjevac, C. Martinez-Perez, C. R. Buckner, P. F. Hach, C. J. Schubert, J. Milucka, M. M. Kuypers, *Environ. Microbiol.* **2016**, *18*, 5288–5302.

13. A. Kappler, C. Bryce, *Environ. Microbiol.* **2017**, *19*, 842–846.
14. C. Peng, C. Bryce, A. Sundman, A. Kappler, *Appl. Environ. Microbiol.* **2019**, *85*, e02826–18.
15. J. C. Cox, D. G. Nicholls, W. J. Ingledew, *Biochem. J.* **1979**, *178*, 195–200.
16. W. J. Ingledew, *Biochim. Biophys. Acta* **1982**, *683*, 89–117.
17. P. Leslie Dutton, *Meth. Enzymol.* **1978**, *54*, 411–435.
18. J. L. Slonczewski, M. Fujisawa, M. Dopson, T. A. Krulwich, *Adv. Microb. Physiol.* **2009**, *55*, 1–317.
19. C. Baker-Austin, M. Dopson, *Trends in Microbiology* **2007**, *15*, 165–171.
20. V. Bonnefoy, D. S. Holmes, *Environ. Microbiol.* **2012**, *14*, 1597–1611.
21. V. Bonnefoy, in *Bioinformatics and Genomics of Iron- and Sulfur-Oxidizing Acidophiles,* in *Geomicrobiology: Molecular and Environmental Perspective,* Eds L. L. Barton, M. Mandl, A. Loy, Springer, Dordrecht, The Netherlands, 2010, pp. 169–192.
22. S. Christel, M. Herold, S. Bellenberg, M. El Hajjami, A. Buetti-Dinh, I. V. Pivkin, W. Sand, P. Wilmes, A. Poetsch, M. Dopson, *Appl. Environ. Microbiol.* **2018**, *84*, e02091–17.
23. K. L. Temple, A. R. Colmer, *J. Bacteriol.* **1951**, *62*, 605–611.
24. A. R. Colmer, M. E. Hinkle, *Science* **1947**, *106*, 253–256.
25. A. R. Colmer, K. L. Temple, M. E. Hinkle, *J. Bacteriol.* **1950**, *59*, 317–328.
26. Y. Sheng, B. Kaley, W. D. Burgos, *Bio-Protoc.* **2017**, *7*, e2130.
27. A. Segerer, A. Neuner, J. K. Kristjansson, K. O. Stetter, *Int. J. Sys. Bacteriol.* **1986**, *36*, 559–564.
28. D. P. Kelly, A. P. Wood, *Int. J. Sys. Evol. Microbiol.* **2000**, *50*, 511–516.
29. D. W. Blowes, C. J. Ptacek, J. L. Jambor, C. G. Weisener, D. Paktunc, W. D. Gould, D. B. Johnson, *The Geochemistry of Acid Mine Drainage,* in *Treatise on Geochemistry,* 2nd ed., Eds H. D. Holland, K. K. Turekian, Elsevier, Oxford, 2014, 131–190.
30. S. Borilova, M. Mandl, J. Zeman, J. Kucera, E. Pakostova, O. Janiczek, O. H. Tuovinen, *Front. Microbiol.* **2018**, *9*, 3134–3134.
31. B. Dold, *Minerals* **2014**, *4*, 621–641.
32. I. Banerjee, B. Burrell, C. Reed, A. C. West, S. Banta, *Curr. Opin. Biotechnol.* **2017**, *45*, 144–155.
33. H. Brandl, R. Bosshard, M. Wegmann, *Hydrometallurgy* **2001**, *59*, 319–326.
34. Y. Hong, M. Valix, *J. Cleaner Prod.* **2014**, *65*, 465–472.
35. A. Schippers, S. Hedrich, J. Vasters, M. Drobe, W. Sand, S. Willscher, *Biomining: Metal Recovery from Ores with Microorganisms,* in *Geobiotechnology I: Metal-Related Issues,* Eds A. Schippers, F. Glombitza, W. Sand, Springer, Berlin Heidelberg, 2014, 1–47.
36. M. Sethurajan, E. D. van Hullebusch, Y. V. Nancharaiah, *J. Environ. Manag.* **2018**, *211*, 138–153.
37. J. Wang, S. Zhu, Y.-S. Zhang, H.-B. Zhao, M.-H. Hu, C.-R. Yang, W.-Q. Qin, G.-Z. Qiu, *J. Cent. South Univ.* **2014**, *21*, 728–734.
38. A. Werner, K. Meschke, K. Bohlke, B. Daus, R. Haseneder, J.-U. Repke, *ChemBioEng Rev.* **2018**, *5*, 6–17.
39. S. Regenspurg, A. Gößner, S. Peiffer, K. Küsel, *Water, Air, Soil Pollut.: Focus.* **2002**, *2*, 57–67.
40. S. Regenspurg, A. Brand, S. Peiffer, *Geochim. Cosmochim. Acta.* **2004**, *68*, 1185–1197.
41. S. Regenspurg, S. Peiffer, *Appl. Geochem.* **2005**, *20*, 1226–1239.
42. I. A. Katsoyiannis, A. I. Zouboulis, *Water Res.* **2002**, *36*, 5141–5155.
43. B. D. Johnson, K. B. Hallberg, *Adv. Microb. Physiol.* **2008**, *54*, 201–255.

44. M. Esparza, J. P. Cárdenas, B. Bowien, E. Jedlicki, D. S. Holmes, *BMC Microbiology.* **2010**, *10*, 229–244.
45. C. Appia-Ayme, N. Guiliani, J. Ratouchniak, V. Bonnefoy, *Appl. Environ. Microbiol.* **1999**, *65*, 4781–4787.
46. R. Quatrini, C. Appia-Ayme, Y. Denis, J. Ratouchniak, F. Veloso, J. Valdes, C. Lefimil, S. Silver, F. Roberto, O. Orellana, F. Denizot, E. Jedlicki, D. S. Holmes, V. Bonnefoy, *Hydrometallurgy* **2006**, *83*, 263–272.
47. A. Yarzabal, G. Brasseur, J. Ratouchniak, K. Lund, D. Lemesle-Meunier, J. A. DeMoss, V. Bonnefoy, *J. Bacteriol.* **2002**, *184*, 313–317.
48. A. Elbehti, G. Brasseur, D. Lemesle-Meunier, *J. Bacteriol.* **2000**, *182*, 3602–3606.
49. M.-T. Giudici-Orticoni, F. Guerlesquin, M. Bruschi, W. Nitschke, *J. Biol. Chem.* **1999**, *274*, 30365–30369.
50. T.–F. Li, R. G. Painter, B. Ban, R. C. Blake II, *J. Biol. Chem.* **2015**, *290*, 18293–18303.
51. C. Cavazza, M. Giudici-Orticoni, W. Nitschke, C. Appia, V. Bonnefoy, M. Bruschi, *Eur. J. Biochem.* **1996**, *242*, 308–314.
52. G. Brasseur, G. Levican, V. Bonnefoy, D. Holmes, E. Jedlicki, D. Lemesle-Meunier, *Biochim. Biophys. Acta* **2004**, *1656*, 114–126.
53. K. Shoji, T. Yamazaki, T. Nagano, Y. Fukumori, T. Yamanaka, *J. Biochem.* **1992**, *111*, 46–53.
54. X. Wang, M. Roger, R. Clement, S. Lecomte, F. Biaso, L. A. Abriata, P. Mansuelle, I. Mazurenko, M. T. Giudici-Orticoni, E. Lojou, M. Ilbert, *Chem. Sci.* **2018**, *9*, 4879–4891.
55. C. Castelle, M. Ilbert, P. Infossi, G. Leroy, M.-T. Giudici-Orticoni, *J. Biol. Chem.* **2010**, *285*, 21519–21525.
56. C. Castelle, M. Guiral, G. Malarte, F. Ledgham, G. Leroy, M. Brugna, M.-T. Giudici-Orticoni, *J. Biol. Chem.* **2008**, *283*, 25803–25811.
57. F. Meschi, F. Wiertz, L. Klauss, A. Blok, B. Ludwig, A. Merli, H. A. Heering, G. L. Rossi, M. Ubbink, *J. Am. Chem. Soc.* **2011**, *133*, 16861–16867.
58. S. Ishii, S. Suzuki, A. Tenney, K. H. Nealson, O. Bretschger, *ISME J.* **2018**, *12*, 2844–2863.
59. M.-T. Giudici-Orticoni, G. Leroy, W. Nitschke, M. Bruschi, *Biochemistry* **2000**, *39*, 7205–7211.
60. G. Brasseur, P. Bruscella, V. Bonnefoy, D. Lemesle-Meunier, *Biochim. Biophys. Acta* **2002**, *1555*, 37–43.
61. P. Bruscella, C. Appia-Ayme, G. Levican, J. Ratouchniak, E. Jedlicki, D. S. Holmes, V. Bonnefoy, *Microbiology* **2007**, *153*, 102–110.
62. M. S. Dodd, D. Papineau, T. Grenne, J. F. Slack, M. Rittner, F. Pirajno, J. O'Neil, C. T. S. Little, *Nature* **2017**, *543*, 60–64.
63. N. Klueglein, F. Zeitvogel, Y.-D. Stierhof, M. Floetenmeyer, K. O. Konhauser, A. Kappler, M. Obst, *Appl. Environ. Microbiol.* **2014**, *80*, 1051–1061.
64. E. E. Roden, D. Sobolev, B. Glazer, G. W. Luther, *Geomicrobiol. J.* **2004**, *21*, 379–391.
65. E. J. Fleming, I. Cetinifá, C. S. Chan, D. Whitney King, D. Emerson, *ISME J.* **2013**, *8*, 804.
66. J. Wang, G. Muyzer, P. L. E. Bodelier, H. J. Laanbroek, *ISME J.* **2009**, *3*, 715 – 725.
67. J. V. Weiss, D. Emerson, S. M. Backer, J. P. Megonigal, *Biogeochemistry.* **2003**, *64*, 77–96.
68. R. Yu, P. Gan, A. A. MacKay, S. Zhang, B. F. Smets, *FEMS Microbiol. Ecol.* **2009**, *71*, 260–271.
69. D. Emerson, E. J. Fleming, J. M. McBeth, *Annu. Rev. Microbiol.* **2010**, *64*, 561–583.
70. E. J. Fleming, R. E. Davis, S. M. McAllister, C. S. Chan, C. L. Moyer, B. M. Tebo, D. Emerson, *FEMS Microbiol. Ecol.* **2013**, *85*, 116–127.

71. C. S. Chan, S. M. McAllister, A. H. Leavitt, B. T. Glazer, S. T. Krepski, D. Emerson, *Front. Microbiol.* **2016**, *7*, 796–796.
72. J. M. Byrne, M. Schmidt, T. Gauger, C. Bryce, A. Kappler, *Environ. Sci. Technol. Lett.* **2018**, *5*, 209–213.
73. S. M. McAllister, R. M. Moore, A. Gartman, G. W. Luther, D. Emerson, C. S. Chan, *FEMS Microbiol. Ecol.* **2019**, *95*, fiz01595; doi: 10.1093/femsec/fiz015
74. J. Miot, K. Benzerara, M. Obst, A. Kappler, F. Hegler, S. Schädler, C. Bouchez, F. Guyot, G. Morin, *Appl. Environ. Microbiol.* **2009**, *75*, 5586–5591.
75. H. H. Hanert, *The Genus Siderocapsa (and Other Iron- and Manganese-Oxidizing Eubacteria),* in *Proteobacteria: Delta, Epsilon Subclass,* Eds M. Dworkin, S. Falkow, E. Rosenberg, K.-H. Schleifer, E. Stackebrandt, Springer-Verlag, New York, 2006, 1005–1015.
76. K. Laufer, M. Nordhoff, M. Halama, R. E. Martinez, M. Obst, M. Nowak, H. Stryhanyuk, H. H. Richnow, A. Kappler, *Appl. Environ. Microbiol.* **2017**, *83*, e03118–16.
77. A. Picard, A. Kappler, G. Schmid, L. Quaroni, M. Obst, *Nature Commun.* **2015**, *6*, 6277; DOI: 10.1038/ncomms7277.
78. C. S. Chan, S. C. Fakra, D. Emerson, E. J. Fleming, K. J. Edwards, *ISME J.* **2011**, *5*, 717–727.
79. S. Kato, M. Ohkuma, D. H. Powell, S. T. Krepski, K. Oshima, M. Hattori, N. Shapiro, T. Woyke, C. S. Chan, *Front. Microbiol.* **2015**, *6*, 1265–1265.
80. S. T. Krepski, D. Emerson, P. L. Hredzak-Showalter, G. W. Luther III, C. S. Chan, *Geobiology* **2013**, *11*, 457–471.
81. B. K. Chiu, S. Kato, S. M. McAllister, E. K. Field, C. S. Chan, *Front. Microbiol.* **2017**, *8*, 1280–1280.
82. D. Emerson, E. K. Field, O. Chertkov, K. W. Davenport, L. Goodwin, C. Munk, M. Nolan, T. Woyke, *Front. Microbiol.* **2013**, *4*, 254–254.
83. M. Seder-Colomina, G. Morin, K. Benzerara, G. Ona-Nguema, J.-J. Pernelle, G. Esposito, E. D. Van Hullebusch, *Geomicrobiol. J.* **2014**, *31*, 64–75.
84. R. Angelova, B. Blagoev, L. Slavov, M. Iliev, V. Groudeva, I. Nedkov, *J. Phys. Conf. Ser.* **2014**, *559*, 012019.
85. S. He, R. A. Barco, D. Emerson, E. E. Roden, *Front. Microbiol.* **2017**, *8*, 1584; doi: 10.3389/fmicb.2017.01584.
86. C. R. Myers, J. M. Myers, *Lett. Appl. Microbiol.* **2004**, *39*, 466–470.
87. S. Pirbadian, S. E. Barchinger, K. M. Leung, H. S. Byun, Y. Jangir, R. A. Bouhenni, S. B. Reed, M. F. Romine, D. A. Saffarini, L. Shi, Y. A. Gorby, J. H. Golbeck, M. Y. El-Naggar, *Proc. Natl. Acad. Sci. USA* **2014**, *111*, 12883–12888.
88. M. J. Edwards, G. F. White, C. W. Lockwood, M. C. Lawes, A. Martel, G. Harris, D. J. Scott, D. J. Richardson, J. N. Butt, T. A. Clarke, *J. Biol. Chem.* **2018**, *293*, 8103–8112.
89. M. A. Firer-Sherwood, N. Ando, C. L. Drennan, S. J. Elliott, *J. Phys. Chem. B.* **2011**, *115*, 11208–11214.
90. D. J. Richardson, J. N. Butt, J. K. Fredrickson, J. M. Zachara, L. Shi, M. J. Edwards, G. White, N. Baiden, A. J. Gates, S. J. Marritt, T. A. Clarke, *Mol. Microbiol.* **2012**, *85*, 201–212.
91. M. Edwards, G. White, J. Butt, D. J. Richardson, T. A. Clarke, *Cell* **2020**, *181*, 665–673.e10.
92. A. S. Beliaev, D. A. Saffarini, *J. Bacteriol.* **1998**, *180*, 6292–6297.
93. J. Liu, Z. Wang, S. M. Belchik, M. J. Edwards, C. Liu, D. W. Kennedy, E. D. Merkley, M. S. Lipton, J. N. Butt, D. J. Richardson, J. M. Zachara, J. K. Fredrickson, K. M. Rosso, L. Shi, *Front. Microbiol.* **2012**, *3*, 37; doi: 10.3389/fmicb.2012.00037.
94. K. Laufer, M. Nordhoff, H. Røy, C. Schmidt, S. Behrens, B. B. Jørgensen, A. Kappler, *Appl. Environ. Microbiol.* **2016**, *82*, 1433–1447.

95. J. Miot, K. Benzerara, G. Morin, A. Kappler, S. Bernard, M. Obst, C. Férard, F. Skouri-Panet, J.-M. Guigner, N. Posth, M. Galvez, G. E. Brown, F. Guyot, *Geochim. Cosmochim. Acta* **2009**, *73*, 696–711.
96. M. Nordhoff, C. Tominski, M. Halama, J. M. Byrne, M. Obst, S. Kleindienst, S. Behrens, A. Kappler, *Appl. Environ. Microbiol.* **2017**, *83*, e00752–17.
97. K. L. Straub, M. Benz, B. Schink, F. Widdel, *Appl. Environ. Microbiol.* **1996**, *62*, 1458–1460.
98. C. Tominski, T. Lösekann-Behrens, A. Ruecker, N. Hagemann, S. Kleindienst, C. W. Mueller, C. Höchen, I. Kögel-Knabner, A. Kappler, S. Behrens, *Appl. Environ. Microbiol.* **2018**, *84*, e02166–17.
99. C. Tominski, T. Lösekann-Behrens, A. Ruecker, N. Hagemann, S. Kleindienst, C. Müller, C. Höschen, I. Kögel-Knabner, A. Kappler, S. Behrens, *Appl. Environ. Microbiol.* **2018**, *84*, e02173–17.
100. C. Bryce, N. Blackwell, C. Schmidt, J. Otte, Y.-M. Huang, S. Kleindienst, E. Tomaszewski, M. Schad, V. Warter, C. Peng, J. M. Byrne, A. Kappler, *Environ. Microbiol.* **2018**, *20*, 3462–3483.
101. E. E. Roden, *Biochem. Soc. Trans.* **2012**, *40*, 1249–1256.
102. K. A. Weber, M. M. Urrutia, P. F. Churchill, R. K. Kukkadapu, E. E. Roden, *Environ. Microbiol.* **2006**, *8*, 100–113.
103. S. Ratering, S. Schnell, *Environ. Microbiol.* **2001**, *3*, 100–109.
104. J. Jamieson, H. Prommer, A. H. Kaksonen, J. Sun, A. J. Siade, A. Yusov, B. Bostick, *Environ. Sci. Technol.* **2018**, *52*, 5771–5781.
105. N. Jakus, N. Blackwell, K. Osenbrück, P. Grathwohl, S. Kleindienst, A. Kappler, *Iron(II)- and Sulfur-Driven Autotrophic Denitrification in a Pyrite-Rich Limestone Aquifer*, Goldschmidt, Barcelona, 2019.
106. N. Pous, S. Puig, M. Coma, M. D. Balaguer, J. Colprim, *J. Chem. Technol. Biotechnol.* **2013**, *88*, 1690–1696.
107. *Environmental performance of agriculture in OECD countries since 1990,* Organisation for Economic Cooperation and Development, 2008.
108. M. O. Rivett, S. R. Buss, P. Morgan, J. W. N. Smith, C. D. Bemment, *Water Res.* **2008**, *42*, 4215–4232.
109. C. F. Mason, *Biology of Freshwater Pollution,* Benjamin Cummings, Prentice Hall, Harlow, 2002.
110. J. Bosch, K.-Y. Lee, G. Jordan, K.-W. Kim, R. U. Meckenstock. *Environ. Sci. Technol.* **2012**, *46*, 2095–2101.
111. R. Yan, A. Kappler, E. M. Muehe, K.-H. Knorr, M. A. Horn, A. Poser, R. Lohmayer, S. Peiffer, *Geomicrobiol. J.* **2019**, *36*, 19–29.
112. *Guidelines for Drinking Water Quality,* World Heath Organization (WHO), Geneva, 2004.
113. C. Peng, A. Sundman, C. Bryce, C. Catrouillet, T. Borch, A. Kappler, *Environ. Sci. Technol.* **2018**, *52*, 5753–5763.
114. P. J. Gonzalez, C. Correia, I. Moura, C. D. Brondino, J. J. G. Moura, *J. Inorg. Biochem.* **2006**, *100*, 1015–1023.
115. B. Kraft, M. Strous, H. E. Tegetmeyer, *J. Biotechnol.* **2011**, *155*, 104–117.
116. J. G. Kuenen, *Nature Rev. Microbiol.* **2008**, *6*, 320–326.
117. M. Oshiki, S. Ishii, K. Yoshida, N. Fujii, M. Ishiguro, H. Satoh, S. Okabe, *Appl. Environ. Microbiol.* **2013**, *79*, 4087–4093.
118. S. He, C. Tominski, A. Kappler, S. Behrens, E. E. Roden, *Appl. Environ. Microbiol.* **2016**, *82*, 2656–2668.
119. M. Blöthe, E. E. Roden, *Appl. Environ. Microbiol.* **2009**, *75*, 6937.
120. D. Emerson, C. Moyer, *Appl. Environ. Microbiol.* **1997**, *63*, 4784–4792.
121. J. Xiong, *Genome Biol.* **2007**, *7*, 245; doi:10.1186/gb-2006–7-12–245.

122. A. Camacho, X. A. Walter, A. Picazo, J. Zopfi, *Front. Microbiol.* **2017**, *8*, 323.
123. F. Hegler, N. R. Posth, J. Jiang, A. Kappler, *FEMS Microbiol Ecol.* **2008**, *66*, 250–260.
124. J. M. Olson, R. E. Blankenship, *Photosynth. Res.* **2004**, *80*, 373–386.
125. K. Petrıckova, M. Petricek, *Microbiology.* **2003**, *149*, 1609–1621.
126. A. Ehrenreich, F. Widdel, *Appl. Environ. Microbiol.* **1994**, *60*, 4517–4526.
127. S. Heising, L. Richter, W. Ludwig, B. Schink, *Arch. Microbiol.* **1999**, *172*, 116–124.
128. L. R. Croal, C. M. Johnson, B. L. Beard, D. K. Newman, *Geochim. Cosmochim. Acta.* **2004**, *68*, 1227–1242.
129. K. L. Straub, F. A. Rainey, F. Widdel, *Int. J. Sys. Bacteriol.* **1999**, *49*, 729–735.
130. C. Bryce, N. Blackwell, D. Straub, S. Kleindienst, A. Kappler, *Microbiology Resource Announcement* **2019**, *8*, e00080–19.
131. A. Kappler, D. K. Newman, *Geochim. Cosmochim. Acta* **2004**, *68*, 1217–1226.
132. J. M. Byrne, G. van der Laan, A. I. Figueroa, O. Qafoku, C. Wang, C. I. Pearce, M. Jackson, J. Feinberg, K. M. Rosso, A. Kappler, *Sci. Rep.* **2016**, *6*, 30969.
133. C. Peng, C. Bryce, A. Sundman, T. Borch, A. Kappler, *ACS Earth Space Chem.* **2019**, *3*, 531–536.
134. C. Peng, C. Bryce, A. Sundman, A. Kappler, *Appl. Environ. Microbiol.* **2019**, *85*, e02826–18.
135. F. Wang, Y. Gu, J. P. O'Brien, S. M. Yi, S. E. Yalcin, V. Srikanth, C. Shen, D. Vu, N. L. Ing, A. I. Hochbaum, E. H. Egelman, N. S. Malvankar, *Cell* **2019**, *177*, 361–369.e10.
136. K. A. Weber, L. A. Achenbach, J. D. Coates, *Nature Rev. Microbiol.* **2006**, *4*, 752–764.
137. D. E. Canfield, B. Thamdrup, J. W. Hansen, *Geochim. Cosmochim. Acta* **1993**, *57*, 3867–3883.
138. F. Widdel, S. Schnell, S. Heising, A. Ehrenreich, B. Assmus, B. Schink, *Nature* **1993**, *362*, 834–836.
139. A. Kappler, C. Pasquero, K. O. Konhauser, D. K. Newman, *Geology* **2005**, *33*, 865–868.
140. C. M. Johnson, B. L. Beard, N. J. Beukes, C. Klein, J. M. O'Leary, *Contrib. Mineral. Petrol.* **2003**, *144*, 523–547.
141. A. D. Anbar, A. H. Knoll, *Science* **2002**, *297*, 1137–1142.
142. M. S. Guzman, K. Rengasamy, M. M. Binkley, C. Jones, T. O. Ranaivoarisoa, R. Singh, D. A. Fike, J. M. Meacham, A. Bose, *Nature Commun.* **2019**, *10*, 1355.
143. T. O. Ranaivoarisoa, R. Singh, K. Rengasamy, M. S. Guzman, A. Bose, *J. Indust. Microbiol. Biotechnol.* **2019**, https://doi.org/10.1007/s1029 5019-02165-7.
144. Y. Jiao, D. K. Newman, *J. Bacteriol.* **2007**, *189*, 1765–1773.
145. J. J. Almagro Armenteros, K. D. Tsirigos, C. K. Sønderby, T. N. Petersen, O. Winther, S. Brunak, G. von Heijne, H. Nielsen, *Nature Biotechnol.* **2019**, *37*, 420–423.
146. C. J. A. Sigrist, L. Cerutti, E. de Castro, P. S. Langendijk-Genevaux, V. Bulliard, A. Bairoch, N. Hulo, *Nucleic Acids Res.* **2009**, *38*, D161–D166.
147. C. Bryce, M. Franz-Wachtel, N. C. Nalpas, J. Miot, K. Benzerara, J. M. Byrne, S. Kleindienst, B. Macek, A. Kappler, *Appl. Environ. Microbiol.* **2018**, *84*, e01166–18.
148. L. R. Croal, Y. Jiao, D. K. Newman, *J. Bacteriol.* **2007**, *189*, 1774–1782.
149. I. H. Saraiva, D. K. Newman, R. O. Louro, *J. Biol. Chem.* **2012**, *287*, 25541–25548.
150. S. Schädler, C. Burkhardt, F. Hegler, K. L. Straub, J. Miot, K. Benzerara, A. Kappler, *Geomicrobiol. J.* **2009**, *26*, 93–103.
151. K. L. Straub, M. Benz, B. Schink, *FEMS Microbiol. Ecol.* **2001**, *34*, 181–186.
152. F. Hegler, C. Schmidt, H. Schwarz, A. Kappler, *FEMS Microbiol. Ecol.* **2010**, *74*, 592–600.

153. L. Pereira, I. H. Saraiva, A. S. F. Oliveira, C. M. Soares, R. O. Louro, C. Frazão. *Biochim. Biophys. Acta* **2017**, *1858*, 847–853.
154. S. Heising, B. Schink, *Microbiology* **1998**, *144*, 2263–2269.
155. C. R. Myers, K. H. Nealson, *Geochim. Cosmochim. Acta* **1988**, *52*, 2727–2732.
156. D. R. Lovley, E. J. P. Phillips, *Appl. Environ. Microbiol.* **1989**, *55*, 3234–3236.
157. D. R. Lovley, E. J. P. Phillips, *Appl. Environ. Microbiol.* **1986**, *51*, 683–689.
158. S. Kato, K. Hashimoto, K. Watanabe, *Environ. Microbiol.* **2012**, *14*, 1646–1654.
159. D. R. Lovley, E. J. Phillips, *Appl. Environ. Microbiol.* **1988**, *54*, 1472–1480.
160. E. J. Beal, C. H. House, V. J. Orphan, *Science* **2009**, *325*, 184–187.
161. D. R. Lovley, E. J. Phillips, D. J. Lonergan, *Appl. Environ. Microbiol.* **1989**, *55*, 700–706.
162. S. Huang, P. R. Jaffé, *PloS one.* **2018**, *13*, e0194007.
163. C. M. Corbett, W. J. Ingledew, *FEMS Microbiol. Lett.* **1987**, *41*, 1–6.
164. J. Kucera, P. Bouchal, H. Cerna, D. Potesil, O. Janiczek, Z. Zdrahal, M. Mandl, *Antonie van Leeuwenhoek* **2012**, *101*, 561–573.
165. A.-E. Rotaru, P. M. Shrestha, F. Liu, B. Markovaite, S. Chen, K. P. Nevin, D. R. Lovley, *Appl. Environ. Microbiol.* **2014**, *80*, 4599–4605.
166. F. Liu, A.-E. Rotaru, P. M. Shrestha, N. S. Malvankar, K. P. Nevin, D. R. Lovley, *Energy Environ. Sci.* **2012**, *5*, 8982–8989.
167. S. Chen, A. E. Rotaru, F. Liu, J. Philips, T. L. Woodard, K. P. Nevin, D. R. Lovley, *Bioresour. Technol.* **2014**, *173*, 82–86.
168. K. L. Straub, M. Hanzlik, B. E. E. Buchholz-Cleven, *Sys. Appl. Microbiol.* **1998**, *21*, 442–449.
169. C. Cai, A. O. Leu, G. J. Xie, J. Guo, Y. Feng, J. X. Zhao, G. W. Tyson, Z. Yuan, S. Hu, *ISME J.* **2018**, *12*, 1929–1939.
170. O. A. Podosokorskaya, V. V. Kadnikov, S. N. Gavrilov, A. V. Mardanov, A. Y. Merkel, O. V. Karnachuk, N. V. Ravin, E. A. Bonch-Osmolovskaya, I. V. Kublanov. *Environ. Microbiol.* **2013**, *15*, 1759–1771.
171. T. Iino, K. Mori, Y. Uchino, T. Nakagawa, S. Harayama, K. Suzuki. *Int. J. Syst. Evol. Microbiol.* **2010**, *60*, 1376–1382.
172. N. Stern, J. Mejia, S. He, Y. Yang, M. Ginder-Vogel, E. E. Roden, *Environ. Sci. Technol.* **2018**, *52*, 5691–5699.
173. D. Adhikari, Q. Zhao, K. Das, J. Mejia, R. Huang, X. Wang, S. R. Poulson, Y. Tang, E. E. Roden, Y. Yang, *Geochim. Cosmochim. Acta* **2017**, *212*, 221–233.
174. Q. Zhao, D. Adhikari, R. Huang, A. Patel, X. Wang, Y. Tang, D. Obrist, E. E. Roden, Y. Yang, *Chem. Geol.* **2017**, *464*, 118–126.
175. J. Clement, J. Shrestha, J. Ehrenfeld, P. Jaffe, *Soil Biol. Biochem.* **2005**, *37*, 2323–2328.
176. J. Shrestha, J. J. Rich, J. G. Ehrenfeld, P. R. Jaffe, *Soil Sci.* **2009**, *174*, 156–164.
177. W. H. Yang, K. A. Weber, W. L. Silver. *Nature Geosci.* **2012**, *5*, 538–541.
178. S. Huang, P. R. Jaffé, *Biogeosciences* **2015**, *12*, 769–779.
179. S. Huang, C. Chen, X. Peng, P. R. Jaffé, *Soil Biol. Biochem.* **2016**, *98*, 148–158.
180. L. J. Ding, X. L. An, S. Li, G. L. Zhang, Y. G. Zhu, *Environ. Sci. Technol.* **2014**, *48*, 10641–10647.
181. M. Egger, O. Rasigraf, C. J. Sapart, T. Jilbert, M. S. M. Jetten, T. Röckmann, C. van der Veen, N. Bândă, B. Kartal, K. F. Ettwig, C. P. Slomp, *Environ. Sci. Technol.* **2015**, *49*, 277–283.
182. Z. M. Summers, H. E. Fogarty, C. Leang, A. E. Franks, N. S. Malvankar, D. R. Lovley, *Science* **2010**, *330*, 1413–1415.
183. O. Sivan, M. Adler, A. Pearson, F. Gelman, I. Bar-Or, S. G. John, W. Eckert, *Limnology and Oceanography* **2011**, *56*, 1536–1544.

184. S. A. Crowe, S. Katsev, K. Leslie, A. Sturm, C. Magen, S. Nomosatryo, M. A. Pack, J. D. Kessler, W. S. Reeburgh, J. A. Roberts, L. González, G. Douglas Haffner, A. Mucci, B. Sundby, D. A. Fowle, *Geobiology* **2011**, *9*, 61–78.
185. H. Osorio, S. Mangold, Y. Denis, M. Esparza, D. B. Johnson, V. Bonnefoy, M. Dopson, D. S. Holmes, *Appl. Environ. Microbiol.* **2013**, *79*, 2172–2181.
186. D. B. Johnson, T. Kanao, S. Hedrich, *Front. Microbiol.* **2012**, *3*, 96.
187. T. D. Brock, J. Gustafson, *Appl. Environ. Microbiol.* **1976**, *32*, 567–571.
188. H. B. Gray, J. R. Winkler, *Chem. Phys. Lett.* **2009**, *483*, 1–9.
189. L. P. Nielsen, N. Risgaard-Petersen, H. Fossing, P. B. Christensen, M. Sayama, *Nature* **2010**, *463*, 1071–1074.
190. D. P. Lies, M. E. Hernandez, A. Kappler, R. E. Mielke, J. A. Gralnick, D. K. Newman, *Appl. Environ. Microbiol.* **2005**, *71*, 4414–4426.
191. L. Shi, K. M. Rosso, T. A. Clarke, D. J. Richardson, J. M. Zachara, J. K. Fredrickson, *Front. Microbiol.* **2012**, *3*, 50.
192. M. E. Hernandez, D. K. Newman, *Cell. Mol. Life Sci.* **2001**, *58*, 1562–1571.
193. K. M. Rosso, J. M. Zachara, J. K. Fredrickson, Y. A. Gorby, S. C. Smith, *Geochim. Cosmochim. Acta* **2003**, *67*, 1081–1087.
194. D. R. Lovley, J. D. Coates, E. L. Blunt-Harris, E. J. P. Phillips, J. C. Woodward, *Nature* **1996**, *382*, 445–448.
195. E. E. Roden, A. Kappler, I. Bauer, J. Jiang, A. Paul, R. Stoesser, H. Konishi, H. Xu, *Nature Geoscience* **2010**, *3*, 417–421.
196. J. Jiang, A. Kappler, *Environ. Sci. Technol.* **2008**, *42*, 3563–3569.
197. A. Kappler, M. Benz, B. Schink, A. Brune, *FEMS Microbiol. Ecol.* **2004**, *47*, 85–92.
198. J. D. Coates, D. J. Ellis, E. L. Blunt-Harris, C. V. Gaw, E. E. Roden, D. R. Lovley, *Appl. Environ. Microbiol.* **1998**, *64*, 1504–1509.
199. D. T. Scott, D. M. McKnight, E. L. Blunt-Harris, S. E. Kolesar, D. R. Lovley, *Environ. Sci. Technol.* **1998**, *32*, 2984–2989.
200. K. P. Nevin, D. R. Lovley, *Environ. Sci. Technol.* **2000**, *34*, 2472–2478.
201. A. Kappler, M. L. Wuestner, A. Ruecker, J. Harter, M. Halama, S. Behrens, *Environ. Sci. Technol. Lett.* **2014**, *1*, 339–344.
202. M. Vargas, K. Kashefi, E. L. Blunt-Harris, D. R. Lovley, *Nature* **1998**, *395*, 65.
203. K. Kashefi, D. R. Lovley, *Science* **2003**, *301*, 934.
204. K. Kashefi, D. R. Lovley, *Appl. Environ. Microbiol.* **2000**, *66*, 1050–1056.
205. J. M. Tor, D. R. Lovley, *Environ. Microbiol.* **2001**, *3*, 281–287.
206. M. Benz, B. Schink, A. Brune, *Appl. Environ. Microbiol.* **1998**, *64*, 4507–4512.
207. F. J. Cervantes, F. A. M. D. Bok, T. Duong-Dac, A. J. M. Stams, G. Lettinga, J. A. Field, *Environ. Microbiol.* **2002**, *4*, 51–57.
208. A. Piepenbrock, S. Behrens, A. Kappler, *Geomicrobiology J.* **2014**, *31*, 917–928.
209. G. Reguera, K. D. McCarthy, T. Mehta, J. S. Nicoll, M. T. Tuominen, D. R. Lovley, *Nature* **2005**, *435*, 1098–1101.
210. Y. A. Gorby, S. Yanina, J. S. McLean, K. M. Rosso, D. Moyles, A. Dohnalkova, T. J. Beveridge, I. S. Chang, B. H. Kim, K. S. Kim, *Proc. Natl. Acad. Sci. USA* **2006**, *103*, 11358–11363.
211. N. S. Malvankar, M. Vargas, K. P. Nevin, A. E. Franks, C. Leang, B. C. Kim, K. Inoue, T. Mester, S. F. Covalla, J. P. Johnson, V. M. Rotello, M. T. Tuominen, D. R. Lovley, *Nature Nanotechnol.* **2011**, *6*, 573–579.
212. M. O. Yee, O. L. Snoeyenbos-West, B. Thamdrup, L. D. M. Ottosen, A.-E. Rotaru, *Front. Energy Res.* **2019**, *7*, 29.
213. L. Shi, T. C. Squier, J. M. Zachara, J. K. Fredrickson, *Mol. Microbiol.* **2007**, *65*, 12–20.
214. J. F. Heidelberg, I. T. Paulsen, K. E. Nelson, E. J. Gaidos, W. C. Nelson, T. D. Read, J. A. Eisen, R. Seshadri, N. Ward, B. Methe, R. A. Clayton, T. Meyer, A. Tsapin, J.

Scott, M. Beanan, L. Brinkac, S. Daugherty, R. T. DeBoy, R. J. Dodson, A. S. Durkin, D. H. Haft, J. F. Kolonay, R. Madupu, J. D. Peterson, L. A. Umayam, O. White, A. M. Wolf, J. Vamathevan, J. Weidman, M. Impraim, K. Lee, K. Berry, C. Lee, J. Mueller, H. Khouri, J. Gill, T. R. Utterback, L. A. McDonald, T. V. Feldblyum, H. O. Smith, J. C. Venter, K. H. Nealson, C. M. Fraser, *Nature Biotechnol.* **2002**, *20*, 1118–1123.

215. B. A. Methé, K. E. Nelson, J. A. Eisen, I. T. Paulsen, W. Nelson, J. F. Heidelberg, D. Wu, M. Wu, N. Ward, M. J. Beanan, R. J. Dodson, R. Madupu, L. M. Brinkac, S. C. Daugherty, R. T. DeBoy, A. S. Durkin, M. Gwinn, J. F. Kolonay, S. A. Sullivan, D. H. Haft, J. Selengut, T. M. Davidsen, N. Zafar, O. White, B. Tran, C. Romero, H. A. Forberger, J. Weidman, H. Khouri, T. V. Feldblyum, T. R. Utterback, S. E. V. Aken, D. R. Lovley, C. M. Fraser, *Science* **2003**, *302*, 1967–1969.
216. L. Shi, D. J. Richardson, Z. Wang, S. N. Kerisit, K. M. Rosso, J. M. Zachara, J. K. Fredrickson, *Environ. Microbiol. Rep.* **2009**, *1*, 220–227.
217. G. F. White, Z. Shi, L. Shi, Z. Wang, A. C. Dohnalkova, M. J. Marshall, J. K. Fredrickson, J. M. Zachara, J. N. Butt, D. J. Richardson, T. A. Clarke, *Proc. Natl. Acad. Sci. USA* **2013**, *110*, 6346–6351.
218. B. Schuetz, M. Schicklberger, J. Kuermann, A. M. Spormann, J. Gescher, *Appl. Environ. Microbiol.* **2009**, *75*, 7789–7796.
219. Y. Liu, Z. Wang, J. Liu, C. Levar, M. J. Edwards, J. T. Babauta, D. W. Kennedy, Z. Shi, H. Beyenal, D. R. Bond, T. A. Clarke, J. N. Butt, D. J. Richardson, K. M. Rosso, J. M. Zachara, J. K. Fredrickson, L. Shi, *Environ. Microbiol. Rep.* **2014**, *6*, 776–785.
220. L. Shi, J. K. Fredrickson, J. M. Zachara, *Front. Microbiol.* **2014**, *5*, 657.
221. D. R. Lovley, J. F. Stolz, G. L. Nord, Jr., E. J. P. Phillips, *Nature* **1987**, *330*, 252–254.
222. D. R. Lovley, T. Ueki, T. Zhang, N. S. Malvankar, P. M. Shrestha, K. A. Flanagan, M. Aklujkar, J. E. Butler, L. Giloteaux, A. E. Rotaru, D. E. Holmes, A. E. Franks, R. Orellana, C. Risso, K. P. Nevin, *Adv. Microb. Physiol.* **2011**, *59*, 1–100.
223. C. O. Obuekwe, D. W. S. Westlake, F. D. Cook, *Can. J. Microbiol.* **1981**, *27*, 692–697.
224. C. R. Myers, K. H. Nealson, *Science* **1988**, *240*, 1319–1321.
225. C. R. Myers, K. H. Nealson, *J. Bacteriol.* **1990**, *172*, 6232–6238.
226. J. K. Fredrickson, M. F. Romine, A. S. Beliaev, J. M. Auchtung, M. E. Driscoll, T. S. Gardner, K. H. Nealson, A. L. Osterman, G. Pinchuk, J. L. Reed, D. A. Rodionov, J. L. Rodrigues, D. A. Saffarini, M. H. Serres, A. M. Spormann, I. B. Zhulin, J. M. Tiedje. *Nature Rev. Microbiol.* **2008**, *6*, 592–603.
227. C. V. Ramana, C. Sasikala, *J. Gen. Appl. Microbiol.* **2009**, *55*, 301–304.
228. J. D. Coates, D. J. Ellis, C. V. Gaw, D. R. Lovley, *Int. J. Sys. Evol. Microbiol.* **1999**, *49*, 1615–1622.
229. K. Kashefi, D. E. Holmes, A.-L. Reysenbach, D. R. Lovley, *Appl. Environ. Microbiol.* **2002**, *68*, 1735–1742.
230. K. Kashefi, D. E. Holmes, J. A. Baross, D. R. Lovley, *Appl. Environ. Microbiol.* **2003**, *69*, 2985–2993.
231. Y. Roh, S. V. Liu, G. Li, H. Huang, T. J. Phelps, J. Zhou, *Appl. Environ. Microbiol.* **2002**, *68*, 6013–6020.
232. J. P. Bowman, S. A. McCammon, D. S. Nichols, J. H. Skerratt, S. M. Rea, P. D. Nichols, T. A. McMeekin, *Int. J. Sys. Evol. Microbiol.* **1997**, *47*, 1040–1047.
233. K. Küsel, T. Dorsch, G. Acker, E. Stackebrandt, *Appl. Environ. Microbiol.* **1999**, *65*, 3633–3640.
234. Q. Ye, Y. Roh, S. L. Carroll, B. Blair, J. Zhou, C. L. Zhang, M. W. Fields, *Appl. Environ. Microbiol.* **2004**, *70*, 5595–5602.
235. V. Gorlenko, A. Tsapin, Z. Namsaraev, T. Teal, T. Tourova, D. Engler, R. Mielke, K. Nealson, *Int. J. Syst. Evol. Microbiol.* **2004**, *54*, 739–743.
236. C. Kato, Y. Nogi, *FEMS Microbiol. Ecol.* **2001**, *35*, 223–230.
237. F. M. Lauro, D. H. Bartlett, *Extremophiles* **2008**, *12*, 15–25.

238. F. Caccavo, R. P. Blakemore, D. R. Lovley, *Appl. Environ. Microbiol.* **1992**, *58*, 3211–3216.
239. J. M. Zachara, J. K. Fredrickson, S.-M. Li, D. W. Kennedy, S. C. Smith, P. L. Gassman, *Am. Mineral.* **1998**, *83*, 1426–1443.
240. H. von Canstein, J. Ogawa, S. Shimizu, J. R. Lloyd, *Appl. Environ. Microbiol.* **2008**, *74*, 615–623.
241. E. Marsili, D. B. Baron, I. D. Shikhare, D. Coursolle, J. A. Gralnick, D. R. Bond, *Proc. Natl. Acad. Sci. USA* **2008**, *105*, 3968–3973.
242. D. Coursolle, D. B. Baron, D. R. Bond, J. A. Gralnick, *J. Bacteriol.* **2010**, *192*, 467–474.
243. N. J. Kotloski, J. A. Gralnick, *mBio* **2013**, *4*, e00553–12.
244. Z. Shi, J. M. Zachara, Z. Wang, L. Shi, J. K. Fredrickson, *Geochim. Cosmochim. Acta.* **2013**, *121*, 139–154.
245. Z. Shi, J. M. Zachara, L. Shi, Z. Wang, D. A. Moore, D. W. Kennedy, J. K. Fredrickson, *Environ. Sci. Technol.* **2012**, *46*, 11644–11652.
246. A. S. Beliaev, D. A. Saffarini, J. L. McLaughlin, D. Hunnicutt, *Mol. Microbiol.* **2001**, *39*, 722–730.
247. J. M. Myers, C. R. Myers, *J. Bacteriol.* **2000**, *182*, 67–75.
248. C. R. Myers, J. M. Myers, *Appl. Environ. Microbiol.* **2002**, *68*, 5585–5594.
249. G. Sturm, K. Richter, A. Doetsch, H. Heide, R. O. Louro, J. Gescher, *ISME J.* **2015**, *9*, 1802–1811.
250. D. R. Lovley, M. J. Baedecker, D. J. Lonergan, I. M. Cozzarelli, E. J. P. Phillips, D. I. Siegel, *Nature* **1989**, *339*, 297–300.
251. D. R. Lovley, D. J. Lonergan, *Appl. Environ. Microbiol.* **1990**, *56*, 1858–1864.
252. D. R. Lovley, *Annu. Rev. Microbiol.* **1993**, *47*, 263–290.
253. X. Qian, T. Mester, L. Morgado, T. Arakawa, M. L. Sharma, K. Inoue, C. Joseph, C. A. Salgueiro, M. J. Maroney, D. R. Lovley, *Biochim. Biophys. Acta* **2011**, *1807*, 404–412.
254. C. Leang, M. V. Coppi, D. R. Lovley, *J. Bacteriol.* **2003**, *185*, 2096–2103.
255. E. Afkar, G. Reguera, M. Schiffer, D. R. Lovley, *BMC Microbiol.* **2005**, *5*, 41; https://doi.org/10.1186/1471-2180-5-41.
256. C. E. Levar, C. H. Chan, M. G. Mehta-Kolte, D. R. Bond, *mBio* **2014**, *5*, e02034.
257. L. Zacharoff, C. H. Chan, D. R. Bond, *Bioelectrochemistry* **2016**, *107*, 7–13.
258. J. R. Lloyd, *FEMS Microbiol. Rev.* **2003**, *27*, 411–425.
259. L. Morgado, M. Bruix, M. Pessanha, Y. Y. Londer & C. A. Salgueiro. *Biophys. J.* **2010**, *99*, 293–301.
260. X. Qian, G. Reguera, T. Ã. Mester, D. R. Lovley, *FEMS Microbiol. Lett.* **2007**, *277*, 21–27.
261. K. Lalonde, A. Mucci, A. Ouellet, Y. Gélinas, *Nature* **2012**, *483*, 198–200.
262. T. Borch, R. Kretzschmar, A. Kappler, P. V. Cappellen, M. Ginder-Vogel, A. Voegelin, K. Campbell, *Environ. Sci. Technol.* **2010**, *44*, 15–23.
263. E. M. Muehe, A. Kappler, *Environ. Chem.* **2014**, *11*, 483–495.
264. Y. G. Zhu, X. M. Xue, A. Kappler, B. P. Rosen, A. A. Meharg, *Environ. Sci. Technol.* **2017**, *51*, 7326–7339.
265. C. Hohmann, E. Winkler, G. Morin, A. Kappler, *Environ. Sci. Technol.* **2010**, *44*, 94–101.
266. E. O. Omoregie, R. M. Couture, P. Van Cappellen, C. L. Corkhill, J. M. Charnock, D. A. Polya, D. Vaughan, K. Vanbroekhoven, J. R. Lloyd, *Appl. Environ. Microbiol.* **2013**, *79*, 4325–4335.
267. K. S. Nitzsche, V. M. Lan, P. T. Trang, P. H. Viet, M. Berg, A. Voegelin, B. Planer–Friedrich, J. Zahoransky, S. K. Müller, J. M. Byrne, C. Schröder, S. Behrens, A. Kappler, *Sci. Total Environ.* **2015**, *502*, 526–536.

268. D. R. Lovley, E. J. P. Phillips, Y. A. Gorby, E. R. Landa, *Nature* **1991**, *350*, 413–416.
269. R. T. Anderson, H. A. Vrionis, I. Ortiz-Bernad, C. T. Resch, P. E. Long, R. Dayvault, K. Karp, S. Marutzky, D. R. Metzler, A. Peacock, D. C. White, M. Lowe, D. R. Lovley, *Appl. Environ. Microbiol.* **2003**, *69*, 5884–5891.
270. T. Zhang, P.-L. Tremblay, A. K. Chaurasia, J. A. Smith, T. S. Bain, D. R. Lovley, *Appl. Environ. Microbiol.* **2013**, *79*, 7800–7806.
271. T. Zhang, T. S. Bain, K. P. Nevin, M. A. Barlett, D. R. Lovley, *Appl. Environ. Microbiol.* **2012**, *78*, 8304–8310.
272. R. T. Anderson, J. N. Rooney-Varga, C. V. Gaw, D. R. Lovley, *Environ. Sci. Technol.* **1998**, *32*, 1222–1229.
273. D. R. Bond, D. R. Lovley, *Appl. Environ. Microbiol.* **2003**, *69*, 1548–1555.
274. J. D. Coates, R. T. Anderson, D. R. Lovley, *Appl. Environ. Microbiol.* **1996**, *62*, 1099–1101.
275. J. D. Coates, R. T. Anderson, J. C. Woodward, E. J. P. Phillips, D. R. Lovley, *Environ. Sci. Technol.* **1996**, *30*, 2784–2789.
276. F. Aulenta, S. Rossetti, S. Amalfitano, M. Majone, V. Tandoi, *ChemSusChem* **2013**, *6*, 433–436.
277. R. T. Amos, B. A. Bekins, I. M. Cozzarelli, M. A. Voytek, J. D. Kirshtein, E. J. Jones, D. W. Blowes, *Geobiology* **2012**, *10*, 506–517.
278. J. G. Lack, S. K. Chaudhuri, R. Chakraborty, L. A. Achenbach, J. D. Coates, *Microb. Ecol.* **2002**, *43*, 424–431.
279. D. B. Senn, H. F. Hemond, *Science* **2002**, *296*, 2373–2376.
280. K. T. Finneran, M. E. Housewright, D. R. Lovley, *Environment. Microbiol.* **2002**, *4*, 510–516.
281. J. R. Lloyd, V. A. Sole, C. V. G. Van Praagh, D. R. Lovley, *Appl. Environ. Microbiol.* **2000**, *66*, 3743–3749.
282. D. R. Brookshaw, V. S. Coker, J. R. Lloyd, D. J. Vaughan, R. A. D. Pattrick, *Environ. Sci. Technol.* **2014**, *48*, 11337–11342.
283. R. S. Cutting, V. S. Coker, N. D. Telling, R. L. Kimber, C. I. Pearce, B. L. Ellis, R. S. Lawson, G. van der Laan, R. A. Pattrick, D. J. Vaughan, E. Arenholz, J. R. Lloyd, *Environ. Sci. Technol.* **2010**, *44*, 2577–2584.
284. D. E. Crean, V. S. Coker, G. van der Laan, J. R. Lloyd, *Environ. Sci. Technol.* **2012**, *46*, 3352–3359.
285. S. K. Chaudhuri, J. G. Lack, J. D. Coates, *Appl. Environ. Microbiol.* **2001**, *67*, 2844–2848.
286. J. G. Lack, S. K. Chaudhuri, S. D. Kelly, K. M. Kemner, S. M. O'Connor, J. D. Coates, *Appl. Environ. Microbiol.* **2002**, *68*, 2704–2710.
287. G. W. Zhou, X. R. Yang, H. Li, C. W. Marshall, B. X. Zheng, Y. Yan, J. Q. Su, Y. G. Zhu, *Environ. Sci. Technol.* **2016**, *50*, 9298–9307.
288. S. Hedrich, D. B. Johnson, *Int. J. Syst. Evol. Microbiol.* **2013**, *63*, 4018–4025.
289. H. Huber, K. O. Stetter, *Arch. Microbiol.* **1989**, *151*, 479–485.
290. G. E. Markosyan, *Biol. Zh. Armenii.* **1972**, *25*, 26–29.
291. F. Walsh, R. Mitchell, *J. Gen. Microbiol.* **1972**, *72*, 369–372.
292. B. D. Johnson, F. F. Roberto, *Heterotrophic Acidophiles and Their Roles in the Bioleaching of Sulfide Minerals,* in *Biomining: Theory, Microbes and Industrial Processes*, Ed. D. E. Rawlings, Springer-Verlag, Berlin, 1997, pp. 259–279.
293. D. B. Johnson, K. B. Hallberg, S. Hedrich, *Appl. Environ. Microbiol.* **2014**, *80*, 672–680.
294. R. S. Golovacheva, G. I. Karavaiko, *Mikrobiologiia* **1978**, *47*, 815–822.
295. P. R. Norris, D. W. Barr, D. Hinson, "Iron and Mineral Oxidation by Acidophilic Bacteria: Affinities for Iron and Attachment to Pyrite", *Biohydrometall., Proc. Int. Symp.,* 1988.

296. P. R. Norris, D. A. Clark, J. P. Owen, S. Waterhouse, *Microbiology* **1996**, *142*, 775–783.
297. P. R. Norris, *Thermophiles and Bioleaching*, in *Biomining: Theory, Microbes and Industrial Processes*, Ed. D. E. Rawlings, Springer, Berlin, 1997, pp 247–258.
298. D. A. Clark, P. R. Norris, *Microbiology* **1996**, *142*, 785–790.
299. K. B. Hallberg, S. Hedrich, D. B. Johnson, *Extremophiles* **2011**, *15*, 271–279.
300. O. V. Golyshina, T. A. Pivovarova, G. I. Karavaiko, T. F. Kondrat'eva, E. R. B. Moore, W.-R. Abraham, H. Lünsdorf, K. N. Timmis, M. M. Yakimov, P. N. Golyshin, *Int. J. Sys. Evol. Microbiol.* **2000**, *50*, 997–1006.
301. W. W. Barker, S. A. Welch, J. F. Banfield, *Am. Mineral.* **1998**, *83*, 1551–1563.
302. H. Zhou, R. Zhang, P. Hu, W. Zeng, Y. Xie, C. Wu, G. Qiu, *J. Appl. Microbiol.* **2008**, *105*, 591–601.
303. A. Segerer, A. Neuner, J. K. Kristjansson, K. O. Stetter, *Int. J. Sys. Bacteriol.* **1986**, *36*, 559–564.
304. T. D. Brock, K. M. Brock, R. T. Belly, R. L. Weiss, *Arch. Mikrobiol.* **1972**, *84*, 54–68.
305. E. Singer, D. Emerson, E. A. Webb, R. A. Barco, J. G. Kuenen, W. C. Nelson, C. S. Chan, L. R. Comolli, S. Ferriera, J. Johnson, J. F. Heidelberg, K. J. Edwards, *PLoS One* **2011**, *6*, e25386.
306. E. K. Field, A. Sczyrba, A. E. Lyman, C. C. Harris, T. Woyke, R. Stepanauskas, D. Emerson, *ISME J.* **2014**, *9*, 857–870.
307. Y. Jiao, A. Kappler, L. R. Croal, D. K. Newman, *Appl. Environ. Microbiol.* **2005**, *71*, 4487–4496.
308. R. Arredondo, A. Garcia, C. A. Jerez, *Appl. Environ. Microbiol.* **1994**, *60*, 2846–2851.
309. L. J. Bird, V. Bonnefoy, D. K. Newman, *Trends Microbiol.* **2011**, *19*, 330–340.

8

Extracellular Redox Chemistry

Inês B. Trindade, Catarina M. Paquete, and Ricardo O. Louro

Instituto de Tecnologia Química e Biológica António Xavier,
Av da República (EAN), PT-2780-157 Oeiras, Portugal
<ines.trindade@itqb.unl.pt>
<cpaquete@itqb.unl.pt>
<louro@itqb.unl.pt>

Metal Ions in Life Sciences, Volume 21 Guest Editors: Peter M. H. Kroneck and Martha E. Sosa Torres
Series Editors: Astrid Sigel, Eva Freisinger, and Roland K. O. Sigel

https://doi.org/10.1515/9783110589771-008

Abstract: Metals are essential for life and the so-called transition metals undergo redox transformations on a biologically accessible potential range. These transformations have an impact in their mobility in aqueous medium, their bioavailability, their toxicity, and their affinity for biological macromolecules. Extracellular redox chemistry is therefore an essential process for the interaction between living organisms and metals. In this chapter we present a survey of the current state of the art with respect to the molecular mechanisms of microbial assimilatory metal uptake with an emphasis for iron. Direct metal uptake by membrane transporters and indirect metal uptake by metallophores are presented. The molecular mechanisms of dissimilatory metal reduction with emphasis for iron and manganese reducers are also described. The modes of extracellular electron transfer are presented in general and then exemplified with the molecular mechanisms known for Gram-negative and Gram-positive bacteria. The implications of the extracellular redox chemistry of microorganisms for the environment, health, and biotechnology are discussed at the end of the chapter and these are framed in the context of the open questions that guide future research directions and reveal new possibilities for diverse applications.

Keywords: cytochromes · dissimilatory metal reducing organisms · extracellular electron transfer · iron · metal ions · metal uptake · siderophores

1. INTRODUCTION

Metal ions play an essential role in metabolic processes, and life as we know it, would not exist without their contribution [1]. The natural selection operating at the level of these chemical elements has made their contribution to the metabolism and structure of living organisms a function of their physicochemical properties, both in terms of the kinetic and thermodynamic aspects of their reactivity [2]. Metal ions are unique among nutrients because they cannot be synthesized or degraded (by metabolic processes). For this reason, bioavailability acts as a selective pressure for the evolution of more efficient capture or disposal of molecular mechanisms. For example, aluminum is highly abundant on the Earth surface, particularly in acidic conditions, but it is not used by living organisms. Its rates of ligand exchange are extremely slow and incompatible with metabolic processes, where it interferes with calcium and magnesium metabolism. This led to the evolution of efficient efflux pumps that transport aluminum out of the cells. As a counter example, iron precipitated out of the water column as banded iron formations (BIFS) caused by the action of photoferrotrophs in the Archaean oceans, and later during the Great Oxidation Event (GOE) caused by the action of water-splitting cyanobacteria (see Chapters 1 and 7) [3]. Nonetheless, despite its low bioavailability, iron still remains an essential element for all organisms with exception of a few rare examples, and organisms go to great lengths to ensure sufficient access to meet their needs (see Chapter 7) [4, 5]. The bioavailability of metal ions is ultimately determined by their affinity for ligands as defined by the Irving-Williams series [$Cu^{2+} > Zn^{2+} > Ni^{2+} > Co^{2+} > Fe^{2+} > Mn^{2+} > Mg^{2+} > Ca^{2+}$] and by the nature of the ligands available in the environ-

ment or biosynthesized by the cells [6]. Given that bioavailability does not necessarily match the metabolic or structural need for metal ions, or on the contrary it can exceed toxic levels, organisms evolved molecular mechanisms that ensure the homeostasis of these elements [7]. Metal homeostasis is ensured by the transport in or out of the cell under the action of metal regulatory systems. These systems can be proteins or riboswitches (conserved untranslated regions of RNA) that bind the metals or their cofactors, and also bind DNA, thus controlling the expression level of genes related to transport and chelation [8]. Adaptation is the key survival strategy that governs life. In microorganisms, in addition to the transport systems, the regulation of lifestyle with transition between planktonic and sessile growth with biofilm formation also impacts on the toxicity of metal ions or is impacted by their presence [9]. On the one hand, quorum sensing among bacteria is disturbed by metal ions and metal nanoparticles leading to destabilization of some biofilms, whereas on the other hand, the retention of toxic metal ions in the extracellular polymeric matrix of biofilms allows cells to survive concentrations that would be toxic to planktonic cells [10]. In this balancing act of need and avoidance, organisms have evolved ingenious molecular systems for the safe collection of the necessary amounts of metal ions from their environment at the right time. This chapter focuses on assimilatory metal uptake and dissimilatory metal reduction.

2. ASSIMILATORY REDOX CHEMISTRY: SCAVENGING FOR METALS

Metal ions such as iron, copper, zinc, and manganese serve diverse vital roles mostly as cofactors of proteins. It is estimated that about 30 to 45 % of enzymes are metalloproteins, with metals being either redox-inert or redox-active [11, 12]. Redox-inert metal ions often bind transiently and either act as substrate activators or as stabilizers of negative charges given their Lewis acid properties. The most abundant examples of the latter are magnesium, zinc, and calcium [13–16]. Redox-active metal ions usually bind strongly to the protein and can act as Lewis acid stabilizers or as the redox centers of a protein. The most common examples of the latter are iron, manganese, cobalt, molybdenum, copper, and nickel [17–19]. Given that often the availability of metals does not match the metabolic needs, all organisms need to scavenge metals from their environment, whether this includes the tug-of-war for iron inside a host, or fighting the odds of metal deprivation in the marine environment (Table 1) [11, 20–22].

2.1. Redox-Inert Metals: Magnesium, Calcium, and Zinc

Magnesium (Mg) plays a central role for life acting as the counter ion for the key biological molecules including the energy-rich ATP and information-encoding DNA and RNA molecules. This metal is stable at the 2+ state and is highly soluble and abundant both inside the cell and in the environment (Table 1) [23]. Magnesium homeostasis is achieved by Mg^{2+} transporters and by Mg^{2+}-

Table 1. Essential metals, properties and bioavailability.

Metal	Common oxidation states	Ionic Radius (Å)*	Redox	Concentration in cells (M)	Concentration in oceans (M)
Mg	+2	0.57–0.89	No	10^{-3}	5×10^{-2}
Ca	+2	1.00–1.34	No	10^{-7}	10^{-2}
Zn	+2	0.60–0.90	No	10^{-11}	10^{-8}
Fe	+2	0.61–0.92	Yes	10^{-7}	10^{-17}
	+3	0.49–0.78			
Cu	+1	0.46–0.77	Yes	10^{-15}	10^{-9}
	+2	0.57–0.73			
Mn	+2	0.66–0.96	Yes	10^{-7}	10^{-9}
	+3	0.58			
Co	+2	0.56–0.90	Yes	10^{-8}	10^{-11}
	+3	0.55			
Mo	+3	0.69	Yes	10^{-6}	10^{-7}
	+4	0.65			
	+6	0.41–0.73			
Ni	+1		Yes		10^{-9}
	+2	0.49–0.69			
	+3	0.56			

Data compiled from [11, 291, 292]. *Ranges for the most common coordination numbers.

responsive signal transduction systems. This way, bacteria have the means to evaluate the levels of Mg^{2+} in their surroundings (extracellularly and in the cytoplasm) and have the means to mount a biochemical response that enables the maintenance of Mg^{2+} levels by increasing or decreasing different Mg^{2+} transporters [24]. Three distinct classes of Mg^{2+} transporters were identified: CorA, MgtE, and MgtA [25–27]. They differ in energy requirements, ability to import and export Mg^{2+}, in the conditions under which they are expressed, and in the environmental cues required for their activation. Most of these transporters function as channels with a pore structure and utilize the electrochemical gradient across the cytoplasmic membrane to transport their substrates [24].

Calcium (Ca) is often compared to magnesium given the similarity in abundance, charge, and preference for hard donors such as oxygen. However, calcium is used much less frequently than magnesium and this is most likely due to the larger size of Ca^{2+} (Table 1) [11, 28]. By contrast, the increased size of the Ca^{2+} cation makes it more suitable for binding numerous of ligands in an irregular geometry enabling it to be particularly suitable for cell-triggering responses (see Chapter 1) [29]. For such important and sensitive role in the cells, calcium homeostasis is tightly maintained and requires an orchestrated activity of export and uptake systems along with Ca^{2+} chaperons or binding proteins [30]. The export of calcium is well studied, and it occurs via P-type ATPases and antiporters [31]. By contrast, calcium uptake systems are barely known and only a few have been identified including two Ca^{2+} channels (in *Escherichia coli* and in *Bacillus subtilis*) and one energy-dependent P-type ATPase (CtpE from *Mycobacterium smegmatis*) [32–34].

Zinc (Zn) is the second most common metal ion found in enzymes, partially because it retains the properties of magnesium. It is stable and inert at the Zn^{2+} state, but it is a stronger Lewis acid than Mg^{2+} and therefore it can bind water and form a hydroxide ion for nucleophilic attack of the substrates [11, 35]. The uptake of zinc usually occurs though high-affinity ABC (ATP-binding cassette) transporters [36]. Encoded by *znu*ABC genes, these transporters consist of ZnuA, a periplasmic-binding protein, ZnuB, a membrane permease and ZnuC, an ATPase. These transporters can also bind manganese and their specificity has been a matter of debate [36–39]. The expression *znu*ABC genes is regulated by zinc and by Zur, a Fur-family (ferric uptake regulator) repressor [40]. A second zinc-uptake system encoded by *zup*T was also identified, but its transport mechanism remains unexplored [41]. Additionally, in pathogenic bacteria, zinc can also be transported indirectly via small chelators or high affinity zinc-binding proteins termed zincophores [39, 42, 43].

2.2. Redox-Active Metals: Iron, Copper, Manganese, Cobalt, Molybdenum, and Nickel

Iron (Fe) has survived in the podium of transition elements throughout the Eras as the most crucial metal for virtually all organisms (except for members of the *Lactobacillus* genus which require little or no iron) [44–46]. Despite its abundance, iron is insoluble in aqueous solutions exposed to an oxygen-rich atmosphere, due to formation of iron oxides, and thus, microorganisms, fungi, and plants have evolved strategies to scavenge this element from different environments including, soil and marine sediments, fresh waters and living organisms (see Chapter 7) [47]. Iron can either be acquired directly in the ferrous form (Fe^{2+}) through the ferrous transport system (Feo) and via ABC-type transporters, or indirectly in the ferric form (Fe^{3+}) via siderophores and/or hemophores [48–51].

Copper (Cu) is considered the "new iron" [47]. The GOE was a catastrophic event that dramatically changed the bioavailability of elements. As the bioavailability of iron dropped, the bioavailability of cupric copper (Cu^{2+}) increased allowing its incorporation in biological systems. This gave rise to a new biochemistry which coincidently aligns with the development of multicellular organisms [52]. Thus, the copper pair Cu^{2+}/Cu^{+} became crucial for life as the redox center in multiple proteins such as cytochrome oxidase (ccb_3, aa_3, caa_3), nitrite reductase, Cu,Zn superoxide dismutase, laccase, azurin, and plastocyanin [53]. Cu^{2+} is highly toxic at very small concentrations, and thus copper levels in the cytosol are very low and tightly regulated (see Chapter 9). Most copper circulates via chaperones (proteins that bind copper), ensuring its safe transport [54]. Additionally, in Gram-negative bacteria copper-containing enzymes are either periplasmic enzymes or are embedded in the cytoplasmic membrane. This avoids the toxicity of copper, since the periplasm is a more oxidizing environment enabling the stabilization copper in the cupric form (Cu^{2+}). While the major export sys-

tems for copper have been identified, Cu^{+} uptake systems are still scarcely studied [37]. The predominant Cu^{+} transporting system involves P-type ATPases [37, 55]. These are transmembrane transporters that maintain cytoplasmic copper levels by coupling unidirectional Cu^{+} efflux to ATP hydrolysis. Based on phenotypic analysis it was suggested that some P-type ATPases can also drive Cu^{+} uptake in addition to the routine efflux function. Additionally, a few proteins have been proposed for directing Cu^{+} uptake and these include porin proteins such as OmpB from *E.coli*, and three proteins from *Pseudomonas aeruginosa*: an outermembrane protein, OprC, an inner membrane protein, PA3789, and a member of the major facilitator superfamily (MFS) PA5030 [53, 56]. Copper can also be transported indirectly via small chelators termed chalkophores [57].

Manganese (Mn) is an essential trace element for all forms of life [58]. For example, it is found in free radical detoxifying enzymes (e.g., superoxide dismutase), in the oxygen evolving complex of photosystem II (see Chapter 1), and also plays a key role for the virulence of pathogenic bacteria [37, 59]. The manganese cycle is composed by two states, Mn^{2+} and Mn^{3+}, where Mn^{2+} is the biologically relevant state. Contrary to iron, Mn^{2+} does not promote the generation of reactive oxygen species and thus it is important in diminishing oxidative stress by substituting Fe^{2+} species [59]. Manganese uptake can occur directly via specialized Mn^{2+} transporters belonging to the ABC-type protein family or via proton-dependent Nramp (natural resistance-associated macrophage proteins)-related transporters [60–62]. Additionally, manganese can be imported through the secretion of Mn^{2+}-binding proteins, also designated as "manganeseophores" by analogy to hemophores [43].

Cobalt (Co) is almost exclusively found as the redox center of B_{12}-dependent enzymes. This cofactor forms a weak Co^{3+}–C bond which can undergo heterolytic cleavage and form Co^{+} and a carbonium ion or undergo homolytic cleavage and form Co^{2+} and a carbon radical. This metal can also be found in methylmalonyl-coenzyme A epimerase as mononuclear Co^{2+} for the activation of substrates [11, 63, 64]. Uptake of Co^{2+} can occur directly using ABC-type transporters of different nature: energy-coupling factor (ECF)-transporters, nickel/cobalt transporters (NiCoT), and/or Ton-B-dependent transporters [65]. Additionally, it also has been observed that cobalt-complexing ligands (cobaltophores) may play a key role in the uptake of this metal specially in different species of cyanobacteria [22].

Molybdenum (Mo) is the only element of the second transition series with known biological importance and plays a key role by acting as the redox center of enzymes involved in the carbon, sulfur, and nitrogen cycles [66]. Molybdenum is found associated with an organic partner (pterin molecule in oxotransferases, Moco center) or integrated in an inorganic cluster when incorporated in the FeMoco cofactor of nitrogenases. It typically cycles between the Mo^{4+} and Mo^{6+} oxidation states although in nitrogenase a spin-coupled Mo^{3+} state has been proposed [67]. The uptake of molybdenum can occur directly via high-affinity ABC-type transporters or indirectly via molybdate-binding proteins, which can store up to eight anions until they can be further utilized in the cell, and/or also by molybdophores, ligands that bind molybdenum [68].

Nickel (Ni) is found in enzymes that play key roles in energy and nitrogen metabolisms (e.g., NiFe-hydrogenase, acetyl-coenzyme A synthase/decarbonylase), in detoxification processes (e.g., urease), carbon dioxide fixation (e.g., carbon monoxide dehydrogenase, methylcoenzyme M reductase), and others (e.g., Ni-superoxide dismutase, glyoxalase I). In these enzymes nickel can be found in the Ni^{+}, Ni^{2+} or Ni^{3+} states [19]. Direct uptake of nickel can occur either through ABC-type transporters or via Ni-specific permeases [65, 69].

2.2.1. Direct Metal Uptake of Redox-Active Metals

Direct uptake of the various metals uses membrane-associated complexes with common organization. In the very rare cases where extracellular metal concentrations are relatively high, passive import of metal ions across the outer membrane can occur through nonspecific porins. However, the most likely scenario is that metal ion contents are low and thus metal uptake requires energy-dependent transporters with inherent specificity [37].

2.2.1.1. ABC-Type Importers

Direct metal uptake through ABC-type transporters is well conserved throughout the bacterial domain regardless of the specificities of the metal. Transporters belonging to the ABC superfamily couple the energy released from ATP hydrolysis to the translocation of a wide variety of substances into or out of cells. ABC exporters are composed by four protein domains or subunits: two hydrophobic membrane-spanning domains (MSDs) that are presumed to constitute the translocation pathway or channel across the membrane and two hydrophilic nucleotide-binding domains (NBDs) that interact at the cytoplasmic surface to supply the energy for active transport [60, 70]. These then require the interaction with an extra-cytoplasmic solute-binding protein (SBP) which dictates the specificity of the transport. SBP can have different structures and different locations. Furthermore, their designation follows different terminologies depending on whether they originate from Gram-positive or Gram-negative bacteria. In Gram-positive bacteria SBPs were grouped as the lipoprotein receptors antigen I, a class of cell-surface receptor proteins, whereas in Gram-negative bacteria SBPs are soluble in the periplasm [71]. These proteins often have negligible sequence similarity and can transport different substrates. However, all have a highly conserved three-dimensional fold which allows their classification according to their ligand specificity. Direct metal ion uptake requires SBPs of cluster type A I whereas indirect metal ion uptake requires SBPs of cluster type A II. SBPs of the two cluster types are distinguished by the fact that cluster type A II has a larger substrate cavity allowing the extra space for the metal-binding molecules. Nonetheless, SBPs of cluster type A I and cluster type A II interact with type II ABC transporters [72]. Type II ABC transporters are larger than type I or type III. They usually import compounds that are present in the environment at very low concentrations by a mechanism that has been described as “buy now, pay later” [71]. Type II ABC transporters have very high affinity for the SBPs regard-

less of whether they are in apo (without the metal) or holo (with metal) forms. This means that SBPs are bound and perform transport constantly ("buy now"). The observation of a basal ATPase activity in this type of transporters together with the displacement of the SBP by ATP indicates that ATP hydrolysis provides the energy to release SBP from the ABC transporter ("pay later") [71]. The SBPs in cluster A I can bind Zn^{2+}, Ni^{2+}, Mn^{2+}, and Fe^{2+}, but in most cases the role and specificity *in vivo* remains unknown since the actual affinities for the different metals were not measured [62, 71]. Besides ABC-transporters, other metal-specific direct import systems have been identified, such as the Nramp Mn^{2+} transporters [62]. However, for many the mechanisms and metal specificity remain undetermined. Notwithstanding, the most explored case of direct metal uptake is the transport of iron through the Feo transport system [37].

2.2.1.2. Iron-Specific Transport: Feo, Transport of Iron(II)

In reducing (anaerobic) and low-pH environments the most stable form of iron is the soluble Fe^{2+} form. In Gram-negative bacteria Fe^{2+} is transported via the Fe(II) transport system (Feo). It is encoded by the *feo* operon that is repressed by Fur (ferric uptake regulator) in the presence of iron and is activated by FNR (fumarate and nitrate reductase transcriptional regulator) under anaerobic conditions. The *feo* operon can encode up to three proteins: FeoA, FeoB, and FeoC. FeoA is a small β-barrel protein with unusually high isoelectric point (*E. coli* FeoA has a pI of 9.4) and for this reason it has been hypothesized that FeoA may be directed into the inner leaflet of the cytoplasmic membrane interacting with the soluble domain of FeoB [73, 74]. However, this interaction remains to be observed together with the role of FeoA in iron uptake. FeoB is a transmembrane protein with three domains: a soluble G-protein domain capable of hydrolyzing GTP, a GDP dissociation inhibitor domain and a transmembrane domain which putatively is responsible for transporting ferrous iron from the periplasm to the cytoplasm [48]. This protein seems to be the most critical for ferrous iron uptake. FeoC is a small cytoplasmic protein containing a winged-helix motif and four widely conserved cysteine (CySH) residues which most likely bind iron. Even though by historical reasons this organization of three proteins is the most widely known, this organization corresponds to only 13 % of what is observed in the known bacterial genomes. Indeed, the most common organization represented in 54 % of the bacterial genomes is FeoAB and then at 11 % FeoB only [75]. There is still no structure of intact FeoB and there is still no knowledge regarding which part(s) of FeoA and/or FeoC interact(s) with the FeoB. Elucidating the site(s) where these interactions take place may contribute to unravelling how Fe^{2+} is transported inside the cell. So far, the current hypothesis is that ferrous iron diffuses freely into the periplasm through porins and then is taken by a gate motif of FeoB while the G-protein domain provides the signaling and energy for active transport into the cytoplasm. FeoA is then thought to take part in transport through interacting with FeoB and FeoC is thought to bind Fe^{2+} and act as a transcriptional regulator [48].

2.2.2. Indirect Uptake of Redox-Active Metals

2.2.2.1. Metallophores

The reactivity of metals that makes them critical for life, comes with the cost of toxicity and therefore, there are hardly any "free metals" in the cell, leading to the need of metal scavenging.

Metallophores are small molecules that bind metals. The most thoroughly studied are siderophores that evolved to selectively bind Fe^{3+} and this can be a consequence of two factors: the evolutionary pressure for iron acquisition in an oxygen-rich atmosphere, and the fact that there are not many biologically relevant metals that can outcompete Fe^{3+}, with the exception for inert Co^{3+} and Al^{3+} [11, 76]. Some siderophores such as pyochelin and ferrioxamine E can bind Co^{3+} and there is also evidence for Co-complexing ligands even though the identity of the organisms producing them and their chemical structures remain unknown [22].

As the affinity for Fe^{3+} decreases, the affinity for other metals increases and thus it is not surprising that small molecules have been found to bind other metals such as vanadium, manganese, copper, and molybdenum. Often these are not termed as siderophores, instead these are called chalkophores (specific for copper-binding) and zincophores (specific for zinc-binding). It was also observed that often metallophores play a role in detoxification in addition to the metal acquisition role [77]. Chalkophores are the best studied examples of non-iron metallophores [78]. The first chalkophore ever isolated was methanobactin from methanotrophic bacteria, which oxidize methane as their sole carbon source. Methanobactin is a chromopeptide containing a mononuclear copper center coordinated by two nitrogen atoms contained in the two oxazolone rings and two thioamide sulfur atoms [79, 80]. Methanobactin binds both Cu^{2+} and Cu^{+} but binding is reductive and at the end only Cu^{+}-methanobactin can be found. The binding constants of copper binding in methanobactins are reported to be in the range 10^{20}–10^{21} M^{-1} with different Cu^{+}:methanobactin species observed depending on stoichiometry and pH [77]. There is still much to unravel regarding the pathway of methanobactins. These compounds, unlike siderophores, are ribosomally produced and post-translationally modified natural products (RiPPs) [77]. However, the biosynthetic machinery of chalkophores appears to be unique in the RiPP class of natural products. Furthermore, methanobactin can also bind other metals in addition to copper, including: Ag^{+}, Au^{3+}, Hg^{2+}, Pb^{2+}, and U^{6+} using a reductive binding mechanism similar to that observed with Cu^{+}; and Cd^{2+}, Co^{2+}, Fe^{3+}, Ni^{2+}, and Zn^{2+}, via a different non-reductive mechanism. Measured binding constants for other metals appear to be lower than that of Cu^{+} by 10–15 orders of magnitude [80].

In comparison with chalkophores, very little is known about the role of other bacterial metallophores including zincophores, cobaltophores, and molybdophores. Some putative zincophores include coelibactin from *Streptomyces coelicolor*, pyridine-2,6-dithiocarboxylic acid, a siderophore produced by *Pseudomonas putida* that can bind Fe^{2+} with higher affinity, yersiniabactin produced by *Yersinia pestis*, and some pathogenic *E. coli* strains [78].

2.2.2.2. Siderophores: Chelating Iron

The best known mechanism of metal scavenging is through the use of siderophores (from the Greek "sidero-"meaning iron, and "-phore" meaning barrel). These are small-molecular-weight compounds (from 500 to 1500 Da) that are secreted outside the cell and present a high affinity and selectivity for Fe^{3+}. They are produced by nearly all types of microorganisms in the tree of life, but they appear to be more prevalent and are better studied in bacteria [81–83]. Even within the bacterial domain, not all are siderophore producers. Some are what is termed "cheaters", meaning they do not produce their own siderophores but are able to scavenge siderophores produced by others. In this case, the scavenged siderophores are designated as xenophores, from the Greek "xénos", meaning "alien or foreign" [84, 85]. The ability to utilize xenophores allows interspecies cooperation within a microbial community but there is also an increased competition for metal acquisition. This was likely the evolutionary pressure that gave rise to the wide range of siderophore structures with respectively different affinities. In order to have a high affinity for Fe^{3+}, negatively charged oxygens are the usual common metal donor atoms and the most common coordination geometry is octahedral. This allows six ligands to be arranged around the Fe center with a minimum amount of repulsion favoring the formation of the thermodynamically stable high-spin Fe(III) species [76]. In some siderophores, the octahedral field may be distorted by the inclusion of a nitrogen or sulfur as donor atom and such modifications reduce the affinity for Fe^{3+} and increase the affinity for other metals. Formation constants (K_f) are used primarily for comparisons of iron affinities between the various siderophores. By convention, the overall equilibria of metal-ligand stability constants are expressed as β_{mlh} values for Reaction (1)

$$mM + lL + hH \rightleftharpoons M_mL_lH_h \quad (1)$$

where M is metal, L is ligand, and H is proton(s). For the wide diversity of siderophores known so far, the corresponding formation constants for one iron binding to one ligand that is fully deprotonated ($K_f \equiv \beta_{110}$) display a range of over 30 orders of magnitude. However, K_f does not consider the effect of proton competition in the iron-siderophore complex and thus, the pFe^{3+} (pM) parameter has been used as a more reliable comparison for the relative affinity of various ligands for Fe^{3+} under physiological conditions [76, 85, 86].

Siderophores can be classified in five classes depending on the chemical moieties that coordinate Fe^{3+}:catecholates, phenolates, hydroxamates, carboxylates, and mixed-type (Figure 1). Catecholates are siderophores characterized by one or more iron-binding catechol moieties (the ortho-isomer of dihydroxybenzene). These have the highest affinities for Fe^{3+} and the most negative reduction potentials. The best known example is enterobactin (also known as enterochelin) a siderophore that is produced by enterobacteria and that holds the record for the strongest iron binding capacity with a β_{110} of 49 and a reduction potential of –750 mV *versus* NHE at pH 7 [87, 88]. Other examples of catecholates include azotochelin produced by *Azotobacter vinelandii* and myxochelin A produced by

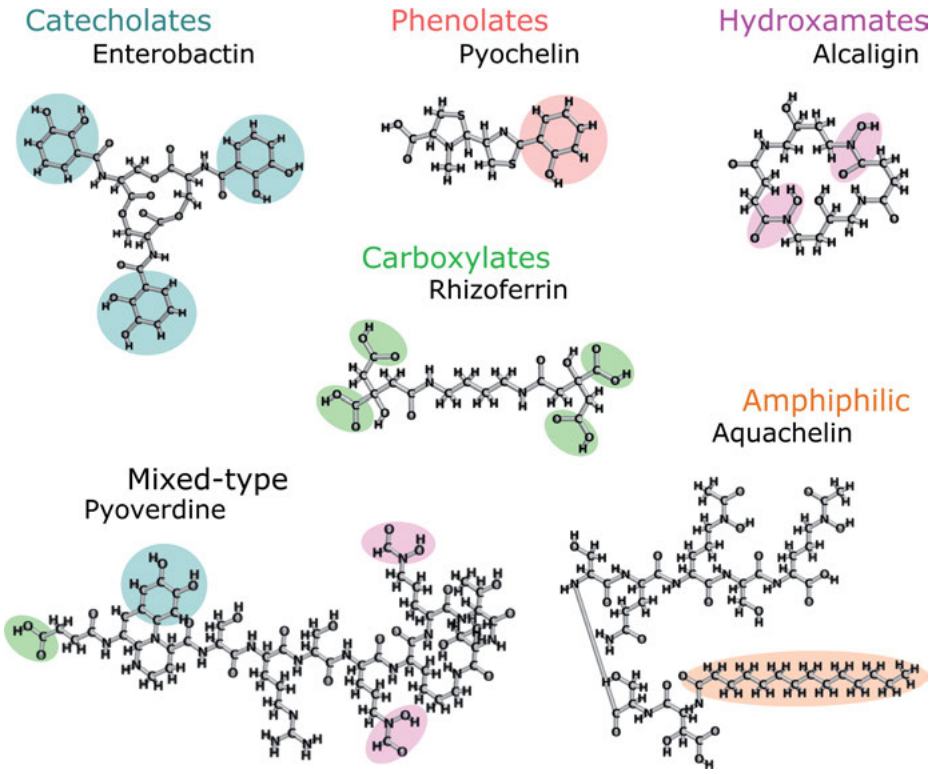

Figure 1. Examples of siderophores highlighting the different classes.

Angiococcus disciformis [89, 90]. Phenolates are siderophores characterized by one or more iron-binding phenol moietie(s) (Figure 1). The most illustrative examples of phenolate-type siderophores are pyochelin, a siderophore produced by *Pseudomonas aeruginosa*, and yersiniabactin produced by *Yersinia pestis* [91, 92]. Hydroxamates are siderophores characterized by one or more iron-binding hydroxamate groups (Figure 1). Some of the most studied hydroxamate siderophores are ferrioxamine E, alcaligin, bisucaberrin, and rhodotorulic acid. Bisucaberrin and alcaligin represent examples on how interesting the coordination chemistry of siderophores can be. These two hydroxamates have a tetradentate nature and thus do not satisfy the preferred octahedral geometry for Fe^{3+} when forming 1:1 FeL complexes. Instead they can form different species (Fe_2L_3, Fe_2L_2) depending on pH and relative concentration ratios of Fe:L [93]. The speciation of these compounds affects their 3D structure when iron-bound and also changes their reduction potential, affecting cell recognition and uptake and also iron release on the inside. Carboxylates are siderophores characterized by an iron-binding α-hydroxycarboxylate functional group. These siderophores tend to be preferred by microorganisms that live in acid environments and are often photoreactive. Rhizoferrin is the prototypical example of this class of siderophores that often resemble EDTA given that they can bind other metals more

strongly than Fe^{3+} [94]. Within each class, siderophores can also be amphiphilic (Figure 1) by containing a fatty acid appendage of variable length [95]. Most of these are produced by marine bacteria and besides the feature of amphiphilicity, this type of siderophores also display photoreactivity due to the presence of α-hydroxy carboxylic acid moieties [22, 96, 97]. This α-hydroxy carboxylic acid moiety is only photosensitive when bound to Fe^{3+}. Upon UV-photolysis (~300 nm) Fe^{3+} in the complex is reduced to Fe^{2+} with concomitant oxidation of the ligand producing a photoproduct which can still coordinate Fe^{3+}. The photoproduct stability constant is lower than the native. This process was first demonstrated in Fe^{3+}-aquachelins but other citrate-based siderophores also undergo photolysis and some examples include Fe^{3+}-coordinated aerobactin, orthobactins and synechobactins [22, 98].

2.2.2.3. Siderophore Pathways: Regulation, Biosynthesis, Extracellular Release, Cell Incorporation, and Metal Release

The siderophore pathway comprises the synthesis of siderophores inside the cytoplasm, extracellular release into the environment, iron complexation, cell incorporation of ferric siderophores and finally, iron release for assimilatory uptake (Figure 2). All these processes require tight regulation of the involved enzymes and transport systems [85]. Regulation commonly involves gene regulation at the transcriptional level by the ferric uptake repressor (Fur) in Gram-negative bacteria and diphtheria toxin regulator (DtxR) in Gram-positive bacteria [99, 100].

The biosynthesis of siderophores occurs when cells are iron-deprived. It occurs inside the cytoplasm via two main pathways: the non-ribosomal peptide synthetase (NRPS) pathway and the NRPS-independent siderophore (NIS) synthetase pathway [101].

Some siderophores produced by the NRPs pathway are yersiniabactin (from *Yersinia pestis*), vibriobactin (*Vibrio cholerae*), mycobactin (*Mycobacterium tuberculosis*), and enterobactin (*E. coli*) [102–104]. This pathway relies on non-ribosomal peptide synthetases (NRPSs), a family of large module-composed enzymes that function in a coordinated and sequential way to synthesize non-ribosomal peptides (NRPs) including siderophores. All modules can exist in the same polypeptide chain (NRPSs, type I), or they exist individually in different interacting proteins (NRPSs, type II). The latter are the most common in bacteria whereas the former are more common in fungi. With the different modules each NRPS selects, activates, and anchors each building block into the NRPS assembly line by peptide bond formation [105]. Each domain in the NRPS enzyme is highly substrate- and function-specific and therefore a genetic analysis predicts which substrates will bind and which siderophores will be produced. This predictability in the modular architecture of NRPSs gave rise to software such as antiSMASH and PRISM which from sequence analysis identify and predict the functionality of NRPS-encoding gene clusters [106, 107]. The knowledge from these predictions is helping in the discovery of novel peptides and is also being used for the reprogramming of biosynthetic machinery for the synthesis of novel peptides with improved and diversified bioactivities [5, 105, 108].

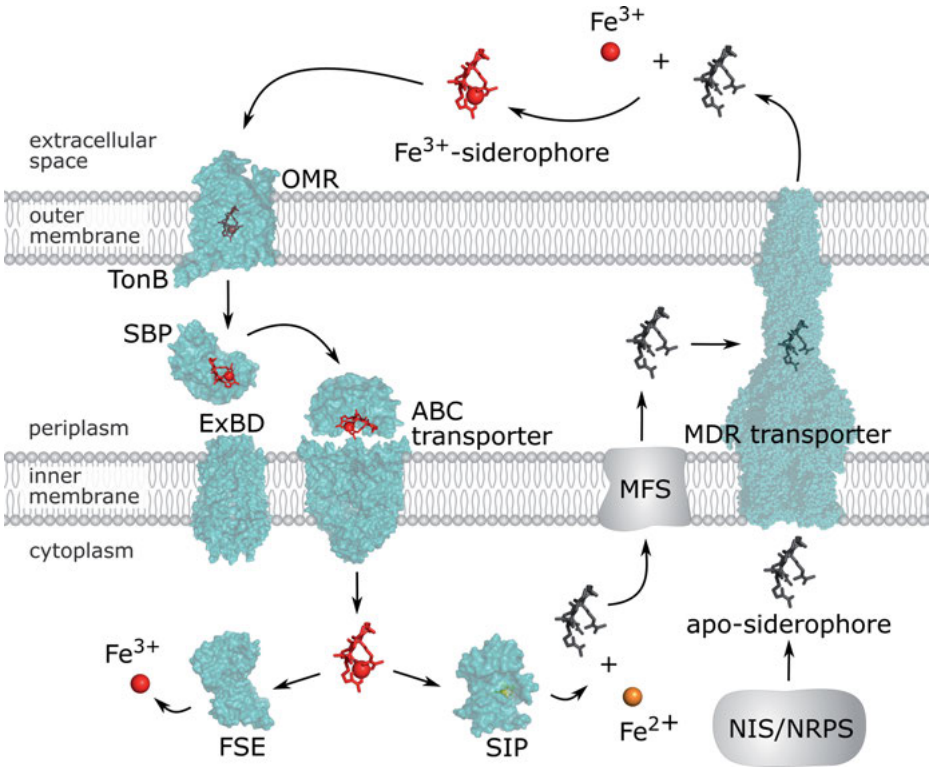

Figure 2. Siderophore pathway. Apo-siderophores are produced via the NIS or the NRPS pathways and then secreted outside via MDR transporters where they will incorporate Fe^{3+} forming ferric siderophores. These are then taken up to the periplasm by energy-dependent (TonB ExBD) OMRs and delivered by SBP to ABC-transporters. Once in the cytoplasm ferric siderophores are either hydrolyzed by FSE or reduced by SIPs, releasing Fe^{3+} or Fe^{2+}, respectively.

The NIS pathway relies on NIS synthetases and usually synthesizes polycarboxylate siderophores. However, other siderophore types (e.g., hydroxamates) are also produced by these enzymes, such as: achromobactin, aerobactin, alcaligin, petrobactin, staphyloferrin A and B, legiobactin, schizokinen, and synechobactin. NIS synthetases are responsible for a single enzymatic reaction, typically activation of citric acid, via adenylation and nucleophilic capture of an amine or alcohol group which by releasing AMP produces a citryl intermediate. These are classified based on the carboxylic acid and hydroxamate-amine substrates: (i) type A NIS which utilize citric acid and mono-amine or amide substrates, with the variant type A′ NIS which are grouped based on the enantioselective nature of substrates and final chirality of the product; (ii) type B NIS, which utilize ketoglutaric acid and a citryl-amine intermediate and; (iii) type C NIS, which are specific for mono-amine or amide substrates with citryl or succinyl intermediates. Multiple sequencing alignments of each type of NIS do not show significant

sequence conservation but it has been proposed that this may be due to the limited number of validated NIS genes [101]. Often, more than one NIS enzyme is required to synthesize a siderophore and usually the biosynthetic pathway through NIS enzymes is discovered by homology searches using the aerobactin NIS synthetases encoded by the *iuc* operon in *E. coli* K-12 [101, 109]. As a model example, the aerobactin synthesis requires two NIS synthetases: Type A IucA synthetase, which catalyzes the condensation of N-acetyl-N-hydroxylysine and citric acid to form N-citryl-acetyl-N-hydroxylysine and type C, IucC, which mediates the addition of another N-acetyl-N-hydroxylysine to the citric acid moiety of N-citryl-acetyl-N-hydroxylysine to form the symmetric aerobactin molecule [101, 110].

Once the apo-siderophores are produced, the size and charge of these compounds prevents passive diffusion and thus, they must be exported via specialized secretion systems into the extracellular space for iron scavenging/complexation [111]. There is still much to unravel regarding the secretion mechanisms of apo-siderophores. However, from the identified secretion systems, the transporters involved belong to three different structural families of bacterial multidrug resistance (MDR) translocases/transporters: the major facilitator superfamily (MFS), the resistance, nodulation, and cell division (RND) superfamily and the ABC superfamily [85]. MFS-transporters are found in all domains of life and move a variety of small compounds including nutrients, metabolites, signaling molecules and even toxins and drugs across biological membranes. They can operate as uniporters, that transport a single substrate and require no energy input; symporters, that transport a substrate together with a coupling ion (typically protons); and antiporters, that transport a substrate and a co-substrate in opposite directions, with the binding of one dependent on the prior release of the other. Both of the latter require external energy input, but unlike the former, they can transport substrates against their concentration gradient [112]. Some examples of MFS transporters that play a role in secreting siderophores include: EntS for the secretion of enterobactin in *E. coli*, YhcA for the secretion of achromobactin in *Erwinia chrysanthemi*, LbtB for the secretion of legiobactin in *Legionella pneumophila*, PvsC for the secretion of vibrioferrin in *Vibrio parahaemolyticus*, SchE for the export of schizokinen in *Anabaena* sp. PCC 7120, CsbX for the secretion of protochelin-like siderophores in *Azotobacter vinelandii*, and SfaA and SbnD for the secretion of staphyloferrin [85, 113–116].

The RND family includes several members that are relevant to antibiotic resistance in Gram-negative bacteria and these function as proton antiporters. Some members of the RND family identified to play a role in the secretion of siderophores are: AcrB, AcrD that transport enterobactin in *E. coli*, ApeX that exports petrobactin in *Bacillus anthracis*, MmpL4 and MmpL5 that export mycobactins and carboxymycobactins from *M. tuberculosis* [117–121].

From the ABC family involved in iron secretion, the following secretion systems have been identified: ExiT that exports exochelin from *Mycobacterium smegmatis* and IroC for the export of salmochelin. This later example, however, has been subject of controversy since independent studies show that IroC is also responsible for the uptake of the ferric salmochelin. Given the current state-of-

the-art regarding the mechanisms of siderophore uptake, it is possible that apo-siderophore release and holo-siderophore (Fe(III) form) uptake may actually be coupled into one mechanism [119, 122–124].

Overall, from the almost uniquely characterized secretion system of enterobactin, it seems that siderophore secretion follows the three-component organization that is shared amongst the majority of multidrug transporters [83, 125]. This three-component organization consists in an inner membrane efflux protein or transporter/translocase (IEPs) (which can be any of the previously described families), an outer membrane efflux protein or channel (OEP) and a periplasmic efflux or accessory protein (PEP) that connects the two [125, 126]. From the data gathered regarding the secretion systems of enterobactin, the hypothesis is that it is exported to the periplasm by the inner membrane protein EntS and/or by RND transporters AcrB, AcrD, and MdtBC and then enterobactin goes through PEP member ArcA and/or MdtA into the OEP member TolC to be exported to the extracellular space [83, 111, 118]. Currently, only one other of the OEP and PEP members has been identified with a role in siderophore secretion: HgdD from *Anabaena* sp. PCC 7120 and MmpS4 & MmpS5 from *M. tuberculosis*, respectively [120, 127]. Once in the extracellular space, apo-siderophores will bind available Fe(III) and then the Fe(III)-siderophore is incorporated back inside the cell. In Gram-negative bacteria, cell incorporation of Fe(III)-siderophores requires specific energy-dependent outer membrane receptors (OMR) since the majority of Fe(III)-siderophores are larger than 600 Da and thus porin-mediated transport is low. Typically, the affinity of these outer membrane transporters to the ferric siderophores is extremely high, in the range of 1–50 nM, allowing for the scavenging of these complexes from the environment. Once in the periplasm they are bound to periplasmic SBPs, which are also designated as siderophore-binding proteins for translocation into the cytoplasmic membrane via ABC-type transporters [76]. In Gram-positive bacteria, the import of ferric siderophores occurs similarly with the exception for the binding to outermembrane transporters [128]. In Gram-positive bacteria Fe(III)-siderophores are transported via SBPs, permease(s), and an ATPase. SBPs are anchored in the membrane and specifically bind siderophores in both Fe(III) and apoforms [129].

Two mechanisms have been proposed for the translocation of Fe(III)-siderophores into the cytoplasm: a displacement mechanism, whereby the initially bound apo-siderophore is replaced by the Fe(III)-siderophore, or by a siderophore-shuttle mechanism where Fe^{3+} is exchanged between the free Fe(III)-siderophore and the bound apo-siderophore and once exchanged, the ferric siderophore can be transported inside the cell [124, 128, 129]. Once inside the cell, given the high affinities for Fe(III), iron release from the Fe(III)-siderophore complex does not occur spontaneously. Instead, iron release from Fe(III)-siderophore complexes can occur via three main mechanisms: the hydrolysis of the Fe(III)-siderophore, proton-assisted dissociation of the siderophore complex and reduction of the Fe^{3+} iron [130, 131]. The hydrolysis of the Fe(III)-siderophore by esterases (FSE, Fe(III)-siderophore esterase, Figure 2), has been observed for various siderophores including bacillibactin (by BesA esterase), enterobactin (by esterase Fes), and fusarinine C (by esterase Sidj) [132, 133]. This

strategy involves great metabolic cost since it requires a constant production of new siderophores for iron acquisition. On the other hand, despite ensuring the recycling of the siderophore, proton-assisted dissociation of the siderophore complex requires a very low pH to guarantee complete dissociation. Siderophores have redox-Bohr effect, thus, the potential increases as the pH is lowered, and in some cases ferric siderophores are sequestered by intracellular compartments that have a lower pH, perhaps as a strategy to facilitate Fe(III)-siderophore reduction [131].

At neutral pH and in the absence of esterases, the release of iron via reduction of the Fe^{3+} iron is the remaining mechanism. Upon reduction of Fe^{3+} to Fe^{2+}, the stability of the complex is decreased given the usual low Fe^{2+} affinity. This will facilitate the kinetics of ligand exchange allowing time- and site-specific delivery of the metal. Reduction of the iron center is proposed to occur via small molecule reducing agents or by a superfamily of assimilatory Fe^{3+} reductases. In bacteria, Fe(III)-siderophore reduction can occur in the cytosol or in the periplasm. In the cytosol, it involves a superfamily of proteins that is widely conserved across bacteria and these are known as siderophore-interacting proteins (SIPs). These can belong to two distinct families: the Fe(III)-siderophore reductase (FSRs) family, and the SIP family [134, 135]. From the FSRs family one protein has been isolated and fairly characterized: FhuF, a Fe(III)-hydroxamate reductase from *E. coli*. FhuF is an atypical [2Fe-2S] ferredoxin which can promote iron release from hydroxamate-type siderophores, namely, ferrichrome, ferrioxamine B and coprogen [136]. For the SIPs family, more members have been identified and characterized and thus these can be further distinguished in two broad groups: one that generates cytosolic reduced free flavins that subsequently reduce the Fe(III)-siderophores, and another that contain stably attached flavins and use NADH and/or NADPH as reducing agents. Once iron is released for incorporation into host proteins, the siderophore ligand can be secreted outside for further rounds of iron uptake.

2.2.2.4. Hemophores, Chaperones, and Others

Hemophores are specialized proteins that are extracellularly secreted and can acquire heme from diverse sources delivering it to specific outer membrane receptors [51]. Hemophores play a key role in the tug-of-war between bacterial pathogens and eukaryotic hosts. There are different types of hemophores including: HasA-type, HxuA-type, NEAT-type, and Rv0203. The HasA-type (heme acquisition system, Has) is the best known and has been identified in several Gram-negative bacteria. Heme transfer occurs from host heme proteins to HasA given the higher affinity of the hemophore to heme, without the formation of a stable protein-protein complex. The HxuA-type is represented by a large 100 kDa protein hemophore from *Haemophilus influenzae* that promotes heme release from hemopexin. However, unlike other hemophores, HuxA does not bind heme. The NEAT (near-transporter)-type hemophores are represented by Isd (iron surface determinant) proteins from the Gram-positive heme uptake pathway. These proteins contain one or more NEAT domains and can acquire heme from methemoglobin (hemoglobin in the Fe^{3+} state). Rv0203 was the most

recently identified hemophore from the *Mycobacterium tuberculosis* (Mtb) heme pathway. This hemophore has no sequence and structural similarities with HasA-type hemophores, but it contains a similar heme-binding motif. Heme from hemophore proteins is then transported to the periplasm via TonB-dependent outer membrane transporters and eventually shuttled across the inner membrane type II ABC-transporters, as previously mentioned [137].

Notwithstanding, evidence has been increasing for other hemophore-like proteins with affinity for other metals such as manganese (manganeseophores) and zinc (zincophores). In different *Burkholderia* species a zincophore (TseZ) and a manganeseophore (TseM) were identified [43]. Other more sophisticated systems for obtaining metals were recently identified such as the ferredoxin uptake system (Fus) a gene cluster encoding proteins that promote the transport of ferredoxin into the bacterial cell and process it proteolytically for iron uptake [138].

3. DISSIMILATORY REDOX CHEMISTRY: POWERING THE METABOLISM WITH METALS

Microbes also have the ability to use metals as terminal electron acceptors. This type of metabolism, called dissimilatory metal reduction, is distinct from the reduction of metals for metal uptake into cells, since it leads to conservation of energy. By coupling the oxidation of dihydrogen (H_2) or organic compounds to the reduction of metals, such as Fe^{3+}, Mn^{4+}, U^{6+}, and Cr^{6+}, some microbes can support growth [139]. There are other organisms that use them for detoxification [140]. Microbial reduction of oxidized forms of metals is crucial not only for the biogeochemical cycles of metals, but also for the fate of organic matter and nutrients present in a variety of environments [141].

The ability of organisms to reduce metals was discovered at the end of the 19th century [142]. However, at that time Fe^{3+} and Mn^{4+} reduction was thought to be the result of a non-enzymatic process [143].

The first organisms shown to be able to couple the oxidation of organic matter to the reduction of metals belong to *Shewanella* and *Geobacter* genera [144, 145]. Nowadays, dissimilatory metal-reducing organisms (DMRO) are continually being discovered. This is mainly due to the fact that dissimilatory metal reducing bacteria can be used for the bioremediation of contaminated environments with metals and in microbial fuel cells for the production of energy [146, 147]. In these devices, instead of using metals, DMRO use an electrode as the terminal electron acceptor, coupling their growth with the transfer of electrons to the electrode (Figure 3).

Dissimilatory metal reduction affects the geochemistry of soils and sediments by allowing the formation of solid minerals, and also contributes to the biogeochemical cycles of metals [148]. In particular, dissimilatory Fe^{3+} reduction has a larger overall environmental impact than microbial reduction of any other metal. Iron respiration has been identified in numerous organisms, including Bacteria and hyperthermophilic Archaea [144, 145, 149, 150], and has been proposed as one of the earliest forms of microbial metabolism to have evolved [151], preced-

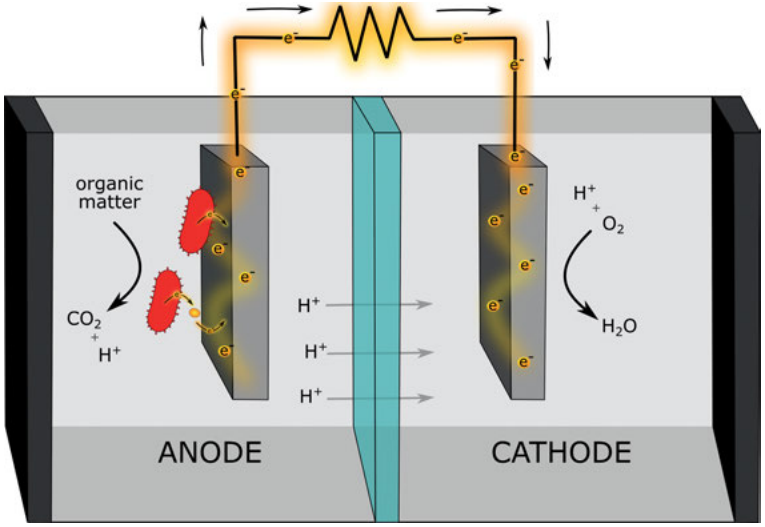

Figure 3. Scheme of a microbial fuel cell with DMRO growing on the anode. Current in the circuit derives from the flow of electrons from the anode to the cathode for the reduction of oxygen. On the anode side direct electron transfer is represented on the top and indirect electron transfer via electron shuttles (yellow circles) is represented on the bottom.

ing the respiration of dioxygen (O_2), nitrate (NO_3^-), and sulfate (SO_4^{2-}) (see Chapters 2 and 7) [87].

3.1. Dissimilatory Metal Reducing Organisms

The best characterized metal reducing organisms are *Geobacteracaea* and *Shewanellacaea*. These organisms are able to use a wide variety of electron acceptors, including metals, and have been in the focus of research for understanding extracellular electron transfer [152, 153]. *Geobacter sulfurreducens* strain PCA and *Shewanella oneidensis* strain MR-1 have become the model organisms for the study of DMRO. While family members of the *Shewanellacaea* are able to metabolize a wide variety of substrates, including monosaccharides, carboxylates, and amino acids as carbon and energy sources under oxic and anoxic conditions, *Geobacteracaea* are restricted to anaerobic respiration, using acetate or short-chained organic acids as carbon and electron donor [154, 155].

The freshwater isolate *Geobacter metallireducens* (formerly known as strain GS15) was the first organism known to conserve energy coupling the oxidation of acetate to iron reduction (Equation 2) [156]:

$$CH_3COO^- + 8\,Fe^{3+} + 4\,H_2O \rightarrow 2\,HCO_3^- + 8\,Fe^{2+} + 9\,H^+ \qquad (2)$$

Geobacter species are also able to reduce Fe^{3+} minerals to the mixed valence mineral magnetite using short chain fatty acids and monoaromatic compounds, such as toluene and benzene as electron donors [157–160].

Desulfuromonas acetoxidans, a marine bacterium that is closely related to *Geobacter* and that was isolated due to its ability to couple the oxidation of acetate to S^0 [161], is also capable of growing on acetate using Fe^{3+} as the sole electron acceptor [162]. Although many organisms have the capacity to reduce Fe^{3+} under anaerobic conditions, only a limited number of organisms are known to couple it to acetate oxidation. Others, including members of *Shewanellacaea* and sulfate reducers are unable to use acetate. These organisms conserve energy to support growth by coupling the oxidation of more complex substrates such as formate, lactate, and pyruvate to the reduction of Fe^{3+} (Equations 3–5):

$$HCOO^- + 2\,Fe^{3+} + H_2O \rightarrow HCO_3^- + 2\,Fe^{2+} + 2\,H^+ \quad (3)$$

$$COHCH_3COO^- + 4\,Fe^{3+} + 2\,H_2O \rightarrow HCOO^- + HCO_3^- + 4\,Fe^{2+} + 5\,H^+ \quad (4)$$

$$COCH_3COO^- + 2\,Fe^{3+} + 2\,H_2O \rightarrow HCOO^- + HCO_3^- + 2\,Fe^{2+} + 3\,H^+ \quad (5)$$

Or they can couple the oxidation of H_2 to the reduction of Fe^{3+} (Equation 6):

$$H_2 + 2\,Fe^{3+} \rightarrow 2\,H^+ + 2\,Fe^{2+} \quad (6)$$

Facultative anaerobic organisms within the genera *Aeromonas* and *Ferrimonas* have also been shown to utilize Fe^{3+} as an anaerobic electron acceptor, but, like *Shewanella* species, they are unable to use acetate as an electron donor [139]. Several *Desulfovibrio* species can incompletely oxidize lactate to acetate and carbon dioxide, and are also able to oxidize H_2 with the reduction of Fe^{3+} [163, 164]. In this case no net growth was observed during reduction of Fe^{3+} [163].

In acidic environments, elemental sulfur (S^0) can also be used as an electron donor for Fe^{3+}-reduction. DMRO such as *Thiobacillus ferrooxidans* and *Sulfolobus acidocaldarius* can reduce Fe^{3+} to support growth [165,166] (Equation 7):

$$S^0 + 6\,Fe^{3+} + 4\,H_2O \rightarrow HSO_4^- + 6\,Fe^{2+} + 7\,H^+ \quad (7)$$

These thermophilic organisms can also reduce Fe^{3+} with glycerol or thiosulfate as the electron donor [167].

Although microbial reduction of Fe^{3+} was observed primarily in low-temperature environments, the identification of *S. acidocaldarius* as a DMRO, provided evidence for the existence of thermophilic Fe^{3+}-reducers. Since then, thermophilic bacteria were also discovered in two geologically and hydrologically isolated Cretaceous- and Triassic-age sedimentary basins in the deep terrestrial subsurface [148, 168]. Two thermophilic Gram-positive bacteria belonging to the Firmicutes class were also identified as DMRO [149, 169]. The discovery of these

organisms has led to the hypothesis that Fe^{3+} respiration existed on Earth in the beginning of life [170].

Although iron reduction is one of the most characterized metal-based respiratory metabolisms, DMRO can also reduce other metals. For example, most of the organisms capable of reducing Fe^{3+} are also able to reduce manganese oxides. Indeed, microbial Mn^{4+}-reduction greatly parallels dissimilatory Fe^{3+}-reduction [148]. This type of reduction has been reported in marine, freshwater, and terrestrial environment, which implies that manganese may play an important role in carbon mineralization [145, 171]. In general, Fe^{3+}- and Mn^{4+}-reducers oxidize the same type of electron donors, however there are some exceptions. These include the Fe^{3+}-reducing *Pseudomonas* sp. that cannot couple the oxidation of H_2 with the reduction of Mn^{4+}, and the Fe^{3+}-reducing proteobacterium *Ferribacter limneticum* that is not able to use Mn^{4+} as an electron acceptor [172, 173].

G. metallireducens was the first organism found to reduce uranium (U), from U^{6+} to U^{4+} (Equation 8):

$$CH_3COO^- + 4\,U^{6+} + 4\,H_2O \rightarrow 2\,HCO_3^- + 4\,U^{4+} + 9\,H^+ \quad (8)$$

Uranium, the heaviest naturally occurring element on Earth, is a very common radioactive element and it exists in all types of rocks [174]. Most Fe^{3+}-reducing bacteria are able to use U^{6+} as an alternative electron acceptor and reduce it to the insoluble U^{4+} mineral, because near neutral pH the potential of the U^{6+}/U^{4+} couple is similar to the potential of Fe^{3+}/Fe^{2+}. Given that U^{6+} is highly soluble in most natural waters and U^{4+} is insoluble, the biological reduction of U^{6+} to U^{4+} is of significant importance in bioremediation, for treating uranium-contaminated waters or soils [174].

Like uranium, gold (Au) is soluble in the oxidized form, Au^{3+} and insoluble in the reduced form, Au^0. Several organisms were shown to have the capacity to reduce Au^{3+}, including mesophilic and hyperthermophilic organisms [175]. However, the reduction of Au^{3+} was not associated with growth, suggesting that the reduction of this metal is a strategy to avoid Au^{3+} toxicity [175].

Although selenium (Se) is not a metal, some DMRO are able to couple their growth with the reduction of selenium compounds, including selenate (SeO_4^{2-}), selenite (SeO_3^{2-}) and elemental selenium (Se^0) [176, 177]. These comprise species of the genera *Bacillus*, *Sulfurospirillum*, *Pseudomonas*, *Clostridium*, *Citrobacter*, and *Flavobacterium* [176, 178–180]. Several organisms can conserve energy to support growth via selenate reduction (Equation 9):

$$4\,CH_3COO^- + 3\,SeO_4^{2-} \rightarrow 8\,CO_2 + 3\,Se^0 + 4\,H_2O + 4\,H^+ \quad (9)$$

While others, including *Pseudomonas* are able to reduce selenate to selenite (Equation 10):

$$CH_3COO^- + H^+ + 4\,SeO_4^{2-} \rightarrow 2\,CO_2 + 4\,SeO_3^{2-} + 2\,H_2O \quad (10)$$

The reduction of selenite to elemental selenium, although identified in numerous organisms since the beginning of the 20th century, was never observed to be

associated with energy conservation. Instead, it is used as a detoxifying mechanism [176, 177, 181].

The reduction of highly toxic and mobile chromium Cr^{6+}, to the less toxic and less mobile Cr^{3+}, can be performed by several organisms including *P. aeruginosa*, *Desulfovibrio vulgaris*, and *S. oneidensis* MR-1 [148, 182, 183]. These organisms reduce Cr^{6+} during anaerobic growth and use this metal as the sole electron acceptor (Equation (11)):

$$3\,CH_3COO^- + 17\,H_2O + 8\,CrO_4^{2-} \rightarrow 6\,HCO_3^- + 8\,Cr(OH)_3(s) + 13\,OH^- \quad (11)$$

Soluble mercury, Hg^{2+}, can be reduced to volatile elemental Hg^0 by many aerobic and facultative aerobic microorganisms as a detoxifying mechanism [148, 184]. In surface waters $Hg(OH)_2$ and $HgCl_2$ are the most common species, while the predominant form in fish is methylmercury [182, 184]. DMRO play an important role in environmental mercury methylation [185]. For example, *S. oneidensis* MR-1 can reduce Hg^{2+} to Hg^0 in the presence of electron donors and acceptors, suggesting that the reduction of Hg^{2+} involves the activity of respiratory chain enzymes [186].

Technetium (Tc) can also serve as an electron acceptor in anaerobic respiration. This radioactive contaminant exists under aerobic conditions in the form of pertechnetate, Tc^{7+}, which is soluble. The reduced form exists as Tc^{4+} that is highly insoluble [148]. The sulfate-reducing organisms *Desulfovibrio gigas* and *D. vulgaris* can convert Tc^{7+} to insoluble adsorbed technetium sulfides [44].

Vanadium (V) is an abundant trace element with a high value for numerous industrial applications. To date, *Pseudomonas* sp. and *S. oneidensis* MR-1 were shown to reduce V^{5+} to V^{4+} under anaerobic conditions [187–189]. In these organisms, sugars, amino acids, lactate, and hydrogen serve as electron donors for the V^{5+} reduction.

3.2. Modes of Extracellular Electron Transfer

The ability of microorganisms to transfer electrons to insoluble metals outside the cell rely on their ability to perform extracellular electron transfer. This type of metabolism allows the microbes to couple their internal metabolism with external charge transport. Up to date two different mechanisms have been proposed for extracellular electron transfer (Figure 3):

(i) Through direct contact between the microbe and the insoluble electron acceptor. This occurs through cell-surface proteins, or conductive nanowires or pili. While cell-surface proteins are produced in the presence of insoluble electron acceptors, pili or nanowires are usually generated under electron acceptor-limited conditions [190]. These structures serve as alternative pathways to extend the direct extracellular electron transfer distance and maximize the efficiency of electron transfer [191, 192].

(ii) Through indirect electron transfer through soluble electron shuttles. These are small redox mediators including anthraquinone 2,6-disulfonate, humic acids and flavins, that are produced by the microorganisms or are available in the environment [193–195].

DMRO can use one or both mechanisms to transfer electrons produced during microbial metabolism to the outside of the cell. During catabolism, electrons are produced and reduce the quinone pool at the inner membrane. This occurs via several quinone reductases, such as formate dehydrogenase or hydrogenase. For the turnover of the quinone pool in DMRO, the reduced quinol is oxidized, and the electrons are transferred to periplasmic proteins that mediate electron transfer to cell-surface proteins for the reduction of metals outside the cell. This requires that electrons are moved from inside the cell to redox proteins on the cell surface [190, 196]. It has been demonstrated that in most DMRO, multiheme *c*-type cytochromes play an important role in these pathways [152, 190, 197]. These proteins can be found associated with the inner membrane, in the periplasmic space, and at the cell surface of numerous DMRO, playing essential roles in extracellular electron transfer [197–207]. At the cell-surface, these proteins are responsible for transferring electrons directly to the insoluble metals, or indirectly with the use of soluble electron shuttles [193, 207, 208].

Different microorganisms evolved distinct pathways to overcome the physical barrier of the cell envelope. Those best characterized and known are the metal-reducing (Mtr) pathway in *S. oneidensis* MR-1 and the porin-cytochrome-mediated (Pcc) pathway of *G. sulfurreducens* [152, 209]. However, distinct pathways were hypothesized in other DMRO (Figure 4).

3.2.1. The Mtr Pathway of Shewanella oneidensis MR-1

The Mtr pathway of *S. oneidensis* MR-1 is composed by six multiheme *c*-type cytochromes: the inner membrane tetraheme cytochrome CymA, the periplasmic tetraheme proteins STC and FccA, the outer membrane porin complex

Figure 4. Scheme of the extracellular electron transfer pathways in (**A**) *S. oneidensis* MR-1, using the structures of STC (PDB 1M1Q), FccA (PDB 1D4D), MtrC (PDB 4LM8), OmcA (PDB 4LMH), and the SAXS model of MtrA [222]. For CymA the model was made with SWISS-MODEL using the template of NrfH (PDB 2J7A); (**B**) *G. sulfurreducens*, using the structure of PpcA (PDB 1OS6), OmcF (PDB 3CU4), OmcS (PDB 6EF8); and (**C**) *T. potens* strain JR using the structure of OcwA (PDB 6I5B). All the structures were made using Pymol. The other cytochromes, for which no 3D-structure is available, are represented in gray with the hemes in red.

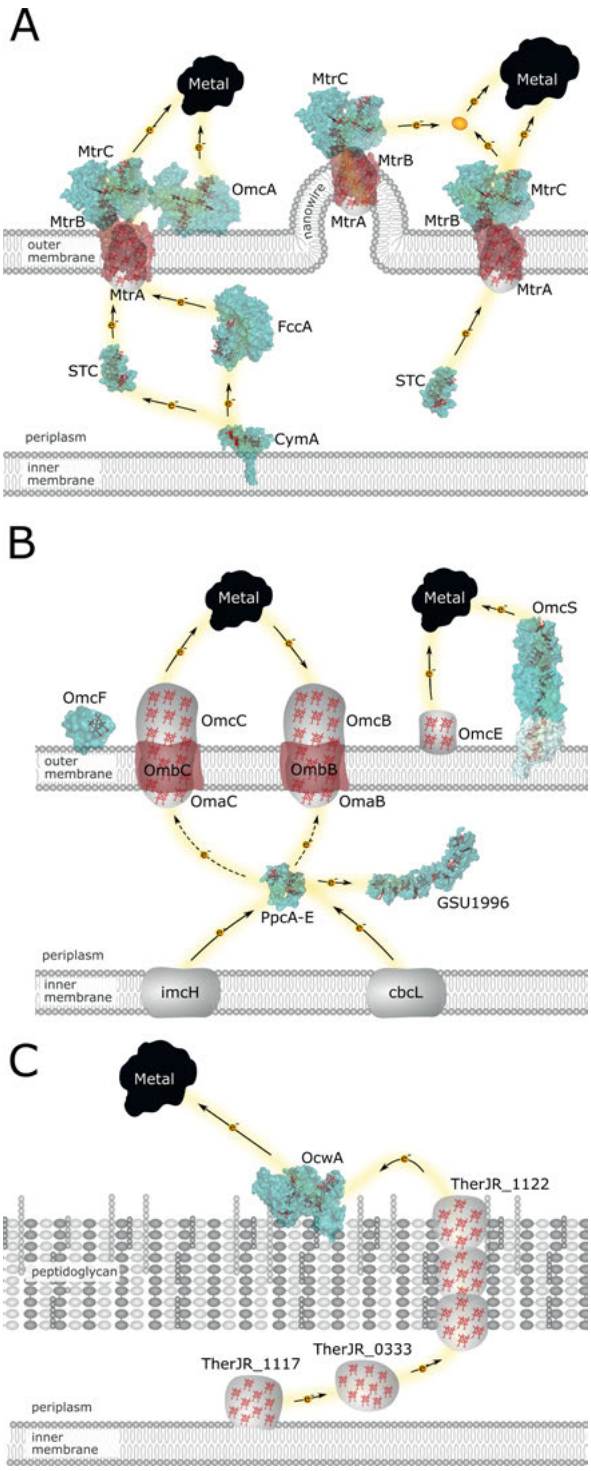

MtrCAB composed by the decaheme cytochromes MtrC and MtrA, and the β-barrel protein MtrB, and the outer membrane decaheme cytochrome OmcA [210] (Figure 4A). Although these proteins were shown to be involved in the extracellular electron transfer pathway to metal oxides and electrodes, there are others that are also important for this process and of other insoluble electron acceptors [211–213].

CymA oxidizes quinol in the cytoplasmic membrane and transfers the electrons to STC and FccA in the periplasmic space that function as mediators to the outer membrane porin complex for the reduction of metal oxides [214]. Besides this, CymA can also transfer electrons to other terminal reductases present in the periplasmic space, such as nitrite reductase and octaheme tetrathionate reductase [215]. Since the knock-out of CymA impairs growth of *S. oneidensis* MR-1 with most used anaerobic electron acceptors, it has been proposed that this tetraheme cytochrome works as a respiratory electron hub in this organism [216, 217].

STC and FccA interact with CymA and MtrA from the MtrCAB complex [214]. Interestingly, these proteins (STC and FccA) interact with both proteins (CymA and MtrA) with the same heme, indicating that they cannot form a stable ternary complex that would span the width of the periplasmic space [214]. Furthermore, they compete for the same binding place in MtrA [215]. It was proposed that the presence of both proteins in the periplasmic space allows the organism to quickly release catabolic electrons to a variety of environmental electron acceptors [203]. It has been shown that FccA, which is also a fumarate reductase, can work as a moonlighting protein, allowing *Shewanella* to quickly switch between reduction of soluble (i.e., fumarate) and insoluble electron acceptors (i.e., metal oxides), bypassing transcriptional regulation [218].

At the outer membrane MtrA, MtrC, and MtrB form a trans-outer membrane porin cytochrome complex of approximately 180 nm that spans the hydrophobic lipid bilayer of *Shewanella* [219]. It has been proposed that MtrB functions as a porin into which both MtrA and MtrC are inserted to allow direct electron transfer. Indeed, this porin protein can only be expressed in the folded state in the presence of MtrA [220, 221]. Recently the overall domain organization of this complex was determined by small angle neutron scattering [219]. This study revealed that the length of MtrAB is approximately 100 Å, the same length as MtrA when isolated from the complex, which suggests that MtrA most likely inserts through the entire length of MtrB [219, 222]. *S. oneidensis* MR-1 contains a series of paralogs of the porin-cytochrome complex MtrCAB, such as the MtrDEF that is preferentially expressed in biofilms and aggregated cells and the SO4360-SO4357 that was shown to function as a terminal reductase at the cell surface [211, 223]. There is redundancy in these extracellular electron transfer pathways, with different proteins displaying overlapping functions [224]. This allows *Shewanella* to use distinct paralog modules of the Mtr respiratory pathway to transfer electrons outside the cell [224, 225].

MtrCAB complexes are well conserved among all analyzed *Shewanella* species, suggesting that this complex is crucial for mineral reduction [226]. *S. oneidensis* MR-1 also produces a second outer membrane protein, the decaheme cytochrome OmcA, that is co-expressed with the complex MtrCAB [227, 228].

OmcA was shown to be important for direct and indirect electron transfer and also for cell adhesion [229–231]. Interestingly, this protein although present in numerous *Shewanella* sp., is not conserved, existing as an undecaheme *c*-type cytochrome, UndA, also localized at the cell surface [232].

The reduction of metals can occur directly with the contact of the outer membrane cytochromes OmcA and MtrC, or indirectly with secreted flavins that mediate electron transfer between the cytochromes and more distant solid electron acceptorsy [193, 233–235]. Recently, it was demonstrated that nanowires from *S. oneidensis* MR-1, usually produced under electron acceptor limiting or low agitating conditions are extensions of the outer membrane [236–238]. These extensions function as electron conduits for the reduction of solid electron acceptors, being composed by both periplasmic and outer membrane proteins [238]. However, in this organism not all compounds are reduced outside the cell by outer membrane cytochromes. Selenite was shown to be reduced by FccA in the periplasm, given that this process was severely suppressed in *Shewanella* mutants lacking this protein [239].

3.2.2. The Pcc Pathway of Geobacter sulfurreducens

Like *Shewanella*, the extracellular electron transfer pathway used by organisms belonging to *Geobacter* genera is composed by numerous multiheme *c*-type cytochromes, that are present in the inner membrane, the periplasmic space and at the outer membrane of these organisms [240, 241] (Figure 4B).

In *G. sulfurreducens*, at least two electron transfer pathways out of the inner membrane were proposed for the reduction of electron acceptors with distinct reduction potentials [198, 200]. While the inner membrane cytochrome ImcH (inner membrane cytochrome for high potential) is required for the reduction of high reduction potential extracellular electron acceptors [198], the CbcL (*c*- and *b*-type cytochrome for low potential) inner membrane cytochrome dominates when the extracellular electron acceptor presents a reduction potential at or below –0.1 V versus SHE [200]. In the periplasmic space, members of the periplasmic triheme PpcA (periplasmic cytochromes)family (PpcA, PpcB, PpcD, and PpcE) were shown to be important for the reduction of different metals [155]. These proteins, together with the dodecaheme cytochrome GSU1996, predicted to function as a nanowire protein in the periplasmic space of *Geobacter*, are proposed to transfer electrons across the periplasmic space of this organism [242].

To transfer electrons outside the cell, *G. sulfurreducens* uses trans-outer membrane porin-cytochrome protein (Pcc) complexes, similar to the porin-cytochrome complex MtrCAB from *S. oneidensis*. These include the porin-like outer membrane protein OmbB and OmbC, the periplasmic octaheme cytochromes OmaB and OmaC and the outer membrane dodecaheme cytochromes OmcB or OmcC [243]. The functional and organizational differences between Pcc and Mtr proteins suggest that these two systems evolved independently to mediate electron transfer across the bacterial outer membrane using the same design principle [243]. It was shown that besides these Pcc complexes *G. sulfurreducens* also contains the *ext* genes that comprise three new clusters, the *ext*ABCD, the *ext*CD,

and the *ext*EFG, proposed to be involved in electron transfer across the outer membrane [244]. Knock-out and complementary studies demonstrated that this organism uses different conduits to transfer electrons outside the cell, and that their use depends on the extracellular substrate [244]. While strains lacking both OmcBC and ExtEFG showed a significant impact in Fe^{3+}-reduction, the deletion of the five gene clusters abolished all metal reduction [244].

At the cell surface, *G. sulfurreducens* contains electrically conductive pili (e-pili) and other *c*-type cytochromes that were shown to be important for metal reduction [245]. Among these are the OmcE, the OmcS and the monoheme cytochrome OmcF [155]. OmcE and OmcS were initially proposed to serve as intermediates to transfer electrons to e-pili [246]. The conductive structures e-pili, assembled from the PilA pilin monomer, were shown to allow the discharge of respiratory electrons at rates that greatly exceed the rates of cellular respiration [192]. However, the recent discovery that the hexaheme cytochrome OmcS from *G. sulfurreducens* can assemble into conductive filaments, revived the discussion on the function and composition of nanowires in *Geobacter* [247–249].

The ability of *G. sulfurreducens* to perform extracellular electron transfer was prevented by the deletion of the gene encoding the monoheme outermembrane cytochrome OmcF [250]. Although this protein is not directly involved in metal reduction, it was demonstrated that it is crucial for the transcription of other outer membrane cytochromes, in particular of OmcB, necessary for metal reduction [250, 251].

Besides multiheme *c*-type cytochromes, other types of proteins were shown to be fundamental for metal reduction. These include the putative porin protein OmpJ and the multicopper protein OmpB, both localized in the outer membrane of *G. sulfurreducens* [252, 253]. The OmpJ protein is required to keep the integrity of the periplasmic space necessary for proper folding and functioning of periplasmic and outer membrane electron transport conduits [252]. Although OmpB is specifically required for the reduction of Fe^{3+} oxides, but not soluble forms of Fe^{3+}, its functional role is still unknown [254]. A homologue of OmpB, designated OmpC, was also shown to be required for iron oxide reduction [255].

G. sulfurreducens can also secrete proteins that facilitate the final steps of electron transfer, analogous to how secreted redox-active molecules accelerate metal reduction [193, 194]. The triheme *c*-type cytochrome PgcA found in the extracellular space of this organism but loosely bound to the outer membrane, was shown to facilitate electron transfer at mineral surfaces [256].

3.2.3. Other Pathways

Besides Gram-negative bacteria, Gram-positive bacteria and Archaea that lack an outer membrane are also capable of reducing insoluble metals. Indeed, until recently, given the thick peptidoglycan cell wall of Gram-positive bacteria it was argued that these organisms were not capable of performing extracellular electron transfer [257].

The Gram-positive *Thermincola potens* strain JR, isolated from the anode of a microbial fuel cell inoculated with anaerobic digester sludge was shown to be

able to use soluble electron shuttles for transferring electrons onto iron hydroxides, although no evidence of excretion of soluble mediators was observed [257]. In contrast, *T. ferriacetica* is capable of directly transferring electrons from acetate to the anode of a microbial fuel cell [258]. Trypsin-shaving experiments together with surface-enhanced Raman spectroscopy of *T. potens* JR allowed the identification of several multiheme *c*-type cytochromes that were proposed to form an extracellular electron transfer pathway to transfer electrons outside the cell (Figure 4C) [259].

This pathway is comprised by the inner membrane decaheme cytochrome TherJR_1117 (Tferr_0075), the periplasmic decaheme cytochrome TherJR_0333 (Tferr_1887), the hexaheme cytochrome TherJR_1122 (Tferr_0070) that is proposed to be embedded in the peptidoglycan cell wall, and the nonaheme cytochrome TherJR_2595 (Tferr_3193) present at the cell surface. It has been proposed that this pathway allows electrons to be transferred across the cell wall, and that the cell surface protein is responsible to transfer electrons with the insoluble electron acceptors. Although until now it is not possible to delete genes in these organisms to confirm the functional roles of the identified cytochromes, some of these proteins were already produced and characterized in detail [207, 260].

The Gram-positive bacterium *Carboxydothermus ferrireducens* can also use direct electron transfer to reduce ferrihydrite [261]. Although no cell-surface proteins have been identified yet, it was demonstrated that pili are expressed during insoluble mineral respiration, and that a cytochrome Fe(EDTA) reductase present at the outer membrane is involved in the pathway [261].

Although the pathways for most DMRO are still unknown, for several of these organisms the proteins that are involved in metal reduction were identified. For example, the periplasmic cytochrome c_3 from *Desulfovibrio* sp. was demonstrated to reduce metals, such as Fe^{3+}, Cr^{6+}, and U^{6+} [262]. Nuclear magnetic resonance studies have shown that in the case of the periplasmic cytochrome c_7 from *Desulfuromonas acetoxidans*, the interaction with Cr^{6+} occurs close to heme IV, the heme that is proposed to be also involved in electron transfer with hydrogenase [262, 263].

4. HEALTH-RELATED APPLICATIONS

Extracellular electron transfer can impact the health of humans and other eukaryotes in numerous ways. For example, the capacity of some bacteria to reduce arsenate present in geological sources to arsenite mobilizes this toxic metal into aquifers putting the health of populations, livestock, and crops at risk [264]. A well-researched case is the contamination of water for drinking and farming in Bangladesh where arsenic levels often exceed by large margins the recommended values of the World Health Organization. The microbial communities responsible for this mobilization of arsenic are constituted by organisms that are also capable of reducing other metals in the environment such as iron [264].

Another example of the importance of extracellular electron transfer in health is its contribution to biofilm stability. *P. aeruginosa* is a notorious opportunistic

pathogen and the formation of biofilms is modulated by the availability of iron. Interestingly, *P. aeruginosa* can produce phenazines that modulate the redox state of extracellular iron favoring ferrous iron, and this way evades therapies that target ferric iron [265]. These therapies benefit from the knowledge gathered on the structure, reactivity, and selectivity of siderophores. Indeed, siderophores have been used in medical applications since the early 1960s, almost since their discovery [76, 266]. They were first applied to the treatment of iron overload diseases or diseases that require excessive blood transfusions including patients suffering for β-thalassemia. Desferrioxamine, a siderophore produced by *Streptomyces pilosus* was the first example used as a chelating agent for excessive iron, forming ferrioxamine (Fe-complexed form) which is water-soluble and can be easily excreted though the kidneys. Desferrioxamine (branded as Desferal) gave then rise to more effective drugs such as deferiprone (branded as Ferriprox) and deferasirox (branded as Exjade) and these are still used for the treatment of iron overload in diseases that include β-thalassemia, hemochromatosis, and sickle cell disease. These drugs are also used for the treatment of aluminum poisoning [267, 268].

Given the high affinity for iron of siderophores, their use in combating infectious diseases can also be extremely powerful. Overall, the potential role of iron in immunity dates back to the early 1940s, and nowadays it is known that eukaryotic hosts produce proteins such as transferrin that keep the levels of circulating iron in the body too low for microbial growth. This process is known as nutritional immunity and therefore, iron acquisition systems are considered virulence factors. This in turn makes them targets for the development of new therapies against infectious diseases or against cancer where cell proliferation requires high amounts of iron [269]. The overall strategy consists in using siderophores for selective drug delivery in a way that is designated "Trojan Horse" strategy [270]. It consists in a siderophore-based antibiotic where a siderophore is joined with an antibiotic which can further bind iron forming an antibiotic-siderophore-Fe^{3+} complex. The use of these siderophores allows for selective delivery of the antibiotic by exploiting the ability of siderophores to carry iron inside the bacterial cell by interacting with specific receptors at the cell surface. Interestingly, this strategy was not a human invention. Instead, these types of siderophore-antibiotic conjugates exist in nature and are usually referred to as sideromycins. Sideromycins are bacterial molecular weapons for killing other competing and undesired bacterial cheaters preventing them from further stealing of xenophores [271, 272].

5. ENVIRONMENTAL APPLICATIONS

The capacity of microorganisms to perform extracellular electron transfer has been harnessed for environmental remediation and industrial biomining [273]. The latter has most frequently been used to obtain copper and gold from low grade ores in mines but many other metals such as cobalt or uranium can be obtained. Bioremediation uses bacteria or plants (called phytoremediation) to

decontaminate soils or aquatic environments, often with dramatic savings in landscape damage and economic cost versus conventional treatments [274]. Of particular relevance is the decontamination of groundwater in nuclear sites by metal-reducing bacteria. A wide diversity of microorganisms is able to interact with numerous radioactive metals and other elements such as uranium, technetium, neptunium, plutonium, americium, strontium, iodine, and cesium. The case of uranium has been intensively studied and different strategies are used by different organisms that are harnessed to remove this radioactive metal from the groundwater [275]. Numerous metal- and sulfate-reducing bacteria are able to use uranium as terminal electron acceptor and therefore precipitate it out of the aquifer.

In the case of plants, but also for some applications with bacteria, biosorption is a promising strategy for decontamination of metal pollution. This rests on the fact that despite the greater emphasis on the affinity of organisms for iron they can also bind with lesser affinity to toxic metals such as V^{4+}, Cr^{3+}, Al^{3+}, Eu^{3+}, Pb^{2+}, Sn^{2+}, and Tb^{3+}. This property mediated by siderophores and metallophores plays an important role in detoxifying the environment for the microbial community. Lower affinity binding causes heavy-metal bound siderophores not to enter the cell efficiently, preventing in this way the uptake of heavy metals [276]. Furthermore, bacteria secrete other metal uptake systems which may play a key role in detoxification mechanisms [277].

Understanding the assimilatory metal uptake is relevant for the field of microbial ecology and environmental restoration where siderophores can be used to enhance the growth of uncultured microorganisms and to manipulate the microbial community in soils [268]. Currently only 0.1 to 1 % of microbes can be cultivated in the laboratory, a microbiology problem regarded as “the great plate count anomaly” which results from the difficulty of replicating in the laboratory some basic microbial requirements. Several strategies have been employed and the co-culture approach of Lewis, Epstein, and coworkers [278] revealed siderophores as the first class of growth factors for uncultured bacteria [268]. It has been reported that the production of siderophores can be an altruistic behavior where siderophore-producing bacteria are invaded with bacteria that do not produce siderophores but have the ability to utilize them to meet their iron requirements [276]. In this way, siderophores allow the proliferation of multiple microorganisms but also alter and exert control in the soil microbial community. Similarly, to promoting the growth of microorganisms, siderophores can also promote plant growth. Acting simultaneously as potential biocontrol agents and/or used for soil bioremediation. Iron starvation can reduce the quantity and quality of crop production. Utilization of certain types of bacteria such as different *Pseudomonas* species can promote plant growth by secreting siderophores such as pyoverdine. This provides plants with an iron source but also reduces the iron availability for plant pathogens [268]. The other areas where understanding metal uptake in bacteria is the potential use of microorganisms in bioremediation.

6. BIOTECHNOLOGICAL APPLICATIONS

The current excitement surrounding extracellular electron transfer stems very much from the fact that "it sits" at the core of an emerging portfolio of technologies based on bioelectrochemical systems. These systems connect the microbial metabolism to an electrical circuit and this way has the potential to transform industrial biotechnology. Most of the efforts in bioelectrochemical systems are focused on the treatment of wastewater that can be coupled with energy production. This allows to decrease the energy demand on wastewater treatment facilities, that usually are energy- and chemical-intensive and require large investments without any revenue generation [279]. Furthermore, bioelectrochemical systems allow a cheap source of power for other sustainable processes, such as the bioelectrosynthesis of biofuels and useful chemicals, biosensing, and desalination of water [280–282]. Indeed, the ability of microorganisms to receive electrons from a cathode allows them to use wastes for the production of ethanol, butanol, and succinate [283]. Furthermore, these systems are currently being explored for the production of fertilizers from source-separated human urine, contributing to the circular economy of nutrients, whereby valuable nutrients such as phosphorus can be recovered from wastes [284]. Another promising use of bioelectrochemical systems is as biosensors, where the microbe can sense or recognize specific elements allowing the detection of bioactive substances or environmental pollutants [281].

The promising application of microorganisms able to perform extracellular electron transfer in biotechnological applications have increased the discovery of this type of organisms as well as the understanding of the mechanistic processes by which they interact and react with external substrates [154, 190, 285]. Still major breakthroughs and improvements are needed to make bioelectrochemical systems a run-of-the-mill technology for energy production and added-value compounds production from wastes [286, 287].

7. GENERAL CONCLUSIONS

From the sections above it is clear that there are numerous issues still open with regard to the mechanistic details surrounding extracellular redox chemistry. For example, details on the molecular mechanisms of numerous of the metal transporters are still lacking. Even the structures of ferric siderophores and other metallophores are still unknown. This mechanistic and structural knowledge has the potential to impact in the development of strategies to manage infection of eukaryotic hosts, or the productivity of agricultural soils. Concerning the dissimilatory reducing mechanisms, the current paradigm is focused on metabolic routes dominated by multiheme cytochromes but other alternatives are cropping up in the literature [288]. This suggests that we may have just scratched the surface of the subject, with important consequences for sustainable waste management, bioremediation of metal-contaminated environments and mining of low-grade ores. Finally, a very exciting prospect derives from the observation that some

organisms engaged in extracellular redox chemistry are enterobacteria, or closely related. It opens the opportunity to manipulate the microbiome in the gut of multicellular eukaryotes by means of extracellular redox chemistry. Given the strengthening perception of the role of the gut-brain axis in neurological disorders this has the potential to open a new front in the management of debilitating psychiatric, age-related, or neurodegenerative diseases [289]. A precedent of natural community electrically interconnected via extracellular electron transfer exists. It was found surrounding a deep-sea vent [290].

ACKNOWLEDGMENTS

This work was supported by Fundação para a Ciência e a Tecnologia (FCT) Portugal [PTDC/BBB-BQB/4178/2014 and PTDC/BIA-BQM/30176/2017], and PhD fellowship PD/BD/135187/2017, the IBT. This work was funded by national funds through FCT Fundação para a Ciência e a Tecnologia, I.P., Project UIDB/04612/2020 and UIDP/04612/2020. This work has received funding from the European Union's Horizon 2020 research and innovation programme under grant agreement No 810856.

ABBREVIATIONS AND DEFINITIONS

ABC	ATP binding cassette
AMP	adenosine monophosphate
ATP	adenosine 5′-triphosphate
BIF	banded iron formation
DMRO	dissimilatory metal reducing organisms
Dtxr	diphtheria toxin regulator
ECF	energy-coupling factor
EDTA	ethylenediaminetetraacetic acid
FNR	fumarate and nitrate reductase transcriptional regulator
FSE	ferric siderophore esterase
Fur	ferric uptake regulator
GDP	guanosine diphosphate
GOE	great oxidation event
IEP	inner membrane efflux protein
MDR	multidrug resistance
MFS	major facilitator superfamily
MSDs	membrane-spanning domains
Mtr	metal reducing
NADH	nicotinamide adenine dinucleotide
NADPH	nicotinamide adenine dinucleotide phosphate
NBDs	nucleotide-binding domains
NEAT	near-transporter

NiCoT	nickel/cobalt transporters
NIS	NRPS-independent siderophore
Nramp	natural resistance-associated macrophage proteins
NRPS	non-ribosomal peptide synthetase
OEP	outer membrane efflux protein
OMR	outer membrane receptor
Pcc	porin-cytochrome
PEP	periplasmic efflux or accessory protein
RiPP	ribosomally produced and post-translationally modified natural products
RND	resistance, nodulation, and cell division
SAXS	small angle X-ray scattering
SBP	solute-binding proteins
SHE	standard hydrogen electrode
SIP	siderophore-interacting protein

REFERENCES

1. R. R. Chrichton, R. O. Louro, *Practical Approaches to Biological Inorganic Chemistry*, Elsevier, Amsterdam, NL, **2019**.
2. J. J. R. Silva, R. J. P. Williams, *The Natural Selection of the Chemical Elements*, Oxford University Press, Oxford, UK, **1996**.
3. A. L. Sessions, D. M. Doughty, P. V. Welander, R. E. Summons, D. K. Newman, *Curr. Biol.* **2009**, *19*, R567–R574.
4. M. Imbert, R. Blondeau, *Curr. Microbiol.* **1998**, *37*, 64–66.
5. C. D. Hardy, A. Butler, *J. Biol. Inorg. Chem.* **2018**, *23*, 957–967.
6. H. Irving, R. J. P. Williams, *J. Chem. Soc.* **1953**, 3192–3210.
7. A. W. Foster, D. Osman, N. J. Robinson, *J. Biol. Chem.* **2014**, *289*, 28095–28103.
8. A. Musiari, M. Rowinska-Zyrek, S. Gallo, R. K. O. Sigel, *Metal Ions in Ribozymes and Riboswitches*, in *DNA in Supramolecular Chemistry and Nanotechnology*, Eds E. Stulz, G. H. Clever, Wiley, Chichester, UK, **2015**, pp. 412–433.
9. K. I. Wolska, A. M. Grudniak, K. Markowska, *Inhibition of Bacterial Quorum Sensing Systems by Metal Nanoparticles*, in *Metal Nanoparticles in Pharma*, Eds M. Rai, R. Shegokar, Springer International, Cham, Switzerland, **2017**, pp. 123–138.
10. S. Grumbein, M. Opitz, O. Lieleg, *Metallomics* **2014**, *6*, 1441–1450.
11. C. Andreini, I. Bertini, G. Cavallaro, G. L. Holliday, J. M. Thornton, *J. Biol. Inorg. Chem.* **2008**, *13*, 1205–1218.
12. K. J. Waldron, J. C. Rutherford, D. Ford, N. J. Robinson, *Nature* **2009**, *460*, 823–830.
13. I. Bertini, C. Luchinat, R. Monnanni, *J. Chem. Inf. Model.* **1985**, *62*, 923–927.
14. J. P. Perreault, S. Altman, *J. Mol. Biol.* **1993**, *230*, 750–756.
15. K. Serec, S. D. Babić, R. Podgornik, S. Tomić, *Nucleic Acids Res.* **2016**, *44*, 8456–8464.
16. D. Staniec, M. Ksiazek, I. B. Thøgersen, J. J. Enghild, A. Sroka, D. Bryzek, M. Bogyo, M. Abrahamson, J. Potempa, *J. Biol. Chem.* **2015**, *290*, 27248–27260.
17. J. Liu, S. Chakraborty, P. Hosseinzadeh, Y. Yu, S. Tian, I. Petrik, A. Bhagi, Y. Lu, *Chem. Rev.* **2014**, *114*, 4366–4369.
18. C. Kisker, H. Schindelin, D. C. Rees, *Annu. Rev. Biochem.* **1997**, *66*, 233–267.
19. J. L. Boer, S. B. Mulrooney, R. P. Hausinger, *Arch. Biochem. Biophys.* **2014**, *544*, 142–152.

20. R. Golonka, B. S. Yeoh, M. Vijay-Kumar, *J. Innate Immun.* **2019**, *11*, 249–262.
21. L. D. Palmer, E. P. Skaar, *Annu. Rev. Genet.* **2016**, *50*, 67–91.
22. J. M. Vraspir, A. Butler, *Ann. Rev. Mar. Sci.* **2009**, *1*, 43–63.
23. C. Sissi, M. Palumbo, *Nucleic Acids Res.* **2009**, *37*, 702–711.
24. E. A. Groisman, K. Hollands, M. A. Kriner, E. Lee, S. Park, M. H. Pontes, *Annu. Rev. Genet.* **2003**, *47*, 625–646.
25. S. P. Hmiel, M. D. Snavely, C. G. Miller, M. E. Maguire, *J. Bacteriol.* **1986**, *168*, 1444–1450.
26. S. P. Hmiel, M. D. Snavely, J. B. Florer, M. E. Maguire, C. G. Miller, *J. Bacteriol.* **1989**, *171*, 4742–4751.
27. R. L. Smith, L. J. Thompson, M. E. Maguire, *J. Bacteriol.* **1995**, *177*, 1233–1238.
28. E. E. Snyder, B. W. Buoscio, J. J. Flake, *Biochemistry* **1990**, *29*, 3937–3943.
29. D. C. Dominguez, *Mol. Microbiol.* **2004**, *54*, 291–297.
30. J. W. Rosch, J. Sublett, G. Gao, Y. D. Wang, E. I. Tuomanen, *Mol. Microbiol.* **2008**, *70*, 435–444.
31. H. K. Gupta, S. Shrivastava, R. Sharma, R. Ross, J. P. Bellenger, T. Wichard, A. B. Kustka, A. M. L. Kraepiel, M. C. Hoffmann, K. Ali, M. Sonnenschein, L. Robrahn, D. Strauss, F. Narberhaus, B. Masepohl, M. Si, C. Zhao, B. Burkinshaw, B. Zhang, D. Wei, Y. Wang, T. G. Dong, X. Shen, *Mol. Microbiol.* **2017**, *101*, 1–14.
32. R. N. Reusch, R. Huang, L. L. Bramble, *Biophys. J.* **1995**, *69*, 754–766.
33. Y. Chang, R. Bruni, B. Kloss, Z. Assur, E. Kloppmann, B. Rost, W. A. Hendrickson, Q. Liu, *Science* **2014**, *344*, 1131–1135.
34. H. K. Gupta, S. Shrivastava, R. Sharma, *Mbio* **2017**, *8*, 1–14.
35. K. A. McCall, C. Huang, C. A. Fierke, *J. Nutr.* **2000**, *130*, 1344S-1349S.
36. K. Hantke, *Curr. Opin. Microbiol.* **2005**, *8*, 196–202.
37. G. Porcheron, A. Garénaux, J. Proulx, M. Sabri, C. M. Dozois, *Front. Cell. Infect. Microbiol.* **2013**, *3*, 1–24.
38. C. A. Blindauer, *Chem. Commun.* **2015**, *51*, 4544–4563.
39. D. A. Capdevila, J. Wang, D. P. Giedroc, *J. Biol. Chem.* **2016**, *291*, 20858–20868.
40. J. Schröder, N. Jochmann, D. A. Rodionov, A. Tauch, *BMC Genomics* **2010**, *11*.
41. G. Grass, M. D. Wong, B. P. Rosen, R. L. Smith, C. Rensing, *J. Bacteriol.* **2002**, *184*, 864–866.
42. A. Proschak, J. Kramer, E. Proschak, T. A. Wichelhaus, *J. Antimicrob. Chemother.* **2018**, *73*, 425–430.
43. D. DeShazer, *Microbiol. Res.* **2019**, *226*, 48–54.
44. J. Henrot, *Health Phys.* **1989**, *57*, 239–245.
45. E. D. Weinberg, *Perspect. Biol. Med.* **1997**, *40*, 578–583.
46. M. Elli, R. Zink, A. Rytz, R. Reniero, L. Morelli, *J. Appl. Microbiol.* **2000**, *88*, 695–703.
47. R. R. Crichton, J. L. Pierre, *BioMetals* **2001**, *14*, 99–112.
48. C. K. Y. Lau, K. D. Krewulak, H. J. Vogel, *FEMS Microbiol. Rev.* **2016**, *40*, 273–298.
49. G. M. Rodriguez, I. Smith, *J. Bacteriol.* **2006**, *188*, 424–430.
50. J. Leong, K. N. Raymond, *J. Am. Chem. Soc.* **1974**, *96*, 1757–1762.
51. C. Wandersman, P. Delepelaire, *Annu. Rev. Microbiol.* **2004**, *58*, 611–647.
52. R. A. Festa, D. J. Thiele, *Curr. Biol.* **2011**, *21*, R877–R883.
53. J. Quintana, L. Novoa-Aponte, J. M. Argüello, *J. Biol. Chem.* **2017**, *292*, 15691–15704.
54. P. Palumaa, *FEBS Lett.* **2013**, *587*, 1902–1910.
55. Y. Fu, F. M. J. Chang, D. P. Giedroc, *Acc. Chem. Res.* **2014**, *47*, 3605–3613.
56. J. F. Lutkenhaus, *J. Bacteriol.* **1977**, *131*, 631–637.
57. S. D. Springer, A. Butler, *Coord. Chem. Rev.* **2016**, *306*, 628–635.
58. D. G. Kehres, M. E. Maguire, *FEMS Microbiol. Rev.* **2003**, *27*, 263–290.
59. J. D. Aguirre, V. C. Culotta, *J. Biol. Chem.* **2012**, *287*, 13541–13548.

60. J. S. Klein, O. Lewinson, *Metallomics* **2011**, *3*, 1098–1108.
61. Glowicz, *Physiol. Behav.* **2017**, *176*, 139–148.
62. K. M. Papp-Wallace, M. E. Maguire, *Annu. Rev. Microbiol.* **2006**, *60*, 187–209.
63. B. Kräutler, *Encycl. Inorg. Bioinorg. Chem.* **2004**, *12*, 1–26.
64. R. Banerjee, S. W. Ragsdale, *Annu. Rev. Biochem.* **2003**, *72*, 209–247.
65. T. Eitinger, *Encycl. Inorg. Bioinorg. Chem.* **2004**, 1–10.
66. R. R. Mendel, *Dalton Trans.* **2005**, 3404–3409.
67. R. Bjornsson, F. A. Lima, T. Spatzal, T. Weyhermüller, P. Glatzel, E. Bill, O. Einsle, F. Neese, S. Debeer, *Chem. Sci.* **2014**, *5*, 3096–3103.
68. J. P. Bellenger, T. Wichard, A. B. Kustka, A. M. L. Kraepiel, *Nat. Geosci.* **2008**, *1*, 243–246.
69. S. B. Mulrooney, R. P. Hausinger, *FEMS Microbiol. Rev.* **2003**, *27*, 239–261.
70. A. J. Rice, A. Park, H. W. Pinkett, *Crit. Rev. Biochem. Mol. Biol.* **2014**, *49*, 426–437.
71. O. Lewinson, N. Livnat-Levanon, *J. Mol. Biol.* **2017**, *429*, 606–619.
72. G. H. Scheepers, J. A. Lycklama A Nijeholt, B. Poolman, *FEBS Lett.* **2016**, *590*, 4393–4401.
73. M. Kammler, C. Schon, K. Hantke, *J. Bacteriol.* **1993**, *175*, 6212–6219.
74. M. L. Cartron, S. Maddocks, P. Gillingham, C. J. Craven, S. C. Andrews, *BioMetals* **2006**, *19*, 143–157.
75. A. E. Sestok, R. O. Linkous, A. T. Smith, *Metallomics* **2018**, *10*, 887–898.
76. R. C. Hider, X. Kong, *Nat. Prod. Rep.* **2010**, *27*, 637–657.
77. G. E. Kenney, A. Rosenzweig, *Annu. Rev. Biochem.* **2018**, *87*, 645–676.
78. T. C. Johnstone, E. M. Nolan, *Dalt. Trans.* **2015**, *44*, 6320–6339.
79. A. A. DiSpirito, J. D. Semrau, J. C. Murrell, W. H. Gallagher, C. Dennison, S. Vuilleumier, *Microbiol. Mol. Biol. Rev.* **2016**, *80*, 387–409.
80. H. J. Kim, N. Galeva, C. K. Larive, M. Alterman, D. W. Graham, *Biochemistry* **2005**, *44*, 5140–5148.
81. C. Correnti, R. K. Strong, *J. Biol. Chem.* **2012**, *287*, 13524–13531.
82. J. C. Renshaw, G. D. Robson, A. P. J. Trinci, M. G. Wiebe, F. R. Livens, D. Collison, R. J. Taylor, *Mycol. Res.* **2002**, *106*, 1123–1142.
83. B. R. Wilson, A. R. Bogdan, M. Miyazawa, K. Hashimoto, Y. Tsuji, *Trends Mol. Med.* **2016**, *22*, 1077–1090.
84. K. T. Schiessl, E. M. L. Janssen, S. M. Kraemer, K. McNeill, M. Ackermann, *Front. Microbiol.* **2017**, *8*, 1–11.
85. M. Miethke, M. A. Marahiel, *Microbiol. Mol. Biol. Rev.* **2007**, *71*, 413–451.
86. W. R. Harris, C. J. Carrano, S. R. Cooper, S. R. Sofen, A. E. Avdeef, J. V. McArdle, K. N. Raymond, *J. Am. Chem. Soc.* **1979**, *101*, 6097–6104.
87. M. Vargas, K. Kashefi, E. L. Blunt-Harris, D. R. Lovley, *Nature* **1998**, *395*, 65–67.
88. W. R. Harris, K. N. Raymond, *J. Am. Chem. Soc.* **1979**, *101*, 6534–6541.
89. B. Kunze, H. Reichenbach, N. Bedorf, W. Kohl, G. Höfle, *J. Antibiot.* **1989**, *42*, 14–17.
90. W. J. Page, M. V. Tigerstrom, *Microbiology* **1988**, *134*, 453–460.
91. J. Brandel, N. Humbert, M. Elhabiri, I. J. Schalk, G. L. A. Mislin, A. M. Albrecht-Gary, *Dalton Trans.* **2012**, *41*, 2820–2834.
92. E. I. Koh, A. E. Robinson, N. Bandara, B. E. Rogers, J. P. Henderson, *Nat. Chem. Biol.* **2017**, *13*, 1016–1021.
93. Z. Hou, K. N. Raymond, B. O'Sullivan, T. W. Esker, T. Nishio, *Inorg. Chem.* **1998**, *37*, 6630–6637.
94. C. J. Carrano, H. Drechsel, D. Kaiser, G. Jung, B. Matzanke, G. Winkelmann, N. Rochel, A. M. Albrecht-Gary, *Inorg. Chem.* **1996**, *35*, 6429–6436.
95. J. S. Martinez, J. N. Carter-Franklin, E. L. Mann, J. D. Martin, M. G. Haygood, A. Butler, *Proc. Natl. Acad. Sci. USA* **2003**, *100*, 3754–3759.

96. J. S. Martinez, A. Butler, *J. Inorg. Biochem.* **2007**, *101*, 1692–1698.
97. A. Butler, *BioMetals* **2005**, *18*, 369–374.
98. K. Barbeau, E. L. Rue, C. G. Trick, K. W. Bruland, A. Butler, *Limnol. Oceanogr.* **2003**, *48*, 1069–1078.
99. B. Troxell, H. M. Hassan, *Front. Cell. Infect. Microbiol.* **2013**, *4*, 1–13.
100. C. A. Kunkle, M. P. Schmitt, *J. Bacteriol.* **2005**, *187*, 422–433.
101. C. S. Carroll, M. M. Moore, *Crit. Rev. Biochem. Mol. Biol.* **2018**, *53*, 356–381.
102. A. M. Gehring, I. Mori, C. T. Walsh, *Biochemistry* **1998**, *37*, 2648–2659.
103. L. E. N. Quadri, J. Sello, T. A. Keating, P. H. Weinreb, C. T. Walsh, *Chem. Biol.* **1998**, *5*, 631–645.
104. T. A. Keating, C. G. Marshall, C. T. Walsh, *Biochemistry* **2000**, *39*, 15522–15530.
105. G. H. Hur, C. R. Vickery, M. D. Burkart, *Nat. Prod. Rep.* **2012**, *29*, 1074–1098.
106. M. A. Skinnider, C. A. Dejong, P. N. Rees, C. W. Johnston, H. Li, A. L. H. Webster, M. A. Wyatt, N. A. Magarvey, *Nucleic Acids Res.* **2015**, *43*, 9645–9662.
107. M. H. Medema, K. Blin, P. Cimermancic, V. De Jager, P. Zakrzewski, M. A. Fischbach, T. Weber, E. Takano, R. Breitling, *Nucleic Acids Res.* **2011**, *39*, 339–346.
108. Z. L. Reitz, C. D. Hardy, J. Suk, J. Bouvet, A. Butler, *Proc. Natl. Acad. Sci. USA* **2019**, *116*, 19805–19814.
109. V. De Lorenzo, A. Bindereif, B. H. Paw, J. B. Neilands, *J. Bacteriol.* **1986**, *165*, 570–578.
110. V. De Lorenzo, J. B. Neilands, *J. Bacteriol.* **1986**, *167*, 350–355.
111. J. L. Furrer, D. N. Sanders, I. G. Hook-Barnard, M. A. McIntosh, *Mol. Microbiol.* **2002**, *44*, 1225–1234.
112. E. M. Quistgaard, C. Löw, F. Guettou, P. Nordlund, *Nat. Rev. Mol. Cell Biol.* **2016**, *17*, 123–132.
113. K. Nicolaisen, A. Hahn, M. Valdebenito, S. Moslavac, A. Samborski, I. Maldener, C. Wilken, A. Valladares, E. Flores, K. Hantke, E. Schleiff, *Biochim. Biophys. ActaBiomembr.* **2010**, *1798*, 2131–2140.
114. M. Hannauer, E. Yeterian, L. W. Martin, I. L. Lamont, I. J. Schalk, *FEBS Lett.* **2010**, *584*, 4751–4755.
115. T. Tanabe, T. Funahashi, H. Nakao, S. I. Miyoshi, S. Shinoda, S. Yamamoto, *J. Bacteriol.* **2003**, *185*, 6938–6949.
116. C. H. Chatfield, B. J. Mulhern, V. K. Viswanathan, N. P. Cianciotto, *Microbiology* **2012**, *158*, 721–735.
117. A. K. Hagan, A. Tripathi, D. Berger, D. H. Sherman, P. C. Hanna, *mBio* **2017**, *8*, e01238–17.
118. T. Horiyama, K. Nishino, *PLoS ONE* **2014**, *9*, e10864.
119. G. Grass, *BioMetals* **2006**, *19*, 159–172.
120. R. M. Wells, C. M. Jones, Z. Xi, A. Speer, O. Danilchanka, K. S. Doornbos, P. Sun, F. Wu, C. Tian, M. Niederweis, *PLoS Pathog.* **2013**, *9*, e1003120.
121. C. M. Jones, R. M. Wells, A. V. R. Madduri, M. B. Renfrow, C. Ratledge, D. B. Moody, M. Niederweis, *Proc. Natl. Acad. Sci. USA* **2014**, *111*, 1945–1950.
122. W. Zhu, J. E. L. Arceneaux, M. L. Beggs, B. R. Byers, K. D. Eisenach, M. D. Lundrigan, *Mol. Microbiol.* **1998**, *29*, 629–639.
123. M. L. V Crouch, M. Castor, J. E. Karlinsey, T. Kalhorn, F. C. Fang, *Mol. Microbiol.* **2008**, *67*, 971–983.
124. K. N. Raymond, B. E. Allred, A. K. Sia, *Acc. Chem. Res.* **2015**, *48*, 2496–2505.
125. H. I. Zgurskaya, H. Nikaido, *Mol. Microbiol.* **2000**, *37*, 219–225.
126. C. Alvarez-Ortega, J. Olivares, J. L. Martínez, *Front. Microbiol.* **2013**, *4*, 1–11.
127. A. Hahn, M. Stevanovic, O. Mirus, E. Schleiff, *J. Biol. Chem.* **2012**, *287*, 41126–41138.
128. T. Fukushima, B. E. Allred, A. K. Sia, R. Nichiporuk, U. N. Andersen, K. N. Raymond, *Proc. Natl. Acad. Sci.USA* **2013**, *110*, 13821–13826.

129. T. Fukushima, B. E. Allred, K. N. Raymond, *ACS Chem. Biol.* **2014**, *9*, 2092–2100.
130. S. Dhungana, A. L. Crumbliss, *Geomicrobiol. J.* **2005**, *22*, 87–98.
131. A. L. Crumbliss, J. M. Harrington, *Adv. Inorg. Chem.* **2009**, *61*, 179–250.
132. R. J. Abergel, A. M. Zawadzka, T. M. Hoette, K. N. Raymond, *J. Am. Chem. Soc.* **2009**, *131*, 12682–12692.
133. M. Gründlinger, F. Gsaller, M. Schrettl, H. Lindner, H. Haasa, *Appl. Environ. Microbiol.* **2013**, *79*, 7534–7536.
134. M. Miethke, J. Hou, M. A. Marahiel, *Biochemistry* **2011**, *50*, 10951–10964.
135. K. Li, W. H. Chen, S. D. Bruner, *Biochemistry* **2015**, *54*, 3989–4000.
136. B. F. Matzanke, S. Anemuller, V. Schünemann, A. X. Trautwein, K. Hantke, *Biochemistry* **2004**, *43*, 1386–1392.
137. S. Cescau, H. Cwerman, S. Létoffé, P. Delepelaire, C. Wandersman, F. Biville, *BioMetals* **2007**, *20*, 603–613.
138. R. Grinter, P. M. Leung, L. C. Wijeyewickrema, D. Littler, S. Beckham, R. N. Pike, D. Walker, C. Greening, T. Lithgow, *PLoS Genet.* **2019**, *15*, e1008435.
139. D. R. Lovley, *ASM News* **2002**, *68*, 231–237.
140. J. R. Lloyd, D. R. Lovley, *Curr. Opin. Biotechnol.* **2001**, *12*, 248–253.
141. D. J. Richardson, *Microbiology* **2000**, *146*, 551–571.
142. W. E. Adeney, *Sci. Proc. R. Dublin Soc.* **1984**, *VIII*, 247–251.
143. D. R. Lovley, *Microbiol. Rev.* **1991**, *55*, 259–287.
144. D. R. Lovley, E. J. P. Phillips, *App. Env. Microbiol.* **1988**, *54*, 1472–1480.
145. C. R. Myers, K. H. Nealson, *Science* **1988**, *240*, 1319–1321.
146. K. Rabaey, J. Rodríguez, L. L. Blackall, J. Keller, P. Gross, D. Batstone, W. Verstraete, K. H. Nealson, *ISME J.* **2007**, *1*, 9–18.
147. B. E. Logan, B. Hamelers, R. Rozendal, U. Schröder, J. Keller, S. Freguia, P. Aelterman, W. Verstraete, K. Rabaey, *Environ. Sci. Technol.* **2006**, *40*, 5181–5192.
148. D. R. Lovley, *Annu. Rev. Microbiol.* **1993**, *47*, 263–290.
149. K. C. Wrighton, P. Agbo, F. Warnecke, K. A. Weber, E. L. Brodie, T. Z. DeSantis, P. Hugenholtz, G. L. Andersen, J. D. Coates, *ISME J.* **2008**, *2*, 1146–1156.
150. J. A. Smith, M. Aklujkar, C. Risso, C. Leang, L. Giloteaux, D. E. Holmes, *Appl. Environ. Microbiol.* **2015**, *81*, 2735–2744.
151. K. A. Weber, L. A. Achenbach, J. D. Coates, *Nat. Rev. Microbiol.* **2006**, *4*, 752–764.
152. L. Shi, H. Dong, G. Reguera, H. Beyenal, A. Lu, J. Liu, H. Q. Yu, J. K. Fredrickson, *Nat. Rev. Microbiol.* **2016**, *14*, 651–662.
153. A. Kumar, L. H. H. Hsu, P. Kavanagh, F. Barrière, P. N. L. Lens, L. Lapinsonnière, J. H. Lienhard, U. Schröder, X. Jiang, D. Leech, *Nat. Rev. Chem.* **2017**, *1*, 1–13.
154. S. Beblawy, T. Bursac, C. Paquete, R. Louro, T. A. Clarke, J. Gescher, *Mol. Microbiol.* **2018**, *109*, 571–583.
155. T. C. Santos, M. A. Silva, L. Morgado, J. M. Dantas, C. A. Salgueiro, *DaltonTrans.* **2015**, *44*, 9335–9344.
156. D. R. Lovley, S. J. Giovannoni, D. C. White, J. E. Champine, E. J. Phillips, Y. A. Gorby, S. Goodwin, *Arch. Microbiol.* **1993**, *159*, 336–344.
157. D. R. Lovley, J. F. Stolz, G. L. Nord, Jr.,E. J. P. Phillips, *Nature* **1987**, *330*, 252–254.
158. S. R. Kane, H. R. Beller, T. C. Legler, R. T. Anderson, *Biodegradation* **2002**, *13*, 149–154.
159. H. Zhang, H. Fu, J. Wang, L. Sun, Y. Jiang, L. Zhang, H. Gao, *PLoS ONE* **2013**, *8*, e62629.
160. E. D. Melton, E. D. Swanner, S. Behrens, C. Schmidt, A. Kappler, *Nat. Rev. Microbiol.* **2014**, *12*, 797–808.
161. N. Pfennig, H. Biebl, *Arch. Microbiol.* **1976**, *110*, 3–12.
162. E. E. Roden, D. R. Lovley, *Appl. Environ. Microbiol.* **1993**, *59*, 734–742.

163. H. S. Park, S. Lin, G. Voordouw, *Antonie van Leeuwenhoek, Int. J. Gen. Mol. Microbiol.* **2008**, *93*, 79–85.
164. D. R. Lovley, E. E. Roden, E. Phillips, J. Woodward, *Marine Geol.* **1993**, *113*, 41–53.
165. A. Das, A. K. Mishra, P. Roy, *FEMS Microbiol. Lett.* **1992**, *97*, 167–172.
166. T. D. Brock, J. Gustafson, *Appl. Environ. Microbiol.* **1976**, *32*, 567–571.
167. D. R. Lovley, *Annu. Rev. Microbiol.* **2012**, *66*, 391–409.
168. S. V. Liu, J. Zhou, C. Zhang, D. R. Cole, M. Gajdarziska-Josifovska, T. J. Phelps, *Science* **1997**, *277*, 1106–1109.
169. D. G. Zavarzina, T. G. Sokolova, T. P. Tourova, N. A. Chernyh, N. A. Kostrikina, E. A. Bonch-Osmolovskaya, *Extremophiles* **2007**, *11*, 1–7.
170. D. R. Lovley, *Origins*, Kluwer Academic Publishers, Dordrecht, NL **2004**, pp. 299–313.
171. K. H. Nealson, C. R. Myers, *Appl. Environ. Microbiol.* **1992**, *58*, 439–443.
172. V. V Balashova, G. A. Zavarzin, *Mikrobiologiia* **1979**, *48*, 773–778.
173. D. E. Cummings, F. Caccavo, S. Spring, R. F. Rosenzweig, *Arch. Microbiol.* **1999**, *171*, 183–188.
174. R. Wufuer, Y. Wei, Q. Lin, H. Wang, W. Song, W. Liu, D. Zhang, X. Pan, G. M. Gadd, *Adv. Appl. Microbiol.* **2017**, *101*, 137–168.
175. K. Kashefi, J. M. Tor, K. P. Nevin, D. R. Lovley, *Appl. Environ. Microbiol.* **2001**, *67*, 3275–3279.
176. J. W. Doran, *Adv. Microbial Ecol.* **1982**, pp. 1–32.
177. Y. V Nancharaiah, P. N. L. Lens, *Microbiol. Mol. Biol. Rev.* **2015**, *79*, 61–80.
178. S. Dhanjal, S. S. Cameotra, *Microb. Cell Fact.* **2010**, *9*, 52.
179. G. A. Burton, T. H. Giddings, P. DeBrine, R. Fall, *Appl. Environ. Microbiol.* **1987**, *53*, 185–188.
180. Y. Wang, X. Shu, Q. Zhou, T. Fan, T. Wang, X. Chen, M. Li, Y. Ma, J. Ni, J. Hou, W. Zhao, R. Li, S. Huang, L. Wu, *Int. J. Mol. Sci.* **2018**, *19*, 2799.
181. V. E. Levine, *Am. J. Bot.* **1925**, *12*, 82–90.
182. J. B. Robinson, O. H. Tuovinen, *Microbiol. Rev.* **1984**, *48*, 95–124.
183. E. C. Butler, L. Chen, C. M. Hansel, L. R. Krumholz, A. S. Elwood Madden, Y. Lan, *Environ. Sci. Process. Impacts* **2015**, *17*, 1930–1940.
184. N. L. Brown, *Trends Biochem. Sci.* **1985**, *10*, 400–403.
185. E. J. Kerin, C. C. Gilmour, E. Roden, M. T. Suzuki, J. D. Coates, R. P. Mason, *Appl. Environ. Microbiol.* **2006**, *72*, 7919–7921.
186. H. A. Wiatrowski, P. M. Ward, T. Barkay, *Environ. Sci. Technol.* **2006**, *40*, 6690–6696.
187. W. Carpentier, K. Sandra, I. De Smet, A. Brigé, L. De Smet, J. Van Beeumen, *Appl. Environ. Microbiol.* **2003**, *69*, 3636–3639.
188. W. Carpentier, *Appl. Environ. Microbiol.* **2003**, *69*, 3636–3639.
189. N. N. Lyalkova, N. A. Yurkova, *Geomicrobiol. J.* **1992**, *10*, 15–26.
190. N. L. Costa, T. A. Clarke, L.-A. Philipp, J. Gescher, R. O. Louro, C. M. Paquete, *Bioresour. Technol.* **2018**, *255*, 308–317.
191. S. Pirbadian, S. E. Barchinger, K. M. Leung, H. S. Byun, Y. Jangir, R. A. Bouhenni, S. B. Reed, M. F. Romine, D. A. Saffarini, L. Shi, Y. A. Gorby, J. H. Golbeck, M. Y. El-Naggar, *Proc. Natl. Acad. Sci. USA* **2014**, *111*, 12883–12888.
192. G. Reguera, *Microb. Biotechnol.* **2018**, *11*, 979–994.
193. E. Marsili, D. B. Baron, I. D. Shikhare, D. Coursolle, J. A. Gralnick, D. R. Bond, *Proc. Natl. Acad. Sci. USA* **2008**, *105*, 3968–3973.
194. H. Von Canstein, J. Ogawa, S. Shimizu, J. R. Lloyd, *Appl. Environ. Microbiol.* **2008**, *74*, 615–623.
195. D. R. Lovley, J. D. Coates, E. L. Blunt-Harris, E. J. P. Phillips, J. C. Woodward, *Nature* **1996**, *382*, 445–448.

196. D. J. Richardson, J. K. Fredrickson, J. M. Zachara, *Biochem. Soc. Trans.* **2012**, *40*, 1163–1166.
197. E. Chen, M. J. Wood, A. L. Fink, D. S. Kliger, *Biochemistry* **1998**, *37*, 5589–5598.
198. C. E. Levar, C. H. Chan, M. G. Mehta-kolte, D. R. Bond, *Mbio* **2014**, *5*, e02034.
199. G. F. White, M. J. Edwards, L. Gomez-Perez, D. J. Richardson, J. N. Butt, T. A. Clarke, *Adv. Microb. Physiol.* **2016**, *68*, 87–138.
200. L. Zacharoff, C. H. Chan, D. R. Bond, *Bioelectrochemistry* **2016**, *107*, 7–13.
201. C. R. Myers, J. M. Myers, *J. Bacteriol.* **1997**, *179*, 1143–1152.
202. E. H. J. Gordon, A. D. Pike, A. E. Hill, P. M. Cuthbertson, S. K. Chapman, G. A. Reid, *Biochem J.* **2000**, *349*, 153–158.
203. G. Sturm, K. Richter, A. Doetsch, H. Heide, R. O. Louro, J. Gescher, *ISME J.* **2015**, *9*, 1802–1811.
204. L. Morgado, M. Bruix, M. Pessanha, Y. Y. Londer, C. A. Salgueiro, M. Brulx, M. Pessanha, Y. Y. Londer, C. A. Salgueiro, *Biophys. J.* **2010**, *99*, 293–301.
205. I. J. Correia, C. M. Paquete, R. O. Louro, T. Catarino, D. L. Turner, A. V. Xavier, *Eur. J. Biochem.* **2002**, *5730*, 5722–5730.
206. R. S. Hartshorne, B. N. Jepson, T. A. Clarke, S. J. Field, J. Fredrickson, J. Zachara, L. Shi, J. N. Butt, D. J. Richardson, *J. Biol. Inorg. Chem.* **2007**, *12*, 1083–1094.
207. N. L. Costa, B. Hermann, V. Fourmond, M. M. Faustino, M. Teixeira, O. Einsle, C. M. Paquete, R. O. Louro, *mBIO* **2019**, *10*, e01210–19.
208. E. D. Brutinel, J. A. Gralnick, *Appl. Microbiol. Biotechnol.* **2012**, *93*, 41–48.
209. D. J. Richardson, J. N. Butt, J. K. Fredrickson, J. M. Zachara, L. Shi, M. J. Edwards, G. White, N. Baiden, A. J. Gates, S. J. Marritt, T. A. Clarke, *Mol. Microbiol.* **2012**, *85*, 201–212.
210. L. Shi, K. M. Rosso, T. A. Clarke, D. J. Richardson, J. M. Zachara, J. K. Fredrickson, *Front. Microbiol.* **2012**, *3*, 1–10.
211. M. Schicklberger, G. Sturm, J. Gescher, *Appl. Environ. Microbiol.* **2013**, *79*, 1150–1159.
212. D. Coursolle, J. A. Gralnick, *Mol. Microbiol.* **2010**, *77*, 995–1008.
213. J. A. Gralnick, H. Vali, D. P. Lies, D. K. Newman, *Proc. Natl. Acad. Sci. USA* **2006**, *103*, 4669–4674.
214. B. M. Fonseca, C. M. Paquete, S. E. Neto, I. Pacheco, C. M. Soares, R. O. Louro, *Biochem. J.* **2013**, *449*, 101–108.
215. M. N. Alves, S. E. Neto, A. S. Alves, B. M. Fonseca, A. Carrêlo, I. Pacheco, C. M. Paquete, C. M. Soares, R. O. Louro, *Front. Microbiol.* **2015**, *6*, 665.
216. J. M. Myers, C. R. Myers, *J. Bacteriol.* **2000**, *182*, 67–75.
217. C. Schwalb, S. K. Chapman, G. A. Reid, *Biochemistry* **2003**, *42*, 9491–9497.
218. C. M. Paquete, I. H. Saraiva, R. O. Louro, *Biochim. Biophys. Acta* **2014**, *1837*, 717–725.
219. M. J. Edwards, G. F. White, C. W. Lockwood, M. C. Lawes, A. Martel, G. Harris, D. J. Scott, D. J. Richardson, J. N. Butt, T. A. Clarke, *J. Biol. Chem.* **2018**, *293*, 8103–8112.
220. R. S. Hartshorne, C. L. Reardon, D. Ross, J. Nuester, T. A. Clarke, A. J. Gates, P. C. Mills, J. K. Fredrickson, J. M. Zachara, L. Shi, A. S. Beliaev, M. J. Marshall, M. Tien, S. Brantley, J. N. Butt, D. J. Richardson, *Proc. Natl. Acad. Sci. USA* **2009**, *106*, 22169–22174.
221. M. Schicklberger, C. Bücking, B. Schuetz, H. Heide, J. Gescher, *Appl. Environ. Microbiol.* **2011**, *77*, 1520–1523.
222. M. A. Firer-Sherwood, N. Ando, C. L. Drennan, S. J. Elliott, *J. Phys. Chem. B* **2011**, *115*, 11208–11214.
223. J. S. McLean, P. D. Majors, C. L. Reardon, C. L. Bilskis, S. B. Reed, M. F. Romine, J. K. Fredrickson, *J. Microbiol. Methods* **2008**, *74*, 47–56.
224. D. Coursolle, J. A. Gralnick, *Front. Microbiol.* **2012**, *3*, 1–11.

225. G. Sturm, K. Richter, A. Doetsch, H. Heide, R. O. Louro, J. Gescher, *ISME J.* **2015**, *9*, 1802–1811.
226. H. Gao, S. Barua, Y. Liang, L. Wu, Y. Dong, S. Reed, J. Chen, D. Culley, D. Kennedy, Y. Yang, Z. He, K. H. Nealson, J. K. Fredrickson, J. M. Tiedje, M. Romini, J. Zhou, *Microb. Biotechnol.* **2010**, *3*, 455–466.
227. J. M. Myers, C. R. Myers, *Science* **1998**, *1373*, 237–251.
228. C. R. Myers, J. M. Myers, *Appl. Environ. Microbiol.* **2002**, *68*, 5585–5594.
229. C. M. Paquete, B. M. Fonseca, D. R. Cruz, T. M. Pereira, I. Pacheco, C. M. Soares, R. O. Louro, *Front. Microbiol.* **2014**, *5*, 318.
230. D. E. Ross, S. L. Brantley, M. Tien, *Appl. Environ. Microbiol.* **2009**, *75*, 5218–5226.
231. B. H. Lower, L. Shi, R. Yongsunthon, T. C. Droubay, D. E. Mccready, S. K. Lower, *J. Bacteriol.* **2007**, *189*, 4944–4952.
232. J. K. Fredrickson, M. F. Romine, A. S. Beliaev, J. M. Auchtung, M. E. Driscoll, T. S. Gardner, K. H. Nealson, A. L. Osterman, G. Pinchuk, J. L. Reed, D. A. Rodionov, J. L. M. Rodrigues, D. A. Saffarini, M. H. Serres, A. M. Spormann, I. B. Zhulin, J. M. Tiedje, *Nat. Rev. Microbiol.* **2008**, *6*, 592–603.
233. D. Coursolle, D. B. Baron, D. R. Bond, J. A. Gralnick, *J. Bacteriol.* **2010**, *192*, 467–474.
234. A. Okamoto, R. Nakamura, K. H. Nealson, K. Hashimoto, *ChemElectroChem* **2014**, *1*, 1808–1812.
235. M. J. Edwards, G. F. White, M. Norman, A. Tome-Fernandez, E. Ainsworth, L. Shi, J. K. Fredrickson, J. M. Zachara, J. N. Butt, D. J. Richardson, T. A. Clarke, *Sci. Rep.* **2015**, *5*, 11677.
236. Y. A. Gorby, S. Yanina, J. S. Mclean, K. M. Rosso, D. Moyles, A. Dohnalkova, T. J. Beveridge, I. S. Chang, B. H. Kim, K. S. Kim, D. E. Culley, S. B. Reed, M. F. Romine, D. A. Saffarini, E. A. Hill, L. Shi, D. A. Elias, D. W. Kennedy, G. Pinchuk, K. Watanabe, S. Ishii, B. Logan, K. H. Nealson, J. K. Fredrickson, *Proc. Natl. Acad. Sci. USA* **2006**, *103*, 11358–11363.
237. S. M. Strycharz-Glaven, R. M. Snider, A. Guiseppi-Elie, L. M. Tender, *Energy Environ. Sci.* **2011**, *4*, 4366–4379.
238. P. Subramanian, S. Pirbadian, M. Y. El-naggar, G. J. Jensen, *Proc. Natl. Acad. Sci. USA* **2018**, *115*, E3246–E3255.
239. D.-B. Li, Y.-Y. Cheng, C. Wu, W.-W. Li, N. Li, Z.-C. Yang, Z.-H. Tong, H.-Q. Yu, *Sci. Rep.* **2014**, *4*, 3735.
240. T. Mehta, M. V. Coppi, S. E. Childers, D. R. Lovley, *Appl. Environ. Microbiol.* **2005**, *71*, 8634–8641.
241. B. A. Methé, K. E. Nelson, J. A. Eisen, I. T. Paulsen, W. Nelson, J. F. Heidelberg, D. Wu, M. Wu, N. Ward, M. J. Beanan, R. J. Dodson, R. Madupu, L. M. Brinkac, S. C. Daugherty, R. T. DeBoy, A. S. Durkin, M. Gwinn, J. F. Kolonay, S. A. Sullivan, D. H. Haft, J. Selengut, T. M. Davidsen, N. Zafar, O. White, B. Tran, C. Romero, H. A. Forberger, J. Weidman, H. Khouri, T. V. Feldblyum, T. R. Utterback, S. E. Van Aken, D. R. Lovley, C. M. Fraser, *Science* **2003**, *302*, 1967–1969.
242. M. N. Alves, A. P. Fernandes, C. A. Salgueiro, C. M. Paquete, *Biochim. Biophys. Acta − Bioenerg.* **2016**, *1857*, 7–13.
243. Y. Liu, Z. Wang, J. Liu, C. Levar, M. J. Edwards, J. T. Babauta, D. W. Kennedy, Z. Shi, H. Beyenal, D. R. Bond, T. A. Clarke, J. N. Butt, D. J. Richardson, K. M. Rosso, J. M. Zachara, J. K. Fredrickson, L. Shi, *Environ. Microbiol. Rep.* **2014**, 1–26.
244. F. J. Otero, C. H. Chan, D. R. Bond, *J. Bacteriol.* **2018**, *200*, 1–20.
245. G. Reguera, K. D. McCarthy, T. Mehta, J. S. Nicoll, M. T. Tuominen, D. R. Lovley, *Nature* **2005**, *435*, 1098–1101.
246. L. Shi, D. J. Richardson, Z. Wang, S. N. Kerisit, K. M. Rosso, J. M. Zachara, J. K. Fredrickson, *Environ. Microbiol. Rep.* **2009**, *1*, 220–227.

247. D. J. Filman, S. F. Marino, J. E. Ward, L. Yang, Z. Mester, E. Bullitt, D. R. Lovley, M. Strauss, *bioRxiv* **2018**, 492645.
248. F. Wang, Y. Gu, J. P. O'Brien, S. M. Yi, S. E. Yalcin, V. Srikanth, C. Shen, D. Vu, N. L. Ing, A. I. Hochbaum, E. H. Egelman, N. S. Malvankar, *Cell* **2019**, *177*, 361–369.e10.
249. D. R. Lovley, D. J. F. Walker, *PeerJPreprints* **2019**, 27773v1.
250. B. C. Kim, B. L. Postier, R. J. DiDonato, S. K. Chaudhuri, K. P. Nevin, D. R. Lovley, *Bioelectrochemistry* **2008**, *73*, 70–75.
251. B. Kim, C. Leang, Y. R. Ding, H. Glaven, M. V Coppi, R. H. Glaven, D. R. Lovley, *J. Bacteriol.* **2005**, *187*, 4505–4513.
252. E. Afkar, G. Reguera, M. Schiffer, D. R. Lovley, *BMC Microbiol.* **2005**, *5*, 41.
253. X. Qian, G. Reguera, T. Mester, D. R. Lovley, *FEMS Microbiol. Lett.* **2007**, *277*, 21–27.
254. T. Mehta, S. E. Childers, R. Glaven, D. R. Lovley, T. Mester, *Microbiology* **2006**, *152*, 2257–2264.
255. D. E. Holmes, T. Mester, R. A. O'Neil, L. A. Perpetua, M. J. Larrahondo, R. Glaven, M. L. Sharma, J. E. Ward, K. P. Nevin, D. R. Lovley, *Microbiology* **2008**, *154*, 1422–1435.
256. L. Zacharoff, D. Morrone, D. R. Bond, D. R. Bond, *Front. Microbiol.* **2017**, *8*, 2481.
257. K. C. Wrighton, J. C. Thrash, R. A. Melnyk, J. P. Bigi, K. G. Byrne-Bailey, J. P. Remis, D.Schichnes, M. Auer, C. J. Chang, J. D. Coates, *Appl. Environ. Microbiol.* **2011**, *77*, 7633–7639.
258. C. W. Marshall, H. D. May, *Energy Environ. Sci.* **2009**, *2*, 699–705.
259. H. K. Carlson, A. T. Iavarone, A. Gorur, B. S. Yeo, R. Tran, R. A. Melnyk, R. A. Mathies, M. Auer, J. D. Coates, *Proc. Natl. Acad. Sci. USA* **2012**, *109*, 1702–1707.
260. N. L. Costa, H. K. Carlson, J. D. Coates, R. O. Louro, C. M. Paquete, *Protein Expr. Purif.* **2015**, *111*, 48–52.
261. S. N. Gavrilov, J. R. Lloyd, N. A. Kostrikina, A. I. Slobodkin, *Geomicrobiol. J.* **2012**, *29*, 804–819.
262. I. A. C. Pereira, A. V. Xavier, *MultiHeme c Cytochromes and Enzymes*, in *Encyclopedia of Inorganic Chemistry*, 2nd ed., Eds R. B. King, R. H. Crabtree, C. M. Lukehart, D. A. Atwood, R. A. Scott, John Wiley & Sons, Chichester, UK, **2006**, pp. 3360–3376.
263. M. Assfalg, I. Bertini, M. Bruschi, C. Michel, P. Turano, *Proc. Natl. Acad. Sci. USA* **2002**, *99*, 9750–9754.
264. E. T. Gnanaprakasam, J. R. Lloyd, C. Boothman, K. M. Ahmed, I. Choudhury, B. C. Bostick, A. van Geen, B. J. Mailloux, *MBio* **2017**, *8*. doi: 10.1128/mBio.01326-17.
265. Y. Wang, J. C. Wilks, T. Danhorn, I. Ramos, L. Croal, D. K. Newman, *J. Bacteriol.* **2011**, *193*, 3606–3617.
266. C. Kurth, H. Kage, M. Nett, *Org. Biomol. Chem.* **2016**, *14*, 8212–8227.
267. R. S. Arze, I. S. Parkinson, N. E. Cartlidge, P. Britton, M. K. Ward, *Lancet* **1981**, *2*, 1116.
268. M. Saha, S. Sarkar, B. Sarkar, B. K. Sharma, S. Bhattacharjee, P. Tribedi, *Environ. Sci. Pollut. Res.* **2016**, *23*, 3984–3999.
269. M. F. Barber, N. C. Elde, *Trends Genet.* **2015**, *31*, 627–636.
270. A. Górska, A. Sloderbach, M. P. Marszałł, *Trends Pharmacol. Sci.* **2014**, *35*, 442–449.
271. T. A. Wencewicz, M. J. Miller, *Sideromycins as Pathogen-Targeted Antibiotics*, in *Antibacterials II*, Eds J. F. Fisher, S. Mobashery, M. J. Fisher, Springer International Publishing, Cham, **2017**, pp. 151–183.
272. V. Braun, A. Pramanik, T. Gwinner, M. Köberle, E. Bohn, *BioMetals* **2009**, *22*, 3–13.
273. A. Schippers, S. Hedrich, J. Vasters, M. Drobe, W. Sand, S. Willscher, *Adv. Biochem. Eng. Biotechnol.* **2014**, *141*, 1–47.

274. O. B. Ojuederie, O. O. Babalola, *Int. J. Environ. Res. Public Health* **2017**, *14*, E1504.
275. C. Roh, C. K. Kang, J. R. Lloyd, *Korean J. Chem. Eng.* **2015**, *32*, 1720–1726.
276. S. O'Brien, D. J. Hodgson, A. Buckling, *Proc. R. Soc. B Biol. Sci.* **2014**, *281*, 0858.
277. S. Abdelbary, M. S. Elgamal, A. Farrag, Trends in Heavy Metals Tolerance and Uptake by *Pseudomonas aeruginosa*, in *Pseudomonas Aeruginosa − An Armory Within*, Ed. D. Sriramulu, InTechOpen, London, UK, **2019**, pp. 1–12.
278. K. Lewis, S. Epstein, A. D'Onofrio, L. L. Ling, *J. Antibiot. (Tokyo)* **2010**, *63*, 468–476.
279. V. G. Gude, *J. Clean. Prod.* **2016**, *122*, 287–307.
280. K. Rabaey, R. A. Rozendal, *Nat. Rev. Microbiol.* **2010**, *8*, 706–716.
281. F. Simonte, G. Sturm, J. Gescher, K. Sturm-Richter, *Extracellular Electron Transfer and Biosensors*, in *Bioelectrosynthesis*, Eds F. Harnisch, D. Holtmann, Springer International Publishing, Cham, **2019**, pp. 15–38.
282. X. Cao, X. Huang, P. Liang, K. Xiao, Y. Zhou, X. Zhang, B. E. Logan, *Environ. Sci. Technol.* **2009**, *43*, 7148–7152.
283. B. E. Logan, K. Rabaey, *Science* **2012**, *337*, 686−690.
284. S. Freguia, M. E. Logrieco, J. Monetti, P. Ledezma, B. Virdis, S. Tsujimura, *Sustainability* **2019**, *11*, 5490.
285. B. E. Logan, R. Rossi, A. Ragab, P. E. Saikaly, *Nat. Rev. Microbiol.* **2019**, *17*, 307–319.
286. A. Prévoteau, J. M. Carvajal-Arroyo, R. Ganigué, K. Rabaey, *Curr. Opin. Biotechnol.* **2020**, *62*, 48–57.
287. S. M. Glaven, *Microb. Biotechnol.* **2019**, *12*, 819–823.
288. S. H. Light, L. Su, R. Rivera-Lugo, J. A. Cornejo, A. Louie, A. T. Iavarone, C. M. Ajo-Franklin, D. A. Portnoy, *Nature* **2018**, *562*, 140–157.
289. J. F. Cryan, K. J. O'Riordan, C. S. M. Cowan, K. V. Sandhu, T. F. S. Bastiaanssen, M. Boehme, M. G. Codagnone, S. Cussotto, C. Fulling, A. V. Golubeva, K. E. Guzzetta, M. Jaggar, C. M. Long-Smith, J. M. Lyte, J. A. Martin, A. Molinero-Perez, G. Moloney, E. Morelli, E. Morillas, R. O'Connor, J. S. Cruz-Pereira, V. L. Peterson, K. Rea, N. L. Ritz, E. Sherwin, S. Spichak, E. M. Teichman, M. van de Wouw, A. P. Ventura-Silva, S. E. Wallace-Fitzsimons, N. Hyland, G. Clarke, T. G. Dinan, *Physiol. Rev.* **2019**, *99*, 1877–2013.
290. M. Yamamoto, R. Nakamura, T. Kasaya, H. Kumagai, K. Suzuki, K. Takai, *Angew. Chemie, Int. Ed.* **2017**, *56*, 5725–5728.
291. G. M. Biggar, *Mineral. Mag.* **1969**, *37*, 299–300.
292. M. A. Saito, G. Rocap, J. W. Moffett, *Limnol. Oceanogr.* **2005**, *50*, 279–290.
293. D. Lide, *CRC Handbook of Chemistry and Physics*, 80th ed., CRC Press, Boca Raton, USA, 1999–2000.

9

Coping with Toxic Metals

Zhiguang Xiao [1] ***and Anthony G. Wedd*** [2]

[1]Melbourne Dementia Research Centre, Florey Institute of Neuroscience and Mental Health, The University of Melbourne, Parkville, Victoria 3052, Australia
<zhiguang.xiao@florey.edu.au>

[2]School of Chemistry and Bio21 Molecular Science and Biotechnology Institute, University of Melbourne, Parkville, Victoria 3010, Australia
<agw@unimelb.edu.au>

Metal Ions in Life Sciences, Volume 21 Guest Editors: Peter M. H. Kroneck and Martha E. Sosa Torres
Series Editors: Astrid Sigel, Eva Freisinger, and Roland K. O. Sigel

https://doi.org/10.1515/9783110589771-009

Abstract: Metal ions, and those of the transition metals in particular, have driven many of biology's catalytic processes since life first evolved. However, this enabling advantage is a double-edged sword: some metal ions are essential but toxic if not processed properly and others are non-essential but toxic if available. The molecular methods that microorganisms have evolved to cope with toxic metal ions are outlined. The toxic ions (Cr, Ag, Au, Cd, Hg) are covered as are the toxic effects of the nutrient metals under dis-homeostasis. Toxic but rare or unavailable elements are not covered, nor are the nutrient and highly soluble metal ions of groups I and 2 (alkali and alkaline earth metals). Brief introductions to some non-nutrient but highly toxic metals and metalloids of groups 13–15 (Al, Tl, Pb, As, Bi) are included.

Keywords: metal ions · bacteria · nutrients · toxicity · homeostasis

1. INTRODUCTION

1.1. The Essential Chemistry of Metal Ions

Metal ions, and those of the transition metals in particular, have driven many of biology's catalytic processes since life first evolved. However, this enabling advantage is a double-edged sword: some metal ions are essential but toxic if not processed properly while others are non-essential, but toxic if available. Consequently, microorganisms have evolved strategies to select and control the advantageous properties of the essential metals and to resist the toxicity of the non-essential ones.

The advantageous properties include:

(i) Mn serving as an electron buffer, e.g., in the water-splitting metallocluster $CaMn_4O_5$ of photosystem II in cyanobacteria;
(ii) Fe in redox-active iron-sulfur clusters and heme compounds;
(iii) Co in vitamin B_{12} and its derivatives that re-arrange C–H and C–C bonds;
(iv) Ni to cleave or form covalent bonds such as those in dihydrogen or urea;
(v) Cu to react with dioxygen;
(vi) Zn to act as a Lewis acid and to induce rigidity in polypeptide chains;
(vii) Mo (and W) to promote oxygen atom transfer reactions.

Toxicity arises when the nutrient metals are not under metabolic control (dishomeostasis) or when toxic metal ions are available and enter cells. The fundamental problems arise from the intrinsic reactivity of the ions:

(i) Common oxidation states I and II lead to first row transition metal cations being 'soft' or 'borderline', meaning that they can bind to thiol groups efficiently. Consequently, as the cytoplasmic spaces of bacteria are reducing, such cations can modify surface protein thiols or molecular thiols such as glutathione. This is also a prime mode of action of the toxic ions Ag^{I}, Au^{I}, Cd^{II}, and Hg^{II} (see Figure 1, set I in Section 1.2 of this chapter).

(ii) Cu, Zn, and Ni cations form stable complexes (i.e., are high in the Irving-Williams series; see Figure 2 in Section 1.3) and may displace native metal ions from their sites.

(iii) Uncontrolled Cu^{I} and Fe^{II} are able to undergo one-electron redox reactions with endogenous species produced by partial reduction of dioxygen to produce the toxic hydroxyl radical [1]. The Fenton reaction (Equation 1; M = Fe) was identified initially and its combination with Reaction (2) provides the Haber-Weiss reaction (Equation 3; M = Fe, Cu):

$$M^{n+} + H_2O_2 \rightarrow M^{n+1} + OH^- + OH^\bullet \quad (1)$$

$$M^{n+1} + O_2^{\bullet -} \rightarrow M^{n+} + O_2 \quad (2)$$

$$O_2^{\bullet -} + H_2O_2 \rightarrow O_2 + OH^- + OH^\bullet \quad (3)$$

$OH^\bullet$ radicals are the result of single-electron interchange utilizing the transient oxidation states of the available transition metal ion. The problem is that two electrons are needed to safely reduce endogenous H_2O_2 to hydroxide (i.e., to the redox state of water) but the metal ion can supply one electron only. The highly oxidizing $OH^\bullet$ radical is capable of initiating radical chain reactions leading to cellular damage.

As the reduced cations are re-formed via reduction of their oxidized product forms in the reducing cytoplasm, catalytic cycles of radical formation are initiated imposing oxidative stress on cells, especially in aerobic respiratory chains where both $O_2^{\bullet -}$ and H_2O_2 are available.

The fundamental importance of the essential chemistry outlined above is emphasized in the geochemical availability of the relevant transition metal ions, the particular roles that have evolved for them (up to 50 % of proteins have a metal ion associated with their activity) and their involvement in the interactions of bacteria with their environments. These aspects are addressed in more detail below.

1.2. Geochemical Availability of Metal Ions

Over geological timescales, the average metal ion content in seawater has reached an equilibrium of inflow and precipitation reactions. It may be assumed

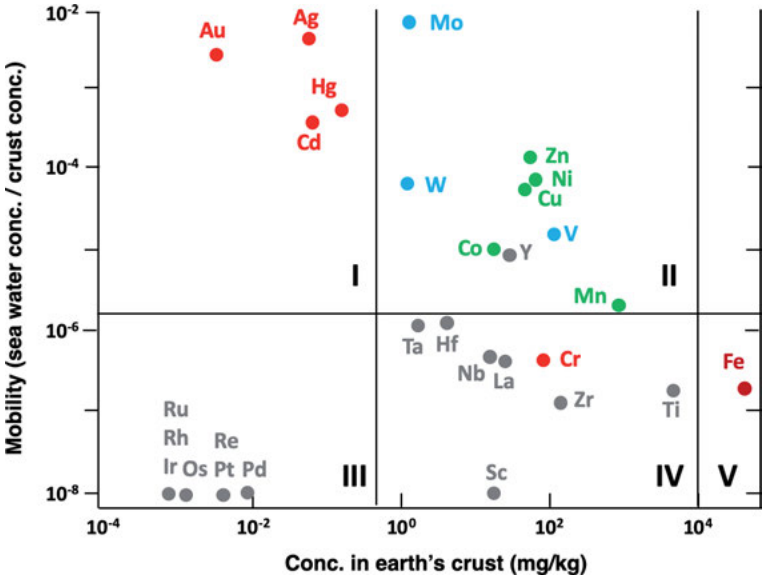

Figure 1. Geochemical availability of transition metals of mobility (estimated as ratio of concentration in seawater (mg/kg) to concentration in earth's crust (mg/kg)) versus concentration in earth's crust. Adapted from [2].

that the ratio of the average concentration of a metal ion in seawater to that in the Earth's crust mirrors its geochemical mobility and, hence, its availability to biology. A plot of mobility versus crust content (Figure 1) separates the transition metals into five sets [2]:

I. Ag, Au, Cd, and Hg have high mobility but low crust content (red dots). Consequent lower availability means that they have not been selected by biology and are toxic when available.

II. Nine metals are both highly mobile and available. Eight of these are the bio-metals V, Mo, W, Mn, Co, Ni, Cu, and Zn. Their oxo-hydroxides (green dots) or oxy-anions (blue dots) are sufficiently soluble.

III. These metallic elements are extremely limited in the crust and of low mobility. They are precious metals, being the later members of groups 7–10.

IV. This set has high crust content but low mobility and are not bio-available. Their stable high oxidation states lead to oxo-hydroxides that are insoluble at biological pH values.

V. Fe is highly abundant but of low mobility (due to insoluble ferric oxo-hydroxides, often referred to generically as 'rust'). These forms have limited availability on the evolved earth. However, Fe was bio-available as ferrous iron under the reducing conditions of the primitive Earth. It is still available as such in anoxic modern environments (e.g., deep seas and lakes) that harbour microorganisms that initiate food chains. High affinity

ferric iron chelators (siderophores) have evolved to make iron available to aerobes.

As Figure 1 demonstrates, the bio-availability of transition metal ions is a consequence of abundance and solubility [2]. Only metals from sets I and II are accessed by microorganisms, with three exceptions:

(i) Set IV element Cr (red dot) can be effectively assigned to sets I/II as a consequence of its soluble oxo-anions. But its rich redox chemistry means that it is intrinsically toxic.

(ii) Set II element Y (gray dot) and its fellow rare earths can be re-assigned to set IV due to the insolubility of trivalent hydroxides in normal environments. However, their presence in enzymes from methanotrophs in volcanic environments has been confirmed recently [3].

(iii) The unique history of the biological chemistry of Fe (brown dot; see set V above) places it effectively in set II.

1.3. Metalation of Metalloproteins

The famous Irving-Williams Series predicts that binding of divalent metal ions to classical ligands will have a common order of affinities with, for example, Cu^{II} and Zn^{II} forming tighter complexes than Fe^{II} or Mn^{II} (Figure 2) [4]. It should be noted that Cu^{I} also forms very stable complexes, especially with the softer biological ligands such as the side chains of the amino acid's cysteine (thiolate) and histidine (imidazole). It is the available valence state of copper in reducing cell cytosols.

The question then is: how do bacteria discriminate to ensure that the right metal occupies its native protein site? The answer is that cells ensure lower availability of the more competitive metals relative to those of the less competitive ones [5]. This would seem to be problematic as many metal ions are buffered at less than one 'free' ion per cell and hence are 'unavailable'. In this context, 'free' means bound by labile ligands such as water. The reality is, however, that metal transfer is favorably 'associative', i.e., rapid exchange can still occur between protein ligand sets of high, but differing, affinities.

Bacterial cells have evolved sensor proteins and metal ion buffers that modulate the free energy of metalation ΔG^0_M so that *apo*-metalloproteins acquire the metal ion M for which ΔG^0_M is favorable (relative to the buffer) [6, 7]. It has been demonstrated that the cobalt chelatase from a *Salmonella* strain has evolved to receive Co^{II} as ΔG^0_{Co} is tuned to be >10 kJ mol^{-1} more favorable than for the other bio-metal ions [7].

The buffered available metal ion concentrations in *Salmonella* cell cytosols vary by 15 orders of magnitude, tuned by the sensor proteins and metal ion buffers [5]. They are in the inverse order of the Irving-Williams series (Figure 2). The nature of the metal ion buffers involved is ill-defined but represents metal ion

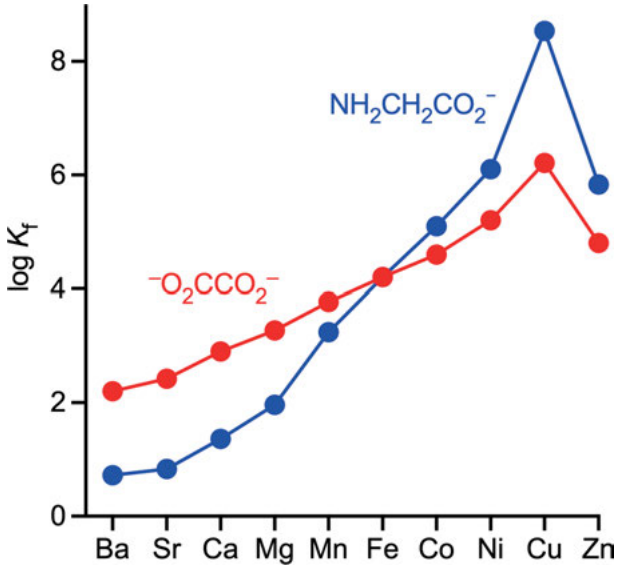

Figure 2. The Irving-Williams series plots the thermodynamic stability of complexes formed by divalent first-row transition metal ions across the fourth period [4]. The log of the formation constant K_f for the 1 : 1 complex is plotted for two bidentate ligands, oxalato ($^-O_2C\text{-}CO_2^-$) and glycinate ($NH_2CH_2CO_2^-$). There is a maximum stability at Cu(II) with Ni(II) and Zn(II) also exhibiting high stability.

populations that are kinetically trapped. It is probable that over-expression of the receiver *apo*-metalloproteins is one component of the overall buffer while the existence of metal 'stores' within certain organelles is another. The latter will be accessible by dedicated metallo-chaperone proteins.

1.4. The Pathogen-Eukaryotic Cell Interface: Nutritional Immunity

Bacterial pathogens encounter a variety of adverse challenges during infection of humans and other mammals. This includes excesses or deficiencies of biometals (Mn, Fe, Cu, Zn) to limit bacterial growth [8–13].

For example, the protein calprotectin constitutes 40 % of the host cytosol in antibacterial white blood cells (neutrophils) and features sites that bind bivalent Mn, Fe, Ni, and Zn with high affinity [8], inducing so-called nutritional immunity. Bacteria have evolved defence mechanisms to resist such attacks when sequestered in the phagosomal compartments of host cells. One of the better understood systems involves pathogenic *Escherichia coli* (Figure 3) [14]. The host injects toxic copper and superoxide ions. The bacterium employs the ligand yersi

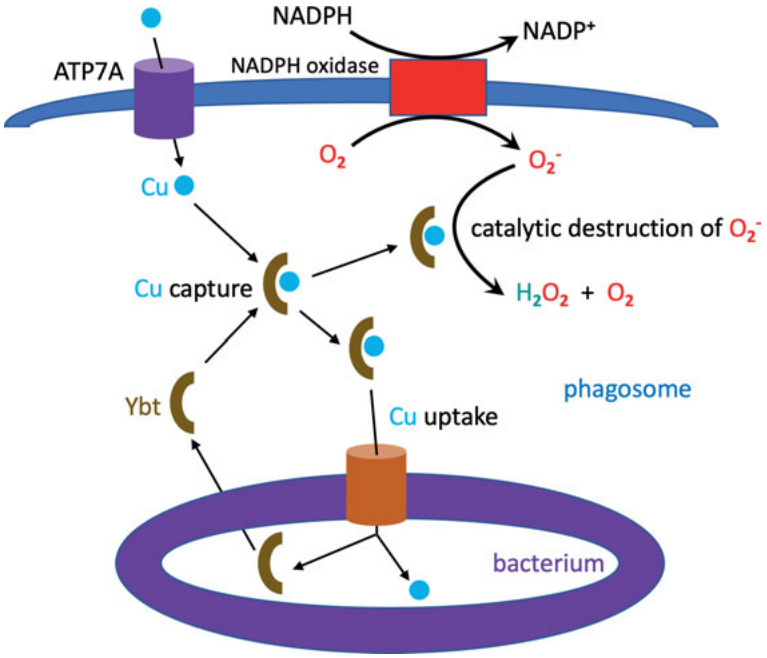

Figure 3. Copper-binding ligand yersiniabactin functions at the host-pathogen interface. The host sequesters invading bacteria into phagosomal compartments. The ligand (khaki crescent) is expressed by *E. coli* and appears to protect by sequestering toxic Cu^{I} ions translocated by the host pump ATP7A. Its redox-active Cu complex can catalyze disproportionation ('dismutation') of superoxide injected as part of host defense. In environments where copper is scarce, the ligand may act as a scavenger of nutrient copper. Adapted from [14].

-niabactin that binds copper ions for both nutritional uptake and for defence against copper toxicity. In addition, the redox-active Cu complex is an efficient superoxide dismutase catalyst, effectively minimizing the assault by superoxide.

This chapter outlines the molecular methods that microorganisms have evolved to cope with toxic metal ions. The toxic ions (Figure 1; red dots) are covered as are the toxic effects of the nutrient metals (green, blue, brown dots) under dishomeostasis. Toxic but rare or unavailable elements (grey) will not be covered, nor will the nutrient and highly soluble metal ions of groups I and 2 (alkali and alkaline earth metals). Brief introductions to some non-nutrient but highly toxic metals and metalloids of groups 13–15 (Al, Tl, Pb, As, Bi) are included.

2. GROUP 5 ELEMENT VANADIUM

Vanadium is the second most abundant soluble transition metal in seawater, existing as the vanadate oxo-anion system $[H_2V^{V}O_4]^{-}/[HV^{V}O_4]^{2-}$. It has few

known biological functions but is present in two classes of enzymes: V-nitrogenases and V-dependent halo-peroxidases [15]. A strain of *Azotobacter vinelandii* expresses only the V-nitrogenase and V concentrations below 10^{-8} M and above 10^{-6} M are, respectively, limiting and toxic to this strain. *A. vinelandii* excretes catechol siderophores for vanadate uptake [16]. Halo-peroxidases catalyze the oxidation of halides by hydrogen peroxide and are used in nature to introduce halogen atoms into organic compounds [17]. They are present across algae, fungi, and bacteria.

Vanadate is a structural and electronic analogue of phosphate. It restricts uptake of the latter and is a potent inhibitor of phosphorylases and ATPases. It can also be toxic by interfering with iron uptake by competing for siderophore ligands and inhibiting the enzyme ferric reductase, essential for uptake of Fe-siderophore complexes [18].

3. GROUP 6 ELEMENT CHROMIUM

As its reduced ores, such as the mineral chromite ($Fe^{II}Cr_2^{III}O_4$), were effectively insoluble in the reducing environment of the primitive Earth, chromium appears to not have been selected by biology. Its mobility remains low on the evolved Earth but industrial scale use has increased its effective concentration. Chromate, $[Cr^{VI}O_4]^{2-}$, is its most oxidised form and is the available form of Cr in seawater. Evidence that it is essential for any prokaryotes is unconvincing [19]. Some strains of anaerobic bacteria utilize chromate as sole electron acceptor but this appears to be an adaption to pollution by industrial Cr^{VI} residues [20].

The stereochemistry and surface charge density of $[Cr^{VI}O_4]^{2-}$ is similar to that of sulfate, $[S^{VI}O_4]^{2-}$, and it appears that both anions are imported and exported via sulfate channels [20, 21]. As it is also isostructural with hydrogen phosphate, $[HP^{V}O_4]^{2-}$, it likely interferes with phosphate metabolism [22]. It undergoes one-electron reduction in many bacteria but the product Cr^{V} is readily oxidised with production of reactive radicals [20, 23, 24]. Consequently, aerobes that are capable of direct reduction of Cr^{VI} to Cr^{III} have been explored for environmental remediation [25]. Promiscuous multi-heme or flavodoxin reductases were identified as responsible for these three-electron reductions [26–28]. The hemotoxicity, genotoxicity, and carcinogenicity of chromium in eukaryotes is believed to be linked to its redox chemistry [29].

4. GROUP 6 ELEMENTS MOLYBDENUM AND TUNGSTEN

Molybdenum is the most abundant soluble transition metal in the oceans (~100 nM; Figure 1) and > 50 molybdo-enzymes are known. The majority is prokaryotic and are key players in the C, N, S, and O biogeochemical cycles [30]. Of particular importance is the reduction of dinitrogen to ammonia (to make N bio-available) and the interconversion of nitrite and nitrate (oxygen atom transfer) for assimilation by plants.

Interplay between the congeners Mo and W is fascinating as their relative availability may have influenced evolutionary processes. While their chemistries are similar, W compounds have lower reduction potentials (hence, are more sensitive to dioxygen) and higher bond strengths and thermal stabilities. On the primitive Earth under so-called euxinic conditions (high sulfide levels, anoxic), W was available as soluble $[W^{VI}O_xS_{4-x}]^{2-}$ species while Mo was tied up as insoluble MoS_2 [31]. Hence, tungsto-enzymes may have evolved initially, consistent with their presence in the hyperthermophilic organisms discovered in the euxinic waters around marine hydrothermal vents.

Sediments containing significant levels of Mo are dated to ~600 million years ago, matching the stage when the oceans became extensively oxygenated and MoS_2 weathered to soluble molybdate $[Mo^{VI}O_4]^{2-}$. It is then that the availability and intrinsic chemistry of Mo became favored over those of W.

While some prokaryotic enzymes are active with either Mo or W bound, W is toxic to most molybdo-enzymes. It acts as an antagonist or inhibitor and substitution leads to low or zero activity [31].

5. GROUP 7 ELEMENT MANGANESE

Manganese is an essential trace element in the majority of bacteria, being present in diverse enzymes. In particular, it provides protection against oxidative stress via Mn-superoxide dismutase and related mechanisms [32]. A primary role of Mn is to compensate for Fe, either when the latter is unavailable or under conditions of oxidative stress. For example, Mn appears to substitute for Fe in mononuclear enzymes in *E. coli*, allowing residual Fe to be used in iron-sulfur and heme enzymes [33]. However, other bacterial systems carefully balance the levels of these metals to achieve optimal growth [11, 33]. Many bacteria need Mn to form pathogenic (Section 1.4) or symbiotic relationships with eukaryotic host cells [34]. *Borrelia burgdorferi* (the cause of Lyme disease in humans) is the single bacterium known to use Mn exclusively in place of Fe. It has no requirement for Fe [35].

Excess Mn is toxic and so cells have both Mn import and export systems [36]. While Mn^{II} is low in the Irving-William series (Figure 2), over-accumulation can cause mis-metallation of enzymes and regulatory sensors (Section 1.3) [33, 37, 38]. On the other hand, excess Zn can disable Mn import in *Streptococcus pneumonia* [39]. Further details of the synergy of Mn and Fe are described in Chapter 6 (Biominerals).

6. GROUP 8 ELEMENT IRON

6.1. History of Iron Transport

Iron is the most abundant element on Earth, forming much of the inner core. This mobile iron generates the planetary magnetic field, protecting it from solar

winds and high energy radiation [40]. It is also the fourth most abundant element in the Earth's crust.

It was available as Fe^{II} under the reducing conditions of the primitive Earth. The iron-sulfur world hypothesis posits that the early chemistry of life occurred on mineral surfaces near hydrothermal vents [41–43] (see Chapter 5). In particular, electron transfer from reduced minerals to acceptors led to reduction of CO and CO_2 that both dissipated the redox gradient and produced organic compounds. Iron-dependent redox enzymes evolved as life developed.

On the evolved Earth, the highly oxidizing conditions imposed by the presence of O_2 mean that Fe is highly abundant but of low mobility (due to insoluble 'rust'). This means that it is the only element to occupy class V of Figure 1. This situation led to the evolution of high affinity Fe^{III} chelators to make iron available to aerobes. These are the so-called siderophores (see Section 6.3).

6.2. Transport of Ferrous Iron

At lower pH values, Fe^{II} is stable and soluble in the absence of O_2 (anoxic conditions). It is transported into many bacteria by the Feo system that evolved on the primitive Earth and is present in Archaea such as *Pyrococcus furiosus* [44, 45]. This system is up-regulated when iron availability becomes limited under anoxic conditions by the regulators Fur and Fnr [46]. In the presence of O_2 (oxic conditions) and under more acidic conditions, a second transport system Efe is induced [47–49].

6.3. Transport of Ferric Iron

Siderophore ligands evolved to extract Fe^{III} from 'rust' under aerobic conditions at typical biological pH values (pH 5–8) [50]. They typically provide protons to activate mineral surface OH^- as labile water, thereby activating multi-dentate ligand fragments as anionic ligands (e.g., catecholato, hydroxamato) that capture the unmasked ferric ions.

Gram-positive and -negative bacteria produce different types of siderophores and, as the outer membranes of these two forms vary, uptake mechanisms also vary. Many bacteria have evolved the ability to 'pirate' siderophores secreted by other bacteria. For further details of these aspects, the reader is referred to Chapters 7, 8.

As discussed in the introductory Section 1.1 (Equations 1–3), uncontrolled Fe^{II} can catalyze the Fenton and Haber-Weiss reactions that produce toxic oxygen radicals [33, 51]. These radicals may damage cell metabolism by oxidation of Fe-S and other metal centers, as well as protein residues and lipids [33].

A readable account of the essential chemistry of iron uptake and homeostasis may be found in the review by Cornelis [52], while other recent developments have been addressed more recently. These include the roles of siderophores be-

yond iron sequestration [53] and the potential of exploiting the pathogen siderophore machinery to treat antibiotic-resistant bacterial infections [54].

7. GROUP 9 ELEMENT COBALT

Cobalt enzymes occur almost exclusively in bacteria, a reflection of evolutionary change imposed by the oxygenation of the atmosphere, beginning about 2.4 billion years ago. This restricted the availability of sulfide minerals versus less accessible oxide minerals and made cobalt less available to higher organisms. A recent increase in the apparent geochemical availability of Co is connected to burning of fossil fuels and its use in steels and industrial processes [55, 56].

The cobalt-containing vitamin B_{12} and other cobalamins, required by humans and other higher animals, is provided by bacteria in the large intestine and by meat and some other sources [57]. It can be seriously deficient for strict vegetarians [58, 59].

A major reason for the limited utility of Co in biology is the kinetic inertness of Co^{III} ($3d^6$) centers (ligand exchange rates ~10^{-5} s^{-1}). The availability of multiple oxidation states (I, II, III) and the low reduction potentials involved implies that unregulated Co may generate oxidative stress. There is preliminary evidence of this in a number of bacterial systems although no evidence of up-regulation of protective genes has been found [60].

The toxicity of unregulated Co has been best defined in *E. coli* and *Salmonella enterica*. Co^{II} out-competes Fe^{II} during the assembly process of Fe-S centers [60, 61]. It does not appear to displace Fe from intact enzymes. However, the challenge of the toxicity of this available metal ion (Figure 1) is highlighted by the existence of a Co (and Ni) defence system RcnR/RcnA in a wide range of Bacteria and Archaea [62].

8. GROUP 10 ELEMENT NICKEL

Nickel is essential to Bacteria and Archaea only, reflecting the same evolutionary issues mentioned above for Co [63]. The exception is the enzyme urease found in plants and some simple eukaryotes. Ni appears to be an essential element for humans but may be associated with the microbiome of the digestive tract [64]. In addition, urease is employed by pathogens to produce ammonia to cope with acid environments. High profile examples are *Helicobacter pylori* in the stomach and *Proteus mirabilis* in the bladder.

Ni-Fe hydrogenases are prominent enzymes in anaerobic metabolism [65]. H_2 produced by bacterial fermentation is oxidized by such enzymes for the establishment of pathogens *H. pylori* and *Salmonella typhimurium* in humans. Further discussion of the roles of bacterial Ni up-take systems and enzymes may be found in [66].

Ni^{II} is high in the Irving-Williams series (Figure 2) and this thermodynamic advantage appears to drive its toxicity via replacement of native metals (such as

Fe and also Zn, if Ni levels are sufficiently high) and also via adventitious binding to proteins, DNA, and lipids [67, 68]. Despite its redox properties, the case that Ni causes oxidative stress is not convincing. The realization that mobile Ni was a universal challenge was the discovery of the Co/Ni defence system RcnR/RcnA in a wide range of Bacteria and Archaea [62].

9. GROUP 11 ELEMENT COPPER

While unavailable on the primitive Earth, copper is both abundant and available on the evolved Earth (Figure 1; set II). Its Cu^{II}/Cu^{I} couple can be tuned to reduce dioxygen and this has been utilized in many oxidase enzymes [69]. However, uncontrolled Cu is able to undergo redox reactions that produce the toxic hydroxyl radical $OH^{\bullet}$ (Section 1.1, Equations 1–3) [70]. In addition, both Cu^{I} and Cu^{II} have high affinities for amino acid ligands (Section 1.3; Figure 2) and have the potential to displace nutrient metals from their native sites or to induce non-native protein folding [71–73].

The latter properties have been long known to prevent fouling of drinking water and ship hulls ('copper-bottomed') and allowed application as bactericidal and fungicidal agricultural sprays. These applications have been extended to the use of copper alloys in surfaces in hospitals [74]. The same properties are exploited by copper ion attack on bacterial pathogens in the 'nutritional immunity' response of phagosomes (Section 1.4; Figure 3).

Bacteria have evolved multiple strategies for the safe import and export of this essential but highly toxic metal [69, 75, 76]. In Gram-negative bacteria, these include the *cue, cus* and *cop/pco* gene clusters [77]. The chromosomally-encoded tolerance operons *cue* and *cus* function in copper export and detoxification [77, 78]. The *cue* system (*Cu e*fflux) includes a trans-membrane P_{1B}-type ATPase (CopA) that facilitates Cu^{I} efflux across the cell membrane to the periplasm. In bacteria such as *E. coli*, a periplasmic multi-copper oxidase CueO catalyzes the oxidation of Cu^{I} to the less toxic Cu^{II}, while a cytoplasmic copper binding regulatory protein (CueR) completes this system that functions predominantly under aerobic conditions [79–82].

The *cus* system (*Cu s*ensing) operates in the absence of dioxygen [83]. It includes four proteins (CusABCF in *E. coli*), together with two regulatory proteins CusR and CusS [84, 85]. CusABC is a tripartite complex that spans the entire periplasmic envelope and facilitates efflux of cytoplasmic Cu^{I} ions, driven by a proton gradient [86–89]. CusF is a copper chaperone that delivers periplasmic Cu^{I} to the complex [90].

In addition to these genomic efflux and detoxification systems, some bacteria have acquired additional copper resistance mechanisms in order to survive in environments with elevated Cu levels. These systems originate from plasmid-borne genes and are termed the *cop/pco* systems (*cop*per resistance, or *p*lasmid-borne *co*pper resistance) [91–95]. Even though these plasmid-borne resistance systems are present in bacteria, it is not yet clear how they impart cellular copper resistance. It has been suggested that the constituent proteins have individual

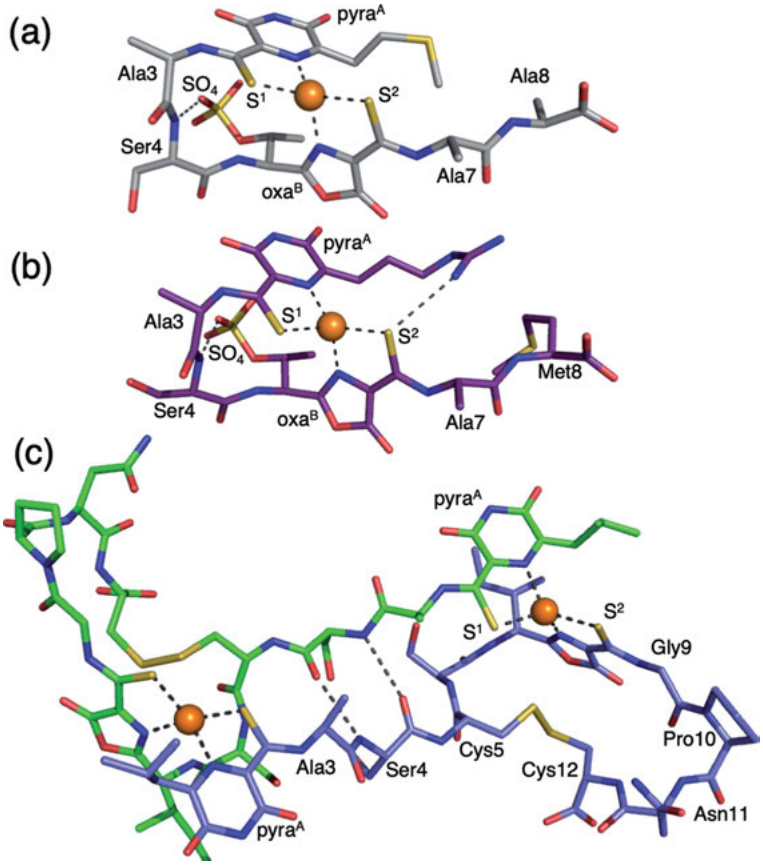

Figure 4. Crystal structures of methanobactins loaded with Cu^{I} ions. (**a**) *Methylocystis hirsute* CSC1 (PDB 2YGI); (**b**) *Methylocystis* strain M (PDB 2YGJ); (**c**) *Methylosinus sporium* NR3K (PDB 4OZ7). The Cu^{I}_{2} dimer in (c) is composed of two symmetry-related monomers. The figures were generated with the PyMol program.

functions in import and efflux of copper into and out of the cytoplasm and that they function in the sequestration of copper in the periplasm. Of these functions, the former activity has been relatively under-investigated due to the fact that there is no known function for copper in the bacterial cytoplasm [96]. Consequently, a definitive model for the individual functions of proteins in the *cop/pco* systems and their contributions to bacterial copper resistance remain poorly characterized.

The *pco* cluster in *E. coli* comprises seven genes, *pcoABCDpcoRSpcoE*, which encode the proteins PcoABCDE, and is regulated by the two-component system, PcoRS [97]. Three soluble proteins (PcoA, PcoC, PcoE) are expressed and translocated to the periplasm, and two copper permeases (PcoB and PcoD) are present in the outer and inner membranes, respectively [98–101]. The *cop* operons found in the copper-resistant bacterium *Pseudomonas syringae* carry six

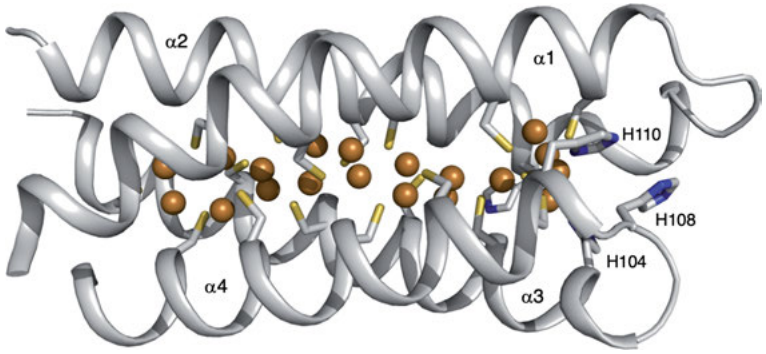

Figure 5. Crystal structure of *Methylosinus trichosporium* copper storage protein CSP3 binding 19 equivalents of Cu^{I}. The four-helix bundle is a monomer (PDB 5ARN) with the N-terminal helix omitted. The brown spheres represent Cu^{I} ions and cysteine and histidine ligands are represented as sticks. The figure was generated with the PyMol program.

genes, *copABCDcopRS*, with equivalent functions and protein products as those of their *pco* counterparts, suggesting conserved mechanisms of copper resistance across these bacteria.

Little is known of the mechanism of uptake of copper by bacterial cells. It is possible that high affinity import systems are not required as copper is sufficiently abundant (Figure 1; set II) in most environments. On the other hand, methanotrophs (proteobacteria that utilize CH_4 as a carbon source) have an exceptional requirement for Cu due to its presence in the enzyme particulate methane monooxygenase [102]. Complex high-affinity peptide ligands, termed methanobactins, have evolved in about 10 % of these bacteria to harvest Cu from the environment under limiting conditions, i.e., performing a similar role to siderophores that acquire ferric iron [103]. Cu^{I} binding occurs at distorted tetrahedral N_2S_2 sites with affinities of ~10^{20} M^{-1}. There is significant structural variation among the known structures (Figure 4) [104]. The mechanisms of dissociation of the Cu ions from such high affinity ligands are currently unknown but are likely to involve associative exchange with another high affinity protein or ligand.

Copper-storage proteins have been isolated from methanotrophs (c.f., ferritins as iron-storage proteins). They are tetramers of four-helix bundles that can accommodate large numbers of Cu^{I} ions within their cysteine-lined cores (Figure 5) [104–105]. Tetranuclear clusters are favored with similar structures to those present in Cu^{I}-metallothioneins. Genetic analysis suggests that these proteins are present in a wide range of bacteria.

As a general strategy to minimize toxic effects, the Cu trafficking pathways in cells involve metallo-chaperone proteins and membrane-bound transporters [69, 75]. Cu ions are tightly bound and specific associative exchange between partners has been demonstrated by two-hybrid assays and by NMR mapping experiments [106, 107]. In the reducing cytosol, metallo-chaperones bind Cu^{I} via coordination to cysteine residues (thiolate) [75]. In the more oxidizing periplasm, Cu^{II} is the

less toxic oxidation state and methionine ligands (thioether) are favored [108]. Significant progress has been made on understanding the molecular nature of membrane-bound export pumps such as CusABC [86–89] and the ATP-ase CopA [109–112]. The conundrum of the apparent absence of a metallo-chaperone in the cytosol of *E. coli* to service CopA with Cu^{I} to export was solved recently: a programmed ribosomal frame shifting generates both the metallo-chaperone Atx1 and the pump CopA from the same gene [113].

10. GROUP 11 ELEMENT SILVER

Silver can occur as the native metal and has been mined through the ages as a precious metal. It has no known biological role but its antibacterial properties were well-known in ancient times through its use in water purification and wound dressing [114, 115]. These properties are currently being re-explored in the form of Ag metal nanoparticles that allow significant dissociation of the toxic Ag^{+} ion. However, serious concerns remain about the safety of such approaches [116, 117].

Silver-resistant bacteria are known. In one notorious case, a Ag^{I} resistance plasmid pMG101 from a *Salmonella* strain induced septicaemia, killing three patients in a hospital burns ward [118].

The operons responsible for resistance are closely related to the Cu systems discussed in Section 9. Under anoxic conditions, the *cue* system in *E. coli* and related cassettes in other Gram-negative bacteria can be utilized as the CopA transporter exports Ag^{I} as well as Cu^{I}. However, this system cannot operate under oxic conditions as Ag^{I} inhibits the multi-copper oxidase CueO, preventing detoxification of Cu^{I} by aerial oxidation to Cu^{II}. Then, the *cus* system is activated, expressing the transporter CusABC and metallo-chaperone CusF, together with two regulatory proteins CusR and CusS. This system has been termed *sil* in *Salmonella* [119]. Further discussion can be found in review [120].

A different mechanism for Ag detoxification via reduction of Ag^{I} to Ag metal has been proposed for a number of bacteria in soil or sediment environments [121, 122].

11. GROUP 11 ELEMENT GOLD

Gold, of course, was one of the first metals known to man, as it occurs naturally in the metallic state and is both durable and attractive to the eye. It is considered to be non-essential to biology but its toxicity has led to the evolution of a variety of resistance mechanisms in bacteria.

Primary gold deposits are laid down by multiple earthquakes that cause flash deposition of minerals due to the rapid pressure drop along fault lines [123]. While species such as Au^{+}_{aq} and $[Au^{I}(SH)_2]^{-}$ are stable and soluble at high temperature and pressure, they are unstable to auto-reduction under milder conditions (Equation 4) [124].

$$2\,[Au^{I}(SH)_2]^- + 2\,H^+ \rightarrow 2\,Au^0 + S^0 + 3\,H_2S \quad (4)$$

Secondary gold deposits appear to have been influenced by bio-mineralization. Bacteria living in bio-films in auriferous soils are subject to gold poisoning [125]. Under surface conditions, defence mechanisms can disperse and re-concentrate the gold [126]. The nature of Au-associated microbial communities is under intensive study [127]. A more detailed account of the geochemistry and biology of gold can be found in review [128].

Bacteria have evolved a range of different strategies to cope with gold toxicity. These include active export and sequestration followed by precipitation [128]. *Salmonella* species have a *gol* operon that handles Au^I in the reducing cytosol and is similar in structure to the *cus* system that exports Cu^I under anaerobic conditions (Section 9) [129].

The proteobacterium *Cupriavidus metallidurans* can survive high concentrations of transition metal ions. In particular, its plasmid-borne *cup* operon is analogous to the *cue* system that handles Cu^I under aerobic conditions (Section 9). However, this system is inhibited by Au^I, leading to accumulation of Cu^I in the cytosol and to synergistic Cu/Au toxicity [130]. Consequently, a chromosomal *cop* operon is up-regulated for full Cu/Au resistance [131].

The periplasmic multi-copper oxidase CopA (not to be confused with the CopA exporter of the *cue* operon (Section 9)) of the *cop* resistance system of *C. metallidurans* can not only oxidize exported Cu^I to less toxic Cu^{II} but also export Au^I for oxidation to Au^{III} [124]. This product spontaneously oxidizes water to precipitate Au metal as nanoparticles (Equations 5 and 6).

$$2\,Au^{I} + O_2 + 4\,H^+ \rightarrow 2\,Au^{III} + 2\,H_2O \quad (5)$$

$$4\,Au^{III} + 6\,H_2O \rightarrow 4\,Au^0 + 3\,O_2 + 12\,H^+ \quad (6)$$

Another strategy is used by *Delftia acidovorans* that is known to dominate, with *C. metallidurans*, the micro-biota associated with gold nuggets. It exports a complex peptide ligand delftibactin that sequesters Au^{III} in its surroundings and promotes reduction to gold metal [127]. This approach echoes that of Cu chelation by yersiniabactin (Section 1.4; Figure 3) and methanobactin (Section 9) and also that of Fe chelation by siderophores (Section 6).

12. GROUP 12 ELEMENT ZINC

Zinc is essential to all known organisms as a non-redox catalytic or structural center. It is a component of about 10 % of all eukaryotic proteins and is present in 70 % of proteins in the human brain [132, 133]. In bacteria, it appears to be important for biofilm formation, motility, antibiotic resistance, metabolic signalling and may be involved in protection against oxidative stress (by protecting important thiol groups).

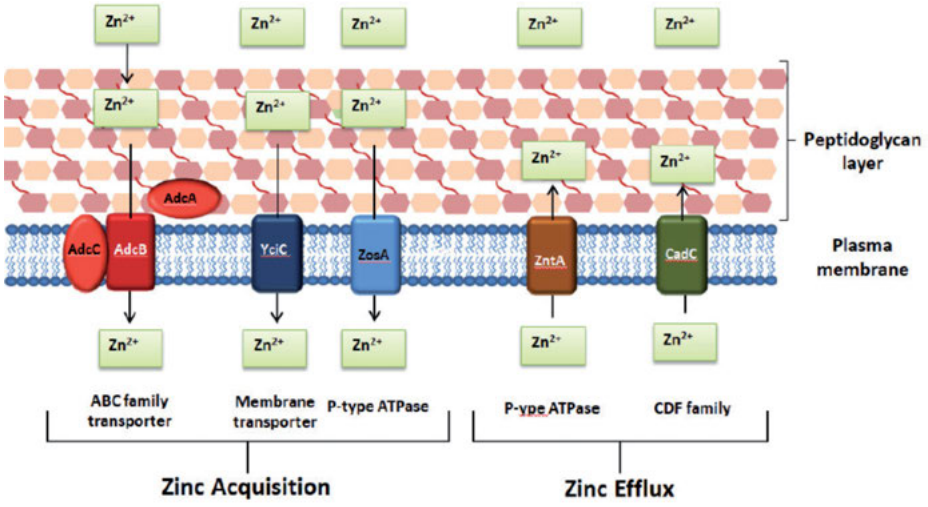

Figure 6. Cartoon illustrating zinc import and export in Gram-positive bacteria. The type of membrane-bound transporter (family) is indicated. The high affinity import transporter is shown in red and low affinity transporters in blue. The export transporters are shown in brown and green. Reproduced from [138], with permission of AIP Publishing; copyright 2018.

Consequently, complex import/export systems have evolved to manage Zn homeostasis. The redox chemistry of release of signalling Zn^{2+} ions from high affinity protein sites and/or as an antioxidant is a recent development (Equation 7).

$$Zn^{II}(S\text{-}Cys)_2 \rightarrow Zn^{2+} + Cys\text{-}S\text{-}S\text{-}Cys + 2\,e^- \quad (7)$$

The overall chemistry underlying the action of Zn in biology is detailed in review [134]. However, like all essential metals, excess Zn is toxic if uncontrolled. For example, a *Synechococcus* cyanobacterium expresses a metallothionein protein in the presence of high levels of Zn. It binds four equivalents of Zn^{II} in a $Zn_4Cys_9His_2$ cluster [135].

As Zn^{II} binds to amino acid ligands with high affinity (Section 1.1; Figure 2), it has the potential to displace metal ions from their natural sites or to structurally distort those sites [39]. This aspect is utilized in the nutritional immunity response of human macrophages against bacterial infection (Section 1.4). Remarkably, it is reported that both zinc starvation and zinc poisoning can be induced against the single pathogen *S. typhimurium*, but that both strategies can be combated effectively by this robust organism [136].

The need for substantial levels of nutrient Zn has led to elaborate mechanisms to control its level and distribution [137, 138]. There are two regulators Zur and ZntR that control, respectively, import and export by monitoring the expression of membrane transporters. A summary of known transporters for Gram-positive and Gram-negative bacteria are shown in Figures 6 and 7 [139–142].

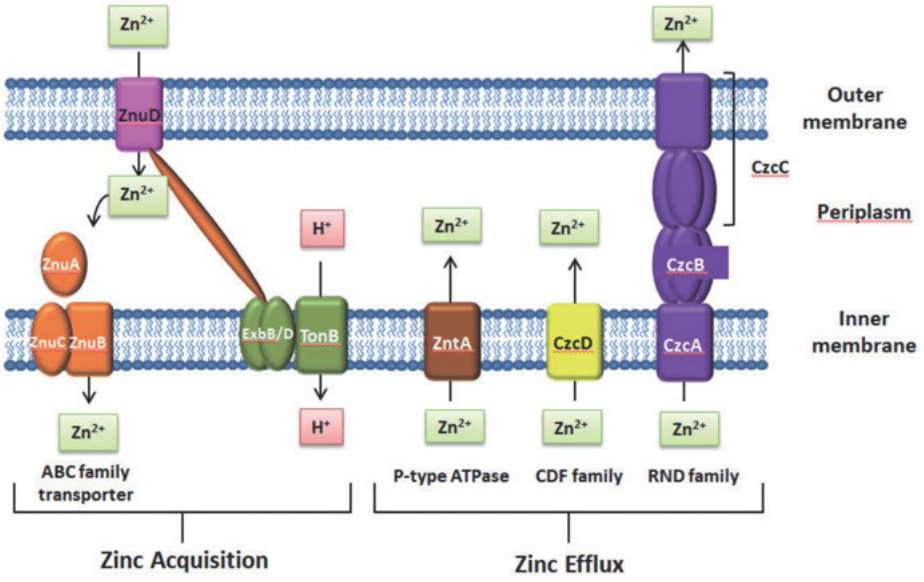

Figure 7. Cartoon illustrating zinc import and export in Gram-negative bacteria. The type of membrane-bound transporter (family) is indicated. High affinity import systems are shown in magenta, orange, and green. The exporters are shown in brown, yellow, and purple. Reproduced from [138], with permission of AIP Publishing; copyright 2018.

Exporter ZntA is a high affinity ATPase in both Gram-negative and -positive bacteria [143, 144]. The essential chemistry of its transport mechanism has been revealed for the transporter from *P. aeruginosa* [145]. Four conserved residues in the transmembrane domains are critical for Zn^{2+} pumping: two Cys and one Asp side chains provide a selective transmembrane binding site while a positively-charged Lys residue acts as a counter ion to prevent proton counter-transport. The flexible metal ion binding site also appears to function in the export of toxic Cd^{2+}, Hg^{2+}, and Pb^{2+} ions (see Sections 13, 14, and 17 below).

The complex homeostasis system for zinc (Figures 6 and 7) allows bacteria to survive in hostile environments such as metal-polluted ponds and mammalian macrophages.

13. GROUP 12 ELEMENT CADMIUM

Cadmium is one of the toxic metals of low natural abundance (Figure 1; set I) that has become problematical as industrial exploitation has outstripped its natural low mobility. The nature of import of Cd^{II} has been examined in a number of bacterial systems, identifying Mn, Zn, and Mg transporters as active uptake sites [146].

The molecular basis of Cd toxicity has been defined for Gram-positive *Streptococcus pneumoniae* whose single cell compartment structure allowed quantita-

tive assessment of perturbation of total metal ion content and homeostasis [147]. Elevated levels of Cd^{II} ions induced oxidative stress, even though the ion itself is redox-inactive. Cd competes for the Mn uptake pump Psa, inhibiting production of protective superoxide dismutase SodA. Cd also upregulates production of the Zn export pumps CzcD leading to depletion of Zn levels. In addition, it appears that binding of glutathione by elevated cytoplasmic Cd diminishes the role of this redox buffer as a metal buffer.

Overall, it appears that many bacteria involve glutathione in the processing of Cd [148]. In contrast to eukaryotes, only a few examples of bacterial Cys-rich metallothioneins are known to bind Cd [149, 150]. On the other hand, the flexible transmembrane metal ion binding site Cys_2Asp present in the *P. aeruginosa* zinc efflux pump ZntA allows it to also export Cd^{2+} as a resistance function [145].

14. GROUP 12 ELEMENT MERCURY

Mercury is another toxic metal of low natural abundance (Figure 1; set I) that has become a nutritional problem through its release by modern industry into biosystems. Its biogeochemical cycle is well-defined (Figure 8), leading to concerns about human ingestion of contaminated plants and fish in the second half of the last century [151].

Figure 8 documents the conversion of inorganic mercuric species into organomercury(II) compounds by methanogens and sulfate-reducing bacteria living in anoxic environments. Cations such as $[CH_3Hg^{II}]^+$ are lipophilic but stable in water. Hence, they can diffuse out of the host and into other microorganisms or be absorbed by higher animals such as plankton (through the exo-skeletons). Hg levels in eukaryotes can be 10^6-fold higher than in surrounding water as it is excreted much more slowly than it is consumed [152]. It consequently accumulates up the food chain.

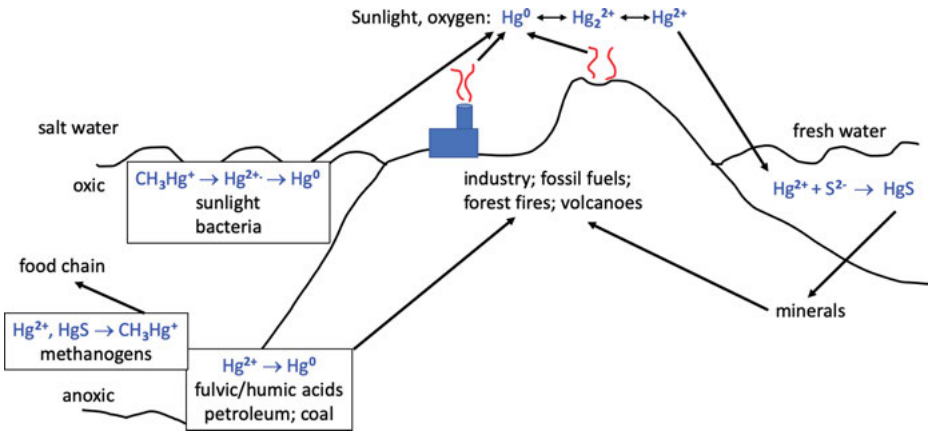

Figure 8. Simple mercury biogeochemical cycle. Adapted from [151].

The *mer* operon that confers resistance to both organic and inorganic forms of Hg is well understood. It has been found in every bacterial genus examined. Variants occur but up to ten mer proteins can be present that combine to bind, transport, and reduce the various forms of Hg^{II}. Each protein provides Cys ligands to bind the soft Hg^{II} electrophile with coordination numbers from 2 to 4 [153].

Inorganic Hg^{II} is transported into the cell for reduction to volatile Hg^0 that can then diffuse away from the cell. Sensor MerR regulates the *mer* operon by initiating transcription upon binding nanomolar Hg^{2+} [154, 155].

In the most common processes, periplasmic MerP sequesters Hg^{2+} ions for import by membrane transporter MerT [156, 157]. The cytoplasmic reductase MerA receives Hg^{II} (bound to a cellular thiol such as glutathione) and effects the reduction to Hg^0 (Equation 8) [158].

$$Hg^{2+} + NADPH \rightarrow Hg^0 + NADP^+ + H^+ \quad (8)$$

Bacteria with resistance to both inorganic and organic mercurials also feature the lyase MerB that releases Hg^{2+} from the latter by protonation (Equation 9) [159].

$$[R\text{-}Hg]^+ + H^+ \rightarrow Hg^{2+} + RH \qquad (R = \text{alkyl, aryl}) \quad (9)$$

Product Hg^{2+} is transported to MerA for reduction and the alkane RH diffuses from the cell. Detailed descriptions of the action of the *mer* operon are available in reviews [151, 160].

15. GROUP 13 ELEMENT ALUMINUM

Aluminum is the third most abundant element on Earth and the most abundant metal in its crust. However, it has no known role in biology. Its non-selection is apparently due to the insolubility of Al^{III} oxo-hydroxo species and that of hydroxo-alumino-silicates, its secondary mineral phases [161, 162]. The industrial and commercial use of Al metal has enhanced its presence in the biosphere.

Its toxicity is invoked when acid soils or 'acid rain' release significant levels of soluble Al [163]. The detailed molecular mechanisms of its impact on bacteria remain unknown. It is known to out-compete Mg^{II} in binding to ATP, may compete with Fe^{III} for siderophore ligands and may act as a pro-oxidant by binding superoxide radical [164–165].

16. GROUP 13 ELEMENT THALLIUM

Thallium has been used in pest control and is being used increasingly in industrial processes. Its main environmental source is smelting and fossil fuel burning and so its presence in the bio-sphere is increasing [166]. Oxidation states Tl^I and Tl^{III} can both be present as aqua cations in natural waters and the particular

balance can depend on local conditions and biota. For example, both oxidation states were found in the waters of Lake Ontario in North America and planktonic bacteria appeared to be responsible for the aerial oxidation of Tl^{I} to Tl^{III} [167].

Tl^{+} and K^{+} have similar ionic radii and one aspect of Tl toxicity may be inhibition of K metabolism. The toxic effects of Tl on certain microorganisms declined with increasing K concentrations [168]. The inhibition to growth of a range of bacterial species has been assessed [168] but the mechanisms of toxicity have not been defined in molecular detail.

17. GROUP 14 ELEMENT LEAD

No level of lead exposure is deemed to be safe for humans [169]. The elimination of lead from petrol, paint, and solder has allowed the average blood lead level in children aged 1–5 years in the USA to drop by about 10-fold over 30 years [170].

Lead defence mechanisms have evolved in bacteria, often as a component of protection against other toxic metals such as Cd and Hg. A dedicated Pb resistance operon *pbr* is present in *C. metallidurans* CH34 [171]. It is a member of the *mer* family (see Section 14) but the detailed mechanism varies to accommodate the different chemistries of Pb^{II} and Hg^{II}. In particular, precipitation of insoluble $Pb_3(PO_4)_2$ in the periplasm and/or exterior eliminates the danger. More details are available in [172, 173].

In *E. coli*, expression of the zinc exporter ZntA (Figure 7) also induces resistance to Pb^{II} and it was suggested that Pb^{II}-glutathione complex anions are the native substrates [174, 175]. However, the flexible transmembrane metal ion binding site in the ZntA from *P. aeruginosa* is able to bind and export Pb^{2+} ions via a three-coordinate $[Pb^{II}Cys_2Asp]$ site that accommodates the apical metal lone pair [145]. A similar situation may apply in *S. aurus* where CadA exports Pb^{II} as well as Cd^{II} and Zn^{II} [143, 174].

18. GROUP 15 ELEMENT ARSENIC

Arsenic is a ubiquitous toxic metalloid widely distributed in soil and groundwater [176]. The metalloid anion arsenate $[As^{V}O_4]^{3-}$ is imported by bacterial phosphate uptake systems and so interferes with phosphate metabolism. Cytoplasmic reduction leads to arsenite $[As^{III}O_3]^{3-}$ and its methylated forms that attack thiol groups. Bacteria have evolved a range of strategies of resistance to arsenic toxicity [177].

19. GROUP 15 ELEMENT BISMUTH

While bismuth drugs have long been used to treat bacterial infections in humans and other animals, the connection of *H. pylori* infection to gastric ulcers has revitalized their use in the treatment of peptic disease. The mechanism of action

is uncertain but may involve formation of a polymeric coating over lesions combined with toxic effects associated with uptake of soluble Bi species by the bacterium [178, 179].

20. GENERAL CONCLUSIONS

Microorganisms have evolved strategies to select and control the advantageous properties of the essential metals and to resist the toxicity of the non-essential metals and, under dis-homeostasis, of the essential metals. Multiple approaches have evolved to cope with the different environments, often extreme, that microorganisms encounter. Despite rapid recent progress, many of these strategies remain unknown, especially those devised by pathogens. The latter have particular impact on human health.

ACKNOWLEDGMENTS

We acknowledge sustained support from the Australian Research Council.

ABBREVIATIONS

ATP	adenosine 5′-triphosphate
ATPase	adenosine 5′-triphosphatase; enzyme that catalyzes the decomposition of adenosine 5′-triphosphate into adenosine 5′-diphosphate and PO_4^{3-}
NADP	nicotinamide adenine dinucleotide phosphate

REFERENCES

1. J. Prousek, *Pure Appl. Chem.* **2007**, *79*, 2325–2338.
2. D. H. Nies, *Metallomics* **2016**, *8*, 481–507.
3. A. Pol, T. R. Barends, A. Dietl, A. F. Khadem, J. Eygensteyn, M. S. Jetten, H. J. Op den Camp, *Environ. Microbiol.* **2014**, *16*, 255–264.
4. D. H. Irving, R. J. P. Williams, *Nature* **1948**, *162*, 746–747.
5. S. Tottey, K. J. Waldron, S. J. Firbank, B. Reale, C. Bessant, K. Sato, T. R. Cheek, J. Gray, C. Dennison, N. J. Robinson, *Nature* **2008**, *455*, 1138–1142.
6. D. Osman, A. W. Foster, K. Svedaite, J. W. Steed, E. Lurie-Luke, T. G. Huggins, N. J. Robinson, *Nature Commun.* **2017**, *8*, 1884.
7. D. Osman, M. A. Martini, A. W. Foster, J. Chen, A. J. P. Scott, R. J. Morton, J. W. Steed, E. Lurie-Luke, T. G. Huggins, A. D. Lawrence, E. Deery, M. J. Warren, P. T. Chivers, N. J. Robinson, *Nature Chem. Biol.* **2019**, *15*, 241–249.
8. M. I. Hood, E. P. Skaar, *Nature. Rev. Microbiol.* **2012**, *10*, 525–537.
9. J. P. Lisher, D. P. Giedroc, *Front. Cell. Infect. Microbiol.* **2013**, *3*, 91.

10. A. Wilks, K. A. Burkhard, *Nature Prod. Rep.* **2007**, *24*, 511–522.
11. A. G. Turner, K. Y. Djoko, C. Y. Ong, T. C. Barnett, M. J. Walker, A. G. McEwan, *Biochem. J.* **2019**, *476*, 595–611.
12. S. M. Damo, T. E. Kehl-Fie, N. Sugitani, M. E. Holt, S. Rathi, W. J. Murphy, Y. Zhang, C. Betz, L. Hench, G. Fritz, E. P. Skaar, W. J. Chazin, *Proc. Natl. Acad. Sci. USA* **2013**, *110*, 3841–3846.
13. J. R. Stephan, F. Yu, R. M. Costello, B. S. Bleier, E. M. Nolan, *J. Am. Chem. Soc.* **2018**, *140*, 17444–17455.
14. E. I. Koh, J. P. Henderson, *J. Biol. Chem.* **2015**, *290*, 18967–18974.
15. P. E. Bishop, D. M. L. Jarlenski, D. R. Hetherington, *J. Bacteriol.* **1982**, *150*, 1244–1251.
16. J. P. Bellenger, T. Wichard, A. B. Kustka, A. M. Kraepiel, *NatureGeosci.* **2008**, *1*, 243–246.
17. J. M. Winter, B. S. Moore, *J. Biol. Chem.* **2009**, *284*, 18577–18581.
18. C. Baysse, D. de Vos, Y. Naudet, A. Vandermonde, U. Ochsner, J. M. Meyer, H. Budzikiewicz, M. Schafer, R. Fuchs, P. Cornelis, *Microbiology* **2000**, *146*, 2425–2434.
19. P. A. Lay, A. Levina, *Chromium*, in *Binding, Transport and Storage of Metal Ions in Biological Cells*, Eds W. Maret, A. G. Wedd, Royal Society of Chemistry, Cambridge, UK, **2014**, pp. 188–222.
20. M. I. Ramirez-Diaz, C. Diaz-Perez, E. Vargas, H. Riveros-Rosas, J. Campos-Garcia, C. Cervantes, *Biometals* **2008**, *21*, 321–332.
21. C. Cervantes, J. Campos-Garcia, S. Devars, F. Gutierrez-Corona, H. Loza-Tavera, J. C. Torres-Guzman, R. Moreno-Sanchez, *FEMS Microbiol. Rev.* **2001**, *25*, 335–347.
22. A. Levina, P. A. Lay, *Dalton Trans.* **2011**, *40*, 11675–11686.
23. R. Codd, J. A. Irwin, P. A. Lay, *Curr. Opin. Chem. Biol.* **2003**, *7*, 213–219.
24. A. Levina, P. A. Lay, *Coord. Chem. Rev.* **2005**, *249*, 281–298.
25. K. H. Cheung, J. D. Gu, *Int. Biodet. Biodegrad.* **2007**, *59*, 8–15.
26. L. Shi, T. C. Squier, J. M. Zachara, J. K. Fredrickson, *Mol. Microbiol.* **2007**, *65*, 12–20.
27. S. Eswaramoorthy, S. Poulain, R. Hienerwadel, N. Bremond, M. D. Sylvester, Y. B. Zhang, C. Berthomieu, D. Van der Lelie, A. Matin, *PLoS ONE* **2012**, *7*, e36017.
28. H. J. Jin, Y. F. Zhang, G. W. Buchko, S. M. Varnum, H. Robinson, T. C. Squier, P. E. Long, *PLoS ONE* **2012**, 7, e42432.
29. D. G. Barceloux, *J. Toxicol. Clin. Toxicol.* **1999**, *37*, 173–194.
30. *Molybdenum and Tungsten Enzymes, Bioinorganic Chemistry*, Eds R. Hille, C. Schulzke, M. L. Kirk, Royal Society of Chemistry, Cambridge, UK, **2017**, pp. v–vi.
31. L. B. Maia, I. Moura, J. J. G. Moura, *Molybdenum and Tungsten-Containing Enzymes: An Overview*, in *Molybdenum and Tungsten Enzymes*, *Biochemistry*, Eds R. Hille, C. Schulzke, M. L. Kirk, Royal Society of Chemistry, Cambridge, UK, **2017**, pp. 1–80.
32. R. Zeinert, E. Martinez, J. Schmitz, K. Senn, B. Usman, V. Anantharaman, L. Aravind, L. S. Waters, *J. Biol. Chem.* **2018**, *293*, 5715–5730.
33. J. A. Imlay, *J. Biol. Chem.* **2014**, *289*, 28121–28128.
34. L. J. Juttukonda, E. P. Skaar, *Mol. Microbiol.* **2015**, *97*, 216–228.
35. B. Troxell, H. Xu, X. F. Yang, *J. Biol.Chem.* **2012**, *287*, 19284–19293.
36. J. E. Martin, L. S. Waters, G. Storz, J. A. Imlay, *PLoS Genet.* **2015**, *11*, e1004977.
37. J. E. Martin, J. P. Lisher, M. E. Winkler, D. P. Giedroc, *Mol.Microbiol.* **2017**, *104*, 334–348.
38. T. H. Hohle, M. R. O'Brian, *Mol. Microbiol.* **2014**, *93*, 736–747.
39. R. M. Counago, M. P. Ween, S. L. Begg, M. Bajaj, J. Zuegg, M. L. O'Mara, M. A. Cooper, A. G. McEwan, J. C. Paton, B. Kobe, C. A. McDevitt, *Nature Chem. Biol.* **2014**, *10*, 35–41.

40. G. Glatzmaier, P. Roberts, *Science* **1996**, *274*, 1887–1891.
41. G. Wächtershauser, *Proc. Natl. Acad. Sci. USA* **1990**, *87*, 200–204.
42. G. Wächtershauser, *Science* **2000**, *289*, 1307–1308.
43. R. J. Williams, *Nature* **1990**, *343*, 213–214.
44. M. Kammler, C. Schon, K. Hantke, *J. Bacteriol.* **1993**, *175*, 6212–6219.
44. Y. Zhu, S. Kumar, A. L. Menon, R. A. Scott, M. W. Adams, *J. Bacteriol.* **2013**, *195*, 2400–2407.
46. M. L. Cartron, S. Maddocks, P. Gillingham, C. J. Craven, S. C. Andrews, *Biometals* **2006**, *19*, 143–157.
47. J. Cao, M. R. Woodhall, J. Alvarez, M. L. Cartron, S. C. Andrews, *Mol. Microbiol.* **2007**, *65*, 857–875.
48. C. Grosse, J. Scherer, D. Koch, M. Otto, N. Taudte, G., *Mol. Microbiol.* **2006**, *62*, 120–131.
49. E. Turlin, M. Debarbouille, K. Augustyniak, A. M. Gilles, C. Wandersman, *PLoS ONE* **2013**, *8*, e56529.
50. V. Braun, H. Killmann, *Trends Biochem.Sci.* **1999**, *24*, 104–109.
51. P. Cornelis, Q. Wei, S. C. Andrews, T. Vinckx, *Metallomics* **2011**, *3*, 540–549.
52. P. Cornelis, *Iron Uptake and Homeostasis in Prokaryotic Microorganisms*, in *Binding, Transport and Storage of Metal Ions in Biological Systems*, Eds W. Maret, A. G. Wedd, Royal Society of Chemistry, Cambridge, UK, **2014**, pp. 303–332.
53. J. R. Behnsen, M. Raffatellu, *Mbio.* **2016**, *7*, e01906–16.
54. B. R. Wilson, A. R. Bogdan, M. Miyazawa, K. Hashimoto, Y. Tsuji, *Trends Mol. Med.* **2016**, *22*, 1077–1090.
55. J. Gal, A. Hursthouse, P. Tatner, F. Stewart, R. Welton, *Environ. Int.* **2008**, *34*, 821–838.
56. L. Leyssens, B. Vinck, C. Van Der Straeten, F. Wuyts, L. Maes, *Toxicology* **2017**, *387*, 43–56.
57. S. Okamoto, L. D. Eltis, *Metallomics* **2011**, *3*, 963–970.
58. R. Pawlak, S. J. Parrott, S. Raj, D. Cullum-Dugan, D. Lucus, *Nutr. Rev.* **2013**, *71*, 110–117.
59. S. P. Stabler, *N. Engl. J. Med.* **2013**, *368*, 2041–2042.
60. F. Barras, M. Fontecave, *Metallomics* **2011**, *3*, 1130–1134.
61. C. Ranquet, S. Ollagnier-de-Choudens, L. Loiseau, F. Barras, M. Fontecave, *J. Biol. Chem.* **2007**, *282*, 30442–30451.
62. A. Rodrigue, G. Effantin, M. A. Mandrand-Berthelot, *J. Bacteriol.* **2005**, *187*, 2912–2916.
63. M. I. Ansari, A. Malik, *Environ. Monit. Assess.* **2010**, *167*, 151–163.
64. M. Patriarca, T. D. Lyon, G. S. Fell, *Am. J. Clin. Nutr.* **1997**, *66*, 616–621.
65. J. C. Fontecilla–Camps, P. Amara, C. Cavazza, Y. Nicolet, A. Volbeda, *Nature* **2009**, *460*, 814–822.
66. P. T. Chivers, *Cobalt and Nickel*, in *Binding, Transport and Storage of Metal Ions in Biological Systems*, Eds W. Maret, A. G. Wedd, Royal Society of Chemistry, Cambridge, UK, **2014**, pp. 381–428.
67. L. Macomber, S. P. Elsey, R. P. Hausinger, *Mol. Microbiol.* **2011**, *82*, 1291–1300.
68. L. Macomber, R. P. Hausinger, *Metallomics* **2011**, *3*, 1153–1162.
69. N. E. Le Brun, *Copper in Prokaryotes*, in *Binding, Transport and Storage of Metal Ions in Biological Systems*, Eds W. Maret, A. G. Wedd, Royal Society of Chemistry, Cambridge, UK, **2014**, pp. 461–499.
70. C. L. Dupont, G. Grass, C. Rensing, *Metallomics* **2011**, *3*, 1109–1118.
71. L. Macomber, J. A. Imlay, *Proc. Natl. Acad. Sci. USA* **2009**, *106*, 8344–8349.
72. K. Y. Djoko, A. G. McEwan, *ACS Chem. Biol.* **2013**, *8*, 2217–2223.

73. C. M. Saporito-Magrina, R. N. Musacco-Sebio, G. Andrieux, L. Kook, M. T. Orrego, M. V. Tuttolomondo, M. F. Desimone, M. Boerries, C. Borner, M. G. Repetto, *Metallomics* **2018**, *10*, 1743–1754.
74. M. Colin, F. Klingelschmitt, E. Charpentier, J. Josse, L. Kanagaratnam, C. De Champs, S. C. Gangloff, *Materials (Basel)* **2018**, *6*, E2479.
75. N. J. Robinson, D. R. Winge, *Annu. Rev. Biochem.* **2010**, *79*, 537–562.
76. S. Tottey, C. J. Patterson, L. Banci, I. Bertini, I. C. Felli, A. Pavelkova, S. J. Dainty, R. Pernil, K. J. Waldron, A. W. Foster, N. J. Robinson, *Proc. Natl. Acad. Sci. USA.* **2012**, *109*, 95–100.
77. C. Rensing, G. Grass, *FEMS Microbiol. Rev.* **2003**, *27*, 197–213.
78. M. I. Samanovic, C. Ding, D. J. Thiele, K. H. Darwin, *Cell. Host Microbe* **2012**, *11*, 106–115.
79. F. W. Outten, C. E. Outten, J. Hale, T. V. O'Halloran, *J. Biol. Chem.* **2000**, *275*, 31024–31029.
80. S. A. Roberts, G. F. Wildner, G. Grass, A. Weichsel, A. Ambrus, C. Rensing, W. R. Montfort, *J. Biol. Chem.* **2003**, *278*, 31958–31963.
81. K. Y. Djoko, L. X. Chong, A. G. Wedd, Z. Xiao, *J. Am. Chem. Soc.* **2010**, *132*, 2005–2015.
82. L. Cortes, A. G. Wedd, Z. Xiao, *Metallomics* **2015**, *7*, 776–785.
83. F. W. Outten, D. L. Huffman, J. A. Hale, T. V. O'Halloran, *J. Biol. Chem.* **2001**, *276*, 30670–30677.
84. S. Franke, G. Grass, C. Rensing, D. H. Nies, *J. Bacteriol.* **2003**, *185*, 3804–3812.
85. S. A. Gudipaty, M. M. McEvoy, *Biochim. Biophys. Acta* **2014**, *1844*, 1656–1661.
86. F. Long, C. C. Su, M. T. Zimmermann, S. E. Boyken, K. R. Rajashankar, R. L. Jernigan, E. W. Yu, *Nature* **2010**, *467*, 484–488.
87. C. C. Su, F. Long, M. T. Zimmermann, K. R. Rajashankar, R. L. Jernigan, E. W. Yu, *Nature* **2011**, *470*, 558–562.
88. C. C. Su, F. Long, E. W. Yu, *Protein Sci.* **2011**, *20*, 6–18.
89. E. H. Kim, D. H. Nies, M. M. McEvoy, C. Rensing, *J. Bacteriol.* **2011**, *193*, 2381–2387.
90. K. N. Chacon, T. D. Mealman, M. M. McEvoy, N. J. Blackburn, *Proc. Natl. Acad. Sci. USA* **2014**, *111*, 15373–15378.
91. D. A.Cooksey, *FEMS Microbiol. Rev.* **1994**, *14*, 381–386.
92. X. X. Zhang, P. B. Rainey, *Environ. Microbiol.* **2008**, *10*, 3284–3294.
93. S. Chillappagari, M. Miethke, H. Trip, O. P. Kuipers, M. A. Marahiel, *J. Bacteriol.* **2009**, *191*, 2362–2370.
94. C. Rensing, S. F. McDevitt, *Met. Ions Life Sci.* **2013**, *12*, 417–450.
95. E. Ladomersky, M. J. Petris, *Metallomics* **2015**, *7*, 957–964.
96. K. Hirooka, T. Edahiro, K. Kimura, Y. Fujita, *J. Bacteriol.* **2012**, *194*, 5675–5687.
97. D. A. Rouch, N. L. Brown, *Microbiology* **1997**, *143*, 1191–1202.
98. D. L. Huffman, J. Huyett, F. W. Outten, P. E. Doan, L. A. Finney, B. M. Hoffman, T. V. O'Halloran, *Biochemistry* **2002**, *41*, 10046–10055.
99. K. Y. Djoko, Z. Xiao, D. L. Huffman, A. G. Wedd, *Inorg. Chem.* **2007**, *46*, 4560–4568.
100. K. Y. Djoko, Z. Xiao, A. G. Wedd, *ChemBiochem* **2008**, *9*, 1579–1582.
101. M. Zimmermann, S. R. Udagedara, C. M. Sze, T. M. Ryan, G. J. Howlett, Z. Xiao, A. G. Wedd, *J. Inorg. Biochem.* **2012**, *115*, 186–197.
102. M. O. Ross, F. MacMillan, J. Wang, A. Nisthal, T. J. Lawton, B. D. Olafson, S. L. Mayo, A. C. Rosenzweig, B. M. Hoffman, *Science* **2019**, *364*, 566–570.
103. H. J. Kim, D. W. Graham, A. A. DiSpirito, M. A. Alterman, N. Galeva, C. K. Larive, D. Asunskis, P. M. Sherwood, *Science* **2004**, *305*, 1612–1615.
104. C. Dennison, *Chemistry* **2019**, *25*, 74–86.
105. N. Vita, G. Landolfi, A. Basle, S. Platsaki, J. Lee, K. J. Waldron, C. Dennison, *Sci. Rep.* **2016**, *6*, 39,065.

106. D. S. Radford, M. A. Kihlken, G. P. Borrelly, C. R. Harwood, N. E. Le Brun, J. S. Cavet, *FEMS Microbiol. Lett.* **2003**, *220*, 105–112.
107. L. Banci, I. Bertini, S. Ciofi-Baffoni, N. G. Kandias, N. J. Robinson, G. A. Spyroulias, X. C. Su, S. Tottey, M. Vanarotti, *Proc. Natl. Acad. Sci. USA* **2006**, *103*, 8320–8325.
108. Y. Xue, A. V. Davis, G. Balakrishnan, J. P. Stasser, B. M. Staehlin, P. Focia, T. G. Spiro, J. E. Penner-Hahn, T. V. O'Halloran, *Nature Chem. Biol.* **2008**, *4*, 107–109.
109. J. M. Arguello, S. J. Patel, J. Quintana, *Metallomics* **2016**, *8*, 906–914.
110. P. Gourdon, X. Y. Liu, T. Skjorringe, J. P. Morth, L. B. Moller, B. P. Pedersen, P. Nissen, *Nature* **2011**, *475*, 59–64.
111. M. Andersson, D. Mattle, O. Sitsel, T. Klymchuk, A. M. Nielsen, L. B. Moller, S. H. White, P. Nissen, P. Gourdon, *Nature Struct. Mol. Biol.* **2014**, *21*, 43–48.
112. C. J. Wijekoon, S. R. Udagedara, R. L. Knorr, R. Dimova, A. G. Wedd, Z. Xiao, *J. Am. Chem. Soc.* **2017**, *139*, 4266–4269.
113. S. Meydan, D. Klepacki, S. Karthikeyan, T. Margus, P. Thomas, J. E. Jones, Y. Khan, J. Briggs, J. D. Dinman, N. Vazquez-Laslop, A. S. Mankin, *Mol. Cell* **2017**, *65*, 207–219.
114. A. D. Russell, W. B. Hugo, *Prog. Med. Chem.* **1994**, *31*, 351–370.
115. J. W. Alexander, *Surg. Infect.* **2009**, *10*, 289–292.
116. H. J. Johnston, G. Hutchison, F. M. Christensen, S. Peters, S. Hankin, V. Stone, *Crit. Rev. Toxicol.* **2010**, *40*, 328–346.
117. S. Lekamge, A. S. Ball, R. Shukla, D. Nugegoda, *Rev. Environ. Contam. Toxicol.* **2020**, *248*, 1–80.
118. A. Gupta, K. Matsui, J. F. Lo, S. Silver, *Nature Med.* **1999**, *5*, 183–188.
119. S. Silver, *FEMS Microbiol. Rev.* **2003**, *27*, 341–353.
120. N. C. Bury, *Silver*, in *Binding, Transport and Storage of Metal Ions in Biological Systems*, Eds W. Maret, A. G. Wedd, Royal Society of Chemistry, Cambridge, UK, **2014**, pp. 556–581.
121. S. L. Percival, P. G. Bowler, D. Russell, *J. Hosp. Infect.* **2005**, *60*, 1–7.
122. H. Wang, N. Law, G. Pearson, B. E. van Dongen, R. M. Jarvis, R. Goodacre, J. R. Lloyd, *J. Bacteriol.* **2010**, *192*, 1143–1150.
123. D. K. H. Weatherley, R. W. Henley, *Nature Geosci.* **2013**, *6*, 294–298.
124. L. Butof, N. Wiesemann, M. Herzberg, M. Altzschner, A. Holleitner, F. Reith, D. H. Nies, *Metallomics* **2018**, *10*, 278–286.
125. F. Reith, M. F. Lengke, D. Falconer, D. Craw, G. Southam, *ISME J.* **2007**, *1*, 567–584.
126. F. Reith, S. L. Rogers, D. C. McPhail, D. Webb, *Science* **2006**, *313*, 233–236.
127. C. W. Johnston, M. A. Wyatt, X. Li, A. Ibrahim, J. Shuster, G. Southam, N. A. Magarvey, *Nature Chem. Biol.* **2013**, *9*, 241–243.
128. F. C. C. Soncini, S. K. Checa, *Gold*, in *Binding, Transport and Storage of Metal Ions in Biological Systems*, Eds W. Maret, A. G. Wedd, Royal Society of Chemistry, Cambridge, UK, **2014**, pp. 582–605.
129. L. B. Pontel, M. E. Audero, M. Espariz, S. K. Checa, F. C. C. Soncini, *Mol. Microbiol.* **2007**, *66*, 814–825.
130. N. Wiesemann, L. Butof, M. Herzberg, G. Hause, L. Berthold, B. Etschmann, J. Brugger, G. Martinez-Criado, D. Dobritzsch, S. Baginsky, F. Reith, D. H. Nies, *Appl. Environ. Microbiol.* **2017**, *83*, e01679.
131. N. Wiesemann, J. Mohr, C. Grosse, M. Herzberg, G. Hause, F. Reith, D. H. Nies, *J. Bacteriol.* **2013**, *195*, 2298–308.
132. C. Andreini, L. Banci, I. Bertini, A. Rosato, *J. Proteome Res.* **2005**, *5*, 196–201.
133. A. Takeda, *Brain Res. Rev.* **2000**, *34*, 137–148.
134. W. Maret, *Free Rad. Biol. Med.* **2019**, *134*, 311–326.
135. C. A. Blindauer, M. D. Harrison, J. A. Parkinson, A. K. Robinson, J. S. Cavet, N. J. Robinson, P. J. Sadler, *Proc. Natl. Acad. Sci. USA* **2001**, *98*, 9593–9598.

136. R. Kapetanovic, N. J. Bokil, M. E. Achard, C. L. Ong, K. M. Peters, C. J. Stocks, M. D. Phan, M. Monteleone, K. Schroder, K. M. Irvine, B. M. Saunders, M. J. Walker, K. J. Stacey, A. G. McEwan, M. A. Schembri, M. J. Sweet, *FASEB J.* **2016**, *30*, 1901–1912.
137. J. P. Barnett, A. Millard, A. Z. Ksibe, D. J. Scanlan, R. Schmid, C. A. Blindauer, *Front. Microbiol.* **2012**, *3*, 142.
138. B. Suryawati, *Zinc homeostasis mechanism and its role in bacterial virulence capacity. AIP Conference Proceedings*, **2021**, 070021 (2018); https://doi.org/10.1063/1.5062819.
139. S. I. Patzer, K. Hantke, *J. Biol.Chem.* **2000**, *275*, 24321–24332.
140. G. Porcheron, A. Garenaux, J. Proulx, M. Sabri, C. M. Dozois, *Front. Cell. Infect. Microbiol.* **2013**, *3*, 90.
141. O. Kolaj-Robin, D. Russell, K. A. Hayes, J. T.Pembroke, T. Soulimane, *FEBS Lett.* **2015**, *589*, 1283–1295.
142. V. G. Pederick, B. A. Eijkelkamp, S. L. Begg, M. P. Ween, L. J. McAllister, J. C. Paton, C. A. McDevitt, *Sci. Rep.* **2015**, *5*, 13139.
143. C. Rensing, B. Mitra, B. P. Rosen, *Proc. Natl. Acad. Sci. USA* **1997**, *94*, 14326–14331.
144. G. Grass, B. Fan, B. P. Rosen, S. Franke, D. H. Nies, C. Rensing, *J. Bacteriol.* **2001**, *183*, 4664–4667.
145. M. J. Gallenito, G. W. Irvine, L. Zang, G. Meloni, *Chem. Commun.* **2019**, *55*, 10844–10847.
146. J.-M. Moulis, J. Bourguignon, P. Catty, *Cadmium*, in *Binding, Transport and Storage of Metal Ions in Biological Systems*, Eds W. Maret, A. G. Wedd, Royal Society of Chemistry, Cambridge, UK, **2014**, pp. 695–746.
147. S. L. Begg, B. A. Eijkelkamp, Z. Luo, R. M. Counago, J. R. Morey, M. J. Maher, C. L. Ong, A. G. McEwan, B. Kobe, M. L. O'Mara, J. C. Paton, C. A. McDevitt, *Nature Commun.* **2015**, *6*, 6418.
148. E. Bianucci, A. Fabra, S. Castro, *Biometals* **2012**, *25*, 23–32.
149. M. J. Daniels, J. S. Turner-Cavet, R. Selkirk, H. Sun, J. A. Parkinson, P. J. Sadler, N. J. Robinson, *J. Biol. Chem.* **1998**, *273*, 22957–22961.
150. B. Gold, H. Deng, R. Bryk, D. Vargas, D. Eliezer, J. Roberts, X. Jiang, C. Nathan, *Nature Chem. Biol.* **2008**, *4*, 609–616.
151. T. Barkay, S. M. Miller, A. O. Summers, *FEMS Microbiol. Rev.* **2003**, *27*, 355–384.
152. N. Ballatori, J. L. Boyer, *Toxicol. Appl. Pharmacol.* **1986**, *85*, 407–415.
153. S. J. Fretham, S. Caito, E. J. Martinez-Finley, M. Aschner, *Toxicol. Res.* **2012**, *1*, 32–38.
154. T. V. O'Halloran, *Science* **1993**, *261*, 715–725.
155. T. O'Halloran, C. Walsh, *Science* **1987**, *235*, 211–214.
156. S. Silver, T. le Phung, *J. Ind.Microbiol. Biotechnol.* **2005**, *32*, 587–605.
157. N. L. Brown, Y. C. Shih, C. Leang, K. J. Glendinning, J. L. Hobman, J. R. Wilson, *Biochem. Soc. Trans.* **2002**, *30*, 715–718.
158. T. Barkay, I. Wagner-Dobler, *Adv. Appl. Microbiol* . **2005**, *57*, 1–52.
159. T. P. Begley, A. E. Walts, C. T. Walsh, *Biochemistry* **1986**, *25*, 7192–7200.
160. S. J. B. Fretham, M. Aschner, *Mercury*, in *Binding, Transport and Storage of Metal Ions in Biological Systems*, Eds W. Maret, A. G. Wedd, Royal Society of Chemistry, Cambridge, UK, **2014**, pp. 747–767.
161. J. D. E. Birchall, C. Exley, J. S. Chappell, M. J. Phillips, *Nature* **1989**, *338*, 146–148.
162. C. Exley, J. K. Pinnegar, H. Taylor, *J. Theor. Biol.* **1997**, *189*, 133–139.
163. R. B. Martin, *Acc. Chem. Res.* **1994**, *27*, 204–210.
164. T. L. Macdonald, R. B. Martin, *Trends Biochem. Sci.* **1988**, *13*, 15–19.
165. C. Exley, *Free Rad. Biol. Med.* **2004**, *36*, 380–387.
166. G. Kazantzis, *Environ. Geochem. and Health* **2000**, *22*, 275–280.
167. B. S. Twining, M. R. Twiss, N. S. Fisher, *Environ. Sci. Technol.* **2003**, *37*, 2720–2726.
168. M. Sager, *Toxicol. Environ.Chem.* **1994**, *45*, 11–32.

169. Centers for Disease Control and Prevention, https://www.cdc.gov/nceh/lead/; https://www.cdc.gov/nceh/lead/acclpp/final_document_030712.pdf. Accessed March 19, 2020.
170. N. Zhang, H. W. Baker, M. Tufts, R. E. Raymond, H. Salihu, M. R. Elliott, *Am. J. Public Health* **2013**, *103*, e72–e77.
171. B. Borremans, J. L. Hobman, A. Provoost, N. L. Brown, D. van Der Lelie, *J. Bacteriol.* **2001**, *183*, 5651–5658.
172. V. M. Cangelosi, V. L. Pecoraro, *Lead*, in *Binding, Transport and Storage of Metal Ions in Biological Systems*, Eds W. Maret, A. G. Wedd, Royal Society of Chemistry, Cambridge, UK, **2014**, pp. 843–882.
173. A. Jaroslawiecka, Z. Piotrowska-Seget, *Microbiology* **2014**, *160*, 12–25.
174. C. Rensing, Y. Sun, B. Mitra, B. P. Rosen, *J. Biol. Chem.* **1998**, *273*, 32614–32617.
175. A. Hynninen, T. Touze, L. Pitkanen, D. Mengin-Lecreulx, M. Virta, *Mol. Microbiol.* **2009**, *74*, 384–394.
176. Y. G. Zhu, M. Yoshinaga, F. J. Zhao, B. P. Rosen, *Ann. Rev. Earth Planet. Sci.* **2014**, *42*, 443–467.
177. S.-C. Chen, G.-X. Sun, B. P. Rosen, S.-Y. Zhang, Y. Deng, B.-K. Zhu., C. Rensing, Y.-G. Zhu, *Sci. Rep.* **2017**, *7*, 7741.
178. M. P. Rigobello, L. Messori, G. Marcon, M. Agostina Cinellu, M. Bragadin, A. Folda, G. Scutari, A. Bindoli, *J. Inorg. Biochem.* **2004**, *98*, 1634–1641.
179. T. O. Negishi, K. Oshima, M. Hattori, M. Kanai, S. Mano, M. Nishimura, K. Yoshida, *PLoS ONE* **2012**, *7*, e43189.

10

The Biochemistry of Rare Earth Elements

Lena J. Daumann [1] ***and Huub J. M. Op den Camp*** [2]

[1]Department of Chemistry, Faculty for Chemistry and Pharmacy, Ludwig-Maximilians-Universität München, Butenandtstrasse 5–13, Haus D, D-81377 München, Germany
<lena.daumann@lmu.de>

[2]Department of Microbiology, IWWR, Faculty of Science, Radboud University Nijmegen, Heyendaalseweg 135, NL-6525 ED Nijmegen, The Netherlands
<h.opdencamp@science.ru.nl>

Metal Ions in Life Sciences, Volume 21 Guest Editors: Peter M. H. Kroneck and Martha E. Sosa Torres
Series Editors: Astrid Sigel, Eva Freisinger, and Roland K. O. Sigel

https://doi.org/10.1515/9783110589771-010

Abstract: Rare earth elements (REE) are essential for our daily lives. It is not only their use in high technologies like smartphones and computers and in renewable energy applications. The interaction of REE with biomolecules and living organisms and the exploitation of their photo-physical properties for a range of applications in biochemistry research and medicine have been studied for many decades. But this is no longer the only reason to make them an attractive group of elements to investigate. An entirely new area of research has emerged in the past ten years after it was established that many bacteria utilize certain REE in their metabolism. This chapter gives an overview on the most recent developments in this field along with an account of the more established uses of REE in biochemistry, biomining, and medicine.

Keywords: lanthanides · rare earth elements · methanotroph · methanol dehydrogenase · medicine

1. INTRODUCTION: PROPERTIES OF RARE EARTH ELEMENTS

"*Among the 102 elements known to men, there are 15 whose properties resemble each other like two drops of water. These are the so-called rare-earth elements. They are situated at the centre of Mendeleyev's table. Their name originates from the Latin* terra rara*, which means "rare earth". For a long time they were considered really rare. Only the investigations of the last two decades have shown that they are far more abundant on the earth's surface than metals like lead, mercury and gold …*" Author's preface, *The Rare-Earth Elements* by D. N. Trifonov, translated 1963 [1].

The rare earth elements (REE) are probably the most misunderstood group of elements in the periodic table. Originally isolated as their oxides, they were named "earths". Scandium (Sc), yttrium (Y), and the elements lanthanum (La) to lutetium (Lu) make up the group of the 17 rare earth elements. Within this group La to Lu are also known as the lanthanides (Ln). Although strictly speaking, lanthanum is not a lanthanide (because the lanthanides are named after this element) it has been included by common usage by IUPAC. These elements occur widely distributed in nature in the form of minerals (Figure 1) for example, xenotime (YPO_4), gadolinite ($(Ce,La,Nd,Y)_2FeBe_2Si_2O_{10}$), bastnaesite ($(Ce,La,Nd,Y)(CO_3F)$) or monazite ($(Ce,La,Nd,Th)PO_4$).

Due to their similar chemical properties REE always occur together in ores, often also with traces of uranium and thorium. As rightly stated by Trifonov above, the REE occur abundantly and widely distributed in the earth's crust. The two most abundant, La and Ce, are of similar abundance as Cu or Zn. Even

Figure 1. Two REE containing minerals. Bastnaesite from Nam Xe in Vietnam on the left and gadolinite from Norway shown in the middle. Ytterby Gruva in Sweden, the place of discovery of many of the REE is shown on the right.

the two rarest, Tm and Lu, are more abundant than I or Ag. The distribution of REE in aqueous environments can vary greatly. Early lanthanides are more abundant than the later ones and those with even atomic numbers along the series are more abundant than their adjacent odd numbered counterparts (Oddo-Harkins rule). Ground water can contain between 5.7 and 410 pmol/kg, riverwater between 15 and 270 pmol/kg REE. In seawater concentrations of 1.6 up to 13 pmol/kg have been reported [2]. However, certain ecosystems, such as volcanic mudpots can contain significantly higher concentrations [3]. Here, high temperatures and low pH favor higher concentrations of REE. It should be mentioned here, that gadolinium levels are on the rise in aquatic ecosystems near larger cities. The reason behind this is the widespread use of Gd-based magnetic resonance imaging (MRI) contrast agents. The trends show that Gd concentrations are rapidly increasing, for example, a study within the San Francisco Bay Area showed that within only 20 years Gd concentrations increased from 8.27 to a staggering 112 pmol/kg [4]. The long term consequences of this anthropogenic introduction of mobile, highly persistent Gd into ecosystems can currently not be foreseen. In addition to the use of gadolinium as an MRI contrast agent, mankind has made substantial use of the remarkable properties of REE. Although possessing very similar properties in coordination chemistry, their different electronic structures have led to them being used in a multitude of different applications in high technologies, medicine, and biochemistry research. The analysis of REE content in biochemical samples (proteins, bacteria, tissues, etc.) can be achieved by a number of different methods [5]. Most widely used are atomic absorption spectroscopy (AAS), inductively coupled plasma coupled with optical emission spectroscopy (ICP-OES) or mass spectrometry (ICP-MS), with the latter being the most sensitive method with a limit of detection (LoD) of 0.1 ppt to 10 ppb. In addition, UV-vis spectroscopy using REE specific dyes has been reported [6] as well as the exploitation of their luminescent properties.

2. SELECTED USES OF RARE EARTH ELEMENTS IN BIOCHEMISTRY RESEARCH

2.1. Interactions of Rare Earth Elements with Biomolecules

The interactions of REE with biomolecules and their applications in biology and medicine have been extensively reviewed and the reader may want to refer to these extensive reference works [7–10]. Long before the biological use of lanthanides by bacteria was discovered, their similar coordination chemistry properties to calcium and interesting spectroscopic and physical properties of REE were exploited by researchers. Therefore, only very recent developments and specific application examples are covered here. As REE are highly charged, hard Lewis acids, hard, negatively charged oxygen donors are preferred when REE readily bind to amino acids and proteins, DNA, and low-molecular-weight ligands such as siderophores, carbohydrates, and cell surfaces (Table 1). In the presence of phosphate, REE form poorly soluble precipitates and thus in (biological) environments the concentration is low [11]. In fact, this property is used in an Australian product called Phoslock™, a modified clay containing lanthanum that was developed to bind phosphate ions from waterways and wastewater and to prevent algal blooms [12].

Table 1. Comparison of coordination properties of Ca(II) and Ln(III) showing similarities and differences.[a, b]

Property	**Ca**	**Ln**
Coordination number (CN)	6–12	6–12
Favored CN	6 or 7	8 or 9
Coordination geometry	flexible	flexible
Donor atom preference	O > N > S	O > N > S
Ionic radius in 6-coordination [13]	1.14	1.172–1.001
Oxidation state in biological environments	+2	+3 (with few exceptions)
Solubility of the phosphates at 25 °C in H_2O	$Ca_3(PO_4)_2$ fairly soluble	$LaPO_4$ poorly soluble; note that the numbers given for the solubility of both compounds vary in the literature, depending on conditions of measurement

[a] Table modified from ref. [7].
[b] REE Sc and Y excluded.

2.2. Nuclear Magnetic Resonance

Paramagnetic lanthanide complexes have found use as shift reagents in nuclear magnetic resonance (NMR) spectroscopy for several decades [7, 14]. Especially useful have been chiral reagents based on low-molecular-weight complexes, like tris[3-(heptafluoropropyl-hydroxymethylene)-d-camphorate Eu(III), for the determination of enantiomeric purity of small organic molecules and natural products [15]. In larger biomolecules like proteins and shorter peptides, lanthanide pseudo contact shifts and residual dipolar couplings have provided researchers with invaluable information on the structure of the biomolecules of interest. Here, either an already existing metal binding site can be used or a lanthanide-binding tag can be employed [16–18]. Binding constants, pK_a values of coordinating ligands and other parameters can be further obtained by NMR titrations. The diamagnetic lanthanides La(III) and Lu(III) may serve as controls for their paramagnetic family members. Recently, NMR spectroscopy with paramagnetic lanthanide compounds has been used to solve the three-dimensional structures of proteins in cells [19]. Shown in Figure 2 is the immunoglobulin-binding domain of protein G (GB1) that was used as a model protein carrying the 2,2′,2″,2‴-[(pyridine-2,6-diyl)bis(methylenenitrilo)]tetrakis(acetic acid) (PyMTA) ligand that can be complexed with lanthanides. The same label has previously been used with Gd(III) for EPR measurements to monitor the dynamics and structure of peptides in cells [20].

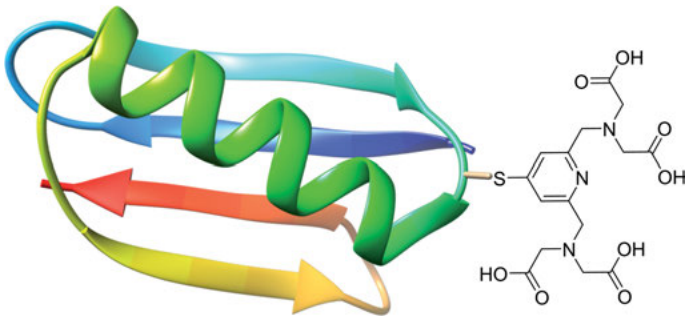

Figure 2. Py-MTA labelled GB1. The chelator tag can be used to complex paramagnetic lanthanides and to gain information of the structure in an intracellular environment. Y(III) can be used as diamagnetic reference [19].

2.3. X-Ray Diffraction

Lanthanides are excellent X-ray scatterers. For this reason they have been widely used in X-ray crystallography of large biomolecules like proteins or DNA/RNA as their anomalous signal can yield helpful phase information. Lanthanides will

readily bind to a Ca(II) site in proteins or replace Mg(II) in other biomolecules such as DNA. Lanthanide-binding tags can also be engineered in specific regions of proteins of interest [16, 21].

2.4. Luminescence

Luminescent lanthanides have attracted attention for their unique photophysical properties making them a vital tool for modern medicinal applications such as time-resolved fluorescence assays and responsive luminescent probes [22–31]. Two very popular lanthanides for applications are Eu(III) and Tb(III) which are especially useful for biological applications due to their long-lived (0.1–3 ms) luminescence (and thus favorable [28, 32] signal-to-noise ratio) and high quantum yields (>10 %) [22, 33]. The emission color depends on the trivalent lanthanide itself and is largely independent of the environment of a lanthanide, while the partially filled 4f shell is responsible for the narrow band emissions and the long lifetimes. The parity rule (*f-f* transitions are Laporte-forbidden) leads to very low molar absorptivities for Ln(III) complexes (>10 $L\,mol^{-1}cm^{-1}$), hence direct excitation is difficult. As a consequence, indirect excitation (via the antenna effect) is often the method of choice. A schematic view of this process is shown in Figure 3, where a ligand chromophore (antenna) absorbs UV-light and then transfers energy from its triplet state to the Ln(III) ion to populate its excited state. In proteins tryptophan residues may be used for this purpose.

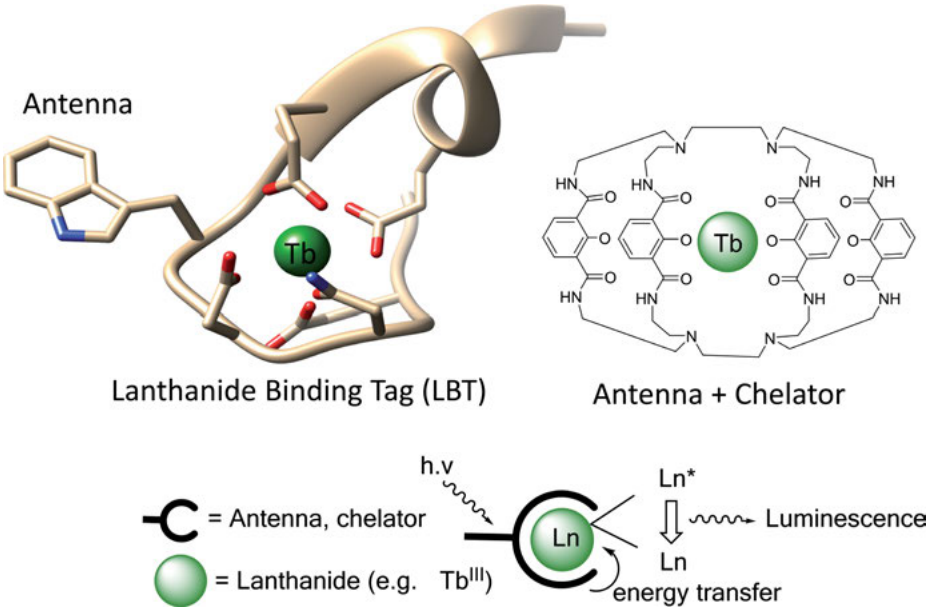

Figure 3. Lanthanide-binding tag (LBT) with tryptophan antenna, a luminescent lanthanide complex that can be used in bioassays and the principle of the antenna effect.

Both Eu and Tb have their own unique properties and advantages. While Tb(III) complexes are in general more luminescent, Eu(III) complexes may provide more information when used as a probe, and other lanthanides might be used as well [27, 34]. The main non-radiative pathway of deactivation is vibronic coupling with solvent molecules. Shielding the lanthanide from water molecules is thus very important. Allen and Imperiali [16] have developed lanthanide-binding tags (LBT) that can not only be used in NMR spectroscopy (*vide supra*) and X-ray crystallography to yield structural information about biomolecules, but also to tag proteins and identify them by the present luminescence. Here, metal binding residues that form a high affinity binding site for lanthanides such as Tb(III) can be engineered onto the proteins of interest [21]. To excite Tb(III), a tryptophan residue may be included in the loop nearby. Another strategy is not to use a peptide LBT but to attach inorganic complexes of an antenna ligand and chelator to biomolecules of interest. For example, the macrotricyclic BH(2,2)IAM ligand (a bicapped ligand with four 2-hydroxyisophthalamide units) based on the 2-hydroxyisophthalamide chromophore was developed by the Raymond group, effectively shielding the Tb(III) ion against water molecules and thus preventing quenching of the luminescence, yielding a very bright luminescent probe for the analysis of biomolecules [22]. In recent years lanthanide-based near infrared luminescence applications have attracted considerable interest due to their increased resolution and favorable signal-to-noise ratios and sensitivity [35, 36]. Luminescence titrations into apo-enzymes can yield binding constants for the active sites of metalloproteins. Srivastava and coworkers have demonstrated this using Eu(III) and the methionine aminopeptidase from *E. coli*. By conducting competition titrations they showed that Fe(II) exhibited a higher affinity than Ca(II) or Eu(III) [37].

3. APPLICATIONS OF RARE EARTH ELEMENTS IN MEDICINE

3.1. Use of Rare Earth Elements for Imaging and Diagnostic Techniques

REE have found extensive use in medical diagnostics [7, 38, 39]. Their luminescent and magnetic properties make them useful for bioassays and as bioresponsive probes [34, 40, 41]. Especially the use of gadolinium in magnetic resonance imaging (MRI) is possibly the most important application of a REE in medical diagnostics. In Germany (2015) and the Netherlands (2016) 13,616 and 4,884 MRI scans, respectively, per 100,000 inhabitants were conducted in one year [42]. During an MRI analysis, sectional images of the proton distribution in the body are taken. For this purpose, the relaxation of the proton nuclear spin in a magnetic field is measured after a radio frequency pulse has been applied. The water content in the human body varies, for example fatty or water-rich, healthy or tumor tissue will look different on an MRI scan, generating a contrast. To en-

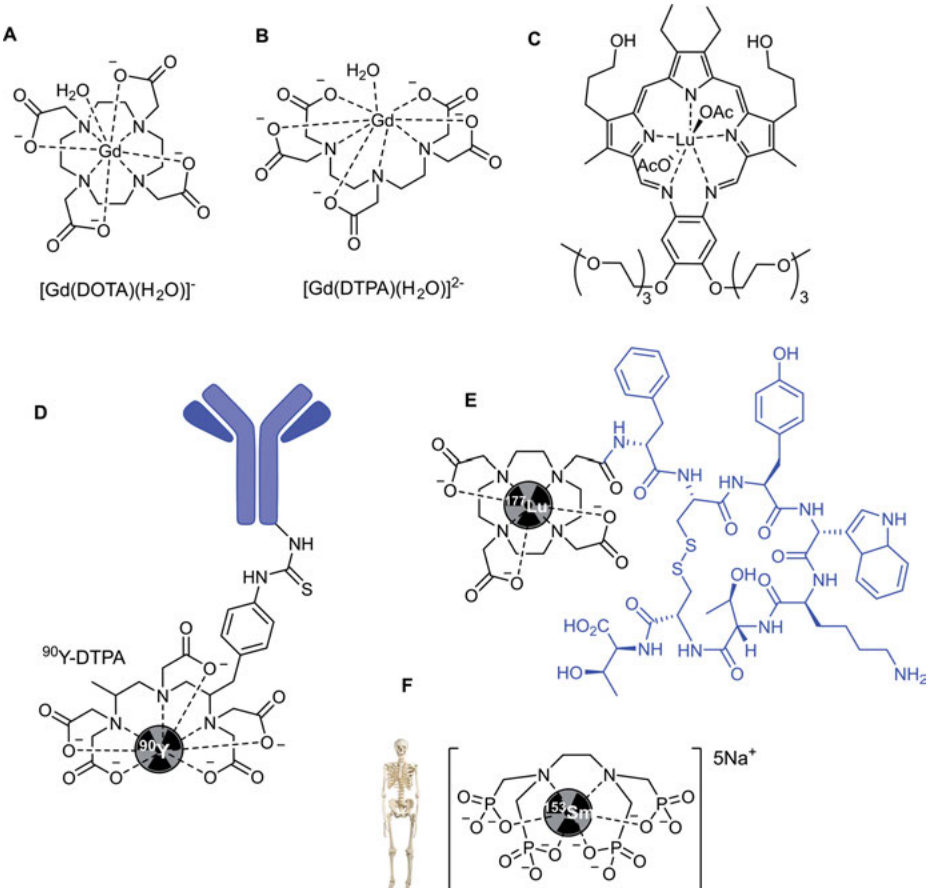

Figure 4. Overview of some lanthanide-based agents used in medical therapy and diagnostics. DOTA = 1,4,7,10-tetraazacyclododecane-1,4,7,10-tetraacetic acid; DTPA = diethylene triamine pentaacetic acid.

hance this contrast paramagnetic compounds are used. One of the most widely used REE for medical diagnostics is Gd(III). Due to the seven unpaired electrons it is an excellent contrast agent for MRI applications and the most efficient of the REE to influence water proton relaxation. However, free Gd(III) not complexed by a (chelate) ligand is toxic: The median lethal dose (LD_{50}) value lies approximately in the concentration range that is applied during an MRI. The amount of gadolinium used in an MRI corresponds to ~0.2 mmol per kg body weight, which corresponds to ~2 g Gd(III)/MRI. Hence, Gd(III) is complexed with chelators so that the resulting complex can be excreted safely via the kidney after a short time. Here, complexes **A** and **B** shown in Figure 4 are widely used. Gadolinium complexes may still be partially hydrolyzed in the body, leading to deposits in tissue [43]. Nephrogenic systemic fibrosis has been discussed to be triggered by Gd-based MRI contrast agents [43, 44]. There is active

interest to improve the safety and functionalities of classical contrast agents. Further, the proton exchange of the -NH or -OH groups of contrast agents can be used to change tissue contrast with the paramagnetic chemical exchange saturation transfer (PARA-CEST) agents [45]. These agents have the potential to be used for imaging of metabolic information (pH, temperature, metabolites such as sugars or metal ions) [34, 41, 45].

3.2. Use of Rare Earth Elements in Therapy

Around 1900 several reports appeared in the literature about the use of cerium compounds (such as cerium oxalate) against vomiting, in fact, Simpson had reported on it in 1854 [7, 46]. Cerium has found further use in antimicrobials such as Ceriform [47]. The burn ointment Phologsam contains samarium complexes as antibacterial ingredient and is available as an over-the-counter ointment in Hungary. Before Heparin was widely available, a neodymium-containing salt was used under the name Thrombodym as anticoagulant [48]. Today, especially the radioactive isotopes find use in medical therapy. The β-emitter ^{90}Y is used embedded in tiny glass particles (~25 μm, TheraSphere®) and injected into patients with liver tumors. Due to the injection in the arteries near the tumor tissue, a localized buildup of the radioactive agent is possible. A more directed therapy of specific tumors is possible with complexes **D** and **E** (Figure 4) that are decorated with directing groups [49]. The samarium isotope ^{153}Sm is used together with the ethylenediamine-N,N,N′,N′-tetrakis(methylenephosphonic acid) ligand (EDTMP) for pain treatment of bone metastases. Due to the phosphonate groups of ^{153}Sm-EDTMP (also known as Sm-lexidronam or Quadramet) it is a bone-seeking drug which accumulates in rapidly growing bone regions. The emitted β-particles alleviate pain by a yet unknown mechanism [38, 50]. The lutetium complex **C** was used in clinical trials as a photosensitizer in the photodynamic therapy of various malignancies such as prostate cancer. By application of light (730 nm) **C** generates reactive oxygen species such as singlet oxygen which then destroys the nearby tumor tissue [51]. Finally, lanthanum carbonate is used in the therapy of hypophosphatemia in patients with decreased kidney function. 2–3 g of this drug (Fosrenol®) is taken orally with meals and dissolves in the stomach. The formed La(III) ions then precipitate phosphates present in the food, after which the precipitates are excreted via the gastrointestinal tract. This excretion relies on the poor solubility of $LaPO_4$ (Table 1). This substance is also used under the name Lantharenol® for elderly cats with kidney problems [52].

4. OTHER APPLICATIONS OF RARE EARTH ELEMENTS

4.1. Rare Earth Elements in Agriculture

For more than four decades, REE have found application as fertilizers in agriculture in China [8]. Formulations like Nongle (“Happy Farmer”) and Changle

("Happiness forever") contain mainly chlorides or nitrates of the four most abundant REE (La, Ce, Pr, Nd) in addition to other essential elements and nutrients like amino acids and ammonium salts. It has been reported that application of REE can increase plant growth, crop yields (enhanced biomass) and starch, fat or sugar contents of different plants [8]. The exact mechanism of action is unknown, but it was proposed that an interaction with the ribulose-1,5-bisphosphate carboxylase (RuBisCO) enzyme is responsible for the positive effect [53]. However, the results of many of these studies have to be judged with caution, as REE were applied either as the nitrate salts or simultaneously with other N-containing compounds (e.g., urea). Further, studies can rarely be reproduced under Western country conditions and thus the reports on the growth-enhancing effects remains ambiguous. The large discrepancies between the studies could also indicate that the phyllosphere, an important factor, was forgotten. Plant symbionts could be one reason behind increased crop yields upon REE addition. Many N_2-fixing bacteria such as *Bradyrhizobium* sp. MAFF211645 are plant symbionts and possess genes (*xoxF*) for lanthanide-dependent enzymes (see also Section 5.2) [54, 55]. Hence, it seems plausible that REE fertilization could help plant symbionts to thrive, which in turn has a beneficial effect on plant growth. Dependent on the microbial composition of the soil and plant phyllosphere it is thus likely that the effects of REE on plants might differ.

The growth-enhancing effect has not only been described for plants but also in livestock animals [8, 56]. Feed additives have shown to increase body weight gain by more than 20 % in pigs, cattle, sheep, and other animals along with an enhanced feed conversion rate. The two most widely used REE are lanthanum and cerium, often in combination. High bioavailability was shown with citrates and these REE salts also have the advantage of being less hydroscopic than the nitrates and chlorides. One such product is available in Switzerland under the name Lancer® from the company Zehentmayer (Figure 5).

The *Panel on additives and products or substances used in animal feed* (FEEDAP) of the European Food Safety Authority (EFSA) had concluded in an investigation published in 2016 that Lancer® was safe for piglets when used below the maximum dose of 250 mg/kg feed [57]. The mode of action has not been elucidated yet but the product is provisionally approved and used in Switzerland.

4.2. Separation and Sequestration of Rare Earth Elements by Biological Means

To acquire, purify, and separate the technologically indispensable REE, biological means have been explored extensively. Francis and coworkers have investigated europium and curium adsorption on the cell surfaces of *Chlorella vulgaris*, *Bacillus subtilis*, *Pseudomonas fluorescens*, and other microorganisms. They showed that Eu(III) and Cm(III) were adsorbed differently depending on the organism and that this process was not always pH-dependent [58].

Specification Lancer 1000

	Method	Specification	Units
Characterisation			
Appearance	visual inspection	yellow powder	
Odor	olfactive inspection	odorless	
Contents			
La	ICP-SFMA (L67)	85300 +/- 8530	mg/kg
Ce	ICP-SFMS (L67)	163000 +/- 16300	mg/kg
Citric acid	enzymat.	35 - 45	%
Na	DIN EN 15510:2007	8 - 12	%
Cl	VDLUFA, MB VII, 2.2.2	8 - 12	%
H2O	Karl Fischer Ph. EU 2.5.12	max. 10	%

Figure 5. Feed additive Lancer® and main ingredients. Picture kindly provided by the company Zehentmayer.

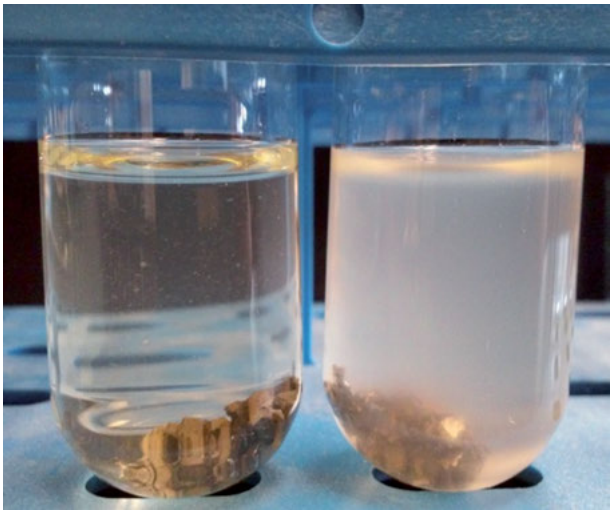

Figure 6. Culture of *Methylorubrum extorquens* with Nd-containing hard drive magnet. On the left a culture at the beginning, on the right after a certain amount of time has passed. Clearly visible is the increase in optical density, a result from bacterial growth on Nd. Picture kindly provided by E. Skovran and H. Vu.

Horiike and Yamashita isolated an acidophilic fungal strain, *Penidiella* sp. T9, and demonstrated that this fungus was able to acquire dysprosium (46 %, 100 mg/L), neodymium (50 %), and other REE during growth at acidic conditions (pH 2.5) [59]. Organisms like these hold promise in recovery of REE from acidic waste waters. La(III) bio-sorption and subsequent desorption was shown by Kazy, Das, and Sar with *Pseudomonas* sp. [60]. This strain has also been shown to be very effective in uranium and thorium accumulation. The La(III) bio-sorption studies showed a pH optimum of 5 and a surprisingly fast accumulation rate of 80 % within the first 30 minutes. The authors further demonstrated that desorption of 98 % of the La(III) was possible by using a 1 M solution of $CaCO_3$. Studies into the mechanism of bio-sorption at the cell walls of microorganisms have identified different possible mechanisms [61]. Lanthanide-binding is proposed to take place at acidic groups on the cell surface (carboxyl, phosphate, and hydroxyl residues). Not only extracellular bioaccumulation but also intracellular biomineralization of REE by microorganisms has been reported recently. Maleke et al. showed in 2019, using transmission electron microscopy coupled with energy-dispersive X-ray spectroscopy (TEM-EDX), that the thermophile *Thermus scotoductus* SA-01 deposited $Eu_2(CO_3)_3$ within its cells [62]. Remarkably, the bacterium *Methylorubrum extorquens* AM1, that uses lanthanides for its methanol metabolism, was shown to store cytoplasmic lanthanum in mineral form (as phosphate) [63]. Martinez-Gomez and coworkers confirmed further, that a TonB/ABC transport system is involved in lanthanide uptake (see Section 5.3). The involvement of this transport system of the same lanthanide-utilizing organism (*Mr. extorquens*) had been established earlier by Ochsner et

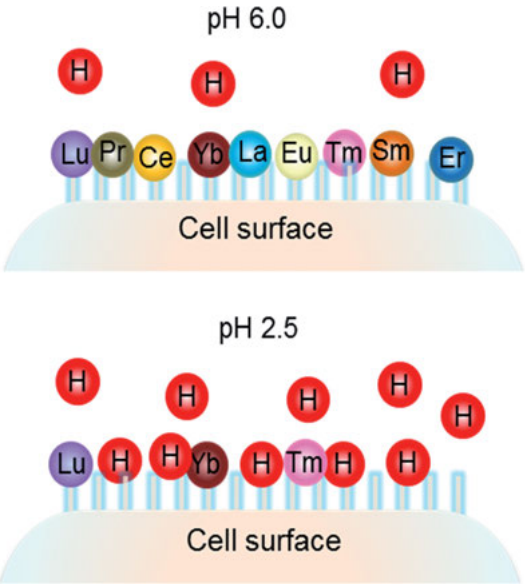

Figure 7. Separation of late REE on a bacterial surface of *Roseobacter* sp. At low pH only the three heaviest REE stay bound to the surface.

al. [64]. It is important to note here, that one has to distinguish between those organisms that accumulate REE non-specifically and those who actively use REE in their metabolism. Especially attractive is also the mobilization of REE directly from minerals or scrap metal. Here the tedious process of dissolving the REE-containing compounds first is omitted. Pure and heterogeneous bacterial cultures and fungi have been tested in the past [65]. Among the REE-utilizing bacteria, *Mr. extorquens* was reported to be able to use neodymium from computer hard drive magnets for growth (Figure 6), albeit at higher concentrations other components of the magnet (Fe, B, Ni) led to cytotoxic effects [66]. Thus, there is still need to engineer these bacteria towards higher metal resistances for future applications.

It was also demonstrated recently that metabolites of microorganisms can be used to leach REE from End-of-Life (EoL) products like fluorescent lamps. In a study with the Kombucha consortium, consisting of yeasts and acetic acid bacteria, by Hopfe et al., the Kombucha-produced metabolites, namely organic acids such as acetic acid and gluconic acid, immobilized Y(III) and Eu(III) from fluorescent phosphor (europium-doped yttrium oxide, YOX) [67]. Remarkably, mixed cultures yielded better results than single strains or the isolated organic acids. Other microbially produced organic ligands such as for example siderophores have been shown to complex and mobilize REE [68, 69]. A high-affinity REE-binding protein has been isolated from the above mentioned lanthanide-utilizing bacteria *Mr. extorquens* [70]. This protein, termed lanmodulin (LanM), exhibits features reminiscent of calmodulin albeit with a remarkable affinity for

lanthanides over calcium. Yttrium and the lanthanides bind to LanM with picomolar affinities and affinities for calcium are in the millimolar range.

Not only recovery but also separation of REE can be achieved using microorganisms. Bonificio and Clarke used *Roseobacter* sp. AzwK-3b cells for the separation of Tm, Yb, and Lu from earlier lanthanides (Figure 7). Here, the cells were immobilized on a filter surface and subjected to a mixture of REE at pH 7. Then the surface was washed with nitric acid (HNO_3) solutions of different pH (6 to 1.5) and it was observed that Tm, Yb, and Lu were desorbed at the lowest pH once all other lanthanides had been already washed off [71].

5. IMPORTANCE OF RARE EARTH ELEMENTS FOR BACTERIA

5.1. Rare Earth Elements in Bacterial C1 Carbon Metabolism (Methanotrophy/Methylotrophy)

First indications for a real role of lanthanides in biological life were obtained when studying the stimulation of expression of the XoxF-type methanol dehydrogenases (MDH) in *Bradyrhizobium* sp. MAFF211645 and *Methylobacterium radiotolerans* by Ce(III) and La(III) [55, 72]. Although the authors discussed the possibility of gene level regulation by lanthanides, the dogma of REE being biologically inert was challenged by the discovery of La(III)-dependent MDHs in the model plant phyllosphere colonizer *Mr. extorquens* AM1 [73, 74] and the thermoacidophilic methanotroph *Methylacidiphilum fumariolicum* SolV [3, 75]. The genome of the latter bacterium only possesses a *xoxF* gene, a homologue of the Ca(II)-dependent MDH gene (*mxaFI*) which was considered to encode for the only enzyme responsible for methanol oxidation in methano- and methylotrophic bacteria. Strain SolV was isolated on a medium containing mud pot water from its original habitat, the Solfatara crater. Growing the pure culture was only possible with this mud pot water added to the medium. The component of the mud pot water responsible for this effect was shown to be inorganic in nature and finally it was shown that the mud pot water could be replaced by REE [3]. Growth of strain SolV was strictly dependent on the presence of Ln(III) in the medium. Cells grown with a range of cerium concentrations showed a proportional response to Ce(III) from 0 to 80 nM. Maximum growth rates obtained with La, Ce, Pr or Nd were identical while REE with higher atomic numbers like Gd resulted in 4-fold slower growth [3]. Thus far, two XoxF-type MDH enzymes were purified from *Methylacidiphilum fumariolicum* SolV and *Methylotuvimicrobium buryatense* 5GB1C and their crystal structures showed a Ln(III) ion in the active site [3, 76, 77]. The discovery of the biological role for lanthanides initiated a new field of research that explored the role of these elements in biological systems and expanded it to enzymes outside methane metabolism. Samples taken from the submerged plume of methane-rich water during the Deepwater Horizon oil spill (Gulf of Mexico, April 20, 2010)

showed a bloom of methanotrophic bacteria together with a depletion of light REEs (La, Ce, Pr, and Nd) from the surrounding seawater [78]. This observation can be explained in terms of the biological role of REE for methanotrophic and methylotrophic bacteria. Furthermore, the addition of REE to cultivation media permitted the isolation of novel and uncharacterized bacteria from a variety of different habitats [79–85].

5.2. Rare Earth Elements in Alcohol Dehydrogenases

The group of MDH enzymes belong to the large class of 8-bladed β-propeller pyrroloquinoline quinone (PQQ)-containing proteins with each blade consisting of a four-stranded anti-parallel β-sheet (Type I). The second type in this class has a 6-bladed β-propeller structure and has no amino acid sequence homology to the other type. Within the group of PQQ-containing proteins both membrane-bound and soluble proteins exist. The membrane-bound PQQ alcohol dehydrogenases (ADHs) may contain multiple cytochrome domains and a [2Fe-2S] site [86, 87].

The soluble proteins within the 8-bladed β-propellertype are localized in the periplasm and on average 600 amino acids in size. A cytochrome *c* protein (cyt c_L) functions as the electron acceptor module [88–93]. The MDHs share their classification with ethanol and higher alcohol dehydrogenases [94, 95]. Since their discovery in 1964 [96, 97], MxaF-MDHs have been studied into great detail [98]. However, based on molecular analysis the MxaF-MDH proteins seem to represent only a minor fraction; most MDHs are XoxF-type proteins [99–102]. This is also supported by detection of mRNA expression levels in environmental samples. In depth phylogenetic analysis of MxaF- and XoxF-type MDH protein sequences available in public databases showed that XoxF-MDHs clustered in five different XoxF families (XoxF1-5) and MxaF-MDHs formed a single separate cluster [90, 103]. The genomes of methano- and methylotrophic microorganism may encode several XoxF-MDH paralogs and orthologs but for MxaF-MDH, if present, only one copy is found. After analysis of the phylogenetic tree it was concluded that the development of the MxaF-type MDH seemed to be a secondary evolutionary event: this MxaF-type descended from a XoxF prototype [90]. Based upon the available crystal structures and the alignment of alcohol dehydrogenases and both types of MDHs a lanthanide motif was proposed; D-x-x-D-[YFW]-D, the third aspartate being the additional ligand for lanthanide binding, replacing the alanine at this position in calcium-dependent enzymes. Taking this into account all ADH types (1 to 9), except type 2a are potential lanthanide-containing enzymes. Recently, evidence was obtained that indeed the ADH-type alcohol dehydrogenases from *Mr. extorquens* AM1 and *Pseudomonas putida* KT2440 are lanthanide-dependent ExaF/PedH enzymes [104, 105]. These findings were further extended by the recent survey of Huang et al. in which *Methyloversatilis* sp. FAM1 and *Methylopila* sp. M107 were shown to possess these enzymes [102]. In the latter survey it was also reported based

on sequence database searches that lanthanide-dependent ADH enzymes occur at similar frequencies compared to their calcium-dependent counterparts.

The XoxF5 cluster forms the largest group and branching of subgroups within this cluster follows the taxonomic position of the microorganisms. All XoxF4-MDHs are from betaproteobacterial Methylophilales species. The XoxF3-MDH proteins comprise a mix of quinoproteins from α-, β- and γ-proteobacteria as well as a MDH from *Candidatus* 'Solibacter usitatus' and represent the deepest branch within the phylogenetic tree. XoxF2-MDHs are thus far restricted to the genera *Methylacidiphilum* and *Methylacidimicrobium*, representing acidophilic methanotrophic Verrucomicrobia, and *Candidatus* 'Methylomirabilis' species, nitrite-dependent methane oxidizers. Besides the XoxF2-MDH, *Candidatus* 'M. oxyfera' contains a XoxF1-MDH. Other XoxF1-MDHs are found in the genomes of α-proteobacterial Rhizobiales species and γ-proteobacterial Xanthomodales species.

5.2.1. The Active Site of Rare Earth Element Dehydrogenases

The overall architecture of MxaF- and XoxF-MDHs (Figure 8), including coordination of the PQQ cofactor, is fully conserved [3, 77, 106]. In the XoxF-MDH of *M. fumariolicum* SolV the diffracting atom at the catalytic site could only be a lanthanide. Changes at the catalytic site involved an aspartate (Asp301, numbering according to the crystal structure of strain SolV) replacing an alanine (in MxaF-MDH) two positions upstream of the catalytic Asp299 (Figure 8).

In addition, a proline and an alanine conserved in MxaF-MDH (Pro264 and Ala176, numbering according to the crystal structure of *Mr. extorquens*) were replaced by a threonine and a glycine, respectively. Quinoproteins markedly differ in substrate specificities [90]. Substrate specificity may be depicted by the volume of the PQQ-containing hydrophobic pocket at the catalytic site [95, 107] with this volume being smallest for MDHs (18 $Å^3$) and larger for ADHs (62–150 $Å^3$). A specific feature of MDHs is the presence of two cysteines (Cys386 and Cys415 numbering according to the crystal structure of *Mr. extorquens*) around loop structure 4. These cysteine residues make a second disulfide bond in the protein structure, next to the Cys103/Cys104 couple.

5.2.2. Mechanism of Alcohol Oxidation

MDHs catalyze the two-electron oxidation of methanol to formaldehyde. Studies on enzyme kinetics of MxaFI-MDHs showed the use of other primary alcohols and formaldehyde as substrates, but with considerable lower substrate affinity and at a lower V_{max}. Assays make use of redox dye-coupled reactions which require a non-physiological high pH (8–11) for maximal activity and ammonia or methylamine is often needed for activation [108]. XoxF-MDHs seem to oxidize methanol with higher rates and higher affinity than MxaF-MDHs [90, 108]. The XoxF-MDH from *M. fumariolicum* SolV has been extensively studied [3, 77, 93, 109, 110]. Besides methanol this enzyme is capable of oxidizing a range of primary alcohols and formaldehyde is converted to formate at high rate and with a

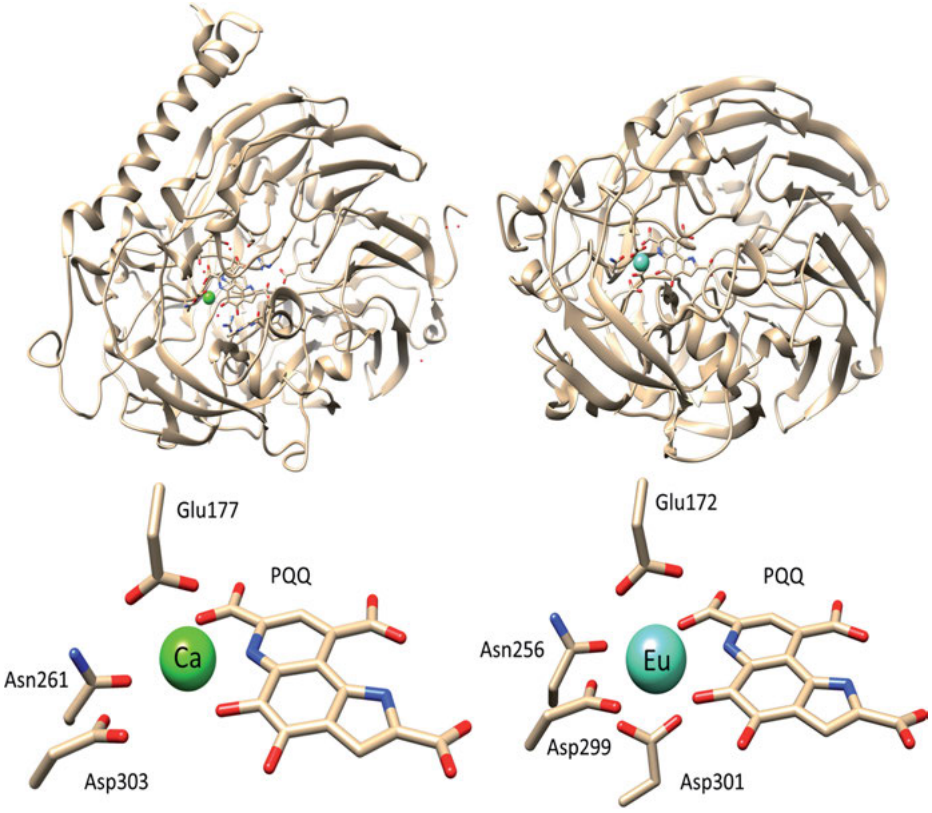

Figure 8. Overall structures of MDH and active sites compared. **Left**: MxaF-type MDH with calcium in the active site. **Right**: XoxF-type MDH with europium.

high affinity. These reactions show optimal activity at neutral pH and no ammonia is needed for activation. Actually, this XoxF-MDH can convert methanol by a four-electron oxidation directly to formate. Other alcohols are oxidized to their corresponding aldehydes. Two mechanisms have been proposed: a hydride (H^-) transfer from the substrate to the redox cofactor as well as nucleophilic attack of PQQ by a methanolate anion (RO^-, or CH_3O^-) forming $PQQH_2$. Model complex studies, density functional theory calculations, crystallographic studies support both of these mechanisms although the hydride transfer seems more plausible (Figure 9) [98, 109, 111–116]. PQQ is then regenerated by transferring the two electrons to distinct cytochromes.

5.2.3. Impact of the Lanthanide Contraction

Not all REE stimulate growth of bacteria equally. Especially the early lanthanides lead to high growth rates in bacteria (Table 2). This is somewhat surprising as the role of the REE is to act as a Lewis acid. The early, naturally more

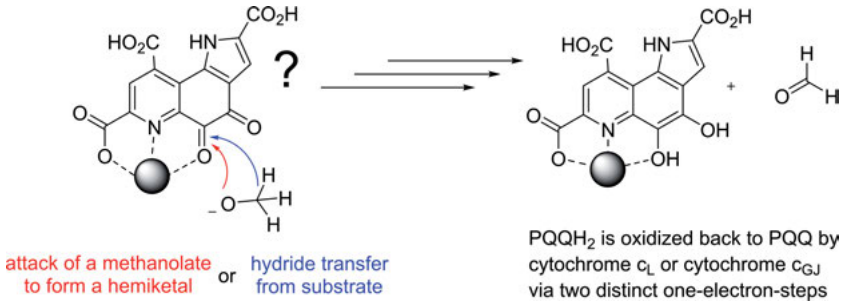

Figure 9. Initial steps of the two proposed mechanisms of methanol oxidation by PQQ containing MDH.

abundant lanthanides exhibit bigger ionic radii than the later ones due to the lanthanide contraction. While the later ones are stronger Lewis acids, they also often exhibit lower coordination numbers and slower ligand exchange rates, properties that might not be beneficial for methanol oxidation catalysis here. Sc and Y are rarely tested in growth experiments, but did not stimulate growth in the few examples that are available in the literature [104]. Surprisingly, in addition to slower growth rates with, for example, Eu(III) compared to La(III), the smaller REE are also depleted from the medium at a slower rate as was shown for strain SolV [6]. The activity of the isolated methanol dehydrogenases are also much higher with the early lanthanides [77, 89, 109].

These observations are in line with the findings during the Deep Water Horizon catastrophe. Here it was observed that during the bloom of methanotrophic bacteria, early lanthanides were depleted from the water around the platform [78]. For *M. fumariolicum* SolV an uptake preference was observed within the series of REE present in the supplemented volcanic mud pot water: Ce and La disappeared more quickly compared to Pr and Nd [3].

5.3. Uptake and Regulation of Rare Earth Elements by Bacteria

Although several bacteria are known that only possess a XoxF-type MDH, the genomes of a large group of methanotrophs and methylotrophs encode for both types of MDHs [75, 79, 80, 90, 117–119]. Studies on microorganisms with both enzymes revealed that lanthanides transcriptionally regulate the expression of *mxaF* and *xoxF* in a number of methylotrophs and methanotrophs [120–123]. Repression of the *mxaF* promotor and induction of the *xoxF* promotor by lanthanides is referred to as the 'lanthanide switch' [124]. The same switch, occurring at low nM lanthanide concentrations, was reported for the PedH/PedE ADH-type alcohol dehydrogenases in *Pseudomomas putida* [104, 125]. In *Methylotuvimicrobium buryatense* it was demonstrated that the MxaY protein serves as a lanthanide sensor, controlling the transcription of genes encoding MxaFI and

Table 2. Selection of bacteria demonstrating the impact of the lanthanide contraction on growth.

Bacterial strain	La	Ce	Pr	Nd	Sm	Eu	Gd	Tb	Dy	Ho	Er	Tm	Yb	Lu
Methylorubrum extorquens AM1 [120]	++	++	++	++	+	/	/	/	–	–	–	/	–	/
Pseudomonas putida KT244 [104]	++	++	+	++	+	/	–	–	/	/	/	/	–	/
Methylotenera mobilis JLW8 mutant [101]	++	++	/	+	+	/	+	/	–	/	/	/	–	/
Methylotenera mobilis JLW8 [101]	++	++	/	++	+	/	–	/	–	/	/	/	–	/
Methylomonas sp. LW13 [101]	++	++	/	+	–	/	–	/	–	/	/	/	–	/
Methylacidiphilum fumariolicum SolV [3, 77]	++	++	++	++	++	+	+	/	/	/	/	/	–	/
Methylobacterium aquaticum 22A [121]	++	/	/	/	/	/	/	/	/	–*	/	/	/	–*

Pm was not tested in all cases. Fast growth (++), medium growth (+), growth not stimulated or poor growth (–), not tested (/) **xoxF* gene expression was not induced and thus growth was not studied with these metals, however, growth is possible in this organism (*mxaF* gene and Ca-MDH). Table adapted from ref. [108].

XoxF through the response regulator MxaB [124]. Recently, it was reported that the effect of lanthanides on XoxF/MxaF-MDH expression was not observed in the presence of copper [126]. For ADH-type lanthanide-dependent alcohol dehydrogenases (PedH/PedE) it was shown that Cu(II), Zn(II), and in particular Fe(II) ions can strongly interfere with the 'lanthanide switch' [127]. This suggests that multiple levels of gene regulation by metals may exist in combination with changing environmental conditions [128, 129]. Concerning the uptake mechanism for lanthanides, differences may exist between bacteria that have both types of MDHs and possess the 'lanthanide switch' and bacteria with only the XoxF-type MDH [6]. For the latter group only transport to the periplasm is needed for incorporation into the catalytic site while for the other group the 'lanthanide switch' will need lanthanides reaching the cytoplasm. Based on research performed with *Mr. extorquens* and *Methylotuvimicrobium buryatense* 5GB1C models were depicted [63, 64, 70, 89, 130, 131]. Outside the cell the lanthanides are bound to a chelator ('lanthanophore') [64, 108]. Transport of the chelator-bound lanthanide to the periplasm takes place by the action of a TonB-type outer membrane transporter. In the periplasm a lanmodulin transfers the lanthanide to the apo-XoxF-MDH. To be able to act as regulator molecules, the lanthanide can be further transported to the cytoplasm by an ABC-type transporter. In the cytoplasm the regulatory cascade can be activated. More research, involving different types of methylotrophic and methanotrophic bacteria, is needed to improve our understanding of the regulatory mechanisms involved.

6. FUTURE DEVELOPMENTS AND APPLICATIONS

Even though many of the REE possess similar coordination chemistry properties, mankind has made substantial use of their different physical properties. Their magnetic properties are explored in medical imaging, structural biology and biochemistry. Many isotopes find application in imaging and therapy and the luminescent properties of REE are extensively used in bioassays and for lanthanide binding tags. REE often form poorly soluble compounds especially with phosphates and are thus considered of low bioavailability. This is exploited in medical and environmental applications like Fosrenol® or Phoslock™. Nevertheless, even though concentrations of REE are low in aquatic ecosystems, their widespread abundance in the earth's crust has prompted microorganisms to evolve REE-dependent enzymes and proteins.

Some early lanthanides have been shown to be relevant or even essential for many methanotrophic and methylotrophic bacteria. While the field of REE-dependent bacterial metabolism is now thriving, there are many unanswered questions on uptake and regulation in bacteria as well as on enzymatic mechanisms that remain.

ACKNOWLEDGMENTS

HOdC was supported by ERC Advanced Grant VOLCANO 669371. LJD thanks the LMU for support. We thank Simon Cotton and Rob Schmitz for critical proofreading and their helpful feedback.

ABBREVIATIONS

AAS	atomic absorption spectroscopy
ADH	alcohol dehydrogenase
DNA	deoxyribonucleic acid
GB1	immunoglobulin binding domain of protein G
ICP	inductively coupled plasma
LBT	lanthanide binding tag
LoD	limit of detection
MDH	methanol dehydrogenase
MRI	magnetic resonance imaging
MS	mass spectrometry
NMR	nuclear magnetic resonance
OES	optical emission spectroscopy
PQQ	pyrroloquinoline quinone
REE	rare earth elements
XAS	X-ray absorption spectroscopy

REFERENCES

1. D. N. Trifonov, *The Rare-Earth Elements*, Pergamon Press (distributed in the Western Hemisphere by Macmillan, New York), **1963**.
2. C. W. Noack, D. A. Dzombak, A. K. Karamalidis, *Environ. Sci. Technol.* **2014**, *48*, 4317–4326.
3. A. Pol, T. R. M. Barends, A. Dietl, A. F. Khadem, J. Eygensteyn, M. S. M. Jetten, H. J. M. Op den Camp, *Environ. Microbiol.* **2014**, *16*, 255–264.
4. V. Hatje, K. W. Bruland, A. R. Flegal, *Environ. Sci. Technol.* **2016**, *50*, 4159–4168.
5. M. R. Ganjali, V. K. Gupta, F. Faridbod, P. Norouzi, *Lanthanides Series Determination by Various Analytical Methods*, Elsevier, Amsterdam, **2016**.
6. C. Hogendoorn, P. Roszczenko-Jasińska, N. C. Martinez-Gomez, J. de Graaff, P. Grassl, A. Pol, H. J. M. Op den Camp, L. J. Daumann, *Appl. Environ. Microbiol.* **2018**, 84:e02887–02817.
7. C. H. Evans, *Biochemistry of the Lanthanides*, Springer Science & Business Media, New York, **1990**.
8. K. Redling, *Rare Earth Elements in Agriculture with Emphasis on Animal Husbandry*, PhD thesis, Ludwig-Maximilians-Universität München, **2006**.
9. *The Lanthanides and Their Interrelations with Biosystems*, *Metal Ions in Biological Systems*, Volume 40, Eds A. Sigel, H. Sigel, Marcel Dekker, Inc./Taylor & Francis/CRC Press, Boca Raton, **2003**, pp. 1–799.

10. S. A. Cotton, J. M. Harrowfield, *Lanthanides in Living Systems*, in *The Rare Earth Elements: Fundamentals and Applications*, Ed D. A. Atwood, John Wiley & Sons, Chichester, UK, **2012**, p. 65.
11. X. Liu, R. H. Byrne, *Geochim. Cosmochim. Acta* **1997**, *61*, 1625–1633.
12. F. Haghseresht, S. Wang, D. D. Do, *Appl. Clay Sci.* **2009**, *46*, 369–375.
13. R. Shannon, *Acta Cryst. Section A* **1976**, *32*, 751–767.
14. W. D. Horrocks, J. P. Sipe, *J. Am. Chem. Soc.* **1971**, *93*, 6800–6804.
15. M. D. McCreary, D. W. Lewis, D. L. Wernick, G. M. Whitesides, *J. Am. Chem. Soc.* **1974**, *96*, 1038–1054.
16. K. N. Allen, B. Imperiali, *Curr. Opin. Chem. Biol.* **2010**, *14*, 247–254.
17. S. Lim, S. J. Franklin, *Cell. Mol. Life Sci.* **2004**, *61*, 2184–2188.
18. J. T. Welch, W. R. Kearney, S. J. Franklin, *Proc. Natl. Acad. Sci. USA* **2003**, *100*, 3725–3730.
19. B.-B. Pan, F. Yang, Y. Ye, Q. Wu, C. Li, T. Huber, X.-C. Su, *Chem. Commun.* **2016**, *52*, 10237–10240.
20. M. Qi, A. Groß, G. Jeschke, A. Godt, M. Drescher, *J. Am. Chem. Soc.* **2014**, *136*, 15366–15378.
21. K. Barthelmes, A. M. Reynolds, E. Peisach, H. R. A. Jonker, N. J. DeNunzio, K. N. Allen, B. Imperiali, H. Schwalbe, *J. Am. Chem. Soc.* **2011**, *133*, 808–819.
22. E. G. Moore, A. P. S. Samuel, K. N. Raymond, *Acc. Chem. Res.* **2009**, *42*, 542–552.
23. G. L. Law, C. M. Andolina, J. D. Xu, V. Luu, P. X. Rutkowski, G. Muller, D. K. Shuh, J. K. Gibson, K. N. Raymond, *J. Am. Chem. Soc.* **2012**, *134*, 15545–15549.
24. J. D. Xu, T. M. Corneillie, E. G. Moore, G. L. Law, N. G. Butlin, K. N. Raymond, *J. Am. Chem. Soc.* **2011**, *133*, 19900–19910.
25. K. N. Raymond, *Abstr. Pap. Am. Chem. Soc.* **2010**, *240*.
26. J. C. G. Bünzli, *Chem. Rev.* **2010**, *110*, 2729–2755.
27. S. V. Eliseeva, J. C. G. Bünzli, *Chem. Soc. Rev.* **2010**, *39*, 189–227.
28. J. C. G. Bünzli, *Chem. Lett.* **2009**, *38*, 104–109.
29. S. Petoud, S. M. Cohen, K. N. Raymond, *Abstr. Pap. Am. Chem. Soc.* **1999**, *217*, U1014–U1014.
30. K. Binnemans, *Coord. Chem. Rev.* **2015**, *295*, 1–45.
31. J.-C. G. Bünzli, *Trends in Chemistry* **2019**, doi: 10.1016/j.trechm.2019.05.012.
32. J.-C. G. Bünzli, S. V. Eliseeva, *Chem. Sci.* **2013**, *4*, 1939–1949.
33. A. P. Samuel, J. Xu, K. N. Raymond, *Inorg. Chem.* **2009**, *48*, 687–698.
34. M. C. Heffern, L. M. Matosziuk, T. J. Meade, *Chem. Rev.* **2014**, *114*, 4496–4539.
35. E. R. Trivedi, S. V. Eliseeva, J. Jankolovits, M. M. Olmstead, S. Petoud, V. L. Pecoraro, *J. Am. Chem. Soc.* **2014**, *136*, 1526–1534.
36. A. Foucault-Collet, K. A. Gogick, K. A. White, S. Villette, A. Pallier, G. Collet, C. Kieda, T. Li, S. J. Geib, N. L. Rosi, S. Petoud, *Proc. Natl. Acad. Sci. USA* **2013**, *110*, 17199–17204.
37. N. Sule, R. K. Singh, P. Zhao, D. K. Srivastava, *J. Inorg. Biochem.* **2012**, *106*, 84–89.
38. B. Jahn, L. J. Daumann, *Chemie in unserer Zeit* **2018**, *52*, 150–158.
39. S. A. Cotton, J. M. Harrowfield, *Lanthanides: Coordination Chemistry*, in *Encyclopedia of Inorganic and Bioinorganic Chemistry*, John Wiley & Sons, Chichester, UK, **2012**.
40. A. D. Sherry, P. Caravan, R. E. Lenkinski, *J. Magn. Reson. Imaging* **2009**, *30*, 1240–1248.
41. M. Woods, D. E. Woessner, A. D. Sherry, *Chem. Soc. Rev.* **2006**, *35*, 500–511.
42. *Eurostat, Healthcare Resource Statistics − Technical Resources and Medical Technology, Use of Imaging Equipment − Number of Magnetic Resonance Imaging (MRI) Scans*, https://ec.europa.eu/eurostat/statistics-explained/index.php/Healthcare_resource_statistics_-_technical_resources_and_medical_technology, **2017**.

43. T. Frenzel, P. Lengsfeld, H. Schirmer, J. Hütter, H.-J. Weinmann, *Investig. Radiol.* **2008**, *43*, 817–828.
44. P. H. Kuo, *J. Am. Coll. Radiol.* **2008**, *5*, 29–35.
45. S. Zhang, M. Merritt, D. E. Woessner, R. E. Lenkinski, A. D. Sherry, *Acc. Chem. Res.* **2003**, *36*, 783–790.
46. *Hospital (Lond 1886)* **1906**, *39*, 368.
47. M. A. Jakupec, P. Unfried, B. K. Keppler, *Pharmacological Properties of Cerium Compounds*, in *Rev. Physiol. Biochem. Pharmacol.*, Vol. 153, Springer, Berlin, Heidelberg, **2005**, pp. 101–111.
48. U. Wilbrand, *Dtsch. med. Wochenschr.* **1953**, *78*, 330–332.
49. F. F. R. Knapp, A. Dash, *Radiopharmaceuticals for Therapy*, Springer India, New Delhi, **2016**.
50. I. G. Finlay, M. D. Mason, M. Shelley, *The Lancet Oncology* **2005**, *6*, 392–400.
51. H. Patel, R. Mick, J. Finlay, T. C. Zhu, E. Rickter, K. A. Cengel, S. B. Malkowicz, S. M. Hahn, T. M. Busch, *Clin. Cancer Res.* **2008**, *14*, 4869–4876.
52. EFSA Panel of Additives and Products or Substances Used in Animal Feed, V. Bampidis, G. Azimonti, M. d. L. Bastos, H. Christensen, B. Dusemund, M. Kouba, M. Kos Durjava, M. López-Alonso, S. López Puente, F. Marcon, B. Mayo, A. Pechová, M. Petkova, F. Ramos, Y. Sanz, R. E. Villa, R. Woutersen, A. Chesson, J. Gropp, G. Martelli, D. Renshaw, G. López-Gálvez, A. Mantovani, *EFSA Journal* **2019**, *17*, e05542.
53. C. Liu, F.-s. Hong, Y. Tao, T. Liu, Y.-n. Xie, J.-h. Xu, Z.-r. Li, *Biol. Trace Elem. Res.* **2011**, *143*, 1110–1120.
54. A. Sy, E. Giraud, P. Jourand, N. Garcia, A. Willems, P. de Lajudie, Y. Prin, M. Neyra, M. Gillis, C. Boivin-Masson, B. Dreyfus, *J. Bacteriol.* **2001**, *183*, 214–220.
55. N. A. Fitriyanto, M. Fushimi, M. Matsunaga, A. Pertiwiningrum, T. Iwama, K. Kawai, *J. Biosci. Bioeng.* **2011**, *111*, 613–617.
56. S. A. Abdelnour, M. E. Abd El-Hack, A. F. Khafaga, A. E. Noreldin, M. Arif, M. T. Chaudhry, C. Losacco, A. Abdeen, M. M. Abdel-Daim, *Sci. Total Environ.* **2019**, *672*, 1021–1032.
57. *European Food Safety Authority (EFSA) Panel on Additives and Products or Substances Used in Animal Feed (FEEDAP), Scientific Opinion on the safety and efficacy of Lancer (lanthanide citrate) as feed additive for weaned piglets, EFSA Journal*, **2013**, *11*, 3206.
58. T. Ozaki, T. Kimura, T. Ohnuki, Z. Yoshida, J. B. Gillow, A. J. Francis, *Radiochim. Acta* **2004**, *92*, 741–748.
59. T. Horiike, M. Yamashita, *Appl. Environ. Microbiol.* **2015**, *81*, 3062–3068.
60. S. K. Kazy, S. K. Das, P. Sar, *J. Ind. Microbiol. Biotechnol.* **2006**, *33*, 773–783.
61. Y. Andrès, A. C. Texier, P. Le Cloirec, *Environ. Technol.* **2003**, *24*, 1367–1375.
62. M. Maleke, A. Valverde, J.-G. Vermeulen, E. Cason, A. Gomez-Arias, K. Moloantoa, L. Coetsee-Hugo, H. Swart, E. van Heerden, J. Castillo, *Front. Microbiol.* **2019**, *10:* 81.
63. P. Roszczenko-Jasińska, H. N. Vu, G. A. Subuyuj, R. V. Crisostomo, J. Cai, C. Raghuraman, E. M. Ayala, E. J. Clippard, N. F. Lien, R. T. Ngo, F. Yarza, C. A. Hoeber, N. C. Martinez-Gomez, E. Skovran, *bioRxiv* **2019**, 647–677.
64. A. M. Ochsner, L. Hemmerle, T. Vonderach, R. Nüssli, M. Bortfeld-Miller, B. Hattendorf, J. A. Vorholt, *Mol. Microbiol.* **2019**, *111*, 1152–1166.
65. F. Barmettler, C. Castelberg, C. Fabbri, H. Brandl, *AIMS Microbiology* **2016**, *2*, 190–204.
66. N. C. Martinez-Gomez, H. N. Vu, E. Skovran, *Inorg. Chem.* **2016**, *55*, 10083–10089.
67. S. Hopfe, K. Flemming, F. Lehmann, R. Möckel, S. Kutschke, K. Pollmann, *Waste Management* **2017**, *62*, 211–221.

68. G. Tircsó, Z. Garda, F. K. Kálmán, Z. Baranyai, I. Pócsi, G. Balla, I. Tóth, *J. Inorg. Biochem.* **2013**, *127*, 53–61.
69. B. E. Allred, P. B. Rupert, S. S. Gauny, D. D. An, C. Y. Ralston, M. Sturzbecher-Hoehne, R. K. Strong, R. J. Abergel, *Proc. Natl. Acad. Sci. USA* **2015**, *112*, 10342–10347.
70. J. A. Cotruvo, E. R. Featherston, J. A. Mattocks, J. V. Ho, T. N. Laremore, *J. Am. Chem. Soc.* **2018**, *140*, 15056–15061.
71. W. D. Bonificio, D. R. Clarke, *Environ. Sci. Technol. Lett.* **2016**, *3*, 180–184.
72. Y. Hibi, K. Asai, H. Arafuka, M. Hamajima, T. Iwama, K. Kawai, *J. Biosci. Bioeng.* **2011**, *111*, 547–549.
73. T. Nakagawa, R. Mitsui, A. Tani, K. Sasa, S. Tashiro, T. Iwama, T. Hayakawa, K. Kawai, *PLoS ONE* **2012**, *7*, e50480.
74. J. A. Vorholt, *Nat. Rev. Microbiol.* **2012**, *10*, 828–840.
75. A. Pol, K. Heijmans, H. R. Harhangi, D. Tedesco, M. S. M. Jetten, H. J. M. Op den Camp, *Nature* **2007**, *450*, 874–878.
76. Y. W. Deng, S. Y. Ro, A. C. Rosenzweig, *J. Biol. Inorg. Chem.* **2018**, *23*, 1037–1047.
77. B. Jahn, A. Pol, H. Lumpe, T. Barends, A. Dietl, C. Hogendoorn, H. Op den Camp, L. Daumann, *ChemBioChem* **2018**, *19*, 1147–1153.
78. A. M. Shiller, E. W. Chan, D. J. Joung, M. C. Redmond, J. D. Kessler, *Sci. Rep.* **2017**, *7*, 1–9.
79. B. Vekeman, D. Speth, J. Wille, G. Cremers, P. De Vos, H. J. M. Op den Camp, K. Heylen, *Microb. Ecol.* **2016**, *72*, 503–509.
80. A. M. Howat, J. Vollmers, M. Taubert, C. Grob, J. L. Dixon, J. D. Todd, Y. Chen, A.-K. Kaster, J. C. Murrell, *Front. Microbiol.* **2018**, *9*, 766.
81. M. Del Rocío Bustillos-Cristales, I. Corona-Gutierrez, M. Castañeda-Lucio, C. Águila-Zempoaltécatl, E. Seynos-García, I. Hernández-Lucas, J. Muñoz-Rojas, L. Medina-Aparicio, L. E. Fuentes-Ramírez, *Microbes Environ.* **2017**, *32*, 244–251.
82. H. Lv, N. Sahin, A. Tani, *Environ. Microbiol.* **2018**, *20*, 1204–1223.
83. M. Taubert, C. Grob, A. M. Howat, O. J. Burns, J. L. Dixon, Y. Chen, J. C. Murrell, *Environ. Microbiol.* **2015**, *17*, 3937–3948.
84. E. Skovran, N. C. Martinez-Gomez, *Science* **2015**, *348*, 862–863.
85. L. Chistoserdova, *World J. Microbiol. Biotechnol.* **2016**, *32*, 138.
86. S. Gómez-Manzo, A. Solano-Peralta, J. P. Saucedo-Vázquez, J. E. Escamilla-Marván, P. M. H. Kroneck, M. E. Sosa-Torres, *Biochemistry* **2010**, *49*, 2409–2415.
87. S. Gómez-Manzo, J. E. Escamilla, A. González-Valdez, G. López-Velázquez, A. Vanoye-Carlo, J. Marcial-Quino, I. De la Mora-de la Mora, I. Garcia-Torres, S. Enríquez-Flores, M. L. Contreras-Zentella, R. Arreguín-Espinosa, P. M. H. Kroneck, M. E. Sosa-Torres, *Int. J. Mol. Sci.* **2015**, *16*, 1293–1311.
88. K. Amaratunga, P. M. Goodwin, C. D. O'Connor, C. Anthony, *FEMS Microbiol. Lett.* **1997**, *146*, 31–38.
89. E. R. Featherston, H. R. Rose, M. J. McBride, E. Taylor, A. K. Boal, J. J. Cotruvo, *ChemBioChem* **2019**, *20,* 2360–2372.
90. J. Keltjens, A. Pol, J. Reimann, H. M. Op den Camp, *Appl. Microbiol. Biotechnol.* **2014**, *98*, 6163–6183.
91. Y. Zheng, J. Huang, F. Zhao, L. Chistoserdova, *mBio* **2018**, *9*, e02430–02417.
92. H. Gon Kim, T. Nhat Phan, T. Sa Jang, M. Koh, S. Wouk Kim, *J. Microbiol. (Seoul, Korea)* **2005**, *43*, 499–502.
93. W. Versantvoort, A. Pol, L. J. Daumann, J. A. Larrabee, A. H. Strayer, M. S. M. Jetten, L. van Niftrik, J. Reimann, H. J. M. Op den Camp, *Biochim. Biophys. Acta* **2019**, *1867*, 595–603.
94. K. Matsushita, H. Toyama, M. Yamada, O. Adachi, *Appl. Microbiol. Biotechnol.* **2002**, *58*, 13–22.

95. H. Toyama, F. S. Mathews, O. Adachi, K. Matsushita, *Arch. Biochem. Biophys.* **2004**, *428*, 10–21.
96. C. Anthony, L. J. Zatman, *Biochem. J.* **1964**, *92*, 614–621.
97. C. Anthony, L. J. Zatman, *Biochem. J.* **1964**, *92*, 609–614.
98. C. Anthony, P. Williams, *Biochim. Biophys. Acta* **2003**, *1647*, 18–23.
99. M. G. Kalyuzhnaya, K. R. Hristova, M. E. Lidstrom, L. Chistoserdova, *J. Bacteriol.* **2008**, *190*, 3817–3823.
100. S. M. Sowell, P. E. Abraham, M. Shah, N. C. Verberkmoes, D. P. Smith, D. F. Barofsky, S. J. Giovannoni, *ISME J.* **2011**, *5*, 856–865.
101. J. Huang, Z. Yu, L. Chistoserdova, *Front. Microbiol.* **2018**, *9:* 1366.
102. J. Huang, Z. Yu, J. Groom, J.-F. Cheng, A. Tarver, Y. Yoshikuni, L. Chistoserdova, *ISME J.* **2019**, *13*, 2005–2017.
103. L. Chistoserdova, *Environ. Microbiol.* **2011**, *13*, 2603–2622.
104. M. Wehrmann, P. Billard, A. Martin-Meriadec, A. Zegeye, J. Klebensberger, *mBio* **2017**, *8*, e00570–00517.
105. N. M. Good, H. N. Vu, C. J. Suriano, G. A. Subuyuj, E. Skovran, N. C. Martinez-Gomez, *J. Bacteriol.* **2016**, *198*, 3109–3118.
106. P. A. Williams, L. Coates, F. Mohammed, R. Gill, P. T. Erskine, A. Coker, S. P. Wood, C. Anthony, J. B. Cooper, *Act. Cryst.* **2005**, *D61*, 75–79.
107. H. Toyama, Z.-W. Chen, M. Fukumoto, O. Adachi, K. Matsushita, F. S. Mathews, *J. Mol. Biol.* **2005**, *352*, 91–104.
108. L. J. Daumann, *Angew. Chem. Int. Ed.* **2019**, *58*, 37, 12795–12802.
109. H. Lumpe, A. Pol, H. J. M. Op den Camp, L. J. Daumann, *Dalton Trans.* **2018**, *47*, 10463–10472.
110. P. Kalimuthu, L. J. Daumann, A. Pol, H. J. M. OpdenCamp, P. V. Bernhardt, *Chem. Eur. J.* **2019**, *25*, 8760–8768.
111. M. Prejanò, T. Marino, N. Russo, *Chem. Eur. J.* **2017**, *23*, 8652–8657.
112. M. Leopoldini, N. Russo, M. Toscano, *Chem. Eur. J.* **2007**, *13*, 2109–2117.
113. X. Zhang, S. Y. Reddy, T. C. Bruice, *Proc. Natl. Acad. Sci. USA* **2007**, *104*, 745–749.
114. Y.-J. Zheng, Z.-x. Xia, Z.-w. Chen, F. S. Mathews, T. C. Bruice, *Proc. Natl. Acad. Sci. USA* **2001**, *98*, 432–434.
115. S. Itoh, H. Kawakami, S. Fukuzumi, *J. Mol. Catal. B: Enzym.* **2000**, *8*, 85–94.
116. A. McSkimming, T. Cheisson, P. J. Carroll, E. J. Schelter, *J. Am. Chem. Soc.* **2018**, *140*, 1223–1226.
117. A. F. Khadem, M. C. F. van Teeseling, L. van Niftrik, M. S. M. Jetten, H. J. M. Op den Camp, A. Pol, *Front. Microbiol.* **2012**, *3*, 345.
118. M. C. F. van Teeseling, A. Pol, H. R. Harhangi, S. van der Zwart, M. S. M. Jetten, H. J. M. Op den Camp, L. van Niftrik, *Appl. Environ. Microbiol.* **2014**, *80*, 6782–6791.
119. W. Versantvoort, S. Guerrero-Cruz, D. R. Speth, J. Frank, L. Gambelli, G. Cremers, T. van Alen, M. S. M. Jetten, B. Kartal, H. J. M. Op den Camp, J. Reimann, *Front. Microbiol.* **2018**, *9*.
120. H. N. Vu, G. A. Subuyuj, S. Vijayakumar, N. M. Good, N. C. Martinez-Gomez, E. Skovran, *J. Bacteriol.* **2016**, *198*, 1250–1259.
121. S. Masuda, Y. Suzuki, Y. Fujitani, R. Mitsui, T. Nakagawa, M. Shintani, A. Tani, *mSphere* **2018**, *3*.
122. M. Farhan Ul Haque, B. Kalidass, N. Bandow, E. A. Turpin, A. A. Dispirito, J. D. Semrau, *Appl. Environ. Microbiol.* **2015**, *81*, 7546–7552.
123. F. Chu, M. E. Lidstrom, *J. Bacteriol.* **2016**, *198*, 1317–1325.
124. F. Chu, D. A. C. Beck, M. E. Lidstrom, *PeerJ* **2016**, *4*, e2435.
125. M. Wehrmann, C. Berthelot, P. Billard, J. Klebensberger, *mSphere* **2018**, *3*, e00376–00318.

126. W. Gu, M. Farhan Ul Haque, A. A. DiSpirito, J. D. Semrau, *FEMS Microbiol. Lett.* **2016**, *363*, fnw129.
127. M. Wehrmann, C. Berthelot, P. Billard, J. Klebensberger, *bioRxiv* **2019**, 670216.
128. W. Gu, J. D. Semrau, *Appl. Microbiol. Biotechnol.* **2017**, *101*, 8499–8516.
129. N. Picone, H. J. M. Op den Camp, *Curr. Opin. Chem. Biol.* **2019**, *49*, 39–44.
130. L. Chistoserdova, *Mol. Microbiol.* **2019**, *111*, 1127–1131.
131. J. D. Groom, S. M. Ford, M. W. Pesesky, M. E. Lidstrom, *J. Bacteriol.* **2019**, 00120–00119.

Subject Index

A

Metal Ions in Life Sciences, Volume 21 Guest Editors: Peter M. H. Kroneck and Martha E. Sosa Torres
Series Editors: Astrid Sigel, Eva Freisinger, and Roland K. O. Sigel

https://doi.org/10.1515/9783110589771-011

B

C

D

E

F

G

H

I

K

L

M

N

O

P

Q

R

S

T

U

V

W

X

Y

Z